150 Topics in Current Chemistry

Relationships and Mechanisms in the Periodic Table

With Contributions by
D. J. Clouthier, P. L. Corio, N. D. Epiotis,
C. K. Jørgensen, D. C. Moule

With 105 Figures and 49 Tables

Springer-Verlag Berlin Heidelberg NewYork
London Paris Tokyo

This series presents critical reviews of the present position and future trends in modern chemical research. It is addressed to all research and industrial chemists who wish to keep abreast of advances in their subject.

As a rule, contributions are specially commissioned. The editors and publishers will, however, always be pleased to receive suggestions and supplementary information. Papers are accepted for "Topics in Current Chemistry" in English.

Editorial Board

Preface

Topics in Current Chemistry was established in 1949 under the
title "Fortschritte der chemischen Forschung" to provide review
articles on topics of current interest in all areas of chemistry.
Originally, contributions were published in English, French and
German. With Volume 13 (1969), the subtitle "Topics in Current
Chemistry" was added and in 1974 (Volume 48) the latter became
the primary title; since then the publication language was ex-
clusively English.

The present 150th volume and its 40th anniversary is an occasion
to briefly reflect the development of this series. Over the years
many distinguished authors from all over the world have con-
tributed to a total of 648 review articles. Organic, inorganic, metal-
organic, physical and biochemical, applied and theoretical aspects
of small and macromolecular molecules — wherever a new develop-
ment or a current interest existed the Editors strived to provide the
scientific community with high quality and up-to-date surveys of
the state of the art.

With the enormous growth in chemical research over these
40 years, research workers need every possible help with the cor-
respondingly large primary literature. The Editors and the Pub-
lisher anticipate that Topics in Current Chemistry will continue to
serve the chemical community as actively as in the past. We wish
to take this occasion to thank all contributors and guest-editors,
past and future.

The Editors   The Publisher

Table of Contents

Are Atoms Significantly Modified by Chemical Bonding?

Christian Klixbüll Jørgensen

Section de Chimie, Université de Genève, CH 1211 Geneva 4, Switzerland

Table of Contents

1 Total Energies

If quantum chemistry can be of any help, when discussing bonds, it is inevitable to discuss total binding energies of all the electrons to one nucleus with the charge Z times the protonic charge, and to two or more nuclei with the charges Z_1, Z_2, Z_3, ... and to consider the chemical bond energy as the (quite small) difference between the latter and the sum of the former (monatomic) energies, in spite of chemists being accustomed to calorimetric determinations of enthalpy differences, or various techniques determining differences of free energy.

Already in the magnesium atom ($Z = 12$) the sum of the 12 consecutive ionization energies found [1] for the gaseous atom and gaseous ions Mg^{+n} is 5450.56 eV or 200.303 hartree, 1 eV being 8065.48 cm^{-1} in the wave-number units used by spectroscopists, 96,485 joule/mole or 23.03 kcal/mole. For (not perfectly understood) reasons, a remarkably general expression for the total binding energy of Z electrons in the neutral atom is the Gombas-Gaspar energy [2, 3]

$$E_{GG} = Z^{2.4} \text{ rydberg} \tag{1}$$

where one rydberg is 13.6058 eV, half of the atomic unit of energy 1 hartree = 27.2116 eV. This expression [3] had already previously been discussed by Foldy [4] and Scott [5]. Neglecting the minute effect of the ratio between the rest-mass of the electron and of the nucleus, Eq. (1) is exact for $Z = 1$, and decreases (as far as observed energies [1] up to $Z = 17$ go, followed by relativistic calculations [6] of more than sufficient precision for our purpose) from $1.10E_{GG}$ for helium to $1.027E_{GG}$ for carbon, and then mildly oscillating between 1.03 and $1.02E_{GG}$ up to rhodium ($Z = 45$) with a shallow minimum close to nickel ($Z = 28$), and then, for relativistic reasons, increasing to $1.063E_{GG}$ for mercury ($Z = 80$) and achieving $1.104E_{GG}$ in fermium ($Z = 100$).

The first question asked by the chemist is how strong the effects of closed electronic shells in the noble gases are. A plausible [3] expression for the closed-shell effect in neon is

$$I_1(F) + 2I_1(Ne) - 2I_1(Na) - I_1(Mg) \tag{2}$$

formed by weighting of the first ionization energy I_1 of the adjacent elements in a way involving six electrons. The resulting 42.6 eV or 1.57 hartree is 1.2 percent of the total binding energy of electrons in the neon atom. The analogous expression is 29.7 eV for argon, 25.8 eV for krypton ($Z = 36$) and 21.7 eV for xenon ($Z = 54$). These values correspond to 0.2 percent for argon, below $6 \cdot 10^{-4}E_{GG}$ for krypton, and $1.1 \cdot 10^{-4}$ for xenon. Unfortunately, it is not possible to evaluate the analogy to Eq. (2) for radon ($Z = 86$) but there is no doubt that it is only a few times $10^{-5}E_{GG}$.

These closed-shell effects are normally at least 10 times larger than the heat of atomization (per atom occurring) which varies between 0.64 eV for Hg and 8.8 eV for W among the metallic elements, and is 7.5 eV for diamond (having two "single bonds" per carbon atom). The dissociation energy of the diatomic molecules N_2, BO, BF, CN, CO, SiO, ZrO, NbO, LaO, CeO, HfO, TaO, ThO and UO is above 8 eV (including a few cases on the limit of the estimated experimental certainty). Only a few triatomic molecules show atomization heats above 12 eV (such as OCO, OCS and

HCN). It is a remarkably general rule that very few compounds have heats of atomization above 4 eV, though the huge heat of atomization of carbon is accompanied by values per atom around 5 to 6 eV in organic molecules with quite few "single bonds" such as HCCH and its trimer, benzene. For comparison, it may be noted that the heat per atom for NaCl-type LiF, hexagonal (wurtzite) BeO, and BN is 4.6, 6.1 and 6.1 eV, respectively. The BF_3 molecule has 5.0 eV and SiF_4 4.8 eV, but the values are well below 4 eV for CF_4 and SF_6.

It might be argued that chemical bonding is an exceedingly small perturbation compared to the total electronic binding energy. However, this would be neglecting that the major part of E_{GG} is due to the 10 inner-most electrons for Z above 20, and to the two 1s electrons for low Z. The first ionization energy I_1 varies across the Periodical Table in a very defined way [1] with the extreme values 3.894 eV for caesium ($Z = 55$) and 24.587 eV for helium. Photo-electron spectra of gaseous molecules ("vertical" I values following the principle of Franck and Condon) vary [7-9] between 16.46 eV in SiF_4 and 5.4 eV in $Cr(C_6H_6)_2$ (with marginally lower I for similar organometallic [10] molecules) showing that the loosest bound orbitals must be quite modified, compared to the gaseous atoms. Hartree-Fock (optimizing one well-defined electron configuration to the closest one can come to the true groundstate of the Schrödinger equation) is an established technique for gaseous atoms [6] and monatomic ions, but the Hartree-Fock treatment of molecules with 2 to, say, 12 nuclei needs an enormous scale of computing, and has approached the goal with all atoms having Z below 10, except perhaps one having Z below twenty [11-13].

The two major imperfections in the Hartree-Fock model are the relativistic effects [14-17] and the correlation effect [18]. As far as the total energy goes, the relativistic effect is the largest for Z above 13, and then increases rapidly, E_R being 1 percent larger than the analogous [6] non-relativistic energy E_{NR} for $Z = 32$, and $1.1 E_{NR}$ for $Z = 96$. The chemistry of elements up to nobelium ($Z = 102$) is only strongly influenced on a few points, such as the difficulty of oxidizing $K = 80$ (this is the Kossel [19-21] electron number used for the definition $z = (Z - K)$ of the oxidation state z of non-catenated, non-metallic compounds [22]) systems thallium(I), lead(II) and bismuth(III), or the surprising fact that the dissociation energy of diatomic Au_2 is half as large as of H_2, and twice the value for Li_2 and I_2.

The correlation effect is 1.1 eV in the groundstate of the helium atom, and 10 times larger in the neon atom. To the first approximation [23]

$$-E_{corr} = (0.7 \text{ eV}) Z^{1.2} \tag{3}$$

proportional to the square-root of E_{GG} and crossing 100 eV around $Z = 66$ (dysprosium). This seems very innocuous to most chemists, though I_1 of all atoms starting with sodium ($Z = 11$) are smaller than $-E_{corr}$ taking out the backbone of the variational principle, since an infinite number of states of identical symmetry type occurs in the interval between the Hartree-Fock groundstate and the lowest (non-relativistic) energy compatible with the Schrödinger equation. However, a much more nagging problem is that the electronic density of the Hartree-Fock wave-function seems to agree quite accurately with the actual three-dimensional distribution, as well as the average $\langle r^2 \rangle$ providing diamagnetism, but it seems almost certain that the "squamp", the squared amplitude of the Hartree-Fock function in the true non-relativistic ground-

3

state, decreases dramatically from its known values 0.99 in helium and 0.93 in neon. An (admittedly rather crude) second-order perturbation argument [23] suggests the squamp to decrease from 0.7 to 0.3 for Z increasing from 30 to 70. If we insist to express molecular orbitals (M.O.) in the model of linear combinations of atomic orbitals (L.C.A.O.) we may have many reasons to worry with a squamp around a-half. Quantum chemistry adds new complications to those present in monatomic entities, but it takes over the whole burden of the many-electron atoms supplying fascinating difficulties [3,24]. It is noted that the typical heats of atomization of compounds (per atom) are 30 to only 2 or 3 percent of $-E_{corr}$ going from $Z = 11$ to 99, once more implying that quantum chemistry (in the deductive, not the classificatory, sense) is hazardous for two-digit Z values.

The *photo-electron spectra* both of inner shells [9,20,25] and of loosely bound penultimate M.O. (which were often considered arbitrary fictions produced by approximate calculations before 1962) have illuminated many obscure fields of quantum chemistry [7,8,10,26,27]. Originally, many organic chemists were feeling uneasy about the methane molecule showing three M.O. having I close to 14 eV, and one close to 23 eV, though this situation is not more distressing than the spherical neon atom having $I_1 = 21.6$ eV due to removal of one 2p electron, and a one-shot ionization energy 48.5 eV with the ionized configuration $1s^2 2s 2p^6$. The inner-shell ionization to form $1s 2s^2 2p^6$ is measured to cost $I = 870.3$ eV, almost 20 eV below the value 890 eV calculated for the Hartree-Fock function with rigid radial functions, but in good agreement with a calculated energy difference between the Ne^+ allowed to modify its radial functions, and the Ne groundstate. This is connected with Eq. 3, the intra-atomic correlation showing up as lower observed one-shot I values than predicted from the Hartree-Fock groundstate, to the extent about [25] 0.8 eV times the square-root of the Hartree-Fock I value (in eV). For the chemist, it is much more interesting that molecules and solids show large additional interatomic relaxation effects. It was believed before 1971 that the "chemical shifts", i.e. the variation of inner-shell I values to an extent typically 4 to 10 eV in compounds of a given element, are due to varying oxidation state, and to Madelung potentials. Many deviations from this rationalization were discovered before 1976, and the major third effect is variation of interatomic relaxation, convincedly seen in I of all inner shells of metallic mercury being 3 eV lower than in the gaseous atom. More extreme behaviour is seen [28] of inner shells of metallic magnesium, calcium, strontium and barium having I values some 5 to 7 eV lower than in the gaseous atoms. We return below to the related ideas of "chemical polarizability".

Numerically, we cannot expect too much from quantum chemistry involving two-digit Z values, if we insist on obtaining information about changes in total energy by combination and re-shuffling of atoms. On the other hand, the last 30 years have seen a rich harvest of rationalizations based on "group-theoretical engineering" and study of manifolds of closely related, low-lying energy levels (including the groundstate). Atomic spectra as developed after the analysis of the neon spectrum by Paschen in 1919 (seven years before the Schrödinger equation) induced familiarity with a gradual transition between two coupling-schemes having two well-defined asymptotic versions. This situation conserves the number of states (the number of mutually orthogonal wave-functions) such as $(2J + 1)$ in each J-level in spherical symmetry, combined in (S, L)-terms having $(2S + 1)(2L + 1)$ states in one extreme of Russell-Saunders

coupling (quite weak spin-orbit coupling) and assign the J-levels to j, j-coupling in the opposite extreme of very strong relativistic effects. This way of thinking has been very important in "ligand field" theory [22, 29–32] where the I^q configuration redistributes its number of states (45 for d^2 or d^8, 120 for d^3 or d^7, ...) in different ways on the Γ_n symmetry types characterizing a given local point-group (in our example O_h as appropriate for regular octahedral MX_6) in one extreme bunched together ("weak field") in the terms of spherical symmetry (such as ^3F, ^1D, ^3P, ^1G and ^1S of d^2 or d^8) and in the other asymptotic treatment, the Γ_n levels are allotted to "strong field" sub-shell configurations, in the octahedral example $(xz; yz; xy)^{q-a} (x^2 - y^2; 3z^2 - r^2)^a$ each having a definite number $a = 0, 1, 2, 3$ or 4 of strongly anti-bonding electrons (in the general d^q case). Γ_n replaces L of spherical symmetry and remains combined with a definite value of S.

When describing chemical bonding, the two major coupling-schemes are valence-bond (V.B.) and M.O. There is a general tendency for (especially main-group) chemists to pull in direction of the V.B. treatment, and (in particular d-group) spectroscopists to prefer the M.O. description. There is the analogous superiority of the V.B. and the "weak field" model at long internuclear distances R between the M and X nuclei, and of M.O. and "strong field" (which is actually M.O. treatment with special emphasis on Slater-Condon-Shortley parameters of interelectronic repulsion separating levels of the same configuration) and, for instance, predicting a difference $2DS_0$ between all states having $S = S_0$ and the average energy of all states $S = S_0 - 1$, stabilizing high S values, like in monatomic entities, but alien to main-group situations is that the basis set of V.B. **is not the same** as M.O. and that the overlap integrals are huge, frequently approaching 1, between V.B. structures, whereas "ligand field" treatment has only one configuration with a partly filled shell, and strictly orthogonal diagonal functions. The argument that taking into account the infinite number of V.B. and of M.O. states produces the same end result, is entirely unreceptive to what an infinite number of states really means in presence of continua of eigen-values. We return in Section 5.2 to this problem.

2 What are Bonds?

This Socratic question has two sides:

2.1 Static Aspects (Internuclear Distances)

Diffraction of X-rays or neutrons by crystals have provided very rich material on internuclear distances R. If explicit determination of angles is not required, electron diffraction of gaseous molecules, or X-ray and neutron diffraction of vitreous materials, solutions, etc. may many times provide acceptable R values. If one asks for the distribution of distances from a given point in a gas of geometrical points, the density in a shell between R and $R + dR$ is proportional to $4\pi R^2 dR = P$. This is also valid in actual compounds and alloys for very long R, but not at all for short R. Fig. 1 is a qualitative probability distribution of R values (normalized by division with P) for nuclei of a given element, or for a combination of two definite elements Z_1 and Z_2. Contrary

5

to early ideas of "pseudo-atoms" such as HCo in $HCo(CO)_4$ to imitate $Ni(CO)_4$ there are no very short R values observed. There is a strong, asymmetric peak at a typical "bond distance" R_0 followed by a very shallow "Van der Waals valley" usually at least 1 Å wide. Then, a stronger oscillating curve takes over, asymptotically converging to a constant height. The high, sharp peak represents "chemical bonds". Noble gases, X-X distances in crystals formed by MX_n molecules, and a few other exceptions may only show the oscillating structure at long R. It is far rarer for an observed R to be 0.2 Å shorter than R_0 (and such cases tend to be chemically very unreactive, such as N_2 and the uranyl ion OUO^{+2}) than to be $R_0 + 0.2$ Å or even $R_0 + 0.3$ Å. If Z_1 and Z_2 show sufficiently differing chemical behaviour to be ascribed highly different electronegativities, it can be argued that R_0 can be significantly separated in two contributions, one from Z_1 and one from Z_2 if approximate additivity can be obtained from the combination of a given Z_1 with many Z in their R_0 values. It cannot be stressed too much that such parameters, e.g. "ionic radii" can always be added a small constant (running up to 0.8 Å for the competing system of "covalent radii") for cations, on the condition of subtracting a similar constant from the anions. This excercise does not work for hydrogen. It must be added, in all fairness, that the system of genuine ionic radii is based on the assumption of direct anion-anion contacts in NaCl-type LiI and in CaF_2-type CeO_2. Nevertheless, one cannot aspire to perfect additivity, as seen from R = 2.105 Å in MgO, 2.222 Å in MnO, 2.602 Å in MgS and 2.612 Å in NaCl-type MnS, showing [33] a deviation almost 5 percent in the additivity. Larger discrepancies are observed in the 10 NaCl-type hydrides and fluorides increasing R smoothly from 2.04 Å in LiH to 3.19 Å in CsH, and from 2.086 Å in LiF to 3.005 Å in CsF, 0.23 Å difference.

The Van der Waals valley on Fig. 1 gets small contributions of varying origin. One source is disordered crystals (like the classical example of 1-chloro-2-bromobenzene having only half a molecule CCCX in the unit cell, X having the apparent Z = 26) and experimental uncertainty, twinning of crystals; etc. It is important to remember [34] that crystallography makes an averaging twice: it determines the time average of the average content of the unit cell. When hydrogen atoms were difficult to detect, many X-X had a hidden hydrogen bond, as known from the symmetric strong hydrogen bonds in FHF^- and in many bridges between carboxylic groups and carboxylate anions [35] as discussed in Sect. 3.1. Genuine Van der Waals distances shortened by
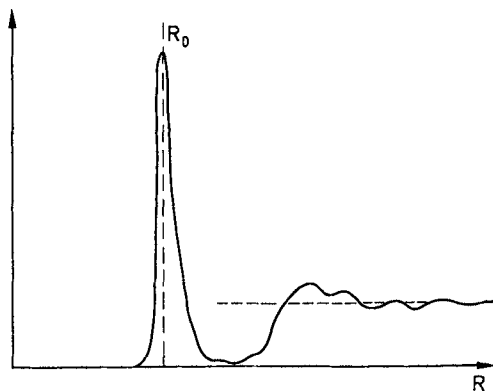

Fig. 1. Typical distribution (normalized by division by $4\pi R^2 dR$) of the (Z_1 to Z_2) internuclear distances in the manifold of all compounds containing the two elements characterized by Z_1 and Z_2 (or the same element $Z_1 = Z_2$). The mean value R_0 for the asymmetric peak is the "average bond length". The stippled curve is the statistical average value for long R

some further interaction are the best documented for sulphur-sulphur and iodine-iodine distances. The heterocyclic thiothiophthenes [36, 37] contain two electrons too little to establish two "single bonds" between three essentially colinear sulphur atoms showing R = 2.36 Å, that is 0.3 Å longer than typical disulphides, but at least 1 Å below S . . . S Van der Waals contacts. Crystalline CdI_2 has very short I-I contacts, but is colourless in contrast to many other layer-type compounds [38] frequently being opaque to visible light (like MoS_2) as known from low-energy gap semiconductors such as silicon, germanium and PbS. Since the *coordination number* N is the number of M-X contacts sufficiently close to R_0 it can be a matter of opinion whether some of the bonds are so long that they rather belong to the Van der Waals valley [39, 40]. For instance, the CsCl type has M-M 1.1547 (a purely geometric factor) times longer than M-X. The cubic type having Cs and Cl identical, represents the common modification of metallic iron, chromium, molybdenum, tungsten, niobium and tantalum, and the question is whether N is 8 or 8 + 6 = 14. In typical compounds, bonds elongated 15 or 20 percent are not usually counted in N.

2.2 Dynamic Aspects
(Dissociation Energies and Free Energies of Complex Formation)

There is no universal relation between the length R of a bond, and the energy needed to dissociate it (if it can be done; or to break N equivalent bonds simultaneously). Most text-books insinuate that bonds are short, when strong. The truth is rather the other way: nearly any bond succeeding in being short (as N_2 compared with P_2 which dimerizes to tetrahedral P_4; or CO and CN) achieves a high dissociation energy. This may be a great part of a secret of the one-digit Z atoms having only two electrons in the inner shell 1s. There has been much effort spent on deriving the force constant (of a diatomic molecule; or a conceptually isolated M-X) from the vibrational wavenumber (infrared or Raman) proportional to $(k/\mu)^{1/2}$ where k is the second differential quotient d^2U/dR^2 of the potential curve U, and μ the reduced mass of the M-X vibrator. Close to the minimum of the potential curve, the agreement between this quantum of vibrational energy and the parabolic shape of U is usually excellent, but it does not really tell much about the Morse-curve letting U (in a gaseous molecule) become horizontal for large R, at a distance above the potential minimum giving the dissociation energy (plus half a vibrational quantum). As well-known from "ligand field" cases [41] of d^5 systems having S = 5/2 (sextet) groundstate and a first excited state S = 3/2 (quartet), the excited state may shrink, having its potential minimum at shorter R than the groundstate. The situation is further complicated in condensed matter (solutions, vitreous and crystalline solids) where there is no Morse limit at longer R, the other atoms present strongly counter-act the expansion of the M-X system. Optical excitation at an energy far above the dissociation of the weakest bond may not always induce dramatic photo-chemistry in condensed matter, for this reason, whereas a similar molecule in a dilute gas at least shows pre-dissociative broadening of the vibronic spectrum at a photon energy exceeding the lowest dissociation energy. One of the disadvantages of determining dissociation energies in the gaseous state is that cations cannot be studied so readily, though studies of appearance potentials in mass-spectra may be helpful.

Photo-electron spectra have allowed us to speak freely about "vertical" (and in fortunate cases "adiabatic" at lower I, without vibronic co-excitation due to changed R values) ionization energies of gaseous molecules, like one has done [1] most of this century for atoms. In spite of a certain resistance among classical physical chemists, it has been recognized [22, 23, 41−44] that a chemical ionization energy I_{chem} can be defined by adding 4.4 or 4.5 eV to the standard oxidation potential E^0 relative to the hydrogen electrode. The most recent value proposed [45] for this constant is 4.42 eV in water, and, for instance, 4.6 eV in acetonitrile. A surprising corollary is that all gaseous atoms absorb energy (and hence do not form bonds in the sense used in molecules) when losing electrons and forming aqua ions in solution, with the marginal exception of lithium atoms. The way out of this dilemma is, that under normal circumstances, electrons are not available with zero energy; they need I_{chem} to be available, that is 4.5 eV per electron in a solution on the limit of developing H_2 (and any system capable of being reduced by n electrons to a species having I_{chem} at least 5.7 eV is able to liberate 0.2 atm. oxygen in equilibrium with the atmospheric air).

The thermodynamic properties of aqua ions can be described, using the words M_{aq}^{+z} in standard state in dilute aqueous solutions. As discussed in Sections 4.2 to 4.5, there is a wide graduation of stoichiometric models of this standard state. The first aqua ion generally recognized [40] was the mixed complex $Co(NH_3)_5(OH_2)^{+3}$ reversibly and rapidly deprotonating (with pK one unit higher than acetic acid) to $Co(NH_3)_5OH^{+2}$. Niels Bjerrum showed in 1909 that the violet $Cr(OH_2)_6^{+3}$ conserves its visible absorption spectrum for many hours in the presence of anions such as Cl^- and NCS^- (though classical measurements of the X^- activity show a proportion of them bound as second-sphere ion-pairs) and rearranging to $Cr(OH_2)_5X^{+2}$ with different absorption band positions. The alums such as $K[Cr(OH_2)_6](SO_4)_2$, $6 H_2O$ have the same transmission and reflection bands. Detection of the exchange of water bound to chromium(III) became possible with stable isotopes, but deuterium did not solve the problem, since the reactive intermediate is $Cr(OH_2)_5OH^{2+}$ forming $Cr(OD_2)_6^{+3}$ after 12 consecutive exchanges of deuterons in a large excess of heavy water. Only when ^{18}O became available, the 20 h half-life of Cr—O bonds confirmed opinions derived from kinetics of outer-sphere complexes transforming to Werner complexes. Such ^{18}O studies were continued by Henry Taube on a large scale, especially on cobalt(III). These results made the slow reactions of octahedral Cr(III), Co(III), Rh(III) and Ir(III) complexes prepared by S. M. Jørgensen (and argued by Alfred Werner to be octahedral a long time before crystallographic structures could be obtained) convincing evidence for chemical bonds, like in other inorganic compounds. Later, it was shown that nickel(II) forms octahedral complexes with bidentate ligands, such as with three phenanthroline (racemizing in minutes) and ethylenediamine (having reactions in the 10 to 1000 seconds range in freezing methanol at −100 °C, and already quite slow at −50 °C).

Eigen developed temperature-sudden-jump techniques allowing the water exchange in aqua ions to be measured in time-scales between 10^{-9} and 1 s. This gave a lot of surprising information, but a difficulty is that it cannot be readily determined how many water molecules are exchanged (rapid rates may refer to the, by far most mobile, ligand) nor how many are present in the aqua ion. With bad luck, sulphate outer-sphere ion-pairs rearranging to $MOSO_3$ or MO_2SO_2 groups may not be easy to distinguish from OH_2 exchange. At 25 °C, the green $Ni(OH_2)_6^{+2}$ was shown to

exchange with half-life 10^{-4} s, whereas at least one water molecule in the copper(II) ion exchanges more rapid than 10^{-9} s, and also more rapid than the zinc aqua ion now known to be $Zn(OH_2)_6^{+2}$ [in contrast to $Zn(NH_3)_4^{+2}$]. One may loosely classify aqua ions in five categories, the first being octahedral $N = 6$ and tetrahedral and quadratic $N = 4$, with a strong preference for both stereochemistry and N. A small second group comprises aqua ions of chromium(II), manganese(III) and copper(II) for which both $N = 5$ and 6 can be defended. A third, rather large group is best known from the trivalent lanthanides [23, 46–48] where $N = 9$ and/or 8 are the major possibilities. The exchange rate (reciprocal 1/e) decreases [49] at 25 °C in the unit 10^8 s^{-1} from 4.96 for terbium, 3.86 for dysprosium, 1.91 for holmium, 1.18 for erbium, 0.81 for thulium and 0.41 for ytterbium, meaning half-lifes in the nanosecond range. Cerium(III) have strong transitions [50] in the ultraviolet due to the excited configuration containing a 5d rather than a 4f electron. Luminescence and absorption spectra [51] of $Ce(OH_2)_9^{+3}$ ethylsulphate show one of the nine Ce—O bonds strongly distended in the excited state (living for 10^{-8} s) and arguments can be given that about 4 percent of the cerium (III) in aqueous solution have $N = 8$. Low concentrations of erbium(III) incorporated in ice [52] may show $N = 8$. Neutron diffraction (of rather concentrated) solutions, using different isotopes of the same element, might have solved this problem. However, both neodymium(III) showing an average $N = 8.5$ (equal amounts [53] of $N = 8$ and 9?) and dysprosium(III) $N = 7.5$ may be somewhat [54] influenced by the high salt concentration. Anyhow, this problem is less fundamental than it would be for a d-group chemist. The numerous crystal structures known of yttrium(III) and lanthanide(III) compounds show a rich variation of N from 6 (very rarely regular octahedral), 7, 8, 9, 10, 11 to 12 (both cuboctahedral, and icosahedral in $M(O_2NO)_6^{-3}$ salts). This is not a specific property of rare earths, it is also found by thorium(IV) and calcium(II), suggesting that the major reason is large ionic size compared to Al(III), Ga(III), Ti(IV) and Mg(II). Neutron diffraction of 1.0 to 3.9 molar calcium chloride solutions [55] indicate a gradual decrease of the average N from 10 to 6.4. These measurements did not allow an estimate of the distribution of adjacent N values for Ca(II), but agree with the calcite-type of $CaCO_3$ having $N = 6$ and the aragonite-type (exclusively found for $SrCO_3$ and $BaCO_3$) $N = 9$. The cubic perovskites $CaZrO_3$ and $SrTiO_3$ have $N = 12$ in cuboctahedral coordination.

A fourth category of aqua ions have also a wide dispersion of N values on an instantaneous picture, but at the same time, they are less defined because of wide dispersion of R, and the water molecules may be far less systematically oriented toward the cation than still true for Ln(III). K^+, Rb^+ and Cs^+ belong to this category, and probably also Tl^+. On the other hand, the silver(I) ion is now known [40] to be $Ag(OH_2)_4^+$ in contrast to linear $Ag(NH_3)_2^+$. An argument that Na^+ and Li^+ rather belong to the third category is that the Kohlrausch ionic conductance of K^+ is 50 percent larger than of Na^+ indicating a smaller effective diameter of the mobile potassium(I) than of $Na(OH_2)_x^+$ using Stokes' law. Ba^{+2} is likely to belong to this lax category, what may be less likely for Sr^{+2}. Since a cation forming a salt soluble in water must have contact with OH_2 at some long distance, there is a fifth category so large that the surrounding water behaves like the second-sphere water around $Cr(OH_2)_6^{+3}$ and $Co(NH_3)_6^{+3}$. Members include $N(CH_3)_4^+$, $N(C_4H_9)_4^+$, $P(C_6H_5)_4^+$ and di-protonated $H_3NCH_2CH_2NH_3^{+2}$ undoubtedly involving hydrogen bonds to the solvent like NH_4^+. However, one should not assume that the influence of the ambient water is quite

negligible on such large cations. It is discussed in Sect. 5.1 that the ionization energy 3.06 eV of gaseous I^- is increased 3.2 eV by the hydration energy to the (adiabatic) $I_{chem} = 6.3$ eV slightly lower than the photo-electron I close to 8 eV found for solid iodides of large cations. By the same token, I $= 6.88$ found [10, 56] for ferrocene $Fe(C_5H_5)_2$ vapour is modified to E^0 of formation of $Fe(C_5H_5)_2^+$ close to $+0.5$ V in aqueous solution, the I_{chem} being 1.9 eV lower than the gas-phase I. Taken at face value, this suggests a hydration energy almost as large as expected, in view of the ten Fe-C distances in the molecule being 2.06 Å and the 10 Fe ... H distances 2.81 Å, corresponding to a diameter about 6 Å and a hydration energy close to 2 eV for the cation of comparable size.

It is far beyond the competence of the writer to discuss the large and complicated difference between liquid water (formed with an heat evolution 0.45 eV per mole) and gaseous H_2O molecules. Nevertheless, some of the most precise inorganic work involves exchange of water in aqua ions with ligands, normally emphasizing differences in free energy $\Delta G \doteq RT(\ln K)$ from formation constants K. When anions are involved, these "constants" depend strongly on the other ions present, and as emphasized by Jannik Bjerrum [57] it is convenient to maintain an ambient salt medium of 1 to several molar $NH_4^+NO_3^-$ or $Na^+ClO_4^-$. The order of magnitude of K $= [CrCl_{aq}^{+2}]/[Cr_{aq}^{+3}]$ $[Cl^-]$ for exchange of one water molecule in chromium(III) aqua ions with one chloride ligand is 0.2. However, Bjerrum pointed out that if the activity of water is not put at 1, as earlier, but the ejection of one water molecule occurs in a solution already 55 molar, the alternative K_{alt} is 55 times larger, or 11. Nickel(II) forms so weak a chloro complex that $Ni(OH_2)_5Cl^+$ can only be detected in above 9 molar hydrochloric acid. Under these circumstances, the activity coefficients vary so dramatically that other weak complexes such as $CoCl_4^{-2}$, $CuCl_3(OH_2)_x^-$ and $CuCl_4^{-2}$ need a special technique [58]. On the other hand, all six ammonia complexes were shown [57] to be formed as octahedral $Ni(NH_3)_n(OH_2)_{6-n}^{+2}$ with K_n decreasing smoothly from 500 to slightly below 1 from n $= 1$ to 6. These results of step-wise complex formation revised earlier ideas derived from the crystallization of solid compounds, and showed (after taking the molarity 55 of water into account) preferential binding of the first ammonia molecule 30,000 to the sixth 50 times, relative to water. It was also noted that the ratio K_1/K_6 is larger than the statistical value 36 one would obtain, if the variation with n is exclusively due to available positions. A more extreme case is palladium(II) where the ammonia complexes $Pd(NH_3)_n(OH_2)_{4-n}^{+2}$ are formed [59] with $K_1 = 4 \cdot 10^9$ normally written $\log_{10} K_1 = 9.6$, and the three subsequent $\log_{10} K_n = 8.9; 7.5$ and 6.8. If K_1 had been much larger, it would have been almost impossible to determine, because pK $= 9.3$ of NH_4^+ implies that the ratio $[NH_4^+]/[NH_3]$ necessarily is $2 \cdot 10^9$ at pH zero, providing a lower limit of free ammonia concentration in presence of ammonium ions. For comparison, it may be noted that $\log_{10} K_1$ for the chloro complex is close to 4 (so the first chloride complex is half a million times weaker than the first ammonia complex) and that K_1 is small, and close to 1 for the first nitrate complex [60]. Complex formation was not detected with ClO_4^- and p-toluenesulphonate "tosylate". The situation of comparable binding of water and chloride, and much weaker than of ammonia, is general for the 3d group (excepting the copper(I) chloro complexes) but not for ions like silver(I), palladium(II) and mercury(II) more similar [59] to copper(I).

Entropy differences contribute to a large extent to the formation constants in aqueous solution, in particular of multidentate amines (of which ethylenediamine is the

simplest case) and biological and synthetic amino-polycarboxylates (such as ethylene-diamine-tetra-acetate). In such cases, very strong complexes can be accompanied by endothermic (such as the dissolution of $NH_4^+NO_3^-$ in water, increasing the entropy strongly) or, at least, much weaker exothermic effects than expected. Such cases of opposite sign of ΔG and of ΔH are striking in fluoride complexes [61] destroying a high degree of order of water around the dissolved F^-. This effect is beyond doubt related to strong hydrogen bonding known not only from salts of FHF^- but also from the species in hydrofluoric acid having $pK = 3$ not involving diatomic HF in water, but the strongly bound [62] ion-pair $OH_3^+F^-$. By the way, H_{aq}^+ is now known from vibrational spectra [63] to be H_3O^+ (as known from crystalline mono-hydrates of perchloric and of p-toluenesulphonic acid). The reason that this species had problems getting accepted (like NH_4^+) is the short life-time close to $2 \cdot 10^{-12}$ s. This means that a water molecule in pure water (necessarily containing 10^{-7} molar H_3O^+ and 10^{-7} molar OH^-) on the average every millisecond goes through the avatar of H_3O^+. When many text-books write $H_9O_4^+$ it is a quite asymmetric [63] adduct $O(H \ldots OH_2)_3^+$ like the hydrogen bonds in ice are asymmetric, not abolishing the individuality of the H_2O molecules (but modifying them quite a lot from the gaseous H_2O).

When 1 eV of free energy G at 25 °C means 16.9 powers of 10 in equilibrium constants, it also means that even the largest complex formation constants known are on the limit of resolution of a theoretical description, if this limit hardly is better than 1 eV (that is $2 \cdot 10^{-5}$ of the total electronic binding energy of a zinc atom). When the first ammonia ligand is $10^{11.3}$ times better bound than the water ligand replaced [59] in the palladium(II) complex, the ΔG is only 0.67 eV, to be compared with ΔH of neutralizing H_3O^+ with OH^- being 0.6 eV. This shows that "bonds" in aqueous solution are not always very similar to those in slowly reacting cobalt(III) and rhodium(III) complexes, of which many isomers can be isolated.

3 Carbon and Other One-Digit Z Elements

3.1 Straightforward Lewis (1916) Behaviour

The paradigm of Lewis [64] was that single bonds are effectuated by *two electrons*. The many difficulties and exceptions to this theory have been discussed at length in this series [40]. Because inorganic solid compounds usually do not contain molecules, the inherent tendency to non-stoichiometry makes it difficult to give the number of inorganic compounds better than a factor 2, but it is certainly above 10^5 and hence, organic compounds are some 10 times more numerous. Since perhaps half of the organic molecules can be reasonably well-described by the Lewis electron pairs, the paradigm is not far from majority, but now recognized to be miles away from universality. It should be added in all fairness that the paradigm was formulated 10 years before Schrödinger published his equation. It started as fixed places for each electron pair in the valence shell (not without connection with the resolution in 1900 of sulphonium cations $(SRR^*R^{**})^+$ with three different substituents in optically active enantiomers, as if they contained an "inversible substituent" compared to a carbon atom with four different substituents) and slowly evolved to a picture of small-amplitude vibrations of the electrons around their equilibrium positions (much like we

consider nuclei in a crystal or molecule). This model was entirely alien to atomic spectroscopy, and the quantum chemistry slowly developing after 1927 was much closer to the ideas of Kossel [19] in 1916, and the spectroscopic version of the Periodic Table [23, 65] established by Stoner in 1924.

The proposal [64] of exactly **four** electron pairs in the well-behaved elements is a relatively less fundamental part of the Lewis paradigm, as seen from the behaviour of hydrogen (**vide infra**) and octahedral species such as SF_6, $Co(NH_3)_6^{+3}$ and $PtCl_6^{-2}$ being slower reacting (more "robust") than many organic compounds. Pauling (having a profound knowledge of crystallography, and a keen interest in quantum chemistry) incorporated 1931 the Lewis paradigm in the hybridization model [40, 41] creating a strong need for allocating 12 electrons to bonding of octahedral species.

There are huge groups of compounds which nicely fit the simplest version of the Lewis paradigm. The best case is acyclic alkanes C_nH_{2n+2} starting with methane, and having a strongly increasing number of isomers for n at least 4. The C—H and C—C bonds are so similar in polarity that nobody felt any need to distort the electron pair close to one of the two atoms. This question might have attracted attention if CF_4 was a more familiar molecule (but "teflon", polymerized CF_2 was a technological "spin-off" of the Manhattan project in 1944, needing hydrogen-free lubricants C_nF_{2n+2} not taking fire in presence of gaseous UF_6 used for ^{235}U isotope separation). Quarternary ammonium cations such as $N(CH_3)_4^+$ are clearly isoelectronic with alkanes, in the example neopentane $C(CH_3)_4$, and the molecule $Si(CH_3)_4$ used as proton magnetic resonance reference, and all the corresponding germanes, stannanes and plumbanes (especially those with only one heavy atom) were perfect subjects. This is also true for diamond, and the isotypic silicon, germanium and grey tin. It is even the case for binary *adamantoid semiconductors* such as GaAs, ZnSe, CuBr, in a sense isoelectronic with Ge (though the beginning polarity in ZnSe makes CuBr a somewhat far-fetched case) and the corresponding InP, InAs, InSb, CdTe ... As implicitly incorporated in the hybridization model, it is striking to recognize one success of the Lewis paradigm in substituted alkanes: regardless of the different size of hydrogen, fluorine, chlorine, bromine and iodine atoms (as seen from C—X bond lengths) the bond angles remain remarkably close to those occurring in a regular tetrahedron. Carbon and nitrogen compounds in this category are also invariantly colourless, with exception of yellow iodoform HCI_3 and red CI_4 (this is, of course, not true for low-energy gap adamantoid semiconductors involving two-digit Z atoms). If N = 4 was exclusively a question of relative atomic size, one would expect the small carbon atom to "rattle" in CI_4 but it does not on the time-scale of Raman spectra.

It is difficult to indicate the highest Z values for which the Lewis paradigm still has legitimate examples. HgI_4^{-2} seems regular tetrahedral in spite of the strong tendency to N = 2 in ClHgCl and IHgI (the yellow, less stable solid contains this molecule, whereas the tomato-red modification of HgI_2 is a cross-linked polymer). It is difficult to tell exactly how regular tetrahedral BiI_4^- is; Gillespie says it contains a lone-pair, but the cubic crystal Cs_2TeCl_6 only shows deviations from regular octahedral symmetry [29] at short, spectroscopic time-scales, though tellurium(IV) and bismuth(III) are closely related by containing two electrons more than a closed d shell. The opposite problem of N above 4 in one-digit Z elements is discussed in Sect. 4.1, alkyl bridges between two Be(II) or Al(III) show N = 5 for carbon, the molecule $Li_4(CH_3)_4$ has N = 6 for carbon (bound to three lithium atoms of a face on the central Li_4 tetra-

hedron, and to three hydrogen atoms) like the molecule $CRu_6(CO)_{17}$. Non-metallic CaF_2-type Be_2C and Li_2O have $N = 8$ for carbon and oxygen. Actually, Be(II) is relatively much more invariant tetrahedral $N = 4$ than carbon.

The compounds complying with the Lewis paradigm exemplify the ideas of Frankland on valency (derived 1850 from studies of pyrophoric $Zn(CH_3)_2$ and other organometallic compounds with M—C bonds) and one of the earliest definitions of valency was that it is 1 for hydrogen atoms. This exception from 4 electron-pairs was quite acceptable to Lewis; after all, the helium atom has only 2 electrons, whereas neon, argon, krypton, xenon and radon have 8 electrons in their outermost shells. Then, hydrogen should invariantly have $N = 1$. Some nagging exceptions were known, such as FHF^-. There are also hydride bridges [39, 40] such as $(OC)_5CrHCr(CO)_5^-$ closely similar to the analogous dimeric chromium(0) complex with iodide bridge. The old paradox diborane $H_2BH_2BH_2$ can be thought of as having two hydride bridges, zirconium(IV) boranate $Zr(H_3BH)_4$ as having three hydride bridges in each of the ligands (providing $N = 12$) and NaCl-type LiH to CsH having $N = 6$ like the cubic perovskites $BaLiH_3$ and $EuLiH_3$ having a regular octahedron for lithium(I) and each H(—I) is bound to two Ba(II) or Eu(II) on each of two Cartesian axes, with R $\sqrt{2}$ times as long as for the two Li-H distances on the third Cartesian axis.

3.2 Multiple Bonds Between One-Digit Z Elements

At the end of last Century, the more aliphatic part of organic chemistry had been very successfully classified with single bonds in R_3CX (X = H, F, Cl, Br, OH, NH_2, SH, ...), double bonds in ketones R_2CO and aldehydes (allowing one or both R to be hydrogen) and "olefins" R_2CCR_2, and triple bonds in nitriles RCN and acetylenes RCCR. Malonic acid can be fully dehydrated to OCCCO having only double bonds. This system provided the most constructive use for the Lewis paradigm. The sum of the multiple bonds is 4 in carbon atoms (with exception of CO having the highest known dissociation energy among all diatomic molecules; it is recently considered as having a triple bond between C^- and O^+ making it isoelectronic with N_2 having the next-highest dissociation energy, and almost cancelling its electric dipole moment). This is true for NR_4^+ as well, but ammonia, primary RNH_2, secondary R_2NH and tertiary amines R_3N were said to have a *lone-pair*. In well-behaved elements maintaining four electron pairs, one way or another, the number of bonds multiplied by their bond-order 1, 2 or 3, and the number of lone-pairs, have the sum 4. Subsequent crystallographic and electron-diffraction studies of molecules have certainly confirmed the indications of lone-pairs in R_3P, R_3As, R_3S^+, R_3Se^+, R_3Te^+, the pyramidal SO_3^{-2}, ClO_3^-, SeO_3^{-2}, BrO_3^-, TeO_3^{-2}, IO_3^-, XeO_3, $Pb(OH)_3^-$, $SnCl_3^-$, $SbCl_3$, $TeCl_3^+$ and the tetragonal pyramidal (like an octahedron lacking a ligand) TeF_5, IF_5 and XeF_5^+. Gillespie [66] elaborated a model, where lone-pairs in main-group compounds occupy somewhat larger spatial angles than bonds to atoms, rationalizing the distorted stereochemistry. As long only one lone-pair is present, photo-electron spectra [9, 26] show one low I of the gaseous molecule. Troubles start, when the Lewis paradigm prescribes two or more lone-pairs; gaseous H_2O has one non-bonding orbital with $I = 12.6$ eV, but the second lone-pair cannot be detected (we are not here speaking about ice) and evidence can hardly be found for three lone-pairs in HF to HI. Recent quantum-

13

chemical results [40] are also opposed to the idea of two distinct lone-pairs in H_2O, and in general to the Lewis paradigm in many carbon to fluorine compounds. It is clear that counting lone-pairs and multiple bonds is based on a unshrinking belief in the sum representing 4 electron-pairs. This is why NaCl-type nitrides, oxides and even some non-metallic carbides with N = 6 are uncanny, and cannot all be swept under the rug as ionic compounds (as MgO and Li_2O perhaps may be). The writer has great sympathy for the pragmatic use of double and triple bonds in organic compounds, but is very reluctant (cf. Sect. 5.2) to greet multiple bonds involving two-digit Z values as more than figments (with a possible and metaphorical acceptance of triple, short V-O and U-O bonds in vanadyl and uranyl ions [67] in analogy to N_2).

3.3 Aromatic Colourless Systems

Formiate HCO_2^- and other carboxylate anions RCO_2^-, nitro-alkanes RNO_2 and benzene C_6H_6 have mild problems with the Lewis paradigm. One of the two oxygen atoms in a carboxylic group might carry the negative charge (having been a OH group before the deprotonation of the acid) and form a single bond to the carbon atom, and the other oxygen form a double bond. This situation of average bond-order 1.5 occurs also in benzene, where each of the two Kekulé structures with alternating single and double C—C bonds is compatible with the counting of electron pairs. The problem of RNO_2 is more a question of nitrogen being as well-behaved as not yearning for five electron pairs (like PF_5). Before Arrhenius, ammonium salts NH_4X had five bonds, like nitric acid $HONO_2$ one single and two double bonds. It may be noted that, by far, most stable nitrogen(V) compounds have N = 3 and hence the average bond order (NO_3^-) 1.33, and that strongly oxidizing N(V) with N = 4 (ONF_3 and NF_4^+) have only single bonds, necessitating N^+O^- in ONF_3 and in two of the three N—O bonds of nitrate.

There is no doubt that the "resonance structures" were conceived as a "mesomeric" migration of electron pairs in analogy to the tautomeric mobility of protons in many compounds. From a purely quantum-mechanical point of view [29] instantaneous pictures of atoms and molecules each show the electrons on scattered positions, like a swarm of bees tending to be close to one or more queens (this metaphor for the nuclei has the weak point that they are thousands of times heavier than the electrons). Only a large number of repeated, differing, instantaneous pictures add up to the "objective" electron density prescribed by the wave-function. Of the nuclei are approximated with geometrical points, three nuclei cannot avoid being co-planar, and hence to exemplify the point-group C_s, but P_4, CH_4, ... cannot avoid almost always having nuclear positions exemplifying the lowest point-group C_1 in the same strong sense that almost all real numbers are irrational, the Cantor cardinality being larger than the rational or even algebraic (non-transcendental) numbers. Only the time average of such instantaneous pictures possesses the point-group T_d. The whole idea of "fluxional" molecules is an extension of tautomerism, such as mercury(II) cyclopentadienide $Hg(C_5H_5)_2$ showing N = 2 on instantaneous pictures, having only one short R to each of the two pentagons C_5 (like a circus seal rotating a hula-hoop with five bells attached on his nose) in contrast to $Fe(C_5H_5)_2$ having ten identical internuclear distances Fe-C to the (admittedly almost freely rotating) pentagons.

We know that nuclear positions are to be taken seriously, but is there really any argument for insisting on resonance between Lewis structures? However much absence of two 1,2-substituted benzene isomers is a doubtful argument, all subsequent vibrational spectroscopy and crystal structures have discouraged the two Kekulé structures to subsist (whereas many protonic tautomers have been fully characterized). In larger aromatic hydrocarbon molecules, the numerous Kekulé structures become rather complex. Already naphthalene can have one of the five $C=C$ between the two central carbon atoms (having no $C-H$), or this central bond can be single, needing three and two double bonds in the two connected hexagons. When a sufficient number of hexagons and other polygons occur, the chemist may ask (like the little child looking for the elegant clothes of the Emperor in the tale of Hans Christian Andersen) whether Lewis structures involving varying bond-order are really the only ingredients needed to describe such systems (Sect. 5.2) and this is the reason why Hückel treatment of aromatic molecules and polyatomic ions (like the well-known ligands $C_5H_5^-$, $C_7H_7^+$ and $C_8H_8^{-2}$) became a strong incentive to M.O. theory (much as "ligand field" ideas later became in the specific field of partly filled d shells) though the straightforward aliphatic compounds were left under V.B. jurisdiction.

Nearly all aromatic hydrocarbons and derived heterocyclic systems, and also the CCO_2 and CNO_2 sub-systems ("moiety" groups) have their nuclei in a plane (let it be $z = 0$) on a time-average picture. Wave-functions (including "orbitals") then have to choose between being "σ" having the same value in the points $(x, y, -z)$ and (x, y, z), or "π" changing sign, when z is multiplied by -1. This is an operation analogous to parity in the presence of an inversion centre at $(0, 0, 0)$ being *even* (g = "gerade") when the wave-function is identical in each couple of $(-x, -y, -z)$ and (x, y, z), or *odd* (u = "ungerade") when it is multiplied by -1. Though the main part of the Hückel treatment frequently is called "π" electron theory, one should not confuse this two-valued quantum number with λ in the linear symmetries replacing l from spherical symmetry, being denoted σ ($\lambda = 0$), π(1), δ(2), φ(3), ... Among the three orbitals of a given p shell, one (angular function proportional to z) is σ and two (x and y) π, but the "π" is (z) and the two "σ" (x and y). Quite general, *if* an orbital can be characterized both by l and by λ, it is "σ" when $(l + \lambda)$ is even, and "π" when $(l + \lambda)$ is odd. Hence, the $(2l + 1)$ orbitals of a given shell distribute on $(l + 1)$ being "σ" and l being "π".

3.4 Organic Colorants

It is, of course, a physiological accident that colourless compounds do not absorb light below 3.2 eV (bees would put this limit at 4 eV, where the ozone layer cuts off the solar spectrum) but the text-book expectation that organic colorants just have their excited "π" system states at lower energy than anthracene and dipyridyl encounters complications. Lewis and Calvin [68] wrote a review: "The Color of Organic Substances" illustrating how the numerous "resonance structures" of V.B. treatment induce a genuine difficulty, that most organic colorants are not only aromatic (though not all planar, as seen from derivatives of orange $C(C_6H_5)_3^+$ called triphenylmethyl colorants, in contrast to the colourless carbinol $C(C_6H_5)_3OH$, where OH can be replaced by H or Cl in a fairly smooth way). There is no predominant "resonance structure" for the groundstate, which can be described by three or more chemical formulae (in the Lewis

sense) all quite plausible. The typical organic colorants fall outside "colourless" organic chemistry by not allowing this choice, and it was argued early that the low-lying excited states are alternative linear combinations of these structures.

A typical triphenylmethyl colorant is Crystal Violet (Gentian violet) $C[C_6H_4N—(CH_3)_2]_3^+$ having three *para*-(dimethylamino) substituents, one on each benzene ring. Changing to a moderate acidic solution, the cation has added a proton, and carry two positive charges, and is green. In very strong acid, the yellow cation has added two protons, having $+3$ charge. Malachite Green $(C_6H_5)C[C_6H_4N(CH_3)_2]_2^+$ has only two p-dimethylamino-substituted rings, and keeps one unsubstituted phenyl group. At pH below 2, the colour changes from green to yellow, the cation with two charges having accepted a proton. The common feature of these cations are that the positive charge no longer is delocalized more or less evenly on the 19 carbon atoms of $C(C_6H_5)_3^+$ but to a large extent is delocalized on the nitrogen atoms, protonated or not. This should be itself "normalize" the cation from the point of view of Lewis, but the paradox remains that the structure having nitrogen in the $+1$ cation of Crystal Violet or Malachite Green carrying the charge, also induces a quinonic situation with four double bonds, one $C=C$ between the central carbon and the ring carrying the positively charged nitrogen, two (and not three) $C=C$ between the six phenyl carbon atoms, and finally $C=N$.

Armstrong pointed out in 1885 that both *para* (1, 4) and *ortho* (1, 2) quinones normally are colored, and suggested typical aromatic colorants to be "quinonoid", a quite successful hypothesis. Among essentially planar aromatic colorants may be mentioned alizarine, the 1,2-dihydroxo derivative (substitution in α- and β-position on one ring) of anthraquinone, which can itself be thought of as anthracene having added an oxygen rather than a hydrogen atom on the two accessible carbon atoms of the middle ring. Before alizarine was synthezised, it was an important agricultural product from the madder root. It is a pH indicator; it is moderately orange under most circumstances, but at high pH, or even at pH around 5 in the presence of dissolved aluminium(III) salts, the solutions turn dark red, and precipitate the aluminium complex on textiles. The red colour is due to the deprotonated anion having lost the protons from the two OH groups, chelating many metal ions as a bidentate ligand.

Among many other colorants, conceptually derived from the three-ring anthracene $C_{14}H_{10}$ Methylene Blue may be mentioned. This cation has a very high molar extinction coefficient $\varepsilon \sim 10^5$ in the red, and has the two middle carbon atoms replaced by one nitrogen and one sulphur atom, and at β-position relative to sulphur (γ-relative to the heterocyclic N) one H replaced by one $N(CH_3)_2$ group on each of the two C_6 rings. Once more, it is a matter of sheer opinion, whether one places the positive charge of the Methylene Blue cation on the sulphur atom, or at several other places. This ambiguity is much more pronounced in the large class of "xanthene dye-stuffs" of which the major fragment is also derived from anthracene. The S atom of Methylene Blue is here an oxygen, and the N now carbon, but nearly always substituted by one α-benzoate group $C_6H_4CO_2^-$ (which may be protonated at low pH). On each of the two external rings of anthracene, an O (or OH) group is situated in β-position. The fluoresceinate anion flu^{-2} is this system without any H attached to the oxygen atoms. With pK $= 6.7$, a proton is fixed in flu^- at the carboxylate group, hardly having any spectroscopic consequences. The neutral flu^0 is formed with pK $= 4.4$, and is a quinonic form (one H on one of the two exterior O, and one on the carboxylic group)

in equilibrium in less polar solvents with a lactonic tautomer, and the cation flu$^+$ formed in aqueous solution with pK $= 2.2$ (and in molten boric acid with great ease, probably establishing ring-C to O-B contacts, like poly-alcohols forming $B(OR)_4^-$ with $B(OH)_3$ becoming a quite strong acid). The long-lived triplet state in boric acid and in very strong aqueous acids [69, 70] has a different fluorescence band, and may also undergo "delayed" fluorescence by (slowly) being thermally excited to the first excited singlet state, having a life-time of only $4 \cdot 10^{-9}$ s and very high quantum yield of fluorescence.

Other xanthene dye-stuffs are Eosine substituted by four bromine atoms on the three-ring moiety of fluorescein, and Rose Bengal [71] having four iodine atoms there, and further on, four chlorine atoms on the benzoate moiety. The various versions of Rhodamine (of great importance for tunable lasers [72]) have in common the two exterior oxygen atoms of fluorescein being replaced by $N(C_2H_5)_2$ substituents. It is evident that this is not the space for summarizing all the chemistry of colorants [73, 74] but for our purpose, the important feature is that, in a certain sense, organic colorants do not have definite chemical formulae, but are ambiguous about *the* place in large poly-atomic cations and anions, where the charge is localized to the first approximation. This reminds one of the (relatively rare) ligands which are not "innocent" in the sense [22] of allowing neighbour atoms with a partly filled d-shell to have a definite oxidation state, which is a far deeper difficulty than just being mixed electrovalent-covalent, as usually the case for inorganic compounds.

It has frequently been pointed out that graphite being black, and a two-dimensional metal, is a limiting case of very large aromatic systems. As we discuss in Sect. 5.3, the chemical bonding characterizing the metallic state, has some precursors in the strongly coloured compounds, not being openly metallic. An interesting case is the photochromic compounds [48, 75, 76] shifting intense absorption bands by spiropyran rearrangement or related modifications in dithizonate complexes of heavy metals. A subject touching the next Section is the molecule C_{60} detected in mass-spectra of volatilized carbon. It seems to have icosahedral symmetry, the quasi-spherical surface covered with pentagons and hexagons, and called buckminsterfullerene (after a famous architect) [77, 78] though it is not absolutely excluded that other symmetries of C_{60} may be nearly as stable, and reorganizing very slowly [77, 79].

3.5 Computer Compounds

Besides quantum-mechanical calculations being feasible for a molecule or ion containing a few nuclei of one-digit Z elements, without any need of experimental input (though in many cases, the internuclear distances are prescribed by extrapolation of known species) there has been a motivation for calculations derived from mass-spectra of cations having a composition unfamiliar to inorganic chemists. For several years, quantum chemistry has been the best (and only) available way of getting information about structure of H_3^+, CH_5^+ (looking as a loose adduct of H_2 and CH_3^+) and many gaseous lithium compounds such as Li_6C, Li_4S and Li_6S. As other examples of such molecules not following customary valency rules may be mentioned the studies by Wu [80] of gas-phase equilibria, involving Li_5O (heat of atomization 13.3 eV), Li_4O (12.0 eV) and Li_3O (10.0 eV). Admittedly, these values are not **much** larger than

17

7.7 eV for Li_2O (compared with 1.0 eV for gaseous Li_2). By the way, the heat of atomization of Li_4 is 3.4 eV, so in this sense, lithium behaves like phosphorus.

Without worrying too much about [11] how CASSCF calculations are performed on CRAY 1, 2, 3 ... computers, it is worth noting that a very fruitful field is *helium chemistry*. Among neutral molecules, it started [81] with HeLiH, but it is now [82] doubted whether the bond-breaking between He and diatomic LiH was not evaluated to 0.08 eV because of insufficient accuracy of the model used in 1969. On the other hand, more elaborate calculations [83] show that HeBeO needs 0.17 eV for dissociating to He and gaseous BeO (which, of course, has an energy of condensation to crystals of 6.7 eV). It is hoped that the triatomic HeBeO may be detected in cool matrices (such as argon solidified by sudden cooling to 4 K).

Nearly all the numerous helium-containing species [84] stable toward dissociation in the gaseous state are cations. Mass spectra clearly show He_2^+, HeH^+ (experimental dissociation energy 1.95 eV), $HeNe^+$, and $HeCN^+$ calculated [85] to need close to 1.6 eV to dissociate in He and CN. Most diatomic MX^+ have relatively high dissociation energies (Chapt. 35 of Ref. [29]) because they dissociate to M^+ and X^0 or to M^0 and X^+. The major part of gaseous MX^{+2} have a repulsive potential curve for large R because of Coulombic interaction between the two most stable fragments M^+ and X^+. However, if the ionization energy I_2 of M^+ is lower than I_1 of X^0 there is no strong repulsion at large R. Actually, $HeBe^{+2}$ is calculated [86] to have the dissociation energy ~0.7 eV and $HeTi^{+2}$ 0.16 eV. It is argued [86] that HeV^{+3} has a metastable potential minimum in spite of Coulombic repulsion (I_3 of V^{+2} is 29.31 eV) and dissociates very slowly, if formed. $HeRh^{+2}$, HeW^{+2}, $HePt^{+2}$ and He_2Pt^{+2} are detected [87] in mass spectra, adding to the complication of MH^+ looking like "supernumerary" isotopes of M^+. With the argument above, all lanthanides have I_3 of Ln^{+2} lower than I_1 = 24.59 eV of helium, with exception of 24.9 eV for Eu^{+2} and 25.05 eV for Yb^{+2}. Hence, at long R, $HeEu^{+3}$ and $HeYb^{+3}$ dissociate repulsively to He^+ and Ln^{+2} (showing that the base helium coordinated to Eu^{+3} or Yb^{+3} is too strongly reducing) whereas the other $HeLn^{+3}$ should have an absolute minimum of the potential curve. The predicted chemistry [82, 84] of helium and neon is quite different from that [21, 29, 88] of krypton (I_1 = 14.00 eV) and xenon (I_1 = 12.13 eV) extensively studied since 1962, though Pauling [89] predicted in 1933 that perxenate XeO_6^{-4} (in analogy to $Sb(OH)_6^-$) and several other compounds can be prepared. For instance, HeF^+ is calculated to be repulsive for all R (HeN^+ seems to have the dissociation energy 0.15 eV and $HeNe^+$ 0.4 eV) whereas calculated ArF^+ (needing [21] gegen-ions such as BeF_4^{-2} or BF_4^- providing a strong Madelung potential for permitting hope of isolation) and numerous salts of KrF^+ and XeF^+ are quite stable. These NgF^+ (noble gas) dissociate to Ng^+ and F^0. The chemistry of helium does not involve bonding to strongly electronegative elements, but rather helium acting as a base coordinating to H^+ and strong anti-bases (Lewis acids) such as gaseous M^{+2} and M^{+3}.

Organo-helium chemistry has been treated [82, 84] with the most refined computing techniques available. The groundstate and low-lying excited states are either triplet (S = 1) or singlet (S = 0) and can have surprisingly different R values for the (absolute or relative) potential minima. For instance, HeC^{+2} has a dissociation energy (producing He^0 and C^{+2}) 0.7 eV comparable to $HeBe^{+2}$ having [86] a much lower I_2 = 18.21 eV of Be^+. Gaseous He_2C^{+2} has a strongly bent (84°) singlet groundstate (to be compared with singlet of CF_2 but triplet of the isoelectronic HCH 135°). R is 1.61 Å to be compar-

ed with the first (excited) triplet 1.17 Å (angle 100°) and, in HeC^{+2}, 1.58 Å for the singlet groundstate and 1.17 Å for the lowest triplet. Though isoelectronic with HCCH, the $HCCHe^+$ is **(trans-)**bent on both angles, the He—C distance 1.10 Å. This species may be detected as ephemeric result of β-decay in tritiated acetylene HCCT. The singlet groundstate of $HeCCHe^{+2}$ is linear, with He—C 1.08 Å, but is 5 eV unstable relative to two HeC^+. The linear doublet groundstate of $HeCC^+$ also has He—C 1.08 Å, but is a relative minimum, 1.7 eV unstable relative to the CC^+ groundstate.

Since helium is the second-most abundant element in the Universe, and carbon the fourth, and since O-(Wolf-Rayet) and B-type stars having surface temperatures above 30,000 K emit intense ultraviolet radiation able to ionize atoms to H^+ and even He^+ over large distance, the organo-helium cations may play an astrophysical rôle. In many (rather dark) clouds, the interstellar space contains familiar and less familiar molecules, such as CO, CH, CH^+, OH, HCO, HCO^+, CCH, NH_3, C_4H^+, H_2CNH, H_2NCN, CH_3OH, CH_3CN, CH_3NH_2, C_2H_5OH, HC_7N, HC_9N, $HC_{11}N$, ... mainly detected via their micro-wave rotational lines. In M- and S-type stars with low temperatures (below 4000 K) as well as in sun spots, diatomic molecules with high dissociation energy are frequently detected via absorption bands, mainly in the visible, such as C_2, CN, SiO, TiO and ZrO. A last example of the contributions of quantum chemistry to astrophysics may be mentioned, the low I_0 = 0.75 eV of gaseous H^-, 0.03 times I_1 of isoelectronic helium, where H^- (having no Hartree-Fock state) has great influence as an electron buffer in stellar atmospheres.

Predictable chemistry of (Z + 1/3) and (Z + 2/3) has had, until now, less involved numerical calculation than helium chemistry has. The need for such novel considerations arose when Gell-Mann in 1964 proposed three types ("flavours") of *quarks*, **u** (up) with charge +2e/3 and **d** (down) and **s** (strange) both with the charge —e/3 to justify the symmetry types and other properties of the roughly 100 known "elementary" particles. Two further quark types are now recognized, **c** (charm, +2e/3) and **b** (beauty, —e/3). This description became well-known [90] after 1974, suggesting that the proton (**u²d**) and neutron (**ud²**) are not anymore structureless than other nuclei characterized by the quantum numbers Z and N = (A — Z) with quark configuration $u^{2Z+N}d^{Z+2N}$. On geochemical time-scales, any negatively charged system is rapidly quasi-permanently fixed on a positive nucleus (most likely ^1H and ^4He in Cosmos) and a quite strong fractionation is predicted [91-94] of the individual "new elements" having their chemical behaviour determined by their (Z ± 1/3) almost independently of their atomic weight, which may easily be 300 to 10^8 amu. Recently, a new proposal is of **uds**-matter [95-97] having roughly twice the density of conventional nuclei and containing comparable amounts of **u, d** and **s** quarks. This may represent the opportunity [23,65,94] to find fractional charge in systems containing (3A + 2) quarks (but atomic weight much above A) in concentrations around one per 10^{20} amu (6000/g) or higher, in specific minerals or sea-bottom manganese nodules. Z is much lower than A, but can well be high above 100 because of differing barriers against fission [92-94]. The parallel description [98] of predicted (Z ± 1/3) chemistry in terms of Mulliken electronegativities of monatomic entities is impeded by difficulties becoming conspicuous by comparison with the chemistry of known elements [94,99].

4 Two-Digit Elements

4.1 Preferred Stereochemistry

It is perfectly legitimate that models of "chemical bonds" have the ambition to predict bond angles and not only to rationalize the bond-breaking (and full atomization) energies, and the internuclear distances R in different categories of compounds. The interest in tetrahedral distribution of nearest-neighbour atoms around carbon and many other elements, and in octahedral coordination of slowly reacting d-group elements, was high at the end of the last century, a long time before crystal structures were available (and confirmed most of the ideas already known). In the hybridization model of Pauling (1931) bond angles were transcribed backwards to be indicators of the hybridization prevailing, as we all are familiar with $N = 3$ sp^2 and $N = 4$ sp^3 labelling. This remodelled version of the Lewis paradigm has many problems, when two-digit Z atoms are involved [40]. However, it may be worthwhile to consider unusual aspects of boron stereochemistry. Beryllium(II) is regularly tetrahedral to an even stricter degree than carbon, so one might have interpolated that B(III) would be similar. Indeed, monomeric BX_3 and BF_4^- show $N = 3$ and 4 like nitrogen(V). How-ever, the cubic crystals CaB_6 isotypic with the semiconducting Sr(II), Ba(II) and Eu(II) hexaborides, and the metallic $M =$ La, Ce, Pr, Nd, Gd and Th showing the conditional oxidation state [22,23,65] Ln[III] and Th[IV] with loose electrons have $N = 24$ for M (beating the record of organometallic compounds such as $U(C_5H_5)_3X$ and $U(C_8H_8)_2$ having $N = 16$) and the boron atoms form a network of octahedral B_6 moieties, connected in the six Cartesian directions with 6 other octahedra. That means $N = 5$ for each boron atom, situated above the plane of 4 B in a square, and completing the pyramid with a fifth B on the top. The same environment of 4 B is found [100] in $B_6H_6^{-2}$ being an octahedron "with nothing in the middle" as known from cluster compounds such as $Nb_6Cl_{12}^{+2}$, $Ta_6Cl_{12}^{+3}$, $Mo_6Cl_8^{+4}$ and one of the modifications of Pt_6Cl_{12}. By the way, boron also forms tetrahedral B_4Cl_4 analogous to P_4. The icosahedral [100] anion $B_{12}H_{12}^{-2}$ has $N = 6$ for each boron situated above a pentagon B_5 and having an axial hydrogen atom. Many other boranes and anions contain more or less complete fragments of a B_{12} icosahedron, as is also true for several crystalline modifications of boron. The carborane anion $C_2B_9H_{11}^{-2}$ functions as a ligand closely similar to $C_5H_5^-$ stabilizing [101] nickel(IV) and cobalt(III) by two C and three B in the $N = 10$ complexes. The effect of carbon substitution in octahedral $C_2B_4H_6$ and icosa-hedral $C_2B_{10}H_{12}$ brings a touch of sanity into carborane chemistry, B being replaced by the isoelectronic C^+, like pyridine in its protonated form is a replacement of C by N^+ in benzene. It may be noted that icosahedral [102] dodecahedrane, aliphatic $C_{20}H_{20}$ has been reported. The text-book comment to boranes is "electron-deficient" in the sense that $N = 5$ in octahedral and $N = 6$ in icosahedral surfaces of the B_n armour cannot obtain 10 or 12 electrons demanded by the Lewis paradigm. Assuming that the B—H requires 2 electrons, neutral boranes of the octahedral type have, on the average, 1 electron available per B—B bond (like H_2^+) and the icosahedral type 0.8 electron. In the anions $B_6H_6^{-2}$ and $B_{12}H_{12}^{-2}$, these values are 7/6 and 13/15, respec-tively. This behaviour indicates that some delocalized M.O. are filled, and other (with L.C.A.O. basis set B 2s; B 2p; H 1s) are empty (as pointed out by Longuet-Higgins)

at higher energy. This field may be rationalized by the polyhedral skeleton electron-pair approach and the tensor surface harmonic theory [103−105] also applicable to metal clusters (cf. Sect. 5.3). Actually, the more exotic aspects of boron chemistry illustrate well the situation of rigidly selected stereochemistry, though the local symmetry is rather low. We now turn to the two classical examples of d-group behaviour investigated by Werner.

4.2 Octahedral Coordination

This stereochemistry is frequently observed in sufficiently large main-group central atoms, such as Mg(II), Al(III), Ti(IV) (here not accounted as a d-group system because of the closed-shell character), Zn(II), Ga(III), Cd(II), In(III), Sn(IV), Sb(V), Te(VI), I(VII), Xe(VIII), Pb(IV) and, in the case of fluoro anions or MF_n also Si(IV), P(V), S(VI), Ge(IV), As(V) and Se(VI). Nevertheless, the overwhelming predominance of octahedral coordination occurs [29, 106] in the Tanabe-Kamimura stable d^3 (S = 3/2), d^5 (S = 5/2), d^6 (S = 0) and d^8 (S = 1) cases [21, 22] V(II), Cr(III), Mn(IV), Mn(II), Fe(III), Co(III), Ni(IV), Ni(II), Mo(III), Tc(IV), Ru(V), Ru(II), Rh(III), Pd(IV), Re(IV), Os(V), Ir(VI), Os(II), Ir(III), Pt(IV) and Au(V). In these d^3 and d^8 systems, 1.2 strongly anti-bonding d-like electron occurs less than the average value 2q/5 in octahedral complexes of d^q amounting to a "ligand field" stabilization of some 1 to 5 eV; and in diamagnetic (S = 0) d^6 systems 2.4 anti-bonding electron less than this average, amounting to 5 to 15 eV, as far as one-electron energy differences go (partly compensated by effects of spin-pairing energy, when decreasing S from 2 to 0). There is no such specific stabilization of d^5 with S = 5/2, so manganese(II) and iron(III) are usually octahedral for the same reasons as the similar magnesium(II) and aluminium(III). N = 6 is very rarely represented by other symmetries. Trigonal-prismatic N = 6 is known from crystalline MoS_2 and WS_2 allowing intercalation of (even large) molecules [38, 107] like graphite does, and bis- and tris-bidentate complexes of certain conjugated "non-innocent" ligands [22] of the maleonitrilo-dithiolate category. The oxidized complexes of apparent high oxidation number have very strong inter-ligand attraction between sulphur atoms, as seen from the almost square disposition of four sulphur atoms belonging to two different ligands.

4.3 Quadratic Coordination

The existence of MX_4 more stable in the point-group D_{4h} than in T_d has been considered, since 1931, as a striking argument for angular directivity in the chemical bonding. Nevertheless, the Madelung constant [22] is 2.1628 on the X site (if the X charge is —e) in the tetrahedral case, only 4 percent larger than 2.0858 in the quadratic case ("square-planar" is slightly redundant, most squares being planar). Nevertheless, this phenomenon is rather restricted to definite central atom configurations [29], mainly diamagnetic d^8 such as nickel(II), copper(III), rhodium(I), palladium(II), silver(III), iridium(I), the classical case platinum(II) of which many trans- and cis-isomers of MX_2Y_2 were isolated last Century, and gold(III); and the bromine(III) BrF_4^-, iodine (III) ICl_4^- and planar $Cl_2ICl_2ICl_2$ isosteric with Au_2Cl_6 and xenon(IV) in the XeF_4

molecule. The common feature of diamagnetic d^8 and p^2 systems is a lone-pair $(3z^2 - r^2)$ or (z) perpendicular on the molecular xy-plane, and strong bonding to those ligand p orbitals making the empty orbitals $(x^2 - y^2)$, or (x) and (y) strongly anti-bonding. According to Gillespie, there are two lone-pairs in XeF_4 taking the Xe 5s orbital into account, but it is rather futile to affirm or deny this [29].

Some quadratic nickel(II) complexes, such as yellow $Ni(CN)_4^{-2}$ having all nine nuclei on two Cartesian axes, can add cyanide to form orange $Ni(CN)_5^{-3}$ remaining diamagnetic, and isosteric with tetragonal-pyramidic, green (S = 1/2) $Co(CN)_5^{-3}$ and similar to $Cu(NH_3)_5^{+2}$. Two bidentate ligands form a rectangular coordination around d^8. This would be a geometric trivial remark, if it was not because dithiocarbamates $Ni(S_2CNR_2)_2$ and dithiophosphates $Ni(S_2P(OR)_2)_2$ show the bond angle SNiS to a given ligand below 80°. On the whole, many quadratic d^8 complexes show properties suggesting minor deviations from strict quadraticity, e.g. of palladium(II) [43, 59].

4.4 Indifferent N Above 6

There is little doubt that the abundance of octahedral main-group complexes is due to the fact that 6 ligands retained on a spherical surface with a central attractor, and having almost any plausible expression of inter-ligand repulsion, is highly stabilized as a regular octahedron. This contributes also to the relative scarcity of N = 5, as seen from gaseous PCl_5 crystallizing as $PCl_4^+ PCl_6^-$ (to be compared with $PBr_4^+ Br^-$). Werner expected all five regular "Pythagorean" polyhedra to be preferred by compounds, but this is not at all true for N = 8 arranged in a cube MX_8. A monomeric entity would be unstable relative to an Archimedean tetragonal anti-prism D_{4d} in any monotonically decreasing inter-ligand repulsion, since turning the four X by 45° in the lower plane relative to the upper square X_4 would increase twelve X-X distances by at least 21 percent, decrease four by less than 11 percent, and let 12 out of 28 remain invariant. The sum of reciprocal X-X distances (using as unit the shortest X-X distance) is 22.79 in the cube and 20.93 in the Archimedean anti-prism. The cubic crystal types like CsCl and CaF_2 stabilize N = 8 by a collective effect of the Madelung potential.

Any models introducing a plausible inter-ligand repulsion conclude that N = 7, 8 (including both the tetragonal anti-prism and competing alternatives), 9, 10 and 11 are remarkably indifferent against the positions of the ligands on the constant distance R from the central nucleus. The Madelung potential in icosahedral MX_{12} is only 0.2 percent larger [29] than in cuboctahedral MX_{12}. These results agree with observations on calcium(II), yttrium(III), all the trivalent lanthanides [23, 46-48, 65], thorium(IV) and uranium(IV). There is hardly any sign of angular directivity, when N is above six.

4.5 Water, Other Solvents, and Glasses

It was already discussed in Sect. 2.2 that aqua ions in solution present a very wide dispersion (classified in five categories) from complexes almost as slowly reacting as organic compounds, e.g. $Rh(OH_2)_6^{+3}$, to species such as Cs^+ and Ba^{+2} where very slight orientation of closest neighbour water molecules (with a rather indeterminate N)

is expected. The kinetic and stereochemical aspects of several aqua ions were reviewed by Hunt and Friedman [108] showing extreme variations of rates of water exchange for, otherwise quite similar, aqua ions. From the point of view of the Lewis paradigm, the best example is $Be(OH_2)_4^{+2}$ at 25 °C (like the following values) having the life-time 0.55 millisecond. Its amphoteric deprotonation in alkaline solution to tetrahedral $Be(OH)_4^{-2}$ is without the complications of $Al_{13}(OH)_{32}^{+7}$ [in solution, disregarding degree of hydration, but probably $AlO_4Al_{12}(OH)_{24}(OH_2)_{12}^{+7}$ known from a crystal structure]. Evidence is available that lithium forms $Li(OH_2)_6^+$ with a life-time of order 10^{-11} s, but it is not excluded that a mixture of adjacent N values occur. As far as crystallization of salts goes, it is striking how unable many anions are to substitute H_2O in main-group aqua ions, as seen from $[Be(OH_2)_4]SO_4$, and $[Al(OH_2)_6]Cl_3$ precipitating from quite cold, concentrated hydrochloric acid (the corresponding chromium(III) salt can be prepared because of slow kinetics) whereas other hexahydrates contain $[Ni(OH_2)_4Cl_2]$, 2 H_2O and $[Gd(OH_2)_6Cl_2]Cl$. The life-time [108] of $Al(OH_2)_6^{+3}$ is 6 seconds, to be compared with 0.55 millisecond for the (otherwise so similar) gallium(III), and 2 microseconds for the isoelectronic $Mg(OH_2)_6^{+2}$.

In recent years, hexaqua ions of several d-group elements have been studied in salts and in acidic solution, such as molybdenum(III) [109], ruthenium(II) and (III) [110, 111] and iridium(III) [112, 113]. Previously, it was believed that quadratic $Pt(OH_2)_4^{+2}$ cannot be prepared (because of inevitable disproportionation to metal and Pt(IV) hydroxo complexes) but it has now been reported [114]. An interesting class of mixed aqua complexes is cis-$Au(CH_3)_2(OH_2)_2^+$ and fac-$Pt(CH_3)_3(OH_2)_3^+$ having very labile water [115] with life-times in the 10^{-5} s range [like $Sn(CH_3)_2(OH_2)_4^{+2}$ and $Ga(CH_3)_2(OH_2)_x^+$] and very moderate pK values. This shows far more pronounced trans-effects than in the isoelectronic mixed ammonia-aqua complexes. Nevertheless, $Au(CH_3)_4^-$ and $Pt(CH_3)_6^{-2}$ are known. There is little doubt that $AuCl_3(OH)^-$ is the anion of a mineral acid (i.e. having negative pK) but gold(III) is far more acidic than all other trivalent elements [116] with the exception of boron(III) and elements in columns V and VII. Text-books tend to say that $PtCl_5(OH_2)^-$ is also a mineral acid, but this derives from studies by Miolati of the dependence of ionic conductance as a function of concentration (by itself an excellent detector of H_3O^+) but pK is as high [117] as 3.8, and of $PtBr_5(OH_2)^-$ 4.4.

In mixtures of alcohols and a few percent of water [118] coloured aqua ions show very weak changes of absorption spectrum from water. At lower H_2O concentrations, the exchange of weakly bound CH_3OH and C_2H_5OH is superposed by the Katzin effect of strong affinity to nitrate (usually very weakly bound in aqueous [60] solution) and chloride (particularly striking in the trivalent lanthanides). From this point of view, water and ammonia seem to have pronounced propensity for replacing univalent anions, in contrast to polar organic solvents. This distinction takes on enormous proportions in octahedral $LnCl_6^{-3}$ and $LnBr_6^{-3}$ only known in acetonitrile solution [119] and in cubic [23] elpasolite-type Cs_2NaLnX_6. Solvent effects on the detailed electron transfer spectra [120] of $IrBr_6^{-2}$ and related robust complexes dissolved as $N(n—C_4H_9)_4^+$ salts in many organic solvents indicate shorter M-X distances (like under strong hydrostatic pressure) in the less polar solvents [121].

Glasses are usually non-stoichiometric mixtures (excepting molten $NaPO_3$) of differing oxides forming borates, silicates, phosphates, ... or, under more special circumstances, mixed fluorides [122-124]. The narrow absorption and luminescence

bands (due to transition between the excited J-levels belonging to $4f^n$ and the ground J-level) have been much studied in glasses [48, 50], partly because of applications in lasers [48, 124, 125] and in luminescent solar concentrators [126]. For our purposes, these spectroscopic studies have confirmed the strong dispersion of both N values and local symmetries [127]. This trend is also found for manganese(II) having a long-lived (1 to 25 millisecond life-time) high-yield broad-band fluorescence from its first excited quartet (S = 3/2) to its sextet (S = 5/2) groundstate [128, 129]. Though a major part of the Mn(II) may be fairly close to regular octahedral symmetry (as is definitely the case for nickel(II) and chromium(III) in fluoride [130] glasses) there may readily occur N = 6 with very low symmetry, or small concentrations of N = 7 and/or 5. Manganese (II) can store energy for some time (say milliseconds) and transfer it to lower-lying levels of simultaneously present lanthanides [129–131].

These observations must be seen against the background that glasses are molten at a fairly high temperature. By gradual cooling, the viscosity increases greatly, and in practice, the mobility of the nuclei is frozen in a rather narrow interval, producing a vitreous solid. Independently of what low temperature the spectroscopic measurements may be performed at, the dispersion of internuclear distances continue to be determined by the condition of glass-formation. Seen from this point of view, it is not surprising that some glasses [48] show high transition probabilities for emission and absorption in lanthanides, but it is in a way more instructive that nickel(II) and chromium(III) remain [130] so invariantly close to regular octahedral. The latter element has been much studied in oxide-type glasses, as reviewed [106] in connection with Cr(III) in glass-ceramics. According to the detailed nature of the immediate surrounding, this $3d^3$ system may sometimes emit a narrow line from the doublet state to the quartet groundstate (as known from ruby $Cr_xAl_{2-x}O_3$ acting as a laser) and/or a broad emission band in the near infrared from the first excited quartet state. The problem with conventional glasses [132] is that none has been found to emit the broadband luminescence with a quantum yield above 0.23 (in a lanthanum lithium phosphate glass). Much higher yields can be obtained [106] in glass-ceramics containing chromium(III). Everyday glass-ceramics are opalescent, but if the precipitated microcrystallites are much smaller than 1000 Å, a limpid glassy material is obtained without significant scattering of light. The micro-crystallites can be cubic spinel-type $MgCr_xAl_{2-x}O_4$ or $ZnCr_xAl_{2-x}O_4$ (gahnite); phases looking like petalite, virgilite, ... It is, to some extent, a conceptual problem to what extent heterogeneous materials are excluded from chemistry. Because of the nuclei, no compound is a fractal structure further down than to the Democrit limit, and even water may be *very* small pieces of ice sliding on a lubricating modification of very low viscosity. The inorganic chemist is accustomed to condensed matter usually not consisting of distinct molecules, and he feels no reason to refrain from discussing chemical bonding in materials that are not necessarily more non-stoichiometric than the minerals are, and most (but not all) properties can be studied without single crystals being available.

5 Categories of Chemical Bonding

Many text-books describe electrovalent, covalent and "metallic" bonding as the three paradigmatic categories of chemical bonding, adding cautiously that most compounds factually are intermediate cases between those asymptotes. As also pointed out by Epiotis in this volume [133] the "metallic" propensities show up even in materials that are not physical metals (conducting, with conductivity not increasing with higher temperature) and have some relation to the mildly diffuse [43] concept of "chemical polarizability" *not* being the first-order electric polarizability in a weak electric field.

5.1 Madelung Potentials, Differential Ionization Energies, and Hydration Energy

It was pointed out by Kossel [19] that the ionization energy of a noble gas is roughly 4 times larger than of the subsequent alkali-metal atom, and later, it became clear [1] that the difference $I_{n+1} - I_n$ is above a rydberg for elements from boron to fluorine, and of order of magnitude 10 eV for most other elements. It is not surprising that the unpolar character of C—H bonds, and the ready substitution of carbon for nitrogen, oxygen and sulphur made organic chemists believe that atoms are roughly neutral in compounds, and the polarity is a mild second-order effect relative to the two-electron bonds. This belief got embodied in the "electroneutrality principle" of Pauling that atoms have fractional charges in the interval $-e$ and $+e$ (though a weak point of this rule is that SF_6 and IrF_6 have F charge between $-0.17e$ and 0). However, inorganic chemists recognized before 1930 that [134] the Madelung potential frequently is capable of compensating the dramatic variation of I_n. The Madelung energy is $-\dfrac{\alpha}{R} z^2$ hartree/bohr $= -z^2$ (14.4 eV/Å)/R with the Madelung constant [22, 29] $\alpha = 1$ for diatomic MX; 3.5 for linear XMX; 7.268 for MX_3 in a plane with X_3 an equilateral triangle; 12.326 for tetrahedral MX_4 and 12.172 for quadratic (cf. Sect. 4.3) and 26.015 for regular octahedral MX_6. In all of these expressions, z is the charge of X (M having $+Ne$). In crystalline NaCl, Madelung performed (an apparent conditionally convergent) summation over an infinite lattice, arriving in a physically justifiable value $\alpha = 1.748$ and for the CsCl-type $\alpha = 1.763$. The concomitant energy is comparable to I_n variation; in alkali-halides, it varies from 12.5 eV for LiF to 6.4 eV for CsI. When applied to the NaCl-type MgO with $z = 2$, a *negative* electron affinity around -8 eV is evaluated for confined O^-, though in practice, a gaseous ion or atom, at the worst, can refuse to bind an electron. It was argued [134] that the CCl_4 molecule cannot be fully ionic (it would dissociate), but that $TiCl_4$ might be, though it was later shown [22, 135] that the Madelung energy of four Cl^- at the observed distance R = 2.18 Å from a central Ti^{+4} would only account for a tiny part of the observed heat of atomization of the molecule. It may be added that the early interest in Madelung energy was stimulated by the attractive theorem that the Coulomb interaction between spherically symmetric, non-overlapping ions can be evaluated from their representation as point charges in their centre (as Newton proved for gravitational attraction). Thus, it was argued [134] that all solid CaX containing calcium(I) would disproportionate to metallic calcium and ionic CaX_2 in close analogy to many copper(I) compounds, and it was

rationalized that Li(I) to Cs(I), Be(II) to Ra(II) and Al(III) only occur in the closed-shell form, the Madelung energy over-compensating the first I_n of the gaseous atom, but being too small to help opening the closed shell.

Rather than a black-or-white choice between electrovalent and covalent bonding, the concept of *differential ionization energies* [22,24,135] allows a quantitative model for a gradual change. Several authors had already remarked that an extended Hückel treatment provides a strong dependence of diagonal elements of the one-electron energy (as function of atomic fractional charge z) and it was suggested [136,137] to define the electronegativity x = dE/dz of an analytical function expressing the total energy of a gaseous ion as function of z. It is an almost obligatory step to consider the average energy of all the states of the electron configuration considered. Actually, the ground-state of the nitrogen atom is 2.4 eV below the barycentre of $1s^2 2s^2 2p^3$ and this difference increases regularily with z in the isoelectronic series, and is 4.3 eV in F^{+2} to be compared with 1.7 eV in P^0 and 2.3 eV in Cl^{+2}, but the effect is much more pronounced [22] in the transition groups, and amounts to 5 eV in $3d^5$ Mn^{+2}, to 10 eV in $4f^7$ Gd(III) and about 6 eV in $5f^7$ Cm(III). The phenomenological barycentre polynomial [22] is a smooth function of z inside each nl-shell (derived from observed barycentre energies):

$$E_{bar} = E_0 + a_0 z + (a_1/2)\, z^2 + (a_2/3)\, z^3$$
$$I(z) = (dE_{bar}/dz) = a_0 + a_1 z + a_2 z^2 \tag{4}$$

where E_0 is the (highly negative) energy of the barycentre of the configuration in the neutral atom (in the example above the groundstate energy of N^0 added to 2.4 eV) and the differential ionization energy $I(z)$ is the differential quotient of the phenomenological barycentre polynomial. The unexpected beauty of Eq. (4) is that the subsequent terms are very small [20]. The Madelung potential can now be added as an explicit coefficient (times z) to $I(z)$ of each atom, and the total energy minimized as a zero-point of the sum of $I(z)$ and the Madelung potential. For a binary compound (also in the case of polyatomic MX_N^{-q}) the z_M and z_X are connected with one free variable (colloquially called the ionicity). This treatment does not succeed in all cases; a major problem is 3d or 4f shells with very large a_1 and a_2 (corresponding to large differences between ionization energy and electron affinity). As also pointed out by Ferreira [24] quantum mechanics does not allow a set of atoms to get lower energy by all having a fractional z, relative to the situation, where some atoms carry the integer z, and others z + 1. The mechanism behind this paradox is that shells with q electrons exhibit $q(q - 1)/2$ parameters of interelectronic repulsion (rather than the classical value $q^2/2$ for an extended distribution) and hence, Nature pays a premium to electrons in shells with particularly large difference between ionization energy and electron affinity. Another difficulty is sharp energy minima at definite z values, such as CF_4 having z exactly +2 for the carbon atom, having no 2p population, but exactly two 2s electrons. The z_M obtained by minimizing $I(z)$ plus Madelung contributions are typically between +1.5 and 3. One can estimate the covalent contributions to this treatment [22,135] bringing, e.g. the z_{Ti} down from 2.64 to roughly 2.2 in $TiCl_4$. The corrected z_M values tend to be inside the interval +1 to +2, in good agreement with the estimates [22] obtained for d-group complexes from the nephelauxetic effect. It must be remembered that the two covalent corrections have opposite signs; one counteracts the implosion

inherent in any electrostatic model, the Madelung potential getting k times stronger, if all distances are divided by k. For short R, the non-overlap assumed is no longer valid, and the local operator of kinetic energy [29, 138, 139] forcefully prevents implosion. The more "text-book-like" covalent contribution is the stabilization already seen in homonuclear molecules. On the whole, the model of differential ionization energies gives a reliable picture of the comparable importance of covalent and electrovalent stabilization in most inorganic compounds.

The hydration energies of gaseous cations and anions transferred from a gaseous state to aqueous solution is closely related to this discussion. If a perfect dielectric surrounds such a spherical ion with radius r, the energy gained is $z^2/2r$ in the unit hartree/bohr; or z^2 (7.2 eV)/(r/Å). It was pointed out by Fajans and Morris [140] that the dissolution of most alkali-halides MX is almost enthalpy-neutral, only CsF and the heavier LiX dissolve rather exothermally. This shows that water cannot act on *both* M^+ and X^- as a perfect dielectric (for our scale of precision, the reciprocal dielectric constant 0.013 of water can be neglected) since if they have comparable radii (r = R/2) the total stabilization corresponds to a Madelung constant $\alpha = 2$, that is 1.15 times the α of the crystal, and if the two radii are different, the aqueous α should be above 2. This problem is intimately connected with the addition of 4.42 eV to E^0 in order to obtain I_{chem} (cf. Sect. 2.2) since the discrepancy can be shifted to the cation or the anion without this constant being accepted. Latimer [141] pointed out that the hydration energies (in eV) of the four X^- fluoride (5.4), chloride (3.9), bromide (3.8) and iodide (3.2) are in excellent agreement with a perfect dielectric (5.41; 3.98; 3.67 and 3.27 eV) if r is taken as the Goldschmidt ionic radius r_{ion}. On the other hand, most cations show a hydration energy close to z^2 (7.2 eV)/(r_{ion} + 0.82 Å). The Latimer constant 0.82 Å may have various interpretations. There may be a sense [43] in which the water does not "wet" the cation in contact, or there may be a local dielectric constant smoothly varying from 78 at large distances, to smaller values at shorter R. Comparison of the influence of positively charged substituents in multidentate ligands [142, 143] on complex formation constants can be shown to be compatible with a local dielectric constant gradually decreasing to 20. However, this occurs at so long R that there might be a value close to 3 in the immediate vicinity of the cation. Anyhow, some aqua ions show somewhat larger hydration energies than the Latimer expression [22, 43, 44].

Pearson [144, 145] suggested the principle that hard anti-bases (Lewis acids) preferentially react with hard bases, and soft bases preferentially with soft anti-bases. In this context, "hard" means essentially pronounced tendency toward electrovalent bonding, as F^-, Li(I), Mg(II), Al(III), Th(IV), ... and "soft" strong covalent bonding of I^-, RS^-, R_3P, R_3As, Cu(I), Pd(II), Ag(I), Pt(II), Au(I), Au(III), Hg(II), Tl(III), ... but Pearson added the novel feature that metallic surfaces ipso facto are soft, including graphite. The various interpretations of the Pearson principle were reviewed in this series [43] but for our purpose, it is important to take up two areas of this field. Ahrland [146] proposed the softness parameter $\sigma_A = (I_{chem}/z)$ as the energy needed to transfer a gaseous atom M to aqueous solution in the form of hydrated M^{+z} and leaving z electrons in the gaseous phase, and then divide this energy by z. Somewhat contrary to the feelings of Pearson, σ_A tends to be higher for the higher of two z values for a given element, e.g. (all values in eV) Fe(II) 2.0 and Fe(III) 3.1; Co(II) 1.8 and Co(III) 3.4; Ce(III) 0.7 and Ce(IV) 2.0; or Tl(I) 2.7 and Tl(III) 4.3. Mercury(II) is

5.1, but gold(I) and (III) are probably higher, but cannot be evaluated in absence of known aqua ions. The only case of $\sigma_A = 0.0$ is lithium(I), a smooth increase occurs to 1.2 for Cs(I). Beryllium(II) is 1.2, and the next four alkaline-earths M(II) close to 0.8, with exception of Mg(II) 1.4 to be compared with 1.6 for Al(III), perceptibly higher than for the rare earths [46]. The hydration energy 11.3 eV of a naked proton gives $\sigma_A = 2.3$ for H(I) in a certain dissonance with the ideas of both Latimer and Pearson. However, it cannot be denied that H^+ has a great affinity to CN^- and to CH_3^- (though not to CO and to C_6H_6 also considered soft ligands by Pearson). We return in Sect. 5.4 to the related question of inorganic symbiosis. As far as E_{bar} from Eq. (4) goes, Pearson now argues [144, 145] that an appropriate parameter of hardness (directly derived from monatomic entities) is $\eta = d^2E_{bar}/dz^2$ (which is not strictly defined at z values representing closed shells). There is a great part of truth in this idea; intrinsically soft systems have vanishing difference between ionization energy and electron affinity (and hard systems a large difference). It may seem a little tough to circumvent the non-differentiability of I(z) at a closed shell by the new definition [144, 145] of η as $(I_3 - I_2)/2$ equal to 67.84 eV for Be^{+2}, 32.55 for Mg^{+2} and the analogous $(I_4 - I_3)/2 = 45.77$ for Al^{+3}. Though the hardness may increase monotonically with η, it seems likely [24] that $\eta/(\eta + k)$ may be more suitable, the ratio varying from 0 to 1 between the extremes (it is noted that a definite energy k must be chosen). This problem is not without similarity to the Mulliken electronegativity $x_M = (I_1 + I_2)/2$ being 26.41 eV for Na^+, much higher [94, 137] than $x_M = (I_0 + I_1)/2$ being 10.41 eV for the fluorine atom. This problem has, to a certain extent, been alleviated by adding the Madelung energy to the differential ionization energy in Eq. (4).

5.2 Covalent Bonds Between Adjacent Atoms

It is evident that interest in spectroscopic properties, and other processes obeying the principle of Franck and Condon (such as photo-electron ionization) motivates the M.O. approach, and that interest in groundstate properties (length and angles of bonds; chemical reactivity and reaction trajectories) predispose in favour of V.B. concepts. Nevertheless, the class of compounds agreeing more or less closely with the Lewis paradigm make a great preference of the latter approach. Life would be much easier for the chemist if, at least, the number of V.B. and of M.O. states involved in the description of a given polyatomic ion or molecule was identical. This situation (occurring in the "weak-field" and "strong-field" description of d^q states for a given q in a definite point-group) would have allowed a "preponderant" set of one or a few V.B. structures in cases not far from Lewis behaviour, much like monatomic systems have a preponderant configuration classifying their low-lying levels, disregarding correlation effects, i.e. configuration intermixing. This dream is turned into a nightmare by the inconsiderate proliferation of permutational states. The sulphate ion SO_4^{-2} has a singlet groundstate, and no excited states below 6 eV. If we "freeze" the S^{+6} and four O^{+6} cores, we have 40 available sites (in the S 3s and 3p, and the oxygen 2s and 2p shells) for 32 electrons, providing $(40!)/(32!)(8!) = 76,904,685$ states. Admittedly, this is somewhat unfair to V.B. ideas. However (foot-note p. 216 of Ref. [41]) the more "chemical" approach of not allowing any positive oxygen constituents is equivalent to distribute 8 electrons on 16 sites, i.e. eight close to S^{+6} and two on each

oxo ligand. Each energy level represented by a definite S value realizes $(2S + 1)$ states. Hence, the unique level with $S = 4$ has 9 states, the 63 septets $(S = 3)$ have 441 states, the 720 quintets $(S = 2)$ 3600 states, the 2352 triplets 7056 states, and the 1764 singlets 1764 states. The latter are, of course, the only ones of interest for our purpose. In many circumstances, the quantum number M_S is important for chemists [22,29]. There are $70^2 = 4900$ states having M_S zero. Each non-zero M_S has the same number of states for $+M_S$ and $-M_S$ such as $56^2 = 3136$ for 1; $28^2 = 784$ for 2; $8^2 = 64$ for 3; and one for $|M_S| = 4$ (by the way, these expressions are also those for the first stratification of "elementary" particles in recent supersymmetry [147] having the J values 0; 1/2; 1; 3/2 and 2). For the chemist, the case of $M_S = 0$ is important for the molecules divided [133] into two sub-systems (such as CH_4 into C and H_4). If the groundstate of the undivided system has $S = 0$, each of the two sub-systems have necessarily $M_S = 0$ (which is the case for 36 out of the 70 states of each of the two sub-systems, if considered as 4 electrons utilizing 8 sites) and hence, 1296 states out of the 4900 states of this description of methane are eligible by having vanishing M_S. They form 626 states with $S = 0$ since each of the two sub-systems have 20 instances of $S = 0$, 15 of $S = 1$ and one of $S = 2$, and S_1 and S_2 of the two sub-systems are identical for any singlet state of the combined system, what can be realized in $1 + 15^2 + 20^2 = 626$ ways. If one insisted [133] that S 3s is an "inert pair", the SO_4^{-2} problem would reduce to 6 electrons on 14 sites, giving 3003 states (like six 4f electrons [23,50] also do). The chemist may take a more down-to-earth attitude that the more important "resonance structures" are the 28 states of S^0 combined with the 28 states of O_4^{-2}; the 56 states of S^+ combined with the 56 states of O_4^{-3} and the 70 states of S^{+2} combined with the 70 states of O_4^{-4}, not bringing very much simplification. This practical chemist may then start to count the number of Lewis-electron bonds between the sulphur atom and each of the four oxygen atoms. For instance, if the S is neutral, $(2,2,1,1)$ bonds are the most plausible to discuss. Around S^+ one expects $(2,1,1,1)$ and around S^{+2} mainly $(1,1,1,1)$. This approach might be stiffened to exclude structures with bond-numbers differing by more than one unit, excluding $S^0(3,1,1,1)$; or by excluding no-bond structures, and hence deleting $S^{+3}(1,1,1,0)$. The molecule NSF_3 (not having a central nitrogen atom like ONF_3) might be allowed to use $S^0(3,1,1,1)$ in what will become a theory of poetry. The first choice for SF_6 would be $S^{+2}(1,1,1,1,0,0)$ with smaller admixture of S^{+3} $(1,1,1,0,0,0)$ and $S^{+4}(1,1,0,0,0,0)$ [though the latter structures are needed to change the fractional charge of fluorine below -0.333] and $S^+(1,1,1,1,1,0)$ is a question of sulphur restrained to only four electron-pairs. Paper is patient, and the chemist may still ask whether we have not got away with only 11 permutations of three predominant "resonance structures", that is six $S^0(2,2,1,1)$, four $S^+(2,1,1,1)$ and one $S^{+2}(1,1,1,1)$, just being determined by conditional reflex.

We know that the S—O distances in sulphate are identical in all available experimental time-scales, and that there is a surrounding electronic density, of which 18 (of the 50 electrons present) give photo-electron evidence of the inner shells. To what extent the "resonance structures" is a helpful metaphor, is dependent on the context, and personal taste. It certainly induces quaint questions: why is sulphate not dark green, having low-lying excited singlets like the superficially similar [148] permanganate MnO_4^- and MoS_4^{-2}, and why does it not have low-lying quintet states? Sidgwick introduced "semi-polar" bonds in 3p group compounds, such as P(V), S(VI) and Cl(VII), to extend the Lewis paradigm to two-digit Z values. In our notation, the

molecule OPF_3 containing 50 electrons like sulphate has the opportunity of semi-polar bonding in $P^+(1,1,1)$ and ancient $P^0(2,1,1,1)$. It is here a fundamental question how polar bonds are to be described: If Lewis pairs are free of any polarity, P—F, P—O, S—O and C—F need ionic "resonance structures" to represent their polarity. It may be determined by the differing electronegativity x (whatever that means [137]); for the inorganic chemist, there is no doubt that x is not an intrinsic property of an element [94] but frequently depends on the oxidation state, x being higher of S(VI) than of S(—II) like x are higher for Cr(VI) and Mn(VII) than for Cr(III) and Mn(II), as already perceived in "group x" of CF_3 being higher than of CH_3). If Lewis bonds can be polar, there is less of an urgent need for semi-polar bonding, though the text-books ask what the fifth orbital is in $P^0(2,1,1,1)$ cases. There is very little firm evidence from nuclear quadrupole and other micro-wave techniques [149] nor from visible and ultra-violet spectra [150] that the "valence-shell is expanded with P 3d electrons", but as discussed in Sect. 5.4, this question is full of ambiguities. We have to be realistic; OPF_3 needs 150 dimensions in the total electronic wave-function; its electronic binding energy is 717 hartree, the heat of atomization close to 0.7 hartree, the first excited state at 0.3 hartree, and the ionization energy of the loosest bound orbitals 0.45 hartree (by the way, the two latter energies are almost the same in the xenon atom with 54 electrons). Compared to the total energy; the first excited and ionized states are not far from the groundstate, but seen with our experience, the first 0.2 hartree is the most interesting.

The indisputable fact that nearly all anhydrous binary halides MX_n either boil below 200 °C and do not conduct electricity in their liquid state; or melt above 400 °C and conduct electricity as molten salts, had early been evidence for a clear-cut distinction between covalent and electrovalent compounds. Already in 1922, Magnus pointed out that the volatile halides have N = n and hence consisting of individual molecules, but earlier columns in the Periodic Table had M so large that, for instance, N = 6 for both NaX, MgX_2 and AlF_3. Hence, the much higher melting and boiling points of these compounds are due to X^- bridging two or more M, as also known from N = 4 for silicon(IV) in the various modifications of SiO_2 to be compared with OCO remaining N = 2 without polymerizing (as H_2CO does). According to Magnus, there is no reason to expect that the gases SiF_4, PF_5 and SF_6 are much more covalent than the isoelectronic AlF_6^{-3}, SiF_6^{-2}, PF_6^- and ClF_6^+.

Varying the internuclear distance R, there is an interval where the M.O. treatment approximately valid at low R becomes useless at larger R, and is superseded by the V.B. treatment. *Anti-ferromagnetic coupling* clearly belongs to the long R situation, where M.O. configurations of great number are mixed in a confusing way. The classical case [151] is the "blue basic rhodo ion" $(H_3N)_5CrOCr(NH_3)_5^{+4}$ where the groundstate has S = 0 followed by S = 1, 2 and 3 at the energy JS(S + 1)/2 with the Heisenberg parameter J = 450 cm^{-1}. The 16 states counted by summation over S(S + 1) are the product of the four [29, 106] states forming the lowest energy level of each of two Cr(III) representing $3d^3$ in local octahedral symmetry. Conceptually, there is no sharp distinction between anti-ferromagnetic coupling and weak bonding at long R, but the V.B. treatment certainly has its heyday there. Of only the three electrons in the lower sub-shell of each Cr(III) are considered (neglecting the anti-bonding two d-like orbitals), the dimer of Cr(III) has 6 electrons distributed on 12 sites, providing 924 states, among which 7 form one septet (S = 3), 175 form 35 quintets, 567 are

incorporated in 189 triplets, and 175 states represent each a singlet. This, quite restricted, M.O. treatment includes [151] mutual electron transfer states such as Cr(IV) & Cr(II) and Cr(II) & Cr(IV), but only considering the lower three orbitals of each Cr. If the whole d^q basis set is included, the 120 states of the separate d^3 becomes 6 electrons on 20 sites, or 38,760 states, having S up to 3. Noodleman [152] discussed the V.B. aspects of more or less weak anti-ferromagnetic coupling between two M.

5.3 Chemical Polarizability and Clusters

Recently, a third category of chemical bonding has been added to covalent and electrovalent bonding, and closely related to chemical polarizability [43] already mentioned above as softness according to Pearson. Though the (roughly additive) electric polarizabilities run parallel [43, 46] with chemical polarizability in the halides X($-$I), gaseous X$^-$ and isoelectronic noble gases this is not at all true for many cations; Cs(I), Ba(II) and La(III) have higher electric polarizabilities than the corresponding Ag(I), Cd(II) and In(III). The values for atoms containing one or two external s electrons are exceedingly high. Epiotis [133] divided the elements in three areas of the Periodic Table, "black" atoms H, B, C, N, O and F; "green" atoms Si, P, S, Cl, As, Se, Br, Kr, Te, I and Xe; and "red" atoms, the colloquially "metallic" elements. This is a very useful reminder that the 2p group is essentially different from the 3p, 4p and 5p groups, in spite of the "diagonal similarities" between lithium and magnesium; between beryllium and aluminium etc. Epiotis [133] argues that 2s and 2p orbitals are almost equivalent for chemical purposes, but that 3s, 4s and 5s orbitals become "inert" in the "green" atoms. There is no doubt that there are relativistic reasons [14-16] for an inert 6s orbital in Tl(I), Pb(II), Bi(III) and Po(IV) but there is no striking difference between their radial extension [6] between 2s/2p and 3s/3p. There is, of course, the difference that the inner shells are far more bulky in the "green" than in the "black" elements. In view of N = 2 to 6 for many hydrides, it may be asked whether hydrogen always is "black". If one accepts the hybridization model rationalizing bond angles, there is a sense in which 3s and subsequent ns are inert. The bond angles are so close to 90° (if not marginally below) in H_2S, H_2Se, H_2Te, PH_3, AsH_3 and SbH_3 suggesting pure p orbital participation. This is most striking contrast to 109.5° in CH_4 only decreased by two degrees in NH_3 (though this molecule has to be observed for less than 10^{-9} s since it is D_{3h} with two density maxima above and below the H_3 plane, if the motion of the nitrogen nucleus is studied) and 5° in gaseous H_2O. Still, N = 4 is frequent of many 3p and 4p group compounds, with point-group T_d (but this may be related to inter-ligand squeezing).

M.O. are not obliged to be L.C.A.O. with a small basis set of atomic orbitals (though they are surprisingly accurate in most 2p group compounds). This fact (which has come into the limelight by the method $X\alpha$ of directly solving the one-electron Schrödinger equation for polyatomic cases) is disclosed by many intense absorption bands (of the type characterizing the organic colorants in Sect. 3.4) and may be more frequent than generally realized. An organic case is tetrahedral $M(C_6H_5)_4^+$ for M = N, P, As and Sb just showing the rather weak bands close to 260 nm (4.8 eV) known from C_6H_6 and (with higher intensities) in pyridine, and its protonated form, and complexes with iridium(III) and other d-group ions [153] as well as from neutral $M(C_6H_5)_4$ with

31

M = Si, Ge, Sn and Pb. On the other hand, $M(C_6H_5)_3$ has a *very* strong band (nm value) 297(N), 261(P), 248(As) and 256(Sb) originally ascribed [154] to the same origin as in other phenyl groups. However, it is more likely [150] that the lone-pair on the three-coordinated elements have a very intense transition to the empty "π" M.O. of the phenyl groups, in analogy to the much higher intensity of the first ultraviolet transition from the non-bonding M.O. of the oxygen atom to the first empty M.O. in acetophenone and benzophenone, compared with acetone; or the "inverted" electron transfer band from reducing central atoms [120,153,155] to low-lying empty M.O. of aromatic ligands. It is likely that the lone-pair of the triphenyl compounds is quite far from being a P 3s or As 4s orbital, and highly delocalized in the phenyl groups. The very high intensity is also found [22] in apparent d^6 and d^8 transitions of iron(II), cobalt(III) and nickel(II) complexes of phosphine and arsine ligands PR_3 and AsR_3. In molecular spectroscopy, extended and highly delocalized empty M.O. are called *Rydberg orbitals* [156,157] in analogy to the 6s → 7p transition in the blue (having given its name to caesium) and subsequent 6s → np (observed in absorption in highly dilute Cs vapour up to 77p) and the $5p^6$ → $5p^56s$ transitions of iodides and the xenon atom [158]. The relatively weak transition in C_6H_6 mentioned above is the only clear-cut transition observed between the filled "π" and empty, anti-bonding "π" M.O. The next three are to a great extent masked by a very strong band close to 210 nm (6 eV) mainly due to an empty Rydberg orbital. This would be considered as linear combination without nodes between the carbon atoms of their six 3s orbitals. However, it may be erroneous to insist on L.C.A.O. treatment of this Rydberg orbital, which may just be an oblate ellipsoid of electronic density. Under strongly reducing conditions, such a Rydberg orbital may accept one electron in the groundstate. Thus, dodecamethyl-cyclohexasilane $[Si(CH_3)_2]_6$ accepts an electron in tetrahydrofuran [159] forming a blue-green radical anion at 50 °C, having nuclear fine structure of the electron paramagnetic resonance indicating interaction of the unpaired electron with 36 equivalent protons, and also the ^{13}C and ^{29}Si nuclei present. This Rydberg orbital is assumed to be L.C.A.O. of empty Si 3d orbitals (illustrating valence-shell expansion) but it may equally well be a roughly ellipsoidal blob. Evidence for such shapeless orbitals includes also realgar As_4S_4 having four equivalent arsenic atoms on the sulphur positions of the, otherwise isosteric, molecule N_4S_4 and four equivalent S atoms on the N positions of N_4S_4. This brings us to the subject of *cluster compounds*. A large number of molecules or anions, having a few other ligands on the surface, have direct bonds [103] between 5, 6, 7, 8, 9 or 11 gold atoms. Schmid [160] also discusses $Au_{13}(PR_3)_{10}Cl_2^{+3}$ having a central gold atom surrounded by a Au_{12} icosahedron, and the rather impressive $Au_{55}[P(C_6-H_5)_3]_{12}Cl_6$ having cubic symmetry. A central gold atom is surrounded by two concentric cages. The first is cuboctahedral Au_{12} (as in cubic close-packed metals) and the second cage consists of 42 gold atoms, arranged in such a way that 12 carry the triphenylphosphine ligands, and 6 the chloride ions. These results may be compared with calculations [161] of the cluster Be_{13} having the heat of atomization (per atom) 0.8 to 0.9 eV, and of Be_{55} 1.3 eV (to be compared with 3.4 eV for the metal). It is noted that 42 of the 55 atoms are in the surface, having about half as many neighbours as interior atoms. A rough model of concentric shells containing $12n^2$ nuclei at $R = nR_0$ produces the sum over the first n atoms $4n^3 + 6n^2 + 2n$ atoms. For large n, the ratio between the number of atoms in the outer-most shell, and all the atoms, is close to (3/n). Hence, for n = 6, about half (exact ratio 36/91) and for n = 12 about a quarter (72/325) of

the atoms are on the surface. The latter system contains 7800 (+ a central) atoms. There is the motivation behind much of the work on cluster compounds that they were expected to represent homogeneously soluble model compounds for heterogeneous catalysis on metallic surfaces. However, even Au_{55} clusters seem small for this purpose. Colloidal gold particles give an intense red colour, when dispersed in glass [162] with an absorption peak at 515 nm. It is possible to produce relatively monodisperse gold and palladium with radii around 10 nm (100 Å) containing some 170,000 atoms and n = 35 in the model above. Such particles (if compact) have 90 percent of the atoms in the interior bulk.

Several of the specific characteristics of enhanced bonding between soft bases and soft anti-bases (Lewis acids, including metallic surfaces) have been tentatively ascribed to *continuum effects* [43] of the kind discussed here, the next Section treats the related problematic of back-bonding, perhaps involving extended orbitals at high energy having only weak relevance in L.C.A.O. models, though these were originally preferred for back-bonding. This subject rarely gives an opportunity to choose between two distinct models, in view of the infinite number of one-electron wave-functions situated in the continuum. Qualitatively, there is no doubt that such effects occur in the presence of "green" and "red" atoms of Epiotis [133].

5.4 The Concepts of Back-Bonding and Inorganic Symbiosis

Chatt made a great effort to explain strong bonding between CO and elements in low (if not negative) oxidation states by bonding from the lone-pair of CO to empty, usually d-like orbitals, of M, or 4s of $Fe(CO)_4^{-2}$, $Co(CO)_4^-$ and $Ni(CO)_4$ *simultaneous* backbonding from d-like filled orbitals of M to the first empty anti-bonding π M.O. of CO. The first time, one hears about this idea, it is difficult to believe fo· /o reasons. The lone-pair has the exorbitant $I = 14.0$ eV (as for krypton) though this surprise is perhaps attenuated when the isoelectronic N_2 is now known to replace water in $Ru(NH_3)_5OH_2^{+2}$ to $Ru(NH_3)_5(N_2)^{+2}$. But CO has the first excited triplet at 6 eV and the first singlet at 8.1 eV, indicating a very high energy of the empty π frequently called π^* also in aromatic systems. If this theory is valid, one must consider backbonding as a collective synergism, and recognize that the radial function of π^* (in L.C.A.O.) must be strongly expanded (because of the virial theorem demanding the kinetic energy to decrease half as much [3, 24] as the potential energy increases, becomes less negative, in any excited state) relative to the C 2p and O 2p orbitals providing the two "π" compounds (they are also $\lambda = \pi$) of the triple bond in $C^- \equiv O^+$. There is one definite instance of CO not back-bonding, $OCBH_3$ (definitely not $COBH_3$) with a total heat of atomization 24.48 eV and a binding [163] between the two fragments BH_3 and CO 1.1 eV. Another case of negligible back-bonding may be $IrBr_5(CO)^{-2}$. In gaseous state, the proton affinity to form HCO^+ is weaker than in XeH^+. The former formyl cation is observed in mass spectra, whereas Susz made the BF_4^- salt of the acetyl cation CH_3CO^+ by reacting CH_3COF with BF_3. It is noted that B(III), Al(III) and Si(IV) are among the rare cases of electron-pair acceptors (Lewis acids) which are *not* [164] electron acceptors (oxidants).

By far the best crystallographic evidence for simultaneous back-bonding is the platinum(II) complex of ethylene [ethene] $PtCl_3(C_2H_4)^-$ prepared by Zeise. The C—C

bond is perpendicular on the $PtCl_3$ plane, and it is tempting to say that the fourth coordination place of Pt(II) is taken by this point rather than by nuclei. On a design, the filled Pt $5d(xz)$ exactly fits the requirements of the empty "π" type M.O. having two node-planes in free C_2H_4, one containing the six nuclei, like the bonding "π" and one in the $PtCl_3$ plane of the complex. It is a moot point to what extent the four protons remain co-planar with the two C in the complex; or if they bend away as in known cases [22] of Pt(II) reacting with C_2F_4 or $C_2(CN)_4$ where it becomes a plausible approximation to imagine two σ-bonds to bidentate $C_2X_4^{-2}$ forming a cyclic platina-cyclopropane ligand. Tetracyano-ethylene is well-known for accepting one electron from moderately reducing species.

Back-bonding may not be restricted to organometallic M—C bonds; PF_3 is more efficient for stabilizing negative d-group oxidation states [165] than CO, and many chemists believe that PF_3 has one or two empty M.O. (perhaps related to the P 3d orbitals invoked in PF_5 and PF_6^-) effective like the first empty M.O. in CO. Vibrational spectra (Raman and infra-red) have been extensively studied of nickel(0) complexes of four ligands selected from the set PH_3, PF_3, PCl_3 and CO. The variation of the force constants show roughly linear inductive effects (NO^+ substitution has much more dramatic effects) and the triple bond C^-O^+ seems indeed loosened in what are, perhaps rightly so, called carbonyl complexes. However, the problem with PR_3 is far more fundamental with alkyl and aryl R substituents. The Pearson-hard cations have only very weak affinity to phosphines (though some complexes may be prepared in non-aqueous solvents) but d^{10} systems such as Ni(0), Cu(I), Ag(I), Au(I) and Hg(II) show extremely high affinities [43] as well as other soft anti-bases $4d^8$ Rh(I), Pd(II), $5d^8$ Ir(I), Pt(II) and Au(III). Actually, there is a conspicuous symphonic behaviour of many soft ligands. We all expect sufficiently reducing ligands (RS^- readily undergoing oxidative dimerization to RSSR, or PR_3 and AsR_3 readily abstracting oxygen atoms) to impede high oxidation states, but this is a delicate balance, $R_2NCS_2^-$ being able [166] to stabilize iron(IV), nickel(IV) and copper(III), what is also true for bidentate phosphines and diarsines. This unexpected co-existence may be described by back-bonding to empty orbitals of the reducing ligands, but a difficulty is that hardly any electronic density is moved, the donation of lone-pair density to M being compensated by back-bonding from M to some non-σ orbitals. Is this a viable analogy to a national economy being kept active by everybody owing money to everybody else? The writer suspects that continuum orbitals [43] play a rôle by allowing the prevailing electron densities to distort in some subtle way not relevant to L.C.A.O. models. It has also been suggested by many text-books that the sharp contrast between fluorides and the "green" set [133] Cl, Br and I is due to back-bonding to empty Cl 3d, Br 4d, and in particular, I 5d orbitals, justifying the high affinity to soft d-group ions. Spectroscopic observations allow 5d to be detected [158] at somewhat higher energy than the empty 6s both in iodides and xenon, but it would rather seem that back-bonding would occur to 6s if it *has* to be L.C.A.O., and it may rather be a diffuse, shapeless continuum orbital.

The question of back-bonding has many ramifications. Colourless $3d^6$ $Cr(CO)_6$ can be photolyzed at low temperature [167] in vitreous matrices to coloured, apparent cases of $N = 5$. However, the band maximum (in nm) depends on the matrix: Ne(624), SF_6(560), CF_4(547), Ar(533), Kr(518), Xe(492) and CH_4(489). These results show clearly that at most one (neon) has no chemical influence, but it seems established that three noble gases form $NgCr(CO)_5$ since a mixed matrix $Ne_{0.98}Xe_{0.02}$ shows two

distinct bands, at 628 nm, and a stronger band at 487 nm, showing greater affinity for Ng = Xe than Ne, but no gradually changing solvent effect. This may be compared with the Cr(0) complex $Cr(CO)_5NH_3$ having a maximum between 420 and 424 nm in three different solids. Taken at the face value, these results [167] indicate that the spectrochemical series increases the sub-shell energy difference Δ in the order [22, 106]: Ne $\ll$ SF_6 < CF_4 < Ar < Kr < Xe $\sim$ CH_4 < NH_3, almost overdoing its trick, since the hypothetical $trans$-$Cr(CO)_4Ne_2$ is extrapolated to have the first spin-allowed d^6 transition at 8000 cm^{-1} (1250 nm) as a stronger case of the large shift toward lower wave-numbers in $Co(NH_3)_5I^{+2}$ compared with $Co(NH_3)_6^{+3}$. We have to accept that the "ligand field" of xenon is not much weaker than of the isoelectronic iodide ligand [$Cr(CO)_5I^-$ has this band [168] at 438 nm] and that the fluoride bridges to C(IV) and S(VI) play a perceptible rôle.

The catenation of S—S—S ... is much more mobile than aliphatic carbon links, but give rise to bidentate ligands [169] such as S_3^{-2}; S_4^{-2} and S_5^{-2}. In view of the notorious tendency of HS$^-$ solutions to form amorphous sulphur (difficult to remove by filtration) it is fortunate that $K_2[Pt(S_5)_3]$ has a crystal structure confirming it as an octahedral platinum(IV) complex. Many complexes are also known of "expanded" dithiocarbamates $R_2NC(SS)S^-$. In all of such cases, the continuum effects [43] may be more appropriate than back-bonding.

An early attempt in this direction was to assume exceptionally strong Van der Waals interactions between atoms with high polarizabilities. One text-book gave a formula for the London forces giving exactly the observed dissociation energy 1.6 eV for the iodine molecule, when the known R and the electric polarizability of iodine atoms were inserted. As a useful reminder for chemists that (A implies B) does not imply that (B implies A), and hence, theories giving some correct results can be entirely unsatisfactory in other aspects, we must express our gratitude that the predicted collapse to a black hole does not take place. The catenated poly-iodides have many aspects of the polysulphides. Linear I_3^- (if it is symmetric with two identical R, it has relations [29] to linear $5p^4$ iodine(I) complexes such as $ClICl^-$, pyICl and pyIpy$^+$ with pyridine, and the xenon(II) compound FXeF) and L-shaped I_5^- may show comparable behaviour.

One can extend [170] the Pearson hard/soft classification by noting the *inorganic symbiosis* (again having sporadic exceptions). Though it is to some extent a result of the preparative chemistry taking place in rather non-polar solvents, it is striking that soft ligands such as H$^-$, CH_3^-, CN$^-$, CO, C_2H_4, C_6H_6, $P(C_2H_5)_3$, $P(C_6H_5)_3$ ... tend to occupy all (or almost all) coordination places once they are bound to a given M (which may not be universally soft). Some ambidentate ligands, such as thiocyanate NCS$^-$ and dimethylsulphoxide $(CH_3)_2SO$ and the acidic central CH_2 group in malonic esters (forming M—C bonds) can be indicators for the soft or hard preferences of the central atom, though it should not be overlooked that kinetics may provide metastable isomers, as when $Co(NH_3)_5NCS^{+2}$ transfer NCS$^-$ (and receives an electron) to $3d^4$ chromium(II) aqua ions, forming $(H_2O)_5CrSCN^{+2}$ taking some minutes to rearrange to $(H_2O)_5CrNCS^{+2}$ studied by Niels Bjerrum. A striking case [170] of inorganic symbiosis is the green $Co(CN)_5^{-3}$ being a Grignard reagent by reacting with benzyl iodide, forming equal amounts of $C_6H_5CH_2Co(CN)_5^{-3}$ and $ICo(CN)_5^{-3}$. The green cobalt(II) complex is also oxidized by H_2 to the colourless Co(III) species $HCo(CN)_5^{-3}$ strictly isoelectronic with the $3d^6$ manganese(I) hydride $HMn(CO)_5$. Contrary to the ammonia

and other ligands attached to cobalt(III), $NCSCo(CN)_5^{-3}$ is the most stable form of ambidentate NCS^- coordination. Said in other words, Co(III) forms a rather hard moiety with $5NH_3$ (and the equilibrium formation constant of $Co(NH_3)_5F^{+2}$ is far higher than for the three heavier halides). On the other hand, $FMn(CO)_5$ is not known (and forms probably MnF_2 and $(OC)_5MnMn(CO)_5$ very rapidly).

Epiotis discusses the question why CF_4 and CH_4 are 1.1 eV more stable [133] than two H_2CF_2, an example of a kind of symbiosis. It is possible that there are many conceivable explanations; the intrinsic dependence of Madelung potentials giving stabilizations proportional to squares z^2 of fractional atomic charges may sometimes overcompensate the less dramatic variation of the differential ionization energy in Eq. (4). This would be compatible with the C—F bonds being more difficult to break, and shorter, as a function of increasing n in CF_nH_{4-n} showing the hard F making C harder. However, there are several other mechanisms possible for symbiosis. One is the choice of S of the groundstate of d^q complexes. Thus, if L is 2,2′ dipyridyl [bipyridine] or phenanthroline, FeL_3^{+2} are stable, dark red, diamagnetic cations, and it is difficult to make them rearrange to yellow $FeL(OH_2)_4^{+2}$ having S = 2, even in a great excess of $Fe(OH_2)_6^{+2}$ also having S = 2, and the unknown bis-complex being unstable by still having S = 2. On the other hand, the diamagnetic $FeL_2(CN)_2$ and $FeL(CN)_4^{-2}$ are quite stable.

The gaseous molecules Li_3O, Li_4O and Li_5O may represent [80] another type of symbiosis, like possibly the preparation of 1,2-dilithiobenzene in unreactive solvents from 1,2-$C_6H_4Br_2$ and four moles of metallic lithium. The five Alkali metals are quite individualistic [171, 172], sodium(—I) being as large as iodide, and Rb^- both being ns^2 systems like Au^-, lithium tending to clustering [133] and caesium(I) co-existing in black crystals having cavities for a single electron (like the F centers rendered irradiated $NaCl_{1-x}(e^-)_x$ blue) and hence being [171, 172] electrides [phlogistonides]. A potassium(I) cryptand electride [193] contains one confined electron *pair* per two cations.

Gaseous diatomic molecules behave differently from condensed matter by having available empty space to accommodate bulky lone-pairs and other extended features of their groundstate electronic density. Like SiO, the BH has a high dissociation energy (3.5 eV) but disproportionates to boranes and solid boron by condensation. It has 6 sites in L.C.A.O. treatment of σ orbitals B 2s, B 2p and H 1s, and two of the three σ orbitals formed, contain 4 electrons, the third remaining empty and strongly antibonding (whereas the two empty B 2pπ orbitals are non-bonding). In empty space, the non-bonding M.O. can sit as a lone-pair on the rear side of the boron, creating a large radius of the electronic density. The dissociation energies of diatomic MX provide many surprises. In condensed matter, atomic size plays a predominant rôle. but nevertheless, the fluorides, chlorides and bromides have dissociation energies varying: BaX > BeX ~ CX $\gtrsim$ CaX, especially surprising by comparison with other carbon compounds. There may be a hint of chemical polarizability in the barium monohalides being so stable. Though ThO dissociating with 8.9 eV may be strongly stabilized by relativistic effects [16] it is striking that LaO and CeO need 8.3 eV, decreasing irregularly across the lanthanides, in spite of preconceived ideas of atomic size (ScO needs only 7.0 eV). On the other hand, BO and BF run very high, 8.4 and 8.0 eV. The unexpected stability of BaX molecules may be related to the results (mainly of Klemperer) that gaseous BaF_2, $BaCl_2$, $BaBr_2$, BaI_2, SrF_2, $SrCl_2$, CaF_2 and also ThO_2 are bent (like ONO) and the other strontium and calcium halide molecules are linear

(like OCO), as one would expect from almost any simple theory. The baroque fact is that the XMX are bent when the ratio r_M/r_X between Goldschmidt ionic radii is above 0.68 ± 0.01. But why is this so?

There is general agreement that low coordination numbers of mercury(II), much smaller than those of calcium(II) [excepting CaF_2-type HgF_2] and very rarely above $N = 4$ characterizing the far smaller beryllium(II), are caused by specific covalent bonding, such as $N = 2$ in NCHgCN; $H_3NHgNH_3^{+2}$; H_3CHgCH_3 and the isoelectronic $NCAuCN^-$ and $H_3CTICH_3^+$. This is, a *fortiori*, true for $N = 1$ in ClO^-, ClOH, KrF^+, XeF^+ and $HgCH_3^+$. There is an interesting discussion [173] about the size of bonding cavities in macrocyclic ligands accommodating nickel(II). Contrary to some text-books, ionic radii is not a concept derived from the quantum chemistry of the ion; the observable is the internuclear distance R (cf. Fig. 1) and it occurs by minimizing the total energy of the compound, not by looking for a threshold value of the exponentially decreasing electronic density for a given distance from one nucleus.

5.5 Energy Bands in Solids

Fifty years after it had been established that water cannot be purified to concentrations of H_3O^+ and of OH^- below 10^{-7} molar, it was realized that both silicon and germanium, which had been considered as feebly conducting metals (like antimony, mercury and bismuth) rather are semiconductors with a very low intrinsic concentration of "charge carriers" at 0 °C (though it increases rapidly with higher temperature). Like one can modify water by adding tiny amounts of bases or acids, one can modify these semiconductors by minute traces of B^- or As^+ or P^+ acting as sources, and traps, for freely mobile electrons. The academic and technological importance of semiconductors after the war gave an enormous impetus to "energy band" theory, which became known as *the* theory for solids. This is short-sighted in many ways [137] since a closer analysis shows that energy bands to solids are what delocalized M.O. are to molecules, and that for sufficiently weak interaction between adjacent atoms, V.B. treatment is the better alternative. For instance, MnF_2, GdF_3 and Er_2O_3 have a partly filled band consisting of 3d-like, or 4f, orbitals, but not the slightest sign of semiconductivity (the text-book excuse used to be "vanishing carrier mobility"). Mott [174, 175] took up this argument for the pale green NaCl-type NiO having all the $3d^8$ transitions expected [22, 41, 176] whereas Li^+ substitution in $Ni_{1-x}Li_xO$ produces grey to black coloration. These materials, containing equivalent amounts x of nickel (III) on an instantaneous picture, conduct electricity to some extent, like the cubic spinel, black magnetite Fe_3O_4 is a metal above the Verwey temperature -154 °C. Mott argued that NiO conducts by "electron hopping" having the large activation energy corresponding to (what is frequently called the Hubbard parameter U) the difference between ionization energy and electron affinity in situ. Mott discovered [174, 175] that some oxides, such as V_2O_3 (corundum-type), VO_2 (distorted rutile with weak tendency toward V . . . V pairs), and Fe_3O_4 have a sharp transition temperature, below which they are almost insulating semiconductors, and above metals. Such materials are now called Mott metals [191].

The extension of the fashionable energy band theory to other crystals than adamantoid semiconductors is frequently justified with the theorem that the one-electron

functions in a closed-shell Slater determinant are invariant for unitary transformations, and hence, there is no effect on the total many-electron wave-function, whether one selects the M.O. or the V.B. representation. This is a rather metachemical statement, since the total wave-function is far from being a Slater determinant (as is also the case for a xenon atom). Present-day thought is rather [177, 178] that the delocalized bands are plausible when the dispersion of one-electron energies in a band is comparable to, or larger than, the Hubbard parameter U of the material. If the ratio between band width and U is small, we have essentially localized f electrons, as occurring in metallic lanthanides, and at 1 atm., metallic americium and subsequent 5f elements. The former alternative is called "itinerant 4f or 5f electrons" and occurs in one of the cubic modifications of cerium, in metallic uranium, neptunium, at least some of the modifications of plutonium, and a high-pressure modification of americium (and praseodymium). Before listening to the energy band catechism, it may be interjected that energy bands belong to a repeated unit cell of a crystal, and that globules of mercury or liquid gallium are metallic. Seen as a question of asymptotic validity of delocalized M.O. rather than V.B. treatment, it is not surprising that grey intermediate shades may occur. It may also be noted that stoichiometric compounds, such as NaCl-type LaS, PrS, GdS, DyS, ErS, LuS and ThS may be metallic, containing for classificatory purposes (in particularly discussing magnetic properties) the number of 4f electrons (Z — 57) defining the conditional [22, 23, 65] oxidation state M[III], and Th[IV]. Many alloys can be stoichiometric, such as CsCl-type LiAg, LiHg, LiTl, MgAg, MgAu, MgTl, AlNi, CaTl, SbTl and TlBi (to be compared with the red semiconductor Cs^+Au^- and the colourless CsBr, CsI, and TlCl). Furthermore, a few compounds [23, 46, 179] such as NaCl-type thulium telluride TmTe have photo-electron spectra indicating an instantaneous picture containing comparable concentrations of $4f^{13}$ Tm[II] and $4f^{12}$ Tm[III]. Metallic lanthanide alloys usually have Eu[II] and/or Eu[III], and Yb[II] and/or Yb[III], and all elements otherwise, starting with Pr[III], exclusively Ln[III]. The 3d-group elements from vanadium to nickel are all itinerant cases.

There has been recent interest in the gradual or abrupt transition from metallic to semiconducting character. Mercury vapour is isolated atoms with $I_1 = 10.44$ eV (close to 10.75 eV for radon) and vanishing I_0. The difference between the liquid and the gas disappears at the critical point [180] 1760 K and $p_{crit} = 1540$ atm. and the supercritical phase has been studied up to 1970 K and 2100 atm. The conductivity depends mainly on the density d (not much on T) and a physical metal is formed for d above 5 g/cm^3. The Mott activation energy of conduction is still 1 eV at 3.5 g/cm^3. Liquid mercury decreases its conductivity slightly from 10^4 Ω^{-1} cm^{-1} at its freezing point to 2000 Ω^{-1} cm^{-1} at 1500 K. In the gas (or supercritical phase) it increases from 10^{-4} to 100 Ω^{-1} cm^{-1} going from $d = 2$ to 6 g/cm^3. Mixtures have also been studied of mercury and caesium vapour [180] (Cs has $T_{crit} = 2060$ K and $p_{crit} = 150$ atm. to be compared with 2570 K and 350 atm. for sodium). The same problem has been studied in cool matrices [181] such as M_xAr_{1-x} for M = Li, Na, K and Rb. The cool (6 K) matrix Cs_xXe_{1-x} is metallic [182] for x above 0.55 and coloured, translucent for lower x. At 38,000 atm., CsI goes tetragonal (like AuCu) and at 56,000 atm. orthorhombic [183, 192] having N = 10 (8 unlike, 2 like neighbours) with similar Cs-Cs, Cs-I and I-I distances, and metallicity occurs at 87,000 atm. The shrinkage of metallic Cs close to 40,000 atm. is ascribed [184] to 6s to 5d demotion. On the other hand, solid xenon does not so easily become metallic as previously expected [185]. These results are interesting

for chemists by the variation of molar volume accessible to measurements at high pressures.

In spite of the fascinating transitions between metallic and non-metallic phases, suggesting the third category of chemical bonding be called [43] "continuum effects", the metallic state is a kind of collective, limiting case of the third category, rather than a third component (electrovalent + covalent + metallic) bonding. Intermediate cases of continuum effects and covalent bonding probably occur in the NaCl-type [177, 186] NdP, GdAs, ErSb, UN, UP, UAs, TiC and UC; and in materials such [38, 107] as MoS_2, $TaSe_2$ and WSe_2. Nevertheless, there is some reason to join the pro-Aristotelian television-watchers (who insist that a compound is toxic or not) and say that a given material is indeed metallic or not. An important class of cubic pyrites [22, 186] which are miscible to a great extent, when semiconductors, such as FeS_2, CoPS, RuS_2, RhPS, OsS_2, IrPS and $PtAs_2$ just to mention a few examples of Fe(II), Co(III), Ru(II), Rh(III), Os(II), Ir(III) and Pt(IV) surrounded in MS_2 by six S, deriving from SS^{-2}, groups, but no miscibility can be detected with the metallic pyrites CoS_2, NiPS, $RhTe_2$, PdAsS, PtAsS and $AuSb_2$ (as well as $NiTe_2$ and $CuSe_2$) even in cases having comparable unit cell parameter. Furthermore, the metallic modifications have, in general, slightly smaller unit cell parameters and molar volumes than extrapolated from analogous semiconducting compounds.

5.6 Born-Oppenheimer Approximation

The high ratios (at least 1836) between the atomic weight of a nucleus and the rest-mass of an electron ensure a result (that would not at all inhere in quantum mechanics of "elementary" particles of comparable masses) that the Schrödinger total wave-function can be written with excellent precision as the product of a translational and an electronic factor, and in the case of more than one nucleus, times factors of rotational and vibrational nature. Though coupling between these factors produce intensities of vibrational "over-tones" and the pre-dissociational broadening of vibronic levels of gaseous molecules at energies larger than the first bond-breaking energy, they are a minor aspect, and it has hardly any importance [187] that any groundstate of a system (not confined in a small volume) immediately is followed by a continuous distribution of translational energies, even if it is a helium atom. However, it has a conceptual importance for a recent controversy [188] about whether a given molecule can be said to possess a definite structure. This vexed problem is connected with the fact that two optically active enantiomers may have exactly the same manifold of internuclear distances R and represent the same point on the potential surface of the electronic groundstate, and actually not being eigen-functions of the Schrödinger equation. However, one must be stoical and recognize that what chemists and crystallographers call "structure" of a polyatomic molecule or ion, is the set (with superposed time-average dispersions) of all R of the kind pictured on Fig. 1, actually also-determining the bond angles between any 3 nuclei. There is still some vigour in this paradox. An empty box, to which are added six nuclei with $Z = 1$ and six with $Z = 6$, and 42 electrons, has not only the benzene groundstate as a potential surface, but also less stable isomers such as prismane, Dewar benzene, and a continuum of three freely mobile acetylene molecules.

Of course, for the practical chemist, the nagging problem is that $N = 2$ has a potential curve (strongly orienting our thought) and $N = 3$ and higher values a $(3N - 5)$-dimensional surface, representing electronic energy as function of the $(3N - 6)$ independent nuclear positions (or R values) remaining after the vibrational and rotational degrees of freedom each have removed 3 variables. Since chemistry is essentially the change of R values, the idea of a single "reaction coordinate" looks slightly supraoptimistic. Actually, accurate calculations of potential surfaces (curves for $N = 2$) of groundstates and excited electronic states are still almost exclusively concentrated [189] on diatomic and triatomic molecules, mainly involving one-digit Z elements.

5.7 Manifolds of Low-Lying States

Chemists are well advised when not requiring nor expecting that quantum chemistry should be a particularly well chosen tool for many of their investigations. It is conceivable (and has certainly not been disproved) that conceptually all chemical facts can be derived from quantum mechanics, but the major problem is of the same kind as the question whether the weather forecast for a definite week in three months' time for a whole continent can be derived with small uncertainty from Newtonian mechanics. The reasons why it is so difficult to answer "yes" or "no" are almost the same in the two situations. At present, the beneficial results of quantum chemistry mainly derive from situations obeying the Franck-Condon principle, the small dispersion of nuclear positions close to the minimum of the potential surface remaining invariant under optical excitation to higher electronic potential surfaces, by photo-electron ionization and by studying the electronic density belonging to this minimum (and the latter studies are still in their very early stages). This is not an accident; quantum mechanics has had, by far, the greatest success treating systems with one nucleus.

The concepts helping thought about chemical bonding have many of the pleasant, and perhaps even more of the unpleasant, sides of mythological tales. The consensus before 1730 about the existence of exactly 7 metallic elements, or (the empirically perfectly verified) non-transmutability of the 30 to 80 Lavoisier elements before 1896 was, if anything, far more complete than any consensus among chemists today [23]. The paradigm of Lewis was the last large-scale myth in chemistry (of the same type as Lavoisier insisting that all acids contain oxygen, and being close to convinced that all bases, including soda and potash, contain nitrogen) not directly inspired by quantum mechanics. Just as Rutherford in 1911 transcribed invariant elements to nuclei (getting their Z in 1913) the Lewis paradigm was such an asset for chemistry teaching that desperate efforts were made [40] to try to reconcile it with quantum chemistry. The main reason why it broke down, was that chemists did not accept restricting its applicability to the huge class of "well-behaved" compounds. The ensuing misunderstandings were of the same kind as a zoologist extending statements about warm-blooded mammals and birds to reptiles and amphibians, ignoring the opportunity of a helpful class distinction.

Chemists have every reason to ask whether quantum chemistry is a suitable tool for solving a given problem. In close analogy to atomic spectroscopy the most pertinent conclusions are about the manifold [22] of low-lying electronic states, including the groundstate. In the same way a two-syllable limerick is *too* short to awake attention,

the most valuable and unexpected conclusions of quantum chemistry (of which it really would not be the business [3] seen from the point of view of the variational principle) are about such manifolds, and the subject of "group-theoretical engineering" and symmetry arguments [29].

Even among organic chemists, there was a strong motivation for studying aromatic, planar molecules (Sect. 3.3) and even organic colorants (though they were considered to be on the intricate side). Partly because of the close relations to atomic spectra, after Kossel [19-23], inorganic chemists were more prepared to think about the set of low-lying levels. This may seem a little unfair to "dull" and colourless CH_4, CF_4, SF_6 and SO_4^{-2}, ClO_4^- and the hexa-aqua ions of zinc(II) and gallium(III). But as any zoologist can tell the chemist, one cannot prevent some problems inviting far more interesting and fruitful comments than other problems. When the zoologist has moved to a safe distance, he may even add with a soft voice that this is true for quantum chemistry too.

Quantum chemistry is now 60 years old. It can help in some situations far more than in others. It would be creating a new myth to pretend that it is the universal explanation of all chemical questions. It should not be hidden from students that it is, to a large extent, concerned with electronic spectra and, to some extent, with local symmetries. As a typical example of uncritical analogies may be mentioned that M-M distances in cluster compounds frequently are compared with the metallic element (though Pauling pointed out that the high N values in metals are accompanied by long R). In an attempt to revive the idea of Bragg that atoms have a roughly constant radius ± 0.1 Å in all solids, Slater [190] noted the exception NaCl-type CsF having Cs . . . Cs 4.25 Å (and CsCl-type CsI 4.56 Å) much shorter than 5.31 Å in metallic caesium (and 4.4 Å in solid xenon). Dynamic (reactivity) aspects are often treated with even more poetic licence than such static properties, gliding smoothly in the $(3N - 5)$-dimensional approximation.

6 References

1. Moore CE (1970) Ionization potentials and ionization limits derived from the analyses of optical spectra, NSRDS-NBS 34, National Bureau of Standards, Washington DC
2. Gaspar R (1967) Int J Quantum Chem 1: 139
3. Jørgensen CK (1988) Chimia 42: 21
4. Foldy LL (1951) Phys Rev 83: 397
5. Scott JMC (1952) Philos Mag 43: 859
6. Desclaux JP (1973): At Data Nucl Data Tables 12: 311
7. Turner DW, Baker C, Baker AD, Brundle CR (1970) Molecular photoelectron spectroscopy, Wiley-Interscience, London
8. Rabalais JW (1977) Principles of ultraviolet photoelectron spectroscopy. Wiley-Interscience, New York
9. Jørgensen CK (1975) Structure and Bonding 24: 1; (1976) 30: 141
10. Green JC (1981) Structure and Bonding 43: 37
11. Roos BO (1987) Adv Chem Phys 69: 399
12. Pyykkö P, Diercksen GHF, Müller-Plathe F, Laaksonen L (1987) Chem Phys Lett 134: 575; 141: 535
13. Robles J, Kemister G (1987) Chem Phys Lett 134: 27
14. Pyykkö P (1978) Adv Quantum Chem 11: 353
15. Pyykkö P, Desclaux JP (1979) Accounts Chem Res 12: 276

16. Pyykkö P (1988) Chem Rev 88: 563
17. Balasubramanian K, Pitzer KS (1987) Adv Chem Phys 67: 287
18. Löwdin PO (1959) Adv Chem Phys 2: 207
19. Kossel W (1916) Ann Physik 49: 229
20. Jørgensen CK (1978) Adv Quantum Chem 11: 51
21. Jørgensen CK (1986) Z Anorg Allg Chem 540: 91
22. Jørgensen CK (1969) Oxidation numbers and oxidation states, Springer, Berlin Heidelberg New York
23. Jørgensen CK (1988) In: Gschneidner KA, Eyring L (eds) Handbook on the physics and chemistry of rare earths, Vol 11, Chapt 75, North-Holland, Amsterdam
24. Jørgensen CK (1988) Quimica Nova (São Paulo) 11: 10
25. Jørgensen CK (1974) Adv Quantum Chem 8: 137
26. Bock H (1964) Angew Chem 76: 697 [Int ed (1964) 3: 686]
27. Bock H, Solouki B (1981) Angew Chem 93: 425 [Int ed (1981) 20: 427]
28. Perera JSHQ, Frost DC, McDowell CA, Ewig CS, Key RJ, Banna MS (1982) J Chem Phys 77: 3308
29. Jørgensen CK (1971) Modern aspects of ligand field theory, North-Holland, Amsterdam
30. Schäffer CE (1968) Structure and Bonding 5: 68; (1973) 14: 69
31. Schäffer CE (1970) Pure Appl Chem 24: 361
32. Brorson M, Jensen GS, Schäffer CE (1986) J Chem Educ 63: 387
33. Shannon RD, Vincent H (1974) Structure and Bonding 19: 1
34. Truter MR (1980) Annual Reports (for 1979) 76 C: 161 Royal Society of Chemistry, London
35. Speakman JC (1972) Structure and Bonding 12: 141
36. Klingsberg E (1963) J Am Chem Soc 85: 3244
37. Klingsberg E (1969) Quart Rev (London) 23: 537
38. Hulliger F (1976) Structural chemistry of layer-type phases Reidel, Dordrecht
39. Jørgensen CK (1983) Revue Chim Min (Paris) 20: 533
40. Jørgensen CK (1984) Topics Current Chem 124: 1
41. Jørgensen CK (1962) Absorption spectra and chemical bonding in complexes, (2. edn 1964) Pergamon, Oxford
42. Rosseinsky DR (1965) Chem Rev 65: 467
43. Jørgensen CK (1975) Topics Current Chem 56: 1
44. Jørgensen CK (1981) Comments Inorg Chem 1: 123
45. Trassati S (1986) Pure Appl Chem 58: 955
46. Jørgensen CK (1979) In: Gschneidner KA, Eyring L (eds) Handbook on the physics and chemistry of rare-earths, 3: 111, North-Holland, Amsterdam
47. Jørgensen CK, Reisfeld R (1982) Topics Current Chem 100: 127
48. Reisfeld R, Jørgensen CK (1987) In: Gschneidner KA, Eyring L (eds) Handbook on the physics and chemistry of rare earths, 9: 1, North-Holland, Amsterdam
49. Cossy C, Helm L, Merbach AE (1987) Inorg Chim Acta 139: 147
50. Reisfeld R, Jørgensen CK (1977) Lasers and excited states of rare earths, Springer, Berlin Heidelberg New York
51. Okada K, Kaizu Y, Kobayashi H, Tanaka K, Marumo F (1985) Mol Phys 54: 1293
52. Couture L, Rajnak K (1984) Chem Phys 85: 315
53. Narten AH, Hahn RL (1983) J Phys Chem 87: 3193
54. Annis BK, Hahn RL, Narten AH (1985) J Chem Phys 82: 2086
55. Enderby JE (1983) Ann Rev Phys Chem 34: 155
56. Furlani C, Cauletti C (1978) Structure and Bonding 35: 119
57. Bjerrum J (1950) Chem Rev 46: 381
58. Bjerrum J (1987) Acta Chem Scand A 41: 328
59. Rasmussen L, Jørgensen CK (1968) Acta Chem Scand 22: 2313
60. Jørgensen CK, Parthasarathy V (1978) Acta Chem Scand A 32: 957
61. Ahrland S (1968) Structure and Bonding 5: 118; (1973) 15: 167
62. Giguère PA (1976) Chem Phys Lett 41: 598
63. Giguère PA (1979) J Chem Educ 56: 571
64. Lewis GN (1916) J Am Chem Soc 38: 762
65. Jørgensen CK (1987) Inorg Chim Acta 139: 1

66. Gillespie RJ (1972) Molecular Geometry, Van Nostrand-Reinhold, New York
67. Jørgensen CK, Reisfeld R (1982) Structure and Bonding 50: 121
68. Lewis GN, Calvin M (1939) Chem Rev 25: 273
69. Reisfeld R, Eyal M, Gvishi R (1987) Chem Phys Lett 138: 377
70. Lewis GN, Lipkin D, Magel TT (1941) J Am Chem Soc 63: 3005
71. Neckers DG (1987) J Chem Educ 64: 649
72. Reisfeld R, Zusman R, Cohen Y, Eyal M (1988) Chem Phys Lett 147: 142
73. Rys P, Zollinger H (1970) Leitfaden der Farbstoffchemie, Verlag Chemie Weinheim
74. Zollinger H, Rys P (1972) Fundamentals of chemistry and application of dyes, Wiley-Inter-science, London
75. Heiligman-Rim R, Hirshberg Y, Fischer E (1962) J Phys Chem 66: 2465; 2470
76. Meriwether LS, Breitner EC, Sloan CL (1965) J Am Chem Soc 87: 4441
77. Fowler PW (1986) Chem Phys Lett 131: 444
78. Matynick DS, Estreicher S (1986) Chem Phys Lett 132: 383
79. Stone AJ, Wales DJ (1986) Chem Phys Lett 128: 501
80. Wu CH (1987) Chem Phys Lett 139: 357
81. Kaufman JJ, Sachs LM (1969) J Chem Phys 51: 2992
82. Koch W, Frenking G, Gauss J, Cremer D, Collins JR (1987) J Am Chem Soc 109: 5917
83. Koch W, Collins JR, Frenking G (1986) Chem Phys Lett 132: 330
84. Frenking G, Cremer D, Jørgensen CK: Structure and Bonding, in press
85. Wilson S, Green S (1980) J Chem Phys 73: 419
86. Hotokka M, Kindstedt T, Pyykkö P, Roos BO (1984) Mol Phys 52: 23
87. Tsong TT (1983) Physica Scripta T 4: 201
88. Seppelt K, Lentz D (1982) Progress Inorg Chem 29: 167
89. Pauling L (1933) J Am Chem Soc 55: 1895
90. Feynman RP (1974) Science 183: 601
91. Jørgensen CK (1978) Structure and Bonding 34: 19; (1981) 43: 1
92. Jørgensen CK (1982) Naturwiss 69: 420; (1984) 71: 151 and 418
93. Jørgensen CK (1983) Nature 305: 787
94. Jørgensen CK In: Liebman JF and Greenberg A (eds) Molecular structure and energetics, in press, VCH publishers, New York
95. DeRújula A, Glashow SL (1984) Nature 312: 734
96. Witten E (1984) Phys Rev D 30: 272
97. Madsen J, Heiselberg H, Riisager K (1986) Phys Rev D 34: 2947
98. Lackner KS, Zweig G (1983) Phys Rev D 28: 1671; (1987) D 36: 1562
99. Liebman JF, Huheey JE (1987) Phys Rev D 36: 1559
100. Barton L (1982) Topics Current Chem 100: 169
101. Warren LF, Hawthorne MF (1967) J Am Chem Soc 89: 470
102. Ternansky RJ, Balogh DW, Paquette LA (1982) J Am Chem Soc 104: 4503
103. Hall KP, Mingos DMP (1984) Progress Inorg Chem 32: 237
104. Mingos DM, Johnston RL (1987) Structure and Bonding 68: 29
105. Kennedy JD (1984) Progress Inorg Chem 32: 519
106. Reisfeld R, Jørgensen CK: Structure and Bonding (1988) 69: 63
107. Tributsch H (1982) Structure and Bonding 49: 127
108. Hunt JP, Friedman HL (1983) Progress Inorg Chem 30: 359
109. Brorson M, Gajhede M (1987) Inorg Chem 26: 2109
110. Joensen F, Schäffer CE (1984) Acta Chem Scand A 38: 819
111. Bernhard P, Ludi A (1984) Inorg Chem 23: 870
112. Beutler P, Gamsjäger H (1976) JCS Chem Comm 554
113. Beutler P, Gamsjäger H, Baertschi P (1978) Chimia 32: 163
114. Elding LI (1970) Acta Chem Scand 24: 1331
115. Harris SJ, Tobias RS (1969) Inorg Chem 8: 2259
116. Skibsted LH, Bjerrum J (1974) Acta Chem Scand A 28: 740 and 764
117. Davidson CM, Jameson RF (1965) Trans Faraday Soc 61: 2462
118. Jørgensen CK (1954) Acta Chem Scand 8: 175
119. Ryan JL, Jørgensen CK (1966) J Phys Chem 70: 2845
120. Jørgensen CK (1970) Progress Inorg Chem 12: 101

121. Jørgensen CK (1962) J Inorg Nucl Chem 24: 1587
122. Lucas J (1985) J Less-Common Metals 112: 27
123. Jørgensen CK (1986) Revue Chim Min (Paris) 23: 614
124. Reisfeld R (1987) Inorg Chim Acta 140: 345
125. Reisfeld R, Eyal M, Jørgensen CK (1986) J Less-Common Metals 126: 187
126. Reisfeld R, Jørgensen CK (1982) Structure and Bonding 49: 1
127. Durville F, Boulon G, Reisfeld R, Mack H, Jørgensen CK (1983) Chem Phys Lett 102: 393
128. Reisfeld R, Kisilev A, Jørgensen CK (1984) Chem Phys Lett 111: 19
129. Jørgensen CK, Reisfeld R, Eyal M (1986) J Less-Common Metals 126: 181
130. Reisfeld R, Eyal M, Jørgensen CK, Guenther AH, Bendow B (1986) Chimia 40: 403
131. Eyal M, Reisfeld R, Schiller A, Jacoboni C, Jorgensen CK (1987) Chem Phys Lett 140: 595
132. Reisfeld R, Kisilev A (1985) Chem Phys Lett 115: 457
133. Epiotis ND: Topics Current Chem, this volume
134. Rabinowitch E, Thilo E (1930) Periodisches System, Geschichte und Theorie. Enke, Stuttgart
135. Jørgensen CK, Horner SM, Hatfield WE, Tyree SY (1967) Int J Quantum Chem 1: 191
136. Iczkowski RP, Margrave JL (1961) J Am Chem Soc 83: 3547
137. Jørgensen CK (1962) Orbitals in atoms and molecules, Academic, London
138. Ruedenberg K (1962) Rev Mod Phys 34: 326
139. Jørgensen CK, Faucher M, Garcia D (1986) Chem Phys Lett 128: 250
140. Morris DFC (1968) Structure and Bonding 4: 63; (1969) 6: 157
141. Latimer WM (1955) J Chem Phys 23: 90
142. Landis T, Schwarzenbach G (1969) Chimia 23: 146
143. Schwarzenbach G (1970) Pure Appl Chem 24: 307
144. Pearson RG (1986) J Am Chem Soc 108: 6109
145. Pearson RG (1987) J Chem Educ 64: 561
146. Ahrland S (1968) Chem Phys Lett 2: 303
147. Wess J (1980) Naturwiss 67: 484
148. Müller A, Diemann E, Jørgensen CK (1973) Structure and Bonding 14: 23
149. Lucken EAC (1969) Structure and Bonding 6: 1
150. Jørgensen CK (1969) Structure and Bonding 6: 94
151. Glerup J (1972) Acta Chem Scand 26: 3775
152. Noodleman L (1981) J Chem Phys 74: 5737
153. Jørgensen CK (1957) Acta Chem Scand 11: 151 and 166
154. Jaffé HH (1954) J Chem Phys 22: 1430
155. Jørgensen CK (1962) Acta Chem Scand 16: 2406
156. Sandorfy C (1979) Topics Current Chem 86: 91
157. Herzberg G (1987) Ann Rev Phys Chem 38: 27
158. Jørgensen CK (1975) Structure and Bonding 22: 49
159. Husk GR, West R (1965) J Am Chem Soc 87: 3993
160. Schmid G (1985) Structure and Bonding 62: 51
161. Petterson LGM, Bauschlicher CW (1986) Chem Phys Lett 130: 111
162. Doremus RH (1964) J Chem Phys 40: 2389
163. Spackman MA, Maslen EN (1986) Chem Phys Lett 126: 19
164. Jørgensen CK (1974) Chimia 28: 605
165. Nixon JF (1985) Adv Inorg Radiochem 29: 41
166. Willemse J, Cras JA, Steggerda JJ, Keijzers CP (1976) Structure and Bonding 28: 83
167. Perutz RN, Turner JJ (1975) J Am Chem Soc 97: 4791
168. McLean RAN (1974) JCS Dalton 1568
169. Müller A, Diemann E (1987) Adv Inorg Chem 31: 89
170. Jørgensen CK (1964) Inorg Chem 3: 1201
171. Dye JL (1984) Progress Inorg Chem 32: 327
172. Dye JL, DeBacker MG (1987) Ann Rev Phys Chem 38: 271
173. Henrick K, Tasker PA, Linday LF (1985) Progress Inorg Chem 33: 1
174. Mott NF (1974) Metal-insulator transitions, Taylor & Francis, London
175. Adler D (1968) Rev Mod Phys 40: 714
176. Jørgensen CK, Lenglet M, Arsène J (1987) Chem Phys Lett 136: 475
177. Manes L, Benedict U (1985) Structure and Bonding 59: 75

178. Naegele JR, Ghijsen J, Manes L (1985) Structure and Bonding 59: 197
179. Campagna M, Wertheim GK, Bucher E (1976) Structure and Bonding 30: 99
180. Hensel F, Franck EU (1968) Rev Mod Phys 40: 677
181. Berggren KF (1974) J Chem Phys 60: 3399; 61: 2989
182. Swenumson RD, Leutwyler S, Even U (1981) Phys Rev B 24: 5726
183. Ruoff AL, Vohra YK, Brister KE, Weir S (1986) Physica 139 B: 209
184. Drickamer HG, Frank CW (1972) Ann Rev Phys Chem 23: 39
185. Jephcoat AP, Mao HK, Finger LW, Cox DE, Hemley RJ, Zha CS (1987) Phys Rev Lett 59: 2670
186. Hulliger F (1968) Structure and Bonding 4: 83
187. Jørgensen CK (1985) J Physique (Colloq) 46 C-7: 409
188. Woolley RG (1982) Structure and Bonding 52: 1
189. Bruna PJ, Peyerimhoff SD (1987) Adv Chem Phys 67: 1
190. Slater JC (1964) J Chem Phys 41: 3199
191. Milligan RF, Thomas GA (1985) Ann Rev Phys Chem 36: 139
192. Vohra YK, Brister KE, Weir ST, Duclos SJ, Ruoff AL (1986) Science 231: 1136
193. Huang RH, Faber MK, Moeggenberg KJ, Ward DL, Dye JL (1988) Nature 331: 599

Chemical Bonding Across the Periodic Table

Nicolaos D. Epiotis

Department of Chemistry, BG-10 University of Washington Seattle, Washington 98195 USA

Table of Contents

Interdisciplinary barriers separating the "organic", "inorganic" and "solid state" subdisciplines of chemistry exist because there is no conceptual apparatus which clearly delineates how the rules of bonding depend on the identity of the atoms comprising a molecule and how they change as we move from one domain to another. We present a theory which is based on a fusion of MO and VB concepts which enables one to do the following: Dissect a molecule into fragments, apportion the valence electrons in the fragment orbitals, and then make "bonds" connecting the fragments. In this way two key elements of the bonding problem become transparent:
(a) The interplay between fragment excitation (investment) and "bond" making (return) in engendering net stabilization (profit) of the system.
(b) The mechanism of bond-making. Nonmetals bind primarily by spin-pairing plus one-electron delocalization due to overlap while metals bind mainly by two-electron delocalization in which overlap is assisted by an overlap-independent mechanism of bonding.

The recognition that the mode of electron delocalization depends on the identity of an atom sets up the stage for a differentiation between structural and reactivity properties expected from organic and inorganic molecules. This point is illustrated by diverse applications and reference to existing experimental and computational data. The article itself can be viewed as a first step towards a reexamination of solid state physics phenomena (most notably conductivity and superconductivity) from a chemist's vantage point after it has been demonstrated that a self-consistent, qualitative understanding of molecular electronics across the Periodic Table is now at hand.

Part I. Theory

1 Introduction

The aim of this article is to present a new way of viewing chemical bonding across the Periodic Table, i.e. a new way of organizing known facts about molecular electronic structure into a coherent pattern and, from this base, attempting predictions of yet undiscovered chemical phenomena. The philosophy that has led to this contribution is that "concepts are more important than numbers", a view explicitly or implicitly stated in the writings of Schrödinger, Wigner, Pauling, Coulson, Fukui, Hoffmann and others [1]. Thus what the reader will find here is a way to think about rather than compute molecules. The importance of what we may call "conceptual theory" (designed for the human mind as opposed to "computational theory" designed for the computer) is that it can be projected at the frontier of experimental research and chemistry is a distinctly experimental science. For example, physical organic chemistry was the frontier of organic chemical research in the 1950's when *ab initio* computations of organic reactions were not possible. In the 1980's, such calculations are almost routine but the experimental frontier has moved: Organic metals, organic superconductors, organic ferromagnets, etc. are far beyond the capabilities of computational quantum chemistry. In short, the development I will describe in this work is the natural consequence of the realization that computational lags far behind experimental chemistry.

Why are we confident in this approach and willing to expose it to scrutiny? Because this contribution fills a gap which is obvious to anyone who has studied chemistry: There exist many *local* models which "work" within a restricted domain but fail when extended beyond it. That is to say, there exists no single, unified theory of bonding. More importantly, because we can now explain precisely what is "wrong" with these local models and how our approach corrects their flaws.

What are the general desirable features of a qualitative theory of chemical bonding which are present in our approach? In setting out to build a unified theory of bonding which annihilates the traditional interdisciplinary barriers separating "organic", "inorganic", and "biological" chemistry from each other and from solid state physics, we demanded that the theory fulfills the following requirements:

(a) It should explain the entire set rather than one or more subsets of calculational *and* experimental data through consistent utilization of one and the same set of basic principles. Local concepts should be specialized applications of the basic theory.

(b) The concepts should be based on equations which can be transcribed to pictures. In this way, the theory can be presented in pictorial format to the chemist who is not a theoretical expert.

(c) The existing tools of computational chemistry are too good and too many so that it would be a waste to shift to a formalism which does not take advantage of them. Hence, the theory must be testable *by translation* by the existing methods of computational chemistry. That is to say, we must propose a "best human thinking" formalism which spawns concepts which are testable by a "best computation" formalism.

(d) The importance of qualitative theory lies in its inspirational value: It can suggest new mechanistic alternatives, new strategies for synthesizing molecules, etc. This means that qualitative theory comes *before* calculation and *before* experiment, i.e. it is a "before theory". Many interpretative tools constructed by classically trained theoreticians are "after theories", i.e. a computation is needed for interpreting the computation itself (e.g. the concept of natural orbitals). To put it crudely, a qualitative theory must be a "back of the envelope theory" which can be routinely implemented so as to precede and inspire new computations and experiments.
As we shall see, our approach combines all four features.

What can we do specifically by using our method which could not be done before? If a molecule is viewed as composite of one or more subfragments, then we can express *explicitly* with "pictures" how *symmetry* dictates *fragment excitation* which produces *optimal bonds* linking the two fragments. We say that our approach projects explicitly the *excitation/bond-making interplay* and we draw the attention of the reader to the four italicized words. Every time we single out a deficiency of a conventional model, we really identify a failure of the model to give proper account of all the effects corresponding to these four italicized words: Molecular Orbital (MO) [2] theory is not *explicit*, Generalized Valence Bond (GVB) [3] theory fails to project the role of *symmetry* (though it accounts quantitatively for its effect), Extended Hückel MO (EHMO) [4] theory fails to properly describe *optimal bonds* (i.e. the mode of electron delocalization), etc. Every time we say that our approach revolutionizes our ideas about chemical bonding, we really mean that the symmetry controlled excitation/bond-making interplay has been made transparent for the first time. Every time the skeptical reader adheres to his own preconceptions and disdains our conclusions, he should check whether his thinking incorporates all four elements just identified.

What is the logic in the development of our approach? First, there were reasons for starting the quest for a unified theory of molecular electronic structure with Valence Bond (VB) [5] theory:

(a) VB theory is a polydeterminantal theory in which the configurations have explicit chemical meaning (unlike those of MO-CI theory) and which can be applied without restriction to any conceivable problem of molecular electronics, at least in principle.

(b) Resonance theory [6], an intuitive version of VB theory, has prepared the chemist well for acceptance of VB theory. Despite the great popularity of MO theory at the present time, one would be hard-pressed to locate an organic chemist who thinks of methane as "eight electrons in four low energy MO's" (MO theory) rather than as "tetravalent carbon making four covalent bonds to four hydrogen atoms" (Lewis concept of electron pair bond and VB theory).

(c) A Restricted Hartree Fock (RHF) Self Consistent Field (SCF) calculation [2d] is effectively a constrained VB calculation and Configuration Interaction (CI) the method by which this constraint is lifted. As a result, VB theory makes a problem which

is conceptually hard within the realm of MO-CI theory easy. For example, square D_{4h} cyclobutadiene is singlet rather than triplet because in the former there are *two* pi bonds (in resonance) while in the latter only *one* pi bond (in resonance with two odd electrons). In MO-CI theory, the same problem has engendered controversies, invocations of "Hund's rule violations", etc. In actuality this is a simple conceptual problem which the choice of a bad starting point (SCF MO theory) has artificially made to appear hard.

(d) The conceptual superiority of VB over MO theory, because of the clear concept of "bonds", is evident even to the most ardent practitioners of MO theory. An excerpt from the published Nobel Prize lecture of R. Hoffmann [7] is revealing: "Molecular orbital theory, . . . is fundamental to our approach . . . Yet when I seek the simplest of all possible ways to tell you of the orbitals of these fragments, I am lead back to the valence bond picture introduced in chemistry by Linus Pauling."

With these ideas in mind, we began back in the middle 1970's with traditional Eyring-Pauling VB theory [5c] and we sought to develop it to a qualitative analytical tool by removing the approximations which caused important conceptual failures which, in turn, predisposed chemists towards acceptance of simpler theories like Hückel MO (HMO) theory [8]. Specifically, we recognized that Resonance Theory is effectively "VB theory without symmetry control" because interaction matrix elements connecting pairs of resonance structure have signs which are the effective carriers of symmetry information and these signs are all taken to be positive in Resonance Theory. Once the signs are properly introduced, the concept of *Configuration Aromaticity* becomes in VB theory what Hückel's Rule is to MO theory. For example, cyclopropenyl cation is "aromatic" because the three lowest energy resonance structures all overlap in phase and they define a Hückel array of configurations which through interaction produce a low energy nondegenerate ground state. By contrast, cyclopropenyl anion is "antiaromatic" because the three lowest energy resonance structures all overlap out of phase and they define a Möbius array of configurations which through interaction generate a high energy doubly degenerate ground state. We say that the former system profits from Configuration Aromaticity while the latter cannot benefit from it. We have shown that an additional factor which makes cyclopropenyl cation so stable and cyclopropenyl anion so unstable as to frustrate all attempts to prepare it is the fact that two different modes of electron delocalization, single electron transfer and double electron transfer, operate in phase in the former and out of phase in the latter system. This causes the interaction matrix elements to have much greater absolute values in the "aromatic" compared to the "antiaromatic" system. Applications of the concept of Configuration Aromaticity can be found in published papers [9,10].

Configuration Aromaticity is a general principle of bonding and not only a stereo-chemical principle. Interaction matrix elements can be viewed as expressions of binding mechanisms and their signs tell us whether the configurations which they connect will interact profitably or not, i.e. Configuration Aromaticity represents the perfect cooperation of different types of binding mechanisms (= different types of matrix elements) in producing a highly stabilized eigenstate. It would be a serious omission not to mention that this concept owes its genesis to a 1965 contribution of Heilbronner [11] which pointed out the implications of the Möbius strip for HMO theory.

: One can go very far indeed with just qualitative VB theory. Applications to stereoselection, spin selection, aggregation selection, Jahn-Teller distortion, etc., were

presented at an early stage of development of our present view-point [9, 10] and after Salem and the Orsay group had clearly shown that a minimal basis set of VB configurations is sufficient to yield interesting insights into the mechanisms of thermal and photochemical reactions [12]. The next important step was the following realization: VB theory can be used to treat simple systems but it becomes impractical in handling conceptually large systems which today are at the focus of interest of the experimentalist. Writing all the necessary VB structures, connecting them with signed "double arrows", and using the concept of Configuration Aromaticity fast becomes an impossible task. Clearly, if progress were to be made, we had to invent some method capable of compacting the problem, so to speak. To put it in different terms, our problem became: How can we replace dozens, hundreds, or even myriads of VB configurations, by one or two "pictures" which describe the collective effect all VB configurations. The conceptual breakthrough was the genesis of Molecular Orbital Valence Bond (MOVB) theory [13, 14, 15] which now allows one to think in an organized way in a manner never heretofore possible.

2 Motivation for the MOVB Method

Figure 1 shows, in schematic form, a constellation of problems as treated by the MOVB method. The definition and solution of these and other problems constitutes the basis of a new electronic theory for chemistry. Some of the questions that arose in my mind about ten years ago and which led to the development of the ideas I will discuss in this monograph were:

(a) Why is it that two-step compete with "allowed" one-step paths in the absence of special constraints and at the moment when Hückel MO theory judges the former to be more unfavorable than "forbidden" paths?

(b) Why is it that we revere benzene as a six-electron "aromatic" pi system at the same time when it is known that six hydrogen atoms do not form a regular hexagon but, rather, they pair to form three H_2 molecules?

(c) Why is cyclopropane strained while at the same time having shorter $C—C$ and $C—H$ bonds than cyclohexane?

(d) Why do we say that hydrazine adopts a gauche conformation because of N lone pair — $N—H$ sigma antibond stabilization (negative hyperconjugation) when replacement of N by As (which precipitously lowers the energy of the sigma antibond and thus must enhance stabilization) drives the system towards a trans conformation?

(e) Why do we invoke negative hyperconjugation to explain the fact that the reaction of CF_4 plus CH_4 to produce $2 CH_2F_2$ is endothermic by about 25 kcal/mole when replacement of C by C_2 renders the same reaction exothermic by about 16 kcal/mole?

(f) Why do we attribute the preference for "outside" rotation of the fluorines in the conrotatory ring opening of trans-3,4-difluorocyclobutene to a more favorable $n_F — \sigma^*_{CC}$ interaction, where $C—C$ represents the breaking sigma bond, when the corresponding transition state. is "tighter" rather than "looser" (than the "inside" transition state) as this interaction would predict?
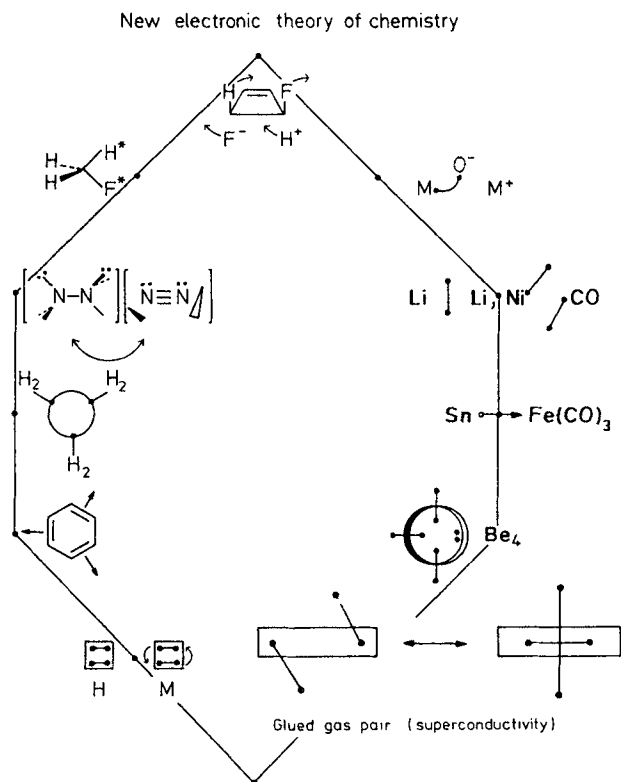
(g) Why is LiOLi linear but CsOCs bent?

New electronic theory of chemistry

Fig. 1. Key problems of modern electronic theory with a pictorial depiction of the MOVB solution

(h) Why does the radical cation of H_2 have a weaker bond than the neutral molecule while exactly the reverse occurs in the case of Li_2? Why is it that Cr_2 with six bond pairs has a weaker bond than V_2 with only four bond pairs and two one-electron bonds?

(i) Why is it that $Fe(CO)_3$-containing molecules often have a characteristic "butterfly" structure when organic molecules show distinct aversion for such a shape and when it is known that acetylene is linear but disilaacetylene is computed to be "butterfly"?

(j) Why is it that computations produce very unusual electron distributions for metal clusters and organometallics often characterized by electron density build-up between negatively charged atoms?

(k) Why is it that a structural modification can turn a normal to a high-temperature superconductor?

It was questions like these that indicated to me that the existing skeleton of "conceptual" applied quantum chemistry had to be replaced by a different framework. It was then that I realized that ab initio VB theory had little to do with Resonance Theory, even in a qualitative sense, and that, as a result, one should expect conventional concepts (based on Resonance Theory) to be intuitive guesses rather than theoretically

53

justified concepts. In this work, we will answer most of the questions I raised above in an effort to demonstrate the cohesion of the method which makes the epithet "unified theory" justified: We will start with methane and we will end with metal clusters. Finally, it would be an omission not to say that, while it was experimental data that provided the inspiration, computational results obtained by other workers (and I would be remiss not to cite the Pople-Schleyer collaboration [16] here) were instrumental in assuring that something essential was not overlooked. Furthermore, pure theoretical contributions in apparently unrelated areas (e.g. intermolecular forces [17-20], solid state physics [21], etc.) defined limits which are correctly reproduced by our theory, e.g. a Van der Waals complex is the zero-overlap limit of the corresponding supermolecule and bonding concepts should be able to describe the entire continuum.

3 What is MOVB Theory?

The recipe for formally implementing MOVB theory is as follows:

(a) A molecule in a given geometry is dissected into two fragments. The most convenient dissection choice is the one for which the local symmetry of the fragments is highest.

(b) The symmetry-adapted fragment orbitals (MO's or AO's) are written from the first principles or computed by using an effective one-electron Hamiltonian of the EHMO variety.

(c) The electrons are distributed so as to generate the MOVB Configuration Wavefunctions (CW's), Φ_i's.

(d) The MOVB CW's are partitioned into sets, T_m's, and each set is diagonalized separately to generate the diabatic states, Θ_{mi},

(e) The diabatic states are, finally, diagonalized to produce the final adiabatic states, Ψ_i.

At this point, it is clear that MOVB theory differs from the conventional methods to the extent that the total wavefunction is not obtained as a linear combination of Φ_i's but as a linear combination of Θ_{mi}'s. It now turns out that there exist choices of partitioning the Φ_i's into T_m's so that each Θ_{mi}, called a *bond diagram*, has explicit chemical meaning and it can be represented pictorially in a simple way. Thus, one arrives at a total wavefunction, Ψ_i, which is a resonance hybrid not of CW's (as in the traditional polydeterminantal theories), but a resonance hybrid of bond diagrams. In this way, we can follow how symmetry dictates bonding changes as the geometry of a molecule changes, in an explicit fashion, *taking into consideration all electrons, all orbitals, and all "effects"* (i.e. all integrals which correspond to chemical bonding mechanisms). A flow chart for illustrating the procedure is given in Scheme 1.

We are now ready to spell out the fundamental postulate of MOVB theory by which mere formalism is transformed to chemical sense: The partitioning of CW's into sets is carried out in such a manner so that each Θ_{m1}, the *ground state* resulting from diagonalizing the Φ_i's of T_m, represents just one way of making interfragmental bonds or

Scheme 1
MOVB Theory flow chart
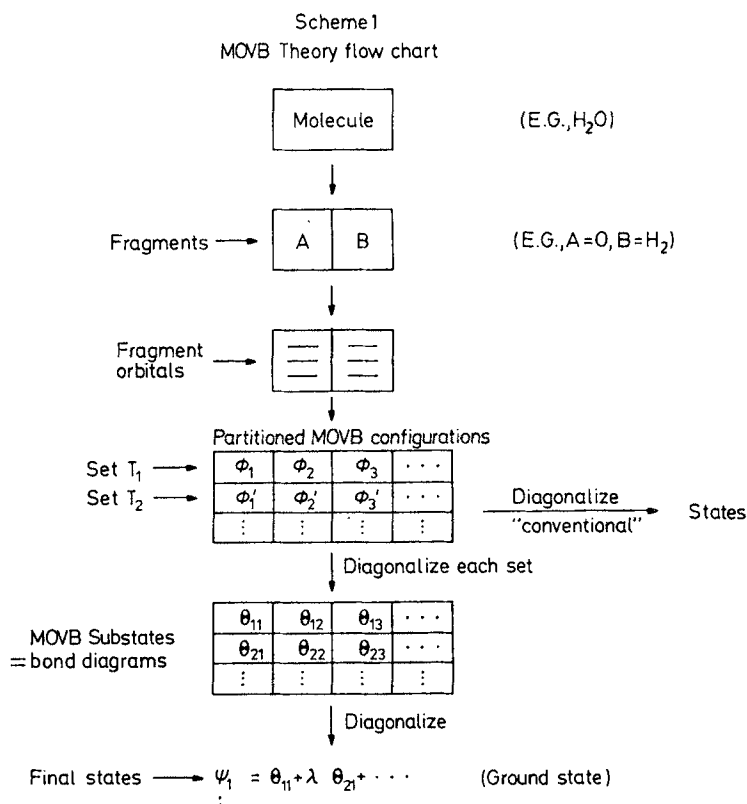
antibonds. With this convention, the approximate form of the *ground* total wave-function becomes:

$$\Psi_1 = \Sigma\lambda_m\Theta_{m1}$$

That is to say, higher diabatic states of appropriate symmetry (e.g. Θ_{mi}'s with $i > 1$) are deemed to be relatively unimportant.

We emphasize now some important aspects of the "mechanics" of MOVB theory and the associated terminology:

(a) With respect to the two fragments which make up the molecule, each individual configuration may contain any one or all of the following elements:

    1. Nonbonding electrons pairs (or odd electrons).

    2. Two-electron DET bonds. Each of them results from in-phase Double Electron Transfer (DET) and it is completely analogous to the classical single bond of singlet ground H_2 (Fig. 2a).

    3. Two-electron DET antibonds. Each of them results from out-of-phase DET and it is completely analogous to the antibond of triplet H_2 (Fig. 2a).

    4. Four electron (or three electron) antibonds. Each of them is due to repulsion arising from the overlap of filled orbitals.

55

Singlet det bond   Triplet det antibond

a $|a\bar{b}| \xleftrightarrow{+} |b\bar{a}|$ $|a\bar{b}| \xleftrightarrow{-} |b\bar{a}|$

	Parent Configuration			Bond diagram	
Nonbond	─┼─	──	⟶	─┼────	1-e Bond
Det bond	─┼─	─┼─	⟶	─┼────┼─	Delocalized det bond
Nonbond	─╫─	──	⟶	─╫─────	Coordinate bond
Det antib.	─┼─	─┼─	⟶	─┼─ ─┼─ Det antib.	
3-e Antib.	─╫─	─┼─	⟶	─╫────┼─ 3-e Bond (?)	
4-e Antib.	─╫─	─╫─	⟶	─╫─ ─╫─ 4-e Antib.	

b
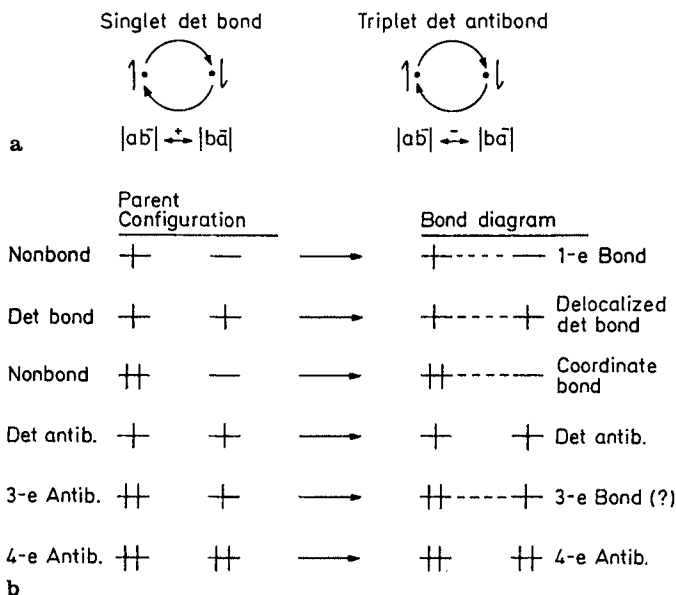
Fig. 2a and b. (a) Illustration of DET bonds and antibonds, (b) Bonding implications of individual configurations and of configuration interaction indicated by dashed lines. A 3-e antibond may end up as a 3-e bond because of configuration interaction

(b) To construct the principal bond diagram, one generates the *parent configuration* by placing electrons in orbitals so as to form the maximum number of bonds and the minimum number of antibonds by occupying as many orbitals having low energy as possible. Then, dashed lines connecting orbitals which belong to the same irreducible representation are added and these now represent how electrons can be shifted in order to generate configurations which will interact with each other, i.e. the dashed lines tell one how "symmetry allowed" delocalization will take place.

(c) A dashed line connecting a doubly occupied with a vacant orbital is said to define a coordinate bond (for lack of a more evocative term). Dashed lines connecting two orbitals with a total of one and three electrons define one- and three-electron bonds, respectively. Finally, a dashed line connecting two orbitals with two electrons defining a DET bond defines a delocalized DET bond. These considerations are illustrated in Fig. 2b.

(d) Higher energy bond diagrams are constructed in an analogous fashion.

(e) When referring to the excitation which is needed for connecting two fragments with bonds specified by the corresponding bond diagram, we always refer to the parent configuration of the bond diagram and we inquire as to whether there exists a delocalization mechanism which can act as to lower the excitation one would calculate by assuming that only the parent configuration exists.

(f) Configuration interaction within each diagram is completely specified by the dashed lines and it represents electron delocalization. This can occur by two different

Example: A = Ni, a = 3d$_{xy}$, a* = 4s
           B = H$_2$, b = σ, b* = σ*
a   AB = NiH$_2$ (bent)

Example: C = Be, c = 2s, c* = 2p$_x$
           D = H$_2$, d = σ, d* = σ*
b   CD = BeH$_2$ (linear)
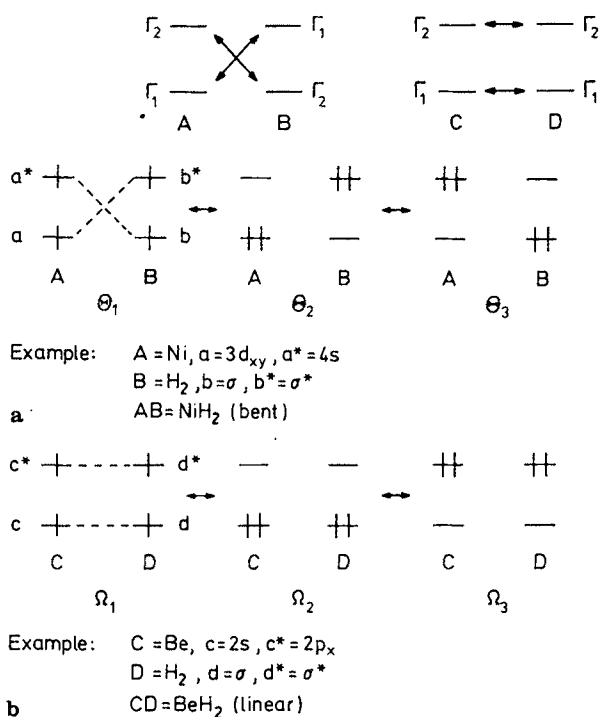
Fig. 3. Bond diagrammatic wavefunctions of A = B and C = D

types of electron transfer mechanisms which are of crucial importance: Single Electron Transfer (SET) and Correlated Electron Transfer (CET) as illustrated below.
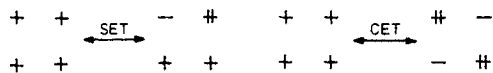
We now give a brief illustration of our approach by showing the bond diagrammatic representation of two different species A = B and C = D. The two systems differ only in the way the four orbitals match in symmetry and this is indicated by the double arrows below.

Each system is a four-orbital-four-electron system and each one is exemplary of an important class of chemical compounds. For example, putting A = Ni and B = H$_2$, we have C$_{2v}$NiH$_2$ and by putting A = Be and D = H$_2$ we have D$_{\infty h}$BeH$_2$. The MOVB representations of the ground state of each of A = B and C = D are shown in Fig. 3. Henceforth, we will exemplify our approach by reference to the A = B system.

According to the "drawing convention" of MOVB theory, dashed lines connecting orbitals belonging to the same irreducible representation imply the set of configurations which can be generated by shifting electrons along them starting from the parent

57

Fig. 4. The MOVB configurations needed for the description of A = B. Configurations 1 to 10 are "contained" in Φ_1. The principal configuration of Φ_1 is Φ_1. Φ_2 and Φ_3 are made up of one configuration (Φ_{11} and Φ_{12}, respectively) each

configuration "projected" by the diagram itself. Thus, in our example, Θ_1 represents two interfragmental *bonds* created by the interaction of Φ_1 to Φ_{10} shown in Fig. 4, Θ_2 represents one interfragmental *antibond* with $\Theta_2 = \Phi_{11}$, and Θ_3 represents one interfragmental *antibond* with $\Theta_3 = \Phi_{12}$. The parent of Θ_1 is Φ_1 and the bond diagram Θ_1 as written "projects" this lowest energy configuration. The approximate total wavefunction is simply a linear combination of these three "bonding schemes", i.e. these three bond diagrams.

$$\Psi = \lambda_1 \Theta_1 + \lambda_2 \Theta_2 + \lambda_3 \Theta_3$$

In fact, for ground state A = B

$$\Psi \simeq \Theta_1$$

This is so because Θ_2 and Θ_3, being antibonds, lie much higher in energy than two bonds. In general, either the "best" or the two leading bond diagrams will be sufficient for most qualitative analyses we shall attempt.

The fundamental difference between MOVB theory and the traditional approaches of building the wavefunction of a molecule is that the former is based on what we may call the "Partition and Successive Elimination Principle". Our position is that, in order to make sense of a polydeterminantal wavefunction, one must build it in such a way so that the initial set of myriads of elements is ultimately reduced to one, or two, or few elements of critical physical importance out of which the final wavefunction is constructed. The initial set is the set of all configurations and the final set is the set of bond diagrams. The latter are nothing else but the low energy substates which will be the dominant contributors to the final wavefunction that can be quantitatively obtained by diagonalizing all substates. The choice of the partition is based on the choice of fragments and the latter is frequently made in such a way as to maximize the symmetry of each fragment, e.g. CH_4 is viewed as C plus H_4 rather than CH_3 plus H. The reason is that, by doing so, we simplify the appearance of the bond diagrams (fewer lines connecting fragment orbitals). In short, we can call our approach the *Substrate Method* to the extent that the qualitative analysis is made by consideration of substates (bond diagrams) rather than individual configurations though the examination of how the principal substate(s) has been formed by configuration interaction plays a key role in the development of general bonding concepts.

4 A New Look at the Periodic Table

What is the conceptual advantage of the MOVB bond diagrammatic representation of the wavefunction of a molecule? The principal bond diagram makes possible an immediate visualization of the energy cost necessary for promoting a fragment to a "valence state" from which it can make a *countable* number of interfragmental bonds. Excitation is an investment, bond making is the capital one generates from the investment, and stability is the net profit associated with the investment. Now, high excitation is justified if the resulting bonds formed by orbital overlap are strong, and vice versa. Hence, the electronic properties of a molecule must be controlled by the intrinsic ability of the constituent atoms to enter into strong or weak overlap interaction. This leads to the following thought: The Periodic Table is a systematic classification of elements which have gradually changing electronic properties. The index to their characteristic properties must then be some measure of the ability of their AO's to sustain overlap interaction. The index of choice is the resonance integral β_{AZ} connecting an AO of atom A with a *fixed* AO of atom Z at the equilibrium bond distance r_{AZ}. According to the Wolfsberg-Helmholz approximation [22], β_{AZ} is proportional not only to the overlap integral t_{AZ}, but also to the valence orbital ionization energies I_A and I_Z:

$$\beta_{AZ} = K(I_A + I_Z) t_{AZ}$$

This means that if, t_{AZ} remains constant, β_{AZ} will decrease as A becomes increasingly electropositive. In actuality, t_{AZ} *also* varies in such a way so as to reinforce this prediction in *main group elements*. Specifically, there is an *abrupt* decrease of t_{AZ} in going from a $2s_A$ (first row) to a $3s_A$ (second row) AO. In contrast, t_{AZ} remains relatively constant in going from a $2p_A$ to a $3p_A$ AO. Accordingly, the atoms from boron to

59

Nicolaos D. Epiotis

Overlap binding abilities of atoms

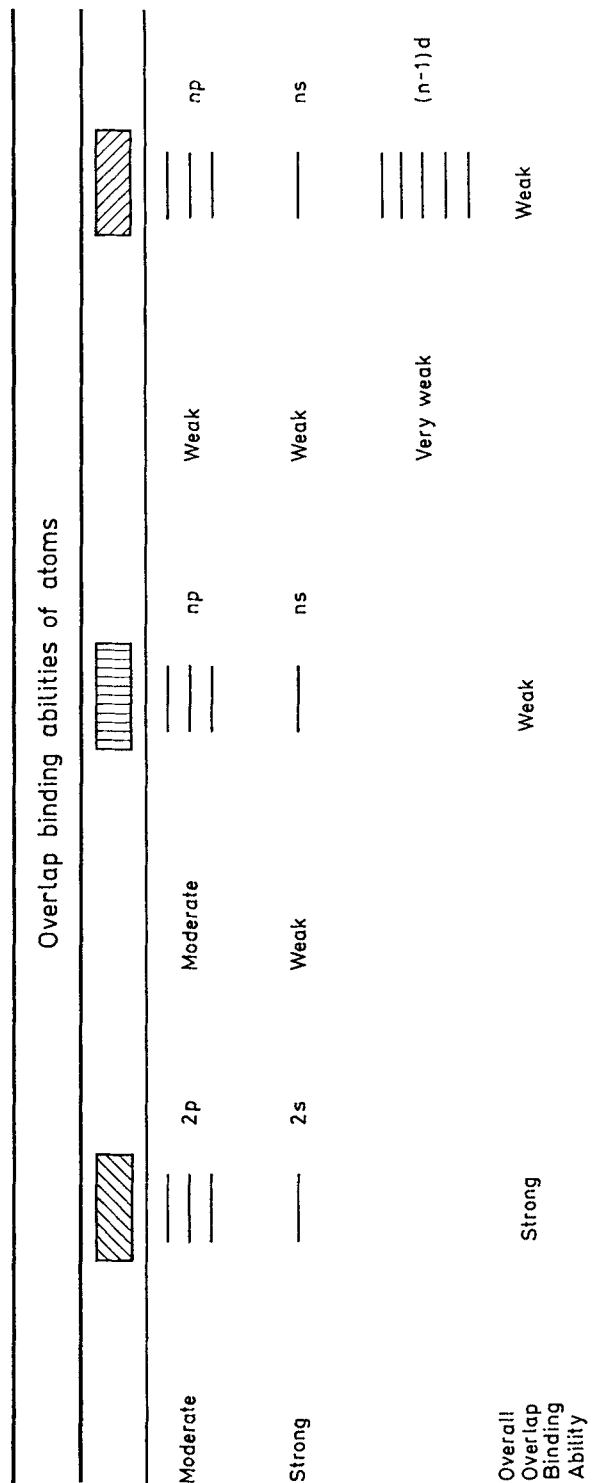|			
Moderate	2p	Moderate	np Weak
Strong	2s	Weak	ns Weak
			Very weak (n-1)d
Overall Overlap Binding Ability	Strong	Weak	Weak

Fig. 5. Color classification of atoms according to their overlap binding ability which depends on atom electronegativity and the radial extension of the valence AO's

fluorine must have substantially greater overlap binding ability than the much more electropositive atoms Li and Be of the same row as well as their second row relatives, namely, aluminum to chlorine. These considerations are more fully developed in Chapter 1 of ref. 14. They naturally lead to a subdivision of the Periodic Table in three colored areas: A black (first row nonmetallic), a green (heavier semimetallic), and a red (metallic). This subdivision is shown in Fig. 5. Henceforth, in preference to introducing new language, we shall use the terms black, green, and red themselves. *Black are strong and green and red weak overlap binders.*

At this point, I open a parenthesis in order to emphasize that the relative overlap binding ability of two atomic AO's of the same n but different l quantum numbers, e.g. ns and np, measured by the corresponding ratio of β_{AZ}'s (hence termed the overlap binding ratio) exhibits a variation across the Periodic Table that is a manifestation of fundamental properties. Thus, a number of workers, namely, Mulliken [23], Jørgensen [24], Pyykkö [23, 24], and Kutzelnigg [25] (see also ref. [8d]) have clearly recognized the fact that the first nodeless orbital without precursors (e.g. 1s, 2p, etc.) has a special position among valence orbitals with the same l quantum number. That is to say, 1s causes an expansion of 2s so that 2s ends up having an R_{max} comparable to that of 2p, etc. The expansion of 4d caused by the 3d precursor has been termed "primogenic repulsion" by Pyykkö [24]. This effect is not relativistic in origin and it is primarily responsible for the decrease of the ns/np ratio in going from first to second row and the decrease of the ns/(n − 1) d ratio in going from the first to the second transition series. The trend continues down a column as a result of three relativistic effects [26].

(a) The Relativistic Contraction.
(b) The Spin-Orbit Splitting.
(c) The Relativistic Self-Consistent Expansion.

Desclaux has tabulated the atomic radius at which the density of a given ns or np *valence AO* has its maximum value (R_{max}) [27]. The quantity $\Delta R_{max} = R_{max}^{av}(np) - R_{max}^{av}$ (ns) is a measure of the *relative* overlap binding abilities of the np and ns AO's. In going from a black to a green or red atom of the same column, a reduction of *overall* overlap binding ability goes hand in hand with (and, in fact, it is due to) an increasing ΔR_{max}, or, in more familiar language, a decreasing s/p overlap binding ratio. What this means is that a black atom will tend to bind by adopting a configuration in which the 2s AO is singly occupied, i.e. the black atom will be excited so that it can take advantage of the great overlap binding ability of the 2s AO. The opposite will be true in the case of green and red atoms in which the ns AO does no offer any great binding advantage *relative* to the np AO. In summary: A mismatch of the valence AO's in terms of R_{max} means that optimum overlap of one implies impaired overlap of a second valence AO of A with the AO's of some fixed fragment Z. In addition, high electropositivity means reduced capacity to promote overlap bonding. Black differs from green and red atoms to the extent that only the latter have the properties just mentioned.

Consider now the prototypical system A = B of Fig. 3a and the three configurations Φ_a, Φ_b, Φ_c shown in Fig. 6 which are contained within Θ_1. Assuming Φ_a to be the perfect pairing configuration, then going from Φ_a to Φ_b and from Φ_b to Φ_c involves disruption of one overlap bond. As a result, we distinguish two limiting cases:

(a) If A and B are strong overlap binders (black atoms), then the energy gap separating Φ_a and Φ_b, ΔE_{ab}, as well as ΔE_{bc} will be very large and Φ_a will be the dominant
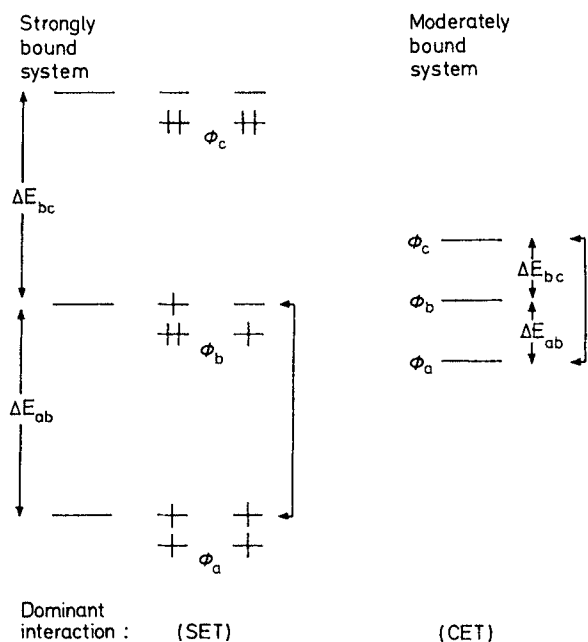
Fig. 6. The two worlds of strongly and moderately bound systems. In the former, the individual configurations are well separated in energy and SET, connecting the two lowest energy configurations, dominates CET because the latter requires interaction of two configurations separated by a large energy gap. In the latter, the energy gap ceases to be the key factor and configuration interaction depends primarily on the size of the interaction matrix element and CET is superior to SET in this sense

contributor with some contribution from Φ_b representing single electron transfer from one fragment to the other.

(b) If A and B are weak overlap binders (green or, better, red atoms), then ΔE_{ab} and ΔE_{bc} will be small and bonding will be due to strong interaction of all three (and others not shown) configurations.

Accordingly, molecules made up of black atoms (e.g organic molecules) define the world of overlap bonding (through spin pairing and single electron transfer) while molecules made up of green or red atoms (e.g organometallics, metal clusters, metals) define a new world which will be the main topic of this article. However, before we enter this new world, let us see how MOVB theory has revolutionized our view of a presumable well-explored territory: The bonding of organic molecules and stereoselection in organic chemistry. We will illustrate our approach by reference to two problems: The "methane problem" and the "strain problem", with the latter one being especially important because it introduces us to a concept, the Echinos Model of cluster electronic structure, which will be pivotal in the development of a theory of superconductivity later on.

Part II. Symmetry Control of Overlap Bonding in Organic Molecules

5 The Methane Problem

In an age when computational accuracy can compete with experimental accuracy in the regime of small molecule chemistry [28], at a time when reliable calculations of organometallic complexes and even metal clusters are feasible [29], and in an era which has seen the proliferation of computer programs capable of performing accurate computations of organic ground states and transition states [30], the question still remains: Do such computations lead to an operationally significant understanding of molecular electronic structure? In attempting to provide an answer, we must come to grips with the stark reality that questions like the following remain unanswered:

Question (a) Why does the C—F bond length, r_{CF}, decrease [31] and the corresponding bond energy, D_{CF}, increase [32] along the series CH_3F, CH_2F_2, CHF_3, and CF_4? [33]
Question (b) Why is the reaction shown below exothermic? [34]

$$2\,H_2CF_2 \rightarrow CF_4 + CH_4 \qquad \Delta H_r = -24.9\ \text{kcal/mole} \qquad (1)$$
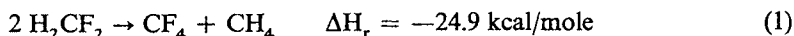
Question (c) Why is it that replacement of C by C_2 changes the above reaction from exothermic to to endothermic? [34]

$$2\,H_2C_2F_2 \rightarrow C_2F_4 + C_2H_4 \qquad \Delta H_r = +15.6\ \text{kcal/mole} \qquad (2)$$
(1,1 Isomer)
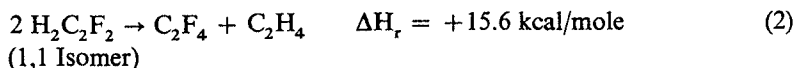
Question (d) Why is it that replacement of C and F by a "heavier" isoelectronic atom, like Sn and Cl, renders reaction (1) endergonic? [35]

$$2\,R_2SnCl_2 \rightarrow SnCl_4 + SnR_4 \qquad \Delta H_r = 7.0\ \text{kcal/mole} \qquad (3)$$
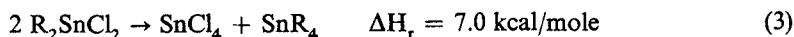
Questions (a) to (c) define the so called "Perfluoro Effect Problem". Questions (a) to (d) define what I will call a general "Methane Problem". If we really understand the electronic structure of methane, then we must be able to provide clear and succinct answer to the above questions. That this is not possible with present-day concepts with regards to the first two, leave alone all four, questions has been recognized independently by various authors. For example, Chambers [33] concludes that "the very range of explanations that have been offered is some indication in itself of the uncertainty which exists in explaining this very fundamental and interesting aspect of fluorine chemistry" in connection with question (a). Smart has reviewed the various conflicting models for bond contraction and bond strengthening in fluoromethanes and concludes that the matter remains unresolved [36, 37]. Note that, to question (a),

we have added three more questions for which we will demand a simple and self-consistent answer. The situation is clear: If a confident understanding of methane is still lacking, i.e. if we still cannot answer questions (a) to (d), how in the world can we claim to understand a conformational equilibrium, a transition state, a metal cluster, etc.?

5.1 The Electronic Structures of the Fluoromethanes

We begin by comparing the MO, VB, and MOVB descriptions of methane which are shown in Fig. 7. At the simplest MO level, we have four occupied bonding and four unoccupied antibonding MO's. At the simplest VB level, we have four sp^3 hybrid carbon AO's forming four bonds with the four hydrogens within the perfect-pairing VB configuration (corresponding to the Lewis structure of methane). These are familiar representations which need no further comment. Now, the steps one must take for the purpose of constructing the principal bond diagram of methane are:

(a) Methane is viewed as a composite made up of two fragments: A *Core*, C, fragment plus a *Ligand*, H_4, fragment. In other words, methane is viewed as "C plus H_4".
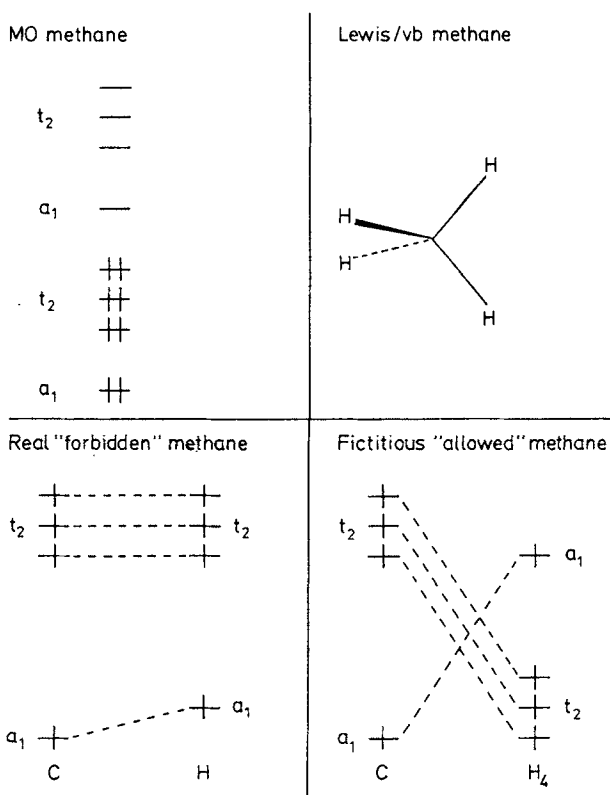
Fig. 7. The MO, classical VB, and MOVB descriptions of methane. Note the "parallel" ("forbidden") and "diagonal" ("allowed") overlap of the orbitals of the two fragments

(b) The symmetry adapted orbitals of the two fragments are drawn and are classified according to the irreducible representation to which they belong. The appropriate group theoretical symmetry label is placed next to each orbital.

(c) The eight valence electrons are placed in the eight valence orbitals so as to generate the maximum number of multicenter bonds.

(d) The four bonds obtained this way are the result of spin pairing within individual configurations plus delocalization brought about by the mixing of the configurations "contained" within the principal bond diagram which is shown in Fig. 7c.

(e) A key thing to note is the large splitting of the ligand a_1 and t_2 orbitals which is a consequence of strong nonbonded H1s—H1s overlap. It is exactly because of this that *both* core and ligand orbitals separate into a high energy t_2 set and a low energy a_1 orbital. The role of nonbonded AO overlap in determining how *direct bonds* are formed is the unappreciated element of molecular stereoelectronics.

(f) The MOVB formula of methane is:

This brings us to the first important point: The advantage of the MOVB theoretical description is that it explicitly reveals that tetrahedral methane is less than perfect: The four multicenter bonds are connecting an *excited* tetravalent carbon to an *excited* H_4 fragment so that the two lowest energy a_1 orbitals of the two fragments can never be simultaneously occupied by two electron pairs. That is to say, the configuration shown below is not contained within the principal bond diagram of methane.

Φ_a
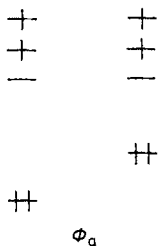
We then realize that real tetrahedral methane is a "forbidden" molecule relative to a hypothetical (nonexisting) "allowed" methane in which the four multicenter bonds are made as indicated by the principal bond diagram of Fig. 7d. Configuration Φ_a is now contained within the *principal* bond diagram of "allowed" methane. Note the hallmarks of "forbidden" and "allowed" molecules: In the former, the dashed lines run parallel in designating the bonds connecting the two fragments while, in the latter, at least a pair of dashed lines cross. These are the fingerprints of "forbidden" and "allowed" transition states insofar as orbital overlap is concerned and, hence, our terminology.

Tetrahedral methane belongs to the T_d point group. Replacement of one H by F yields CH_3F which now belongs to the C_{3v} point group. The question is: What is the *effective symmetry* of the four bonds connecting carbon to H_3F? We will argue that the *effective symmetry* is not C_{3v} but T_d, that is to say, the four bond orbitals of the

Θ_U

$2p_y$ e		e	q_4
$2p_x$			q_3
$2p_z$ a_1		a_1	$q_2(H)$

"Parallel"
overlap pattern –
"forbidden"
bonding

e n_2
n_1

$2s$ a_1 a_1 $q_1(F)$

C H_3F

Θ_D

"Diagonal"
overlap pattern –
"allowed"
bonding
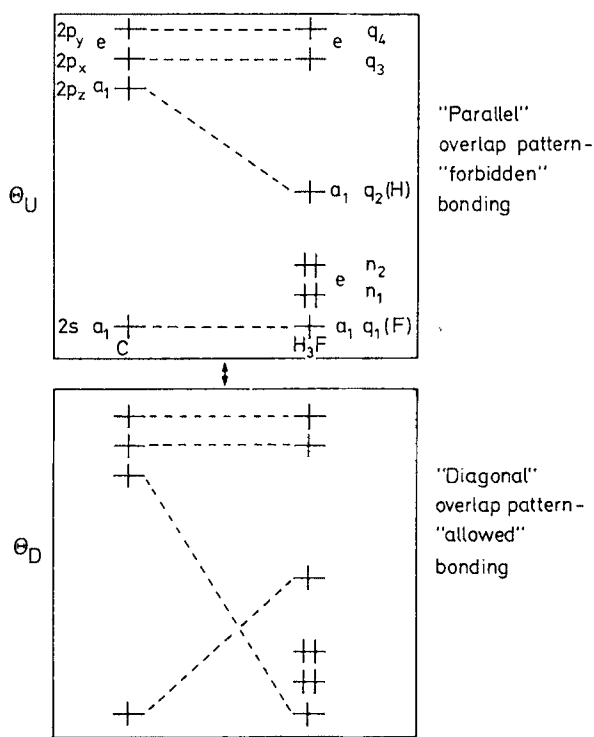
Fig. 8. Bond diagrammatic representation of CH_3F. Note how one contributor involves "parallel" a_1 overlap (as in methane itself) and the second contributor "diagonal" a_1 overlap. Which contributor dominates is determined by the detail structure of the a_1 ligand (H_3F) MO's. The q_1 MO has principal F2p and the q_2 MO principal HIs character and this is what is meant by the symbols in the parenthesis

H_3F fragment in CH_3F very much resemble the four bond orbitals of the H_4 fragment in CH_4.

The two principal bond diagrams of CH_3F necessary for correctly describing hybridization are shown in Fig. 8. It is immediately obvious that Θ_U represents four interfragmental bonds much like those of T_d methane (Fig. 5c). By contrast, Θ_D represents four bonds made in acompletely different fashion. We say that the four bonds within Θ_U are "T_d bonds" while those within Θ_D are "C_{3v} bonds". If it turns out that there are *compelling reasons* for declaring Θ_U the dominant bond diagram, then we will be forced to conclude that bonding in CH_3F resembles that within CH_4, i.e. although CH_3F has lower symmetry than CH_4, nonetheless, both molecules are roughly equally "forbidden" because the effective symmetry of both is T_d. Now, Θ_U will be the dominant bond diagram if the H_3F fragment orbitals have the shapes shown in Fig. 9a rather than the shapes shown in Figure 9b. So, the final question reduces to the following: Is there any reason to expect that q_1 and q_2 will look as shown in Fig. 9a rather than as in Fig. 9b, given that q_3 and q_4 are invariant?

It may now be appropriate to slow down and go over, step-by-step, the construction of the principal bond diagrams of CH_3F shown in Fig. 8. First, we subdivided the
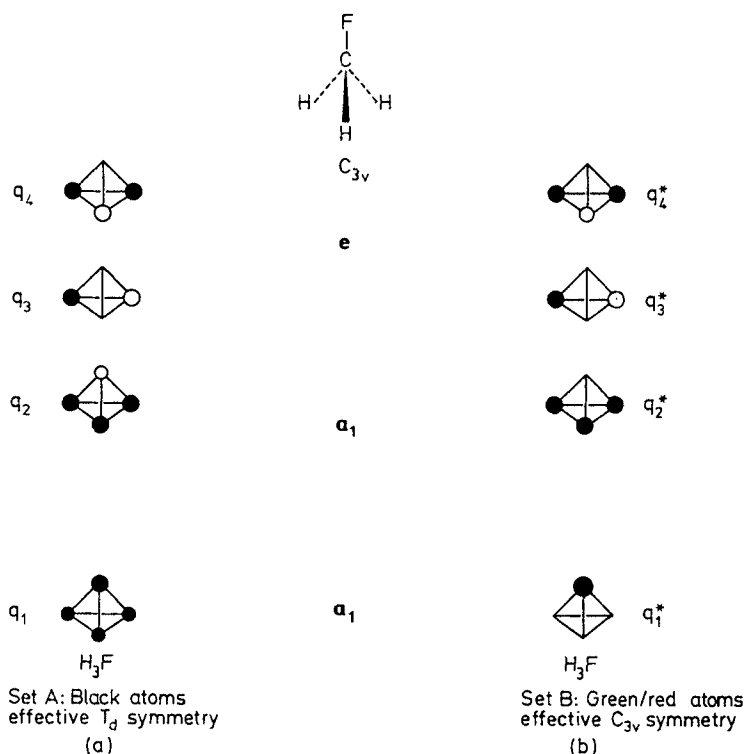
Fig. 9. Ligand MO's of CH₃F generated under two different constraints: Zero H—F overlap interaction (Set A) and strong H—F overlap interaction (Set B). The two different assumptions affect only the structures of the a_1 MO's. Note that the a_1 MO's contain both H and F AO's while the e MO's are pure H MO's

molecule into two fragments, namely, C plus H₃F, then we wrote the AO's of C and we constructed the MO's of H₃F starting from the AO basis shown below.
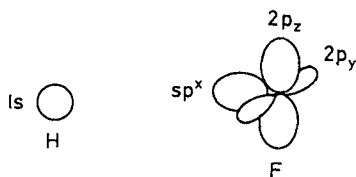
Specifically, F is assigned one valence sp AO and two lone pair 2p AO's while neglecting the lone pair sp AO which points away from the carbon center and H is assigned one valence 1s AO, as usual. As a result, we obtain four valence MO's (q_1 through q_4) and two lone pair MO's (n_1 and n_2). Next, symmetry labels are affixed on the individual orbitals, the electrons are fed therein, and bonds are made subject to the orbital symmetry restrictions (i.e. only orbitals carrying the same symmetry label can overlap and define a bond). Now, Θ_U represents one way of making four bonds and Θ_D a second way for accomplishing the same. The only difference between Θ_U and Θ_D comes about because the four a_1 singly occupied orbitals can be coupled either

in "parallel" (Θ_U) or in diagonal (Θ_D) fashion simply because there are two spin independent ways of coupling four electrons into two bonds and delocalizing them accordingly. Remembering now what each dashed line signifies, we can redraw the two original bond diagrams as shown in Fig. 10 so that now the "parent configuration" of each one is the dominant configuration of the set of configurations contained within each bond diagram. These pictures make clear that Θ_U represents "forbidden" and Θ_D "allowed" bond formation. The rest of the bonds, i.e. the two e bonds do remain invariant in a one-electron sense. The following trends are now evident:

(a) In CH_4, the H_4 ligand fragment MO's all span atoms of the same type. As a result, there is an analogy between VB electron pair C—H bonds and MOVB multicenter C—H bonds (Fig. 7). This analogy ceases to exist in CH_3F where two of the H_3F ligand MO's (q_1 and q_2) span two different types of atoms. As a result, q_1 is really a mixture of VB electron pair C—F and C—H bonds, with the former making a dominant contribution, and q_2 is the same mixture with the latter now making a major contribution. Thus, in general, *MOVB bonds do not have the same meaning as VB bonds.*

(b) Reduction of symmetry from T_d in methane to C_{3v} in fluoromethane is really signaled by the fact that we can now superpose Θ_D on Θ_U (Fig. 10) for a proper description. The physical meaning of this additional bond diagram is that symmetry reduction causes fragment deexcitation through charge transfer from q_2 to q_1 and electron demotion from C2p to C2s and this fact is portrayed in the principal configuration
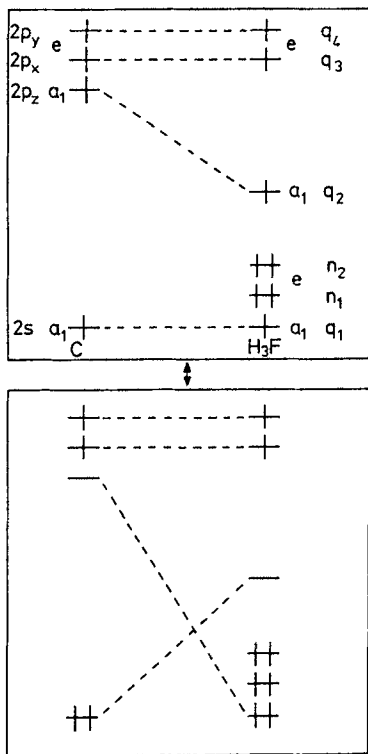
Fig. 10. Equivalent bond diagrammatic representation of CH_3F where now the dominant contributor configuration of Θ_D is the one which places two electron pairs in the two lowest energy a_1 orbitals of the two fragments

projected by Θ_D in Fig. 10. However, a price must be paid: In this principal configuration, the electron pair used for making an MOVB bond of principal C—F character now resides in q_1, the electron pair used for making an MOVB bond of principal C—H character now resides in C2s, and as a result, one CF-type and one CH-type MOVB bond has partly ceased to exist. Furthermore, because of the engendered overlap repulsion of the C2s and q_1 pairs, we say that the two aforementioned MOVB bonds are antagonistic and we expect the CH and CF bond lengths of CH_3F to be *both longer* than those in CH_4 and CF_4, respectively, where this antagonism no longer exists (but *vide infra*). These ideas are described in section III of Chapter 4 of reference 14. MOVB theory is a theory which shows in an explicit fashion how symmetry controls fragment excitation for the purpose of bond making and which projects the interplay of these two factors.

(c) CH_3F has two *pure* C—H MOVB bonds of e symmetry, one *impure* C—H MOVB bond of a_1 symmetry and one *impure* C—F MOVB bond also of a_1 symmetry with the latter two being antagonistic regardless of how small or large the contribution of θ_D is, i.e. this statement is based exclusively on symmetry considerations. Henceforth, the term C—H bond will be taken to mean pure MOVB bond, the term "C—H" bond to mean impure C—H bond and the term VB C—H bond will refer to the usual VB description with which the chemist is well familiar.

Let us return to the original question: Will the symmetry MO's of the H_3F fragment look like q_1 and q_2 or like q_1^* and q_2^*? But, the approximate explicit expressions of these orbitals are:

$$q_1 = Q_1 \ (\lambda_1 = \text{Large})$$

$$q_1^* = Q_1 \ (\lambda_1 = \text{Small})$$

$$q_2 = Q_2 \ (\lambda_2 = \text{Large})$$

$$q_2^* = Q_2 \ (\lambda_2 = \text{Small})$$

$$Q_1 = N[f + \lambda_1(s_1 + s_2 + s_3)]$$

$$Q_2 = N[(s_1 + s_2 + s_3) - \lambda_2 f]$$

where s_i are hydrogen and f fluorine valence AO's. As a result, the question becomes: What will be the value of mixing coefficient λ_i? If it is large, we have θ_U dominant and effective T_d symmetry while, if it is small, we have effective equalling real C_{3v} symmetry. There exist two important factors which cause λ_i to be large:

(a) The geminal nonbonded overlap of the H and F valence AO's is very large, much like the geminal overlap of AO's of atoms attached on a central first row atom[37]. Replacement of C by Si will reduce nonbonded overlap and the value of λ_i.

(b) The central atom controls the value of λ_i to the extent that a large λ_i means that the now delocalized q_1 and q_2 can yield large overlap integrals with the C2s and C2p$_z$ AO's, respectively, provided that these AO's have radii of maximum electron density which are very similar (i.e. provided that the central atom is a strong overlap binder). Because q_1 and q_2 span the same AO's (by virtue of being delocalized), a mismatch of

the radial extensions of C2s and C2p would create a situation in which optimal C2s-q_1 overlap would necessitate poor $2p_z$-q_2 overlap, or vice versa. In such a case, q_1 and q_2 would become localized q_1^* and q_2^* so as to engender fragment deexcitation since now only one (rather than two) strong interfragmental bond could be formed. Hence, we say that *even in the absence of direct H—F interaction*, the q_1 and q_2 MO's will be delocalized as a consequence of the fact that C2s and C2p are both strong overlap binders. In other words, the nature of the AO's of the central atom alone can control the effective symmetry of the molecule. When C is replaced by Si, the unequal radial extensions of 3s and 3p causes increased localization of q_1 and q_2, and SiH_3F tends to have effective C_{3v} symmetry.

The MOVB theoretical analysis is over. We will now construct the principal bond diagrams, Θ_U, of the fluoromethanes and we shall let them speak for themselves. The "effective T_d symmetry" bond diagrams of CH_3F, CH_2F_2, CHF_3, and CF_4 are shown in Fig. 11 and 12. All we have to do now is count the ligand valence MO's of exclusive F character which make bonds in conjunction with the upper 2p AO's of the core fragment. The count is zero for CH_3F, one for CH_2F_2 (b_1 bond), two for CHF_3 (the two e bonds) and three for CF_4 (the three t_2 bonds). This means that the percentage of C—F polar bonds, i.e. the percentage of C—F bonds formed via utilization of the more electropositive C2p AO, is: 0.0, 50.0, 66.6, and 75.0, in CH_3F, CH_2F_2, CHF_3, and CF_4, respectively. Had Θ_D been dominant (see Fig. 10), the percentage of C—F bonds made through utilization of C2p would have been 100, 100, 100, and 75 for CH_3F,
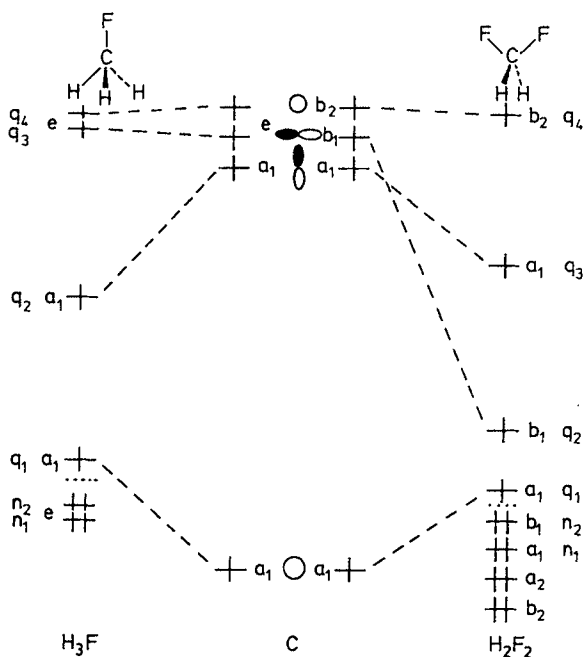
Fig. 11. Principal bond diagrams of CH_3F and CH_2F_2 including the fluorine 2p lone pairs. In CH_3F, the "C—F" a_1 multicenter bond finds no matching lone pair MO of the same symmetry while, in CH_2F_2, each of "C—F" and C—F has one matching lone pair MO
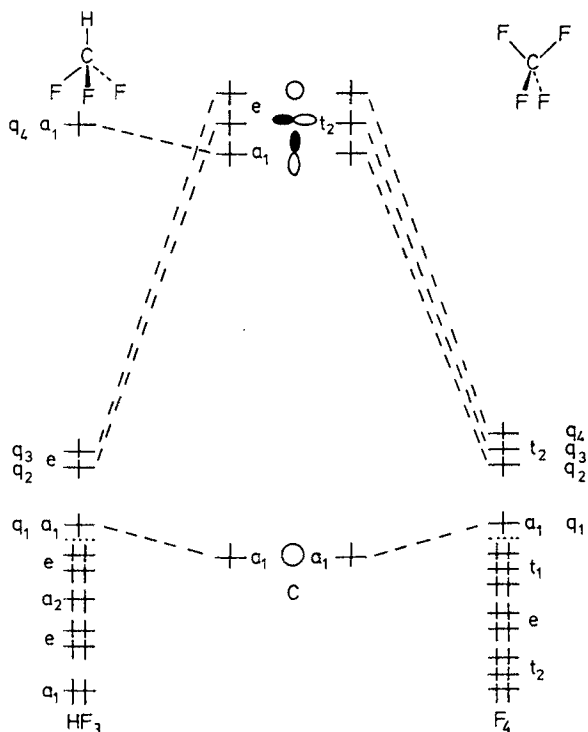
Fig. 12. Principal bond diagrams of CHF_3 and CF_4. In the former, two e C—F bonds are matched by two e lone pairs and one a_1 "C—F bond" by one a_1 lone pair. In CF_4, only three (t_2) C—F bonds are matched by (t_2) lone pairs

CH_2F_2, CHF_3 and CF_4, which is quite a different trend. Furthermore, we see that the percentage of "C—F" bonds, each of which is antagonized by a "C—H" bond of a_1 symmetry, is 100, 50, 33.3, and zero within the same series of molecules because "C—F"—"C—H" bond antagonism exists only in CH_3F, CH_2F_2, and CHF_3 which have symmetry lower than T_d. Since the bond of the diatomic H—F is the prototype of an *optimal* polar bond resulting from the coupling of the relatively electropositive H1s and the relatively electronegative F2p AO and, at the same time, it is not antagonized by any other bond, we say that "H—F type bonding" becomes increasingly prevalent in sweeping from CH_3F to CF_4.

Since only total energy arguments are valid in any qualitative discussion of molecular electronic structure and since the problems we defined in the introduction call for some kind of comparison of nonisomeric and normally noncomparable molecular species, we now see a simple way of attaining this last goal. Recognizing that, ideally, electropositive ligands prefer to bind to electronegative AO's of a core fragment and vice versa (e.g. H prefers to bind to C2s and F to C2p thus generating polar bonds) we can see that the total number of *optimal* C—H *and* C—F bonds are three, two, one, and zero in CF_4, CHF_3, CH_2F_2, and CH_3F, respectively, that is to say the number of optimal bonds equals the number of optimal C—F bonds, remembering that the term "optimal" means that the bond is polar plus there is no antagonistic interaction be-

tween this bond with some other existing bond on symmetry grounds alone. Hence, total energy arguments can be made by reference only to C—F bonds in the case of fluorocarbons.

With this background, here are now the direct and specific answers to questions (a), (b), and (d): First, the CF bond length decreases steadily in going from CH_3F to CF_4 paralleling the percentage of optimal C—F bonds. Second, reaction (1) is exothermic because the number of optimal product bonds exceeds that of reactant bonds, i.e. CH_2F_2 has one, CH_4 one, and CF_4 three optimal bonds and one plus one is less than one plus three. Third, in (1), the *effective symmetry* of each *reactant* is the *same* as the *effective symmetry* of each *product*, namely T_d, despite the fact the the reactants belong to lower symmetry point groups than the products. As a result, *there is no "forbiddenness" reduction as we go from products to reactants*, the products have more optimal C—F bonds and, hence, more favorable overall bonding, and the reaction is *exothermic*. By contrast, in (3), the effective symmetry of each species is identical to the actual symmetry which is attested by the point group, *the reactants are less "forbidden" than the products*, and the reaction becomes *endothermic*. In Table 1, we show data which clearly indicate that when the components are red "metallic" atoms, there is ligand *antisymbiosis*, i.e. changing the central atom from black to red changes the trend defined by Eq. (1). We can explain the same thing in alternative language: When the constituent atoms are green or red, as in (3), the best placement of ligands is the one in which a sigma donor and a sigma acceptor group are placed on the same atom so that charge donation from the donor to the acceptor has the *concomitant* effect of converting the central atom from tetra- to di-valent (cental atom deexcitation). This is precisely what the bond diagrams of Fig. 10 tell us when Θ_D becomes dominant (green and red component atoms).

Table 1.

Reaction	ΔE (kJ/mole)
$HgMe_2 + HgCl_2 \rightarrow 2\ MeHgCl$	—28.5
$HgMe_2 + HgI_2 \rightarrow 2\ MeHgI$	—17.2
$Cr(CO)_6 + Cr(PhH)_2 \rightarrow 2\ (CO)_3Cr(PhH)$	—6.0
$Cr(CO)_6 + Cr(HMB)_2 \rightarrow 2\ (CO)_3Cr(HMB)$	—50.2
$SnMe_4 + SnCl_4 \rightarrow 2\ Me_2SnCl_2$	—29.3

Data taken from ref. [35]. HMB = Hexamethylbenzene.

5.2 Bonds and not Lone Pairs are Responsible for Symbiosis

We have outlined the MOVB interpretation of the four chemical trends defined within the initial four questions as well as additional trends which have long been regarded as puzzling. What remains to be done is to now use MOVB theory to show clearly what exactly is wrong with previously attempted rationalizations of these phenomena. We proceed in two steps: First, we show why we have totally neglected the lone pairs in the bond diagrams of Fig. 11 and 12 and why the correct explanation has little to do with lone pairs. Second, we show why the preoccupation with lone pairs

in seeking answers to the stated questions is the result of logical as well as theoretical misunderstandings.

We begin by asking the reader to consider a carbon 2p AO which is making a bond with a valence fluorine AO, q, which is oriented favorably towards 2p, under the observation of a lone pair contained within a fluorine AO, n, which overlaps minimally with 2p.
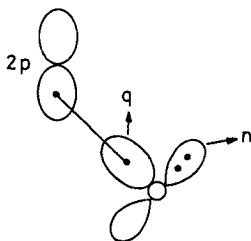
The way in which the C—F bond is formed is described in MOVB theory by a linear combination of two bond diagrams as shown in Fig. 13. Now, suppose that we carry out two calculations, one by eliminating the doubly occupied n AO and a second in which the entire system is properly treated. The change in energy in going from the first to the second calculation will reflect nothing else but the fact that we improved the C—F bond. This improvement will now be either *small* or *colossal* depending on how efficiently q and n overlap with 2p in the coordinate system of choice. That is to say, if we orient q and n as we did above, the improvement will be small and vice versa. Hence, *the "lone pair effect" will depend upon some arbitrary choice of the initial set of AO's.* Now, the important thing to understand is that regardless of what we called "valence AO" and "lone pair AO" in the beginning, we will always end up with a resonance hybrid of Θ_1 and Θ_2 which will represent one bond formed via some optimal valence AO q' and one lone pair housed within an optimal lone pair AO n'. Whatever physical interpretation we advance should always be definition-invariant.

The way in which lone pairs enter into play can be understood by examining the principal diagrams of the four fluoromethanes. These are shown in Fig. 11 and 12 under the assumption that the principal bond diagram of CH_3F, CH_2F_2, and CHF_3 is Θ_U. These diagrams show explicitly the "observer" symmetry-adapted lone pair MO's (constructed from the 2p fluorine AO's) which will hybridize with the sigma symmetry-adapted interfragmental bonds as decreed by symmetry. This hybridization is represented by writing additional bond diagrams in the fashion illustrated in Fig. 13.
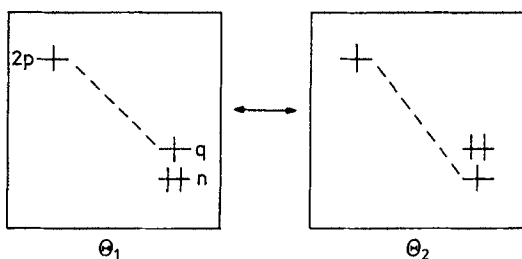
Fig. 13. Bond pair-lone pair hybridization according to MOVB theory and the necessity for conceptual invariance of the definitions of "bond AO" and "lone pair AO"

Now, assuming that $\lambda_1 = \lambda_2 = k$ and symbolizing by u and d the coefficients of Θ_U and Θ_D, we redefine an optimal C—F MOVB bond as one which fulfills these *three* conditions:

(a) The ligand group orbital spanning F atoms responsible for the bond has either unique symmetry or it has the same symmetry as another ligand group orbital spanning X atoms but the mixing coefficient k is zero. An example of the first type is q_2 of CH_2F_2 and an example of the second type is q_1 when it is totally uncontaminated by hydrogen AO's $(k = 0)$.

(b) The ligand orbital identified in (a) couples with an upper core AO or MO to make the bond. An example is the C2p-q_2 coupling in CH_2F_2.

(c) There exists an associated "observer" MOVB lone pair orbital (henceforth called F lone pair) spanning F atoms with the same symmetry as the ligand identified in (a). The result is C—F bond — F lone pair hybridization. An example is the hybridization of the C2p-q_2 bond with the n_2 lone pair, both having b_1 symmetry, in CH_2F_2.

Finally, we define an optimal C—H bond as the one which involves an uncontaminated ligand orbital spanning the H atoms which couples with a lower core AO or MO in making a multicenter MOVB bond. An example is the a_1 symmetry bond of methane viewed as "C plus H_4".

With the recipe just specified, let us count the optimal bonds in the four fluoromethanes assuming the Θ_U is the dominant contributor. From Fig. 11 and 12, the count is simply zero, one, two, and three for CHF_3, CH_2F_2, CHF_3, and CF_4, respectively. Now, let us count again assuming that k and the u:d ratio are zero and that Θ_D is the dominant contributor. The results are now entirely different: One, three, four, and three for the same series. It is now clear that our prediction of the enthalpy sign of reaction (1) will depend on the "method" of counting. Assuming Θ_U dominance, reaction (1) is predicted to be exothermic because the products have more optimal bonds. On the other hand, the same reaction is predicted to be endothermic by assuming Θ_D dominance. So, the operationally important thing in making predictions about symbiosis is our ability to count correctly. That is to say: Should we count by reference to Θ_U or by reference to Θ_D? We will count by reference to the former when k and u:d is large in which case the effective symmetry of a molecule is higher than the apparent one. We will count by reference to Θ_D when k and u:d tend to zero, in which case effective equals apparent symmetry. By doing so, any emerging argument automatically contains the effect of sigma bonding plus the effect of any symmetry-allowed hybridization. Realizing now that the bond pair-lone pair hybridization described in Fig. 13 contains $n_F - \sigma^*_{CF}$ negative hyperconjugation, we conclude that explaining bond contraction in fluoromethanes and fluorine symbiosis on carbon by negative hyperconjugation is accidentally correct because the latter effect is simply an inseparable part of optimal bond formation. However, the distinction between nonoptimal and optimal sigma bonding exists even in the absence of lone pairs, i.e. it still exists after eliminating criterion (c) above. Hence, we conclude that the celebrated trends discussed before are principally due to sigma bonding.

Finally, we argue that whatever legitimate lone pair effects exist beyond hybridization are caused by differential symmetry constraints. To see this point, we refer the reader to Fig. 11 and 12 and we recall that up until now, we counted optimal bonds by assuming constancy of the nonoptimal "C—F" and "C—H" bonds. Obviously this is not the case. For example, such nonoptimal bonds exist in CH_3F, CH_2F_2,

and CHF_3 and they are òbserved by zero, one, and two optimal C—F bonds, respectively, as well as by zero, one and one (more delocalized) lone pairs of a_1 symmetry, respectively. Recognizing that more C—F optimal bonds means more charge withdrawal from carbon and that a lone pair can coordinate with a proton, we say that in sweeping from CH_3F to CHF_3, there will be a pronounced tendency to convert the nonoptimal to optimal bonds by setting k equal to zero and increasing the contribution of Θ_D so that, for example, the H of CHF_3 acts now as an electron donor with respect to the C2s AO to counteract the electron density depletion and, at the same time, the lone pair of a_1 symmetry coordinates with the now vacant H1s AO. To put it simply, in sweeping from CH_3F to CHF_3, the optimal bonds and the existing lone pairs act as to "protonize" the hydrogen and turn the "C—H" (and concomitantly the "C—F") bond into an optimal bond. In other words, CH_3F and CHF_3 are both C_{3v}, but the former approaches effective T_d symmetry (i.e. it is "forbidden") more than the latter partly because of a lone pair effect. The increase of s character in the carbon AO directed to H plus the intramolecular hydrogen bonding is what causes the CH bond to be *shorter* in CF_3H than in CH_4 [39] despite bond antagonism in the former but not in the latter.

5.3 The Electronic Basis of Symbiosis: New Predictions

We now translate the key conclusions of our analysis in a language familiar to the chemist by reference to the prototypical reaction shown below in which each species is bent with constant angle and D and A stand for "sigma donor" and "sigma acceptor", respectively.

$$2\ MAD \rightarrow MA_2 + MD_2 \qquad (4)$$
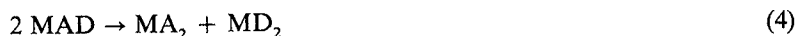
Each molecule is viewed as an M core plus an AD or A_2 or D_2 ligand fragment with M having àn upper m* and a lower m orbital while D and A have an a and a d valence orbital, respectively. Now, our contribution has been to point out that this Lewis representation is misleading and that the appropriate molecular formulae depend on the nature of all three species M, D, and A. Specifically, there exists a gradation between two limits:

(a) When M is a strong overlap binder, D mixes with A and vice versa in MAD so that each one ends up having properties intermediate between D and A. The benefit of this mixing (delocalization) is that the lower ligand MO, z, can overlap strongly with the lower m orbital of M and the same is true of the upper ligand MO, z*, and m*. This permits the formation of two good semipolar interfragmental bonds which tend to be shielded from each other because neither can z overlap effectively with m* nor z* with m (prevention of interbond overlap repulsion). At the same time, maximization of the overlap of M with AD requires that the acceptor/donor aspect of the ligands is lost. This state of affairs does not exist on the product side where each species has one nonpolar and one polar interfragmental˙bond. Hence, the correct Lewis formulae are the ones shown below, with the asterisks indicating that D is really

acting as a group with properties intermediate between a donor and an acceptor, etc., in MAD only.

$$2 \quad \overset{M}{\diagup \diagdown}_{*A \quad D*} \quad \longrightarrow \quad \overset{M}{\diagup \diagdown}_{A \quad A} \quad + \quad \overset{M}{\diagup \diagdown}_{D \quad D} \qquad (5a)$$
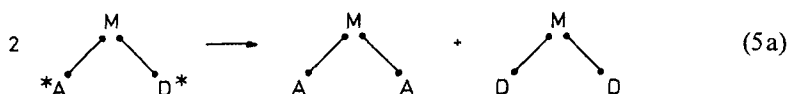
The approximate bond diagrammatic description of the reaction is shown in Scheme 2 a where we have assumed zero nonbonded interaction. First, note that M is divalent and each ligand, D and A, is univalent in the parent configuration of reactant and product bond diagrams. Then, observe the ligand hybridization that takes place in MAD producing z and z* ligand MO's which approach degeneracy half way between the one-electron energies of the d and a orbitals. This is called indirect ligand hybridization in MAD and it is energetically *beneficial*, i.e. it represents the best MAD can do to maximize its stability. Ligand hybridization is also imposed by strong nonbonded interaction which splits the x/x* and y/y* degeneracy and the z/z* near-degeneracy. This is called direct ligand hybridization in MAD and it is energetically *deleterious* because it tends to turn the two semipolar to two nonpolar bonds in MAD while it has less impact on MA_2 and MD_2. In previous papers, we emphasized the latter component as the two effects cannot be easily separated. In any event, the important thing is that, at the limit of M being a very strong overlap binder, the mixing of the ligand

Scheme 2

(a)

(b)

77
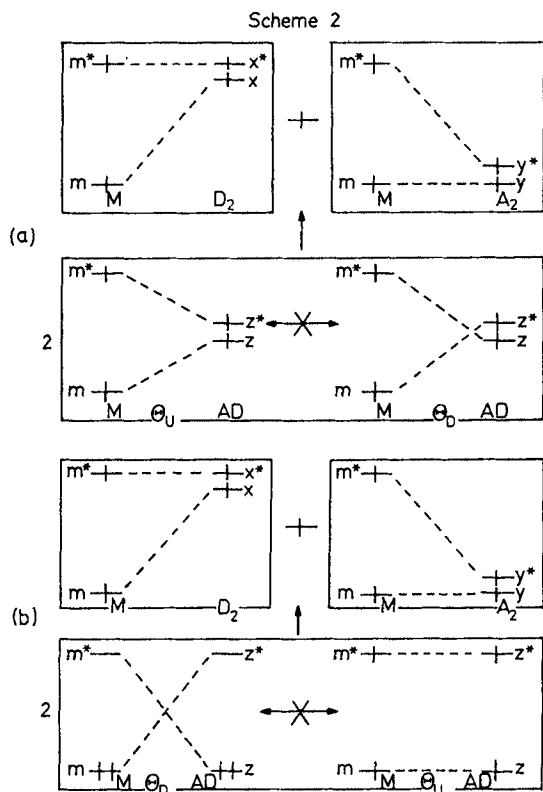
orbitals d and a is very strong, the principal bond diagram is Θ_U, the ratio of the co-efficients of Θ_U and Θ_D, $u:d$, large and the effective symmetry of MAD is not C_s but rather C_{2v} like that of MA_2 and MD_2. The reaction is exothermic because one polar plus one nonpolar is better than two semipolar covalent MOVB bonds. In other words, the products are more stable than the reactants because the reactants have more stars. The pattern of orbital overlap in all three molecules (when the ligand fragment MO's are nondegenerate) is characteristic of a Woodward-Hoffmann "forbidden" system.

(b) When each of M, A, and D becomes a weak overlap binder (and for M to become such the effective m — m* gap should be large), the wavefunctions representing the three molecules change. The approximate bond diagrammatic representation is now shown in Scheme 2b. Observe the dehybridization of the ligand AD orbitals ($z = a$ and $z^* = d$) and the fact that an electron pair occupies the m core orbital (which we assume that is contracted relative to m* and incapable of strong overlap binding (by definition) in the parent configurations of the reactant and product bond diagrams. Furthermore, observe that a pair is now placed within an antibonding ligand MO in MA_2 and MD_2 and this, in VB theory, implies charge transfer from one ligand to the other as does the placement of an electron pair in the lower ligand MO of MAD. At this limit, the mixing of the ligand orbitals tends to zero (directly and indirectly), the principal bond diagram is Θ_D, the $u:d$ ratio tends to zero and the effective symmetry of MAD is C_s. In direct contrast to the situation in (a), Θ_D describes now weaker bonds (no "spin-pairing" in the parent configurations) formed with overcompensating M fragment relaxation (= deexcitation). The key idea now is that generation of zero-valent M effectively triggers charge transfer from one ligand to the other. As a result, the reactants are now more stable than the products because a donor-acceptor relationship of the ligands exists only in the former. The chemical formulae which express the critical *difference* between reactants and products are:

$$2 \quad \overset{\cdot\cdot}{M} \quad \longrightarrow \quad \overset{\cdot\cdot}{M} \quad + \quad \overset{\cdot\cdot}{M}$$
$$\underset{+}{D} \quad \underset{-}{:A} \qquad \underset{+}{A} \quad \underset{-}{:A} \quad \underset{+}{D} \quad \underset{-}{:D} \tag{5b}$$

It is now obvious that the situation described in (b) is nothing else but an intermediate stop to the limiting case of two-bond exchange represented by the following formulae.

$$2 \quad \overset{\cdot\cdot}{M} \quad \longrightarrow \quad \overset{\cdot\cdot}{M} \quad + \quad \overset{\cdot\cdot}{M}$$
$$D\overset{\cdot}{\bullet\!-\!\bullet}A \qquad A\overset{\cdot}{\bullet\!-\!\bullet}A \qquad D\overset{\cdot}{\bullet\!-\!\bullet}D \tag{5c}$$
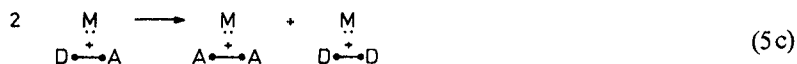
Note that it is only at this limit that any bond contraction effect goes to zero because the M—D and M—A bonds in the reactants and the products have equal legth: Infinity. Furthermore, observe the change of the enthalpy sign in going from negative at the (5a) to positive at the (5c) limit for, e.g. M = CH_2, D = H, A = F.

Our analysis makes now obvious the following connection: As M tends to divalency and as the M—A and M—D overlap bonding gets stronger, reaction (4) will tend to be exothermic while, as M tends to become zerovalent and the overlap component of the M—A and M—D bonds weak, the exact reverse will occur. This leads then to the following partial rule: For constant A and D ligands, the exothermicity of reaction (4) will be a function of the effective promotional energy that takes zerovalent M with electronic configuration m^2 to divalent M with electronic configuration $m^1 m^{*1}$.

For row comparisons, this quantity can be approximated by the singlet-triplet gap of M computed at the geometry of MAD, or MA_2, or MD_2. We can now explain the huge enthalpic change in going from reaction (1) to (2) recognizing that M = C and $M = C_2$, respectively, and realizing that each reaction is a double redistribution of the ligands (i.e. four DA are rearranged to two D_2 plus two A_2 units). We say that the enthalpy switches from negative to positive by about 40 kcal/mol because C is ground divalent with an accessible tetravalent state while C_2 is ground singlet (in which essentially two ground divalent carbons are linked by two bonds) with a very high lying tetravalent state appropriate for ethylene formation. On top of it, the two sets of ligands (F_2 and H_2) become segregated in $C_2H_2F_2$ but they are forced to close proximity in CH_2F_2. Hence, nonbonded interaction of H with F is minimized in the former which then approaches its apparent point group symmetry more than the latter.

A theory which only explains but cannot predict is not a theory. The approach we outlined forms the basis for a wide range of predictions which can be easily tested by ab initio computations. For example, the singlet-triplet gap of M shown below computed at the idealized geometry
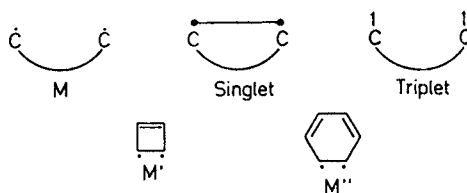
of MAD or MA_2 or MD_2 geometry is expected to be related to the enthalpy of reaction (4). One immediate prediction is that M' (resembling square cyclobutadiene with a small singlet-triplet gap) should favor symbiosis while M'' (resembling regular hexagonal benzene with a large singlet-triplet gap) should favor antisymbiosis. Given a list of singlet-triplet carbene energy gaps (M = CXY), one can design at will reactions in which M will dictate either symbiosis or antisymbiosis depending on its nature and irrespective of the presence or absence of lone pairs on X and Y, etc. Existing ab initio computational data are consistent with our analysis [39].

6 The Strain Problem

"While it is easy to look at a molecule and conclude it is strained, a simple and unified understanding of strain still evades us." This is the pessimistic conclusion of Liebman and Greenberg [40] justified nonetheless by the very fact that answers to questions like the following still evade us.

(a) Why do you call cyclopropane "strained" [41] when at the same time the C—C bond distance in this molecule is shorter than in "unstrained" cyclohexane? [42]

(b) It is known that electropositive substituents stabilize "strained" cyclopropane but electronegative substituents stabilize "strained" cyclobutane relative to isomeric forms [43]. Why is that so and can we predict other substituent effects in advance of calculation or experiment?

(c) Why does the C^{13}—H NMR coupling constant of a cycloalkane correlate with strain [44] and acidity [45] some times and why does the correlation break down some other times? [46]

(d) Why are there odd-even distinctions in the stability of rings containing hetero-atoms? [47]

(e) Why are organic polyhedra so unstable (e.g. tetrahedrane) while inorganic polyhedra (e.g. B_4Cl_4) so commonplace? [48]

We say that these and many more related questions define a "strain problem" and we now show how MOVB theory handles such a problem.

6.1 The Echinos Model

In a typical problem, we will be asked to consider a number of geometrical arrangements of the cluster A_m, where A is an atom or a fragment, predict the one which constitutes the global minimum, and explain why this particular geometry is favored over the others. The molecular shapes which will be at the focus of our attention will be linear or chain, two-dimensional cyclic, and three-dimensional polyhedral geometries. Hence, restricting our attention to an sp AO basis, we classify our AO's in such a way so as to differentiate between *Surface AO's* and *Needle AO's* as follows:
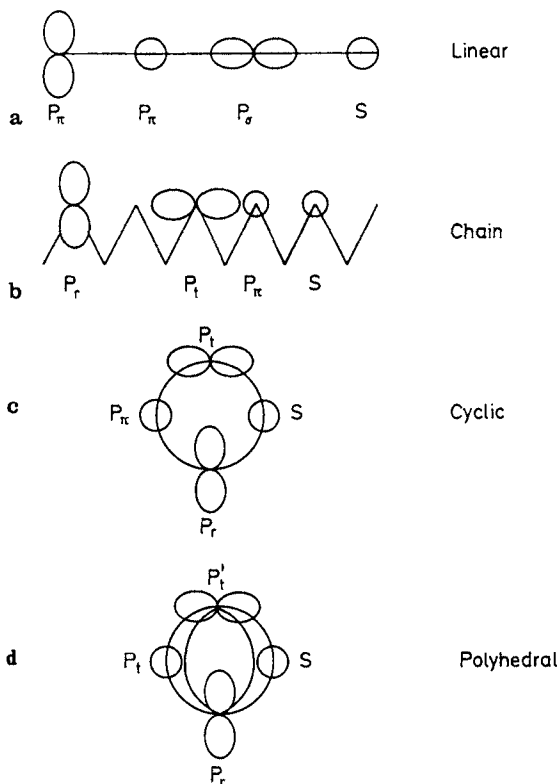
Fig. 14. The AO basis set for treating clusters. In each case, the AO's can be subdivided into Needle and Surface AO's according to the Echinos MOVB model as defined in the text

(a) In the case of *linear* A_m, as defined in Fig. 14a, we have:

    1. Surface AO's: $p\sigma$ and $p\pi'$ AO's.

    2. Needle AO's: s and $p\pi$ AO's.

In the case of *chain* A_m, as defined also in Fig. 14b, we have:

    3. Surface AO's: p_t and $p\pi$ AO's.

    4. Needle AO's: s and p_r AO's.

(b) In the case of *regular polygonal* A_m, as defined in Fig. 14c, we have:

    1. Surface AO's: p_t and $p\pi$ AO's.

    2. Needle AO's: s and p_r AO's.

(c) In the case of *regular polyhedral* A_m, the same definitions apply as in (b) only $p\pi$ becomes p'_t.

With these definitions, it is now clear that the Surface or Needle AO's of each type will generate *MO ladders* in which we shall be able to classify the individual MO's according to the point group of A_m. Henceforth, we shall symbolize each MO ladder by (x), where $x = p\pi$, p_t, etc., and each ladder MO by $(x)_i$. Furthermore, we shall recall that, in the case of an A_m cluster, there will always be m ladder MO's for each (x). Finally, the interaction of the two Surface ladders will produce the *Surface manifold*, denoted by S, and the interaction of the two Needle ladders will produce the *Needle manifold*, denoted by N. The specific process and the necessary symbolic notation for the polygonal case are shown in Fig. 15a. We have now reached the point where we have really generated two *fragments*, S and N, which contain a given total number of electrons. Hence, *we generated a problem that can be easily treated by MOVB theory to the extent that the total wavefunction of the system will be a linear combination*
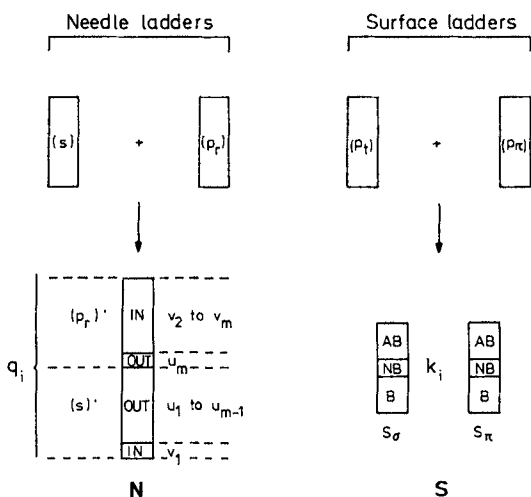
Fig. 15. The interaction of Needle Ladder MO's to produce the Needle MO manifold. The (s)' ladder is the (s) ladder after interaction with the (p_r) ladder, etc. The MO's from q_1 to q_m have principal 2s and those from q_{m+1} to q_{2m} principal character. The v_i MO's point inside the circle and the u_i MO's point outside the circle. The surface MO ladders cannot interact, by symmetry, in the case of a cyclic two-dimensional cluster. As a result, the Surface manifold is made up of one sigma and one pi manifold, the MO's are symbolized by k_i and they can be labelled Bonding, Antibonding, and Nonbonding, by reference to noninteracting p_t or $p\pi$ AO's

of bond diagrams which depict the different arrangements of electrons in the fragment S and N that may generate bonds or antibonds between these two fragments. In other words, the wavefunction of a three-dimensional polyhedral A_m will be nothing else than a depiction of how a set of needles can penetrate a spherical surface where the verb "penetrate" should be taken to mean "make bonds with". Of course, the wavefunctions of two-dimensional cyclic or chain and one-dimensional linear A_m will be related cases. An Echinos is a species in which a spherical surface is penetrated by radially disposed needles and affords the best insignia of the N—S dissection which will now form the basis for application of MOVB theory. Hence, the name of this bonding model: "The Echinos Model".

A number of properties of the N and S manifolds make possible considerable simplifications in our thinking about the electronic structures of clusters and these will now be illustrated by the reference to D_{mh} regular polygons, keeping in mind that parallel trends exist in the case of regular polyhedra and that the picture is not qualitatively altered when a transition is made to lower symmetry two- and three-dimensional solids.

(a) *Properties of the N Manifold*

An N manifold of a cluster A_m contains 2m MO's m of which are derived from the (s) and m from the (p_r) ladder. Each N orbital is symbolized by q_i. Their most important properties are:

(1) The q_i MO's can be subdivided into a lower energy set of $m (s)_i'$ MO's, with principal s character, and a higher set of $(p_r)_i'$ MO's with major p character.

(2) In interacting the $(s)_i$ and $(p_r)_i$ to produce the q_i MO's we can say that the former set is stabilized by the latter or the latter is destabilized by the former.

(3) Since each $(s)_i$ MO has the same symmetry and number of nodes as the corresponding $(p_r)_i$ MO, the strongest orbital interactions within the Needle fragment will be $(s)_i$ — $(p_r)_i$ interactions and each q_i MO will have a shape dictated by symmetry. Accordingly, the q_i Needle MO's can also be classified into "outside", u_i, and "inside", v_i, MO's depending on whether they point outwardly or inwardly with respect to the periphery of the polygon. There is a definite pattern of alternation of u_i and v_i MO's which is dictated by symmetry and which is shown in Fig. 15b. This pattern can be easily understood if we recognize that each Needle ladder has only one MO with no nodes, namely, the lowest energy MO. Hence, each ladder has one totally bonding MO, $(x)_1$, and m — 1 partly antibonding MO's $(x)_i$ with i > 1, where the subscript next to the ladder symbol denotes a ladder MO. Because of this, we have these combinations:

$$(s)_1 + (p_r)_1 \rightarrow q_1, \text{ or } v_1$$

$$(s)_i + (p_r)_i \rightarrow q_2 \text{ to } q_m, \text{ or, } u_1 \text{ to } u_{m-1} \qquad i \neq 1$$

$$(s)_1 - (p_r)_1 \rightarrow q_{m+1}, \text{ or, } u_m$$

$$(s)_i - (p_r)_i \rightarrow q_{m+2} \text{ to } q_{2m}, \text{ or, } v_2 \text{ to } v_m \qquad i \neq 1$$

An illustration of how in- and out-of-phase combinations of $(s)_i$ and $(p_r)_i$ MO's produce u_i and v_i MO's is shown in Fig. 16a.
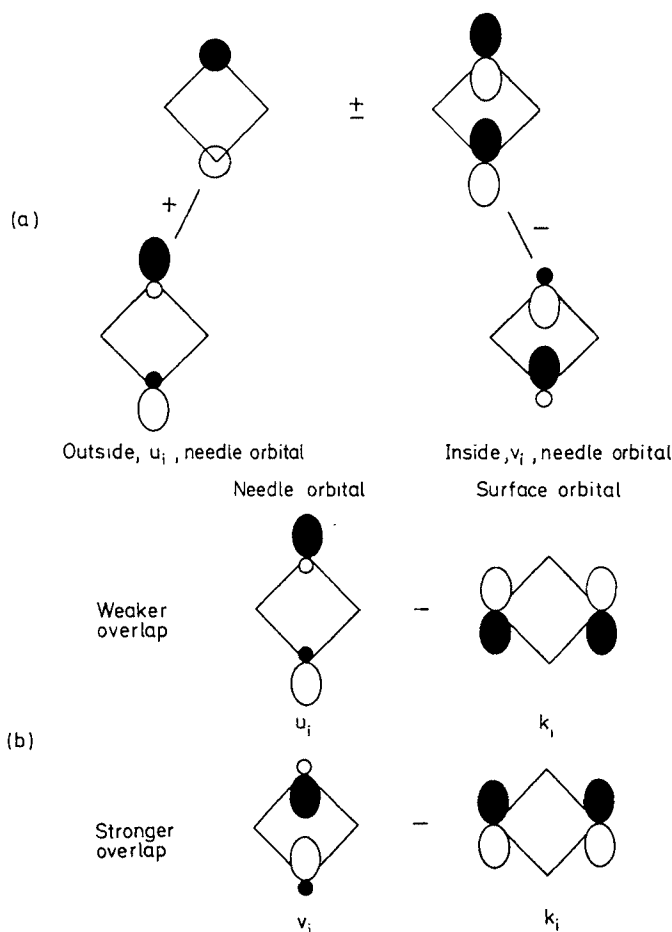
Fig. 16a and b. (a) Illustration of how an $(s)_i - (p_r)_i$ interaction produces MO's pointing outside or inside a cluster surface, (b) Illustration of why an "inside" Needle can overlap better than an "outside" Needle orbital with a Surface orbital of the right symmetry

(4) The N fragment uses preferentially the u_i MO's for binding ligands and the v_i MO's for binding the S fragment, to the extent possible.

(5) The directionality of the u_i and v_i MO's is a function of m and also of the overlap binding abilities of the atomic AO's. As m increases, $(s)_i - (p_r)_i$ mixing decreases and, at the limit m = inf., the hybrid u_i and v_i become unhybridized s and p_r AO's.

(b) *Properties of the S Manifold*

An S manifold of a cluster A_m contains m MO's derived from the (p_t) and m from the $(p\pi)$ ladder. Each S orbital is symbolized by k_i. Some properties are:

(1) The k_i MO's can be subdivided into bonding, nonbonding, and antibonding relative to the energy of an isolated p AO and by reference to the HMO theory with neglect of overlap.

(2) The $(p_t)_i$ cannot, by symmetry, interact with the $(p\pi)_i$. However, as m increases, $p\pi - p\pi$ overlap remains roughly constant while $p_t - p_t$ overlap increases.

(c) *Interaction of N and S Manifolds*

The interaction of the two manifolds is brought about by p_t — p_r and p_t — s overlap integrals. As m increases, the former increases up to m = 4 and then steadily decreases while the latter increases continuously. At the limit m = inf. the p_r — p_t interaction is abolished and only the p_t — s interaction remains.

With this background, we can now tackle the most general problem in cluster chemistry, namely, the electronic structure of the polymer $(AH)_m$ which can be regarded as the "product" of the union of H_m and A_m. We know how to develop a description of A_m, namely, by writing the N and S manifolds and then constructing the principal bond diagram of A_m. In generating $(AH)_m$, all we have to do is make the appropriate electronic promotions and "couple" A_m to H_m. In MOVB theory, the total wavefunction of $(AH)_m$ will then appear as a linear combination of bond diagrams, each of which will have three MO manifolds, i.e. each will consist of three fragments:
(a) The ligand L fragment (L = H_m).
(b) The core N fragment.
(c) The core S fragment.
The key simplification afforded by Echinos MOVB theory is now that, because of the choice of the AO basis, the L fragment can make strong *sigma* bonds only with the N fragment. That is to say, the ligands will be deposited at the ends of the needles simply because only the *direct* Ligand AO-Needle AO overlap is large, the Ligand AO'Surface AO overlap being comparatively much smaller in most cases of interest. In other words, the N fragment will make principal usage of the u_i MO's bind the ligands, to the extent possible, simply because the u_i's point *toward* while the v_i's point *away* from the ligands.

6.2 The Construction of the Principal Bond Diagram of a Cluster

Consider the four-orbital-four-electron pi system of cyclobutadiene. In VB terms, this can be described by a linear combination of twenty VB configurations (or, "resonance structures"). The two Kekule VB configurations are shown below, where a, b, c, and d are the four AO's.
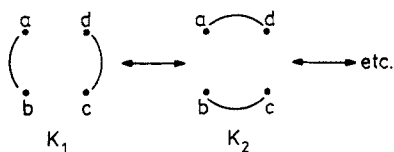
In MOVB theory, the same system can be approximately described by a linear combination of bond diagrams Θ_1 and Θ_2 as shown below:
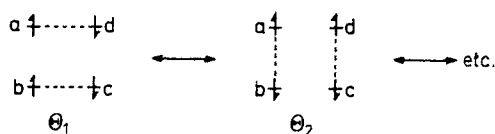
Now, instead of the illustrator system above, consider the prototypical three fragment system ABC in which A has one orbital, r, B has two orthogonal orbitals, u and v, and C has one orbital, k, all of which have the same symmetry and, thus, can interact in a cyclic manner. The situation is entirely analogous to the cyclobutadiene case only now the orbitals have different energies. Assuming that u lies below and v lies above r and k, we can repeat the above exercise and write the Kekule VB configurations and the MOVB description as follows:

VB Theory:

$$(7)$$

MOVB Theory:

$$(8)$$
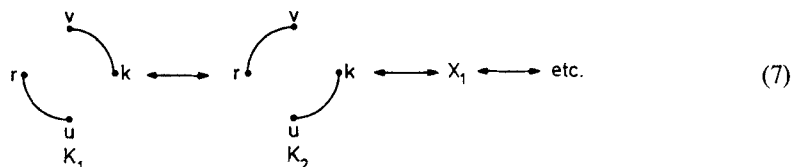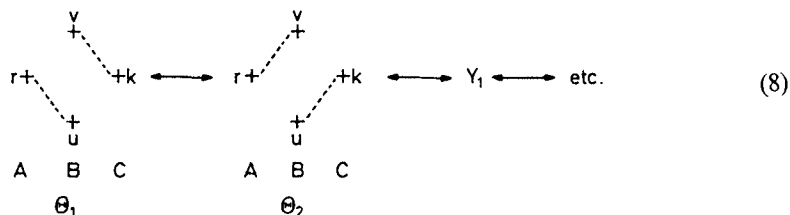
In VB description, K_1 and K_2 are the Kekule configurations and X_n represents the additional "ionic" configurations. In the MOVB description, Θ_1 is the optimal linear combination of nine VB configurations, generated by "moving" electrons along the dotted lines, Θ_2 has analogous meaning and Y_n represents the additional ("extrinsic") configurations which are not contained in Θ_1 or Θ_2. For completeness, we add that there are two K_n and eighteen X_n in the VB description while each of Θ_1 and Θ_2 is made up of nine VB configurations but two of them are common and there are four Y_n. Each bond diagram, Θ_n, projects as written the presumed dominant configuration, i.e. the dominant configuration in Θ_1 is K_1 and thatin Θ_2 is K_2.

In Eq. (8), Θ_1 and Θ_2 had as their principal contributors K_1 and K_2, respectively. In going from the *arbitrary* ABC to the *Echinos* LNS three-fragment system the situation changes. If we set L = A, N = B, and S = C, then Θ_1 and Θ_2 are properly written as shown below. What has happened is that the Θ's in LNS have different principal configurations.

$$(9)$$
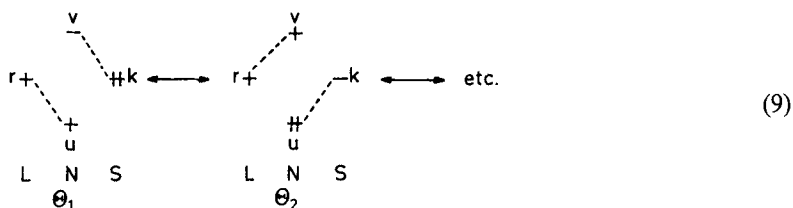
The reasons are basic:

(a) r and u or v belong to different fragments and span different atoms. Hence, charge transfer is coulombically unfavorable and, as a result, the principal contribution to bonding comes from "spin pairing". The situation is exactly analogous to that encountered in H_2. Note that "spin-pairing" ("covalency") will be dominant regardless of how strong or weak the L—N bond is.

. (b) u or v and k belong to different fragments but span, at least in part, the same atoms. Thus, there exists no significant coulombic preference for placing two electrons in either u (or v) or k or for putting one in u (or v) and the other in k. Furthermore, v, which can overlap strongly with k (u cannot do so; see, e.g. Fig. 16 b), lies high in energy. Hence, N—S bonding will be of the "coordinate" type. Three things now need to be emphasized:

(a) Θ_1 in (8) is formally exactly the same as Θ_1 in (9) and the same is true of Θ_2. We merely changed the reference configuration in our drawing.

(b) Θ_1 in (8) is different from Θ_1 in (9) only, insofar as it portrays our guess that the "doubly covalent" (Φ_R) configuration is dominant in the former but the "covalent-coordinate" (Φ_C) configuration is dominant in the latter.

The same goes for Θ_2.

(c) The problem does not change if each of the r, u, v, and k MO's is doubly or triply degenerate. We will simply have to write more bond diagrams for a complete representation as indicated in Scheme 3. We will refer to Scheme 3 as we add detail to the simple first order MOVB analysis.

With this background, we are now prepared to spell out a simple procedure for constructing the principal bond diagram of a cyclic $(AH)_m$ system. The recipe is as follows:

(a) The dominant configuration, which is the "parent" of the principal bond diagram, Θ_1, is the "LN covalent-NS coordinate" configuration, Φ_{11}.

(b) In Φ_{11}, each of the MO's of the L fragment is occupied by one electron, with the sum of electrons being m (L = H_m). The remaining electrons of the NS fragment (NS = A_m) are then distributed as follows: Electron pairs are placed in sequence in the $q_1 = v_1$ MO of N, then first in the *bonding* and next the *non-bonding* MO's of S, and, finally, in the MO's of N starting with $q_2 = u_1$ and ending with q_j. Subsequently, odd electrons, one per N MO, are placed starting with q_{i+1} and moving upward.

(c) Dashed lines are written which connect singly occupied MO's of the same symmetry (to produce "covalent" bonds) and pairs of MO's, one containing a hole and the other a pair, also of the same symmetry (to produce "coordinate" bonds). The resulting picture is the principal bond diagram.

Scheme 3
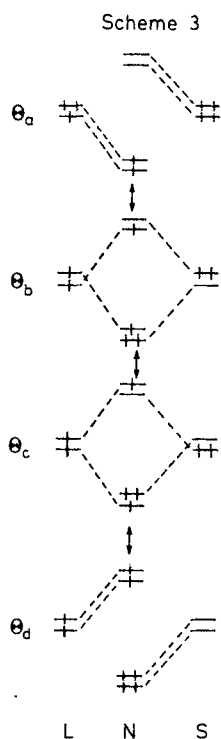
6.3 The Electronic Structures of $(CH_x)_m$ Cyclic Systems

Depending on m in $(CH)_m$, one can have the following types of polygons:

$(CH)_m$ Polygons

	Even		Odd	
	m = 2N (N = Even)	m = 2N (N = Odd)	m = 2N+1 (N = Even)	m = 2N+1 (N = Odd)
	EE	EO	OE	OO
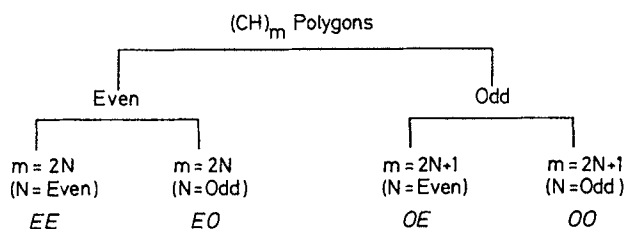
Now, each class of polygons differs from all others in the type of (s), (p_r), $(p\pi)$, on the one hand, and (p_t) manifolds, on the other. The (s), (p_r), $(p\pi)$ manifolds are generated by the in-phase overlap of the AO's and are called $(x)^+$ manifolds. By contrast, the (p_t) manifold is generated by the out-of-phase overlap of the AO's and it is called $(x)^-$. Now, it can be shown that the consequences are the following:

(a) Since an $(x)^+$ manifold is of the Hückel type regardless of whether m is even or odd and since an $(x)^-$ manifold is of the Hückel type if m is even and of the Möbius type if m is odd, then m = Even differs from m = Odd systems in a fundamental sense: In the former, both manifolds are Hückel but, in the latter, there is complementarity in the sense that the $(x)^+$ manifold is Hückel but the $(x)^-$ is Möbius.

(b) The classification of $(x)^+$ or $(x)^-$ MO's into Bonding (B), Nonbonding (NB), and Antibonding (AB), *by reference to HMO theory without overlap*, depends not only on whether m is even or odd but also on whether N is even or odd in the recursion formulas $m = 2N$ and $m = 2N + 1$.

It should now be clear that what we really deal with are *four* different problems because *eveness and oddness impose different orbital symmetry constraints.*

The principal bond diagrams of the simplest representatives of the four $(CH)_m$ polygon classes are displayed in Fig. 17. If we denote the dominant configuration which parents the bond diagram Θ_n by the symbol Φ_{n1}, then Φ_{11} represents the dominant configuration of the principal bond diagram Θ_1. With this in mind, we can now define the following terms:

M = Number of polygon vertices = Total number of C—C electron pairs.

T = Number of *electron pairs* in the S fragment in Φ_{11}.

R = Number of *electron pairs* in the N fragment in Φ_{11}.

(S) = Number of *odd electrons* in the s-type MO's of N, $(s)'_i$, in Φ_{11}.

(P) = Number of *odd electrons* in the p-type MO's of N, $(p_r)'_i$, in Φ_{11}.
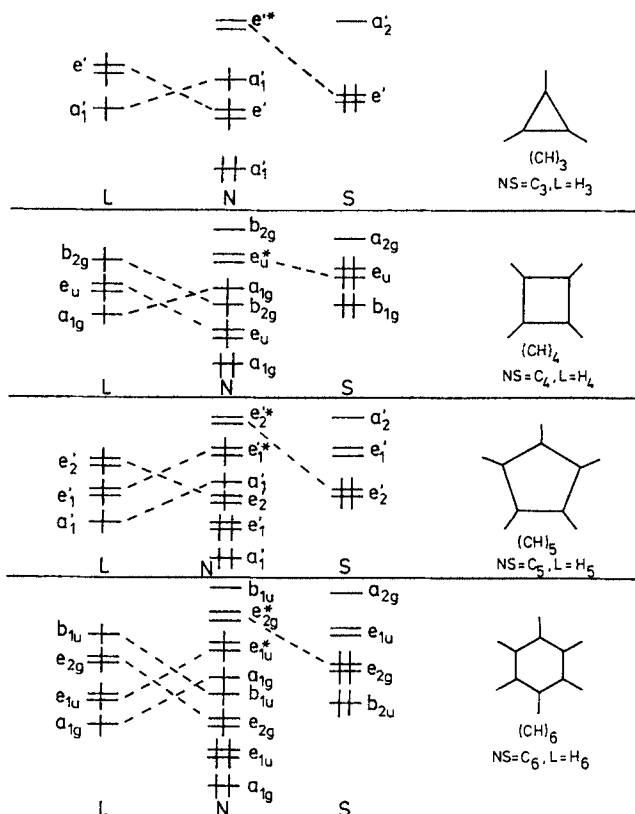
Fig. 17. The principal bond diagrams of D_{mh} $(CH)_m$, with m = 3–6, carbocyclics. Note that no antibonding k MO of S is occupied. The T:R ratio is read directly off each diagram

The reader can now verify that for *any* $(CH_x)_m$ polygon (x = 1, 2), the following equations hold:

$$T = (S)$$

$$R = (P)$$

$$T + R = (S) + (P) = M$$

On this basis, we can now define two key indices, V and Q:

(a) In the N fragment, $q_1 = v_1$ is bonding but $q_2 = u_1$ to $q_{m+1} = u_m$ are approximately nonbonding with respect to adjacent carbons. On the other hand, all occupied S MO's are bonding except in the EE family. Hence, the number of skeletal electron pairs (i.e. C—C bonding electron pairs) per CH is:

$$V = (T_b + 1)/M .$$

The subscript b emphasizes that T_b are bonding pairs.

(b) $Q = T:R = (S):(P)$
Note that T is the number of electron pairs in S regardless of whether they are bonding, nonbonding or antibonding. Now, since the ratio (S):(P) is proportional to the fractional s character of the Needle MO's which are directed towards the Ligand MO's for the purpose of binding each C to the corresponding H and since this fractional s character is directly proportional to the C^{13}—H NMR coupling constant J, we have:

$$Q = T:R = (S):(P) \propto J$$

In order to make strong N-L (N = Needle, L = Ligand) bonds, we must populate as many outside pointing N MO's from u_1 to u_m as possible (*because these have principal s character*) with odd electrons. But, every single electron deposited in these orbitals means that a corresponding electron pair must be deposited in the S fragment because (S) = T. *The more bonding orbitals S has, the larger the value of T and, by necessity, the larger the value of (S)*. Accordingly, we arrive at the following conclusion: J is a measure of the ability of a carbon atom to make strong CH *and* CC bonds, i.e. *is a measure of the overall bonding of all atoms within the cyclic system (CH)$_m$*, in addition to being an index of the strength of the C—H bond itself. Each of these statements is also equivalent to the statement that J is a measure of the electron pair acceptor ability of the S fragment, i.e. it is a fingerprint of the orbital pattern of S. Equally important, since T pairs have *exclusive* p character and R pairs *principal* s character, *J is a measure of atomic excitation, $s^2p^2 \rightarrow s^1p^3$, necessary for bond formation* because J is proportional to T:R. In conclusion, a large J means strong CH *and* CC bonding at the expense of large excitation, and *vice versa*. The J value of a ring informs us what precisely is the compromise between the desire of atoms to make strong bonds and the necessity for excitation for the purpose of doing so. We shall now see that the value of J, i.e. the type of compromise struck in $(CH)_m$ rings, depends on the "orbital structure" of S, or, more generally, on symmetry.

The correct MOVB wavefunction of a cyclic $(CH)_m$ system is:

$$\Psi = \lambda_1\Theta_1 + \lambda_2\Theta_2 + \lambda_3\Theta_3 + \ldots$$

If λ_1 is much larger than any of the other coefficients, we are justified in writing an approximate wavefunction as follows:

$$\Psi^0 = \Theta_1 .$$

If every one of the four types of rings is represented in this fashion, the principal bond diagrams of Fig. 17 predict that the T:R ratios and, hence, the J values, will vary in the following way:

$$
\begin{array}{lllll}
m = & 3 & 4 & 5 & 6 \\
T:R = & 2:1 & 3:1 & 2:3 & 3:3
\end{array}
$$

As we pointed out, these are rough estimates obtained by approximating the wavefunction of each cyclic system by the "guessed" principal bond diagram. Let us now see what happens if we sharpen our analysis. We illustrate our approach by reference
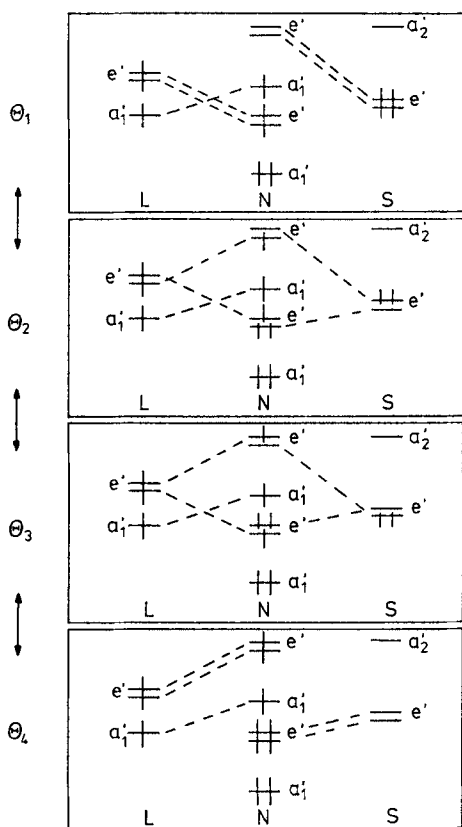
Fig. 18. Detailed bond diagrammatic representation of $(CH)_3$. In Θ_4, the nature of u_1 and u_2 (outside pointing) precludes strong delocalization of the two e' pairs, while at the same time, the nature of v_2 and v_3 (inside pointing) precludes strong C—H bond formation via the two odd e' electrons

to $(CH)_3$. In this case, there will be four bond diagrams necessary for a good description and these are shown in Fig. 18. Note that these four diagrams taken in combination describe hybridization, i.e. each one there has the same number of odd electron-odd electron and pair-hole bonds but the four differ in the way these bonds are made. Now, it is clear that because the S are bonding low energy MO's, there is simply no motivation for relocating one or two electrons pairs from e' of S to e' of N because, by doing so, we are now forced to make one or two L—N bonds using the inside pointing e'^* MO of N. The reader should verify that each of the higher energy bond diagrams, Θ_n, provides little stabilization of e pairs at the cost of very significant Ligand—Needle C—H bond weakening relative to Θ_1. In one sentence: By writing the representation of $(CH)_3$ as shown in Fig. 17, we conclude that θ_1 is an apt description in itself, that two pairs will reside in the S fragment and that the T:R ratio should be close to that predicted. We note that Fig. 18 is nothing else but a specific example of the general situation depicted in Scheme 3. By repeating this procedure, we obtain the following results for the other three rings:

(a) In Θ_1 of (CH_4) (Fig. 17), the e_u pairs of S are nonbonding electron pairs. As a result, a bond diagram which places one or both of them in the much lower energy e_u MO's of N at the expense of now making weaker L—N bonds via the e_u^* MO's of N will be a significant contributor. The situation is that depicted in Scheme 3 with $\Theta_n = \Theta_1$, etc. Briefly, two pairs will reside mostly in S and partly in the N fragment with the L—N bonds readjusting appropriately. Hence, T:R should be lower than 3:1.

(b) In Θ_1 of $(CH)_5$ (Fig. 17), the pairs of S occupy strongly bonding orbitals and there will be no motivation for relocating them. By contrast, two pairs occupy low lying outside pointing N orbitals which are optimal for ligand binding. As a result, there is now motivation for relocating them to very low lying antibonding MO's of S. The situation is that depicted in Scheme 2 with $\Theta_1 = \Theta_d$, etc. In one sentence: The two e_1' N pairs will reside mostly in N and to some small extent in S with the L—N bonds readjusting appropriately. Hence, the T:R should be a little higher than 2:3.

(c) In $(CH)_6$, we have a situation much like that encountered in $(CH)_3$, i.e. the principal bond diagram is an apt descriptor and the T:R ratio close to the exact one.

Our final predictions are then the following.

$$m = 3 \quad 4 \quad 5 \quad 6$$
$$T:R = 2 \quad <3 \quad >0.7 \quad 1.0$$

The same approach can be used to study $D_{mh}(CH_2)_m$ systems only now each H_2 unit contributes a sigma $(1s + 1s)$ and a pi $(1s - 1s)$ AO so that there are m L_σ and m L_π MO's. The former match q_i N MO's in making m sigma N—L_σ bonds and the latter match $(p\pi)_i$ S MO's in making m pi N—L_π bonds (Fig. 19).

The NMR J constants for cycloalkanes have been determined a long time ago and the results are given below.

$$m = 3 \quad 4 \quad 5 \quad 6 \quad 7 \quad 8 \quad 9 \quad 10$$
$$J = 161 \quad 134 \quad 128 \quad 124 \quad 123 \quad 122 \quad 121 \quad 118$$

We propose that the J's are characteristic indices of the *four* different families of cyclic molecules (EE, OE, EO, OO) and that, understanding the physical significance of J

91

$(CH_2)_3$ ... L_σ ... N ... S_σ ... S_n ... L_n

$(CH_2)_4$ ... L_σ ... N ... S_σ ... S_n ... L_n

$(CH_2)_5$ ... L_σ ... N ... S_σ ... S_n ... L_n

$(CH_2)_6$ ... L_σ ... N ... S_σ ... S_n ... L_n
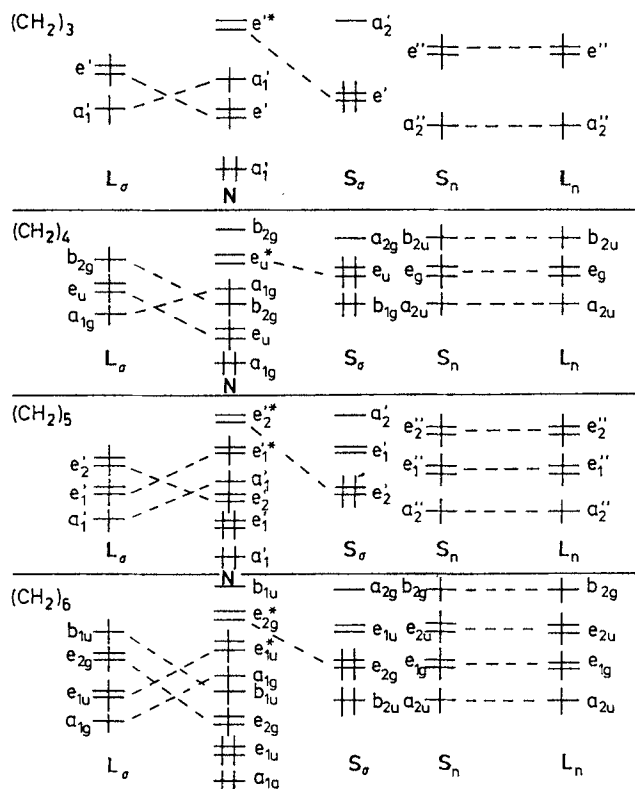
Fig. 19. The principal bond diagrams of $D_{mh}(CH_2)_m$ carbocyclics

is tantamount to understanding the electronic structure of these molecules. If we confine our attention to cyclopropane and cyclohexane, we say that the simple bond diagrams of Fig. 19 (analogous to those of Fig. 17) lead to an immediate understanding of how the D_{mh} sigma frames differ: *Cyclopropane has a larger $T:R$ ratio and this means that it has stronger bonds and higher atomic excitation than cyclohexane.* In cyclopropane, one can deposit electron pairs in low lying bonding MO's of S so that all the outward-pointing N MO's can be used to bind the ligands. This is not possible in cyclohexane. On the other hand, starting with three ground carbons and six s and six p electrons one ends up with four s and eight p electrons in cyclopropane while starting with six ground carbons and twelve s and twelve p electrons one ends up with twelve s and twelve p electrons in cyclohexane, i.e. on needs to excite the carbon atoms more in order to make cyclopropane. A strained molecule is the one in which the outlay of atomic excitation is not properly compensated by bond formation and an unstrained molecule is one in which the best balance of atomic excitation and bond formation is struck. *Cyclopropane is strained because the carbons are too excited and not because the bonds are weak and cyclohexane is strain free because the requirement for atomic excitation is not so steep as in cyclopropane.*

With these ideas in mind, it is now easy to see why cyclohexane avoids planarity and adopts a D_{3d} chair geometry by puckering. Specifically, we recognize that planar

cyclopropane and planar cyclohexane are the opposite faces of the same coin: In the former case, a large T:R ratio and a large J constant tells us that *too much* atomic excitation was spent for obtaining *strong* C—H and C—C bonding. By contrast, in the case of planar cyclohexane, the much smaller T:R ratio tells us that *too little* atomic excitation has produced *weak* C—H and C—C bonds. Accordingly, both D_{3h} cyclopropane and D_{6h} cyclohexane are strained for the opposite reasons. But now, D_{6h} can be converted to D_{3h} cyclohexane and this transformation readjusts primarily the orbital manifold of the Surface fragment (due to sigma-pi mixing) with the consequence that now five electron pairs can be deposited in the lowest energy orbitals of the S fragment so that strong C—H bonds can be made via utilization of the outside pointing u_i MO's of the N fragment. In other words, one important contributor bond diagram of D_{3d} cyclohexane has a T:R ratio of 5:1 and this increases the T:R ratio of the hybrid to an optimal value corresponding to a J constant which is still much smaller than that of cyclopropane.

We have already seen that J informs us of the overall atomic excitation within a cycloalkane and this is why it correlates with both strain *and* CH bond length (Table 2). However, there can be no correlation between J and CC bond lengths. The latter depend on the number of *bonding* electron pairs in S, T_b, not on T. Hence, it is the index V, not J, that informs us about the variation of CC bond lengths. Experimental results are in agreement with expectations (Table 2). However, while J often correlates with strain and carbon acidity in cycloalkanes, there is simply no reason to assume that this will always be true. An example will serve to illustrate this point.

Table 2.

	Strain per carbon (kcal/mole)	T:R	V	r_{CC} (Å)[b]	J (Hz)[c]	r_{CH} (Å)[b]
△	9.2	2:1	3:3	1.510	161	1.089
▢	6.5	3:1	2:4	1.555	134	—
⬠	1.3	2:3	3:5	1.546	128	1.114
⬡	0.0	3:3	4:6	1.536	124	1.121
◺	33.0	5:1	4:4	1.473[d]	—	1.069[d]
⬛	20.0	8:4	3:8	1.55[e]	155	1.06[e]

[a] Ref. [40]; [b] Ref. [42] unless otherwise stated; [c] Ref. [46] and Foote CS: Tetrahedron Lett. 1963: 579; [d] Ref. [53]; [e] Fleischer EB (1964) J. Am. Chem. Soc. 86:3889

Problem. Cyclopropane and cubane have roughly the same J values, 160 Hz and 155 Hz, respectively. Yet, cubane is 10.8 kcal/mole per carbon more strained and 10^3 more acidic than cyclopropane! [46)] Why did the J correlation with strain and acidity break down?

Answer. The principal bond diagram of cubane is shown in Fig. 20. The T:R ratio is 2:1, exactly like in cyclopropane. However, the S fragment is now *excited* to the extent that there is a "hole" in it, the t_{1u} hole. This t_{1u} S orbital is forced to remain unoccupied so that a triple antibond with the occupied t_{1u} N orbital is averted. We say that *the N footprinted the S fragment.* Cubane is much more strained than cyclopropane because S must be excited to avoid repulsion with N and this is reflected by the V indices: Cyclopropane has a much large V index and this is the reason it is so much less strained than cubane (Table 2). Cubane is more acidic than cyclopropane because the electron pair left behind by proton removal can be effectively accommodated in the S hole. Calculations [49)] and PE spectroscopic experiments [50)] have provided evidence for the existence of a hole. Thus, the first two ionizations arising from t_{2u} and t_{2g} are followed by a 4.9 eV gap before the next ionization arising from e_g occurs! The message is clear: When two molecules have comparable J's but very different strain energies look for S holes to be the answer.

6.4 Why are Boron Polyhedra Stable?

Why is boron so notorius for forming bridged structures and polyhedra? Again, we suggest that the popular viewpoint is not the correct one. For instance, what diborane did to chemists is to lead them to believe that there is something magic
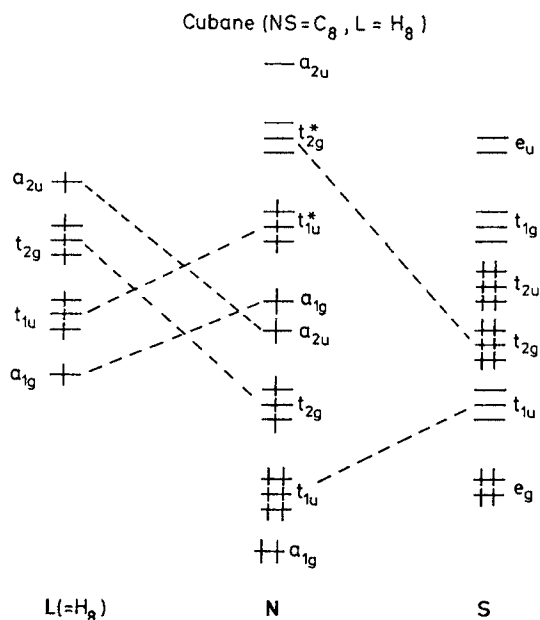
Fig. 20. The principal bond diagram of cubane. Note creation of the Surface t_{1u} hole by the Needle t_{1u} pairs

about electron deficient bonding, e.g. two-electron three-center bonding. But, at the limit, this pattern of bonding is nothing else but multicenter bonding and the vast majority of all molecules larger than diatomic can be formulated as two fragments connected by multicenter bonds. For example, we can view H_3^+ as "H_2^+ plus H" and methane as "C plus H_4" and the bonds of the principal bond diagrams of the two species are multicenter bonds. So, from the standpoint of capability for multicenter bond formation with whatever electron count boron is the *same* as every other atom.

In a previous paper, we have explained why diborane is bridged but the isoelectronic $C_2H_6^{+2}$ is not [51]. The answer was: The behavior of B is different from that of C because s → p promotion in B is much cheaper than in C [52]. We will now try to convince the reader that tetrahedrane, $(CH)_4$, is highly strained but its boron analogue, $(BH)_4$, and its derivatives are stable species (the structures of which have been determined by now conventional spectroscopic techniques) only because the atomic excitation price that must be paid for bond making is much less in the latter case. The principal bond diagram of T_d $(CH)_4$ shown in Fig. 21 renders the problem trivial. The reason is that removal of the four nonbonding electrons from this diagram produces the principal bond diagram of $(BH)_4$. Now T_d $(CH)_4$ is highly strained but $(BH)_4$ is stable and $(BCl)_4$ a known compound. *The difference cannot be*
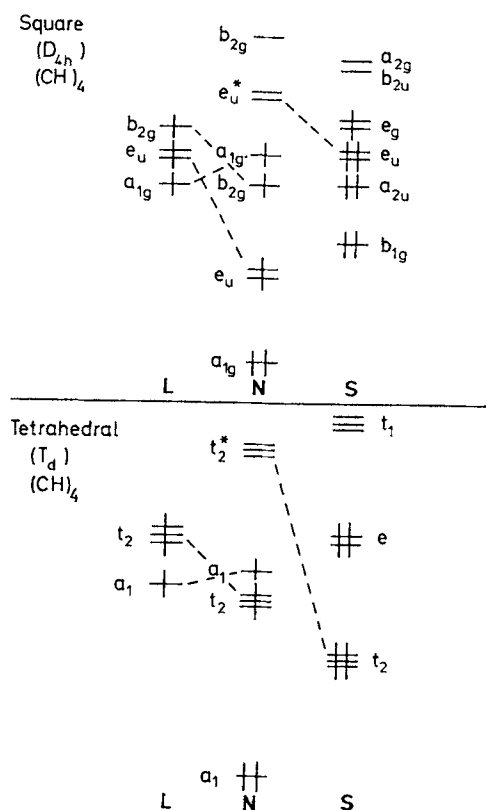
Fig. 21. Principal bond diagrams of D_{4h} and $T_d(CH)_4$, cyclobutadiene and tetrahedrane, respectively

the four nonbonding e electrons of the S fragment. Rather, the difference must be reduction of the atomic excitation in going from C to B which allows formation of the isomer which has the *strongest bonds* and *this is the tetrahedral molecule non the cyclic or "strain-free" isomer*! Again, asking the chemist to believe that tetrahedrane has stronger overall bonding relative to the less strained analogues seems iconoclastic. But consider the logical structure of the MOVB interpretation. Tetrahedrane is by far more strained than cyclopropane itself because the former has a 5:1 and the latter a 2:1 T:R ratio, i.e. tetrahedrane requires much more excitation than cyclopropane (Table 2). At the same time, the C—C bond length varies in the order cyclohexane > cyclopropane > tetrahedrane (Table 2). The C—C bond length of tetrahedrane is taken from an ab initio computational paper by Pople and Hehre [53] and it seems very reasonable given the fact that the C—C bond length of the tetra-t-butyl derivative is 1.485 Å [54]. On the other hand, the V index predicts that the C—C bond lengths of cyclopropane and tetrahedrane should be comparable but this index does not take into account the fact that overlap repulsion between N and S orbitals of the same symmetry which are occupied by three or four electrons is reduced as the mixing of the (s) and (p_r) ladders increases causing a more pronounced outwards-pointing of the Needle u_i MO's and greater avoidance of N—S overlap repulsion. This is precisely what happens as one goes from cyclopropane to tetrahedrane and each p_r can overlap with three (rather than two) s AO's.

Part III. Overlap Dispersion

7 Correlated Electron Motion in Molecules

It is not an exaggeration to say that most of the conceptual framework of chemistry is based upon the notion of *Single Electron Transfer* (SET). From a very early stage, the chemist focuses attention on the hydrogen molecule or some other diatomic as the illustrator of the fundamental principles of bonding. As a result, he learns to write "covalent" and *singly* "ionic" structures, in the Pauling fashion, in attempts to understand why one bond is stronger than another, e.g. why HF has a stronger bond than H_2 [55]. Then, he becomes acquainted with double bonds, as the sigma and pi carbon—carbon bonds in ethylene, and treats them as two independent single bonds. The trend continues when a transition is made to Frontier Orbital Hückel MO (HMO) theory [56, 57]. Here the HOMO-LUMO interaction of two fragments, when translated to VB language, is nothing other than the situation encountered in the treatment of the single bond of a diatomic, only now atom AO's are replaced by fragment MO's [58]. This equivalence is illustrated in Fig. 22. The original work of Dewar in PMO theory [59] and contributions by Hoffmann [60], Fukui [56], and others [61] have eastablished this type of approach, essentially an Extended HMO (EMHO) approach, as the principal *qualitative* theoretical tool for rationalization and prediction. In this work, we raise the issue of whether the Independent Bond Model (IBM) and the notion of SET are qualitatively (let alone quantitatively) justified. Can it be that electrons move

Fig. 22. Perturbation MO orbital interaction diagram and its MOVB equivalent description

in pairs rather than one at a time? Can it be that there is really nothing like a "single bond"?

Consider the prototypical $A = B$ system and its principal bond diagram depicted in Fig. 4. We recognize the intraction of Φ_1 and Φ_3 defines Correlated Electron Transfer (CET) while the $\Phi_1 - \Phi_8$ interaction defines Single Electron Transfer (SET). Now, in a recent work, we showed the following:

(a) Matrix elements over MOVB configurations can be written explicitly in a pictorial, diagrammatic fashion.

(b) The interaction of two configurations Φ_i and Φ_j depends on two factors: The interaction quantity $R_{ij} = H_{ij} - ES_{ij}$ and the energy gap separating them, D_{ij}. The qualitative trends which can be obtained from studying the variation of H_{ij} are significant only in terms of what they tell us about R_{ij}. The best way to make R_{ij} large is to create a situation in which large negative terms which are *overlap independent* contribute to H_{ij}. That is to say, the key realization is that whenever we make H_{ij} large by virtue of increasing overlap, a corresponding term ES_{ij} contributes in exactly the opposite direction. Hence, this is an inefficient way of enhancing the $\Phi_i - \Phi_j$ interaction. The best solution is to get coulombic (non-overlap) assistance! Such strong assistance is only possible in the case of CET and it is due to a term which is the repulsion integral connecting two configurations the interactions of which reproduces induced dipole-induced dipole, i.e. dispersion, stabilization when interfragmental overlap is zero. Hence, CET is nothing else but the process of making *one* bond while assisted by the coulomb interaction of the two transition dipoles. The VB analogue for $A = Ni$, $B = H_2$ is shown in Fig. 23.

(c) The condition for making R_{ij} large is CET. But this has an adverse consequence: When we start from a perfect-pairing configuration (e.g. Φ_1 in Fig. 4), SET causes disruption of one while CET causes disruption of two DET bonds. Hence, the D_{ij} factor will end up favoring SET when there is strong overlap of the two fragments and the perfect-pairing (Φ_1) attains much lower energy than the no-bond (Φ_3) configuration.

(d) "Connecting" (b) and (c) and recalling that the superiority of R(CET) over R(SET) is due to a dispersion (non-overlap) phenomenon, it is apparent that all that is needed for CET to take over is that the D_{ij} factor does not act overwhelmingly against it. Hence, we expect CET to dominate SET in system where fragments are connected by modestly strong DET bonds. But, whar are the likely candidates that may fulfill this last condition? Our answer has already been given: Molecules made up of green, or still better, red atoms or molecules containing weak or weakened bonds connecting black stoms (which normally form strong sigma bonds and, thus, cannot support CET), e.g. pi bonds.
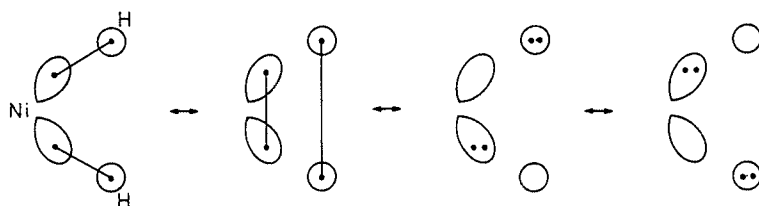
Fig. 23. Overlap Dispersion in NiH_2

7.1 The Concept of Overlap Dispersion

The wavefunction of our prototypical system $A = B$ (Figs. 3, 4) can be written as:

$$\Psi = \lambda_1 \Theta_1 + \lambda_2 \Theta_2 + \lambda_3 \Theta_3 \qquad \lambda_1 > \lambda_2, \lambda_3$$

If A were a black group and both the α and α^* orbitals were capable of generating strong overlap interaction, then the major configuration interaction would involve Φ_1 (belonging to the even set) and the CT configurations Φ_7 and Φ_8 (belonging to the odd set). However, if A is an electropositive atom in which, additionally, the a orbital does not have the spatial extension necessary for strong overlap with the orbitals of B, i.e. A is a red atom, then the major configuration interaction will involve the configurations of the even set, i.e. the configurations which, through interaction, define CET. We now want to take a close look at the consequences of CET and get better acquainted with the principal actors of the bonding mechanism we shall name *Overlap Dispersion*.

The critical CET configuration interaction we shall consider is shown schematically in Fig. 24. The following aspects are noteworthy:

(a) In Φ_y, each fragment is an open shell species in which the two electrons have half of the time parallel spins and benefit from exchange correlation. The two open shell species combine to form two interfragmental DET bonds. By contrast, in Φ_z, the two electrons of each fragment have always antiparallel spin, something which

$$\Phi_x = |a\bar{a}b\bar{b}|$$

$$\Phi_y = |\bar{a}b\bar{b}^*a^*| - |\bar{a}bb^*\bar{a}^*| - |ab\bar{b}^*a^*| + |a\bar{b}b^*\bar{a}^*|$$

$$\Phi_z = |\bar{a}b\bar{b}^*a^*| - |\bar{a}\bar{b}b^*a^*| - |ab\bar{b}^*\bar{a}^*| + |a\bar{b}b^*\bar{a}^*|$$

$$H_{xy} = 2W - Z$$

$$H_{xz} = 2Z - W$$

$$W \alpha \underbrace{\langle a|b^*\rangle \langle b|\hat{H}|a^*\rangle}_{I \qquad II} + \underbrace{\langle b|a^*\rangle \langle a|\hat{H}|b^*\rangle}_{III \qquad IV} + \underbrace{(ab^*|ba^*)}_{V} = \text{Overlap term}$$

$$Z = (aa^*|bb^*) = \text{Dispersion term}$$
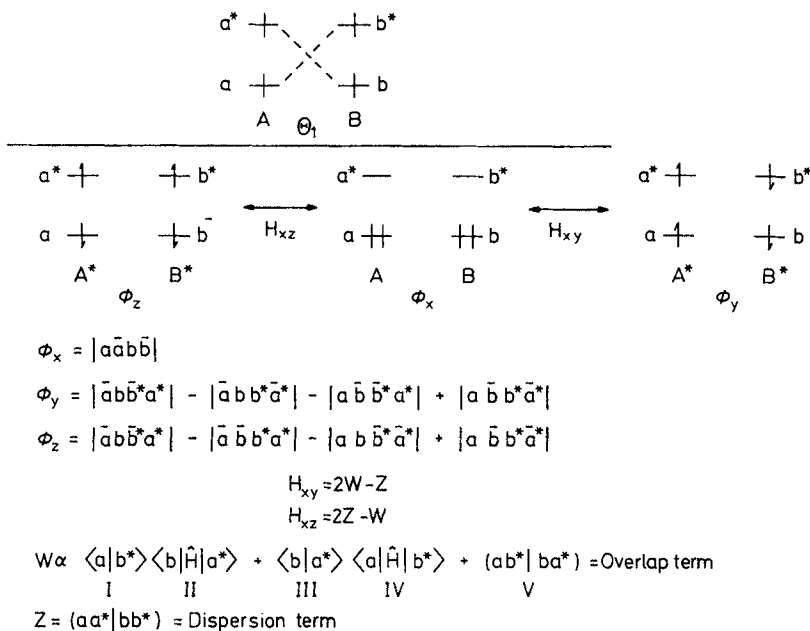
Fig. 24. Principal bond diagram of $A = B$ and the key bielectronic configuration interaction responsible for Overlap Dispersion

generates severe interelectronic repulsion. Furthermore, the two open shell species combine to form two interfragmental DET antibonds.

(b) Each configuration differs from the one with which it interacts by two occupied spin orbitals and each interaction matrix element represents a two-electron hop. Now, each matrix element is a difference of two terms which have opposite signs: One term is an overlap term, W, and it represents formation of two CET bonds and the other term is a bielectronic repulsion integral, Z, which represents the interaction of two transition dipoles. As a result, each matrix element leads to strong configuration interaction by combining in phase (algebraic addition) Overlap and Dispersion. Hence, the name of the bonding type is *Overlap Dispersion*.

(c) The overlap term responsible for CET bond formation within each interaction element is different from the overlap term responsible for DET bond formation within Φ_y to the extent that the two electrons which generate the single bond by exchanging their spins are now kept further away from each other. This can be seen by comparing the overlap terms within H_{xy} and H_{yy}:

$$H_{xy} = 2\langle a|b^*\rangle \langle b| H |a^*\rangle + 2\langle b|a^*\rangle \langle a| H |b^*\rangle + \underline{(ab^*|ba^*)} + \underline{(ab^*|ba^*)} + \ldots$$

$$H_{yy} = 2\langle a|b^*\rangle \langle a| H |b^*\rangle + 2\langle b|a^*\rangle \langle b| H |a^*\rangle + \underline{(ab^*|ab^*)} + \underline{(ba^*|ba^*)} + \ldots$$

The key difference is that the repulsive bielectronic terms (underlined) in H_{xy} are smaller than those in H_{yy}.

(d) The conditions for the maximization of the Dispersion term are:

(i) The orbitals a and a* must extend in the same region of space.
The same must be true of b and b*.

(ii) The geometry of A and B should be such so that the transition dipoles associated with the a $\rightarrow$ a* and b $\rightarrow$ b* excitations interact to a maximum extent.

(e) The H_{xy} (and H_{xz}) matrix element can be represented by using arrows to indicate the motion of electrons within Φ_y (and Φ_z) that generates the additive overlap and dispersion terms (Fig. 25). Unlike other representations with which the reader may be familiar, we now need two *pairs* of arrows which indicate the two different paths by which a pair of electrons can be relocated from one to another pair of orbitals. The picture shown in Fig. 25 embodies the concept of Overlap Dispersion.

The final conclusion is that Overlap Dispersion constitutes the mechanism of binding A and B provided that A and B can only form weak DET bonds and this mechanism can be expressed in VB language as shown in Fig. 26. We end this section by recalling previous important contributions to the theory of *intermolecular* forces [17] which force upon us the following conclusion: *polarizability* [63] *is a measure of the capacity of an atom or fragment to support CET.* Since there is a sharp increase of atomic polarizability as one moves away from the first row of the
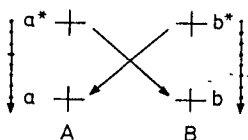
Fig. 25. Pictorial depiction of matrix element responsible for Overlap Dispersion

Periodic Table from B to Ne (and from H and He), the physical picture of bonding developed here is entirely consistent with the available information regarding atomic properties: The red and green atoms which we have signaled out as supporters of CET *do* have large atom polarizabilities. Computational support for the concept of Overlap Dispersion has been presented in the original paper [64].

A⥃B ⟶ A⟩ ⟨B ⟶ A⁺ ⁻B ⟶ A⁻ ⁺B   **Fig. 26.** Overlap Dispersion in an A = B system

7.2 The Electronic Structure of Ferrocene

We are now prepared to provide a very explicit description of the way a metal binds organic molecules to form a coordination compound. We proceed as follows:

(a) We view ferrocene as "iron metal plus cyclopentadiene dimer", i.e. as "Fe plus Cp_2".

(b) We write the symmetry orbitals of Fe and Cp_2 and we allocate the electrons so that, with minimal excitation of the two fragments, we accomplish the following:

1. We make the maximum number of DET bonds by coupling the odd electrons of the two fragments.

2. We match the maximum number of electron pairs of one fragment with high energy holes of the second fragment.

3. We minimize the number of four-electron antibonds.
This is the recipe for generating the dominant configuration, Φ_p, which will be the parent of the principal bond diagram.

(c) The principal bond diagram, Θ_1, is produced by connecting the orbitals of the same symmetry with dashed lines. This is now a representation of the optimal linear combination of all configurations that can be generated by moving electrons along the dashed lines.

The principal bond diagram of ferrocene is shown in Fig. 27. Note that, in the parent configuration "projected" by the bond diagram as written, each Cp ring is in its ground state electronic configuration while Fe is excited to the extent that it has been forced to have a d^8 configuration with all electrons paired. Now, the important thing is that the bonding of ferrocene is due to the fact that two DET bonds connect the two fragments but, equally important, there is Overlap Dispersion produced by the *simultaneous* delocalization of one electron from Fe to Cp_2 and one from Cp_2 to Fe. Starting with the Φ_p configuration and moving two-electrons at a time, one left and and one right in all possible ways, amounts to the conceptual generation of the T_1^{even} substrate. Repeating this process starting with the configuration which differs from Φ_p by *one electron* transfer from one Fe to one Cp_2 orbital, amounts to generating the T_1^{odd} substrate. The best approximation to the truth is:

$$\Psi = \Theta_1 \simeq c_1 T_1^{even} + c_2 T_1^{odd} + \ldots$$

101
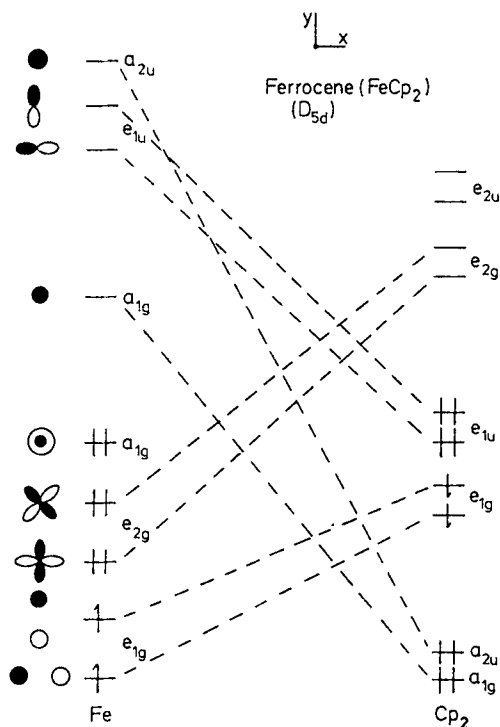
Fig. 27. The principal bond diagram of ferrocene which is read to mean the following: Delocalization occurs by moving two electrons in opposite directions along the dashed lines

The reader should note how the concept of "single bond" becomes meaningless at this level of theory. Each individual bond helps the formation of a second which, in turn, reinforces the first. *The concept of Overlap Dispersion is based upon the realization that CET is better than SET.*

7.3 Are d Orbitals "Overlap-Inert"?

Atoms of the first row of the Periodic Table differ from all other atoms in one fundamental way: They are *orbitally homogeneous*. This term denotes the fact that the valence AO's of these atoms have comparable radii of maximal electron density, R_{max}, and, thus, are equally available for overlap with the orbitals of some other atom. By contrast, all other atoms are *orbitally inhomogeneous*, with the effect becoming increasingly acute down a column within the main group atoms while it progressively becomes moderated down a column within the trasition series. To put it crudely, both the 2s and the 2p · AO's of carbon are equally available for overlap with the orbitals of some fixed atom while, in silicon, the 3s is contracted relative to the 3p and this contraction increases in going all the way down to Pb. Indeed, Pb has active 6p AO's but a "dead" 6s AO insofar as overlap is concerned. Similarly, Ni has "dead" 3d AO's an active 4s AO and overextending 4p AO's.

Table 3.*

Atom	R_{max} (au)		
	ns	np	(n − 1) d
C	1.220	1.217	—
Si	1.793	2.177	—
Sn	2.067	2.590	—
Ni	2.378	—	0.641
Pt	2.529	—	1.257

* All data taken from Ref. [27].

R_{max} data taken from the Desclaux tabulation are shown in Table 3. R_{max} is an *atomic* property and atoms within molecules readjust the radii of their AO's in order to optimize bonding. However, regardless of how the atoms change their appearance within molecules *their atomic identity is never totally lost.* This is an important point which we must explain carefully.

Consider a Ni atom which is in the process of making two bonds using the 4s and one 3d AO with some orbitally homogeneous fragment B. Now, the two fragments must approach each other so that 4s will overlap optimally with some orbital u of B and 3d will also overlap optimally with a second orbital v, of B. However, such a simultaneous optimization is not possible because Ni is orbitally inhomogeneous. That is to say, we have two AO resonance integrals, γ_{ab}, as shown below, and, if we optimize the first, then the second becomes zero. The reason is that the inter-fragmental distance r_{NiB} has been set by R_{max} of 4s and at this distance the 3d AO cannot overlap with B AO's. The situation is graphically illustrated below:

$$\gamma_{du} = K(I_d + I_u) s_{du} \qquad I_a = \langle a| \hat{H} |a\rangle$$
$$\gamma_{sv} = K(I_s + I_v) s_{sv} \qquad s_{ab} = \langle a | b\rangle$$
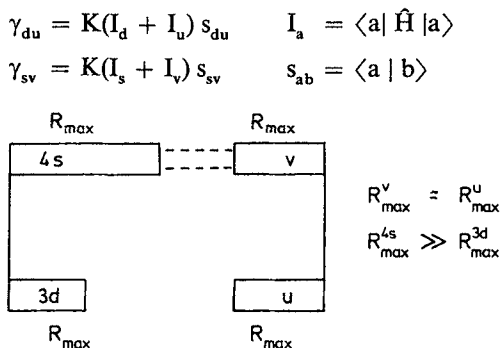
In crude language, we can say that, when two atoms, at least one of which is orbitally inhomogeneous, are bonded, their teeth do not match.

What we have described above is the situation that would obtain if the atoms were to enter molecule formation with their AO's frozen. While this is not the case, the problem we delineated above cannot be annihilated. For example, consider what Ni would try to do so that its 3d AO becomes capable of bonding. This orbital will expand so that the AO overlap integral s_{du} will change from zero to some nonzero value. But, at the same time, the one electron orbital

energy of 3d will be raised, i.e. I_d will become smaller in absolute magnitude. This will raise the total one-electron energy of the system and at the same time it will tend to return the γ_{du} to its original zero value. Reduction of inter-electronic repulsion may still make the 3d orbital expansion within the molecule the thing of choice but this expansion should in no way lead us to expect that the 3d AO's will now bind strongly by overlap. Hence, logic dictates that, though the 3d-u overlap can be appreciable, the corresponding 3d-u resonance integral will be small because I_d had to be reduced. Now, Overlap Dispersion is the bonding mechanism which recognizes these indisputable trends and which tells us that *metals do not have to rely on overlap to make strong bonds with organic fragments.*

Consider the binding of Ni with H_2 to form the triatomic NiH_2. Simplifying for the moment, the problem, we write the abridged principal bond diagram, the key configuration interaction that brings about Overlap Dispersion, and the critical matrix elements shown in Fig. 26 with A = Ni, B = H_2, d_{xy} = a, s = a*, σ = b, σ* = b*. Consider now what happens under two different conditions:

(a) The $3d_{xy}$ remains as in the atom highly contracted relative to the 4s AO. Then both I and III terms go to zero and, in addition, the bielectronic repulsion integral Z will be very small because $3d_{xy}$ and 4s do not span the same space. In such a case, neither overlap nor dispersive binding of significant magnitude is possible.

(b) The $3d_{xy}$ expands relative to the 4s AO. Now, I becomes appreciable while III is still negligible. However, Z now becomes large. The system is bound by Overlap Dispersion due to the overlap interaction of 4s and v and the dispersive interaction brought into play by Z.

Our final conclusion: The overlap-active orbital of a metal is the ns AO and d orbitals tend to be "overlap-inert". We suggest that this type of binding is present, to a lesser or greater extent, in all molecules which contain atoms which have valence AO's of unequal spatial extension, i.e. all atoms except B, C, N, O, F, Ne, H and He! There are now some indications that d orbitals tend to be "overlap inactive":

(a) Cyclobutadiene complexes of the type $(C_4R_4)ML_3$ have a low barrier to rotation about the metal-C_4 axis [65]. In a more general sense, many organometallic complexes exhibit fluxional behavior because the "bonds" formed by the metal d orbitals do not restrain rotation, sliding, and other relative motions since they are not conventional overlap bonds [66].

(b) There should be little energetic preference for linear or bent H_2 fragments within the organometallic molecule L_2PtH_2. The bond diagrams for bent and linear singlet PtH_2 (Fig. 28) show that the principal configuration parenting the diagrams is different, but, in both cases, there is an s—σ bond linking the two fragments.

The dispersion is brought into play by two different orbitals d_{xy} in the bent and p_x in the linear form. Again, the s orbital of the metal is the critical one for overlap interaction and it is involved in both geometries. As a result, the cis and trans forms of $(PH_3)_2PtH_2$ are found to be nearly equienergetic [67]. That is to say there is no thermo-dynamic trans effect in this case.

(c) Scott and Richards suggest that the $3d^{n-1}4s^1$ configuration of the metal gives rise to the ground state of the hydrides and that the d electrons are largely non-bonding from ScH to FeH [68].

y
└─z

— b₂ pₓ
       πᵤ
— a₁ p_y
— b₁ p_z σᵤ

Pt
H   H

H——Pt——H

a₁ s σ_g

a₁ d_{z²} σ_g

b₁ d_{zy}
            π_g
a₂ d_{zx}

b₂ d_{xy}
            δ_g
a₁ d_{x²-y²}

b₁

a₁

σᵤ

σ_g

H₂   Pt   Pt   H₂
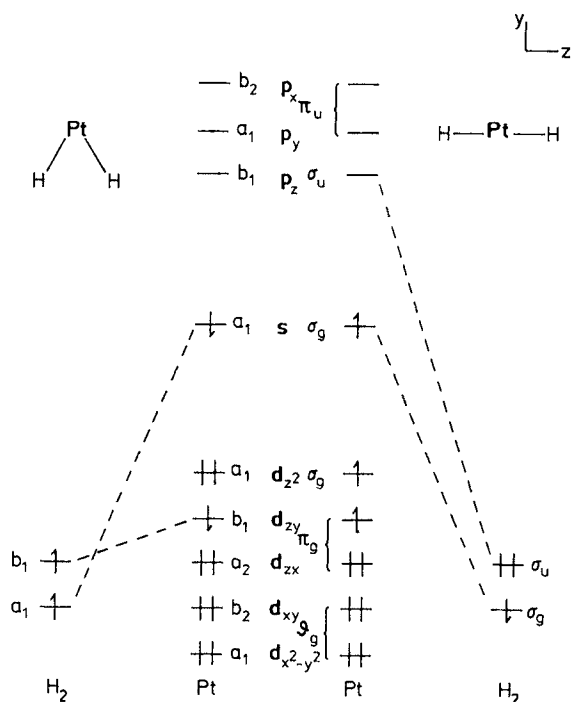
Fig. 28. Principal bond diagrams for bent and linear HPtH. Note how the linear form requires participation of a 6p AO of high energy and this is why one Pt—(H₂) bond becomes nearly ionic

(d) $Ni(CO)_4$ is a prototypical organometallic molecule. Ionization from the 1s carbon AO of CO requires much more energy than the same process within $Ni(CO)_4$, i.e. there is a very large breakdown of Koopmans' theorem in this and related molecules [69]. The reason is that the positive charge generated by electron ejection is stabilized by the responding metal atom within $Ni(CO)_4$ via monoelectronic polarization. The situation is very different from that encountered in organic molecules where the frozen orbital approximation works well in Photoelectron Spectroscopy. These facts are trying to tell us that Ni and metals in general act via polarization, monoelectronic and bielectronic dispersion), because their d AO's cannot generate strong overlap bonding.

(e) There have been several high quality calculations of small metal diatomics or clusters where the authors fully recognized that the important metal orbital insofar as overlap is concerned is the ns AO [70]. Others have realized that d orbitals, though they may not overlap substantially, are very critical for reproducing quantitatively bond energies [71].

(f) If the d orbitals of Fe were strongly overlap-active, the hydrogens of the cyclopentadienyl rings of ferrocene would bend *away* from the iron metal. That the opposite happens is testimony of the fact that the strongest overlap interaction is due to the metal 4s vacant AO which can interact with the totally symmetric sigma MO of the cyclopentadienyl rings that span the ring hydrogens. We suggest that this type of bending is diagnostic of primary overlap involvement of a totally symmetric AO of the

central atom because the additional p- or d-type AO's cannot overlap strongly with the appropriate ring MO's to define DET bonds, in the language of MOVB theory. Many such cases of counter-intuitive bending are known in organometallic chemistry [72, 73].

The fact that Overlap Dispersion is a hard concept to grasp because of the overexposure of chemists to theoretical models of the EHMO variety is made obvious by the fact that, faced with logical dilemmas posed by the experimental data, chemists often retrench to familiar theoretical concepts of overlap binding. An example will serve to illustrate this point. There are at least three types of compounds for which the strength of the bond connecting the metal with the organometallic fragment is clearly related to the ground $d^n s^2 \rightarrow$ excited d^{n+2} promotional energy, if one recognizes that past a certain point along the series one creates (three- or four-electron) antibonds rather than electron pair bonds. Such a correlation holds for:

(a) The M—CO bond strengths of $M(CO)_n$.
(b) The M—Cp bond strengths of MCp_2 (Table 4).
(c) The CO IR frequencies of M(CO) [74].

Table 4. Average M-Cp Bond Dissociation Energies and Metal Promotional Energies to the d^n Valence State.*

M	D (M-Cp) (kJ/mole)	Ground $\rightarrow d^n$ Promotion (cm^{-1})
V	420.0	20.202
Cr	340.3	35.398
Mn[a]	265.6	44.978
Fe	351.7	32.873
Co[b]	323.5	27.497
Ni[a]	300.9	14.728

* Pilcher G, Skinner HA (1982) Thermochemistry of organometallic compounds. In: Hartley FR, Patai S (eds) The chemistry of the metal-carbon bond. Wiley, New York. The d^n state is the one corresponding to the metal configuration principally responsible for bonding, i.e. the parent configuration of the principal bond diagram.
[a] Two metal-ligand 3-e antibonds; [b] One metal-ligand 3-e antibond

What do these correlations try to tell you? That one has to take the electron pair (or the odd electron) off the ns metal AO, which can overlap with a totally symmetric doubly occupied ligand MO thus producing a four- (three-) electron antibond, and "hide" it in an $(n - 1)$ d metal AO which is contracted (relative to the ns) and, thus, cannot form an antibond with the ligand fragment. But if this is so, one cannot turn around and claim that d orbitals act like ordinary carbon s and p AO's generating bonds through overlap. It is exactly because they do *not* overlap substantially that they become the repository of the original ns electron pair at the

expense of promotion energy. The correlations I mentioned are testimonies of overlap dispersion and not overlap bonding as workers who have been well aware of these trends have advocated. Going one step further: The bond strengths referred to above correlate with the promotional energy for $d^n s^2 \rightarrow d^{n+2}$ conversion and they both correlate with the heat of formation of metal gaseous atoms when the metal belongs to the first transition series. But the heat of formation of gaseous metal atoms reflects bonding within the *metal crystal* and metal—metal bonds in the crystalline state have long been regarded as due to non-overlap factors and, in particular, to cohesive forces of the dispersion type. Hence, we are pleased to see that metals bind each other in the solid by dispersion and they bind organic molecules by molecules by modified dispersion, namely Overlap Dispersion.

7.4 The Isosynaptic Principle. A Dictionary for Inorganic Stereochemists

We now focus our attention on organometallic chemistry and ask the question: Are there common denominators in main group chemistry of the "heavy" elements (green or red atoms) and in organometallic chemistry, i.e. the chemistry of molecules containing red atoms? In establishing useful analogies one must determine the number and types of *active orbitals* as well as the number of *active electrons* of a given fragment, i.e. one must identify the *active electrons* and *active holes*. The first step is to define a useful *first order* approximation, which we shall term the *First Order Bonding* (FOB) approximation, according to which the black or green or red atom of the highest row is a representative not only of itself but also of the other atoms of the same column which have the same color. That is to say, C (black) is representative only of itself and so is Si (green). Ge* (red) is representative of Ge, Sn and Pb (all red), Co* (red) is representative of Co, Rh, Ir (all red), and Li* (red) is representative of Li, Na, K, Rb, Cs, Fr (all red). This approximation will allow us to present the fundamental concepts in a simple way in a first stage and then include the refinements (second order differentiations of bonding properties) in a later stage. The second step is to recognize that in the first transition row, from Sc to Zn, the $(n-1)$ d AO's are very much contracted relative to ns AO ($n=4$). The same is true of the second and third transition rows although, ultimately, in the third row the magnitude of the effect is significantly reduced and this becomes a cause for a second-order distinction between atoms of the same color (*vide infra*). Finally, we recall that a red metallic atom within an organo-metallic complex is expected to have the same binding properties as an appropriate main group metallic atom of the *same color*, i.e. they will both tend to bind via Overlap Dispersion. Thus, the MOVB dictionary of analogies will be fundamentally different from those previously suggested by a number of workers, since in their contributions an effort was made to define inorganic (red) — organic (black) analogies [75], something in direct contradiction with the essence of our arguments, i.e. that Overlap Dispersion is different from Overlap binding.

We now focus attention on metal carbonyl compounds and we construct the principal bond diagrams of $M(CO)_n$ fragments with the hope that we could equate $M(CO)_n$ to main group green or red atoms by identifying the number of electrons and the types of metal orbitals of $M(CO)_n$ which are free to participate in the

bonding of some other atom or fragment Z. Always, in accordance with fundamentals discussed before, we require that the principal bond diagrams be constructed subject to the following restrictions:

(a) Each CO is binding to the metal center primarily by using the non-bonding sp-like AO of carbon which contains two electrons and the low lying π^* antibonding MO's.

(b) The metal is excited by relocating the electrons normally occupying the totally symmetric ns AO in the ground state to the $(n - 1)$ d AO's so that metal-ligand overlap repulsion (otherwise caused by the overlap of the metal ns and the ligand totally symmetric MO) is avoided.

(c) To the extent possible, d electron pairs on the metal should be alotted to d orbitals which have minimal overlap with the occupied $(CO)_n$ orbitals. This is the requirement for *protection against metal-ligand overlap repulsion*. The same requirement guarantees that odd electrons or electron pairs that must unavoidably be placed in d orbitals which overlap strongly with the occupied $(CO)_n$ orbitals will acquire significant s or p character via effective hybridization. Hence, orbitals and electrons of the former type will not contribute to binding Z while orbitals and electrons of the latter type will be principally utilized in making $M(CO)_n$—Z bonds because the s and p AO's have greater radial extension than the contracted d AP's of the metal.
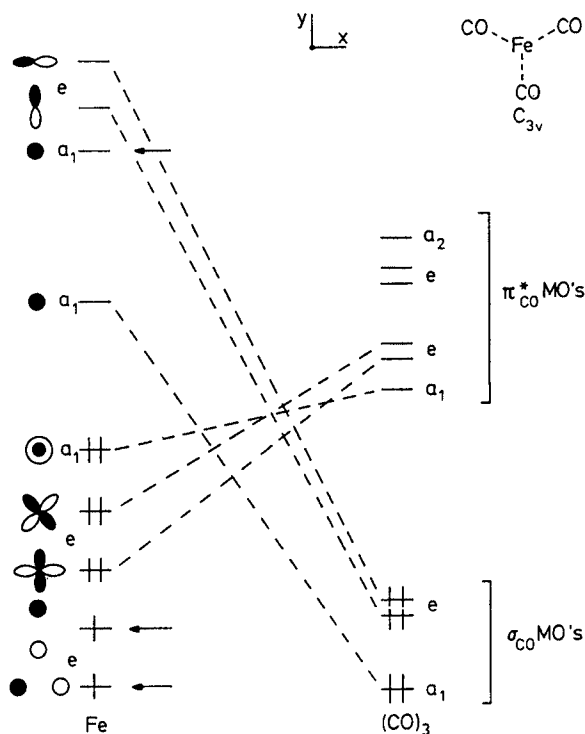
Fig. 29. Principal bond diagram of $Fe(CO_3)$. Arrows indicate orbitals and electrons available for binding with some fragment Z

The principal bond diagram of $Fe(CO)_3$ in which all important sigma-occupied and pi-unoccupied MO's of the carbonyl are allowed to take part in the bonding looks like the one shown in Fig. 29, with the arrows indicating the orbitals and electrons available for bonding some other fragment, Z. On the basis of Fig. 29, we now conclude that there are three Fe AO's and two electrons available for binding and that $Fe(CO)_3$ is isosynaptic to ground Si or Ge* in which the ns AO with its two electrons have been artificially deleted. This has occurred because the Fe $3d_{z^2}$ AO, which has the same symmetry as the Si 3s AO, and its two electrons has been tied up by a ligand hole of appropriate symmetry. So, $Fe(CO)_3$ is very much like Si or Ge* with a stereochemically inactive ns electron pair. Hence, we obtain the following relationship:

$$Fe(CO)_3 \; \circ\!\!\rightarrow \; Si, Ge^* .$$
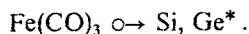
It should be noted that the principal bond diagram features a $3d_{z^2}$ pair and a 4s hole with the latter coupled to the ligand fragment a_1 pair. In this way, we bypass metal-ligand overlap repulsion but we create severe d-interelectronic repulsion in the configuration "projected" by the principal bond diagram in which the metal has s^0d^8 occupancy. However, delocalization of the d-electrons of the metal into the vacant ligand MO's and *concomitant* donation from the doubly occupied a_1 to the 4s hole provides a mechanism by which this unfavorable situation is partly remedied. This mechanism is Overlap Dispersion.

Consider now the isoelectronic principle as understood by most people: One says that, e.g. C and Si are valence-isoelectronic and expects that C_2H_2 and Si_2H_2 have similar structures, but they do not! Then, consider the "frontier isolobal" analogies developed by a number of workers over the years. One says now that, e.g. HC and $Ir(CO)_3$ are not, of course, isoelectronic but "frontier isolobal" [76]. However, $(HC)_4$ and $[Ir(CO)_3]_4$ are structurally very different; the former *organic* species definitely prefers a D_{4h} over a T_d structure while the latter *inorganic* molecule has the opposite preference [77]. Now, the reader might recognize that in defining "frontier isolabal" analogies using MO theory we are in constant danger of making an error if we cannot properly count *all* active electrons and holes of the two fragments. Thus, one may argue that $Ir(CO)_3$ is not isolobal to H—C, as proposed by Hoffmann, but to N. This again would not work because N_4 is unstable relative to $2 N_2$ while $[Ir(CO)_3]_4$ is a stable tetrahedral cluster. It is then clear that the contribution of this paper is to point out that isoelectronic or frontier isolobal analogies exist only between species of *the same metallic character*, i.e. species which have the same color, and that this can only be sensed by a theory of bonding which *explicity* projects the competition between fragment excitation and inter-fragmental bond-making and the dependence of electron delocalization on color itself. MOVB theory is such a theory and the MOVB bond diagram its simple coveyor. Clarly, what the practicing chemist needs are analogies which incorporate color. We suggest that such relationships be called *isosynaptic analogies*, i.e. analogies which identify two species A and B which upon combination with some atom or fragment Z will form molecules AZ and BZ in which A and B and bound to Z in a reasonably similar fashion. A dictionary of iso-synaptic relationships can then only be created if one realizes that black atoms are different from green

and red atoms and that additional effects create shades of green and red. Pursuing the example of $Ir(CO)_3$, we say that it is isosynaptic neither to HC nor to N but to P or As*, always according to the FOB approximation. By working in the manner illustrated above for $Fe(CO)_3$, we have constructed a table of isosynaptic relationships which we now submit for scrutiny, testing, and further development (Table 5). The

Table 5. The Isosynaptic Analogies. A First-Order MOVB Dictionary

$M[CO]_n$	d^7 Mn, Tc, Re	d^8 Fe, Ru, Os	d^9 Co, Rh, Ir	d^{10} Ni, Pd, Pt
M(CO)	--	Li^{+*} g	Li^* g	Be^* g
$M(CO)_2$	Li^* g or $^2P^o$	Be^* $^3P^o$	Al^* g or ^2D	$SiGe^*$ ^1D
$M(CO)_3$	Al^* g	$SiGe^*$ g	P^*Sb^* g or $^2D^o$	S^*Po g or ^1D
$M(CO)_4$	P^*Sb^* $^2D^o$	S^*Po g	Cl^* g	Ar^* g

* The assumed $M(CO)_n$ fragment geometries are $C_{\infty h}$, C_{2v}, C_{3v}, and C_{2v} for n = 1, 2, 3, and 4, respectively. The symbol g indicates the atomic ground state and other symbols denote alternate valence states.

reader is cautioned that AZ and BZ may have the *same* shape even if A and B are *not* isosynaptic. The difference between A and B can then be perceived only by examination of the electronic wavefunction of the global minimum. For example, CH_4 and GeH_4 are both tetrahedral while C and Ge are not isosynaptic. We now exemplify the connection between main group and inorganic chemistry by reference to a few experimental and theoretical results taken from the literature.

(a) In Scheme 4, we start with linear acetylene (organic). Replacement of each C by Si leads to the "butterfly" structure. To see why this happens consider the bond diagrammatic representations of linear and butterfly C_2H_2 are shown in Fig. 30. As in H_2O, the linear form has strong bonds by keeping the C_2 fragment excited while the opposite is true of the butterfly form. However, in stark contrast to H_2O, the linear form is now preferred because the $1\pi_u - 1\sigma_u$ gap of C_2 is relatively small. Replacement of C (black atom) by green or red atoms will tend to change the geometry from linear to butterfly. This is indeed what happens when C is replaced by Si [78] according to computations. Next, we can replace H (black) by weaker overlap binders (green or red) in Si_2H_2 and assume that the original shape of Si_2H_2 will be retained. For similar reasons, we can replace Si by green or red atoms and expect to get a derivative of the original geometrical structure. Finally, we can take these new derivative molecules and replace main group green or red atoms by their $M(CO)_n$ analogues according to Table 5. The resulting inorganic complexes

Scheme 4

H——C≡≡≡≡C——H

Replace | C by Si

Si⟨⟩Si (C_{2v}) (with H top and bottom)

Add | S   Replace H· by M≡P·   Replace H· by S=P· Replace H· by RS·   H· by Li·

Si⟨S⟩Si (H top, H bottom)   Si⟨M/P⟩Si (P top, M bottom)   Si⟨P/S⟩Si (Li bottom)   Si⟨R/S⟩Si (R top, S bottom)

Si •→ Os(CO)₃   Si •→ Fe(CO)₃   Si •→ Fe(CO)₃   Si •→ Fe(CO)₃
S •→ Os(CO)₄   Si •→ Ru(CO)₃
                    P •→ Co(CO)₃
                    Li •→ AuPPh₃

Orpen et Al   Lang et Al   Fischer et Al   Marko and Marko-
1978   1983   1984   Monostory
                                   1981
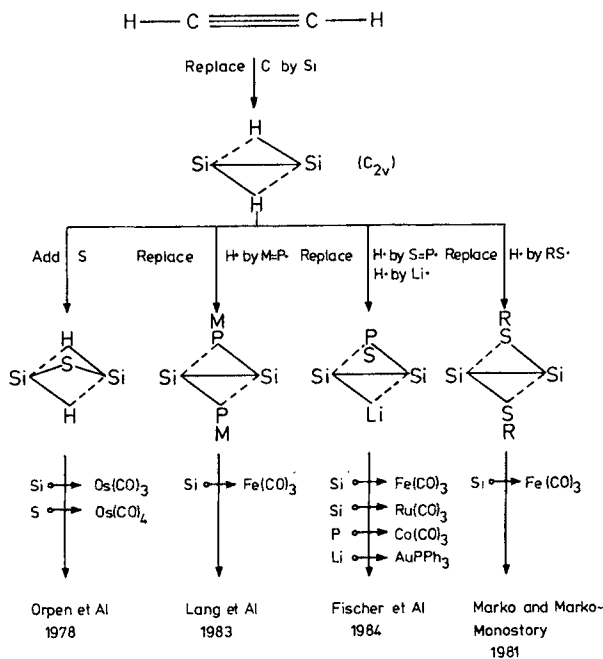
(a) Orpen AG, Rivera AV, Bryan EG, Pippard D, Sheldrick GM, Rouse KD: J. Chem. Soc. Chem. Commun. 1978: 723
(b) Lang H, Zsolnai L, Huttner G (1983) Angew. Chem., Int. Ed. Engl. 22: 976
(c) Fischer K, Müller M, Vahrenkamp H (1984) Angew. Chem., Int. Ed. Engl. 23: 140
(d) Marko L, Marko-Monostory B (1981) in: von Gustorf EAK, Grevels F-W, Fischler I (eds) The organic chemistry of iron, Academic, New York, vol 2
(e) The Fischer et al. compound can be alternatively viewed as a derivative of the "precursor" of the Orpen et al compound (Si_2SH_2) in which the two hydrogens were replaced by the univalent $Li^{\cdot}$ and $LP^{\cdot}$, where L is a two-electron donor ligand simulating the effect of one sulfur lone pair. This "precursor" along with the isosynaptic relationships for $LP^{\cdot}$ and $Li^{\cdot}$ yields also the Fischer et al. compound.

have all been prepared in the laboratory and all have the same shape as their main group parents!

(b) In Table 6, we list the geometries of Ge_n clusters determined computationally by Pacchioni and Koutecky [79]. It can be seen that the $(Os(CO)_3)_n$ analogues ($Ge \circ\!\!\rightarrow Os(CO)_3$) have the same gross structures!

(c) C is tetravalent in linear C_2H_2 but Si is divalent in butterfly Si_2H_2 and in its derivative SSi_2H_2, which is then a Lewis Acid-Lewis Base. Hence, $(Os(CO)_4)$ $(Os(CO)_3)_2H_2$ must have properties of both a Lewis acid and a Lewis base as it

$(CO)_3Fe$—CO—$Fe(CO)_3$ (with CO top and CO bottom) $\xrightarrow[FeCO_3 \circ\!\!\rightarrow Si,Ge^*]{}$ M—CO—M (with CO top and CO bottom) $M = Si, Ge^*$

111
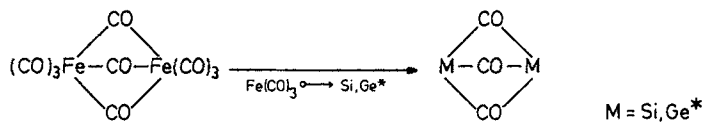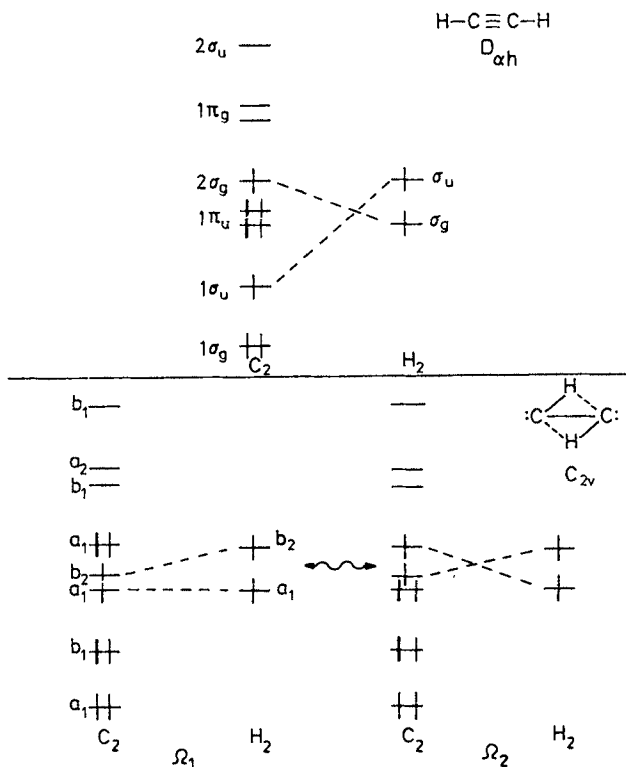
Fig. 30. Bond diagrammatic descriptions of linear and "butterfly" C_2H_2

has been recently demonstrated [80]. This same fact is responsible for the catalytic activity [81].

(d) Consider the case shown below, where we use line drawings devoid of any true "electronic" meaning.

Taking M = Ge for illustrative purposes, we discover through construction of the appropriate bond diagram that the molecule $Ge_2(CO)_3$ can be nothing other than a propellane in which each Ge is in each ground state and at least one CO is coordinated, i.e. the proper electronic structure is:

Table 6.

Os(CO)$_3$ o——► Si,Ge* o—||—► C
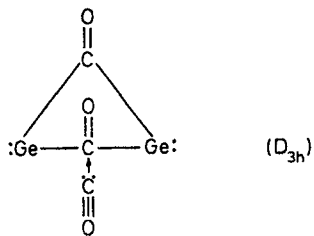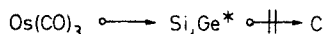
n =	$\left[Os(CO)_3 \right]_n$	Ge$_n$ [a]	C$_n$ [b]
4		Rhombus	Rhombus
5		Tetragonal Pyramid	Trigonal Bipyramid
6	Monocapped Trigonal Bipyramid	Monocapped Trigonal Bipyramid	Distorted Octahedron
7	Monocapped Octahedron		Pentagonal Bipyramid

The Geometries of Clusters
* Best singlet geometries; [a] Pacchioni G, Koutecky J (1984)
Ber. Bunsen Ges. Phys. Chem. 88: 242; [b] Slanina Z, Zahrad-
nik R (1977) J. Phys. Chem. 81: 2252

There is no Ge—Ge Bond, exactly like there is no Fe—Fe bond in Fe$_2$(CO)$_9$, according to calculations [82].

This example has a broader significance for it teaches us why some propellanes are global minima and others highly strained secondary minima (which nonetheless can be isolated) [83]. To understand this, compare the bond diagrams of C$_2$(CH$_2$)$_3$ and Ge$_2$(CO)$_3$ (Fig. 31) C$_2$ is isoelectric to Ge$_2$ and CH$_2$ and CO are isolobal:
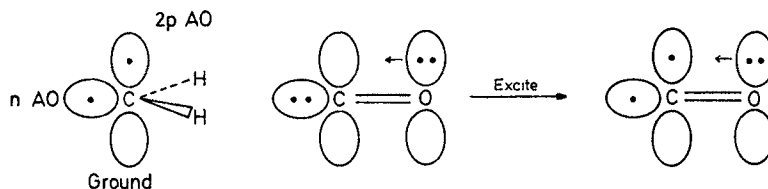
First some technical details: If we symbolize each propellane by ML$_3$M (M = C, Ge and L = CH$_2$, CO), the basis AO's are the valence AO's of each M and the n and 2p AO's of each L with a total of 14 electrons. The bond diagram for C$_2$(CH$_2$)$_3$ and drawings of the orbitals can be found in our previous published work. In Fig. 31, we indicate the type of each set of ligand MO's (n-type and 2p-type) assuming for simplicity, zero L—L nonbonded overlap.

Second, the fundamental differences:

1. In C$_2$(CH$_2$)$_3$, C$_2$ acts primarily as a *septet* with one weak C—C bond (a$_1'$ doubly occupied orbital). By contrast, in Ge$_2$(CO)$_3$, Ge$_2$ acts mainly as a *quintet* with no net Ge—Ge bond. C$_2$ makes *six* "covalent" bonds to (CH$_2$)$_3$. Ge$_2$ extends only *four* "covalent" bonds to (CO)$_3$.

113
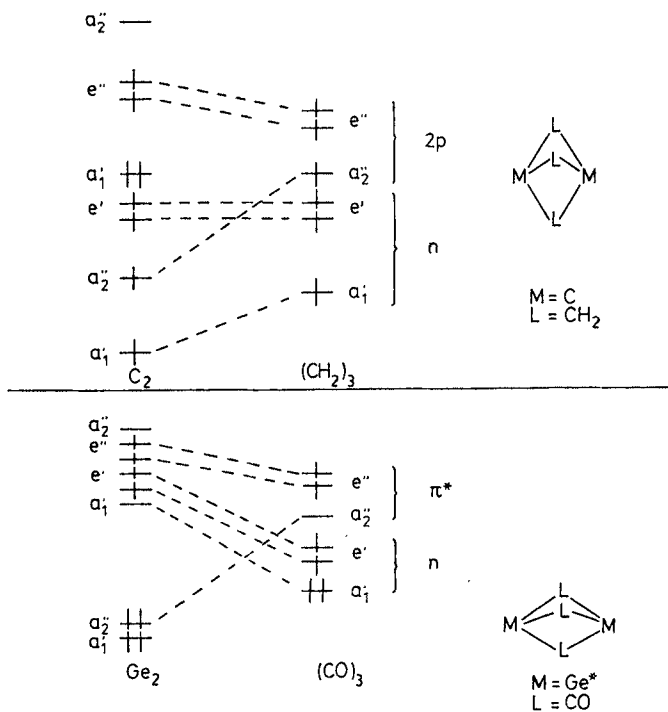
Fig. 31. Principal bond diagrams of an organic and an inorganic propellane

2. In $C_2(CH_2)_3$, there are three "covalent" T-type bonds (a_1', e'). In $Ge_2(CO)_3$, there are only two T-type (e') bonds. A T-type bond is on involving ligand MO's which are directed to the midpoint of the M—M line and, by its nature, tends to "clamp" M and M together. As a result, the MLM angle increases in going from $C_2(CH_3)_3$ to $Ge_2(CO)_3$. The reason is the fact that, in the former, the a_1' "covalent" bond "clamps" strongly the two carbons because the lowest energy a_1' C_2 MO is essentially $2s_1 + 2s_2$. In the latter case, the corresponding Ge_2 MO accommodates an electron pair and is not involved in core-ligand binding. It is replaced by an essentially $2p_1 + 2p_2$ MO which is involved only in coordinate bonding and which has less "clamping ability". The double occupancy of the bonding σ_g MO and its anti-bonding partner, the σ_u MO, of Ge_2, is ultimately responsible for the long Ge—Ge distance and large GeCGe angle.

3. Each of $C_2(CH_2)_3$ and $Ge_2(CO)_3$ has *six* core-ligand bonds. However, the former has six "covalent" while the latter four "covalent" plus two "coordinate" bonds.

Now, we can understand the fundamental differences between "organic" and "inorganic" chemistry. If one binds 2 C's and 3 CH_2's, or, equivalently, 5 C's and 6 H's, the global minimum is the unstrained isomer shown below produced by spin pairing.
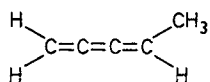
By contrast, one can use two ground state Ge and three :CO of which only two are excited to build a propellane-type structure in which one :CO is coordinated to Ge_2. We understand that bridging can be a mechanism by which bridgehead atoms (Ge in our example) are kept deexcited! It will be encountered whenever the bridge-head atoms are weak overlap binders. Furthermore, we point out that the terms "covalent bond" (i.e. bond due to spin-pairing) and "coordinate bond" have been used in the case of the organometallic species out of sheer chemical expedience. The correct term for describing the bonding of the Germanium propellane is Overlap Dispersion "parented" by a configuration in which "covalent and coordinate bonds" link the two fragments.

We now connect this discussion to experimental reality. We just predicted that triply bridged M $(CO)_3$ M, where M is green Si or red Ge, Sn or Pb may be an isolable species. When M = Si and when two carbonyls are replaced by different Si and RP green fragments, we expect to get the propellane-like $Si_3(PR)$ (CO). Replacement of all three silica by the isosynaptic analogue $Fe(CO)_3$ would then produce the propellane-like $Fe(CO)_3[Fe(CO)_3(CO)(PR)]Fe(CO)_3$. Knoll et al. were able to prepare such a molecule and determine its structure [84].

7.5 Organic Transition States

In a typical bimolecular pericyclic reaction, such as cycloaddition of two olefins, reactant bonds stretch, product bonds are partially formed, and overlap inter-action is weakened at the transition state. Hence, each reactive carbon atomic center effectively changes color form black to green. Our intent now is to exemplify the key role of Overlap Dispersion in pericyclic transition states using the language of VB rather than MOVB theory. To this extent, we show in Table 7 the semi-empirical qualitative VB wavefunctions of a Hückel ("forbidden") and a Möbius ("allowed") four orbital-four electron system. Recognizing that the interaction of the Kekule structures with the "diagonal charge transfer" structures represents a form of correlated double electron transfer called Relay Electron Transfer (RET) while the "charge alternant" structures define CET (Overlap Dispersion), we see immediately that these latter two types of structures contribute only to the Möbius species. Hence, the rule: The superiority of an "allowed" over a "forbidden" complex is due to the fact that RET and CET (Overlap Dispersion) occur more efficiently in the former. Now, because the double electron transfer resulting in charge alternation correlates electronic motion better than that resulting in diagonal charge transfer, we can focus our attention on the former. The question now becomes: What happens when Overlap Dispersion is obstructed at the transition state of an "allowed" reaction? We can see the following trends:

(a) Because carbon is a black atom of low polarizability, i.e. because it cannot efficiently support CET, the energetic advantage of a concerted "allowed" over a stepwise diradical mechanism will be small in pericyclic reactions contrary to what is implied by Hückel MO theory. This is why it has been repeatedly demonstrated that stepwise can be competitive with one-step "allowed" reactive channels [85].

Table 7. NDO VB Wavefunctions of Four-Electron-Four-Orbital Hückel (HAO) and Möbius (MAO) AO Systems

		E (eV)	C1	C2	C3	C4	C5	C6	C7	C8	C9	C10	C11	C12	C13	C14	C15	C16	C17	C18	C19	C20	C21	C22	
HAO Singlet		-13.7	0.65	0.38	⊘	-0.23	-0.23	-0.23	0.23	0.23	0.23	0.23	-0.23	0.23	0	0	0	0	0	0	0	0	0	0	Ψ₁
		-10.8	-0.29	0.51	⊘	0.24	0.24	0.24	0.24	0.24	0.24	0.24	0.24	0.24	0	0	0	0	0.10	0.10	0.10	0.10	0.28	0.28	Ψ₂
		-9.3	0	0	⊘	-0.26	-0.26	0.26	-0.26	0.26	0.26	0.26	-0.26	0.26	-0.25	0.25	0.25	-0.25	0	0	0	0	-0.33	0.33	Ψ₃
HAO Triplet		-12.9	0.47	0.27	-0.38	-0.23	0.23	-0.23	-0.23	0.23	-0.23	0.23	-0.23	0.23	0.19	0.19	-0.19	-0.19	⊘	⊘	⊘	⊘	⊘	⊘	Ω
MAO Singlet		-19.3	0.50	0.29	⊘	-0.24	0.24	-0.24	0.24	0.24	0.24	0.24	-0.24	0.24	0.15	0.15	-0.15	-0.15	0	0	0	0	0.21	0.21	×
MAO Triplet		-9.9	0.57	0.33	-0.46	-0.21	0.21	-0.21	-0.21	-0.21	-0.21	-0.21	-0.21	0.21											Φ

* Reproduced from ref. 14.

(b) Ground state reactants have optimal covalent bonds. On the way to transition state for *concerted* bond exchange, old bonds are broken and new bonds are made in a synchronous fashion. This process can only be achieved by *net* reduction of overlap of the AO's of the active centers because interbond overlap repulsion dominates the resonance interaction. The only way to compensate for the net loss of overlap bonding is to fall back on some other mechanism of bonding with is overlap independent. This mechanism of bonding is dispersion. At the level of VB theory, it is brought about by the interaction of covalent with the doubly ionic VB structures in which there is charge alternation. If, for whatever reason, these charge-alternant structure are blocked from participation, there is no longer any reason to expect concerted bond exchange and we focus our attention entirely on stepwise mechanisms via diradical or dipolar intermediates which are principally described by covalent and singly ionic VB structures, respectively. Having realized that the most efficient mixing of covalent and charge-alternant structures occurs at pericyclic "allowed" transition states, one can fully expect that reactions in which geometric constraints preclude pericyclic overlap will occur by stepwise mechanism. Thus, for example, the reason that calculations have found the Woodward-Hoffmann 2s + 2a cyclo-addition transition state to lie above the transition state leading to a transoid diradical [86] is not a consequence of "steric effects" as commonly thought but the result of the fact that there can be no pericyclic overlap in such a complex since the pi bond of one reaction partner *must* be broken by virtue of rotation at some *intermediate* stage of the reaction.

(c) Unsymmetrical substitution of a reaction partner in an "allowed" peri-cyclic reaction should be more effective than symmetrical substitution in accelerating the reaction because it effectively causes lowering of the energy of the charge-alternant structure which plays the key role in stabilizing the "allowed" transition state complex. It has been long known that an unsymmetrical 1,1-disubstituted alkene, which is an inferior acceptor compared to the symmetrical 1,2-disubstituted isomer, reacts faster with a donor diene [87]. Recent results obtained by Professor Sauer's group in Regensburg are also consistent with these arguments [88].

7.6 Bond Cooperativity

The implication of the MOVB analysis presented in Sect. 7 is that there exist two different worlds of bonding.

(a) The world of strongly bound systems in which the principal configuration is the perfect pairing configuration and this contains most of the information about the electronic structure of the system. The SET delocalization mechanism is superior to the CET delocalization mechanism but it makes a relatively small contribution to the total wavefunction. This is why stereoselection credited to better SET delocalization in one of two isomers under comparison (e.g. trans versus gauche 1,2-difluoroethane) is weak (e.g. the conformational preference for gauche over trans 1,2-difluoroethane is of the order of 1 kcal/mol) [89]. Systems of this type are made up of sigma bonded black atoms.

(b) The world of moderately bound systems in which the principal configuration may be a perfect pairing or a closed shell configuration which by itself accounts

117
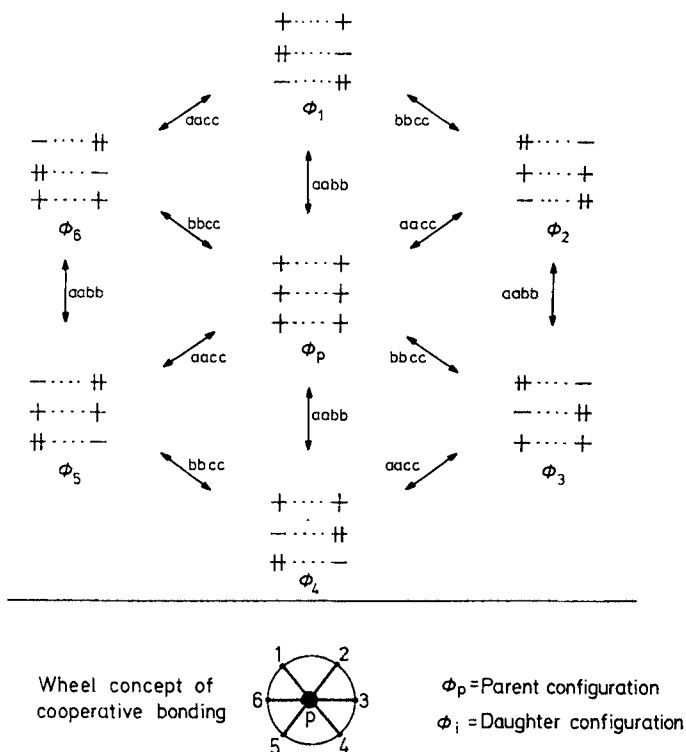
Fig. 32. The Wheel concept of cooperative bonding: All configurations interact with each other through Φ_p and through each other. For example, configurations 1 and 6 interact through p, through 2 and p, through 2, 3, and p, ... , through 2, 3, 4, and 5. This means that every bond cooperates at least in part with each other one

for only a small fraction of the total binding energy. In such systems CET becomes superior to SET and the bonding can be described only in terms of configuration interaction of a special type: Starting from a parent principal configuration, electrons move two at a time in a correlated sense in order to produce what we call Overlap Dispersion bonding. The hallmark of Overlap Dispersion is bond cooperativity to the extent that every single DET or coordinate bond assists every other such bond via CET delocalization. This situation is illustrated in Fig. 32. A corollary is that the way an atom exists in a molecule of this type depends on the total number of bonds (and the total number of electrons) within the parent configuration of the molecule, e.g. Ni in NiCO is going to be different from Ni in Ni(CO)$_4$[90]. We will now try to demonstrate that bond cooperativity exists in the ground states of molecules which are made up of green and/or red atoms. We will load the case *against* bond cooperativity and we will find that the thermochemical evidence is consistent with its presence in molecules of the type defined above.

We begin by considering the three reactions shown below where repetition (10 and 11 are the same) was deemed desirable so that the reader clearly sees the analogy with the case to follow.

$$CH_2\!=\!CH_2 + H\cdot \rightarrow \underset{\underset{H}{|}}{CH_2}\!-\!\dot{C}H_2 \qquad \Delta E_1 = -39 \text{ kcal/mole} \qquad (10)$$

$$CH_2\!=\!CH_2 + H\cdot \rightarrow \underset{\underset{H}{|}}{CH_2}\!-\!\dot{C}H_2 \qquad \Delta E_2\ (= \Delta E_1) = -39 \text{ kcal/mole} \qquad (11)$$

$$\underset{\underset{H}{|}}{CH_2}\!-\!\dot{C}H_2 + H\cdot \rightarrow \underset{\underset{H}{|}}{CH_2}\!-\!\underset{\underset{H}{|}}{CH_2} \qquad \Delta E_3 = -98 \text{ kcal/mole} \qquad (12)$$
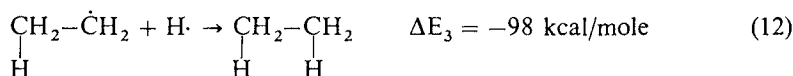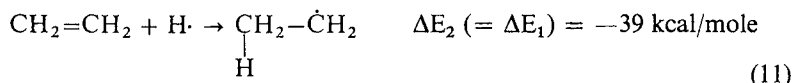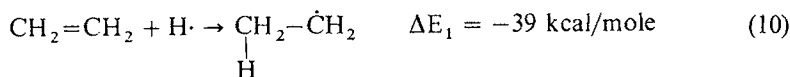
Reaction (12) is known to be more exothermic than (10). The reason is that addition of the first H (in 10) necessitates promotion of one electron from π to π^* in $CH_2\!=\!CH_2$. We call this spatial excitation and we recognize that this has a mono- as well as a bi-electronic component. Addition of a second H (in 12) [after H has already been inserted (in 11) and has caused spatial excitation of $CH_2\!=\!CH_2$] is more exothermic than simply addition of H to $CH_2\!=\!CH_2$ (in 10) because spatial excitation of a reactant is no longer required. The difference between ΔE_1 and ΔE_3 is nothing else but the thermodynamically defined strength of the pi bond of ethylene and all this basic VB argumentation is probably already familiar to the reader.

Since we have argued that bonding in moderately bound molecules is cooperative, we could explain similar trends in such systems in a completely different fashion: A second bond will always be stronger than the first because of bond cooperativity, everything else being equal. That is to say, even if spatial excitation were to remain constant, reaction (12) would be more exothermic than reaction (10) because the first formed bond assists the formation of the next one. Now, the spatial excitation factor is an indisputable reality and what we have to show is that bond cooperativity does exist. We can demonstrate the existence of such a phenomenon if we could produce a set of data which show that, while reaction (10) requires *less* spatial excitation than reaction (12), the latter is nonetheless *equally* or *more* exothermic than the former because it profits from bond cooperativity.

$$A + X \rightarrow AX \qquad (13)$$

$$A + Y \rightarrow YA \qquad (14)$$

$$YA + X \rightarrow YAX \qquad (15)$$

In other words, we expect that, although A needs much less spatial excitation than YA, nonetheless (15) is more exothermic than (13) because, in (15), Y cooperates with X. *The condition for such observation is that A is a green or red atom.*

We now descirbe one such example. Specifically, attachment of H_2 to ground Si atom (to produce C_{2v} SiH_2) can be achieved with zero monoelectronic excitation

to a first approximation. All we have to do is couple ground state triplet Si to triplet H_2 and generate the parent configuration of the bond diagram Θ. Configuration interaction (described by Θ, etc.) takes care of the rest. To the extent
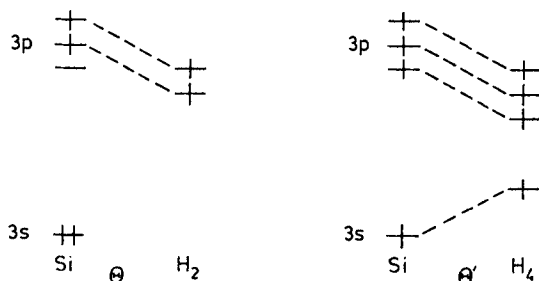
that Θ is the principal bond diagram, no spatial excitation of Si is needed for effecting the binding. However, addition of H_2 to SiH_2 (to produce T_d SiH_4) now requires promotion of one electron from 3s to 3p in Si as a comparison of Θ and Θ' reveals. Hence, addition of H_2 to Si should be much more exothermic than addition of H_2 to SiH_2. Nonetheless, the experimental results given in Table 8 clearly show that this is not the case. Thus, some other factor X has neutralized the spatial excitation factor. We suggest that factor X is bond cooperativity: The two SiH bonds in SiH_2 assist the formation of two new SiH bonds in SiH_4 and this counterbalances the spatial excitation requirement.

In Table 8 we show further experimental and computational results which constitute evidence for cooperativity. In all cases, attachment of Y on A necessitates that A in YA must become spatially excited to accept X. As a result, one would expect on the basis of standard VB reasoning that A + X will be more

Table 8.

Reaction	ΔH_r (kcal/mole)
Si + H_2 → SiH_2	−50.0
(a)	
SiH_2 + H_2 → SiH_4	−49.8
Si + F_2 → SiF_2	−248.5
(b)	
SiF_2 + F_2 → SiF_4	−245.5
$PtPH_3$ + CO → $PtPH_3CO$	+63.0
(c)	
$PtPH_3HCH_3$ + CO → $PtPH_3HCH_3CO$	+54.5
$PtPH_3$ + CH_4 → $PtPH_3HCH_3$	−18.0
(d)	
$PtPH_3CO$ + CH_4 → $PtPH_3COHCH_3$	−26.4
$PtPH_3$ + H_2 → $PtPH_3HH$	+2.4
(e)	
$PtPH_3CO$ + H_2 → $PtPH_3COHH$	−3.7

* Entries (a) and (b) taken from: Walsh R (1981) Acc. Chem. Res. 14: 246; Entries (c) to (e) are computational data taken from: Koga N, Morokuma K (1986) J. Am. Chem. Soc. 108: 6136

exothermic than YA + X. The fact that the exothermicities are either roughly equal or the second greater than the first within each pair despite the greater excitation requirement of the second reaction is strong indication of bond cooperativity in all these systems. In all cases, *the "central atom" is green (Si) or red (Pt)*. Note also that bond cooperativity works *against* any nonbonded repulsion effects which will be more accentuated in the more ligated species, e.g. nonbonded repulsion would tend to make the exothermicity of adding H_2 to Si larger than the exothermicity of adding H_2 to SiH_2.

Carter and Goddard found that adding triplet CH_2 to $^4Ru^+$ is *less* exothermic than addition of the same fragment to $^3RuH^+(Cl^-)$ by 17.5 kcal/mol [91]. We can simplify things be neglecting Cl^- in the following discussion. Since no nonelectronic orbital excitation of Ru^+ is required for coupling it to one, two, or three monovalent ligands, one possible explanation of these results is that attachment of H on $^4Ru^+$ to generate $^3Ru^+$—H has excited Ru^+ and this excitation can now be profitably used to bind CH_2. As a result, excited Ru^+ in $^3Ru^+$—H binds more strongly than unexcited Ru^+ the CH_2 unit. Let us see how this argument comes about.

$^4Ru^+$ has three spins pointing in the same direction while in ^3Ru—H one of the three spins must (in part) become opposite to the other two in the process of Ru^+—H bond formation.

This process is termed *exchange correlation loss* and it amounts to *bielectronic excitation* of Ru^+ by H. This argument has been produced by exclusive consideration of bonding within the *perfect-pairing configuration*. The alternative, of course, is that the greater exothermicity of the RuHCl plus CH_2 reaction is due to bond cooperativity, a phenomenon which is the result of *configuration interaction*. We now argue that *loss of exchange correlation is necessary for generating strong configuration interaction which, in turn, produces overlap dispersion and bond cooperativity*.

The loss of exchange correlation in the process of molecule formation is always an investment which creates returns: Overlap Dispersion bonding in moderately bound systems. This can be easily seen by reference to the system $M=CH_2$, which can be built from triplet M [with orbitals d (b_1) and s (a_1)] and triplet CH_2 [with orbitals p (b_1) and n (a_1)] in the following fashion. In the first stage, exchange correlation obtains in both ^3M and $^3CH_2$. Upon coupling the two fragments into an overall singlet so that two bonds are made, exchange correlation is partly lost because the wavefunction Φ_1, has two (out of four) primitive functions in which spins alternate. This is shown below where E.C. stands for "Exchange Correlation".

$$\Phi_1 = N \{|\bar{s}d\bar{n}p| - |\bar{s}dnp| - |sd\bar{n}p| + |s\bar{d}n\bar{p}|\}$$

No E.C.   E.C.   E.C.   No E.C.

However, Φ_1 can now interact with Φ_3.

$$\Phi_3 = |d\bar{d}n\bar{n}|$$

The interaction matrix element is:

$$H_{13} = N \ \langle |d\bar{d}n\bar{n}| \ |\hat{H}| \ |\bar{s}d\bar{n}p| \rangle - \langle |d\bar{d}n\bar{n}| \ |\hat{H}| \ |\bar{s}d\bar{n}p| \rangle$$

$$\begin{array}{cc} \text{Yields} & \text{Yields} \\ W_1 - Z & -W_1 \end{array}$$

It is seen that the spin-uncorrelated function of Φ_1 $|\bar{s}d\bar{n}p|$ creates a large $W_1 - Z$ term, i.e., loss of exchange correlation yielded a beneficial dispersion term $(-Z)$ which adds algebraically to an overlap term W_1. We must conclude that exchange correlation loss is actually the conveyor of a stabilizing mechanism. Overlap Dispersion, the consequence of which is bond cooperativity. Hence, the only physically meaningful comparison is between spatial excitation and bond cooperativity when attempting to understand how the A—X bond dissociation energy depends on the "environment" of A, always remembering that bond cooperativity can be observed only in moderately bound systems.

The difference between the Carter-Goddard explanation and our is a fundamental one. The enhancement of the exothermic binding of CH_2 to Ru^+ by attachment of H on the metal center is traced to the perfect pairing configuration, Φ_1, by these workers while it is attributed to configuration interaction in which electrons hop in pairs by us. But, this bond cooperativity should vanish in systems which are strongly bound and all the examples we cited as evidence of bond cooperativity were systems containing green and red atoms. On the other hand, the Carter-Goddard argument should remain unaltered because the perfect pairing configuration does not depend on atom color, only the configuration interaction does. To put it crudely, if all molecules "organic", "organometallic", "inorganic", etc., are bound in such a way so that in all cases the perfect pairing configuration by itself provides an apt description of bonding then we should not expect bond cooperativity at all. We now show that, in addition to the strong hints for the existence of such an effect by the data of Table 8. bond cooperativity disappears when the perfect pairing configuration does become an apt description of bonding in black, strongly bound systems. To understand this, first consider what happens as we go from Si to SiH_2, and then to SiH_4. Attachment of two H's on Si to generate ground singlet SiH_2 does not necessitate orbital promotion of Si and it yields 154 kcal/mole. Attachment of two more H's on SiH_2 now requires 3s → 3p Si promotion and, so, we expect the addition to yield *less* than 154 kcal/mole. In contrast, what is found is that the total energy released is 154 kcal/mole! As we said before, we credit bond cooperativity for this extra bond strengthening. The situation remains essentially unaltered when we go from Si to SiF_2 and then to SiF_4 via sequential addition of two F's despite the fact that the singlet-triplet gap and. hence, the required orbital promotional energy, is much greater in SiF_2 than in SiH_2. The situation changes when we take a look at the carbon analogues. Thus, addition of two H's to C necessitates excitation of C to yield as a final product ground triplet CH_2 which can then add two more hydrogens *without* the requirement of orbital promotion. As a result, the addition of two hydrogens to C yields 181.4 kcal/mole which is much less than the 215.7 kcal/mole yielded by the addition of two hydrogens to CH_2. Accordingly, this case is not at all comparable to either of the sequential additions of H's or F's to Si. More importantly, addition of two F's to C to produce ground singlet CF_2 does not require orbital promotion of

C and it yields 252 kcal/mole. However, in contrast to the Si case, further addition of two F's to CF_2 requires promotion but the energy yield is now 218 kcal/mole, i.e. it is less than the amount of energy released by adding two F's to C. We must conclude that unlike the Si case, there is no bond cooperativity which can render the addition of two F's to CF_2 as exothermic or more exothermic than the addition of two F's to C. The reason for this difference is that carbon is black and Si green and the binding mechanisms are different. The difference of the binding mechanisms is lost if one considers only the perfect pairing configuration. This is strongly hinted by the computational results of Carter and Goddard. Specifically, the computed bond dissociation energy of $^4Ru=CH_2$ is 27.6 kcal/mole at the GVB-Perfect Paring level only to become 68.0 kcal/mole at the GVB-CI level! That is to say, configuration intereaction is mostly responsible for the binding of the two pieces.

7.7 Anti Overlap Dispersion

Much like there exist situations in which the overlap (W) and dispersion (Z) terms contribute in phase (Overlap Dispersion), there also exist situations in which the two terms tend to cancel each other. We refer to this phenomenon as Anti Overlap Dispersion and the simplest example we can give is two-electron delocalization in the *sigma space* of Li_2 due to the interaction of the two configurations shown in Fig. 33a. The symbolic notation is given in Fig. 33b where one pair of arrows undoes what the other does in contrast to the case of Overlap Dispersion where one set of arrows reinforces what the second does. It follows then that the CI principally responsible for the binding of Li_2 is that depicted in Fig. 33c. Since the two electrons are coupled through overlap into a weak bond in both configurations and since the interaction of them causes pure dispersion, this binding mechanism is a form of Overlap Dispersion. Our interpretation of the electronic structure of Li_2 is then embodied in formula *B* shown below which has two Li cations bridged by a pair of electrons and which is completely different from the formula of H_2.

$$
\begin{array}{ccc}
\text{H} \bullet \!\!-\!\!\!-\!\!\!- \bullet \text{H} & \overset{-2}{\underset{+1}{\text{Li}} \, (\,\colon\,) \, \overset{+1}{\text{Li}}} & \overset{-2}{\underset{+1}{\text{Li}} \, (\,\colon\,) \, \overset{+1}{\text{Li}}} \\
 & & \underset{-2}{\underset{+1}{\text{Li}} \, (\,\cdot\,) \, \underset{+1}{\text{Li}}} \\
A & B & C
\end{array}
$$
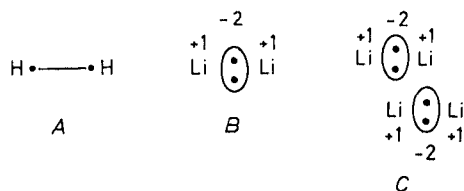
Our conclusion that H_2 and Li_2 differ much like day differs from night insofar as bonding is concerned is consistent with the following facts:

(a) Two Li_2 molecules can approach each other as indicated by formula *C* without barrier to form rhombic Li_4 which is more stable than the reactants by 15.4 kcal/mol [92]. By contrast rhombic H_4 lies 151 kcal/mol above $2\,H_2$ [93]!
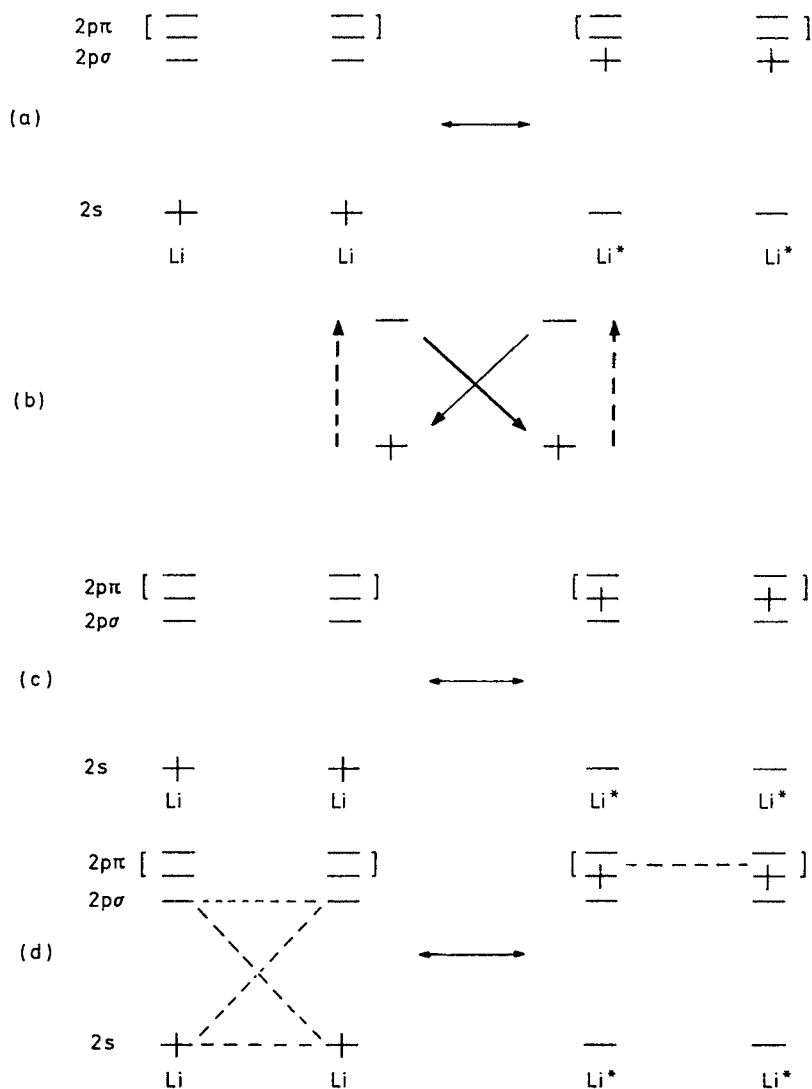
Fig. 33a–d. (a) CI due to two-electron excitation (2s → 2pσ/2s → 2pσ) within the sigma space of Li_2. (b) Pictorial depiction of the interaction matrix element of (a). (c) CI due to 2s → 2pπ/2s → 2pπ excitation (dispersion). (d) Bond diagrammatic representation of Li_2

(b) Many Li_2 molecules associate to form a solid while each H_2 repels a second H_2 (bond overlap repulsion) and intermolecular association is precluded.

(c) Li_2^+ has a *stronger* bond than Li_2 while H_2^+ has a *weaker* bond than H_2 [94a]. All these and many more differences between Li_2 and H_2 are due to the fact that the binding of the former is essentially classical coulombic with "islands" of positive and negative charge density appearing because of the "gasification" or "interstitiali-

124

H—H----H—H-----H~H----H—H

H↔H Homopolar Overlap Bond Causes
Repulsion of H_2 Units (Peierls Distortion).

Li (:) Li
       Li
Li (:) Li (⊙•)   etc.
Li (:) Li   Li

Li Li Homopolar Ionic Bond
Causes Aggregation of Li_2 Units.
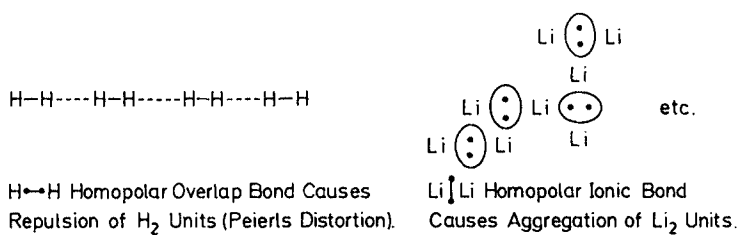
zation" of the electrons due to the CI mechanism described above. Space alimitations preclude a fuller discussion to which we shall return in a separate paper [94b].

Part IV. Overlap Induction

8 The Concept of Ionic Overlap Induction

Consider the smallest $(RLi)_n$ polymer 1 (Fig. 34) in which n $= 2$. If Li is thought of as an H analogue, i.e. if Li is thought of as having only a 2s AO and no 2p AO's and that this pseudo-Li binds by an overlap mechanism, then the stable geometry of $(RLi)_2$ should be two RLi molecules separated by infinite distance. The reason is that the two symmetry MO's of R_2 and the two symmetry MO's of pseudo Li_2 match only in a linear but not a bridged geometry and if $(RLi)_2$ is conceived as the product of the union of triplet Li_2 and triplet R_2, then union should occur at infinite Li—Li distance at which triplet pseudo Li_2 has its minimum. So, deletion of the 2p AO's of Li and enforcement of overlap binding predicts that RLi should be a monomer much like RH. The next choice is to delete the 2p AO's of Li but replace overlap by ionic binding in which case we predict a cyclic structure, D, in which the charges

$$\begin{array}{ccccc}
\bar{R}: & & & R & \\
& & & | & \\
+Li & Li+ & +1/2\ Li & \bullet & Li +1/2 \\
& & & \downarrow & \\
R: & & & R: \\
\underline{} & & & \underline{} \\
D & & & E
\end{array}$$
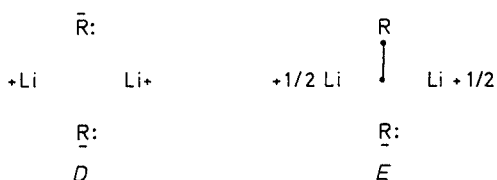
alternate and this is consistent with the fact that $(RLi)_2$ is computed to have a bridged geometry [95]. Now, what we will argue is that the mechanism of binding of $(RLi)_n$ clusters is neither overlap nor ionic but one that we will call *Ionic Overlap Induction*, an analogue of Overlap Dispersion. This bonding mechanism critically depends on the presence of the Li 2p AO's and it leads to a Lewis description of the bridged $(RLi)_2$ species as indicated by formula E. In this molecule, the R_2 unit has accepted one electron from the Li_2 unit with the following results:

(a) Li_2^+ is bound by induction as described before. This means that one electron "glues" electrostatically two Li cations. This electron is called an *interstitial electron*.

(b) One R radical makes an overlap bond with the Li_2^+ unit. The remaining R: anion is then attached electrostatically to RLi_2^+.

(c) The $(RLi)_2$ dimer is really a composite of R_2^- radical anion and Li_2^+ radical cation covalently bound. The important thing is that a covalent bond is formed which is directed from an atom (C of R) to the midpoint of the line connecting
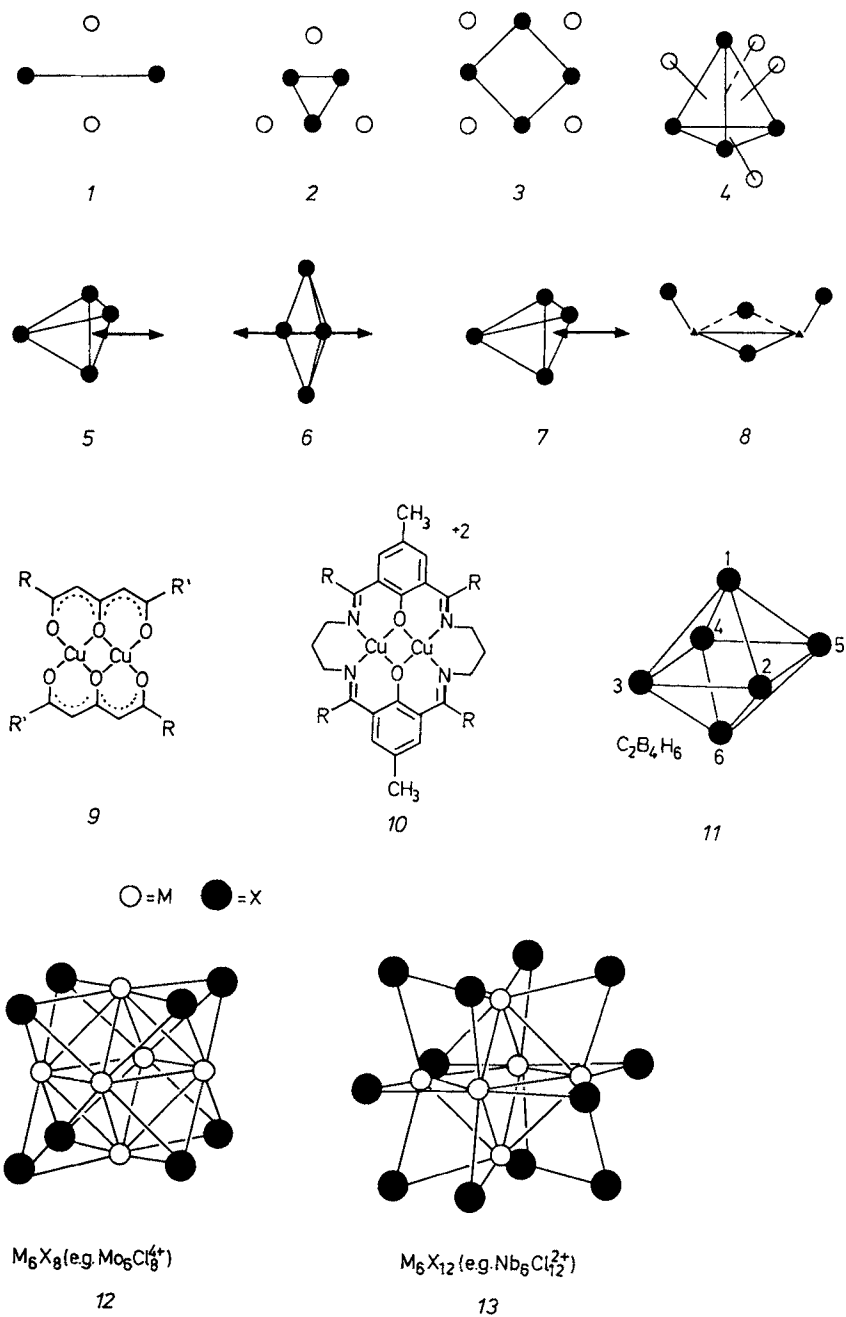
Fig. 34. Geometries of organometallic and inorganic complexes discussed in the text. White circles represent alkyl groups, black circles Lithium atoms, and black triangles carbon atoms in *1* to *8*

two other much more electropositive atoms. We call such bonds *interstitial bonds* and this mechanism of binding *Ionic Overlap Induction*.

In Fig. 35a, we show the principal bond diagrams for $(RLi)_2$ in a D_{2h} (bridged) geometry, with $HT = NS = Li_2$ and $GT = R_2$ according to the Echinos model (see section 6). The orbitals of the N subfragment of HT are labeled q_i, those of the S subfragment by k_i, and the orbitals of GT by r_i. The fact that the HT and GT fragments cannot form *two* multicenter bonds because q_2 and k_2 have different symmetry from r_2, immediately tells us that the bonding of $(RLi)_2$ is not an "exercise in overlap". Note the following:

(a) The $(RLi)_2$ dimer is represented by two principal bond diagrams, Θ_1 and Θ_2, each one having one multicenter bond connecting $HT = NS$ with GT.

(b) In each of Θ_1 and Θ_2, one electron has been transferred from the host to the Recall now the fact that organic chemists represent a molecule either by drawing resonance structures or by drawing the corresponding resonance hybrid.
For example:

$$CH_2 = CH - \overset{+}{C}H_2 \longleftrightarrow \overset{+}{C}H_2 - CH = CH_2$$
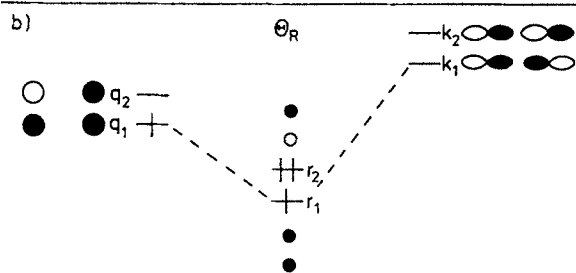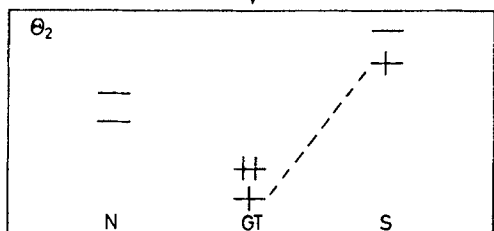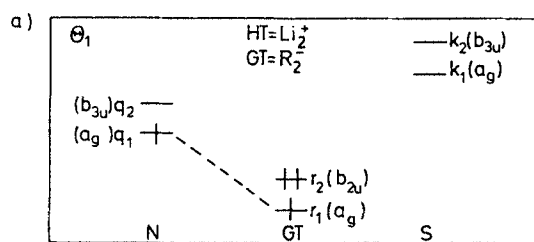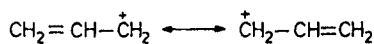
Fig. 35a and b. (a) Bond diagrammatic representation of rhombic R_2Li_2 (*1*). (b) Shorthand resonance bond diagram

is equivalently represented by

$$\text{CH}_2^{\cdot-} \stackrel{+}{\text{CH}}_2^{\cdot-} \text{CH}_2$$
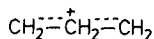
In a completely analogous fashion, the reasonance bond diagram Θ_R (formerly called the "detailed bond diagram")[13,14] shown in Fig. 35b is equivalent to the two individual bond diagrams of Fig. 35a plus the "extrinsic configurations" not contained in Θ_1 and Θ_2[13,14,96].

(c) The resonance diagram, Θ_R, of Fig. 35b tells us that there is one HT electron which may occupy either q_1 of N or k_1 of S. This is the *interstitial electron* and the interfragmental multicenter bond linking N and S to GT is the *interstitial bond*.

We now show that the type of bonding described by Θ_R is Ionic Overlap Induction, the monoelectronic analogue of Overlap Dispersion.

The principal contributor to Θ_1 is configuration Φ and the principal contributor to Θ_2 is configuration X shown below.
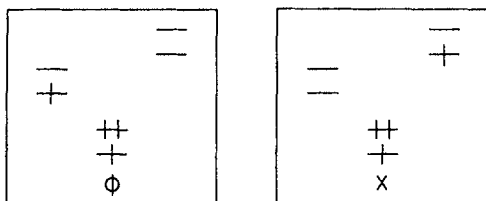
In order to simplify the problem, we consider the two odd electrons in the field of all the remaining nuclei and electrons (including the b_1 pair in r_2). Omitting normalization, we obtain:

$$\Phi = |r_1 \bar{q}| + |q_1 \bar{r}_1|$$

$$X = |r_1 \bar{k}_1| + |k_1 \bar{r}_1|$$

The interaction matrix element, H, is:

$$H = W + Y \tag{16}$$

where W is a negative overlap term which represents overlap bonding due to Relay Electron Transfer (RET), a correlated electron transfer mechanism, and Y is a negative induction term representing the polarization of one Li *atom* by a second Li *cation*.

$$W = \langle r_1 | k_1 \rangle \langle q_1 | \hat{H} | r_1 \rangle + \langle q_1 | r_1 \rangle \langle r_1 | \hat{H} | k_1 \rangle + (r_1 k_1 | r_1 q_1)$$

$$Y = \langle q_1 | \hat{H} | k_1 \rangle + (r_1 r_1 | k_1 q_1)$$

We now write an arrow representation of this matrix element, much as we did for the case of Overlap Dispersion. Note how an electron from q_1 ends up in k_1 by two different mechanisms ("routes") which operate "in-phase". The dashed arrow path represents RET and the single-solid arrow path represents induction.
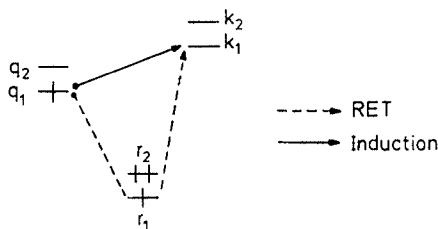
In summary, we read the resonance bond diagram Θ_R as implying that there is one electron permanently transferred from HT to GT so that it generates an electric field responsible for overlap induction which manifests itself by one *interstitial electron* and one *interstitial bond*. Induction-assisted RET bonding involving q_1 and k_1 is equivalent to DET bonding now involving an interstitial orbital, p, located at the midpoint of the line connecting the two Li centers.

8.1 The Electronic Structure of $(RLi)_4$

The resonance bond diagram, Θ_R, of D_{4h} $(RLi)_4$ (species *3* in Fig. 34) is shown in Fig. 36. We note the following:

(a) HT $= Li_4$ and GT $= R_4$ with one electron transferred from HT to GT and now occupying the r_4 MO of R_4.

(b) There are two interstitial electrons holding the four Li *species* (atoms and cations) together and two "full" interstitial e_u bonds and one "weak" interstitial a_1 bond (participation of only radial, q_i, MO's) fastening three R radicals on the Li network with a fourth R: anion being attached coulombically on the same Li network. The simplest Lewis structure corresponding to Θ_R is:
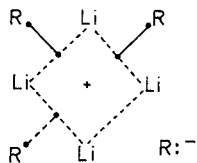
We now open a parenthesis in order to point out that the orbitals of N, S, and GT are "first-principles orbitals" which can be written without recourse to calculations. So, here is a set of clarifications:

(a) There are four radial MO's (q_1 through q_4) spanning the four 2s AO's and four more radial MO's (q_5 through q_8) spanning the four 2p AO's of the four Li atoms and these are drawn in Fig. 37a.
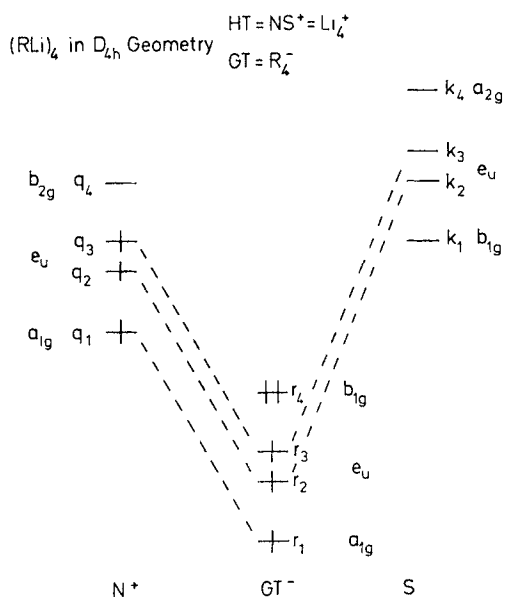
Fig. 36. Resonance bond diagram of R_4Li_4 (3)
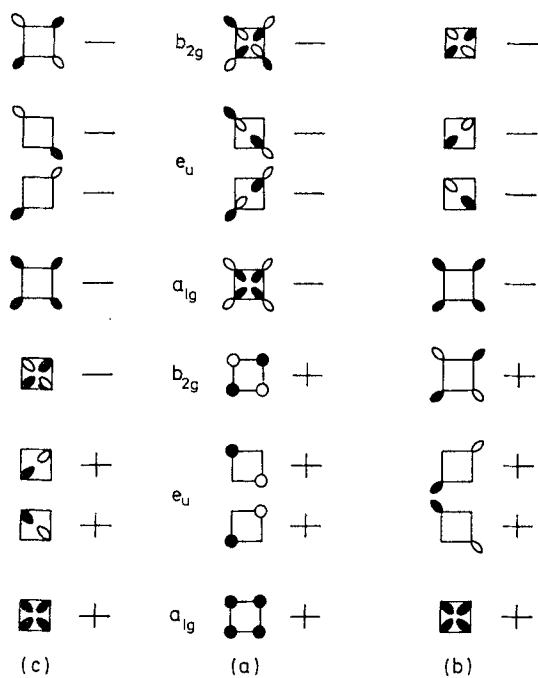
Fig. 37 a–c. (a) The radial 2s-type and 2p-types MO's of square Li_4 prior to interaction. **(b)** The resulting q_i MO's after mixing of the orbitals in **(a)** via overlap in square Li_4. **(c)** The resulting q_i MO's after mixing of the orbitals in **(a)** via induction under the influence of an electric field created by the expulsion of one electron, i.e., we are now dealing with square Li_4^+

131

(b) On symmetry grounds alone q_i (i = 1–4) can only interact with q_{i+4}. The type of mixing depends on the occupancy of the lowest four N MO's.

(c) If each of q_1 through q_4 contains one electron, then the mixing of the upper with the lower set, i.e., the mixing of q_1 with q_5, etc., will be determined by *overlap*. If the four Li's are brought close enough together so that there is appreciable overlap, one obtains the eight N MO's shown in Fig. 37b. Note the pattern of "outside" versus "inside" pointing of the resulting MO's. By contrast, if there are fewer than four electrons within q_1 through q_4, i.e. if Li_4 has lost one, two, or three electrons, and there is no appreciable Li—Li spatial overlap, one obtains the eight N MO's shown in Fig. 37c. The mixing of q_1 with q_5, etc., is now due to induction. Note how, in contrast to the previous case, q_1 through q_4 all point "inside".

(d) In $(RLi)_4$, the four Li stay sufficiently away from each other and one electron is transferred from Li_4 to R_4. Hence, the four lowest q_i orbitals shown in Θ_R of Fig. 36 are the ones displayed in Fig. 37c.

(e) The four tangential MO's of the S fragment spanning the four $2p_t$ AO's are shown in Fig. 38a.

(f) In the construction of the θ_R of $(RLi)_4$ shown in Fig. 36, we have used the schematic q_i and k_i MO's which are shown in Fig. 38.
The important thing to note is that none of these MO's of Fig. 38 encourages placement of the four R groups at the *corners* of an Li_4 square because none of the q_i's is directed strongly outward (as is the case with the "overlap hybrids" of Fig. 36b) and, of course, because the tangential k_i MO's dictate placement of R at the bridging sites. We believe that, once the art of drawing symmetry adapted MO's has been mastered, construction of cluster MO's is easy. What is more difficult is to expose how hybridization depends on electric charge and this can only be made transparent by a CI-type theory like MOVB theory. We end this digression by emphasizing that, of the q_i N MO's (i = 1 to n), "full interstitial MO's" are only those for which there is a corresponding k_i MO of the same symmetry in the S manifold. This last recognition will permit us to write bond diagrams using *only the 2s Li AO's* and immediately recognize the number of "fully" interstitial electrons. For example, we can rewrite Θ_R of Fig. 36 by omitting the S MO manifold while recognizing that only q_2 and q_3 have corresponding k_i MO's of the same

Fig. 38a and b. (a) Tangential, k_i, MO's of the Surface fragment. (b) Radial inwards pointing, q_i, MO's of the Needle fragment generated by induction

symmetry (k_2 and k_3). Asterisks placed next to the appropriate MO's (q_2 and q_3 in our example) will be taken to indicate that these are "fully" interstitial MO's containing "fully" interstitial electrons. Henceforth, in enumerating interstitial bonds, we will count only the "fully" interstitial bonds whenever a distinction between weak and full interstitiality can be made and we will use the term interstitial in this sense.

Ab initio calculations reveal that *3* is a bound tetramer of appreciable stability. However, the best geometry of $(RLi)_4$ is not *3* but *4* (Fig. 34). Construction of the resonance bond diagram for the geometry in which an Li_4 tetrahedron is face-capped by an R_4 tetrahedron reveals three interstitial electrons and three interstitial bonds (Fig. 39), as compared to two interstitial electrons and bonds in the planar system in which square Li_4 is sidecapped by square R_4. Hence, the tetrahedral geometry should be favored, as it is found to be the case [97].

We end this section by making two important points which one should keep in mind while examining the bond diagrams of clusters of the type discussed in this paper. The first is that the overlap and the induction components of the bonding may come both in one "installment", e.g. as two additive terms (W and Y) within a single energy expression (Eq. 10), or in two "installments", e.g. as two additive terms appearing at different stages of the construction of the final ground eigenstate. The former situation has been encountered in the case of $(RLi)_2$ and the latter one in the case of $(RLi)_4$ with the difference being due to the fact that Ionic Overlap Induction is due to the mixing of HT s and pσ with themselves and with GT AO's in $(RLi)_2$ while it is brought about by the mixing of HT s, p_r, and p_t with themselves and with GT AO's in D_{4h} $(RLi)_4$ and we arbitrarily defined pσ to be a tangential AO in $(RLi)_2$ when we could as well have chosen pσ to be a radial AO. The

$(RLi)_4$ in T_d geometry   HT = NS$^+$ = Li$_4^+$
GT = R$_4^-$

Fig. 39. Resonance bond diagram of R_4Li_4 (*4*)

physical mechanism which corresponds to Ionic Overlap Induction in D_4 $(RLi)_4$ can be described as follows:

1. Transfer of one electron from the Li_4 host to the R_4 guest fragment creates a charged circle, Li_4^+.

2. The electric field of the charged circle dictates that the lower "s-type" radial MO's mix with the upper "p-type" radial MO's in the N fragment so that each lower energy radial MO, q_1 to q_4, ends up pointing inside the circle. At this stage, we have bonding due to induction.

3. The r_i MO's of R_4^- can now overlap with the lower energy N radial MO's, q_i, as well as with the S tangential MO's, k_i, of Li_4^+ in order to create interstitial bonding due to RET if all three MO's, q_i, r_i, and k_i have the same symmetry. However, RET is now unassisted by induction (which has already set up RET by causing the lower q_i's to point inside the circle) because the electric field of the Li_4^+ circle cannot induce the separate mixing of q_i and k_i, i.e., we have an analogous situation to that described by Eq. (1) only now Y is zero but this term has already appeared in the equation describing the stabilization of the host Li_4^+ due to induction through the mixing of the "s-type" and "p-type" radial MO's.

4. In summary, induction turns the low energy radial MO's of the N fragment inside. As a result, each R group can be deposited on the bridging sites so that an r_i MO of R_4^- can now overlap with both a q_i MO of N (due to induction) as well as a k_i MO of S.

A second important point that should be finally made is that the q_i MO's of Fig. 37b and 37c have been drawn assuming overlap but no induction in the former and induction but no overlap in the latter. A comparison of the MO shapes reveals that, in an intermediate situation, the two mixing mechanisms will operate either in phase (e.g. q_1) or out-of-phase (e.g. q_2, q_3, q_4) and, in the latter case, one or the other will dominate. We will come back to this point later on.

8.2 Examples of Interstitial Bonding

If $(RLi)_4$ is viewed as $(Li_4)^+(X)^-$ where $X^- = R_4^-$, then Fig. 40 clearly shows that $^4R_4^-$ is isosynaptic to ground $^4C^-$ and $^6C_2^-$! That is to say, all of $^4R_4^-$, ground $^4C^-$, and ground $^6C_2^-$ have three singly occupied MO's which precisely match the three singly occupied t_2 MO's of the $^4Li_4^+$ tetrahedron in defining three interstitial bonds. Hence, we predict that tetrahedral CLi_4 is neither covalent (like CH_4) nor ionic $(C^{-4}Li_4^{+4})$ and that one low energy form of triplet C_2Li_4 will have a completely different structure from triplet C_2H_4 which will look as if one end of the C_2 moiety has penetrated a face or a side of an Li_4 tetrahedron, e.g. structure 5 shown in Fig. 34. However, there is one key difference: Interstitialization in $(RLi)_4$ is due to tangential and radial AO's (Overlap Induction) while in CLi_4 it is due only to tangential AO's (i.e., there is *no* Overlap Induction). This critical point is dicussed in section X.

The preferred structure of $(RLi)_4$ is the "cubane" structure 4 with an associated count of *eight* electrons. However, construction of the resonance bond diagram reveals that exactly the same bonding mechanism will occur for a count of
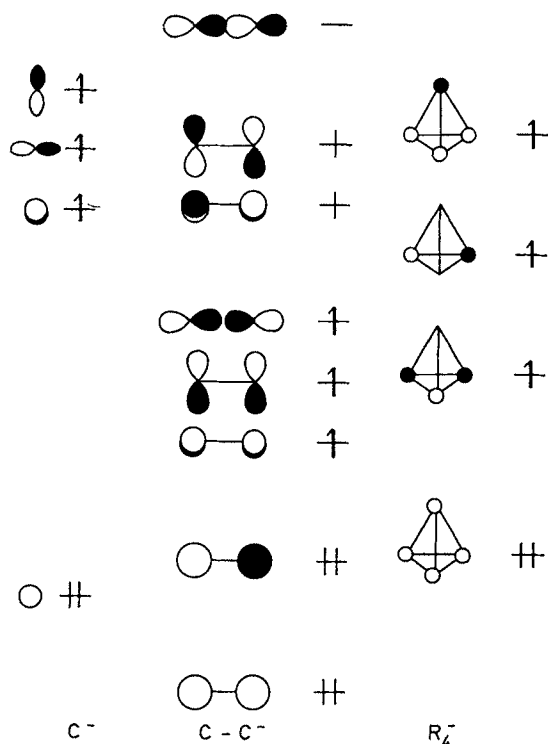
Fig. 40. Illustration of the isosynaptic relationship of ground $^4C^-$, $^6C_2^-$, and $^4R_4^-$. The three electrons shown in boldface are contained in MO's which have the right symmetry for matching three singly occupied t_2 MO's of tetrahedral Li_4^+, thus generating tetrahedral CLi_4, 5, and 4, respectively

sixteen electrons, if low lying vacant metal AO's participate in the bonding. Indeed, $(Pb^+)_4(OH)_4$, which can be viewed as $(Pb^+)_4^+(OH)_4^-$, is known to have a "cubane" structure [98]. Furthermore, it should be noted that, according to the isosynaptic relationship, both $Re(CO)_2$ and CuL ($L = AsEt_3$) are analogous to Li. As a result, $[Re(CO)_2]_4H_4$ and $(CuL)_4I_4$ have exactly the same structure as Li_4R_4 [99, 100].

With this background, it is now easier to appreciate how Ionic Overlap Induction differs from the conventional covalent and ionic bonding models.

(a) Unlike other bonding mechanisms, Ionic Overlap Induction combines overlap, induction, and ionic bonding operating "in-phase" in one package. If any one of the three ingredients becomes unsatisfactory, this bonding mechanism is replaced by ionic bonding, if the constituent atoms have very different electronegativities, or, by Overlap Dispersion, if the opposite is true. An example may be the change of geometry as one goes from $(CH_3Li)_4$ to $(CH_3K)_n$ [101].

(b) Ionic Overlap Induction is the bonding type exemplified by $(RLi)_4$ but it is overlap bonding that is exemplified by the "aromatic" H_3^+ although both species are commonly referred to as "electron deficient". The tendency of boron towards bridging (absent in stable organic molecules) can be ascribed to the lower 2s → 2p promotion energy relative to carbon [102]. The fact that close boron polyhedra have the guest attached to the vertices of the host [e.g. $HT = B_6^{-2}$, $GT = H_6$ in $(BH)_6^{-2}$]

135

speaks in favor of overlap bonding. Thus, it is very likely that diborane exemplifies overlap bonding (much like H_3^+) with Ionic Overlap Induction becoming dominant in Al_2Cl_6.

(c) We can represent Li_2^+ with the interstitial electron in the σ_g symmetric (S) MO as in F and Li_2^+ with the interstitial electron in the σ_u antisymmetric (A) MO as in G.

$$Li\text{———}\bullet\text{———}Li^+ \qquad Li\!\!\!\overset{\frown}{}\!\!\!Li^+$$
$$\quad\;\; F \qquad\qquad\qquad\qquad G$$
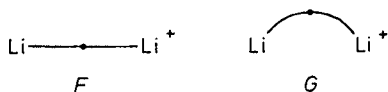
We expect the preferred structure of $CH_3Li_2^+$ will be the one in which planar CH_3 radical, with maximally strong C—H overlap bonds, makes an interstitial bond with Li_2^+ (G). This is much better than having a pyramidal CH_3 radical, with weakened C—H overlap bonds (due to the greater 2p AO character of the carbon valence AO's form an interstitial bond with Li_2^+ (F). Schleyer and coworkers have performed calculations which indicate that $CH_3Li_2^+$ prefers a D_{3h} geometry rather than the "nonclassical" C_s geometry preferred by CH_2^+ [103]. The antisymmetric interstitial bond of D_{3h} $CH_3Li_2^+$ is shown in bond diagrammatic form in Fig. 41 a.

There exist two intresting experimental facts that are compatible with the concept of the Ionic Overlap Induction. First, NMR experiments have revealed that *there is* ^{13}C—^7Li [104] but *there is not* ^6Li—^7Li [105] spin-spin coupling in $(CH_3Li)_4$. The presence of the former is the result of the interstitial *overlap* bond while the absence of the latter is the result of induction *(non-overlap)* binding of Li and Li^+. The second point is that the MOVB analysis suggests that a transition from Ionic Overlap Induction to pure ionic bonding should be observed as the electronegativity of X in $(LiX)_n$ increases. This proposal is very much consistent with computational
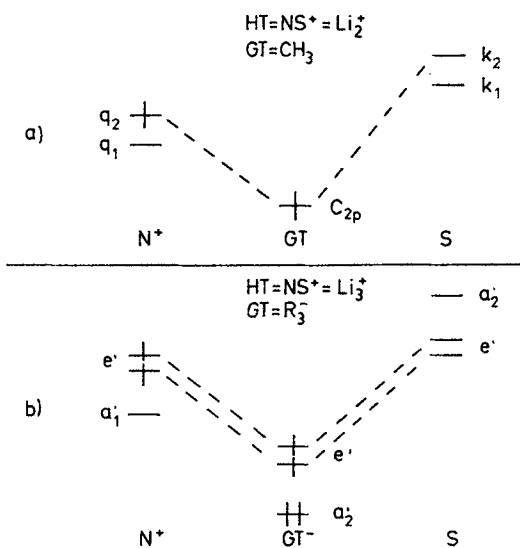
Fig. 41a and b. Resonance bond diagram of $CH_3Li_2^+$ (a) and R_3Li_3, *2* (b)

data [106a)] which show that the MIX term in a Morokuma-style investigation of the principal mechanism of binding in $(LiX)_n$ is extremely large when X is electropositive (e.g. X = BeH) and negligible when X is highly electronegative (e.g. X = F). Furthermore, the fact that a classical electrostatic model predicts that the LiX tertamer (X = F, OH, NH_2, etc.) will prefer a D_{4h} rather than the observed and calculated T_d geometry [106b)] is testimony of the fact that Ionic Overlap Induction dies out slowly and that even at the ionic limit there is some small, yet stereochemically meaningful, tendency for electron "interstitialization".

8.3 Dilithiomethane and the Organometallic Banana Bond

We can represent Li_2^+ by one VB structure which immediately tells us that Li_2^+ is a building block with one interstitial electron residing in an *Interstitial Orbital* (IO) placed *between* the two atomic nuclei. Now, by using a conceptual minimal IO basis set, we can represent doublet Li_2^+ is a similar fashion as illustrated below, each circle representing an IO.
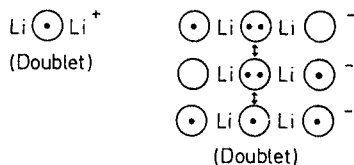
We now illustrate how we go about constructing an IO basis set for two prototypical systems, Li_2^+ and Li_2^-. The first step is the construction of symmetry adapted group orbitals, x_i. Omitting normalization and denoting 2s by s and 2pσ by p, we have:

$$x_1 = s_1 + s_2$$
$$x_2 = s_1 - s_2$$
$$x_3 = p_1 + p_2$$
$$x_4 = p_1 - p_2$$

These orbitals are now allowed to mix through a Hamiltonian which describes the electric field produced by one electron and two positive cores in Li_2^+ and a Hamiltonian which describes the electric field produced by three electrons and two positive cores in Li_2^-. The resulting symmetry adapted MO's differ in the two cases and they are given by the following expressions, in which the upper sign of y_2 and y_4 pertains to the Li_2^+ case and the lower sign of the same orbitals to the Li_2^- case. Clearly, the MO's of the two species are different as a result of the different active electric fields in the two cases.

$$y_1 = x_1 + \lambda x_3$$
$$y_2 = x_2 \mp \lambda x_4$$
$$y_3 = x_3 - \lambda x_1$$
$$y_4 = x_4 \pm \lambda x_2$$

The final step is hybridization of y_3 and y_4 in Li_2^+ and of y_2 and y_3 in Li_2^- to produce two new orbitals, t_3 and t_4 in Li_2^+ and t_2 and t_3 in Li_2^-, which together with the unperturbed y_i MO's form a set of IO's, t_i, which we may now use for writing Lewis structures for molecules which contain L_2^+ or Li_2^- building blocks or analogous one- or three-electron fragments. The entire process is schematically depicted in Fig. 42. The shapes of the IO's are drawn in Fig. 43. For most problems of interest, Li_2^+ within a molecule can be described using only t_1 or t_2 and Li_2^- within a molecule can be treated using only t_1, t_2, and t_3. A warning of utmost importance: All analyses should be made using the symmetry adapted y_i MO's and then translated into IO (t_i) language. Failure to do so and unwarranted simplification (e.g. assigning one spherical IO per Li atom in an Li_n cluster) is bound to lead to erroneous conclusions regarding molecular electronic structure. With this background, we will now investigate the bonding of a "simple" organometallic monomer. Dilithiomethane.

Consider triplet methylene and singlet Li_2 put together to make dilitiomethane by the MOVB procedure: We argue that one electron will be transferred from Li_2 to $^3CH_2$ so that coupling of the two resulting radical ions will yield a molecule which can be represented by the formula shown below. The predicted shape is a highly distorted tetrahedron with a large LiCLi angle or a planar structure with a much smaller LiCLi angle. In the tetrahedral geometry the two radical ion fragments are joined by a "b_2" interstitial bond. In the planar geometry, the interstitial bond
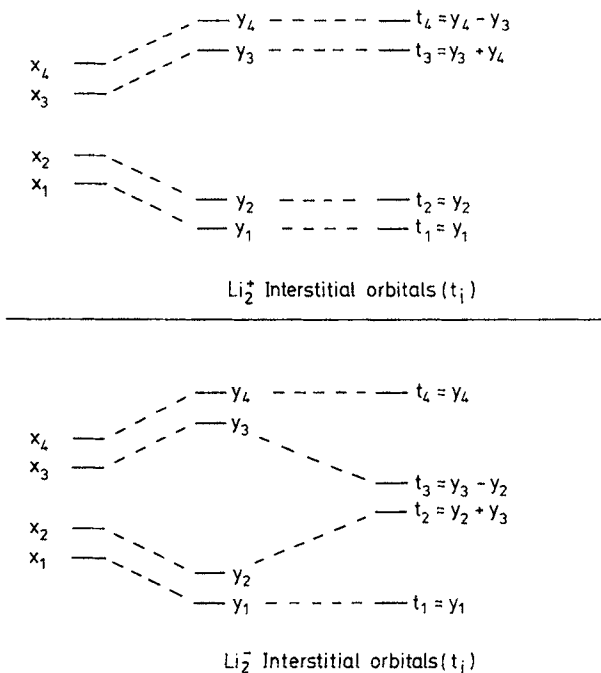
Fig. 42. Generation of Interstitial Orbitals (IO's) starting from canonical atom-centered orbitals, x_i, as described in the text

has a_1 symmetry. The notation $t_1 \rightarrow a_1$ means "t_1 upon symmetry adaptation yields an a_1 MO".
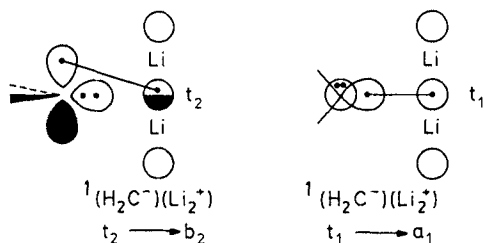
What will be the structure of the lowest energy triplet state? To make the ground singlet state we obeyed the wishes of the electropositive Li_2 to be transformed to interstitial Li_2^+ by donating one electron to $^3CH_2$ so that ultimately interstitial bond formation joining the resulting radical ions produces the most stable species. To make the ground triplet state the direction of charge transfer is simply reversed: We now transfer one electron from $^3CH_2$ to Li_2 to generate the stable interstitial $^2Li_2^-$ which needs comparatively small energy to be promoted to the interstitial $^4Li_2^-$ having the configuration $2\sigma_g^1 2\sigma_u^1 1\pi_u^1$. Coupling of $^2CH_2^+$ and $^4Li_2^-$ by one interstitial bond results in the formation of a molecule which can be represented by the formula shown below. The predicted shape is either a distorted tetrahedron or a distorted planar system with the remarkable property that the Li_2 unit is negatively charged against all intuitive ideas based upon the notion of ionic bonding. In both geometries, there is one "a_1" interstitial bond.
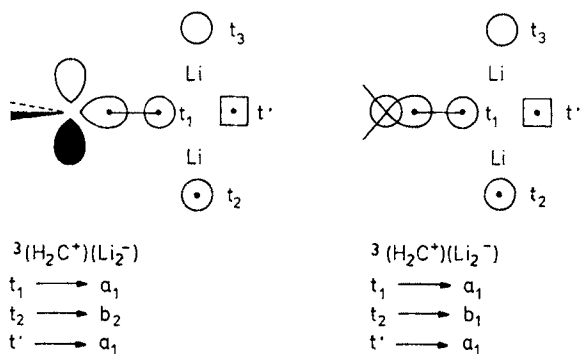
We say that singlet as well triplet CH_2Li_2 is bound by *Overlap Induction*, i.e. induction "interstitializes" the electrons of the ion metallic fragment and these are then used to form covalent interstitial bonds with the second nonmetallic or semimetallic fragment. These ideas are consistent with calculational results of Schaefer and Laidig [107] which predicted the following:

(a) Singlet and triplet tetrahedral CH_2Li_2 are separated by a very small energy gap and the same is true for singlet and triplet planar CH_2Li_2. This implies that *both spin isomers at a fixed geometry have the same number of covalent bonds*, a situation in contrast to that encountered in organic chemistry where the lowest triplet state has one less covalent bond than the singlet ground state with the geometries of the two
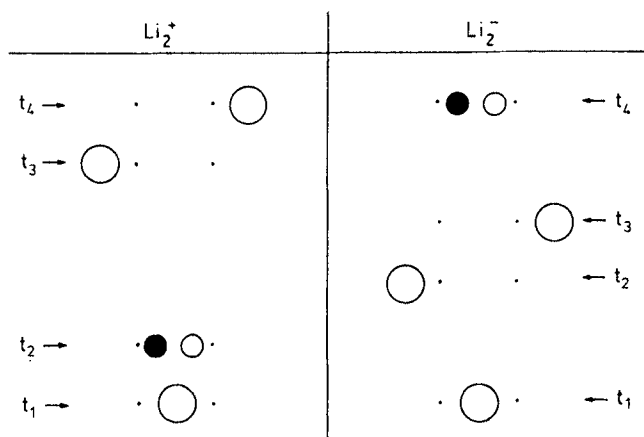
Fig. 43. The shapes of the interstitial orbitals of Li_2^+ and Li_2^-

species being radically different (e.g., planar singlet D_{2h} ethylene is about 3.3 eV more stable than perpendicular triplet D_{2d} ethylene) [77]. The reason for this is that both spin isomers, in either tetrahedral or planar geometry, have two normal C—H overlap bonds and one interstitial bond.

(b) The calculated dipole moments clearly demonstrate that the CLi bonds have C^-Li^+ polarization in the singlet but, astoundingly, C^+Li^- polarization in the triplet states.

(c) The LiCLi angle is 120.3° in the tetrahedral and 101.7° in the planar singlet reflecting the fact that the interstitial bond in the former uses a carbon 2p AO while that in the latter a carbon sp^2 AO. For exactly the same reason, the C—Li bond is much shorter in the planar than in the tetrahedral $^1A_1$ form.

A word of caution: The atomic charges we use are *formal charges* assigned by considering the dominant electronic configuration of the molecule in question. Because of the considerable radial extension of metal AO's, the integrated electron density may be considerably different. Also, additional polarization effects will play a role in shaping the final electron densities, e.g. the t' odd electron of Li_2^- will most certainly be polarized towards the CH_2^+ unit in triplet CH_2Li_2 and the same will be true of the electron pair bond of a_1 symmetry.

In our discussion above, we payed special attention to the interstitialization mechanism and some of its physical consequences. We now add a layer of important details which will enable us to make specific "hard" predictions which computations can test. Specifically, we recognize that, in describing the singlet dilithioethylenes, we neglected for the moment the contribution of the empty π_g and π_u MO's of the Li_2^+ units which have b_2 and a_1 symmetries and thus can hybridize with interstitial MO's of the same symmetry in tetrahedral and planar dilithiomethane, respectively. Focusing our attention on the planar species, we recognize that the complete bond diagram describing the bonding of the carbon to the two Li's will be:
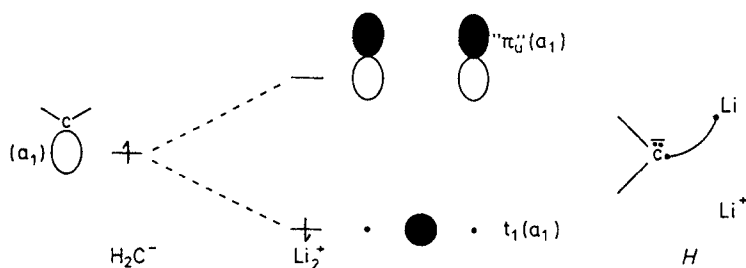
This diagram says that the odd electron on Li will spend part of the time between the two Li centers in the interstitial orbital t_1 and part of the time on top of Li in a 2p AO. Hence, the best Lewis formula describing this state of affairs is formula H which shows that one C—Li bond is actually a banana bond bent in the direction of the Li cation. The banana bond reflects that fact that one normal covalent bond has been inductively polarized by a neighboring cation. Its presence is indirectly attributable to the fact that the interstitial MO of Li_2^+ has no nodes.

The situation changes only quantitatively in the tetrahedral form. Here, the interstitial MO of the Li_2^+ unit has a node which means that the interstitial electron will be localized "inside" the Li—Li segment but close to the two nuclei. Hybridization of this t_1 with π_g will give rise to bonding that will very much resemble classical bonding. Namely, one C—Li covalent bond will be bent towards the Li cation to a very small extent so that now ionic overlap induction through present could be mistaken for classical bonding.

We can now make a number of predictions. Recognizing that the interstitial t_1 and the normal π_u MO of Li_2^+ play exactly the same roles in planar dilithiomethane as the radial interstitial and the tangential MO's in planar D_{4h} $(CH_3Li)_4$ and recognizing that the CH_2^- unit of dilithiomethane is monovalent like CH_3, we see that planar dilithiomethane resembles a fragment of planar D_{4h} alkyllithium tetramer. However, because the interstitial MO of a_1 symmetry of the former has no nodes while the interstitial MO's of e_u symmetry of the latter have one node (see Fig. 36 and 37), we expect banana bond formation to be much more pronounced in planar CH_2Li_2 than in $(RLi)_4$ in D_{4h} or T_d geometry and also than in tetrahedral CH_2Li_2. A "perfect" MCSCF calculation with a "perfect" orbital basis and full geometry optimization which is subsequently decoded by Bader's method [109] should reveal carbon—lithium bond paths in planar dilithiomethane consistent with banana bond formation. The same analysis will reveal deceptively normal—looking bond paths in the alkyllithium tetramers but it will inescapably lead to the dicovery of intuitively unexpected bond paths in other polylithio orbanometallics. For example, planar CH_2Li_2 should dimerize with two banana C—Li bonds effectively fusing to form a bond path connecting two negatively charged carbons. This is what recent calculations suggest [110] and a detailed discussion will be presented elsewhere.
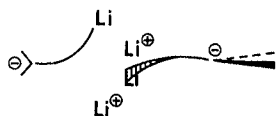
The bonding of polylithioalakanes is not pure ionic and the operationally significant formulae describing them are not point-charge formulae. In our discussions, we have made no commitment regarding the extent of single electron transfer from Li_2^+ to CH_2^- within the interstitial bond. Rather, we claim that such a bond exists no natter how polarized it may be, i.e. the operationally significant formula of dilithiomethane is (CH_2^-) •—• (Li_2^+) and not $(CH_2)^{-2}(Li_2)^{+2}$. Obviously, as the interstitial bond becomes more ionic, banana bond formation will tend to disappear.

8.4 Anti Ionic Overlap Induction

Consider our exemplary D_{4h} alkyllithium tetramer in which one unit of electron charge has been transferred from the Li_4 to the R_4 fragment. We can view this species as an inner spherical shell containing four positively charged ($+0,25$ charge) lithia plus an outer spherical shell containint four negatively charged (-0.25 charge) alkyl groups. Restricting our attention to the radial AO's of s and p type (radial s/p basis), it is clear that the electric field generated by this charge distribution will cause the mixing of p into s AO's so that the resulting hybrid AO points *inside the inner sphere* thus localizing electrons between Li centers. This becomes responsible for interstitial bonding. In a pictorial fashion, we can symbolize the process as shown in Figure 44a: Three conventional covalent R—Li bonds have been polarized by the R^-Li^+ dipole in (a).

Tetrahedral CLi_4 in which one unit of electric charge has been transferred from Li_4 to C is the inside-out version of the above. Now, the inner spherical shell contains the carbon nucleus at its center with the carbon AO's reaching to the surface of a sphere which is charged with one unit of negative charge and the outer shell contains four positively charged ($+0.25$ charge) lithia. If only a radial s/p basis is used, the electric field now causes formation of a hybrid Li AO which points *outside the outer sphere*. The Li electrons are no longer interstitialized and they are placed on top of the Li centers. This inductive mechanism now operates in direct opposition to overlap bonding between C and Li as illustrated in Fig. 44b. That is to say, strong C—Li overlap requires that s mixes with p with one sign (with the resulting hybrid pointing *inside the outer sphere*) while induction requires that it mixes with the opposite sign. We call this phenomenon Anti Ionic Overlap Induction. Changing from an s/p to an s/p/d radial basis changes the situation: Now, mixing of s with d_{z^2} can cause interstitialization as illustrated in Fig. 44c. However, the key difference between CLi_4
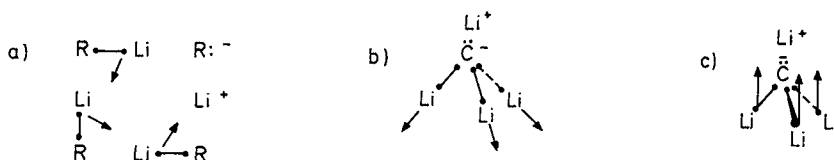
Fig. 44a–c. The way in which an electric field set up by a single electron transfer from lithium to carbon polarizes the valence electrons of the remaining Li atoms engaged into "covalent" bonding with carbon. Arrows indicate how the Li electron will move under the influence of a field. (a) $(RLi)_4$ case (b) CLi_4^- with no d-orbital involvement. (c) CLi_4^- with d-orbital (and higher energy orbital) involvement

and $(RLi)_4$ remains: The former enjoys Overlap Induction while the latter is unlikely to escape Anti Overlap Induction.

The above considerations lead to the formulation of a rule: The preferred geometry of an M_xA_y species in which M is metal atom and A is, e.g. H, B, C, N, O, or F or a group made up of these atoms will be the one in which M_x forms an inner core to which an outer mantle of A_y is attached. It is only in this way that Ionic Overlap Induction can occur "within" an s/p radial basis. Application of the rule to CLi_4 predicts the C_{2v} or C_{3v} geometry shown below in which three multicenter bonds connect carbon anion with Li_4^+ with the carbon lone pair pointing away from the Li_4^+ unit. The C_{2v} is the geometry featured by the hypervalent SF_4 and found to be preferred by $SiLi_4^{111}$ which lies further away from the ionic limit than CLi_4.

C_{3v} C_{2v}
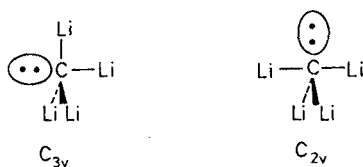
Some things need to be emphasized:

(a) A proper account of polarization can only be given by a complete metal AO basis up to the continuum. Our discussion of the s/p and s/p/d AO bases have only qualitative significance. Interstitialization can only be well reproduced by a complete s/p/d/etc. basis.

(b) Dispersion and induction depend on the polarizability of the atoms which constitute a molecule, i.e. they depend on the spectrum of the excited states of each atom. Replacement of, say, Li by the isoelectronic Be^+ will tend to annihilate Overlap Induction (and Overlap Dispersion) or Anti-Overlap Induction (and Anti-Overlap Dispersion) because the 2s → 2p promotion energy increases from 14,903 to 31,928 wave numbers. Atom oxidation is an excellent way for switching from a polarization-dependent bonding mechanism to bonding via "spin-pairing" because this tends to institute large gaps between the atomic states.

(c) The new idea described and emphasized in this chapter is Overlap Induction. Because the bond diagram of each interstitially bound molecules contains the configuration which when taken by itself described pure ionic bonding (e.g. to obtain $H_2C_2^{-2}Li_2^{+2}$ transfer one electron from t_2 to C2p in the MOVB formula for tetrahedral dilithiomethane given in Sect. 9), there is a continuum connecting interstitial bonding with pure ionic bonding. Because of the large electropositivity of Li, organolithium species may not be the best illustrators of interstitial bonding but we have used them to exemplify our approach in preference to organometallics containing less electropositive and/or more polarizable metal atoms because Li has one valence electron and four valence AO's so that the electron and orbital bookkeeping is relatively simple.

Part V. New Concepts

9 The MOVB Chemical Formulae

The Lewis concept of the electron-pair bond, invented before the birth of quantum chemistry, is still a dominant influence: The language of chemistry *is* the dash or dot formulae which represent how atoms are connected by bonds. In this work, we have introduced a new language and the formulae we write to represent molecules are no longer the Lewis ones. To emphasize this point, we show in Table 9 the formulae for typical nonmetallic and metallic systems which project their fundamental difference insofar as bonding is concerned.

(a) The formula for H_2 projects overlap bonding through "spin pairing"[112]. This is a typical Lewis electron-pair bond. By contrast, the formula for Li_2 projects homopolar ionic bonding discussed before.

(b) The formula for H_2^+ projects the fact that the bond is due to resonance interaction while the bond of Li_2^+ is really electrostatic with one electron flanked by two Li cations. To comprehend this difference consider what happens when $A^{\cdot}$ and A^+ (A = H, Li) are brought together from infinity to the equilibrium bond distance of A_2^+. In a first stage, the energy of AA^+ and A^+A drops due to induction

Table 9. Formulae for Nonmetallic and Metallic Chemical Systems

Nonmetallic	Metallic
H ⟵⟶ H	Li (⦂) Li
⊕ H ·H ⟵⟶ H· H ⊕	Li ⊙ Li⊕
$CH_2 = C = O$	Ni: ⟍ :CO

 a Carbon penetrates face of Li_4 tetrahedron. Alternative structure has carbon penetrate side of Li_4 tetrahedron.

and in a second stage there is the $AA^+ \langle - \rangle A^+A$ overlap interaction. In H_2^+, the first energy lowering is miniscule and the second comparatively large while the opposite is true in the case of Li_2^+. In formal language, we say that the CI defined below occurs predominantly via the induction p_{ij} matrix elements which are larger than the change transfer (overlap) d_{ij} matrix elements.

$$
\begin{array}{cccc}
p_x \; - & - \; p_x & - & - \\
s \; + & - \; s & - & + \\
\text{Li} & \text{Li}^+ & \text{Li}^+ & \text{Li} \\
\end{array}
$$

(with d_{12}, p_{14}, p_{23}, d_{34} labels)

$$
\begin{array}{cccc}
+ & - & - & + \\
- & - & - & - \\
\text{Li}^* & \text{Li}^+ & \text{Li}^+ & \text{Li}^* \\
\end{array}
$$
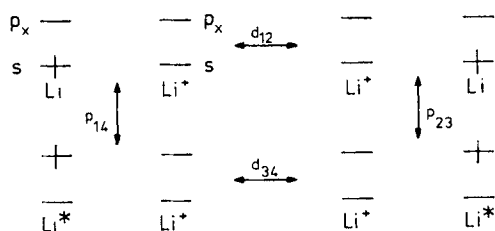
(c) Divalent triplet CH_2 can be coupled to divalent excited triplet $:C \equiv O$ to form $CH_2 = C = O$ by spin pairing. By contrast, though Ni and $C \equiv O$ can do just the same, their mechanism of bonding is entirely different approaching homopolar ionic bonding as indicated by our formula.

(d) The formula for, e.g. planar dilithiomethane is not the $H_2C^{-2}(Li_2)^{+2}$ representation but rather a formula which alerts the reader of the presence of interstitial (or, banana) bonding. Dilithiomethane is a qualitatively different problem compared to disubstituted methane where the substituents are first row non-metals.

(e) Triplet ethylene is D_{2d} but triplet tetralithioethylene is expected to be an overall zwitterionic triplet "carbene" with a quadruplet Li_4^+ cluster hosting a quadruplet carbyne at one end with an anionic carbyne (isoelectronic to $R-N$) on the other side.

We can now see the problems that plague methods which are currently in use:

(a) According to EHMO theory, the formulae of H_2 and Li_2 are qualitatively the same and the same is true of H_2^+ and Li_2^+. Furthermore, the formula of NiCO will be similar to that of CH_2CO, perhaps with dashed replacing the solid lines to imply "half-baked" covalency.

(b) GVB computations have been incorrectly interpreted by Goddard who suggests that Li_2 and Li_2^+ are similar to H_2 and H_2^+ insofar as bonding is concerned. The stronger bond of Li_2^+ compared to Li_2 is attributed to the fact that an electron pair bond depends on $2S^2$ while an odd electron bond on S (S = AO overlap integral) and when S is small the latter quantity is larger [113]. That this is wrong can be easily seen by the fact that ethylene has a stronger pi bond than ethylene radical cation despite the fact that the pi AO overlap is only 0.25 or so [114]. Li_2 is *not* a two-electron/two-orbital but rather a two-electron/four-orbital problem with the 2p AO's being critical for bringing into play overlap-independent binding mechanisms and the same holds true for Li_2^+. Here, I would like to point out that, though no specific reference can be given, the German theoreticians (W. Kutzelnigg, J. Hinze, and others) had long ago recognized that the stronger bond of Li_2^+ relative to Li_2 is due to the superiority of "one-electron over two-electron polarization".

(c) Falling back on conventional ideas, a number of workers have promulgated the notion of "ionic" bonding in organolithium species despite the fact that their stereochemical properties suggest otherwise. For example, at the limit of pure "ionic" bonding the energy separation of planar and tetrahedral dilithiomethane should approach zero and this should remain insensitive to substituent effects. The fact that replacement of the two hydrogens can enhance or reverse the preference for tetrahedrality signals that something more is involved [115].

Computational chemists will readily attest that it is nowadays hard to compute metal clusters but trivial to compute ground state closed-shell organic molecules. On the other hand, we have seen that it is equally hard to *understand* the electronic structures of metals and alkanes. The MOVB formulas for methane and derivatives differ from the Lewis structure in a fundamental way:

$$2 \overset{\overset{\displaystyle H}{|}}{\underset{\underset{\displaystyle F^*}{|}}{F-C}}-H^* \longrightarrow \overset{\overset{\displaystyle F}{|}}{\underset{\underset{\displaystyle F}{|}}{F-C}}-F \quad + \quad \overset{\overset{\displaystyle H}{|}}{\underset{\underset{\displaystyle H}{|}}{H-C}}-H$$
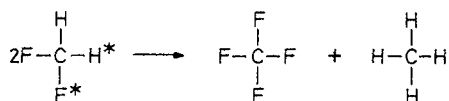
H* is "H admixed to F" and F* is "F mixed with H" so that neither H* is a sigma donor nor F* a sigma acceptor any longer. The meassage of these new formulas is very straightforward: In order to bypass the necessity of ligand "contamination" so as to avoid bond interference and create the strongest possible C—H and C—F bonds, electronegative groups should be attached on the same carbon. Replacement of F by CH_3 leads to an analogous situation and the formation of a simple rule for predicting the most stable structural isomer of an *alkane*: The most stable structural isomer is predicted to be the one which has the largest number of methyls per carbon. Thus, for example, isobutane is more stable by roughly two kcal/mole relative to n-butane because of greater aggregation of methyls on a single carbon.

10 New Stereoelectronic Concepts for Organic Reactions

The concepts outlined in Sect. 5 and in related published papers can be put to work in order to uncover new stereoselectronic principles of organic chemistry. We illustrate our approach by reference to the cyclobutene → 1,3-butadiene pericyclic transformation which, according to the Woodward-Hoffmann rules [60], proceeds thermally in a conrotatory fashion. The detailed theory has been presented in Chapter 15 of ref. 14.
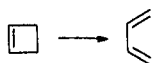
We begin with two background items:
(a) In CH_2, a 90° rotation of the H_2 unit can be defined which amounts to maintaining a sigma-type bond connecting carbon and H_2 while replacing a pi-type bond

formed via the $2p_z$ by one formed via the $2p_y$ carbon AO. The MOVB bond diagrammatic representation of this process, called pi rebonding, is shown in Fig. 45a. It is now immediately obvious that, if the positions of the four carbons of cyclobutene remain fixed, the ring opening raction shown above can be thought of as rebonding of two H_2 units attached on C_3 and C_4.
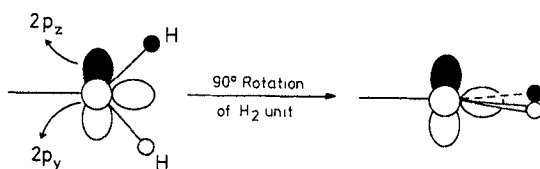
(b) The overlap of two nodeless symmetry MO's is maximized if the atoms spanned by one are "inside" those spanned by the second. If the two symmetry MO's possess one node, their overlap is maximized if the first set of atoms are outside those of the second set. This point is schematically illustrated in Fig. 45b.

We begin by constructing the principal bond diagrams for the reactant cyclobutene and the product which, for the time being, we take to be Cisoid-1,3-butadiene. Each species is viewed as "C_4 plus H_6" and the reaction itself is visualized as synchronous 90° rotation of each of two H_2 units about the bisectors of the HCH angles on C_3 and C_4. The fragment orbitals will be either of sigma or pi symmetry and so will be the multicenter bonds connecting the C_4 and the H_6 fragment. Denoting pi and sigma C_4 MO's by π_i and w_i, respectively, and H_6 MO's by x_i, we obtain the diagrams shown in Fig. 46. For better
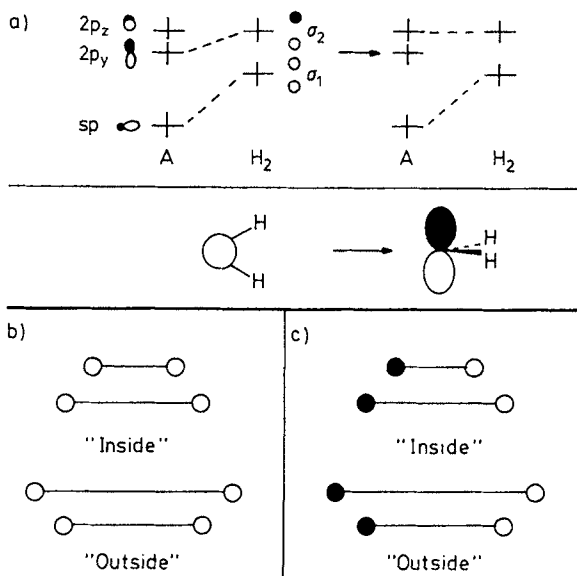
Fig. 45a–c. (a) Bond diagrammatic representation of pi rebonding. (b) The overlap of two nodeless MO's is stronger "inside". (c) The overlap of two antibonding MO's is stronger "outside"

comprehension, we have grouped the fragment orbitals into pi and sigma rather than drawing them in order of increasing energy. Furthermore, we have assumed that sigma orbitals of C_4 find their symmetry matches in H_6 in defining the sigma ponds linking the fragments. The symmetry aspect of pi bond formation (between C_4 and H_6) in cyclobutene is self-evident.

The next step is to identify the critical fragment MO's and associated electrons involved in the transformation. There are identified and they are drawn in Fig. 47 for the conrotation reaction intermediate complex. Accordingly, the critical electronic rearrangement occuring in going from reactant to product can be represented by the simplified (abridged) bond diagrams shown in Fig. 48. The abridged wavefunction of the conrotation transition state will be a linear combination of the bond diagrams Θ_1 and Θ_2 (see Fig. 48) and additional extrinsic configuration, Φ_i, for the appropriate nuclear coordinates.

$$\Psi_{CON} = \lambda_1 \Theta_1 + \lambda_2 \Theta_2$$

We now address the problem first brought to focus of attention by the important work of Dolbier [116] and Kirmse and Houk [117] and their groups: Why is it that a cyclobutene in which each H_2 is replaced by XY undergoes conrotatory ring
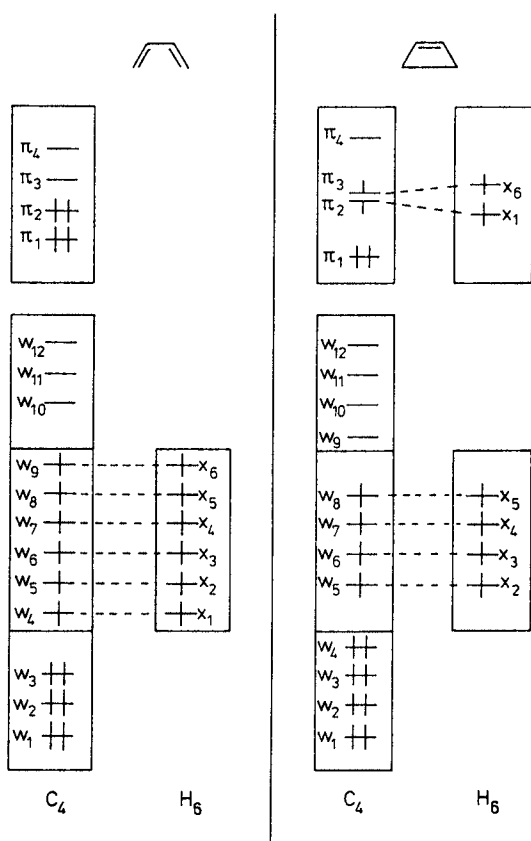
Fig. 46. Principal bond diagrams of 1,3-butadiene and cyclobutene (schematic)
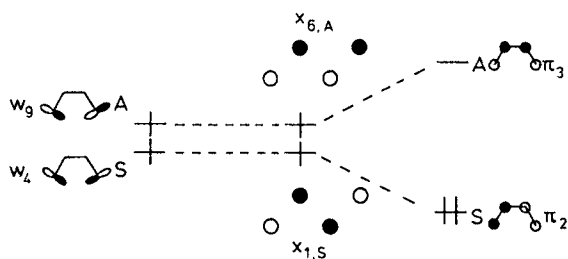
Fig. 47. The critical sigma- and pi-type orbitals involved in the conrotatory ring opening of cyclobutene
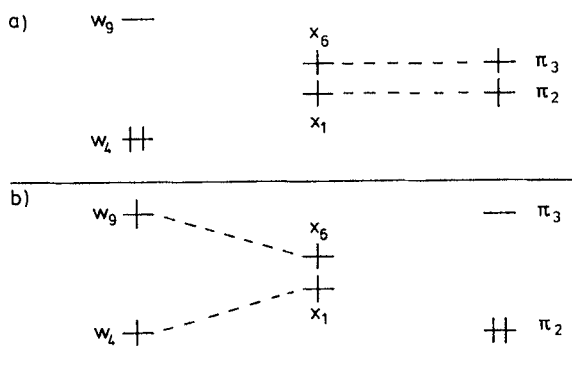
Fig. 48a and b. (a) Simplified bond diagrammatic representation of cyclobutene, Θ_1 **(b)** Simplified bond diagrammatric representation of 1,3-butadiene, Θ_2.

opening in such a way so that the more electronegative of X and Y end up rotating "outside" even if this may require that the bulkier Y rotates "inside"?
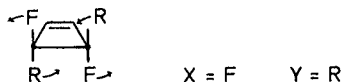
To answer this question, we observe that replacement of the two H_2 units by two HF units in cyclobutene will change four of the six H_6 orbitals, from x_1, x_6, x_3, and x_2 to m^*, m, n^*, and n as shown in Fig. 49, where in parenthesis we show the orbital of C_4 which matches each of them symmetrywise. For example, x_1 matches π_2 and together they define a core (C_4)-ligand (H_6) interfragmental bond, etc. We can now visualize clearly what will happen to the two critical bonds, $n^* - \pi_3$ and $m - \pi_2$, of trans-3,4-difluorocyclobutene as the system arrives to the transition state and rebonding begins to occur.

One may envision two different reaction paths which can take cyclobutene to the diene product. In one (Path A), the four carbons remain coplanar and rotation of the two H_2 units occurs while the $C_1C_4C_3$ angle opens up. This, of course, is
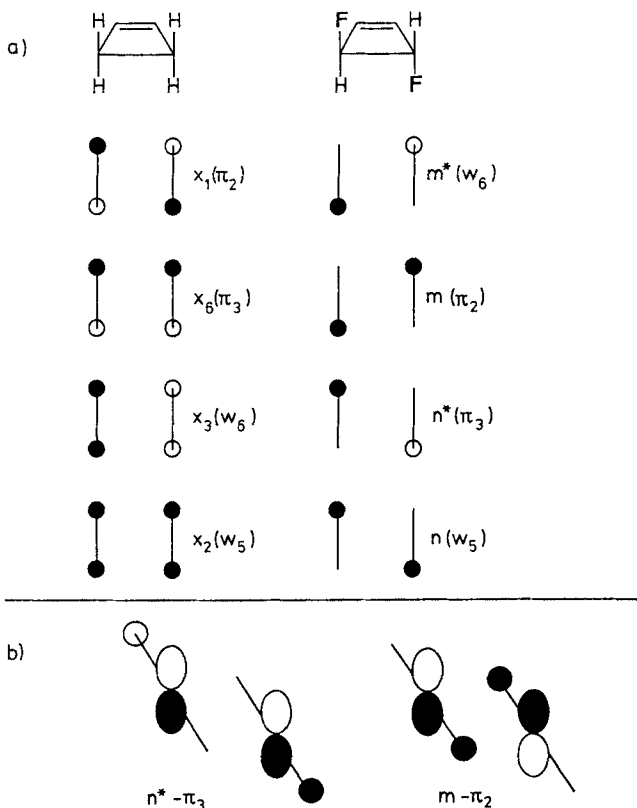
Fig. 49 a and b. (a) The way in which the H_4 ligand fragment MO's change in going to H_2F_2. In parenthesis, we indicate the matching core (C_4) orbitals with which the corresponding ligand fragment orbitals define a bond. (b) Optimal bond formation at the conrotation transition state requires "outside" rotation of F's (because the C_3—C_4 interaction is antibonding in π_3) and "inside" rotation of H's (because the C_3—C_4 interation is bonding in π_2)

unfavorable because it would lead to a highly congested cisoid diene. The second path (Path B), involves the same nuclear motions as before only now coupled to rotation about the C_1–C_2 bond, a process leading to a gauche and ultimately to a transoid diene. Clearly, this is a much more plausible path and this is what calculations bear out [118]. Returning now to our conrotatory transition state complex wavefunction, we can see that there are two dimensions to the problem:

(a) The stereochemistry of the reaction is determined by the symmetry labels of the orbitals x_1 and x_6. When they are S and A, respectively, reactant bonds transform to product bonds. This is the case of conrotation. If the labels ar inverted (disrotation), this is no longer possible. The situation, illustrated with appropriate diagrams, has been discussed in the original work using the ring opening of cyclopropyl cation as an example.

(b) If each H_2 is replaced by an HF unit so that now there is a choice between "inside" and "outside" conrotation of F or H in trans-3,4 difluorocyclobutene, the preferred motion is determined by the relative energies and nodal properties of the

π_2 and π_3 MO's at some intermediate stage. The optimal reaction path is the one for which one F_2 symmetry MO best matches the *higher energy* π_3 so as to *deplete* while one H_2 symmetry MO best matches the *lower energy* π_2 so as to *add* electron density to it in Θ_1, keeping in mind that F is viewed as a *sigma* acceptor and H as a *sigma* donor, in a relative sense. Now, this matching can occur for either plus 90° or minus 90° rotation of each HF unit but the preferred mode of rotation will be the one which maximizes the overlap of the paired orbitals. For the reaction path B defined above, the matching illustrated in Fig. 49 leaves no doubt about the choice: The F's must be "outside" so that their antisymmetric combination (n* MO) matches best (= maximally overlaps with) an orbital (π_3) which is $C_3 - C_4$ antibonding while, at the same time, the H's must be "inside" so that their symmetric combination (m MO) matches best an orbital which is $C_3 - C_4$ bonding (π_2). The reader may verify that Path A would create a preference for exactly the opposite. However, nonbonded repulsion of the "larger" F's will oppose this tendency. Nonetheless, a calculational test of this prediction may produce interesting results.

In conclusion, much like in Sect. 5, our explanations have to do with symmetry control of bond making and nothing to do with "steric effects", "coulomb effects", "lone pair effects", etc., as suggested in the literature. The inside-outisde orbital overlap differentiation is identical in spirit to the one implied by the work of Bürgi and Dunitz [119]. Sections 5, 6, and 10 define a new organic sigma stereoelectronic theory. In sharp contrast to metallic systems, symmetry arguments alone suffice in dealing with the problems defined in these three sections and so we expect the trends to be well reproduced by EHMO calculations [120].

11 Electron Transfer in Biology

The principal configuration of the resonance bond diagram of $(RLi)_2$, i.e. the "picture" obtained by removing the dashed lines from Θ_R in Fig. 35, has a vacant q_2 MO in Li_2^+ and a half-occupied r_1 MO in R_2^-. Hence, sequential delivery of two electrons will place the first in the vacant q_2 (which is delocalized over the two Li's) and the second in the singly occupied r_1 thus creating an odd unpaired electron in q_1. Had the bonding of $(RLi)_2$ been completely ionic, the single configuration $R^{-2}Li^{+2}$ representing the system would have two equivalent holes in Li_2^{+2}. Hence, $(RLi)_2$ should display two different reduction potentials if it is bound by Ionic Overlap Induction but only one (or, better, two having the same value) reduction potential if it is bound by "classical" coulomb forces (ionic bonding limit).

With this background, we now turn our attention to the so-called Type III copper protein considered as a two-electron donor to molecular oxygen in the biological electron-transfer systems [121]. The characteristic feature of the Type III copper is the ESR non-detectable nature in spite of its divalent oxidation state. This has been attributed to the magnetic interaction between two copper(II) ions located in a proximity at the active site of the protein [122]. Accordingly, binuclear copper(II) complexes have been considered as possible candidates of models of the active site of Type III copper proteins. A few electrochemical studies have been carried out on binuclear copper(II) complexes and they revealed that these complexes are divided into two groups: i.e. those whose two copper(II) ions are reduced to copper(I)

at the same potential [123, 124], and those whose two copper(II) ions are reduced step-wise to copper(I) at different potentials [125, 126]. An example of the former group is the binuclear copper(II) complexes of the triketones, e.g. *9* (Fig. 34) [123]. A typical example of the latter group is the macrocyclic binuclear copper(II) complex *10* (Fig. 34) [125, 127]. These complexes show two reduction waves corresponding to the reductions to Cu(II)–Cu(I) and to Cu(I)–Cu(I). The differences between the two reduction potentials fall in the range of 400–700 mV depending on the sub-stituents R. Such a two-stepped reduction was explained in terms of the stabilization of the Cu(II)–Cu(I) state. In fact, the crystals of [Cu^{II}Cu^I (fsaltn)] ClO$_4$ were isolated and characterized. In this complex, the unpaired electron is delocalized over the two copper atoms, since the ESR spectrum in solution shows a seven-lined hyperfine
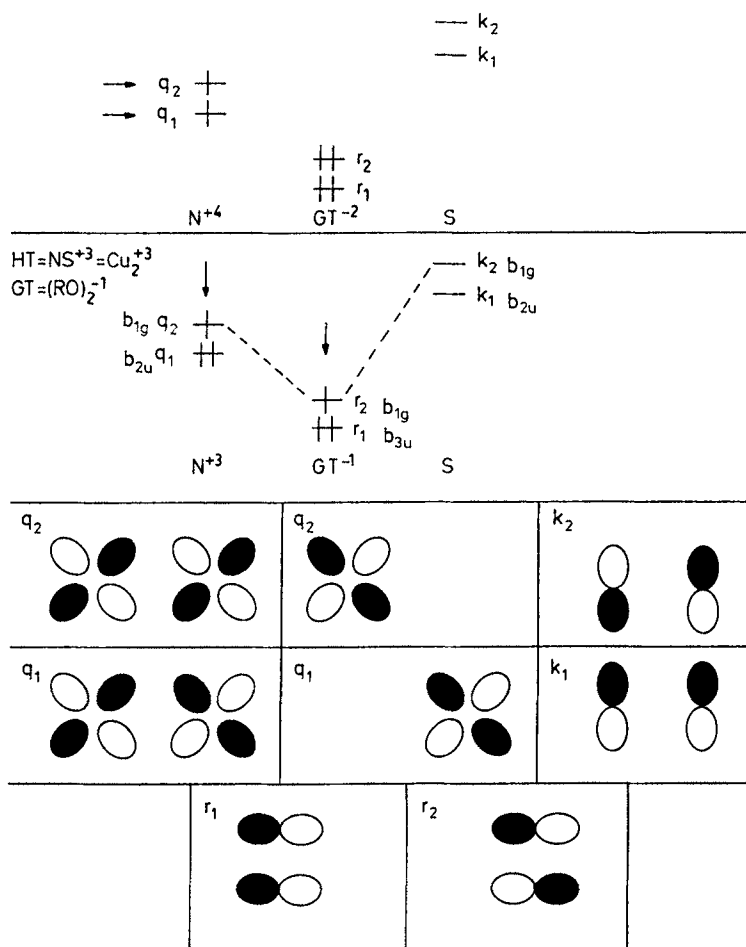
Fig. 50a and b. (a) Pure ionic binding of $(Cu^I)_2$ to $(RO)_2$. (b) Resonance bond diagram describing overlap induction in the same complex, $Cu_2(RO)_2^{+2}$. The various orbitals are drawn schematically with both permissible drawings of the q_i MO's shown. In the resonance bond diagram, we use the canonical q_i's (outer set) but this is only a matter of convenience

152

structure and the electronic spectrum shows an intervalence CT band at approx. 10×10^3 cm^{-1}.

The bond diagrams of Fig. 50 provide a simple explanation of these observations: In Fig. 50a, we portray the $(CuOR)_2^{+2}$ system as if it were ionically bound and we indicate by arrows how the reduction potential equivalence for converting each Cu^{+2} to Cu^{+1} comes about. In Fig. 50b, we portray the same system as if it were bound by Ionic Overlap Dispersion. Now, the first electron must be delivered to the empty q_2 and the second one to the singly occupied r_2 thus creating an odd unpaired electron delocalized on the two copper ions. In other words, one of the observed reduction potentials corresponds to reduction of oxygen atom! The intervalence CT band corresponds to promotion of an electron from q_1 to q_2. Our suggestion is that Fig. 50a is a description of the bonding of type *9* complexes and Fig. 50b is a description of type *10* complexes with the environment of the $(CuOR)_2^{+2}$ moiety determining whether pure ionic bonding or Ionic Overlap Induction will be the best bonding choice. Note how the ligands are much more electron rich, thus favoring unilateral presence of Cu^{+2}, in type *9* complexes.

12 Heterogenous Catalysis

The features of Ionic Overlap Induction, namely, the fact that it combines "inphase" coulomb attraction, charge-induced dipole stabilization, and overlap bonding necessitate a new language for the description of the chemical and physical consequences of this binding mechanism. By representing the total system under consideration as a Host-Guest composite, by realizing that each of the two fragments, HT and GT, has component atoms or subfragments (e.g. in $(RLi)_4$, HT $= Li_4$, GT $= R_4$, the components of HT are the four Li's, etc.), and by denoting a unit of positive charge by h^+ and a unit of negative charge by h^-, we recognize the following:

(a) $(RLi)_4$ can be written as $R_4(h^-)Li_4(h^+)$ or as $R_4(h^{-m})Li_4(h^{+m})$ where $1 \leqq m < n$. We do *not* know what the precise value of m will be in a given system but it should be such so that formation of the maximum number of full interstitial bonds is possible. Thus, $m = 1$ in T_d but m equals either one or two in $D_{4h}(RLi)_4$.

(b) Each of h^{+m} and h^{-m} is viewed as a particle. Circulation of one or more h^{+m} particles zips together by induction the "metallic" components of HT. By doing so, h^{+m} finds itself at various distances from h^{-m}, the optimum average inter-particle separation being determined by Coulomb's law.

(c) The components of HT are additionally fastened to the components of GT not only by the attractive interactions of h^{+m} and h^{-m} but also by multicenter overlap bonds.

(d) Interstitial electrons and interstitial bonds are the result of h^{+m} circulation within the metallic HT fragment under observation by h^{-m}. This circulation is overlap-independent and this is why HT-GT systems viewed through conventional conceptual lenses seem to be "hypovalent", "normal" (CLi_4), or, "hypervalent"

(CLi_6): The conventional concepts of bonding (and associated electron counts, valence considerations, etc.) break down because they are either *overlap* or *ionic* bonding concepts. Specifically, unlike the case of pure overlap binding in which different electron counts are associated with different geometries (e.g. Walsh rules for predicting the stereochemistry of AH_n molecules, etc.), different electron counts can now be associated with the same geometry. As evidence, we cite the cases of the prototypical $Mo_6Cl_8^{+4}$ and $Ta_6Cl_{12}^{+2}$ molecules (*12* and *13* in Fig. 9) for which the construction of resonance bond diagrams reveals the presence of three and five, respectively, interstitial bonds [128]. Now, it is well known that other species with different electron counts have the same structures as *12* or *13* as indicated in Table 10. The reason is that part of the bonding is due to induction (caused by the circulation of h^{+m} particles) and "classical" coulomb attraction, i.e. bonding is largely due to overlap-independent mechanisms which place either zero or, at best, small restriction on the electron count. In other words, the close energy spacing of the MO's of weakly bound systems makes possible the occupation of close lying orbitals by one, two, or more electron pairs with the final geometry being determined by the occupation of the critical interstitial MO's.

We will now consider the implications of the concept of overlap induction for heterogeneous catalysis. Specifically, we will examine the interaction of an ethylene

Table 10.

	Species		Electron Count[*]	Geometry
A	$Mo_6Cl_8^{+4}$	a	40	M_6 Octahedron in X_8 cube
	$Nb_6I_8^{+2,+3}$	b	36,35	M_6 Octahedron in X_8 cube
	$Ag_6(Ag^+)_8$	c	60	M_6 Octahedron in $(Ag^+)_8$ cube
B	$Ta_6Cl_8^{+2,+3,+4}$	d,b	40,39,38	M_6 Octahedron in X_{12} cube
	$Zr_6Cl_{12}^{0,+3}$	b	36,33	M_6 Octahedron in X_{12} cube
	$Sc_6Cl_{12}^{-3}$	b $\leftarrow$	33	M_6 Octahedron in X_{12} cube
	Pt_6Cl_{12}	e	72	M_6 Octahedron in X_{12} cube
C	Ge_9^{-2}	f	38	Sq. Tricap. Trig. Prism(D_{3h})
	Bi_9^{+5}	f	40	Sq. Tricap. Trig. Prism(D_{3h})
	Sn_9^{-4}	f	40	Sq. Cap. Antiprism (C_{4v})

[*] Electron counts, in families A and B, by assuming that each Cl or I is a one valence electron species and Ag^+ has zero valence electrons; [a] Brosset C (1946) Arkiv. Kemi Mineral. Geol. 22A: 1; [b] Corbett JD (1981) Acc. Chem. Res. 14: 239; [c] Kim Y, Seff K (1978) J. Am. Chem. Soc. 100: 6989; [d] Vaughan PA, Sturdivant JH, Pauling L (1950) J. Am. Chem. Soc. 72: 5477. Burbank RD (1966) Inorg. Chem. 5: 1491; [e] Brodersen K, Thiele G, Schnering HG (1965) Z. Anorg. Allgem. Chem. 337: 120; [f] Corbett JD, Critchlow SC, Burns RC (1983) Polyatomic zinc anions stabilized through crypt complexation of the cation. In: Cowley AH (ed) Rings, clusters, and polymers of the main group elements. American Chemical Society, Washington, DC

monomer with a platinum surface and we will attempt to write down a reasonable mechanism for the conversion of ethylene to ethane. We begin by defining the principal actors of the drama: These are the ethylene monomer and the Pt atom in any of the s^1d^9 (ground), or s^2d^8, or d^{10} electronic configurations realizing that these are separated by relatively small energy gaps. We can now see the following series of events:

(a) Ethylene is adsorbed on *one* Pt atom via Overlap Dispersion and this complex is electronically very similar to the Pt-Ethylene gas phase complex. [70]

(b) One Pt atom transfers one electron to ethylene (E) and the resulting radical anion, E^-, is coordinated to a Pt_2^+ unit in a manner completely analogous to the case of $(RLi)_2$, i.e. the E plays the role of R_2 and Pt_2, with two active 6s electrons, plays the role of Li_2, which has two active 2s electrons, one of which is relinquished to R_2 in the process of forming the $R_2^- Li_2^+$ species via ionic overlap induction.

$$
\begin{array}{ccc}
 & \overset{\displaystyle H_2}{\underset{\displaystyle C}{}} & \\
+1/2 & \big\uparrow & +1/2 \\
Pt & \big| & Pt \\
 & \underset{\displaystyle H_2}{(-1):\overset{\displaystyle \bullet}{C}} & \\
 & I &
\end{array}
$$
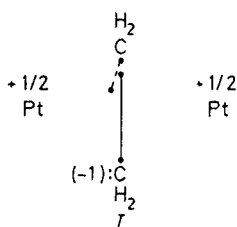
(c) A 1,2 hydrogen shift now occurs within *I*. The resulting product is *J* where CH_3CH is affixed by overlap induction on Pt_2^+.

$$
\begin{array}{ccc}
 & \overset{\displaystyle CH_3}{\underset{\displaystyle (-1):CH}{}} & \\
+1/2 & \updownarrow & +1/2 \\
Pt & & Pt \\
 & J &
\end{array}
$$
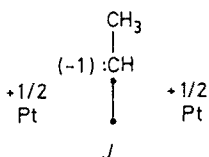
(d) The itinerant h^+, which glues together by induction not only the two Pt centers shown in *I* and *J* but also neighboring Pt atoms, renders one of the neightboring Pt's very reactive towards C—H oxidative addition. The reason is that this "activated" Pt is now partly positive and metal cations are known to insert very efficiently into C—H bonds [71]. Hence, we envision:

$$
\begin{array}{ccccc}
 & & \overset{\displaystyle CH_3}{\underset{\displaystyle (-1):\overset{\displaystyle \bullet}{C}}{}} & & \overset{\displaystyle H}{\underset{\displaystyle |}{}} \\
 & +1/2 & & +1/2 & \\
J\!-\!-Pt\!\longrightarrow\! Pt & & \updownarrow & Pt\!-\!-\!-\!-\!-\!-Pt & \\
\uparrow & & & & \updownarrow \\
\text{Neighbour} & & K & & \text{Neighbour}
\end{array}
$$
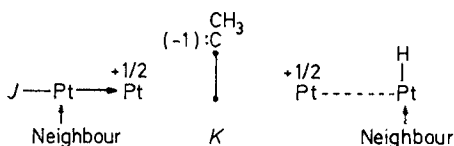
(e) K rearranges to L which is now analogous to $(RLi)_3$), i.e. 2 in Fig. 34.

$$
\begin{array}{ccc}
{}^{+1/3} & & {}^{+1/3} \\
Pt & CH_3 & Pt \\
& {}^{(-1)}\!C & \\
& Pt & \\
& {}^{+1/3} & \\
& L &
\end{array}
$$
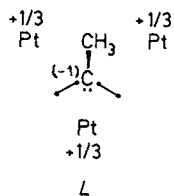
R_3^- within $R_3^- Li_3^+$ is isosynaptic to $CH_3\!-\!C^-$ within $CH_3 C^- Pt_3^+$ as can be deduced from the resonance bond diagram of $(RLi)_3$ given in Fig. 51. Pt is analogous to Li because both have an ns odd electron in their ground configurations. We propose that L is the correct electronic structure of the observed ethylidyne intermediate observed in the heterogeneous reaction of ethylene and hydrogen over Pt metal which chemists represent by conventional Lewis structures such as the one show below.
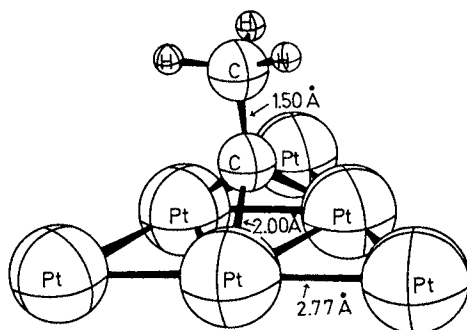
(d) Attachment of ethylidynes on the metal surface by Ionic Overlap Induction activates the metal surface by endowing it with itinerant h^+ particles. In turn, these cause interstitialization of hydrogen atoms originally attached on individual Pt atoms. As a result, we obtain:

$$
\begin{array}{ll}
CH_3 & \\
\mid & \\
:C(h^-) & (h^+) \\
\parallel & \quad\downarrow \qquad\qquad Pt\text{------}Pt \\
Pt_3\text{-----}Pt & \qquad\qquad\quad\uparrow \\
& \qquad\quad\bullet \quad\quad H_2C = CH_2 \\
& \qquad\quad H \\
& \qquad\quad M
\end{array}
$$
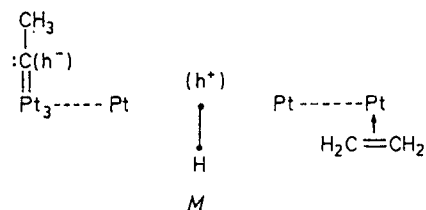
The interstitial hydrogen can easily migrate and add to a nearby coordinated ethylene:

$$CH_3$$
$$|$$
$$C:(h^-)$$
$$||$$
$$Pt_3 \longrightarrow Pt \qquad (h^+) \qquad Pt$$
$$|$$
$$CH_2$$
$$|$$
$$CH_3$$

N
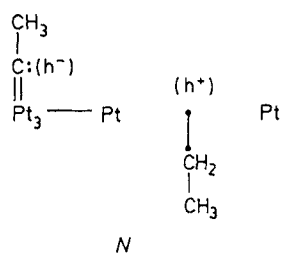
Note again that H atom in *M* and CH_3CH_2 radical in *N* are attached on Pt_2^+ via Ionic Overlap Induction only now h^+ is further removed from h^- compared, for example, to rhombic $Pt_2^+H_2^-$ in which the two h particles lie close together.

(e) Reaction of *N* with a second interstitial hydrogen leads to the ethane product.

A word of caution: By no means do we imply that what we described above is the detailed mechanism of ethylene hydrogenation on Pt surfaces. What we suggest is that the ultimately correct mechanism will very likely contain steps (a) to (e) and versions thereof as integral parts. The reader is referred to the important work of Somorjai for the experimental facts [129].
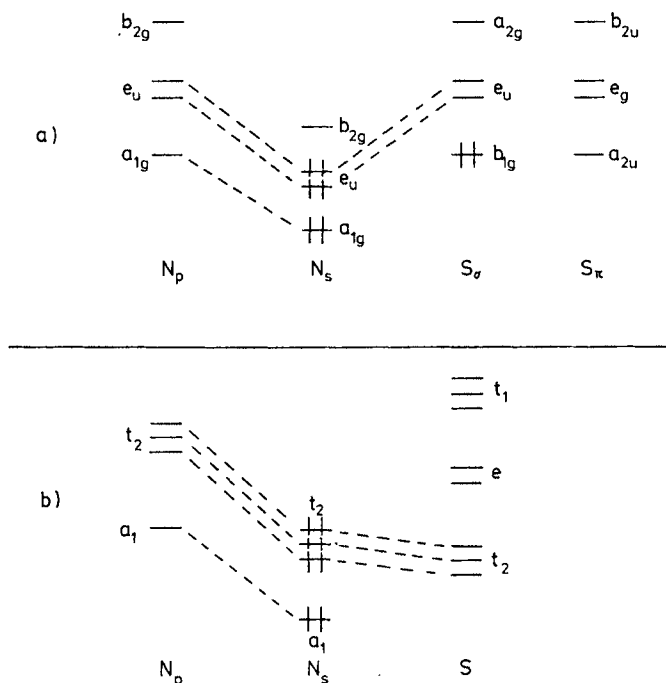
Fig. 51. Echinos bond diagrammatic representation of D_{4h} (a) and T_d (b) Be_4

13 The Gas Pair and the Electronic Structure of Metal Clusters

In Sect. 7.7, we saw that Li_2 can be represented by a formula in which an electron pair is flanked by two Li cations. We call this electron pair a *gas pair* to indicate that the two electrons have been effectively detached from the atomic nuclei, i.e. they have been *gasified*, and we now show how such a gasification which causes electron pairs to move to interstitial positions with respect to atomic nuclei may occur in metal clusters and, of course, in metals themselves. In order to simplify the drawings and the discussion, we use D_{4h} Be_4 as our example with the Echinos Model discussed in Sect. 6 being the basis of the theoretical analysis.

We work as follows: Starting with the set of four 2s AO's of the four Be atoms, we generate the four symmetry MO's which are then said to constitute the MO manifold of "fragment" N_s. We repeat the process with the radial and the tangential in-plane 2p AO's in order to obtain the MO manifold of "fragments" N_p and S_σ. The principal bond diagram of the D_{4h} Be tetramer is then the one shown in Fig. 51a. The question now is: What is the physical significance of the interaction of the configurations contained within the principal bond diagram? The answer can be very easily given by viewing the Be_4 system as a circle containing the four Be atoms with a perimeter of finite thickness and then referring to Fig. 52 which shows the key delocalization of electrons starting with the parent configuration $a_{1g}^2 b_{1g}^2 e_u(N_s)^4$. The two key events are the following:
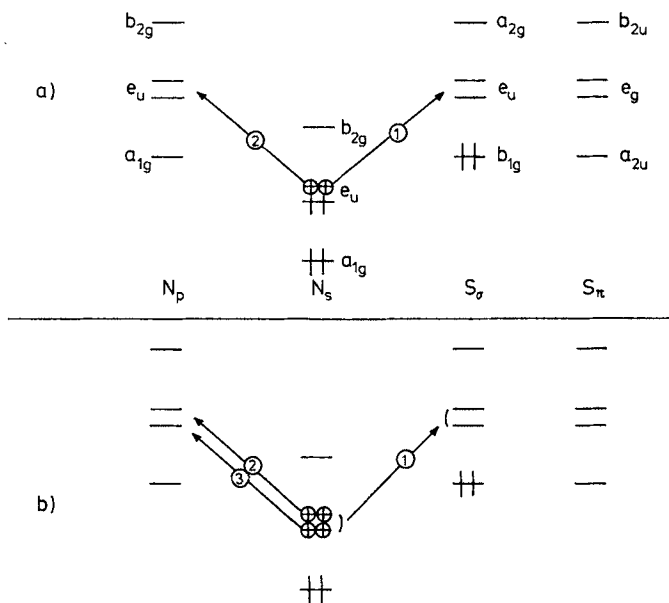
Fig. 52a and b. (a) Formation of a gas pair in D_{4h} Be_4. Process 1 corresponds to ejection of an electron outside the perimeter of the circle. Process 2 causes electron movement within the perimeter (induction). Process 2 is triggered by 1. (b) Correlated ejection of two electrons corresponds to Overlap Dispersion bonding

(a) $e_u(N_s) \rightarrow e_u(S_\sigma)$ electron transfer (process 1 in Fig. 52) generates overlap bonding moving electron density *outside* the perimeter.

(b) The electric field generated by process 1 will now dictate the mode of $e_u(N_s) \rightarrow e_u(N_p)$ electron transfer (process 2 in Fig. 52a). The CI which describes processes 1 and 2 is shown explicitly below and it is clear that process 2 represents either Overlap Induction or Anti Overlap Induction depending upon the action of
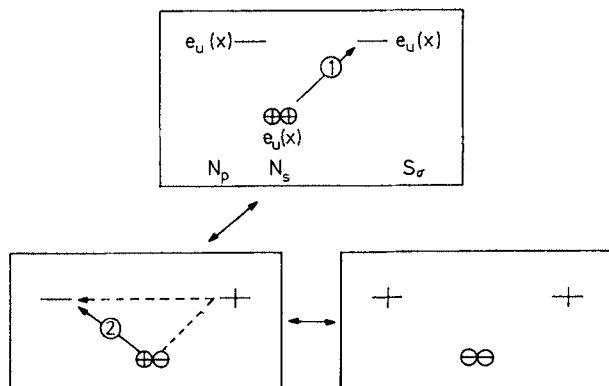
the electric field. If Overlap Induction occurs, the $e_u(N_s) \rightarrow e_u(N_p)$ electron transfer will cause electron density to move strongly inside the perimeter while, if Anti Overlap Induction occurs, the probability of the same electron transfer will tend to zero. Regardless of what the case is, the motion of the two $e_u(N_s)$ pairs is correlated. This happens because process 1 for the first pair is coupled to the same process for the second through Overlap Dispersion as illustrated in Fig. 52b. Hence, the key CI defined by the principal bond diagram of Fig. 51a is that corresponding to processes 1, 2, and 3 shown in Fig. 52b. This simple picture says that one pair moves by attracting the other one.

We can determine by calculation towards which of the two extremes our system finds itself by carrying out an MCSCF calculation with full geometry optimization and then examining the shape of the doubly occupied e_u MO. If the hybrid AO's point strongly inside, we have manifestation of Overlap Induction and electron pair interstitialization (gasification) but, if there is weak inside, weak outside, or zero hybridization, we have manifestation of Anti Overlap Induction. We expect the tendency for interstitialization to increase as we go from a small cluster (like Be_4) to the Be solid. The only relevant calculations which can be cited in connection with this problem are those of Whiteside at al. [130]. They find that tetrahedral is more stable than square planar Be_4, something which is easily explicable through comparison of the two bond diagrams of Fig. 51: The T_d has three t_2 while the D_{4h} species has only two e_u incipient gas pairs. More interesting is the fact that the AO composition of the t_2 orbitals of the tetrahedral species implies that we are closer to Anti Overlap Induction because the admixture of radial 2p AO's in these orbitals is very small and it comes with signs that cause AO hybridization directing electron density outside the sphere containing the tetrahedron. Of course, these calculations were carried out with different aims in mind and not at a level which is sufficiently high to accurately locate the Be_4 cluster on the bonding spectrum delineated

159

Be₄ (Planar, D₄ₕ) | (RLi)₄ (Planar, D₄ₕ)
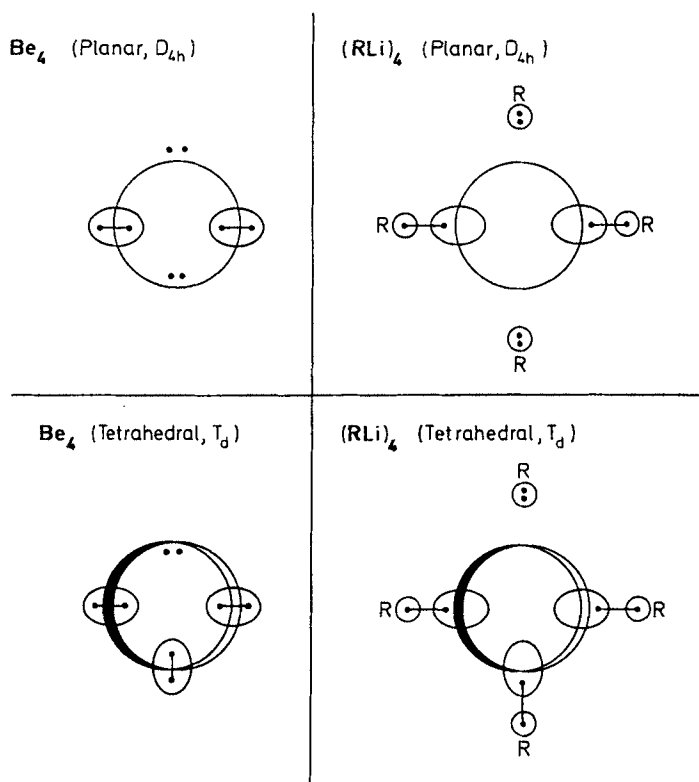
Fig. 53. Gas pairs in Be₄ and (RLi)₄ systems

here. As discussed elsewhere, correlation (gasification) of the a_1 pair (described by superposition of additional bond diagrams) is expected to move tetrahedral Be₄ towards Overlap Induction. The unexpected analogy between (RLi₄) and Be₄ is illustrated in Fig. 53.

14 Conclusion

What have we accomplished by MOVB theory? We have replaced intuitive concepts like "Aromaticity", "Hyperconjugation", and "Strain", etc. by a single interpretative framework and we have demonstrated what is wrong with these ideas. We have shown that there exist bonding mechanisms other than "covalent" and "ionic" which are employed by metal-containing molecules.

Why did MOVB theory make all this possible? Because it is a theory which projects how symmetry orchestrates the interplay of atom excitation and bond making and how there can be different types of bond making corresponding to different mechanisms of electron delocalization. Furthermore, it is a CI theory and only in the language of CI can concepts like dispersion, induction, etc., be expressed in a clear and pictorial fashion.

Why cannot other approaches do the same? "Perfect" MO theory is not conceptually explicit. Part Two illustrates this problem. Its approximate version, EHMO theory, cannot be even applied to any of the problems of Parts Three, Four and Five because of the integral approximations made at this level (e.g. neglect of bielectronic, etc., terms). GVB theory cannot show explicity how symmetry controls the situation because if does not employ canonical symmetry orbitals.

What made all this possible? In essence the University tenure system which permits "risky" research. The work described here advocates a non-approximate state viewpoint of chemical bonding and it represents a complete abandonment of the approximate orbital viewpoint which we favored some ten years ago.

What are the prospects? I have argued that "conceptual theory" is important because it can project one to the experimental frontier where explicit computations are impossible. With the completion of this work, we are now stepping on the threshold of problems which are at the focus for worldwide interest. One such problem is that of high temperature superconductivity. Noting that the highest T_c within a transition series (except La) is observed for a metal which has the largest diatomic bond dissociation energy (V, Nb, Ta) [131] and noting that the exciting high T_c phases are copper oxides, we can immediately appreciate the potential role of the gas pair in normal and of the interstitial bond in high temperature superconductivity. For large metal dimer bond dissociation energy implies strong Overlap Dispersion, i.e. highly stabilized gas pairs, and because one illustrator of Ionic Overlap Induction has been a copper oxide system drawn from biology!

What are the final messages that we want to leave with the reader? First, organic chemistry is, by and large, the chemistry of overlap bonds but the way in which symmetry orchestrates such bonding is difficult to perceive by using conventional approaches. Second, there is no such thing as independent bond formation. The most important consequence of this is that a molecule having some covalent and some ionic bonds is not the "in-between" species chemists believe it to be: The covalent and ionic bonds are not independent to the extent that the latter set up an electric field to which the covalent bonds respond. The operationaly significant question then becomes: How can covalency benefit from the presence of a field? Our response to this are the concept of Overlap Induction. The need for such a conceptual development should be evident to every chemist who has realized that point charges placed on atoms do not reproduce the behavior of the composite system unless one deals with the limiting case of pure ionic bonding, a rather rare occurrence.

A final thought: The concepts of Overlap Dispersion and Overlap Induction owe their existence to a simple observation: The VB matrix element connecting two configuration can be thought of as the algebraic sum of two terms, A and B, where for appropriate choice of fragments, A is overlap-dependent and B overlap-independent. The first time this author realized the significance of this observation was when he attempted a VB treatment of aromaticity and antiaromaticity. [132] In

161
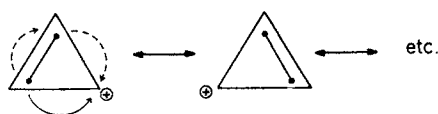
writing the three equivalent configurations of aromatic cyclopropenyl cation, one realizes that there exist *two ways* of shifting electrons in going from one to the other configuration as illustrated below. In this example, the two "arrow pushing" paths both correspond to overlap terms, A and B, which add. In the antiaromatic case B subtracts from A. A is a single and B is a double (RET) electron transfer. In a sense, it is ironic that a problem ("aromaticity"), which can be simply understood by means of Huckel MO theory, prepared us for coping with problems (metal bonding, superconductivity, etc.) which are treatable only at the level of "perfect" theory.

15 References

1. Epiotis ND (1988) J. Mol. Struct. (THEOREM) in press.
2. (a) Hund F (1927) Z. Physik. 40: 742 (1927) 42: 93 (1928) 51: 759
   (b) Mulliken RS (1928) Phys. Rev. 32: 186 (1928) 32: 761 (1929) 33: 730
   (c) Bloch F (1928) Z. Physik. 52: 555
   (d) Hartee DR (1928) Proc. Cambridge, Phil. Soc. 24: 89. Fock V (1930) Z. Physik. 61: 126
3. Goddard WA III, Dunning TH Jr, Hunt WJ, Hay PJ (1973) Accounts Chem. Res. 6: 368
4. (a) Wolfsberg M, Helmholz L (1952) J. Chem. Phys. 20: 837
   (b) Hoffmann R, Lipscomb WN (1962) J. Chem. Phys. 36: 2179, 3489 (1962) J. Chem. Phys. 37: 2873
   (c) Hoffmann R (1963) J. Chem. Phys. 39: 1392
5. (a) Heitler W, London F (1927) Z. Phys. 44: 455
   (b) Slater JC (1963) Quantum theory of molecules and solids. McGraw-Hill, New York, vol 1
   (c) Glasstone S, Laidler KJ, Eyring H (1941) The theory of rate processes. McGraw-Hill, New York
   (d) Pauling L (1960) The nature of the chemical bond, 3rd edn, Cornell University Press, Ithaca, New York
6. Wheland GW (1955) Resonance in organic chemistry, Wiley, New York
7. Hoffmann R (1982) Angew. Chem., Int. Ed. Engl. 21: 711
8. (a) Hückel E (1931) Z. Physik. 70: 204 (1932) Z. Physik. 76: 628
   (b) Hückel E (1937) Z. Electrochem. 43: 752
   (c) Heilbronner E, Bock H (1968) Das HMO-Modell und Seine Anwendung, Verlag Chemie, Weinheim
   (d) Epiotis ND, Cherry WR, Shaik S, Yates RL, Bernardi F (1977) Topics Curr. Chem. 70: 1
9. Epiotis ND (1983) Nouv. J. Chim. 8: 11
10. Epiotis ND (1983) Nouv. J. Chim. 8: 421
11. Heilbronner E: Tetrahedron Lett. 1964: 1923
12. Salem L (1982) Electrons in chemical reactions. Wiley-Interscience, New York
13. Epiotis ND (1982) Lect. Notes Chem. 29: 1
14. Epiotis ND (1983) Lect. Notes Chem. 34: 1
15. (a) Epiotis ND (1983) Pure Appl. Chem. 55: 229
    (b) Epiotis ND, Larson JR (1983) Isr. J. Chem. 23: 53
    (c) Epiotis ND (1984) J. Am. Chem. Soc. 106: 3170
    (d) Epiotis ND, Larson JR, Eaton H (1984) Croatica Chem. Acta 57: 1031
    (e) Jug K, Epiotis ND, Buss S (1986) J. Am. Chem. Soc. 108: 3640
    (f) The idea that a total wavefunction can be constructed from substates (configuration packets) rather than configurations was first put to application in: Epiotis ND (1978) Theory of organic reactions. Springer, Berlin Heidelberg New York
16. Hehre WJ, Radom L, Schleyer PvR, Pople JA (1986) Ab initio molecular theory. Wiley, New York

17. (a) Buckingham AD (1959) Quart. Rev. 13: 183
    (b) Buckingham AD (1970) in: Eyring D, Henderson D, Jost W (eds) Physical chemistry —
        An advanced treatise. Academic, New York
    (c) Hirschfelder JO, Curtiss CF, Bird RB (1964) Molecular theory of gases and liquids. Wiley,
        New York
18. Murrell JN (1974) in: March NH (ed) Orbital theories of molecules and solids. Clarendon, Oxford, Chapt 7
19. Morokuma K (1977) Accounts Chem. Res. 10: 294
20. Hobza P, Zahradnik R (1980) Topics Curr. Chem. 93: 53
21. Ehrenreich H (1987) Science 235: 1029
22. McGlynn SP, Vanquickenborne LG, Kinoshita M, Carroll DG (1972) Introduction to applied quantum chemistry. Holt, New York
23. Pyykkö P: J. Chem. Res. (S) 1979: 380
24. Pyykkö P (1979) Physica Scripta (Sweden) 20: 647
25. Kutzelnigg W (1984) Angew. Chem., Int. Ed. Engl. 23: 272
26. Pyykkö P, Desclaux JP (1979) Accounts Chem. Res. 12: 276
27. Desclaux JP (1973) Atom. Data Nucl. Data Tables 12: 311
28. Schaefer HF III (1984) Quantum chemistry: The development of ab initio methods in molecular electronic structure theory. Clarendon, Oxford
29. Pacchioni G, Koutecky J (1984) J. Chem. Phys. 81: 3588
30. Binkley JS, Frisch MJ, DeFrees DJ, Raghavachari K, Whiteside RA, Schlegel HB, Fluder EM, Pople JA (1983) Gaussian 82, Carnegie-Mellon University; Whiteside RA, Frisch MJ, Pople JA (1983) The Carnegie-Mellon quantum chemistry archive, 3rd edn. Carnegie-Mellon University
31. Brockway LO (1937) J. Phys. Chem. 41: 185, 747
32. Patrick CR (1964) Advan. Fluorine Chem. 2: 10
33. For review and data tabulation, see: Chambers RD (1973) Fluorine in organic chemistry. Wiley-Interscience, New York
34. (a) Benson SW, Cruickshank FR, Golden DM, Hougen GR, O'Neal HE, Rodgers AS, Shaw R, Walsh R (1969) Chem. Revs. 69: 279
    (b) Cox JP, Pilcher G (1970) Thermochemistry of organic and organometallic compounds. Academic, New York
    (c) JANAF thermochemical tables (1971) Dow Chemical Corp, Springfield, VA
35. Pilcher G, Skinner HA (1982) Thermochemistry of organometallic compounds. In: Hartley FR, Patai S (eds) The chemistry of metal-carbon bond, Wiley, New York
36. Smart BE (1986) in: Liebman JF, Greenberg A (eds) Molecular Structure and Energetics. VCH, Dearfield Beach, vol 3 p 141
37. Liebman JF, Greenberg A (unpublished results)
38. See Ref 13 p 264
39. Schleyer PvR, Reed AE (1988). J. Am. Chem. Soc. 110, 453.
40. For a discussion of the components of "strain" as well as a thought-provoking presentation of "strained" organic molecules, see: Greenberg A, Liebman JF (1978) Strained organic molecules, Academic, New York
41. This section is devoted to a discussion of "angle strain" or "Bayer strain":
    (a) Bayer A (1885) Chem. Ber. 18: 2269
    (b) Huisgen R (1986) Angew. Chem., Int. Ed. Engl. 25: 297 Furthermore, the term "bond length" is uniformly assumed to mean "interatomic distance".
42. Callomon JH, Hirota E, Kuchitsu K, Lafferty WJ, Maki AG, Pote CS (1976) Structure data of free polyatomic molecules. In: Helwege K-H (ed) Landolt-Börnstein numerical data and functional relationships in science and technology, Springer, Berlin Heidelberg New York
43. (a) Dill JD, Greenberg A, Liebman JR (1979) J. Am. Chem. Soc. 101: 6814
    (b) Clark T, Spitznagel GW, Klose R, Schleyer PvR (1984) J. Am. Chem. Soc. 106: 4412
44. Closs GL, Larrabee R: Tetrahedron Lett. 1965: 287
45. (a) Shatenstein AI (1963) Advan. Phys. Org. Chem. 1: 155
    (b) Streitwieser A Jr, Hammons JH (1965) Prog. Phys. Org. Chem. 3: 41
    (c) Cram DJ (1965) Fundamentals of carbanion chemistry. Academic, New York
    (d) Fort RC, Schleyer PvR (1966) in: Advances in acicyclic chemistry. Academic, New York, p 358

46. Lauh T-Y, Stock LM (1974) J. Am. Chem. Soc. 96: 3712
47. Peterson PE (1972) J. Org. Chem. 37: 4180
48. Gillespie RJ (1979) Chem. Soc. Rev. 8: 315
49. Schulman JM, Fischer CR, Solomon P, Venanzi TJ (1978) J. Am. Chem. Soc. 100: 2949
50. Bodor N, Dewar MJS, Worley SD (1970) J. Am. Chem. Soc. 92: 19
51. Lammertsma K, Olah GA, Barzaghi M, Simonetta M (1982) J. Am. Chem. Soc. 104: 6851
52. Epiotis ND (in press)
53. Hehre WJ, Pople JA (1975) J. Am. Chem. Soc. 97: 6941
54. Irngartinger H, Goldmann A, Jahn R, Nixdorf M, Rodenwald H, Maier G, Malsch KD, Emrich R (1984) Angew. Chem., Int. Ed. Engl. 23: 993
55. Pauling L (1960) The nature of chemical bond, 3rd edn. University Press, Ithaca, New York, Sect 6-5
56. Fukui K (1965) Theory of orientation and stereoselection. Springer, Berlin Heidelberg New York
57. Fleming I (1976) Frontier orbitals and organic chemical reactions. Wiley, New York
58. Fukui K, Fujimoto H (1968) Bull. Chem. Soc. Japan 41: 1989 (1969) 42: 3399
59. Dewar MJS (1969) The molecular orbital theory of organic chemistry. McGraw-Hill, New York
60. Woodward RB, Hoffmann R (1970) The conservation of orbital symmetry. Verlag Chemie, Weinheim
61. The independent recognition of orbital symmetry control of reaction stereochemistry by many brilliant investigators is documented in: Epiotis ND, Shaik S, Zander W (1980) in: de Mayo P (ed) Rearrangements in ground and excited states, Academic, New York vol 2
62. Epiotis ND (in press)
63. Schmidt PC, Bohm MC, Weiss A (1985) Ber. Bunsen Ges. Phys. Chem. 89: 1330
64. Epiotis ND (in press)
65. Davies RE, Riley PE (1980) Inorg. Chem. 19: 674
66. Cotton FA, Hanson BE (1980) in: de Mayo P (ed) Rearrangements in ground and excited states. Academic, New York vol 2 Chapt 12
67. Obara S, Kitaura K, Morokuma K (1984) J. Am. Chem. Soc. 106: 7482
68. Scott PR, Richards WG (1976) Chem. Soc. Spec. Per. Rep. 4: 70 See also: Armentrout PB, Halle LF, Beauchamp JL (1981) J. Am. Chem. Soc. 103: 6501
69. Mitcheson GR, Hillier IH (1979) J. Chem. Soc. Faraday II 75: 929 See also: Saddei D, Freund H-J, Hohlneicher G (1981) Chem. Phys. 55: 339
70. Bursten BE, Cotton FA, Hall MB (1980) J. Am. Chem. Soc. 102: 6348
71. Dixon RN, Robertson IL (1978) Mol. Phys. 36: 1099
72. Redhouse AD (1982) in: Hartley FR, Patai S (eds) The chemistry of the metal-carbon bond. Wiley, New York, Chapt 1
73. Jemmis ED, Schleyer PvR (1982) J. Am. Chem. Soc. 104: 4781
74. Bach SBH, Taylor CA, Van Zee RJ, Vala MT, Weltner W Jr (1986) J. Am. Chem. Soc. 108: 7104
75. (a) Halpern J (1968) Adv. Chem. Ser. 70: 1 (1968) Discuss. Faraday Soc. 46: 7
    (b) Foust AS, Foster MS, Dahl LF (1969) J. Am. Chem. Soc. 5631: 5633
    (c) Hawthorne MF (1968) Acc. Chem. Res. 1: 281
    (d) O'Neil ME, Wade K (1982) in: Wilkinson G, Stone FGA, Abel EW (eds) Comprehensive organometallic chemistry. Pergamon, Oxford, vol1 Chapt 1
    (e) Wade K (1976) Advan. Inorg. Chem. Radiochem. 18: 1
    (f) Mingos DMP (1982) in: Wilkinson G, Stone FGA, Abel WW (eds) Comprehensive organometallic chemistry, Pergamon, Oxford, vol 3 Chapt 19
76. The term "isolobal" is used here in the sense that orbitals of different l value act similarly in bonding provided that they belong to the same irreducible representation
77. Wilkes GR (1965) PhD Thesis, University of Wisconsin, Madison
78. (a) Kalcher J, Sax A, Olbrich G (1984) Int. J. Quantum Chem. 25: 543
    (b) Lischka H, Köhler H-J (1983) J. Am. Chem. Soc. 105: 6646
    (c) Binkley JS (1984) J. Am. Chem. Soc. 106: 603
    (d) Luke BT, Pople JA, Krogh-Jespersen MD, Apeloig Y, Chandrasekhar J, Schleyer PvR (1986) J. Am. Chem. Soc. 108: 260
79. Pacchioni G, Koutecky J (1984) Ber. Bunsen Ges. Phys. Chem. 88: 233

80. Plotkin JS, Alway DG, Weisenberger CR, Shore SG (1980) J. Am. Chem. Soc. 102: 6156

81. Adams RD (1983) Acc. Chem. Res. 16: 67

82. Heijser W, Baerends EJ, Ros P (1980) Faraday Symp. Chem. Soc. 14: 211

83. Wiberg KB (1984) Acc. Chem. Res. 17: 379

84. Knoll K, Orama O, Huttner G (1984) Angew. Chem., Int. Ed. Engl. 23: 976

85. Berson JA (1980) in: deMayo P (ed) Rearrangements in ground and excited states. Academic, New York, vol 1 p 311

86. Bernardi R, Olivucci M, Robb MA, Tonachini G (1986) J. Am. Chem. Soc. 108: 1408

87. Huisgen R, Grashey R, Sauer J (1964) in: Patai S (ed) The chemistry of alkenes. Wiley-Interscience, New York, p 739

88. Sauer J: private communication

89. Epiotis ND (1988) New. J. Chem. 12, 231, 257.

90. For recent computational results on $Ni(CO)_n$, where n = 1–4, see: Bauschlicher CW, Bagus PS, Nelin CJ, Roos BO (in press) J. Chem. Phys. and references cited therein.

91. Carter EA, Goddard WA III (1986) J. Am. Chem. Soc. 108: 2180

92. Beckman H, Koutecky J, Botschwina P, Meyer W (1979) Chem. Phys. Lett. 67: 199

93. Rubinstein M, Shavitt I (1969) J. Chem. Phys. 51: 2014

94. (a) Konowalow DD, Rosenkrantz M (1979) Chem. Phys. Lett. 61: 489
    (b) The independent works of: Gatti G, Fantucci P, Pacchioni G (1987) Theoret. Chim. Acta 72, 433 and of Cao WL, Gatti C, MacDougall PJ, Bader RFW (to be published) report non-nuclear density maxima in alkali clusters in consonance with the ideas described here. We thank Professor Bader for kindly sending us a preprint of this work.

95. Graham G, Richtsmeier S, Dixon DA (1980) J. Am. Chem. Soc. 102: 5759

96. For example, one extrinsic configuration has one electron in each of q_1 and k_1.

97. (a) Weiss E, Lucken EAC (1964) J. Organomet. Chem. 2: 197
    (b) Weiss E, Hencken G (1970) J. Organomet. Chem. 21: 265

98. Wilson RD, Bau R (1976) J. Am. Chem. Soc. 98: 4687

99. Hentz FC, Tyree SY Jr (1964) Inorg. Chem. 3: 844

100. Wells AF (1936) Z. Krist. 94: 447

101. Weiss E, Sanermann G (1968) Angew. Chem., Intl. Ed. Engl. 7: 133

102. Epiotis ND (in press)

103. Jemmis ED, Chandrasekhar J, Schleyer PvR (1979) J. Am. Chem. Soc. 101: 527

104. McKeever LD, Waach R, Doran MA, Baker EB (1968) J. Am. Chem. Soc. 90: 3244

105. Brown TL, Seitz LM, Kimura BY, (1968) J. Am. Chem. Soc. 90: 3245

106. (a) Hodoscek M, Solmajer T (1984) J. Am. Chem. Soc. 106: 1854
    (b) Sapse A-M, Raghavachari K, Schleyer PvR, Kaufmann E (1985) J. Am. Chem. Soc. 107: 6483. An exception is $(LiNH_2)_4$ which prefers a D_{4h} geometry.
    (c) Epiotis ND (to be published)

107. Laidig WD, Schaefer HF III (1978) J. Am. Chem. Soc. 100: 5972. See also ref. 50.

108. Dunning TH, Hunt WJ, Goddard WA III (1969) Chem. Phys. Lett. 4: 147

109. Bader RFW (1985) Acc. Chem. Res. 18: 9

110. Ritchie JP, Bachrach SM (1987) J. Am. Chem. Soc. 109: 5909

111. Schleyer PvR (private communication)

112. Actually, "spin pairing" means Double Electron Transfer (DET).

113. Upton TH, Goddard WA III (1978) J. Am. Chem. Soc. 100: 5689

114. (a) Lorquet AJ, Lorquet JC (1968) Bull. Classe Sci. Acad. Roy. Belges 54: 617
    (b) Rodewell WR, Guest MF, Clark DT, Shuttleworth D (1977) Chem. Phys. Lett. 45: 50

115. Collins JB, Dill JD, Jemmis ED, Apeloig Y, Schleyer PvR, Seeger R, Pople JA (1976) J. Am. Chem. Soc. 98: 5419

116. Dolbier WR Jr, Koroniak H, Burton DJ, Bailey AR, Shaw GC, Hansen SW (1984) J. Am. Chem. Soc. 106: 1871

117. Kirmse W, Rondan NG, Houk KN (1984) J. Am. Chem. Soc. 106: 7989

118. Rondan NG, Houk KN (1985) J. Am. Chem. Soc. 107: 2099

119. The attack of carbonyl by nucleophile is a simple example of an "outsie" stereochemical preference: Burgi HB, Dunitz JD (1983) Acc. Chem. Res. 16: 153

120. This section will be better understood if the reader is well versed in the construction of symmetry adapted fragment orbitals. See: Jorgensen WL, Salem L (1974) The organic chemist's book of orbitals. Academic, New York
121. (a) Makino N, MacMahill P, Mason HS, Moss TH (1974) J. Biol. Chem. 249: 6062
     (b) Andreassen LE, Reinhammer B (1979) Biochim. Biophys. Acta 568: 145
122. Fee JA (1975) Structure and Bonding 23: 1
123. (a) Fenton DE, Schroeder RR, Lintvedt RL (1978) J. Am. Chem. Soc. 100: 1931
     (b) Fenton DE, Lintvedt RL (1978) J. Am. Chem. Soc. 100: 6367
124. Gisselbracht JP, Gross M, Alberts AH, Lehn JM (1980) Inorg. Chem. 19: 386
125. Addison AW (1976) Inorg. Nucl. Chem. Lett. 12: 899
126. Gagne RR, Kreh RP, Dodge JA (1979) J. Am. Chem. Soc. 101: 6917
127. (a) Gagne RR, Koval CA, Smith TJ (1977) J. Am. Chem. Soc. 99: 8367
     (b) Gagne RR, Koval CA, Smith TJ, Cimolino MC (1979) J. Am. Chem. Soc. 101: 4571
128. Epiotis ND (to be published)
129. Zaera F, Gellman AJ, Somorjai GA (1986) Acc. Chem. Res. 19: 24
130. Whiteside RA, Krishnan R, Pople JA, Krogh-Jespersen M-B, Schleyer PvR, Wenke G (1980) J. Comp. Chem. 1: 307
131. Morse MD (1986) Chem. Rev. 86: 1049
132. First recognized by Mulder J. J. C., Oosterhoff L. J. Chem. Commun. 1970, 49, 52.

Periodic Group Relationships in the Spectroscopy of the Carbonyls, Ketenes and Nitriles: The Effect of Substitution by Sulfur, Selenium, and Phosphorus

Dennis J. Clouthier[1] and David C. Moule[2]

1 Department of Chemistry University of Kentucky Lexington. KY 40506-0055 U.S.A.
2 Department of Chemistry Brock University St. Catharines. Ontario CANADA. L2S 3A1

Sufficient data are now available to study trends in the spectra of molecules on substitution with progressively heavier atoms down the periodic table. We have chosen the carbonyls and ketenes for review of the effect of replacement of the oxygen by sulfur or selenium and the nitriles for which there is information on substitution of nitrogen by phosphorus. The basic spectroscopy of these chromophores is reviewed for the ground and electronic excited states, correlating observed trends and differences. Using this information, conclusions are drawn concerning the spectroscopic effects of substitution by heavy atoms. In particular, it is observed that such substitutions have predictable effects on the ground state but often surprising and interesting changes are found in the excited state. In most cases, more information can be gleaned from the electronic spectra of the heavy atom substituted chromophores due to lower transition energies, stronger spin-orbit coupling effects and favorable changes in excited state geometries. Future advances in our understanding of molecular spectroscopy are likely to come from the pursuit of the spectra of other chromophores substituted with heavy atoms.

1 Introduction

The spectroscopy of polyatomic molecules has been extensively studied. In the microwave region, precise measurements of the rotational constants and derivation of the molecular structures of stable molecules, transient species, radicals, ions and van der Waals complexes have been widely explored [1]. Such laboratory studies have been extended to the observation of the microwave emission lines of molecular species in the interstellar medium [2]. In some cases, it has even been possible to assign interstellar lines to molecules which have not been observed in the laboratory [3]. In the infrared, high resolution FTIR spectrometers and laser sources have made it possible to study the rovibrational energy levels of a large number of stable and unstable polyatomic species, yielding refined force field, centrifugal distortion and structural information. Electronic spectroscopy, in the UV-visible, has also developed rapidly since the pioneering interpretation of the rotational sub-band structure in the spectrum of formaldehyde in 1934 by Dieke and Kistiakowsky [4]. Spectrographic Fourier transform and laser techniques coupled with powerful computer methods for the simulation and analysis of complex spectra have broadened our understanding of the excited states of molecules. Sub-Doppler resolution and the spectral simplification afforded by supersonic expansion cooling have pushed the frontiers of high resolution spectroscopy to larger and larger molecules.

Molecular spectroscopy has been reviewed many times from many points of view. The comprehensive volumes by Herzberg [5] cover the vibrational and electronic spectra of polyatomic molecules in detail. Comparisons of molecules have generally been done on the basis of the type of rotor (linear, symmetric, asymmetric top, etc.) in the microwave, the type of functional group in the infrared, and isoelectronic series in the UV-visible. Such correlations have proven to be extremely useful in studying the spectra of new compounds.

One aspect of comparative molecular spectroscopy which appears to have received little attention is trends in the spectra of molecules on substitution with progressively heavier atoms down the periodic table, which we shall call periodic group relationships. For example, we might ask what effects are apparent in the spectra of aldehydes, RCHO, on substituting sulfur, selenium or tellurium for oxygen. On the one hand, we might predict that the ground state structures would be qualitatively similar for this series. In contrast, considerations of the electronic orbital energies suggest that the first electronic transitions would occur in substantially different regions of the electromagnetic spectrum. It has become increasingly clear in recent years that the spectra of molecules substituted with heavier atoms are not simple clones of the spectra of the lighter parent species. It is for this reason that we have chosen to attempt to correlate the diverse information available, in order to gain some insight into the spectroscopic trends on substitution by heavier atoms. Much of our interest in this topic comes from a parallel and often collaborative research effort on spectroscopic studies of the $C=O$, $C=S$ and $C=Se$ moieties. The many satisfying correlations and the more delightful sharp contrasts between these species have prompted us to examine the general trends for other functional groups.

Unfortunately, spectroscopic data on conventional organic functional groups substituted with heavy elements are limited. The primary reason for the lack of study seems

to be the instability of compounds containing multiple bonds between elements of the second and subsequent periods of the periodic table [6]. In general, the instability is with respect to polymerization, so that studies of the monomer are only feasible in matrices or at low pressures in the gas phase. Microwave spectroscopy has been extensively employed in the detection, yield optimization and determination of the molecular structures of such transient gas phase monomers. Of particular note are the extensive investigations by Kroto and co-workers which he has eloquently described in a published Tilden lecture [7]. Infrared spectra have been observed for fewer of these unstable species and the least data are available in the UV-visible region.

Out of the substantial number of simple functional groups known in organic chemistry, we have chosen three for this work: the carbonyls $R'R''C=O$, the ketenes $R'R''C=C=O$ and the nitriles, $RC\equiv N$. At this time, there do not appear to be sufficient spectroscopic data on periodic group relationships for other chromophores to warrant attempting to draw any general conclusions.

1.1 Scope

This work is, by necessity, selective rather than exhaustive. It is not mean as a general review of the literature but rather an overview of the various conclusions which can be drawn from many diverse pieces of data. We have limited consideration to the spectra of simple molecules observed in the gaseous state, for which the effects of inter-molecular interactions are minimal. Primary attention has been devoted to microwave, infrared and UV-visible spectra, although the results of Raman, photoelectron, millimeter-wave and other spectroscopic techniques have been included where appropriate. We have also attempted to correlate spectroscopic results with general chemical notions of bonding and molecular orbital theory.

2 Carbonyls, Thiocarbonyls, and Selenocarbonyls

The spectroscopy of formaldehyde has been reviewed by Moule and Walsh [8] and more recently by Clouthier and Ramsay [9]. The assignments of the electronic transitions out to 100,000 cm^{-1} (100 nm) have been surveyed in some detail by Robin [10]. Other excellent sources include Herzberg [5] and a review of the photophysics of formaldehyde and the carbonyls by Lee and Lewis [11]. The spectroscopy of the simple thiocarbonyl compounds and their photophysical behaviour has been discussed by Steer [12]. As these studies provide an excellent source for an understanding of the dynamics of the CH_2O/CH_2S pair, the emphasis in the present work will be on the recent developments in the spectroscopy of CH_2Se, the aliphatic carbonyl and thiocarbonyl compounds, and the formyl and thioformyl halides. Many of the simple thiocarbonyl compounds are unstable. Only recently have they been detected by the technique of flash pyrolysis. In this method a molecular precursor such as a cyclic dimer or trimer is passed at low pressures through a tube furnace where it is pyrolyzed into fragments which flow directly into a laser excitation cell or a multiple pass absorption cell. Detection of the unstable species is through its absorption or laser excitation spectrum. The method does require that the thiocarbonyl compounds

be sufficiently long-lived that a steady state concentration is achieved. This require-ment places a lower limit on the lifetime of the molecule of about one second.

2.1 Formaldehyde, Thioformaldehyde, Selenoformaldehyde

CH_2O: The emission from formaldehyde was detected as a pale blue glow in the cool flames of ether by Sir Humphrey Davy [13] in 1817. The spectroscopy of formal-dehyde began some 109 years later when Emeleus [14] succeeded in obtaining a photographically recorded ultraviolet spectrum. This molecular system has now become the prototype for many types of spectroscopic studies. This is partly because of the ease with which the molecule can be synthesized, and partly because the analysis of the electronic spectra is a tractable yet nontrivial problem.

CH_2S: The prototype molecule for the thiocarbonyl series, CH_2S, has received a great deal of experimental and theoretical attention in the last ten years. Spectroscopic studies on this interesting species have been impeded by the fact that the molecule is unstable in the gas phase under laboratory conditions. It must be synthesized through pyrolysis or photolysis and detected immediately after it is formed. The molecule is sufficiently long lived, under low pressure conditions, that its spectrum can be recorded in absorption by flowing it into a large volume multiple reflection cell directly from a pyrolysis system. It can also be studied under supersonic jet conditions. In these experiments, the precursor compound is mixed with He or Ar at a pressure of 2 to 3 atmospheres and pyrolyzed before it enters the jet chamber. From an experi-mental point of view, studies of the molecule in the vapor phase present few diffi-culties, except for the vacuum ultraviolet region, where the pyrolysis side-products absorb and interfere. A number of precursor compounds have been used to generate CH_2S. The order of preference appears to be; C_3H_6S (trimethylene sulfide), $(CH_3)_2S$ (dimethyl sulfide) and $(CH_2S)_3$ (s-trithiane). Cracking temperatures for the pyrolyses range from 750–850 °C. Thioformaldehyde was first detected [15] as a fragment in a mass spectral study of the pyrolysis products of polymethylene sulfide. At about the same time, Callear et al. [16] flash photolyzed a group of sulfur-containing mole-cules and observed a transient absorption at 212 nm which they attributed to CH_2S. Unambiguous identification of the species came in 1970 with the microwave study of Johnson and Powell [17].

CH_2Se: The preparation of stable aliphatic selones was first reported in 1976 by Bartow and coworkers [18]. They found it was possible to stabilize these molecules in the liquid phase by attaching bulky substituents such as the t-butyl group or ring structures directly to the selenocarbonyl function. Halogens are known to stabilize the thiocarbonyl group, and the same year Haas et al. [19] reported the properties of monomeric selenocarbonyl difluoride, CF_2Se. Selenoacetaldehyde [20] and seleno-formaldehyde [21] were detected in the gas phase somewhat later by the combined tech-niques of photoelectron and microwave spectroscopy.

2.1.1 The Ground State

Formaldehyde, thioformaldehyde and selenoformaldehyde are planar molecules with C_{2v} symmetry. Structural parameters have been derived from the microwave

data; they are collected together in Table 1. Brown and coworkers [22] observed the microwave spectra of six isotopic species of selenoformaldehyde and derived a substitution structure from the rotational constants. As the A constant could not be determined accurately from the spectrum, the planarity constraint $I_A = I_C - I_B$ was used.

Table 1. Ground state structural parameters.[a]

Structural parameter	CH_2O[c]	CH_2S[c]	CH_2Se[d]
$r(C=X)$[b]	1.2072(5)	1.6138(4)	1.7531
$r(C-H)$	1.1171(10)	1.0962(6)	1.0904
$\sphericalangle(HCH)$	116.23(10)	116.26(10)	117.93

[a] in Å or degrees. [b] X = O, S or Se. [c] r_z, ref. 9. [d] r_s, ref. 22.

Under the symmetry operations of the C_{2v} point group, the six fundamental vibrational modes of CH_2O transform as:

$$\Gamma_v = 3a_1 + b_1 + 2b_2$$

The three totally symmetric modes $\nu_1(CH)$, $\nu_2(C=O)$ and $\nu_3(HCH)$ give rise to type-A infrared bands, while the in-plane antisymmetric modes $\nu_5(CH)$ and $\nu_6(HCO)$ generate type-B bands in the spectrum. The out-of-plane wagging mode ν_4 gives rise to a distinctive type-C band. Figure 1 shows a representation of the CH_2X molecule, the symmetry axes and the principal axes.
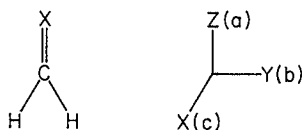
Fig. 1. The molecular structure of the CH_2X molecule, X = O, S, Se, including the symmetry and principal axes

The six fundamental bands of formaldehyde and thioformaldehyde have been analyzed by a combination of infrared and laser Stark techniques. The vibrational frequencies of CH_2O, CD_2O, CHDO, CH_2S and CD_2S have been collected together by Clouthier and Ramsay [9] and are given in Table 2. At this time the ground state vibrational spectrum for CH_2Se has not been observed, although hot bands have been recently discovered [24] in the LIF spectrum of CH_2Se/CD_2Se. Ab initio values [23] have been derived using a double zeta basis set, plus polarization functions. The scaled values for the fundamentals are given in Table 2.

Table 2. Ground state vibrational frequencies.[a]

Mode	Approx. description	CH_2O[b]	CHDO[b]	CD_2O[b]	CH_2S[b]	CD_2S[b]	CH_2Se[c]	CD_2Se[d]
$\nu_1(a_1)$	CH stretch	2782.5	2120.7	2055.8	2971.0	2158.5	2988	—
$\nu_2(a_1)$	CX stretch[e]	1746.0	1724.3	1701.6	1059.2	936.2	901[d]	788
$\nu_3(a_1)$	HCH bend	1500.2	1400.0	1105.7	1457.3	1171.8	1397	—
$\nu_4(b_1)$	wag	1167.3	1058.8	938.0	990.2	781.2	978[d]	768
$\nu_5(b_2)$	CH stretch	2843.5	2844.1	2159.7	3024.6	2262.7	3059	—
$\nu_6(b_2)$	HCH rock	1249.1	1028.4	989.3	991.0	757.4	914	—

[a] in cm^{-1}. [b] ref. 9. [c] ref. 23. [d] ref. 24. [e] X = O, S or Se.

2.1.2 The $S_1(n, \pi^*)$ Excited State

In absorption, CH_2O displays a many-banded spectrum in the near-ultraviolet region, which extends from 353 to 230 nm. Figure 2 shows the system under low resolution. Rotational analyses of several of the stronger bands of CH_2O were accomplished long before the details of the vibrational structure were fully understood. In a pioneering study, Dieke and Kistiakowsky [4] photographically recorded the CH_2O spectrum at high resolution and established rotational assignments and the spectroscopic constants for several of the combining vibronic states. They were able to determine, for the first time, a set of structural parameters (bond lengths and bond angles) for the ground electronic state. Moreover, they demonstrated that the electronic moment for the transition was directed perpendicular to the C=O bond direction. This information was used to establish the identity of the n and π^* molecular orbitals involved in the excitation process.

The ground electronic configuration of CH_2O can be written:

$$\ldots (\sigma)^2(n')^2(\pi)^2(n)^2 \qquad \tilde{X}^1A_1$$
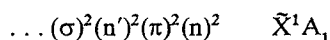
where n is the nonbonding orbital localized on the oxygen center and is of b_2 symmetry, π is the carbonyl bonding orbital of b_1 species, and n' is the second non-
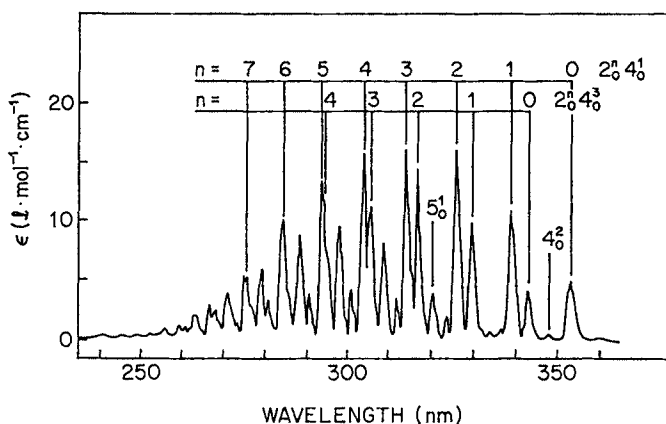
Fig. 2. Low resolution absorption spectrum of CH_2O

bonding a_1 orbital. In the lowest energy excitation process, the outermost electron in the n orbital is promoted to the lowest antibonding orbital π^* in the carbonyl group. The electron configuration and the overall symmetry for the upper state become:

$$\ldots (\sigma)^2 (n')^2 (\pi)^2 (n)^1 (\pi^*)^1 \qquad \tilde{A}^1 A_2$$

A schematic representation of the valence π, n, n' and π^* molecular orbitals is given in Fig. 3. The selection rules for electric dipole radiation do not permit the $\tilde{X}^1 A_1$ and $\tilde{A}^1 A_2$ states to combine. As a result, the 0_0^0 transition is formally electric dipole forbidden. (M_b^a denotes a vibronic transition involving "a" quanta in the upper state and "b" quanta in the lower state, while a level is designated M^a. In the case of the 0—0 origin transition, the mode is labelled 0 and the transition 0_0^0.)

Aside from the intensity in the n $\rightarrow \pi^*$ system which arises from allowed magnetic dipole transitions, the other source for the oscillator strength comes from vibrational-electronic coupling (Herzberg-Teller interaction). Molecular motion in CH_2O results in a breakdown of the Born-Oppenheimer separation of the electronic and vibrational wavefunctions. As a consequence, the wavefunctions of the antisymmetric in-plane vibrations v_5 and v_6 of b_2 species couple with the electronic wavefunction of the $\tilde{A}^1 A_2$ state to form vibronic states of B_1 species. These vibrational levels attach to the 0^0 zero-point energy of the $\tilde{A}^1 A_2$ state to form 5^1, 5^3, 6^1, etc., vibronic states which couple to the higher valence and Rydberg electronic states of the molecule. It is through this dipole-dipole mixing that intensity is induced into the first absorption system. The direction of polarization is that of the donor transition, in this case, $^1 B_1 \leftarrow \tilde{X}^1 A_1$. Bands resulting from the activity of single quanta of v_5 and v_6 would be x polarized and would follow type-C rotational selection rules. Likewise, the antisymmetric vibration v_4 of b_1 species couples the $\tilde{A}^1 A_2$ state with higher B_2 electronic states. This provides for y polarized intensity and type-B bands. These possibilities are shown schematically in Fig. 4. Both x and y polarized transitions are perpendicular to the C=O bond direction z. The weakness of the absorption system

$2b_2(n)$

$2b_1(\pi^*)$

$5a_1(n')$

$1b_1(\pi)$
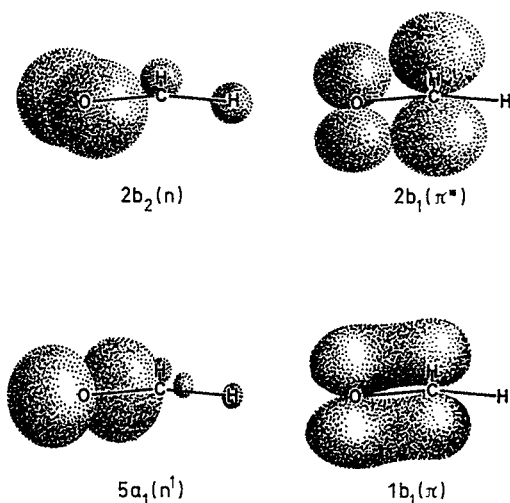
Fig. 3. A schematic representation of the σ, n, n' and π^* MO's of CH_2O
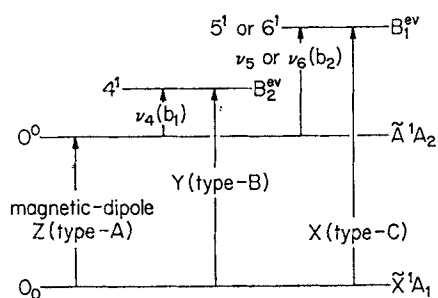
Fig. 4. Possible vibronic transitions in the $\tilde{A}^1A_2 \leftarrow \tilde{X}^1A_1$ electronic transition of CH_2X molecules

and the observation by Dieke and Kistiakowsky [4] of perpendicular polarization is consistent with a forbidden electronic transition made allowed by vibronic coupling.

The interpretation of the vibrational fine structure in the formaldehyde spectrum developed more slowly. Aside from the well developed progressions in a frequency of 1182 cm^{-1} which were assigned to the ν_2' carbon-oxygen stretching mode, the other intervals observed in the spectrum were not readily interpreted. The hot bands did not form intervals which correlated with the ground state vibrational frequencies. Furthermore, the band structure in absorption and emission did not display the expected mirror image relationship. The major problem was the abnormally small vibrational spacing of 125 cm^{-1} which separated the first two bands in the spectrum.

The way out of these difficulties was pointed out by Walsh [25] and was worked out in more detail in a brilliant analysis by Brand [26]. A correlation diagram of the one electron MO energy (Walsh Diagram) for formaldehyde shows that the π^* orbital becomes more stable when the OCH or HCH angles distort from the planar $120°$ configuration to a $90°$ right pyramid. (Walsh's rules work on the principle that s orbitals are more stable than p orbitals with the same quantum number). As the molecule distorts from the plane, the form of the π^* orbital changes from a pure p atomic orbital on the carbon center to an sp^3 hybrid which results in a decrease in energy. It is the presence of the electron in the π^* orbital which is responsible for the non-planar structure of $\tilde{A}^1A_2$ formaldehyde.

A nonplanar molecule would have two distinct equilibrium configurations which are related to each other by an inversion of the nuclei. The potential function for the out-of-plane displacement of the oxygen atom would contain a double minimum, with the height of the central barrier providing a measure of the stability of the molecule
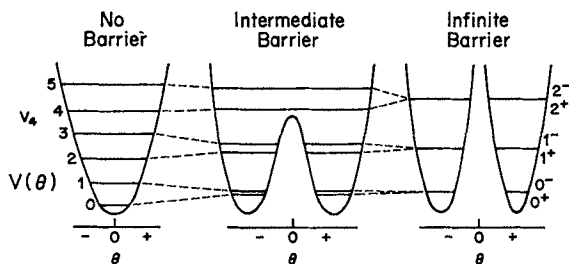
Fig. 5. Correlation diagram for the energy levels of rigidly planar and flexible nonplanar structures

brought about by the nonplanar distortion. Figure 5 shows the correlation of the energy levels for a planar, slightly nonplanar and rigidly nonplanar molecule.

It is clear that the vibrational quanta for out-of-plane bending are highly anharmonic, with the spacing between the levels displaying a small-large-small behavior. When the height of the barrier is increased, this anharmonicity increases and the $v = 0$ and $v = 1$ levels draw together. In the high barrier approximation these levels become degenerate and they are labelled 0^+ and 0^-. They become the first two members of the inversion manifold.

A number of different empirical functions have been used to fit double minimum potentials. The most popular model function contains three adjustable parameters:

$$V(Q) = Q^2/2 + A \exp(-a^2Q^2) \tag{1}$$

and may be considered to be a Gaussian function superimposed on a quadratic potential. Eigenvalues for this problem have been tabulated by Coon, Naugle and McKenzie [27] in terms of a reduced frequency, a variable barrier height and a shape factor. To transform the normal coordinate Q to the internal coordinate (the angle between the CO bond and the projection of the line bisecting the HCH angle) the differential relationship is often used:

$$dQ = G_{44}^{1/2} d\theta \tag{2}$$

This expression allows for the variation of the reduced mass as a function of θ, and takes account of the fact that the coordinates of the large amplitude bending mode are curvilinear, rather than rectilinear. In the excited state, formaldehyde is a
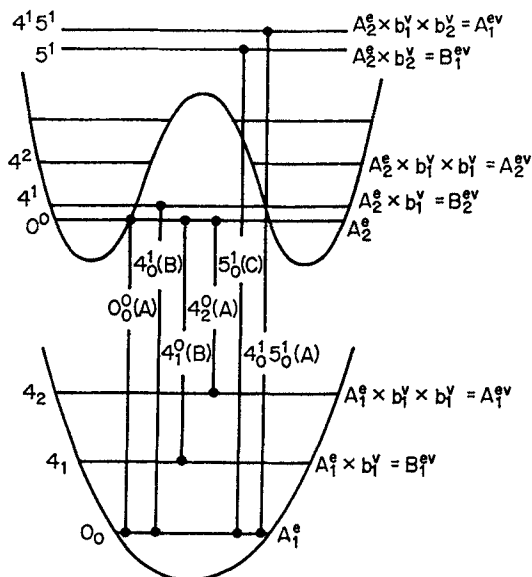
Fig. 6. The allowed vibronic transitions between a planar ground state and a nonplanar excited electronic state

176

floppy-flexible molecule [28] and the symmetry of the vibrational wavefunctions must be classified according to the operations of the nonrigid point group, G_4. As this group is isomorphous with the C_{2v} point group, it is possible to use the A_1, A_2, B_1 and B_2 symmetry symbols to designate the symmetry species.

The possible vibronic transitions between a planar $\tilde{X}^1A_1$ electronic state and a nonplanar $\tilde{A}^1A_2$ excited state are illustrated in Fig. 6. The potential for the Q_4 mode is shown as a single minimum function for the ground state and as a double minimum function for the excited state. Quanta of the in-plane antisymmetric modes v_5 and v_6, are symbolized by the 5^1 level. Since the levels 1^1, 2^1, 3^1, etc. attach to the 4^1, 5^1, 6^1, etc. states without altering the vibronic symmetry, they are not illustrated in the diagram.

The $\tilde{A}^1A_2 \leftarrow \tilde{X}^1A_1$ transition is forbidden by electric dipole radiation, although magnetic dipole and electric quadrapole transitions are possible. Among the strong perpendicular bands in the UV spectrum Dieke and Kistiakowsky [4] noted a few weaker bands of very different contour which they assigned as type-A (parallel polarization). These bands, which bear the assignment 0_0^0 and 4_0^2, are allowed by the vibronic selection rules. From a variety of experimental data and the process of elimination. Callomon and Innes [29] assigned these features to magnetic-dipole transitions. Figure 7 shows a typical type-A band.
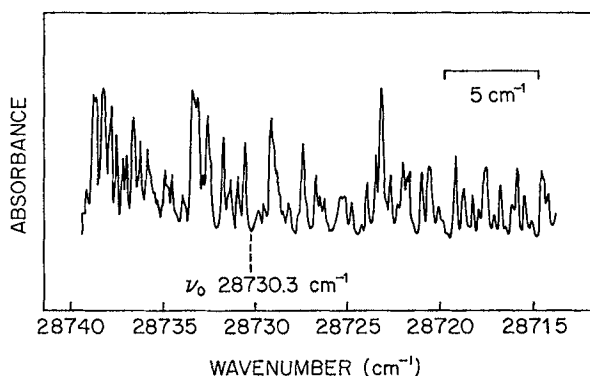
Fig. 7. The type-A band 4_0^2 of CH_2O

The type-B bands of y polarization give rise to the bulk of the intensity of the near UV system. The responsible vibronic coupling mechanism, which is illustrated in Fig. 4, allows odd quanta of the out-of-plane vibration, v_4, of b_1 species, to attach to the origin to form pseudo-origins of B_2 vibronic symmetry. These vibronic transitions owe their intensity to a borrowing (or stealing) of oscillator strength from allowed transitions to higher electronic B_2 states. The first Rydberg transition, which bears the orbital assignment n → 3s, is of the correct symmetry and appears to have sufficient strength to be the source for the intensity of the type-B system. The bands of x polarization are somewhat weaker. A mixing of the $n\pi^*$ state with the $n'\pi^*$ state of B_1 symmetry via the v_5 and v_6 vibrations of b_2 species would account for the x polarized intensity and for the type-C bands.

The Franck-Condon consequences of a planar ground electronic state combining with a nonplanar excited state are that the normal coordinate which most closely corresponds to the coordinate which defines the structural displacement will be active in the spectrum. In this case, it is the out-of-plane mode v_4. Odd quanta of v_4, viz., 4_0^1, 4_0^3, 4_1^0, etc. will appear as type-B bands whereas the 0_0^0, 4_0^2, 4_0^4, etc. transitions will give rise to type-A (magnetic dipole) bands. The 125 cm^{-1} interval between the first band (type-A) and the second band (type-B) which have assignments 0_0^0 and 4_0^1 respectively, is then the separation between the first two members of the inversion doubling manifold $0^+ - 0^-$. These bands act as sub-origins for extensive progressions in v_2, the carbonyl stretching mode. Figure 2 shows the arrangement. A similar progression in v_2, of C-type bands, attaches to a sub-origin at $+2968$ cm^{-1}. This interval was assigned to the antisymmetric CH stretching mode v_5. The v_3 mode, HCH bending, does not appear to be active. It has been detected, however, as a perturbation on the $2^1 4^1$ level. Table 3 gives the vibrational frequencies for formaldehyde and its isotopomers in the $\tilde{A}^1 A_2$ state.

Table 3. Vibrational frequencies[a] for the $\tilde{A}^1 A_2$ state.[b]

Mode	Approx. description	CH$_2$O	^{13}CH$_2$O	CHDO	CD$_2$O	CH$_2$S	CD$_2$S
$v_1(a_1)$	CH stretch	2846	—	2154	2079	3034	2139
$v_2(a_1)$	CX stretch[c]	1183	1158	1189	1175	820	771.3
$v_3(a_1)$	HCH bend	1293.1	1290	—	—	1316	1013
$v_4(b_1)$	wag[d]	124.5	123.1	96.1	67.0	371.1	275.3
$v_5(b_2)$	CH stretch	2968.3	—	2923.9	2234	3081.3	2324.9
$v_6(b_2)$	HCH rock	904	899	777	706	799	599

[a] in cm^{-1}. [b] ref. 9. [c] X = O or S. [d] $0^+ - 0^-$.
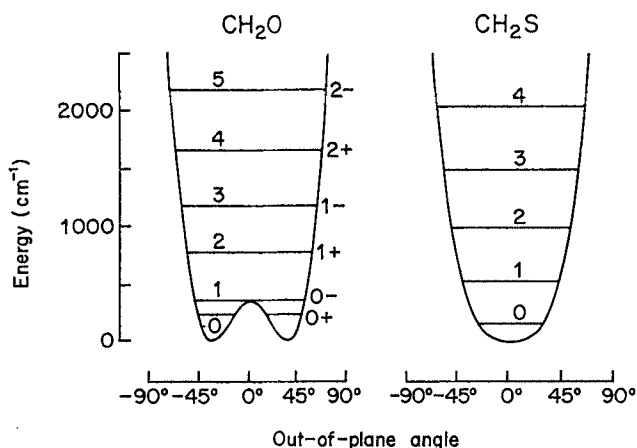
Fig. 8. Potential curves for the out-of-plane bending of CH$_2$O and CH$_2$S

Table 4. Inversion levels and structural parameters for the $\tilde{A}^1A_2$ state.[a, b]

	CH_2O	$^{13}CH_2O$	CD_2O	CH_2S	CD_2S
T_0	28 188.2[c]		28 302.5[c]	16 394.6	16 483.5
4^0	0.0	0.0	0.0	0.0	0.0
4^1	124.5	123.1	67.0	371.1	275.3
4^2	542.3	535.9	386	834.8	618.5
4^3	947.9	936.6	667.1	1 342.3	1 005.5
4^4	1 429.3	1 412.4	1015	1 881.4	1 430.5
$r(C=X)$[d]	1.323	1.331	1.328	1.682	1.707
$r(C-H)$	1.098	1.095	1.105	1.077	1.076
$\measuredangle(HCH)$	118.4	118.2	118.2	120.7	120.4
$\theta(min.)$	34.0	33.9	33.3	0.0	0.0
barrier	350.3	347.9	333.2	0.0	0.0

[a] in cm^{-1}, Å, and degrees. [b] ref. 9. [c] from $4_1^0 + 4_1$. [d] X = O or S.

Jones and Coon [30] fitted the inversion level data with the quadratic-Gaussian model function Eq. (1). They obtained a barrier height of 336 cm^{-1} for the $\tilde{A}^1A_2$ state and, from Eq. (2), an out-of-plane angle of 33.6°. The potential function has been further refined by allowing the HCH angle and the CO and CH bonds to vary as the carbonyl bond swings away from the molecular plane. The most detailed of these calculations are those of Jensen and Bunker [31] who made use of a semirigid-invertor Hamiltonian in which the rotational-inversion motions were treated simultaneously. Their results are presented in Table 4 and Fig. 8.

Judge and King [32] recorded the visible absorption spectrum of thioformaldehyde under conditions of long path length. Figure 9 shows a low resolution spectrogram.

The first bands in the spectrum were found to have a characteristic double headed appearance, and were assigned without difficulty to the $T_1 \leftarrow S_0$ triplet singlet $n \rightarrow \pi^*$ system. At somewhat higher energies, (16 394 cm^{-1}), the CH_2S spectrum displayed a band which has the line-like head characteristic of a type-A transition. The H_2/D_2 isotope effect identifies this band as the 0_0^0 transition of the $S_1 \leftarrow S_0$ system. It was assigned to the pure magnetic dipole transition. A somewhat stronger band at $+371$ cm^{-1} was observed which bears the K-type sub-band structure of a perpendicular transition. This was shown to be a type-B band and was assigned to 4_0^1. The observed interval is $(0^-) - (0^+)$. These bands are not too dissimilar in appearance to the 0_0^0 and 4_0^1 bands in CH_2O. A major difference is their intensities. In formaldehyde, the 4_0^1 Herzberg-Teller band has many times the strength of the magnetic dipole band. Here they have comparable intensities. As the strengths of the magnetic dipole transitions in CH_2O and CH_2S are expected to be similar, the differences in band intensity would have to be related to different vibronic coupling efficiencies in the two molecular systems.

All three band types are found in the spectrum of CH_2S. What is unusual is that Judge and King [33], in 1979, were able to bring the vibrational analyses of the excited state of $\tilde{A}^1A_2$ thioformaldehyde to a level which surpassed that of the lower ground electronic $\tilde{X}^1A_1$ state. Vibrational frequencies for the CH_2S/CD_2S pair are collected together in Table 3. Of interest are the levels of the wagging mode v_4. The intervals contained in Table 4 display the small-large variation expected for a large amplitude
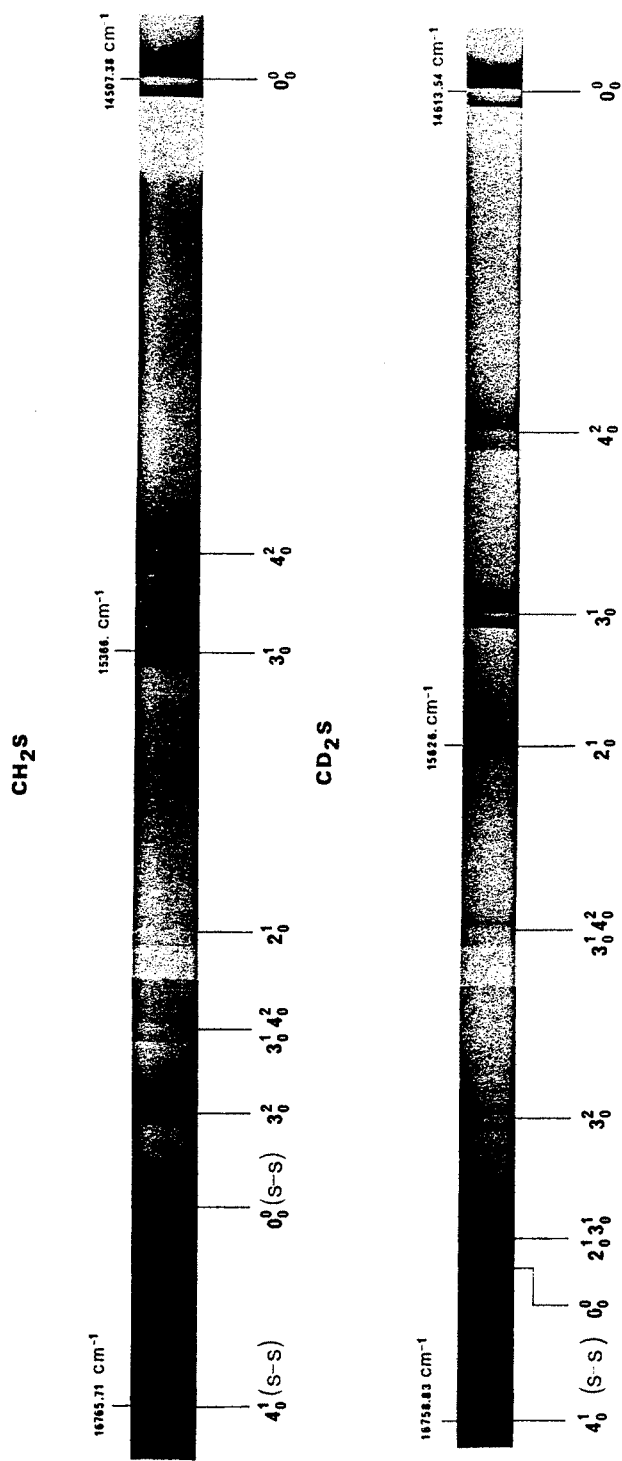
Fig. 9. Low resolution spectrogram of thioformaldehyde

vibration. A fit of this data to the invertor-rotational Hamiltonian shows that the potential does not contain a central barrier. That is, the molecule is planar in its equilibrium configuration. This is in contrast to the 350 cm^{-1} barrier and 34° out-of-plane angle of the $\tilde{A}^1A_2$ state of CH_2O. Structural parameters based on the rotational analyses of the 0_0^0 bands of CH_2O/CH_2S are given in Table 4.

2.1.3 The $T_1(n, \pi^*)$ Excited State

Among the weak bands on the long wavelength side of the near ultraviolet system of formaldehyde, Cohen and Reid [34] and shortly thereafter Brand [26] observed a few bands which had a rotational profile which was different from the other bands of the singlet-singlet system. From their temperature insensitivity, these bands were assigned to the triplet-singlet, $\tilde{a}^3A_2 \leftarrow \tilde{X}^1A_1$ transition. A powerful technique for distinguishing bands of triplet multiplicity from singlet bands is magnetic rotation spectrocopy. In this method an external magnetic field is applied along the axis of an absorption cell. The plane of polarized light is rotated by singlet-triplet transitions in the presence of a magnetic field. Since singlet-singlet transitions are unaffected by magnetic fields, the two systems can be separated from each other by introducing crossed polarizers at the ends of the cell. The result is that the singlet-triplet bands have the appearance of an emission spectrum, whereas the singlet-singlet spectrum is totally extinguished.

According to the spin selection rule $\Delta S = 0$, the singlet-triplet transition is forbidden. Intensity is introduced through a higher order coupling of the spin and orbital parts of the wavefunctions. Hougen [35] has described the effect of spin-orbit coupling on the rotational structure. Formaldehyde lacks axial symmetry about the $z(C=O)$ direction, and the electronic orbital angular momentum is not defined. The spin couples only weakly to the principal inertial axes (Hund's case b coupling), yielding three close-lying spin levels, F_1, F_2 and F_3, for a given rotational state. Birss and coworkers [36] have analyzed the rotational structure. They observed that the main contribution to the intensity of the rotational profile came from S, Q, and O form branches ($\Delta N = +2, 0, -2$) which were superimposed on parallel $\Delta K = 0$, type-A sub-origins. That is, the upper triplet wavefunctions act as if they have A_1 symmetry. In the case of the 4_0^2 band of CH_2O, very weak branches with $\Delta K = +2$

Table 5. Inversion levels[a] and structural parameters for the $\tilde{a}^3A_2$ state.

	CH_2O^c	CD_2O^c	CH_2S^c	CD_2S^c	CH_2Se^d	CD_2Se^d
T_0	25194:3	25312.9	14507.4	14613.5	12171.0	12262.7
4^0	0.0	0.0	0.0	0.0	0.0	0.0
4^1	36	9.9	311.8	222.7	297	208
4^2	538.2	448.8	711	516	681	493
4^3	777.2	569.5	1126.2	828.9	1074	793
4^4	1175.0	889.4	1544.1	1148	1475	1104
$r(C=X)^b$	1.307	1.316	1.683	1.686	—	—
$r(C—H)$	1.084	1.077	1.082	1.083	—	—
$\angle(HCH)$	121.8	121.5	119.3	119.2	—	—
$\theta(min.)$	41.1	43.0	11.9	13.0	—	—
barrier	775.6	769.0	4.1	5.7	13.1	16.2

[a] in cm^{-1}. [b] $X = O$, S or Se. [c] ref. 9. [d] ref. 24.

were observed. According to the Hougen expressions, the intensities in these branches depend upon a transition moment which is perpendicular to the z axis. The experimental intensity ratio of the perpendicular to parallel components was estimated to be 0.1. This observation indicates that it is the mixing of the $\tilde{a}^3A_2(n, \pi^*)$ state with the $^1A_1(\pi, \pi^*)$ state which is responsible for the parallel component of the band strengtth. The pathway for the perpendicular part of the band is believed to come from the $^1B_1(n', \pi^*)$ valence state. Structural parameters for $\tilde{a}^3A_2$ formaldehyde are given in Table 5.

The selection rules for vibronic transitions in a triplet-singlet transition do not allow for the activity of single quanta of the antisymmetric v_4, v_5 and v_6 modes, although double quantum additions are possible. For this reason, vibrational information for the $\tilde{a}^3A_2$ states is sparse. Table 6 gives the available vibrational frequencies.

Table 6. Vibrational frequencies[a] for the $\tilde{a}^3A_2$ state.

Mode	Approx. description	CH$_2$O[c]	CD$_2$O[c]	CH$_2$S[c]	CD$_2$S[c]	CH$_2$Se[d]	CD$_2$Se[d]
$v_2(a_1)$	HCH bend	—	—	1320	1012	1312	996
$v_3(a_1)$	C=X stretch	1283.0	1249.3	859	798	704	667
$v_4(b_1)$	wag[e]	538.2	448.8	711	516	681	—
$v_6(b_2)$	HCH rock[f]	—	—	—	—	812	563

[a] in cm^{-1}. [b] X = O, S or Se. [c] ref. 9. [d] ref. 24. [e] 4^2. [f] $6^2/2$.

Figure 9 shows that the singlet-triplet spectrum of thioformaldehyde has about the same strength as its companion spin-allowed system. The C=S stretching mode was observed to be strongly active at $+859/798$ cm^{-1} in the CH$_2$S/CD$_2$S pair. In contrast to formaldehyde, the HCH mode appears clearly in the spectrum as a weak band at $+1320/1012$ cm^{-1}. While the double quantum of the out-of-plane mode, 4^2, in the two isotopomers was sufficient to establish the form of the V_4 potential, additional inversion levels would be desirable. The application of the rigid-bender model yielded a low central barrier of 4.1 cm^{-1} and an out-of-plane angle of 11.9 degrees. The potential function for nonplanar distortion is broad and flat at its base with a central maximum well below the zero-point level. Rotational analyses [37] of the 0_0^0 bands of CH$_2$S and CD$_2$S led to the structural parameters of Table 5. Figure 10 shows a photograph of the origin band of CH$_2$S recorded under high resolution and the rotational assignments.

A weak absorption spectrum between 825 and 695 nm was observed by Judge and Moule [38] in the pyrolysis products of dimethyl selenide (CH$_3$)$_2$Se. The carrier was found to be a thermally unstable species and was identified from its band spectrum as selenoformaldehyde. The vibrational fine structure was consistent with that of a singlet-triplet transition. The spectrum was assigned to the $\tilde{a}^3A_2 \leftarrow \tilde{X}^1A_1$ transition. Glinski et al. [39] recently observed this same electronic transition as a phosphorescence emission spectrum which was generated from a reaction of molecular fluorine with dimethyl selenide. Figure 11 shows the spectrum.
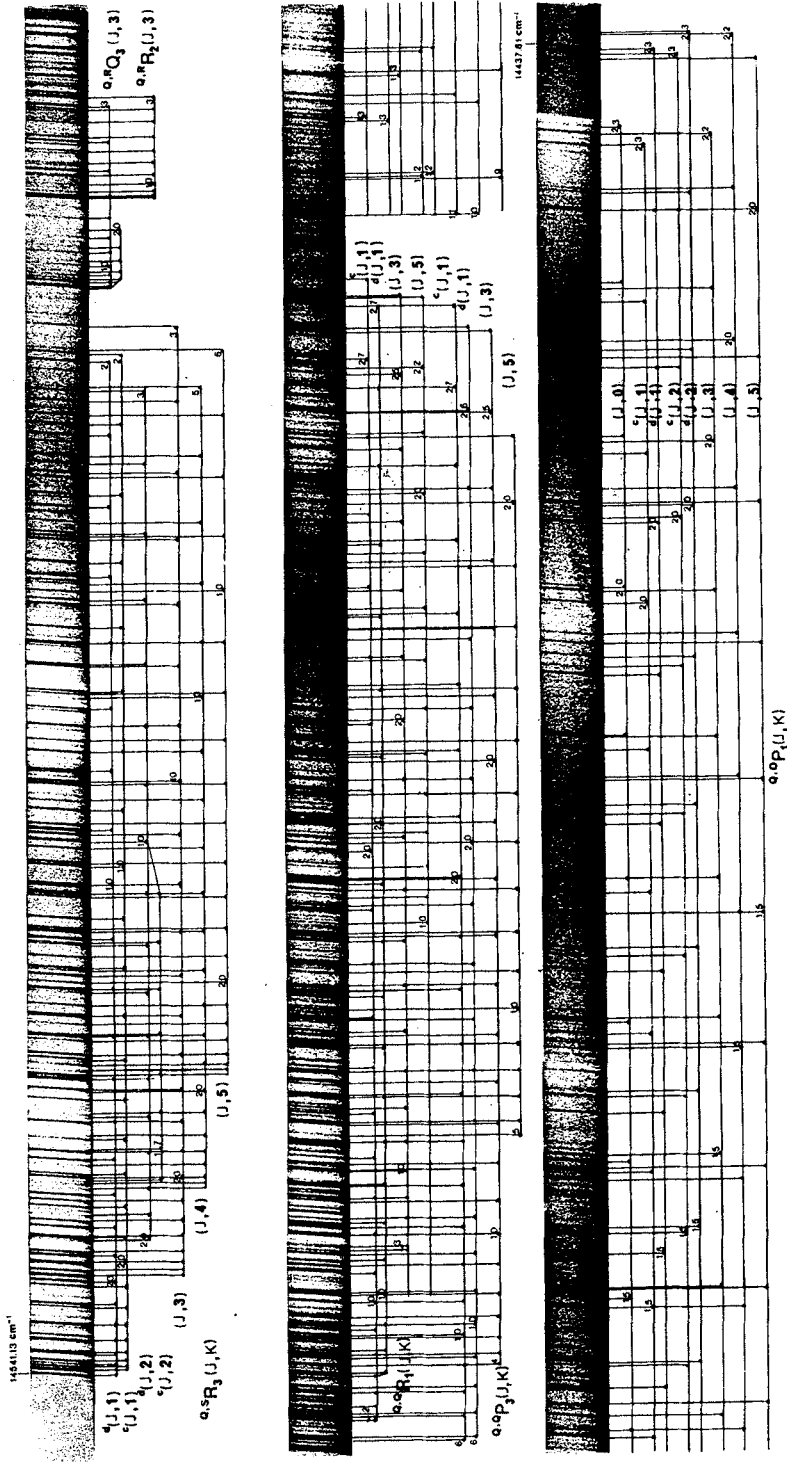
Fig. 10. The rotational structure of the $T_1 \leftarrow S_0$ 0^0_0 band of CH_2S
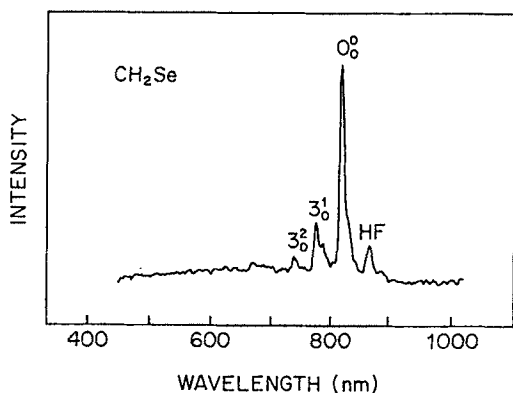
Fig. 11. Chemiluminescence spectrum of CH_2Se from the $(CH_3)_2Se—F_2$ reaction

The strongest bands in both the long path length absorption and the emission spectra were observed at 12171 cm^{-1}. From the mirror image relationship these bands were assigned to the 0_0^0 transition. Recently[40], an excitation spectrum has been recorded at high sensitivity. Figure 12 shows the spectrum. Quantum additions of v_2(HCH), v_3(CSe), $2v_6$ and $2v_4$ were observed to attach to the origin. The most interesting feature in the excitation spectrum is the weak structure observed between 13900 and 14000 cm^{-1}. The 20 to 30 cm^{-1} intervals are correctly spaced for the K-type sub-bands of a perpendicular transition. As vibronic-spin-orbit selection rules preclude the appearance of such transitions in the triplet-singlet spectrum, this structure is assigned to the singlet-singlet 4_0^1 band.
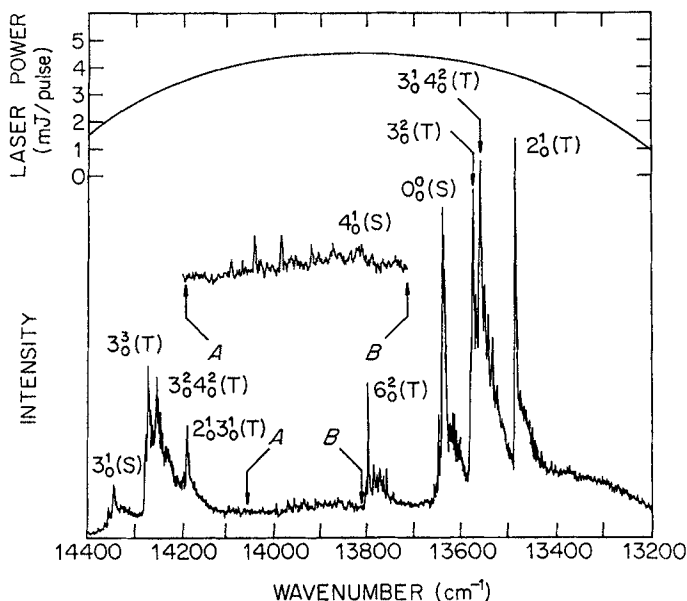
Fig. 12. The laser excitation spectrum of CH_2Se. The inset is a higher sensitivity scan of the $S_1 \leftarrow S_0$ 4_0^1 Band

184

2.1.4 Higher Excited States

The electronic states of CH_2O have been reviewed by Robin [10] and by Clouthier and Ramsay [9] and will not be treated here in detail. The first study of the vacuum UV spectrum was done by Price [41] in 1935. He observed many line-like bands which could be fitted into two Rydberg series which converged on a common limit. These progressions were assigned to the promotion of the n electron to the Rydberg 3s, 4s, ... , 3p, 4p, ... , orbitals. Under conditions of higher resolution, the transitions to the 3p orbitals could be resolved into two separate band systems, with the lower energy member displaying a double headed band contour which is characteristic of a type-A band. This series can be assigned as terminating on the p_y Rydberg component. The more diffuse neighbor would be the result of a promotion to the p_z Rydberg component. The transition to the third component $3p_x$ is electric dipole forbidden. Lessard and Moule [42] observed two sharp bands in the 143 nm region of the CD_2O spectrum which had type-C rotational profiles. These were assigned to the Herzberg-Teller active antisymmetric modes, v_x and v_6 which were attached to the 0^0 level. From frequency estimates for these modes, they predicted the origin of the $n \rightarrow 3p_x$ transition to lie at 67779 cm^{-1}. Recently, Taylor et al. [43] observed in a high resolution electron scattering experiment a peak at 8.374 eV (67539 cm^{-1}), which they assigned to an electric quadrupole transition terminating on the 0^0 level of the $^1A_2(n, 3p_x)$ Rydberg state. The discrepancy between the two frequency estimates for the $n \rightarrow 3p_x$ third Rydberg transition could be cleared up by observing the two-photon multiphoton ionization spectrum, as pointed out by Robin [10]. In the two-photon experiment, the 0^0_0 transition is allowed and should give rise to a strong band.

The CH_2O absorption in the 175 nm region is dominated by a strong band which was assigned by Allison and Walsh [44] to the Rydberg transition derived from $n \rightarrow 3s$ excitation. In addition to the normal vibrational fine structure at $+1577$ and $+2660$ cm^{-1}, which was assigned to the 2^1 and 1^1 vibrational quanta, diffuse bands appeared at $+346$ and $+822$ cm^{-1}. These intervals are too small to be accounted for by harmonic vibrations. It has been suggested [8] that the upper electronic state is
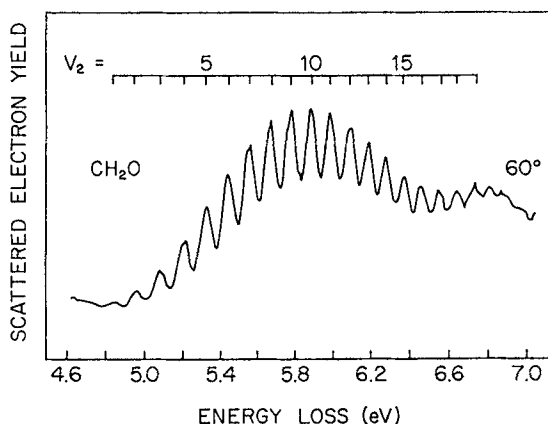
Fig. 13. The energy loss spectrum of CH_2O in the 4.6–7.0 eV region

nonplanar, thus giving rise to strongly anharmonic vibrations in v_4, or that it is distorted from C_{2v} geometry along the y direction with a double minimum in the v_6 potential. The ab initio calculations of Bell and Crighton [45] predict no such change in frequency for the antisymmetric vibrations. The low frequency structure must involve an unusual perturbation in the $\tilde{B}^1B_2$ Rydberg state. Excitation from the n orbital to the σ^* orbital has long been thought to give rise to an absorption in the 170 nm region. Theory [46] has placed this transition at 96 to 104 nm, and it is expected to appear as a shape resonance.

A many banded absorption is observed in the 144–136 nm region which broadens and shifts to longer wavelengths with the addition of a high pressure of inert gas. The calculations of Langhoff et al. [47] assign this system to an excitation from the second nonbonding n' (a_1) orbital to the antibonding π^* (b_1) orbital. The presence of the overlapping 3p and 3d Rydberg transitions obscures this part of the spectrum and as a result definitive vibrational assignments have not been made.

The identification of the $\pi \rightarrow \pi^*$ system in the short wave length absorption spectrum is one of the unanswered questions in the spectroscopy of formaldehyde. The most detailed calculations place the transition at 87270 cm^{-1} (10.82 eV). Because the $^1A_1$ state is calculated to lie above the first ionization potential, it would be autoionized by its ionization continuum. Theory [48] also predicts that the molecule is unbound along the CO coordinate in the upper state.

A number of triplet levels have been observed under high resolution electron impact [43]. As illustrated in Fig. 13, the 4.83 to 6.73 eV region displays an extensive progression of bands in an interval of 855 cm^{-1}, which was assigned to the CO stretching mode, v_2. A Franck-Condon calculation based on the intensity distribution shows that the CO bond undergoes an increase of $+0.21$ Å on electronic excitation. In the $n \rightarrow \pi^*$ promotion, an electron is lifted from a nonbonding into an antibonding π^* orbital. The bond order of the CO group drops from 2.0 to 1.5. This is accompanied by a decrease in v_2 from 1746 to 1183 cm^{-1} and an increase in r(C=O) of 0.116 Å. The large increase in bond length and the low vibrational frequency establishes the responsible state as $\tilde{b}^3A_2(\pi, \pi^*)$.

The major experimental difficulty with the UV and vacuum UV studies of the CH_2S/CH_2Se species is the chemical instability of their $\tilde{X}^1A_1$ ground states. These compounds must be synthesized and then immediately observed in a fast flow system. By its very nature, the pyrolysis reaction produces a complex mixture of side products. While these impurities are usually transparent in the visible and near IR, they do interfere and obliterate the far UV region below 200 nm. Because of the high oscillator strength, it is possible to record the spectrum of CH_2S with a 10 cm cell. A spectrophotometer recording is shown in Fig. 14. The onset of the absorption is characterized by an extensive system of bands [49] which can be grouped into a progression of 11 members in a frequency interval of 483 cm^{-1}. The low energy members were observed to have discrete rotational fine structure. In appearance, this spectrum is very similar to the electron scattering spectrum of CH_2O, Fig. 13, as the assignment is to the same valence excitation $\pi \rightarrow \pi^*$. However, in H_2CS, the transition is spin allowed, $\tilde{B}^1A_1 \leftarrow \tilde{X}^1A_1$.

The length and strength of the progression allow it to be assigned to activity of the C=S mode. The drop in frequency is compatible with a change in bond order from 2 to 1 as a result of the π to π^* electron excitation.
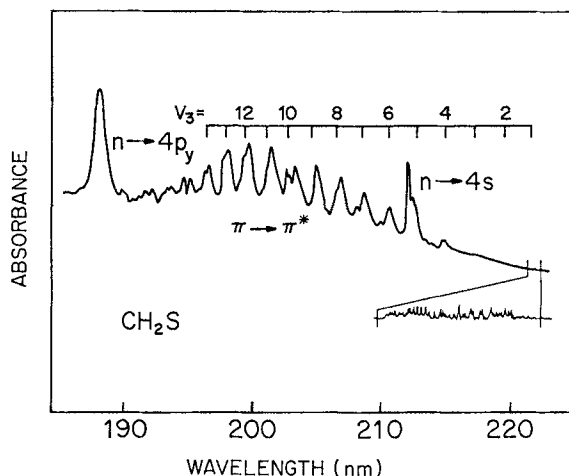
Fig. 14. The UV absorption spectrum of CH_2S

The bands of the valence transition merge into a strong line-like absorption [50] at 212 nm. On the basis of its Franck-Condon profile, it was assigned to the first Rydberg transition, $\tilde{C}^1B_2(n, 4s) \leftarrow \tilde{X}^1A_1$. A rotational analysis of the 0^0_0 bands of CH_2S/CD_2S led to a planar r_0 structure: $r(C=S) = 1.6047$ Å, $r(CH) = 1.1119$ Å and $\angle(HCH) = 122.68°$. Excitation to the first Rydberg state is accompanied by a $5.81°$ increase in HCH angle, but more surprisingly a 0.007 Å decrease in the $C=S$ bond length. Two additional members of the Rydberg complex were observed at higher energies as narrow but diffuse bands. These bands are the result of excitation to the Rydberg $4p_y$ and $4p_z$ orbitals. Table 7 collects together the data for formaldehyde and thioformaldehyde.

The UV spectrum of selenoformaldehyde has not been observed. Ab initio estimates [51] of the transition energies are included for the sake of comparison. Of interest is the prediction that the lowest triplet state at 1.42 eV is derived from $\pi \to \pi^*$ excitation. Perturbations arising from the $^3A_1(\pi, \pi^*)$ state have not been observed among the vibronic levels of the $^3A_2(n, \pi^*)$ state.

2.2 Carbonyl, Thiocarbonyl, Selenocarbonyl Halides

Carbonyl and formyl halides: CF_2O, $CClFO$, and CCl_2O are stable gases and are commercially available. CBr_2O is a liquid and is prepared by the reaction of tetrabromomethane with concentrated sulfuric acid. The replacement of a halogen atom by hydrogen decreases the molecular stability. Formyl fluoride, CHFO, is usually generated, as needed, by the fluorination of dry formic acid with NaF. CHClO is unstable, and must be prepared in a flow system. The procedure is to pass formic acid vapor over solid PCl_5 immediately before it is to be used. The bromine compound, CHBrO, is very short lived. It has been prepared in the vapor phase by the photolysis of a bromine-formaldehyde mixture.

187

Table 7. Observed and calculated singlet and triplet excitation energies[a] of CH_2O, CH_2S and CH_2Se.

State	Excitation[d]	CH_2O[b]			CH_2S[b]		CH_2Se[c]
		Optical	El. Loss	Theory	Optical	Theory	Theory
$^1A_1$		0.0	0.0	0.0	0.0	0.0	0.0
$^3A_2$ } $n \rightarrow \pi^*$		3.124	3.50	3.41	1.799	1.84	1.62
$^1A_2$ }		3.495	3.94	3.81	2.033	2.17	2.02
$^3A_1$ } $\pi \rightarrow \pi^*$		—	5.53	5.56	—	3.28	1.42
$^1A_1$ }		—	—	11.41	5.60	7.92	4.94
$^3B_2$ } $n \rightarrow Ns$		—	6.827	7.32	—	5.72	5.46
$^1B_2$ }		7.089	—	7.38	5.841	5.83	5.25
$^3A_1$ } $n \rightarrow Np_y$		—	7.790	8.09	—	6.58	5.98
$^1A_1$ }		7.965	—	8.11	6.60	6.62	6.66
$^3B_2$ } $n \rightarrow Np_z$		—	7.955	8.29	—	—	5.86
$^1B_2$ }		8.115	—	8.39	6.82	—	5.48
$^3A_2$ } $n \rightarrow Np_x$		—	—	9.06	—	—	6.83
$^1A_2$ }		8.50	8.374	9.07	—	—	5.88
$^3B_1$ } $n' \rightarrow \pi^*$		—	—	8.14	—	6.38	—
$^1B_1$ }		8.68	—	9.03	—	7.51	—

[a] in eV. [b] ref. 9. [c] ref. 51. [d] $N = 3, 4$ or 5.

Thiocarbonyl and thioformyl halides: Of the thiocarbonyl compounds, only thiophosgene, Cl_2CS, is commercially available. It is a volatile, pungent, red-colored liquid. The compounds CClFCS and CF_2CS are also stable in the vapor phase, due to the electron withdrawing substituents. They are prepared by the partial or complete fluorination of CCl_2S by a halogen exchange reaction with SbF_3. Likewise, CBrClS and CBr_2S are synthesized by the direct bromination of thiophosgene through a BBr_3 exchange. The dimer of CF_2S can be purchased as the liquid, which can be cleanly pyrolyzed to form the monomer. CHClS is the only known thioformyl halide. This species is unstable in the vapor phase and exists under low pressure conditions for about 5 s. It was prepared in poor yield by the flash pyrolysis of chloromethyl methyl sulfide.

Selenocarbonyl halides: Only two selenocarbonyl halides are known, CF_2Se and CCl_2Se. Selenocarbonyl difluoride is formed by the pyrolysis of $B(SeCF_3)_3$ in the presence of KF. Chlorination with Cl_2 gives the dichloride.

2.2.1 The Ground State

The structural parameters for the ground electronic states of the carbonyl, thiocarbonyl and selenocarbonyl halides are collected together in Table 8, along with an estimate of the experimental precision which is given in parentheses. Average structures r_z, r_{av}, or r_g, which combine the microwave and electron diffraction parameters, are quoted wherever possible for the sake of comparison. Only electron diffraction data, yielding r_α^0 values, are available for CF_2Se and CBr_2O. For absorption in the microwave, the species must possess a permanent electric dipole moment. The IR spectrum of CF_2S was recorded without difficulty, yet its small dipole moment of 0.080 debye made its microwave detection difficult. The unstable species CHClS and CHBrO have not been characterized by either microwave or by electron diffraction methods.

The stable carbonyl and thiocarbonyl halide molecules have been studied by IR as well as Raman spectroscopy. Normal coordinate analyses based on force constants transferred from other molecules (Urey-Bradley type), or from ab initio calculations, have aided in the vibrational assignments. Some of the unstable molecules which have been observed in the microwave have been characterized by infrared spectroscopy. The somewhat lower sensitivity of this method means that long path lengths of the gas may be needed. The identification of the various stable and unstable species in the microwave spectrum is simplified by the fact that the absorption lines are usually well resolved from each other. The widths of the bands in the infrared may make the transient species difficult to detect against the stronger absorptions of the stable side products. IR and Raman spectroscopies do have the advantage that they can be used on solid and liquid samples. Since the bands in a low temperature rare gas matrix have a narrower profile, the infrared spectrum is usually simplified over the room temperature gas phase spectrum. Moreover, the vibrational frequencies are only mildly perturbed by solid state effects. For example, CF_2Se has not been observed in the vapor phase, yet its vibrational dynamics are known from its matrix isolation spectrum. Table 9 gives the vibrational data for the carbonyl, thiocarbonyl, seleno-carbonyl and formyl halides.

2.2.2 The $S_1(n, \pi^*)$ Excited State

C_{2v} Type Molecules: The low energy electronic transition in the $C=X$ chromophore is the result of an $n \rightarrow \pi^*$ electron promotion. This is a forbidden transition in C_{2v} type molecules. As discussed in 2.1.2, the observed intensity results from a vibronic coupling of S_1 to higher electronic states of the molecule. The energy levels, symmetry and coupling schemes for CH_2O are illustrated in Fig. 4. Magnetic dipole transitions have

Table 8. Structural parameters[a] for the carbonyl, thiocarbonyl, selenocarbonyl and formyl halides.

Molecule		C_{2v} Molecules $X_2C=Y$			
		$r(C=Y)$	$r(C-X)$	$\angle(X-C-X)$	Ref.
CF_2O	r_z	1.1717(13)	1.3157(8)	107.71(8)	[52]
CF_2S	r_{av}	1.5894(17)	1.3165(11)	107.05(16)	[53]
CF_2Se	r_α^0	1.743(3)	1.314(2)	107.5(4)	[53]
CCl_2O	r_z	1.1785(26)	1.7424(13)	111.83(11)	[54]
CCl_2S	r_z	1.602(5)	1.728(3)	111.2(4)	[55]
CBr_2O	r_z	1.178(9)	1.923(5)	112.3(4)	[56]
CBr_2S	r_α^0	1.597(5)	1.894(9)	111.6(4)	[57]

Molecule		C_s Molecules $XZC=Y$[b]					
		$r(C=Y)$	$r(C-X)$	$r(C-Z)$	$\angle(YCX)$	$\angle(YCZ)$	Ref.
CHFO	r_{av}	1.188(4)	1.11(2)	1.346(3)	130(4)	122.3(2)	[58]
CHClO	r_z	1.1853(3)	1.0944(3)	1.7716(2)	126.49(4)	123.07(1)	[59]
CClFO	r_{av}	1.173(2)	1.334(2)	1.725(2)	123.7(2)	127.5(3)	[60]
CClFS	r_s	1.5931(8)	1.3387(14)	1.7178(9)	123.58(12)	127.28(9)	[61]

[a] in Å and degrees. [b] X = atom of lower atomic weight, Z = atom of higher atomic weight.

not been observed in the halide molecules. This is partly because of the low Franck-Condon factors for the 0_0^0 band relative to the higher bands in the spectrum as a result of the unusual activity in the carbon-halogen stretching and bending modes. The nonbonding MO in the halides also appears to affect the magnetic dipole transitions. Calculations [76] at the CNDO/2 level show that while the n MO in CH_2O has a node across the CO bond (antibonding), the nonbonding orbital is nodeless (bonding) in CF_2O. The result, for CF_2O, is that the magnetic dipole strength from the carbon center cancels the contribution from the oxygen end of the molecule thereby reducing the 0_0^0 band intensity.

Unlike CH_2O, all but a few of the observed bands [77,78] in the CF_2O and CCl_2O spectra may be accounted for by y polarized (B-type) transitions. It would appear that the main pathway for intensity borrowing involves the out-of-plane v_4 wag and that higher Rydberg states of B_2 species are responsible for the induced electric dipole strength. The weakness of the C-type transitions is somewhat surprising. $M_b^a 6_1^1$ sequence bands have been observed [79] in the room temperature excitation spectrum of CCl_2S. From their band heads and the value of v_6 in the ground state, it is possible to predict the positions of the 6_0^1 C-type bands. Weak bands observed in the −78 °C spectrum of CCl_2S have been given this assignment. The jet spectrum [80] of CBr_2S should be of help in this respect since it provides a clear view of the weaker vibronic features in the $S_1 \leftarrow S_0$ transition of a thiocarbonyl halide. While the 6_0^2 overtone bands in the dibromide system are found to attach to the stronger bands throughout

Table 9. Vibrational frequencies[a] of the ground electronic states of the carbonyl, thiocarbonyl, selenocarbonyl and formyl halides.

	C_{2v} Molecules $X_2C=Y$						
Molecule	C=Y str. (a_1)	C—X str. (a_1)	XCX bend (a_1)	Wag (b_1)	C—X str. (b_2)	XCX bend (b_2)	Ref.
CF_2O	1929.9	965.6	582.9	619.9	1243.7	774.0	[62,63]
CF_2S	1368	787	526	623.4	1189	417	[64]
CF_2Se	1287	705	432	575	1207	351	[65]
CCl_2O	1828.2	567	285	580	851.0	440	[66]
CCl_2S	1139.0	503.5	288.5	471.0	818	305	[67,68]
CCl_2Se	991	437	260	—	805	248	[69]
CBr_2O	1828	425	181	512	757	350	[66]
CBr_2S	1116.3	367	183	415	697	230	[70]

	C_s Molecules $XZC=Y$[b]						
Molecule	C=Y str. (a′)	C—X str. (a′)	C—Z str. (a′)	ZCY bend (a′)	ZÇX bend (a′)	Wag (a″)	Ref.
CClFO	1868	1095	764.2	501	415	667	[71]
CClFS	1257.7	1014.7	611.9	427.1	322.6	539	[72]
CHFO	1836.8	2981.0	1064.8	1342.5	662.5	—	[73]
CHClO	1784.1	2929.2	738.8	1307.0	458.0	932.1	[59]
CBrClS	1130	764	438	256	236	441	[74]
CHBrO	1789.6	2912.5	646.0	1276.2	—	894.0	[75]

[a] in cm^{-1}. [b] X = atom of lower atomic weight, Z = atom of higher atomic weight.

the spectrum, the expected 6_0^1 C-type bands are missing. This is somewhat surprising since the vibronic coupling mechanisms should be similar in the two molecules. The general conclusion is that the $n \to \pi^*$ transitions in the carbonyl and thiocarbonyl halide molecules are y polarized and that the bands are governed by type-B selection rules.

The energy level diagram which shows the arrangement of the y polarized vibronic transitions in CH_2O was given in Fig. 6 and can be used here. The majority of the observed bands can be assigned to transitions which begin on 4_0 (ground electronic state zero-point level) and terminate on the $4^1(0^-)$, $4^3(1^-)$, $4^5(2^-)$ . . . levels of the out-of plane mode Q_4. At room temperature, the 4_1 level is usually populated and transitions to the $4^0(0^+)$, $4^2(1^+)$, $4^4(2^+)$ . . . levels are also observed. Transitions which involve quanta of v_4 are active because of Herzberg-Teller vibronic coupling. The length of the progression depends on the extent to which the S_1 state becomes nonplanar. Attached to these pseudo-origins are quanta in the totally symmetric modes $v_1(C{=}X)$, $v_2(C{-}Y)$, and $v_3(YCY)$. As the n and π^* MO's of the $C{=}X$ group extend and interact with the orbitals on the halogen centers, quite large changes are observed in the $C{-}X$ and XCX bonding coordinates. As a result, v_2 and v_3 are active in forming progressions. These quanta attach to each other to form various overtone or combination states and the vibrational energy manifold quickly becomes dense and complex. For this reason, the spectrum at $+1000 \text{ cm}^{-1}$ above the T_0 origin is usually congested and too complicated to be assigned with certainty.

The height of the barrier to molecular inversion represents one of the more important pieces of dynamical information. The most reliable values for the height come from the $(v^-) - (v^+)$ inversion doubling splittings in Q_4. These are usually derived from the hot band intervals by the ground state combination difference $\delta_1 = (1^-) - (1^+) = 4^3 - 4^2 = 4_0^3 - 4_1^2 + 4_1$. An ideal case [68] is CCl_2S, where it is observed that each of the cold bands $(v'' = 0)$ is accompanied by a hot band satellite at some 471 cm^{-1} to lower energies. This makes it possible to measure the inversion doubling splitting for many of the higher vibronic energy levels. The inversion splittings may be used as an aid in the assignment since the magnitude of δ increases dramatically for each quantum of v_4. For example, in the $\tilde{A}^1A_2$ state of CCl_2S, the splittings increase as $\delta_0 = (0^-) - (0^+) = 0.4$, $\delta_1 = (1^-) - (1^+) = 12.9$, $\delta_2 = (2^-) - (2^+) = 139.9 \text{ cm}^{-1}$. The magnitude of δ, the inversion splitting associated with each of the upper levels, is a way of establishing the v_4 quantum numering.
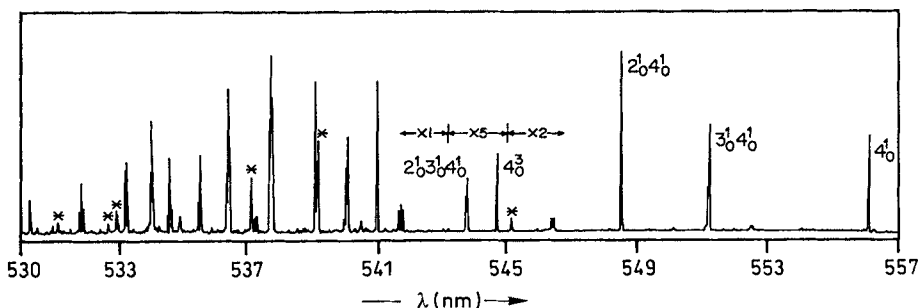
Fig. 15. The laser excitation spectrum of jet-cooled CBr_2S. The asterisks denote impurity bands

Qualitative information about the shape of the double minimum potential can be obtained from the strength and the length of the individual band progressions. The Franck-Condon principle states that the most probable transitions in absorption are those which occur vertically upwards. For planar-planar states in a forbidden electronic transition, the 4_0^1 pseudo-origin would be strong, while the next member, 4_0^3, would be weak or absent. The $S_1 - S_0$ system for CH_2S described in section 2.1.2 is an example. In the planar-nonplanar case illustrated in Fig. 6, the transitions from the ground state terminate on high levels of the double minimum potential. The result is a weak 4_0^1 pseudo-origin and a progression of stronger 4_0^3 and 4_0^5 bands. The molecule CF_2O is an example [77] where the barrier is very high (8200 cm^{-1}). In this case the progressions in v_4 dominate the spectrum and can be tracked out for 6 members with surprisingly little anharmonicity. It is only at $v' = 4$ that a perceptible inversion splitting is evident. It was this $\delta_4 = 0.3$ cm^{-1} splitting which was used to determine the barrier height.

The intensity relationship among the bands is another important aspect. It is possible to assume that the normal modes are well behaved, and an intensity ratio such as $I(n_0^1 4_0^1)/I(4_0^1)$ is determined by the component of the structural displacement along the Q_n normal coordinate ($n = 1, 2, 3$). To convert these normal coordinate displacement vectors to changes along the internal coordinates (bond lengths and bond angles) it is necessary to perform a Duchinski transformation [81]. If little internal coordinate mixing occurs in the formation of normal coordinates (valence vibrations), the Duchinski rotation will be small and the band intensities within each progression can be related directly to the structural changes. If the internal coordinates are strongly mixed, it is possible for the intensity profiles to show constructive or destructive interference. That is, strong activity may be observed in a vibrational mode in which the corresponding change in the bond length is small. In the case [68] of CCl_2S, the $v_2(CCl)$ mode is found to be strongly active in the spectrum. When Duchinski rotation is taken into account, the bond undergoes only a modest displacement of $+0.022$ Å. The major contribution to the intensity, about 80%, is associated with the $+0.10$ Å extension in the length of the $C=S$ bond.

A number of techniques may be employed as aids in the assignment of the vibrational fine structure:

a) If the species is stable with a low boiling point (CF_2O, CCl_2O, CF_2S) it is often possible to record the spectrum at low temperatures (-78 °C) and at long path lengths (60 m). At this temperature the ground state levels with $+500$ cm^{-1} of vibrational energy or greater will be sufficiently depopulated that the cold bands ($v'' = 0$) can be clearly distinguished. For less volatile molecules (CCl_2S, CBr_2S), supersonic jet spectroscopy has proven to be fruitful in reducing the band congestion and clarifying the spectrum.

b) Structural changes occur in the YCY end of these molecules as a result of halogen participation in the n and π^* MO's, and progressions in v_1, v_2, and v_3 may be formed which build onto the 4_0^1 and 4_0^3 pseudo-origins. These origins are usually located by extrapolating the band positions back to a common point through the use of Deslandres tables.

c) The isotope effect, where it can be measured, is another powerful tool. In the case of thiophosgene, the chlorine isotopomers 35,35/35,37/37,37 have natural abundances of 9/6/1. Since the bands in the spectrum appear with an almost atomic
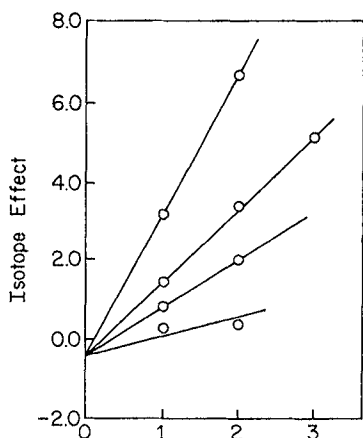
Fig. 16. The chlorine 35/35 35/37 isotope effect in S_1 CCl_2S

line-like profile, the two more abundant species can readily be identified. It is possible to group the vibrational modes in CCl_2S into those which are only moderately sensitive to chlorine isotope substitution, $v_1(C=S)$ and v_4 (out-of-plane), and those which show a marked isotope effect, $v_2(CCl)$ and $v_3(ClCCl)$. A plot of the 35,35/35,37 chlorine isotope effect on the vibrational modes is shown in Fig. 16.

d) The identification of transitions which originate on the 4_1 level and terminate on levels bearing a 4^0, 4^2 of 4^4 assignment fixes the inversion doubling splitting parameters. Since the inversion splittings δ_0, δ_1 and δ_2 are sensitive to the barrier height, they can be used to establish the v_4 quantum numbering in a complex band system.

e) Ab initio calculations have improved to the extent that it is now possible to obtain good estimates for the vibrational frequencies and molecular structures for both of the combining states. This information can be combined into a polydimensional Franck-Condon analysis from which a theoretical band spectrum can be synthesized.

C_s Type Molecules: The formyl, thioformyl, and the Br, Cl and F mixed halides have reduced symmetry and are grouped together. The vibrational modes either lie in the molecular plane (a'), or are directed out of the plane (a''):

$$\Gamma_v = 5a' + a''$$

In the electronic ground state, the 5 in-plane vibrations give rise to IR-active A/B hybrid bands. The v_6 fundamental produces a C-type band which can be identified by its line-like Q branch. While the ground electronic state has total symmetry A', the n, π^* upper state is of A'' species. The 0_0^0 transition is allowed as a C-type band, as are the quantum additions of $v_1 \ldots v_5$. Odd quanta of v_6, viz. 6^1, 6^3, etc. are forbidden in the first order, but may appear as vibronic A/B hybrids. Even though the electronic transition is formally allowed, the oscillator strengths are not that different from the C_{2v} molecules discussed earlier. It would appear that the local environment is more important in determining the transition strength than is the overall symmetry. The electron promotion process involves the n and π^* orbitals which are of a' and a''

species. Electric dipole radiation requires electrical charge translation and is unable to effectively connect these orbitals together, so the electric dipole transitions are weak. Additional band congestion is observed in C_s molecules since the symmetry allowed C-type bands are often of the same strength as the vibronically induced A/B hybrids. In addition, the reduced symmetry allows all five a′ modes to be active. Transitions to both upper and lower members of the inversion manifold are now possible, which leads to a doubling of the bands and further complexity. In those cases where the barrier is relatively low it is possible to resolve the $(0^+) - (0^-)$ doublets as two separate bands. For example,[82] in CHClO the 6_0^1 transition appears as an A/B band $+119.6 \text{ cm}^{-1}$ above the 0_0^0 C-type origin. This information, along with a 6^2 level at $+653.4 \text{ cm}^{-1}$, established the barrier height to be 616.3 cm^{-1}. An advantage of the lower C_s symmetry is that the barrier determination can be made without recourse to hot band structure. When the atoms are heavier, such as in CClFS, the inversion splitting becomes so small [83] that all three bands are brought together in a single contour. In this case, the splitting could be determined by comparison of calculated and observed band contours. The inversion splitting $\delta_1 = 0.3 \text{ cm}^{-1}$ came from the separation between the A/B and C-type bands.

2.2.3 The $T_1(n, \pi^*)$ Excited State

Triplet-singlet transitions are forbidden by the spin selection rule, $\Delta S = 0$. These systems have not been observed [89] in the formyl or carbonyl halides even at very long path lengths and high gas pressures, although the $T_1 \leftarrow S_0$ absorption in CH_2O can be recorded without too much difficulty. Intensity is introduced into these

Table 10. Vibrational frequencies[a] of the S_1 excited electronic states of the carbonyl, thiocarbonyl, selenocarbonyl and formyl halides.

Molecule	C_{2v} Molecules $X_2C=Y$						
	C=Y str. (a_1)	C—X str. (a_1)	XCX bend (a_1)	Wag (b_1)	C—X str. (b_2)	YCX bend (b_2)	Ref.
CF_2O	1056.2	834.1	470.0	669.1	1252.1	—	[77]
CF_2S	1100.6	736.5	385.8	557.9	—	—	[84]
CF_2Se	1129	662	388	539	—	—	[85]
CCl_2O	1152	552	301	439.5	—	—	[78]
CCl_2S	907.4	480.0	245.0	279.6	—	189	[79]
CBr_2S	890	250	160	383	242	166	[80]

Molecule	C_s Molecules $XZC=Y$[b]						
	C=Y str. (a')	C—X str. (a')	C—Z str. (a')	ZCY bend (a')	ZCX bend (a')	Wag (a'')	Ref.
CClFS	877.3	964.0	583.0	348.3	223.8	409.3	[83]
CHFO	1112	—	—	1286	450	462	[86]
CHClO	1153.8	—	633.6	—	306.3	779.5	[82]
CBrClS	890	540	423	159	207	273	[80]
CHClS	848.0	—	556.3	1338.7	230.2	119.7	[87]

[a] in cm^{-1}. [b] X = atom of lower atomic weight, Z = atom of higher atomic weight.

Table 11. Electronic origins, $S_1 - T_1$ energy separations, barrier heights, and out-of-plane angles of the S_1 states of $X_2C=Y$ and $XZC=Y$ molecules.[a]

	T_0	Barrier	θ(min.)	$\Delta E(S_1 - T_1)$	Ref.
CF_2O	39252	8200	31.8	—	[77]
CF_2S	23477	3076	30.5	1286	[84]
CF_2Se	19689	2483	30.1	671	[85]
CCl_2O	33631	3170	32.5	—	[78]
CCl_2S	18716	620	32	1224	[68]
CBr_2S	17992	465	19	1133	[80]
$CHClO$	32754	1609	48.6	—	[82]
$CHClS$	18792	616	25	1558	[87]
$CClFS$	21657	1556	38	—	[83]
$CBrClS$	18363	538	26	1247	[80]
$CHFO$	37490	2550	29.7	—	[88]

[a] in cm^{-1} and degrees.

forbidden transitions by a coupling of the triplet levels to singlet electronic levels of the molecule through the spin-orbit operator. In the case of CH_2O, which was outlined in section 2.1, it was a coupling of the $\tilde{a}^3A_2(n, \pi^*)$ and $^1A_1(\pi, \pi^*)$ states which was responsible for the intensity and the band polarizations. The oscillator strength of a $T_1 \leftarrow S_0$ transition $(f(n \rightarrow \pi^*))$ can be derived [90] from perturbation theory as:

$$f(n \rightarrow \pi^*) = H^2 \cdot f(\pi \rightarrow \pi^*) \cdot v(n \rightarrow \pi^*)/v(\pi \rightarrow \pi^*) \cdot [E(^1A_1) - E(\tilde{a}^3A_2)]^2 \qquad (3)$$

where $f(\pi \rightarrow \pi^*)$ is the oscillator strength of the $^1A_1(\pi, \pi^*) \leftarrow \tilde{X}^1A_1$ allowed transition. $E(^1A_1) - E(\tilde{a}^3A_2)$ is the energy difference between the perturbing $n\pi^*$ and $\pi\pi^*$ states, and H is the matrix element $\langle ^1A_1| H_{so} |\tilde{a}^3A_2\rangle$ which connects the two states together. The reduction in triplet-singlet absorption strength in the keto-halides is unexpected since the spin-orbit operator H_{so} contains the atomic spin-orbit operator ξ which varies as the fourth power of the atomic number. It would be anticipated that the higher Z of the halogen substituents would contribute a heavy atom effect and enhance the singlet-triplet transition probability. CNDO/2 theory [76] has been used to rationalize this anomaly. It was found that the halogen orbitals in the π MO are antibonding relative to the carbonyl 2p orbitals. As a result, the Cl and F substituents have the effect of reducing the spin-orbit matrix elements of the keto-halides relative to those of the dihydro compound.

The effect of replacing sulfur by oxygen is dramatic. As was pointed out earlier, the strength of the triplet-singlet transition in CH_2S is roughly the same as that of the corresponding singlet-singlet transition. Two factors in Eq. (3) contribute to the observed oscillator strengths in the thiocarbonyl compounds. The higher spin-orbit coupling constants of sulfur relative to oxygen, 382 versus 152 cm^{-1}, are partly responsible. The other factor is the position of the $^1A_1(\pi, \pi^*)$ state. This state has not been observed for CH_2O although it has been predicted by theory to lie at 11.4 eV

195

(109 nm). In CH_2S it can be observed without much difficulty at 5.60 eV (221 nm). The different perturbation gaps in the two molecules of 8.28 and 3.80 eV respectively, lead to a 5-fold enhancement of the oscillator strength in the thioketo compounds relative to the corresponding keto compounds. The effect of halogen substitution can be clearly observed in CCl_2S where the $f(T_1 \leftarrow S_0)/f(S_1 \leftarrow S_0)$ oscillator strength ratio has been measured to be $1/6$. The reduction in the triplet-singlet strength, as described earlier, must come from interference effects introduced through the chlorine MO coefficients.

The vibrational fine structure which is observed within the $T_1 \leftarrow S_0$ systems of the thiocarbonyl halides displays frequency and intensity patterns which are similar to those observed in the $S_1 \leftarrow S_0$ systems. Indeed, a useful technique is to use the singlet-singlet spectrum as a template against which to compare and assign the triplet-singlet spectrum. This was particularly useful in the analyses [80] of the CBr_2S and CBrClS molecules, where the spectra are badly congested with $S_1 \leftarrow S_0$ hot band structure. A major distinction between the two systems is the different band patterns which are a consequence of the different selection rules, rather than large frequency differences between the excited singlet and triplet states. The vibronic-spin-orbit selection rules which operate for transition to the triplet state do not allow for the activity of odd quanta of the antisymmetric vibrations. The lack of vibronically induced bands does have the effect of simplifying the $T_1 \leftarrow S_0$ spectrum. Perhaps the greatest difficulty with the assignment of room temperature spectra is that the hot bands of the singlet-singlet system are often more intense and lie in the same region as the triplet-singlet bands, and the multiplicity of each band must be established.

Of the halide molecules studied to date, thiophosgene has been the most thoroughly investigated. It has the advantage that it is stable and is commercially available. Moreover, the narrowness of the lines under high resolution allows the built-in isotope effect to be exploited. The problem of spin multiplicity in CCl_2S was solved [79] by the techniques of magnetic rotation spectroscopy (MRS) and laser induced fluorescence spectroscopy (LIF). Thiophosgene fluorescence can be readily observed in an excitation cell at pressures of several torr, yet it cannot be made to phosphoresce under these conditions. The LIF spectrum then has the capability of discriminating between the bands of the two systems. Conversely, the MRS technique registers only bands of triplet multiplicity. It was through these mutually exclusive techniques that the singlet and triplet bands were separated from each other. The differences in the vibronic selection rules may also be of assistance. For example, in CCl_2S, the v_4'' ground state vibration has a frequency of 471.10 cm^{-1} and is active in forming hot band intervals in both spectra. In the singlet-singlet system, the interval $4_0^3 - 4_1^2 = 484.0$ cm^{-1}, whereas in the triplet-singlet case it becomes $4_0^2 - 4_1^3 = 466.3$ cm^{-1}. That is, the hot band intervals are larger than v_4'' in the singlet system and are smaller than v_4'' in the triplet system. The differences in selection rules allow the vibrational levels of the $\tilde{a}$ and $\tilde{A}$ states to be locked into similar schemes. Inversion doubling splittings are derived from the ground state combination differences as $\delta_1 = (1^-) - (1^+) = 4^3 - 4^2 = 4_1^3 - 4_0^2 + 4_1$, from which the barrier heights can be extracted.

The vibrational frequency data and T_0 values for the carbonyl and thiocarbonyl series of molecules are collected together in Tables 12 and 13. The $v(C{=}S)$ stretching frequency is different in the singlet and triplet (n, π^*) states with the triplet being

Table 12. Vibrational frequencies[a] of the T_1 excited electronic states of the thiocarbonyl and seleno-carbonyl halides.

Molecule	C_{2v} Molecules $X_2C=Y$						
	C=Y str. (a$_1$)	C—X str. (a$_1$)	XCX bend (a$_1$)	Wag (b$_1$)	C—X str. (b$_2$)	YCX bend (b$_2$)	Ref.
CF_2S	1186	729	391	566	—	—	92)
CF_2Se	1156	671	397	543	—	—	85)
CCl_2S	923	474	247	298	—	—	79)
CBr_2S	895	258	154	336	—	—	94)
Molecule	C_s Molecules $XZC=Y$[b]						
	C=X str. (a′)	C—Y str. (a′)	C—Z str. (a′)	ZCX bend (a′)	ZCY bend (a′)	Wag (a″)	Ref.
CHClS	865	—	—	—	221	—	87)
CBrClS	934	570	442	143	238	258	94)

[a] in cm^{-1}. [b] X = atom of lower atomic weight, Z = atom of higher atomic weight.

slightly higher. DiGiorgio and Robinson [91)] noted that the higher frequency for $v_2(C=O)$ in the $\tilde{a}^3A_2$ state of CH_2O relative to the $\tilde{A}^1A_2$ state (1283/1183 cm^{-1}) could be used as a diagnostic test of the spin multiplicity. The barrier heights for the two spin states are also somewhat different. Formaldehyde shows the greatest effect: $\tilde{a}^3A_2/\tilde{A}^1A_2 = 776/350 \cdot cm^{-1}$. For thiophosgene, which is the best understood case in this series, the barrier heights are 726 and 620 cm^{-1}. It would appear that the effect of halogen substitution is to make the structure and the dynamics of the singlet and triplet states more alike. This observation should not be too surprising, since the positions of the electronic origins of the two systems vary in a similar way. The $T_0(S_1) — T_0(T_1)$ intervals are collected together in Table 11. It is clear that the stabilization energy conferred on the triplet state over the corresponding singlet state depends on the type and extent of the halogen substituent and on the nature of the chromophore itself. In the case of CH_2O or CH_2S, the π^* orbitals are confirmed in the C=O or C=S region. The addition of halogen groups, which are capable of back bonding to the carbonyl MO's, creates additional space for the antibonding

Table 13. Electronic origins, barrier heights, and out-of-plane angles of the T_1 states of $X_2C=Y$ and $XZC=Y$ molecules.[a]

Molecule	T_0	Barrier	θ(min.)	Ref.
CF_2S	22191	>3100	—	92)
CF_2Se	19018	2923	31.4	85)
CCl_2S	17492	726	32	93)
CBr_2S	16859	524	17.5	94)
CBrClS	17116	541	25	94)
CHClS	17234	—	—	87)

[a] in cm^{-1} and degrees.

electrons, thereby lowering the repulsive energy and the energy required for spin interchange.

2.2.4 Higher Excited States

The far UV spectra of CF_2O and CCl_2O have been observed in absorption. These spectra are quite different in appearance from those of CH_2O, in that the bands are broad and featureless. In particular, the characteristic line-like Rydberg systems n → 3s, 3p, 3d, 4s . . . which are found in CH_2O are absent in the spectra of the corresponding halides. The loss of structure can be related to the Franck-Condon profiles associated with the bands. The progressions in the ν(CX) and ν(XCX) stretching and bending modes which appear in the photoelectron spectrum demonstrate that the n MO extends into the halogen ends of these molecules. The lowest Rydberg transitions which promote n electrons would give rise to similar band profiles. The loss of the Rydberg progressions in the far UV spectra could be the result of weak 0_0^0 structures and band congestion rather than spectral diffuseness.

The π → π* transition is of interest. Workman and Duncan [96] observed a featureless continuum at 9.67 eV in CF_2O. Recent calculations on the Rydberg and valence transitions [95] assign this absorption to the $^1A_1(\pi, \pi^*) \leftarrow \tilde{X}^1A_1$ system. This band is some 5000 to 10000 cm^{-1} lower in energy than that of the corresponding dihydro compound. The excitations to the π, π* states so long sought in the keto compounds are readily apparent in the thioketo and selenoketo compounds. In the CX_2S and CX_2Se species the π → π* transitions lie in the near UV. Figure 17 shows the spectrum of CClFS, a typical example, while Table 14 collects the data. The halogenated are readily apparent in the thioketo and selenoketo compounds. In the CX_2S and CX_2Se species the π → π* transitions lie in the near UV. Figure 17 shows the spectrum of CClFS, a typical example, while Table 14 collects the data. The halogenated derivatives behave in an interesting way. On going from CH_2S to CF_2S, the origin bands move to lower energies, whereas the general effect [10] of fluorine substitution is to shift transitions to higher energies.

The photophysical behavior of the $\tilde{B}^1A_1(\pi, \pi^*)$ state is of particular interest because emission and photochemical processes have been observed from this state, contrary to Kasha's rule. The S_2 states are also ideally positioned for optical-optical double
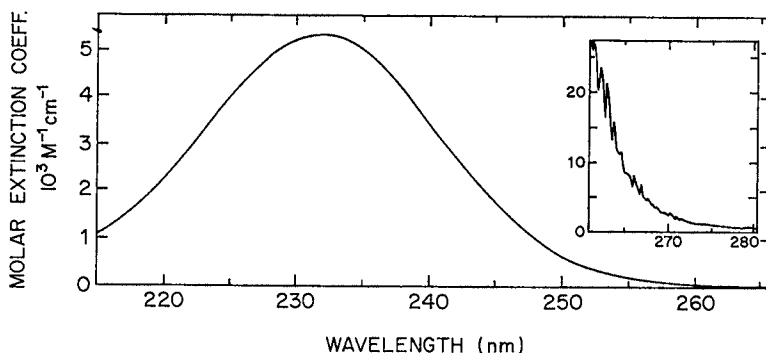
Fig. 17. The $\tilde{B}^1A_1 \leftarrow \tilde{X}^1A_1$ transition in CClFCS

resonance (OODR) studies. In such experiments, the molecule is prepared in a specific vibronic level of the S_1 state by a laser and the $S_2 - S_1$ transition is probed by pulses from a second laser.

The S_2 structure and dynamics of the two thiocarbonyl halides which display emissive behavior, CCl_2S and $CClFS$, have at this time not been fully characterized. The Franck-Condon factors seem to be responsible since the bands in the origin area of the spectra are exceedingly weak relative to the stronger higher energy continua. The major difficulty is that the antibonding electron introduces repulsive forces into the molecule which are spread throughout the structure, causing large changes in the $C=S$, CCl, and ClCCl coordinates. Excitations where the n electron is promoted to an antibonding π^* orbital lead to a reduction in bond order from 2 to 1.5 and to corresponding changes in $C=S$ bond length and stretching frequency. Excitation to the π, π^* state reduces the bond order even further, to a value of 1. Furthermore, the Walsh postulate predicts that the molecule should be nonplanar and that the potential function describing Q_4 should contain a double minimum. A major question is the relative barrier heights of the S_2 and S_1 states.

Spectroscopic information on the S_2 states is given in Table 14. The CClFS analysis [99] shows that the progression in the $v_1(C=S)$ stretching frequency is long and the value drops from 1257 to 566 cm^{-1} on excitation. The v_6 progression displays harmonic intervals of 448 cm^{-1}, with an inversion splitting $\delta_3 = 1.3$ cm^{-1}. The barrier is estimated to be greater than 2000 cm^{-1}.

The bands in the $n \to \pi^*$ and $\pi \to \pi^*$ systems of CCl_2S resemble each other in that the line-like heads of the individual 35,35/35,37 isotopomers can be identified. Moreover, the stronger bands are accompanied by hot bands in the v_4 interval of 471 cm^{-1}, from which the inversion doublings can be extracted. Judge and Moule [87] were able to identify a band in the absorption spectrum at 34278 cm^{-1} which had a $\delta = 0.11$ cm^{-1} and an isotope effect of -0.28 cm^{-1}. These values can be compared to those of the 4_0^1 band of the $S_1 \leftarrow S_0$ system with $\delta_1 = 0.42$ and isotope effect of -0.43 cm^{-1}. As the inversion splitting is smaller than that observed for the n, π^* state the barrier must be somewhat higher in the π, π^* state. Their analysis placed the S_2 barrier height at 729 cm^{-1}, which is to be compared to the S_1 value of 597 cm^{-1}. Dixon and Western [97] identified 23 bands by OODR methods. Their results are given in Table 14. They placed the origin at 33991 cm^{-1},

Table 14. Spectroscopic parameters[a] for the S_2 excited states of the thiocarbonyl and selenocarbonyl halides.

	CCl_2S	CClFS	CF_2S	CF_2Se
T_0	33991	35277	39868	42400[b]
Barrier	—	>2000	—	—
v_1	340	566	—	—
v_2	249	—	729	—
v_3	212	590	400	—
v_4 `	—	311	554	—
v_6	292	448	—	—
Ref.	97,98	99	100	85

[a] in cm^{-1}. [b] vertical excitation energy.

which is 286 cm^{-1} lower than the previous value. It is puzzling that the v_4 progression was not active in the OODR spectrum and that the strong absorption band at 34287 cm^{-1} was not observed.

2.3 Acetaldehyde, Thioacetaldehyde, Selenoacetaldehyde

CH_3CHO: Acetaldehyde is the prototype species for a wide variety of aliphatic carbonyl compounds. The photochemistry and electronic spectroscopy have been reviewed by Lee and Lewis [101]. The electronic structures in the carbonyl group of acetaldehyde are similar to those of formaldehyde in that the low lying valence and Rydberg levels have about the same energy. For example, n $\rightarrow$ π^* excitation in both species gives rise to a weak absorption at 350–250 nm. The first Rydberg n $\rightarrow$ 3s excitation is found as a line-like feature at 182 nm, compared to the 174 nm band of CH_2O.

The internal dynamics of the methyl group immensely complicates the spectroscopy of these molecules. Of course, this aspect of the problem also provides much of the spectroscopic interest. When the methyl hydrogens of acetaldehyde oscillate around the CC axis, they experience forces arising from the CHO frame of the molecule which vary sinusoidally. As a result, the potential function for internal rotation can be represented by a cosine function in which the crest to trough distance measures the height of the potential barrier. Since the energy barrier to methyl rotation is low in acetaldehyde, the internal motion is one of hindered internal rotation, rather than torsional oscillation.

CH_3CHS: The properties of monomeric thioaldehydes have been difficult to determine, because under normal experimental conditions they polymerize into cyclic dimers and trimers. Kroto and Landsberg [102] were able to produce monomeric thioacetaldehyde as a product from the pyrolysis of 1,3,5-trimethyl-s-trithiane. The species is unstable, and was generated and detected in a fast flow system. The various species which coexist in this system at low pressures are summarized in Fig. 18.
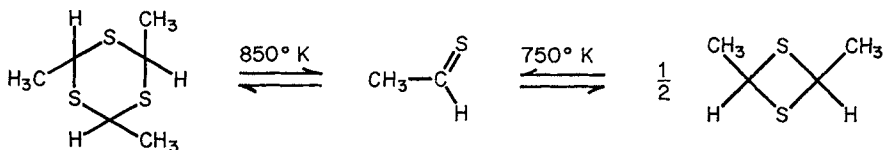
Fig. 18. The formation of thioacetaldehyde

CH_3CHSe: Hutchinson and Kroto [103] succeeded in preparing the trimer of selenoacetaldehyde by the addition of hydrogen selenide to cold acidified acetaldehyde. On pyrolysis, this material yielded the unstable monomeric species CH_3CHSe, which was detected and characterized by its microwave spectrum.

2.3.1 The Ground State

The microwave spectrum of acetaldehyde has been studied by Kilb, Lin and Wilson [104]. Effective bond lengths and angles have been derived from this data by Harmony et al. [105] and are shown in Table 15. The coordinates used in describing the structure are defined in Fig. 19. Note that the methyl hydrogen, H_2, and the oxygen atom, X, lie in the molecular plane in an eclipsed conformation.

Table 15 also gives the structure for $\tilde{X}^1A'$ thioacetaldehyde. This was derived as a substitution structure [102] from eight isotopomers of thioacetaldehyde. In the case of selenoacetaldehyde, Hutchinson and Kroto [103] were unable to obtain accurate A rotational constants, although they did derive substitution parameters for the $r(C=Se)$ and $\alpha(CCSe)$ molecular fragments.
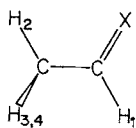
Fig. 19. Coordinates which define the structure for CH_3CHX molecules, X = O, S, Se

Table 15. Molecular parameters[a] for acetaldehyde,[b] thioacetaldehyde[c] and selenoacetaldehyde[d] in the ground state.

Parameter	CH_3CHO	CH_3CHS	CH_3CHSe
$r(C=X)^e$	1.213(10)	1.610(9)	1.758(10)
$r(C-C)$	1.504(10)	1.506(7)	
$r(CH_1)$	1.106(10)	1.089(4)	
$r(CH_2)$	1.091(5)	1.090(6)	
$r(CH_3)^f$	1.085(5)	1.098(8)	
$\alpha(CCX)$	124.0(0.5)	125.3(1.1)	125.7(0.3)
$\alpha(CCH_1)$	114.9(1)	119.4(1.2)	
$\alpha(CCH_2)$	110.6(0.5)	111.2(1.4)	
$\alpha(CCH_3)$	110.3(0.5)	110.1(0.9)	
$\alpha(H_3CH_4)$	108.9(0.5)		

[a] in Å and degrees. [b] r_{eff}, ref. 105. [c] r_s, ref. 102. [d] r_s, ref. 103. [e] X = O, S, Se.
[f] $r(CH_3) = r(CH_4)$.

If the internal torsional motion of the methyl group is fixed, acetaldehyde can be classified under the symmetry operations of the C_s point group. The 15 small amplitude normal vibrational coordinates decompose as:

$$\Gamma_v = 10a' + 5a''$$

Vibrational spectra of Hollenstein and Gunthard [106] were combined by Wiberg et al. [107] with vibrational force fields from ab initio 6–31 G* calculations to establish the vibrational frequencies for acetaldehyde. These are given in Table 16.

It is the dynamics of the internal motion of the methyl group which is of most interest in the acetaldehyde molecule. Since the CH_3 rotor has a threefold symmetry axis, the potential energy is usually approximated by the Fourier series expansion:

$$V(\theta) = V_3/2(1 - \cos 3\theta) \qquad (4)$$

where θ is the angle of rotation of the methyl group and V_3 is the height of the threefold barrier. The torsional potential then becomes $H = Fp^2 + V_3/2(1 - \cos 3\theta)$, where p is the internal angular momentum given by $p = -id/d\theta$ and F the reduced moment of inertia which is evaluated from the molecular structure.

The triple minimum nature of the potential leads to a tripling of the torsional levels. As the barrier to methyl rotation is relatively low, the internal motion is one of hindered internal rotation. This has the effect of removing the 3-fold degeneracy of the zero-point level. As a consequence of this torsional flexibility, the symmetry properties of the molecular Hamiltonian must be defined by the nonrigid point group G_6. This point group is isomorphous with the C_{3v} group and the torsional wave functions can be labelled by the symmetry symbols a_1, a_2, and e. When the barrier is high, the levels form a stack with uniform spacing and are classified by a set of torsional-vibrational quantum numbers $v = 0, 1, 2 \dots$. In the order of increasing energy, the levels divide into pairs of nondegenerate and degenerate microstates (a_1, e), (e, a_2), (a_1, e), ... Figure 20 shows a potential function for internal rotation.

The barrier to internal rotation of the methyl group of acetaldehyde was initially determined by Kilb et al. [104] from an analysis of the microwave spectrum. Since then, the values of the potential constants have been continually revised. Recently, Crighton and Bell [108] combined the available microwave and infrared data with ab initio theory and refined the torsional parameters. Table 17 collects their internal rotation parameters.

Table 16. Fundamental frequencies[a] for $\tilde{X}^1A'$ acetaldehyde[b] and thioacetaldehyde.[c]

Mode	Description	CH_3CHO	CH_3CDO	CD_3CHO	CD_3CDO	CH_3CHS
v_1 (a')	CH_3 stretch	3014	3014	2262	2262	—
v_2 (a')	CH_3 stretch	2923	2922	2120	2125	—
v_3 (a')	CH_1 stretch	—	2059	—	2054	—
v_4 (a')	C=X stretch	1746.0	1743	1754	1736	1389
v_5 (a')	CH_3 bend	1429.9	1432	1038	—	—
v_6 (a')	CH_1 bend	1394.9	1080	1387	1151.0	—
v_7 (a')	CH_3 bend	1352.6	1356	1131	1029	—
v_8 (a')	C—C stretch	1114	1109	960	940	—
v_9 (a')	CCX bend	877	840	750	747.5	—
v_{10} (a')	CCX bend	506	500	444	436	—
v_{11} (a'')	CH_3 stretch	2964.4	2965	2224	2222.7	—
v_{12} (a'')	CH_3 rock	1435.8	1432	1062	1046.3	—
v_{13} (a'')	CH_1 wag	1107.3	1043	1027	948	—
v_{14} (a'')	C=X wag	764.1	674	624	571	—
v_{15} (a'')	torsion	143	—	—	116	116

[a] in cm^{-1}. [b] ref. 107. [c] ref. 117. [d] Subscripts 1 and 3 refer to Fig. 19.
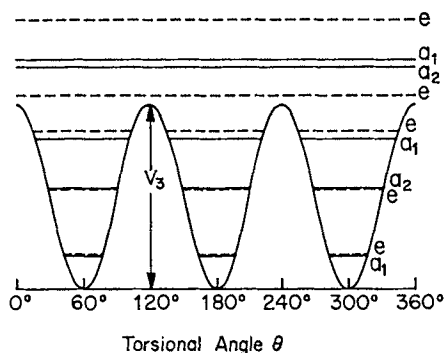
Fig. 20. Potential function for methyl group internal rotation

Torsional Angle θ

Table 17. Internal rotation parameters[a] for $\tilde{X}^1A'$ acetaldehyde, thioacetaldehyde and selenoacetaldehyde.

Parameter	CH_3CHO[b]	CH_3CHS[c]	CH_3CHSe[d]
F	7.8588	6.9950	6.7275
V_3	415.0	534.3	560.3
V_6	22.3	—	—
$1e-0a_1$	142.0	161.4	—
$2a_1-0a_1$	258.3	306.6	—
$3e-0a_1$	356.7	394.2	—

[a] in cm^{-1}. [b] ref. 108. [c] ref. 117. [d] ref. 103.

In this class of compounds, many of the microwave lines are observed to be doublets as a result of methyl group internal motion. These splittings are sensitive to the potential barrier and may be used to determine its height. Kroto and co-workers [102, 103] used this rotational information to obtain the reduced mass, F, and the barrier, V_3, for thioacetaldehyde and selenoacetaldehyde. For the isotopomers of thioacetaldehyde, $^{12}CH_3{}^{12}CH^{32}S/12CH_3{}^{12}CD^{32}S/^{12}CD_3{}^{12}CH^{32}S/^{12}CH_3{}^{12}CH^{34}S/$ $^{13}CH_3{}^{12}CH^{32}S/^{12}CH_3{}^{13}CH^{32}S$, the V_3 parameters were observed to vary as 549.8/ 559.6/525.0/552.6/552.6/552.6 cm^{-1}. The large variation among these terms was attributed to a coriolis interaction with the other low frequency vibrations or to the neglect of the shape factor term, V_6.

2.3.2 The $S_1(n, \pi^*)$ Excited State

Although there were some early attempts to analyze the vibrational fine structure contained in the near ultraviolet vapor phase spectrum of acetaldehyde, these studies were generally unsuccessful because of the diffuse and congested nature of the bands. It has only been in the last several years that the problem has been resolved by the powerful techniques of supersonic jet-laser excitation spectroscopy.

Rao and Rao [109], the first investigators, placed the origin of the singlet-singlet system at 320.4 nm. Somewhat later, Innes and Giddings [110] revised this value upwards to 348.4 nm by comparing the contours of the spectra in absorption and
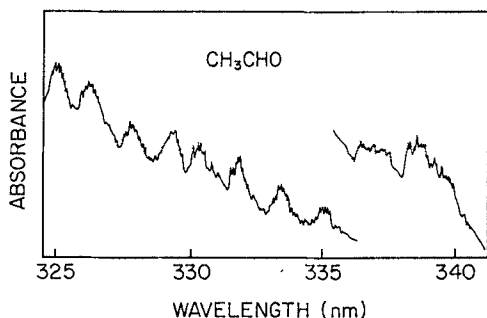
Fig. 21. Low resolution absorption spectrum of acetaldehyde

emission. More recently, Hubbard et al. [111] combined a medium resolution absorption spectrum with a resolved laser fluorescence spectrum to place the origin at 346.4 nm. None of these studies were able to positively locate the 0_0^0 band. The problem was solved by supersonic jet spectroscopy. Noble, Apel and Lee [112] observed the excitation spectrum of jet cooled CH_3CHO which was free from the complications of thermally induced torsional fine structure. Although they disagree with much of the vibrational analysis of Hubbard et al., they did obtain similar values for the V_3 barrier in the $\tilde{A}^1A''$ state. Figure 22 shows a low resolution spectrum recorded under jet conditions.

The apparent simplicity of the jet spectrum over the room temperature absorption or excitation spectrum is remarkable and the origin is clearly visible as the lower frequency member of a doublet at 29771 cm^{-1}.

Rigid acetaldehyde belongs to the C_s point group and the origin transition 0_0^0 is formally allowed as a type-C band. Additions of quanta of the v_1–v_{10} vibrations also result in type-C bands. The out-of-plane antisymmetric modes of a″ species generate type-A/B bands. The high resolution excitation spectrum, when compared with the calculated spectra (Fig. 23), demonstrates that the origin band is indeed
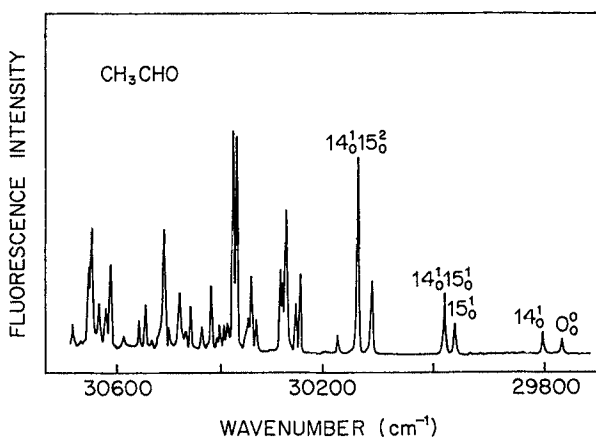
Fig. 22. Low resolution fluorescence excitation spectrum of jet-cooled CH_3CHO
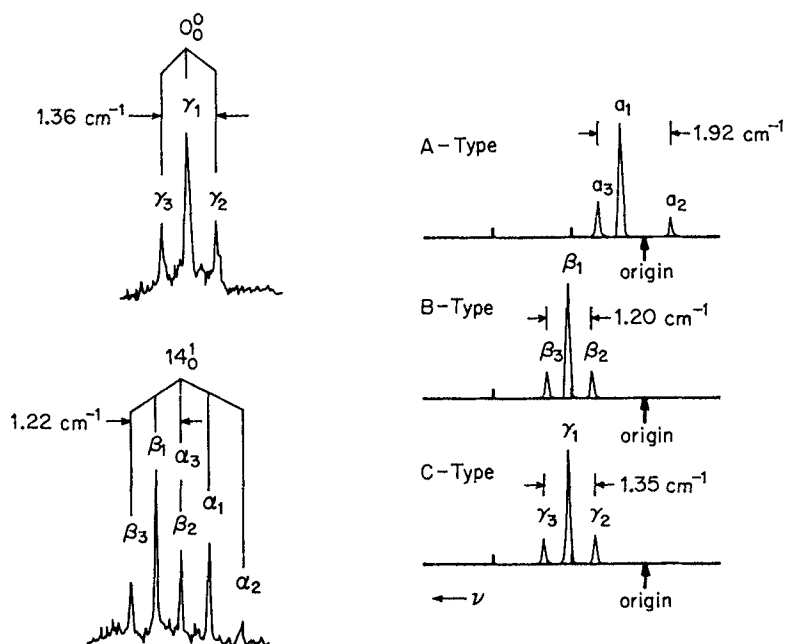
Fig. 23. The 0_0^0 and 14_0^1 bands of CH_3CHO under high resolution and the calculated excitation spectra for type —A, —B and —C bands

type-C, whereas the $+33$ cm^{-1} component is an A/B hybrid. The polarizations of the two bands and their separations are compatible with vibronic assignments to the first two members of the v_{14} inversion manifold, 0^+ and 0^-. Such a small inversion splitting shows that the $\tilde{A}^1A''$ molecule is indeed nonplanar at the carbonyl carbon. In more recent work, Baba et al. [113] used a combination of pulsed laser excitation and pulsed supersonic expansions to record the spectrum at shorter wavelengths. From a fit of the levels of a quadratic Gaussian model function (Eq. (1)), to the observed levels, they concluded that the barrier to molecular inversion was 541 cm^{-1}. In the first excited singlet electronic state, acetaldehyde is pyramidal and the double minimum function for out-of-plane distortion resembles that of form-aldehyde in its first triplet state.

The strength of the next band at $+195$ cm^{-1} was not anticipated, as it signifies strong Franck-Condon activity in a low frequency mode. The vibrational assignment for this interval came from the spectrum of CD_3CHO where this frequency was observed to fall to $+157$ cm^{-1}. The CH_3/CD_3 isotope effect identifies the interval as v_{15} (methyl torsion). Moreover, the strength of the bands indicates that there is a conformational change when the molecule is excited to the higher electronic state. Noble and Lee [114] were able to fit the energy levels derived from Eq. (3) to the torsional levels attached to the 0^0 (0^+) and 14^1 (0^-) inversion levels of the aldehyde wagging mode, v_{14}. Somewhat surprisingly, the two barriers were nearly equal (668 and 653 cm^{-1}), which must be an indication that methyl torsion-hydrogen wagging motions are not strongly coupled. Parameters for the $\tilde{A}^1A''$ state of acetaldehyde are given in Table 18.

Table 18. Spectroscopic parameters[a] for $\tilde{A}^1A''$ acetaldehyde.

Parameter	CH_3CHO^b	CH_3CDO^b
F	6.40	6.24
V_3	691	645
$1e-0a_1$	194	193
$2a_1-0a_1$	345	330
$3e-0a_1$	487	451
$0^- -0^+$	32	21
$1^+ -0^+$	405	387
$1^- -0^+$	635	580
$2^+ -0^+$	936	879
$2^- -0^+$	1319	1200
V_0 (barrier)	541	578
$v_{10}(CCO)^c$	374	367
$v_4(C=O)^d$	1119	1173
T_0	29771	29813

[a] in cm^{-1}. [b] ref. 113. [c] ref. 114. [d] ref. 111.

The length and the strength of the progression in methyl torsion is undoubtedly the most interesting and unusual aspect of the spectrum. If the methyl group were to retain its ground state conformation in the $\tilde{A}^1A''$ state and eclipse the carbon-oxygen bond, the torsional transitions would not be active in the spectrum. That the $15^{2a_1}0a_1$ transition gives rise to a strong band signifies that the methyl group undergoes a torsional displacement on electronic excitation. To gain insight into the conformational changes which occur during the n → π* process, Baba and Hanazaki[115] performed ab initio SCF calculations and evaluated the potential functions for hydrogen wagging and methyl torsion. Their results are shown in Fig. 24, where the full lines represent the theoretical potentials and the dotted lines are those derived from experiment. Three cases were considered, namely: (a) the ground electronic state $S_0(\tilde{X}^1A')$ with a planar frame, (b) a planar excited state $S_1(\tilde{A}^1A'')$, and (c) an excited state $S_1(\tilde{A}^1A'')$ in which the frame was distorted into a pyramidal configuration.

Their calculations correctly predict that in the $\tilde{X}^1A'$ ground state the methyl hydrogen eclipses the carbonyl group with a barrier to internal rotation of 481 cm^{-1}. What is more interesting is that for the planar $\tilde{A}^1A''$ excited state, the methyl hydrogen antieclipses the oxygen atom (60° torsional angle) with a barrier of 208 cm^{-1}. When the angle between the CO bond and the molecular frame was increased from 0° to 32°, the calculated barrier height for methyl torsion increased from 208 to 732 cm^{-1}, and the equilibrium torsional angle from 60° to 72°. That is, for the molecule which is clamped into a planar CCHO framework, the electronic excitation process leads to an eclipsing-antieclipsing change in conformation and a reduction in barrier height. When the frame is able to relax into a pyramidal conformation, the barrier height increases from its ground state value by 50 percent. Experimental values for the two states $S_0(\tilde{X}^1A')/S_1(\tilde{A}^1A'')$ are 415/668 cm^{-1}. As a result of the difference in methyl conformation predicted from the ab initio theory, torsional transitions be-
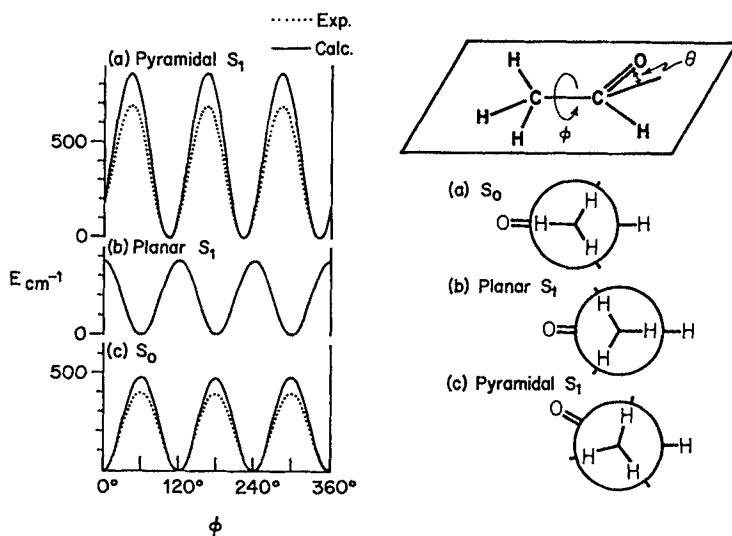
Fig. 24. Potential curves for the internal rotation in CH_3CHO

tween the two states should be highly Franck-Condon active. Thus, the source of the long progressions in the v_{15} torsional mode becomes clear. It is the consequence of an eclipsing-antieclipsing conformational difference in the two states.

Judge et al. [116] recorded the n → π^* absorption spectrum of CH_3CHS under similar conditions of flow rate and pressure as that used in the microwave studies. At a total path length of 72 m they observed a discrete band system at 620–570 nm, which they assigned as the $\tilde{a}^3A'' \leftarrow \tilde{X}^1A'$ transition. Laser excitation experiments [117] have shown that, while the lower excited triplet state is phosphorescent, the singlet companion $\tilde{A}^1A''$ state does not fluoresce.

2.3.3 The $T_1(n, \pi^*)$ Excited State

Schuh et al. [118] were able to observe the resolved phosphorescence from CH_3CHO by taking advantage of the much longer 25 µs emission from the triplet state relative to the 5 ns component from the corresponding singlet state. In their experiment CH_3CHO was optically excited into its $\tilde{A}^1A''$ singlet state at 320 nm where it underwent direct emission or intersystem crossing to the triplet state. The resulting emission was resolved into fluorescent and phosphorescent components by observing the temporal development of the spectrum. From the onset of the phosphorescence they were able to estimate that the $\tilde{a}^3A'' \leftarrow \tilde{X}^1A'$ system origin lay in the region of 369 nm. Moule and Ng [119] studied CH_3CHO in absorption at path lengths up to 168 m and temperatures down to −90 C. They established that many of the 363 to 351 cm^{-1} bands were temperature insensitive with a simple band pattern. An analysis of this band structure, when combined with the known torsional parameters of the lower state, led to a value of $V_3 = 625$ cm^{-1} for the $\tilde{a}^3A''$ state, which is to be compared to the 668 cm^{-1} barrier for the $\tilde{A}^1A''$ state. The strength of the progression in methyl torsion is an indication that the CH_3 conformations are very different in the

excited triplet and ground electronic states. As vibronic-spin-orbit selection rules do not allow for odd quanta of the aldehyde wagging mode, v_{14}, to be active in the spectrum, the 0^- and 1^- components of the inversion manifold were not observed and the barrier to inversion of the aldehyde hydrogen was not established for the $\tilde{a}^3A''$ state.

The laser phosphorescence excitation spectrum of thioacetaldehyde, which is shown in Fig. 25, has nearly the same profile as the absorption spectrum and both spectra appear to contain the same vibrational information. The spectrum consists of two sets of band clusters centered at 608 and 593 nm. They form an interval of $742\ cm^{-1}$ which was assigned to the C=S stretching mode, v_6. The clusters are too wide to be assigned to individual vibronic transitions. Rather, as in the case of CH_3CHO, each cluster consists of a series of transitions in the torsional mode, v_{15}. As the spectra were recorded at room temperature, the assignment had to be made by comparing the observed intervals with the ground state levels determined from the microwave parameters of Kroto et al. [102]. This process established the origin, 0^0_0, as a weak band at $16294\ cm^{-1}$. The assignment of the upper state levels could not be made directly because of spectral congestion. Instead, the spectral profile (band intensity and band positions) was synthesized from estimates of the V_3 torsional potential. The agreement between the calculated and the observed torsional contours, shown in Fig. 26, is satisfactory for the transitions which terminate on the lower 15^{0a_1} and 15^{0e} levels, but is poor for the higher transitions. An analysis of the data for the isotopic species showed that the source of the difficulty was a strong coupling between the large amplitude hydrogen wagging mode, v_{14}, and the torsional mode, v_{15}. Table 19 collects the torsional parameters which were extracted from the $\tilde{a}^3A'' \leftarrow \tilde{X}^1A_1$ transition.

The $94\ cm^{-1}$ barrier in CH_3CHS is quite low compared to the $625\ cm^{-1}$ barrier in $\tilde{a}^3A''\ CH_3CHO$. The difference may be understood from the ab initio calculations of Baba et al. [115]. For $\tilde{A}^1A''\ CH_3CHO$, they found that a pyramidal distortion of the aldehyde group did influence the torsional barrier which increased from 208 to $732\ cm^{-1}$ when the oxygen atom was displaced out-of-plane by $32°$. From this correlation with acetaldehyde, it follows that the low V_3 value for thioacetaldehyde must be the consequence of a planar or pseudo-planar CCHS framework. The v_{14} wagging
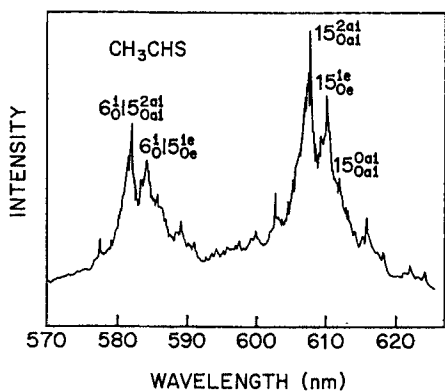
Fig. 25. Laser phosphorescence excitation spectrum of CH_3CHS
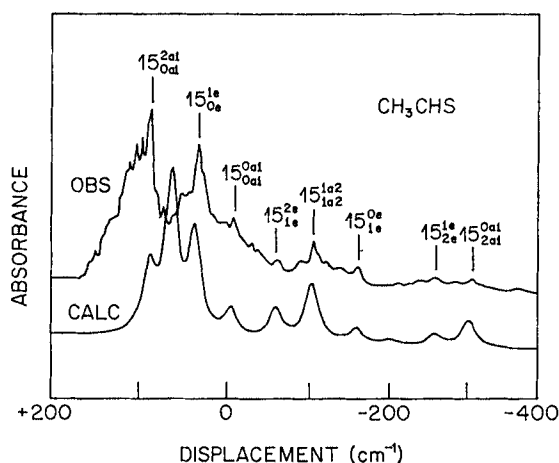
Fig. 26. Observed and calculated torsional clusters in the singlet-triplet spectrum of CH_3CHS

motion, which is largely an out-of-plane displacement of the aldehyde hydrogen, must be confined to a broad potential which contains a low central barrier, not unlike that of thioformaldehyde in the $\tilde{a}^3A_2$ electronic state.

Smeyers et al. [120] have performed an ab initio study of the joint large amplitude methyl rotation and hydrogen wagging vibrations in the $\tilde{X}^1A'$ and $\tilde{a}^3A''$ states of CH_3CHS. They found the eclipsed and antieclipsed conformers to be the preferred structures for the lower and upper electronic states, respectively. The calculated barrier heights to methyl rotation of $118.3/455.6$ cm^{-1} for the respective states are in good agreement with the experimental values of $94.2/534.3$ cm^{-1}. The barrier to inversion of the aldehyde hydrogen in the $\tilde{a}^3A''$ state was calculated to be very low, 67.4 cm^{-1}. As a consequence, the potential function of Fig. 27 is flat and resembles a square well.

It has been known for some time that shifts in the phase angle occur on electronic excitation in simple molecules with hindered internal rotation. For example, in the case of acrolein, the trans isomer is the most stable form of the S_0 molecule, while it is the cis form which is more stable in the excited S_1 state. A simple explanation

Table 19. Spectroscopic parameters[a] for the $\tilde{a}^3A''$ states of acetaldehyde and thioacetaldehyde.

Parameter	CH_3CHO^b	CH_3CHS^c
F	6.81	5.3608
V_3	625	94.18
$1e$—$0a_1$	183.2	48.7
$2a_1$—$0a_1$	335.8	79.5
$v_4(C=X)$	—	742
T_0	27240.4	16293.8

[a] in cm^{-1}. [b] ref. 119. [c] ref. 117.

209
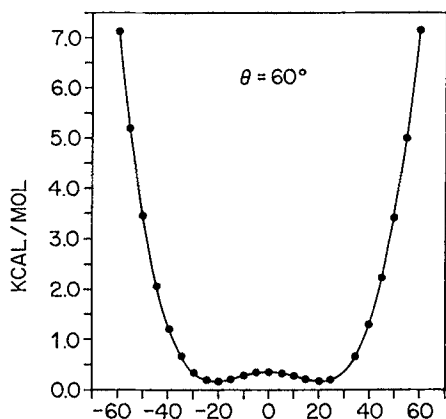
Fig. 27. The hydrogen wagging potential function of $\tilde{a}^3A''$ CH_3CHS

comes from a consideration of the π type MO's. In acrolein, the arrangement of the orbitals is not unlike that of the butadiene system, with four out-of-plane p-type AO's centered on the oxygen and three carbon atoms, forming four π-type MO's. In order of increasing energy the nodes in these orbitals would be defined by (a) $+ + + +$, (b) $+ + - -$, (c) $+ - - +$, (d) $+ - + -$. In the S_0 state the orbitals (a) and (b) would be fully occupied. The S_1 and T_1 states would have configuration $(a)^2(b)^1(c)^1$. If the relative stabilities of the two isomers are determined by π-type interactions between the end groups, it is clear that (b) and (d) would be antibonding, whereas (a) and (c) would be bonding. This simple MO picture predicts that the trans isomer would be the preferred conformer for the S_0 state while the cis isomer would be more stable in the S_1 state.

These simple ideas can be applied to molecules which have methyl groups adjacent to an $n \rightarrow \pi^*$ chromophore, such as acetaldehyde, nitromethane and methyl glyoxal. If the methyl group in these molecules is assumed to have a three-fold symmetry, the $\sigma(CH)$ MO's can be decomposed into the sum $2a' + a''$ of the C_s point group. The out-of-plane a'' MO is constructed from a pair of 1s orbitals and has a node at the molecular plane. It has the resemblance of a p orbital. Three other p orbitals on the C and S centers are required to complete the description of the pseudo π network. Figure 28 shows the arrangement. If weak π-type interactions of the type
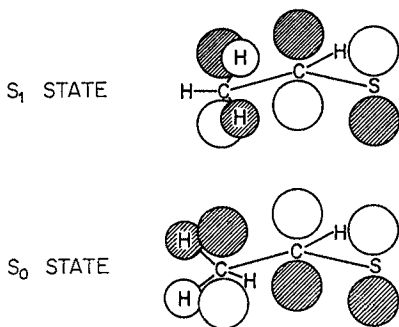
Fig. 28. Conjugative model for the pseudo-π orbitals in the S_0 and S_1 states of thioacetaldehyde

210

which are observed in glyoxal or acrolein occur between the ends of the molecule, then it follows that the eclipsed conformer of thioacetaldehyde will be the stable form in the ground electronic state, while the antieclipsed conformer would be the preferred form for the S_1 excited state.

2.3.4 Higher Excited States

The vacuum ultraviolet region of acetaldehyde has been studied by Walsh [121] and by Lucazeau and Sandorfy [122]. Both groups suggested that the complicated structure at 160 to 190 nm was due to the presence of two different electronic transitions. They assigned line-like structure at 182 nm to the $n \rightarrow 3s$ Rydberg excitation, and the weaker bands at longer wavelengths to the $n \rightarrow \sigma^*$ valence transition. Crighton and Bell [123] rephotographed CH_3CHO and its deutero isotopomers under conditions of higher resolution. They were able to identify all of the weak features in the spectrum as part of the Rydberg system and could find no evidence for a second $^1B_2$ electronic state. As in the case of formaldehyde, $n \rightarrow \sigma^*$ excitation is believed to lie at higher energies.

The line-like profile of the bands is an indication that the structural changes associated with the Rydberg transition are not nearly as severe as those of the lower $n \rightarrow \pi^*$ valence process. It follows that the molecule retains its ground state conformation in the $\tilde{B}^1B_2(n, 3s)$ excited state with the methyl hydrogen eclipsing the oxygen. Within the envelope of the 0_0^0 band, a group of violet-degraded bands was observed which were assigned to sequence transitions in the torsional mode. The torsional transitions were deconvoluted from each other by a fitting procedure which used asymmetric top type-B contours derived from ab initio determined rotational constants. Observed and calculated band clusters are illustrated in Fig. 29.

This procedure led to the excited state parameters $V_3 = 880 \text{ cm}^{-1}$ and $V_6 = 77 \text{ cm}^{-1}$. Ab initio calculations confirmed the experimental expectations that the
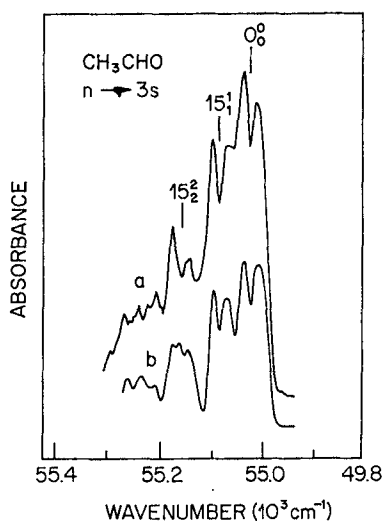
Fig. 29. Torsional rotational envelopes for the origin band of the 182 nm system of CH_3CHO. (a) experimental (b) calculated
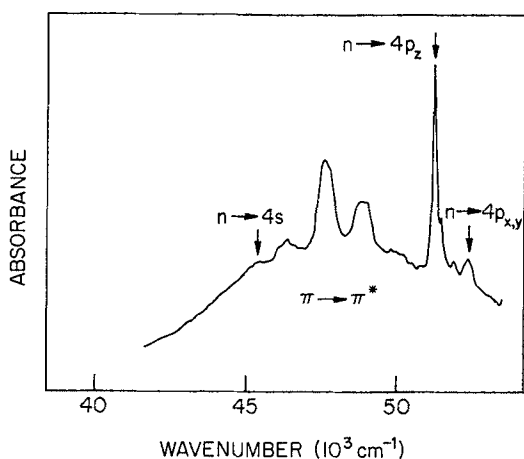
Fig. 30. The ultraviolet spectrum of CH_3CHS

CCHO frame of the molecule was planar and the methyl hydrogens eclipsed the oxygen atom.

The ultraviolet spectrum of thioacetaldehyde, CH_3CHS, shown in Fig. 30, displays 5 diffuse bands in the Rydberg region which can be grouped into a progression of about 1150 cm^{-1}. This is the vibrational interval expected for the $C=S$ stretching mode for an $n \to 4s$ Rydberg transition. However, the intensity and the width of the absorption give the system the appearance of the valence $\pi \to \pi^*$ transition. As these Rydberg and valence states are both of the same symmetry, the excited state must be of a mixed $(n, 4s)-(\pi, \pi^*)$ character.

2.4 Acetone, Thioacetone

C_3H_6O: Acetone is one of the more important molecules of organic chemistry. It is a stable, readily available solvent.

C_3H_6S: Thioacetone, on the other hand, is a difficult compound to work with because of the odor associated with the trace compound 2,2-propanedithiol, which is omnipresent. This impurity is readily formed by the addition of hydrogen sulfide to thioacetone. It is said [124] that the odor of thioacetone is so obnoxious that Baumann and Fromm had to abandon their work with the compound because of protests of the city of Freiburg, Germany. Thioacetone is a red liquid which is stable at 0 °C.

2.4.1 The Ground State

The microwave spectrum of acetone was first studied by Swalen and Costain [125] who determined the dipole moment and a structure for the molecule. This work was extended by Peter and Dreizler [126]. At about the same time, Nelson and Pierce [127] observed the spectrum of its isotopomers and reported an r_s geometry. More recently, Iijima [128] determined a zero-point average structure from moments of inertia obtained by microwave spectroscopy and bond distances from gas electron diffraction. Table 20 gives the zero-point average parameters which have been corrected for the

Table 20. Zero-point average struc-
ture^a for $\tilde{X}^1A_1$ acetone.^{b}

Parameter	r_g
r(CC)	1.517(3)
r(CO)	1.210(4)
r(CH)	1.091(3)
α(HCH)	108.5(0.5)
α(CCC)	116.0(0.25)

^{a} in Å and degrees. ^{b} ref. 128.

effects of the large amplitude torsional motion. The equilibrium structure of acetone was shown to be a double eclipsed conformation in which the hydrogens from the methyl groups lay in the molecular plane of the frame.

The addition of two methyl groups to the carbonyl moiety creates two low frequency, large amplitude torsional modes which greatly complicate the molecular dynamics. In the absence of torsional level splitting (high barrier approximation), the wavefunctions can be classified according to the operations of the C_{2v} group. The joint motions of both rotors can be grouped into a clockwise-clockwise mode, $v_{12}(a_2)$, and to a clockwise-anticlockwise mode, $v_{17}(b_1)$. The effective barrier opposing the joint methyl rotations, which is central to the dynamics of this problem, was determined from the microwave line splittings. A more complete picture of the potential surface was obtained by the addition of infrared data, since this technique yields information about the higher energy levels from which higher order interaction terms (top-top coupling) can be extracted. The far infrared spectrum of acetone was first reported by Fately and Miller [129] and then by Smith et al. [130]. Figure 31 shows the recent high resolution infrared spectra of acetone which have been recorded and analyzed by Groner et al. [131]. From the predictions of the double rotor Hamiltonian, the strong band at 125.16 cm^{-1} was assigned to the $v_{17}(b_1)$ fundamental and the remaining bands to sequence or overtone transitions within the v_{17} torsional manifold. It is improbable that the $v_{12}(a_2)$ mode is active for symmetry reasons. From a fit of the data to the calculated levels, the effective barrier was determined to be 291 cm^{-1}. The ab initio SCF results of Crighton and Bell [132] were found to satisfactorily reproduce the observed frequencies.

Under the operations of the C_{2v} point group, the 24 vibrational modes can be decomposed into the representations:

$$\Gamma_v = 8a_1 + 4a_2 + 5b_1 + 7b_2$$

Vibrational frequencies for acetone and thioacetone-d_6 are given in Table 21. These are collected from the infrared and Raman studies of Dellipanane and Overend [133] and the force field calculations of Hollenstein and Gunthard [134].

Experimental data are quite sparse for thioacetone. Rotational constants and a barrier height for methyl torsion were estimated by Kroto et al. [135] from the microwave spectrum. They obtained an effective barrier height of 454.7 cm^{-1} from the torsional fine structure splittings in the $J(3) \leftarrow J(2)$ line, which is to be compared to the 291 cm^{-1}

barrier of acetone. Garrigou-Lagrange et al. [136] recorded solution infrared and Raman spectra of the d_0 and d_6 species and with force field assistance assigned the skeletal frequencies. Table 21 gives their results.
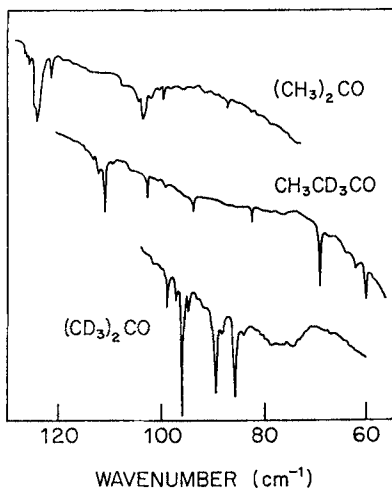
Fig. 31. Far infrared spectra of acetone vapor

Table 21. Vibrational frequencies[a] for ground state acetone and thioacetone.

Mode	Approx. description	$(CH_3)_2CO^c$	$(CD_3)_2CO^d$	$(CH_3)_2CS^e$	$(CD_3)_2CS^e$
v_1 (a_1)	CH stretch	3004	—	—	—
v_2 (a_1)	CH stretch	2937	2109	—	—
v_3 (a_1)	C=X[b] stretch	1731	1732	1269	1257
v_4 (a_1)	CH deform	1435	1088	1422	1025
v_5 (a_1)	CH deform	1355	1036	1359	1062
v_6 (a_1)	CH deform	1072	887	—	—
v_7 (a_1)	CC stretch	777	689	704	—
v_8 (a_1)	CCC bend	385	321	380	—
v_9 (a_2)	CH stretch	2972	2229	—	—
v_{10} (a_2)	CH deform	1426	1017	1447	1025
v_{11} (a_2)	CH deform	872	763	992	775
v_{12} (a_2)	torsion	112	—	—	—
v_{13} (b_1)	CH stretch	2972	2227	—	—
v_{14} (b_1)	CH deform	1454	1050	1437	1044
v_{15} (b_1)	CH deform	1090	—	1087	1044
v_{16} (b_1)	C=X wag	484	405	436	369
v_{17} (b_1)	torsion	120	—	—	—
v_{18} (b_2)	CH stretch	3018	2264	—	—
v_{19} (b_2)	CH stretch	2920	2123	—	—
v_{20} (b_2)	CH deform	1410	1242	1422	1025
v_{21} (b_2)	CH deform	1364	1035	1353	—
v_{22} (b_2)	CH deform	1216	1004	1195	1207
v_{23} (b_2)	CH deform	891	—	896	691
v_{24} (b_2)	C=X deform	530	475	—	345

[a] in cm^{-1}. [b] X = O or S. [c] ref. 134. [d] ref. 135. [e] ref. 136.

2.4.2 The $S_1(n, \pi^*)$ Excited State

Acetone has a moderately strong absorption system in the near ultraviolet extending from 330 to 220 nm with a maximum at about 275 nm. There is vibrational fine structure at the long wavelength end, but this rapidly becomes diffuse and merges into a continuum. Noyes et al. [137], in 1934, made a partial analysis of the discrete part of the spectrum. Their analysis placed the 0_0^0 band at 30839 cm^{-1}. Recently, Baba et al. [138] recorded the fluorescence excitation spectrum in a supersonic jet. Figure 32 shows their spectrum. The 0_0^0 bands are very clear in the spectra of the two compounds $(CH_3)_2CO/(CD_3)_2CO$ at $30435/30431 \text{ cm}^{-1}$. The 4 cm^{-1} red shift on deuteration is somewhat surprising since D for H substitution usually produces blue shifts. It must be that the isotope effects resulting from decreases in the out-of-plane wag $\nu_{16}(b_1)$ are more than offset by increases in frequency of the torsional modes. Three somewhat harmonic quanta in a single torsional mode (either $\nu_{12}(a_2)$ or $\nu_{24}(b_1)$) were observed at $+172$, $+341$ and $+473 \text{ cm}^{-1}$. If the minor features due to top-top coupling are not considered, the problem can be treated in one dimension using Eq. (4) to give an effective barrier height of 466 cm^{-1}.

The torsional activity is similar to that found in the spectrum of CH_3CHO. A single progression of bands in one of the two torsional modes is observed to attach to the electronic origin. It follows, on Franck-Condon grounds, that only one methyl group internally rotates on excitation to the upper electronic state. If the two torsional angles in the lower state are defined as 0ˑ, 0ˑ, (both methyls in an eclipsed configuration) then the conformation in the upper state would be 0°, 60°, (eclipsed-anticlipsed). Such a model would explain the observed polarizations of the bands. Baba et al. [138] were able to obtain the rotational contours of the bands under conditions of relatively high resolution. A fit of the possible band types to the contours showed that the bands are mainly of type-C character (transition dipole directed out of the molecular plane). Furthermore, the first band in the spectrum was assigned to a transition which terminated on 0^+. Based on C_{2v} symmetry, this could only appear as a magnetic dipole transition. Single quanta of the torsions $\nu_{24}(b_1)$ and $\nu_{12}(a_2)$ would give rise to type-B and type-A bands, respectively. Baba et al. needed a second order vibronic mechanism to explain the band polarizations. A way
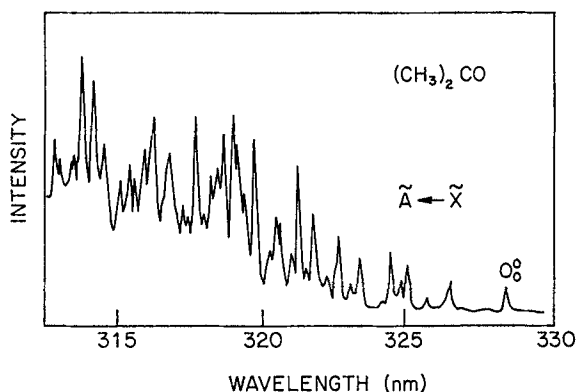
Fig. 32. Fluorescence excitation spectrum of jet-cooled acetone

out of this quandary would be to assume that the symmetry of the upper state is reduced to C_s (0°, 60°). Under C_s selection rules, the origin transition would be allowed as a type-C band, as would the quantum additions of the totally symmetric vibrations.

On Franck-Condon grounds, the oxygen out-of-plane wagging mode v_{23} should form a well developed progression. The identification of five levels was sufficient to establish the form of the quadratic Gaussian function Eq. (1) and the height of the barrier opposing planarity as 466 cm^{-1}.

Spectra of thioacetone in solution were recorded by Fabian and Meyer [139]. They assigned a single absorption at 499 nm to n → π* excitation. Recently, vapor phase absorption spectra have been recorded by Paone et al. [140] as shown in Fig. 33.

Under conditions of moderate resolution, the spectrum in the region of the singlet-singlet system origin is diffuse and structureless. As the molecule does not fluoresce strongly, supersonic jet spectroscopy may not be possible for this system.
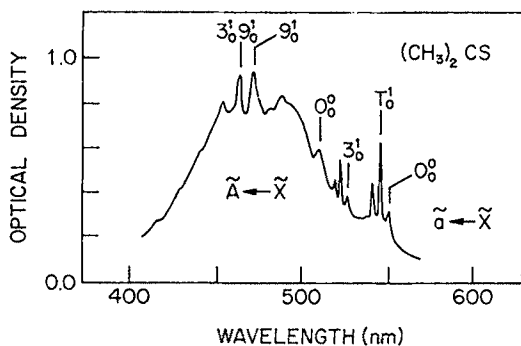
Fig. 33. Visible spectra of thioacetone

2.4.3 The $T_1(n, \pi^*)$ Excited State

The long wavelength side of the visible absorption spectrum of thioacetone displays a series of line-like bands starting at 575 nm. Figure 34 shows the corresponding laser phosphorescence excitation spectrum in the same region, which is similar in profile. The starting point for the vibrational assignment was the identification of repeating intervals of about 70 cm^{-1} in the spectrum. This clustering was assigned to the activity of the $v_{12}(a_2)$ and $v_{17}(b_1)$ torsional modes. Under higher resolution, the bands show the distinct rotational outline of S form ($\Delta N = +2$) and Q form ($\Delta N = 0$) branches.

The 0_0^0 system origin at 17384 cm^{-1} forms the first member of the torsional progression. The four bands within the torsional envelope appear to have a regular intensity pattern. It was possible to treat the problem in one-dimension using Eq. (4). Effective barriers, V_3, of 462/167 cm^{-1}, were derived for the $\tilde{X}/\tilde{a}$ states. The simplicity of the spectrum suggests that, like acetone, only one methyl group undergoes a 60° rotation on electronic excitation. In all probability, the conformation of the ground state is eclipsed-eclipsed and the first excited triplet state is eclipsed-antieclipsed.
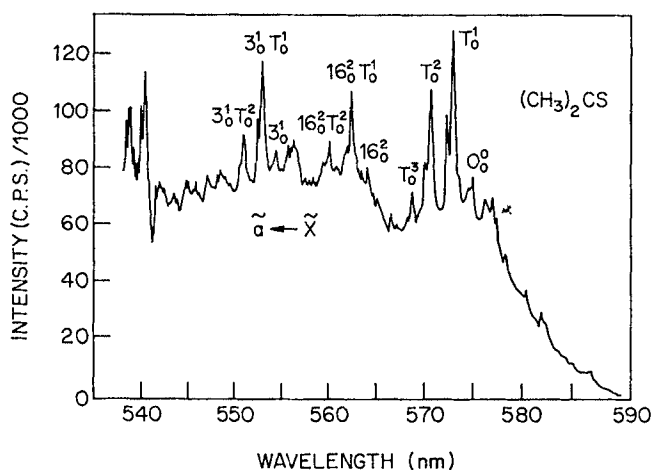
Fig. 34. Laser phosphorescence excitation spectrum of thioacetone

2.4.4 Higher Excited States

Survey spectra of thioacetone in the 260 to 185 nm region, recorded by Paone et al. [140] are shown in Fig. 35. The band at 226 nm (5.49 eV) is given the assignment $n \rightarrow 4s$, based on the calculated value of 5.23 eV. The spectrum resembles the first Rydberg transition in CH_2S, with the 0_0^0 band dominating as a sharp line-like feature. The bulk of the vibrational activity is contained in the three modes $v_8(CCC)$, $v_3(CS)$ and $v_{15}(CH_3)$. The lack of progressions in the torsional mode indicates the conformations of the methyl groups are not altered on electronic excitation.

The $\tilde{B}$ state results from $\pi \rightarrow \pi^*$ excitation and manifests itself as a broad, featureless absorption which lies beneath the $n \rightarrow 4s$ Rydberg transition. In profile, the spectra are reminiscent of those of CH_2S. The conformational changes which occur on the $n \rightarrow \pi^*$ first electronic excitation are believed to be a consequence of
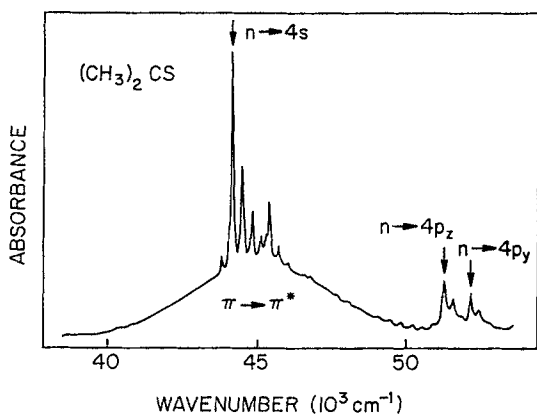
Fig. 35. Ultraviolet absorption spectra of thioacetone

217

populating a π* orbital which also occurs on π → π* excitation. It follows that the conformation in this state should be eclipsed-antieclipsed or antieclipsed-antieclipsed. In either case, the torsional modes should be active in forming band progressions. The result would be a highly congested spectrum and would account for the seemingly diffuse and featureless nature of the observed spectrum. Supersonic jet laser excitation studies would be of help here.

The $\tilde{D}^1B_2 \leftarrow \tilde{X}^1A_1$ and $\tilde{E}^1A_1 \leftarrow \tilde{X}^1A_1$ transitions which result from n → $4p_z$ and n → $4p_y$ excitations were observed at 6.40 and 6.52 eV, respectively. Both systems display single quantum additions of v_8, the CCC in-plane bending mode.

3 Ketenes, Thioketenes, and Selenoketenes

CH_2CO: Ketene is the prototype for this series of compounds. It is readily prepared by the pyrolysis of acetone, acetic anhydride and other simple precursors. The monomer has limited stability due to the ease with which it dimerizes. The haloketenes and other small, substituted ketenes are reactive enough to be considered transient molecules. Ketene has been studied spectroscopically since the first report of its liquid phase Raman spectrum in 1936 by Kopper [141]. The main interest comes from the comparison with formaldehyde. Although the molecular structure of ketene is only marginally larger, with one extra atom, the microwave, infrared and UV-visible spectra are much more complex than those of CH_2O.

The electronic spectroscopy of ketene is of particular interest because the upper state is photochemically active, leading to the formation of singlet and triplet methylene. There has been much controversy over the wavelength dependence of the relative yields of the two species of methylene, which to this day has not been satisfactorily resolved. For such a relatively simple molecule, the difficulties in unraveling its spectroscopy continue to be both surprising and challenging.

CH_2CS: Thioketene was first reported by Howard [142] in 1962 as an unstable product of the thermolysis of t-butylthioacetylene. Subsequent microwave [143] and photo-electron [144] work confirmed that the molecule could be prepared by pyrolysis of a number of precursors including hexamethyltrithiane, dithioacetic acid and 1,2,3-thia-diazole. All reports confirm the relative instability of the species in the gas phase, with a reported half-life of five minutes at pressures of 0.04 Torr [145]. Spectroscopic studies of thioketene have not advanced nearly as rapidly as those of thioformaldehyde, possibly because of the difficulties anticipated by analogy to ketene. It has been found possible to stabilize the CCS moiety by the addition of bulky substituents [146,147]. However, few of the less stable, small, substituted thioketenes have been reported and spectroscopic studies are limited.

CH_2CSe: The preparation of gas phase selenoketene was first reported by a group of microwave spectroscopists [155] in 1978. Pyrolysis of 1,2,3-selenodiazole gave a species whose microwave spectrum in the 18 to 40 GHz region, including transitions of the ^{80}Se and ^{78}Se species in natural abundance, was consistent with that expected for CH_2CSe. Further observations of deuterium substituted species [159] confirmed the identification and established the structure of the molecule. Selenoketene is a transient species, like thioketene, which dimerizes and polymerizes rapidly at room temperature. Few other selenoketenes have been prepared.

3.1 The Ground State

A diagram of the geometry and axis conventions for ketene is shown in Fig. 36. The molecule has a planar structure with C_{2v} symmetry. The molecular orbitals in the ketene molecule are not directly analogous to those of formaldehyde, as was recognized in early ab initio studies [148]. Ketene is a 22 electron system with 16 valence electrons. The molecular orbitals can be classified according to their behavior under the symmetry operations of the molecular point group, C_{2v}. Detailed MO calculations have established that the ground state orbital occupancy is:

$$1a_1^2 2a_1^2 3a_1^2 4a_1^2 5a_1^2 6a_1^2 7a_1^2 1b_2^2 1b_1^2 2b_2^2 2b_1^2$$
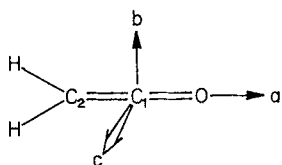
Fig. 36. The molecular structure of ketene with the principal axes. The Cartesian axes are $z = a$, $y = b$ and $x = c$

The calculated orbital energies [149] and approximate descriptions are given in Table 22. The n and π designations are less applicable to the ketene molecular orbitals than in the formaldehyde case. However, they serve as a useful guide for purposes of comparison.

The two molecular orbitals of b_1 symmetry are formed predominantly by out-of-plane p_x orbitals on oxygen and the two carbons. Population analysis shows that these orbitals can be described as lone-pair orbitals on oxygen as well as π bonding between the carbons. The carbon-oxygen π bond is formed mainly by the b_2 orbitals, with the π lobes *in the plane of the molecule*. However, these simple descriptions are misleading since the b_2 orbitals also contribute to the methylene carbon-hydrogen sigma bonds, and the b_1 orbitals give an appreciable amount of triple bond character to the C=O bond. A simplified diagram of the bonding is shown in Fig. 37.

$3b_1$

$3b_2$

$2b_1$

$2b_2$
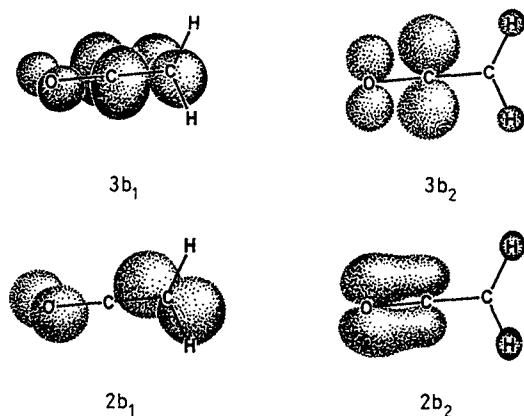
Fig. 37. Schematic representation of the higher energy HOMO and LUMO orbitals of ketene

Table 22. Calculated energies and approximate descriptions of the molecular orbitals of ketene [149].

Orbital	Energy (DZ + P) (au)	Approximate description
$1a_1$	—20.6333	O inner shell
$2a_1$	—11.4035	C inner shell
$3a_1$	—11.2488	C inner shell
$4a_1$	—1.4713	C_1—O σ bond
$5a_1$	—1.0708	C_1—C_2 σ bond
$6a_1$	—0.7557	$\sigma(CH_2) + \sigma(C_1—C_2)$
$7a_1$	—0.6830	$n + \sigma(C_1—C_2)$
$1b_2$	—0.6573	$\pi_y(CO) + \sigma(CH_2)$
$1b_1$	—0.6415	$\pi_x(CC) + n(O)$
$2b_2$	—0.5609	$\pi_y(CO) + \sigma(CH_2)$
$2b_1$	—0.3674	$\pi_x(CC) + n(O)$

The bonding in thioketene and selenoketene is expected to be qualitatively similar to that in ketene, although few detailed calculations have been reported. Some idea of the similarities can be gleaned from a comparison of the photoelectron spectra of ketene and thioketene. The interpretation of the two spectra, from the recent results of Bock et al. [144], is shown in Fig. 38. The expected close resemblance is found, although the $2b_1$-$2b_2$ energy separation is substantially reduced in the thioketene molecule.

There has been considerable theoretical effort devoted to calculating the relative energies of the possible ketene and thioketene isomers, primarily in the study of the Wolff rearrangement. The structures of the various valence isomers are shown in Fig. 39. For ketene the computed stabilities follow the order I > II > VI > III, with the ketene structure clearly the most stable [150]. In contrast, early minimal basis set calculations [151] predicted mercaptoacetylene (II) to be the most stable C_2H_2S isomer with thioketene slightly above and thiirene (III) less stable than thioformylmethylene (VI). More thorough ab initio studies [152,153] now agree that the order of stability is I > II > III, illustrating once more the inherent dangers in relying on the predictive powers of calculations whose basis set sensitivity has not been fully explored. In any event, experimental results [143,154,155] support the conclusion that ketene, thioketene and selenoketene are the most thermodynamically stable species on the relevant C_2H_2X surfaces.

H_2CCO

H_2CCS
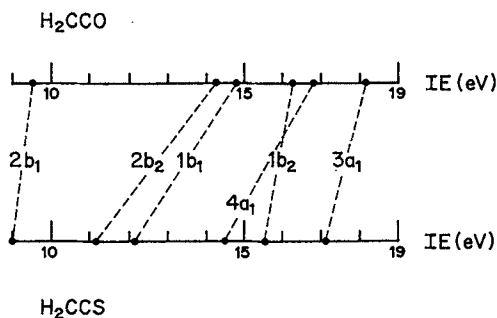
Fig. 38. Photoelectron ionization potential correlation diagram for ketene and thioketene
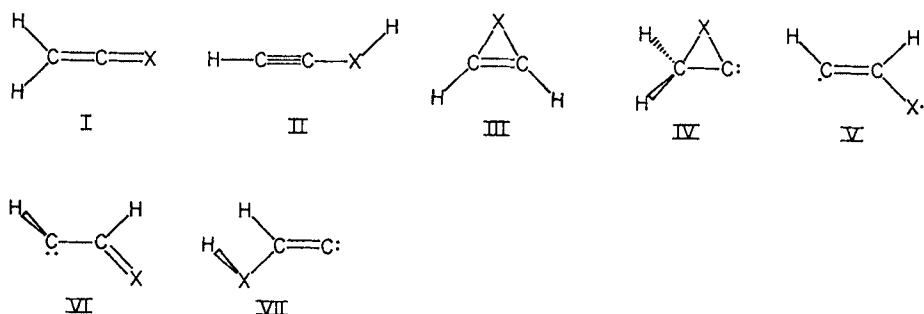
Fig. 39. Possible C_2H_2X isomers

The gas phase substitution structures and dipole moments of CH_2CO, CH_2CS, and CH_2CSe have been determined by microwave absorption spectroscopy. The results are summarized in Table 23.

The gas phase infrared spectra of ketene and thioketene have been reported and a few bands of selenoketene have been observed in matrix isolation studies [160]. These molecules have C_{2v} symmetry with their rotational axes oriented as shown in Fig. 36. The nine fundamental vibrations factorize such that the totally symmetric vibrations v_1-v_4 belong to the a_1 species, the out-of-plane vibrations v_5 and v_6 to the b_1 species, and the in-plane vibrations v_7-v_9 to the b_2 species. The a_1 fundamentals give type-A parallel bands, while type-C and type-B perpendicular bands are found for the b_1 and b_2 fundamentals, respectively. Since ketene and thioketene are near-prolate symmetric tops, the rotational structure of the IR bands is only minimally complicated by asymmetry splittings.

The analysis of the IR spectrum of ketene has occupied many workers since the earliest report in 1937 [161]. The rotational and vibrational structure is complicated by numerous Fermi and Coriolis interactions which are only beginning to be understood [162]. In very recent work, Duncan et al. [163] set out to determine the general harmonic force field of ketene using extensive high-resolution IR data from many isotopic species. They concluded that no acceptable force field for ketene could be derived purely from the available data and had to resort to ab initio calculations to complete the analysis. These authors point out that of the A_1 fundamentals of CH_2CO, $^{13}CH_2CO$, $CH_2^{13}CO$ and CD_2CO only v_1 of CD_2CO is unperturbed. The presence of such extensive perturbations in a molecule as small as ketene does not bode well for high resolution studies of other molecules in this series. Infrared spectra of thioketene have only been published very recently [164,165]. Using

Table 23. Molecular substitution structures and dipole moments.

Molecule	C=X (Å)	C=C (Å)	C—H (Å)	∢ HCH (deg)	μ (D)
CH_2CO [156,157]	1.1618(30)	1.3159(30)	1.0740(18)	122.17(20)	1.414(10)
CH_2CS [158]	1.554(3)	1.314(3)	1.090(6)	120.3(5)	1.02(1)
CH_2CSe [155,159]	1.706	1.303	1.0908	119.7	0.90(5)

multiple reflection techniques Kroto and McNaughton [164] were able to observe the high resolution FTIR spectrum of CH_2CS and rotationally analyzed two perpendicular bands. The fundamental frequencies were established and are presented in Table 24 along with those of ketene.

Table 24. Gas phase fundamental frequencies[a] of ketene and thioketene.

Vibration	CH_2CO[b]	CH_2CS[c]
$v_1(a_1)$ C—H stretch	3070.4	3020
$v_2(a_1)$ C—X stretch	2152.6	$850(v_4)$
$v_3(a_1)$ HCH bend	1387.5	1331
$v_4(a_1)$ C=C stretch	1116.0.	$1757(v_2)$
$v_5(b_1)$ CH_2 wag	587.3	701[d]
$v_6(b_1)$ C=C=O bend	528.4	378[d]
$v_7(b_2)$ C—H asy. str.	3165.3[e]	3107
$v_8(b_2)$ CH_2 rock	977.8[f]	922
$v_9(b_2)$ C=C=O bend	439.0[f]	340

[a] in cm^{-1}. [b] all frequencies from ref. 162 except as noted.
[c] all frequencies from ref. 164 except as noted. [d] ref. 166.
[e] ref. 167. [f] ref. 168.

3.2 The Excited States

The near UV-visible absorption spectrum of ketene consists of a large number of broad, diffuse bands superimposed on a continuum. High resolution studies under a variety of conditions have failed to reveal any evidence of structure in these bands [169]. Dixon and Kirby [169] have analyzed the low-frequency vibrational progressions observed among the diffuse bands in terms of two transitions: $^1A'' \leftarrow {}^1A_1$ in the 260 to 385 nm region and $^3A'' \leftarrow {}^1A_1$ in the 385 to 475 nm region. Subsequently, Laufer and Keller [170] re-examined the spectrum and concluded that only the $^1A'' \leftarrow {}^1A_1$ band system is evident. They argue that the excited triplet and singlet electronic term values are less than 19 200 and 21 300 cm^{-1}, respectively. Despite considerable effort [171], ketene has not been reported to fluoresce or phosphoresce. Therefore, it has not been possible to directly determine the lowest excited state geometry, vibrational energy levels, or the nature of the electronic transition of ketene by experimental methods.

There have been a variety of theoretical studies of the excited states of ketene, culminating in a recent, very detailed set of calculations by Allen and Schaefer [172]. The calculated vertical excitation energies for a variety of low-lying electronic states are given in Table 25. The lowest energy transitions are predicted to involve excitation of an electron from the $2b_1$ (HOMO) out-of-plane n-type orbital to the $3b_2$ (LUMO) in-plane π^*-type molecular orbital (see Fig. 37). Geometry optimization yields an in-plane bent structure of C_s symmetry for these excited states as depicted in Fig. 40. The calculated geometries and adiabatic excitation energies are given in Table 26. Dixon and Kirby [169] argued that the long progressions with

350 to 500 cm^{-1} intervals in the electronic spectrum are upper state skeletal bending vibrations. Franck-Condon arguments then predict a bent excited state geometry. Consideration of the Walsh diagram for AB_2 molecules led these authors to conclude that the bending was in-plane, in agreement with later calculations.

Allen and Schaefer [172] also calculated the excited state vibrational frequencies as shown in Table 27. The major frequency changes on excitation are predicted to occur for the $C=C$ and $C=O$ stretches, although there is some uncertainty concerning the $^1A''$ state a$''$ modes, due to mixing with the ground state.

Table 25. Theoretical (DZP+R—CISD) vertical excitation energies for the low-lying electronic states of ketene [172].

Electron configuration	State	Energy (cm^{-1})
... $1b_2^2 1b_1^2 2b_2^2 2b_1^2$	$^1A_1$	0
... $1b_2^2 1b_1^2 2b_2^2 2b_1^1 3b_2^1$	$^3A_2$	29830
	$^1A_2$	30904
... $1b_2^2 1b_1^2 2b_2^2 2b_1^1 3b_1^1$	$^3A_1$	44677
	2^1A_1	56054

Table 26. Geometries and adiabatic excitation energies calculated for ketene ground and lowest excited states.[a]

Parameter	$^1A_1$	$^3A''$	$^1A''$
r(C=O)	1.1466	1.1716	1.1742
r(C=C)	1.3101	1.4660	1.4620
r(C—H$_1$)	1.0735	1.0735	1.0728
r(C—H$_2$)	1.0735	1.0780	1.0766
∢(CCO)	180.00	129.25	129.81
∢(H$_1$CC)	119.01	119.94	120.02
∢(H$_2$CC)	119.01	119.60	118.99
Energy (cm^{-1})	0	16719	19015

[a] bond lengths in Å, angles in degrees, calculated at the DZP SCF level; adiabatic excitation energy in cm^{-1}, calculated using DZP CIDVD wavefunctions; all data from ref. 172.
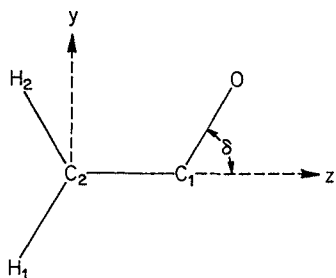
Fig. 40. C$_s$ planar structure for excited state ketene

Table 27. Calculated DZP SCF vibrational frequencies[a] for the ground and excited states of ketene [172).

Description	$^1A_1$	$^3A''$	$^1A''$
asym. C—H str.	3467	3458	3469
sym. C—H str.	3355	3319	3332
C=O stretch	2360	2093	2108
HCH bend	1537	1554	1556
CH_2 rock	1094	1158	1189
C—C stretch	1245	1027	1052
CCO bend	618	508	509
CH_2 wag	702	680	1383[b]
HCCO torsion	486	396	483[b]

[a] in cm^{-1}. [b] differs from the triplet state due to mixing with the ground state. An alternate calculation gives 599 and 427 cm^{-1}.

One experimental approach to further understanding the excited states of ketene would be to study a related molecule with a bound upper state and resolvable structure in the absorption spectrum. Such a study has been attempted by Clouthier [173), who theorized that thioketene might have a discrete spectrum which could be rotationally analyzed to establish the upper state geometry and symmetry. Several factors suggested this approach. Previous experience with thiocarbonyl compounds had shown that substituting sulfur for oxygen substantially lowered the excitation energy for the electronic transitions to n, π^* states, usually shifting them from the UV into the visible. Such low-lying states are more likely to be bound than those at higher energies, as is thought to be the case for thioformaldehyde, in contrast to the well-known photochemical activity of formaldehyde.

Ab initio calculations [152) on thioketene were also encouraging, suggesting that the lowest triplet state is about 15000 cm^{-1} above the ground state and has an in-plane bent geometry with an elongated C=C bond, analogous to the results for ketene. Thus, comparisons of the excited states of the two species were likely to be meaningful. Finally, suitable methods for preparing thioketene were available based on the pyrolysis of 1,2,3-thiadiazole as in Eq. (5).

$$\begin{array}{c} H-C-N \\ \| \quad \| \\ H-C \quad N \\ \diagdown / \\ S \end{array} \rightarrow CH_2CS + N_2 \tag{5}$$

Although thioketene is unstable, successful microwave and IR studies showed that it could be handled in the low pressure gas phase with relative ease.

The electronic spectrum of thioketene was successfully recorded using spectrographic techniques. Low resolution comparison spectra of the lowest electronic transitions of ketene and thioketene are shown in Figs. 41 and 42. The thioketene spectrum is at much longer wavelengths and shows well-resolved vibronic structure. Unfortunately, very high resolution spectra of CH_2CS and CD_2CS show no evidence

of any rotational structure, suggesting that the excited state is predissociated. All attempts to excite fluorescence in the thioketene bands were unsuccessful.

Analysis of the vibronic structure of the thioketene spectra does provide information on the excited state structure. Pronounced hot band progressions in v_9'', the in-plane bending mode, are found in the spectra of both thioketene and dideuterothioketene. No evidence of intervals involving the ground state out-of-plane bending mode v_6'' could be found, although v_6'' and v_9'' have comparable Boltzmann factors. Long progressions involving low frequency excited state intervals most readily assigned as activity in v_9' were also observed. The strong Franck-Condon activity in the hot and cold bands in both isotopic species provides good evidence for the geometry change to an in-plane bent structure in the excited state.

The vibronic structure in the spectrum is consistent with but does not prove that the transition is $^1A'' \leftarrow {}^1A_1$. Attempts to assign the bands using selection rules appropriate to other electronic transitions either failed or were inconclusive. In the absence of further information, the exact nature of the electronic transition cannot be determined although it can be assigned as $\tilde{A} \leftarrow \tilde{X}$ with reasonable certainty. A careful search, out to 800 nm, was made for the corresponding triplet-singlet transition but no further bands were observed. In sharp contrast to the spectra of formaldehyde and thioformaldehyde, the triplet-singlet system in thioketene is too weak to be observed by
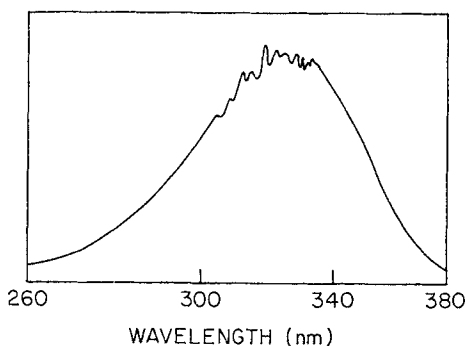
Fig. 41. The ultraviolet absorption spectrum of ketene
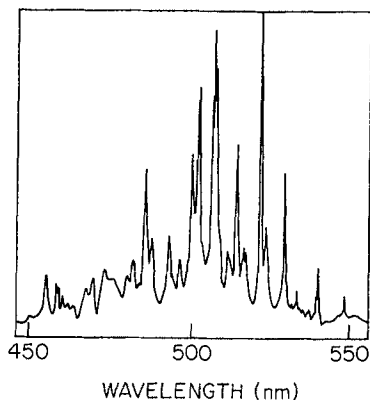
Fig. 42. The visible absorption spectrum of thioketene

225

conventional absorption spectroscopy using long-path multiple reflection techniques.

All the experimental evidence suggests that the lowest excited states of ketene and thioketene are analogous. Both are devoid of discrete rotational structure and do not detectably fluoresce. The observed vertical excitation energies are in agreement with the results of high level ab initio calculations for a $2b_1 \rightarrow 3b_2$ electron promotion. Finally, both transitions exhibit extensive progressions in low-frequency bending modes implying a change in geometry on excitation. From these results it can be concluded that both molecules have an in-plane bent excited state geometry, in agreement with the early work of Dixon and Kirby [169]. The absence of any evidence for thioketene triplet-singlet bands agrees with the reassessment of the ketene vibronic spectrum by Laufer and Keller [170] as a single band system.

The major discernible difference in the two band systems is the length of the bending progressions and consequent width of the electronic transition. The thioketene bands span a narrow region of about 8000 cm^{-1} centered at 500 nm, whereas the ketene spectrum covers some 17000 cm^{-1} centered at about 370 nm. This large difference probably reflects to some degree the limited pressure-path attainable with thioketene due to its instability, but also suggests more extensive Franck-Condon activity and a more distorted excited state in the ketene case. Such a conclusion is consistent with the ab initio results.

Although a number of other electronic transitions have been reported for ketene, UV spectra are not available for thioketene and none of the electronic transitions of selenoketene have been identified. A similar lack of data on the transitions in substituted species makes further comparisons of their spectroscopy unrewarding.

4 Nitriles and Phosphaalkynes

The nitriles are a well known functional group for which there is a substantial spectroscopic data base. The phosphorus analogs, $RC \equiv P$, are obscure oddities to most chemists and yet there is a surprising amount of spectroscopic information available for the molecules with simple R— groups. Although generally unstable with low pressure gas phase lifetimes of minutes to hours, the phosphaalkynes are sufficiently long-lived to be studied under flow and often static conditions.

HCN: Hydrogen cyanide is the nitrile prototype. The simple linear molecular structure and well separated vibrational frequencies have made it an ideal candidate for high resolution spectroscopic studies, particularly in the microwave and infrared regions. Intensive investigations, particularly of isotopically substituted species, have yielded very precise sets of vibration-rotation constants for the electronic ground state. This work was critically reviewed for the triatomic cyanides by Chadwick and Edwards [174] in 1973. Since that time the state-of-the-art has been subject to major advances which are reflected in further refinements of the spectroscopic data base.

One of the most interesting aspects of the spectroscopy of HCN is the possibility of intramolecular isomerization to form the isocyanide, HNC. Although this class of organic compounds is well known, the simplest member, HNC, was first detected in a matrix by Milligan and Jacox [175] in 1963. The first gas phase detection was by observation of IR emission from HNC and DNC in the reaction of active nitrogen

with a variety of organic substances [176]. Subsequently, the species was observed by microwave [177] and IR [178] absorption spectroscopy. These observations have stimulated a variety of studies of the large amplitude internal bending potential function for the isomerization process.

Studies of the excited states of HCN have been hampered by the necessity of working in the notoriously difficult region beyond 200 nm. In a now classic paper, Herzberg and Innes [179] analyzed the rovibronic structure of the absorption bands in the 160 to 200 nm region and established that the first excited singlet state has a bent geometry. Various other transitions further in the vacuum ultraviolet have been studied since then. The subject was reviewed by Ashfold et al. [180] in 1979.

HCP: The prototype phosphaalkyne, HCP, was the first member of this group of compounds to be synthesized. Gier [181] reported, in 1961, that HCP could be prepared by passing phosphine through a low intensity rotating arc struck between graphite electrodes. The resulting colorless, very reactive gas could be stored without decomposition at temperatures below $-124\,°C$, and had an IR spectrum consistent with the $H—C\equiv P$ structure. Later workers showed that essentially pure HCP could be generated by pyrolysis of CH_3PCl_2 and low temperature distillation of the products. When exposed to glass, HCP is quite stable at room temperature at pressures below a few Torr. Studies of the microwave, infrared and UV-visible spectra of HCP have been reported.

Fifteen years after Gier reported the preparation of HCP, a second member of the phosphaalkyne family, CH_3CP, was identified by Kroto et al. [182] using microwave spectroscopy. Subsequently, the same group prepared and recorded the microwave spectra of FCP, CF_3CP, NCCP, HCCCP, H_2CCHCP and C_6H_5CP [183]. Clearly, $C\equiv P$ is a viable functional group and a whole family of such molecules exists. The chemical reactions and properties of the phosphaalkynes are now being explored in a number of laboratories.

4.1 The Ground State

The prototype nitrile, HCN, is a linear molecule of $C_{\infty v}$ symmetry in the electronic ground state. The orbital occupancy of the 14 electrons is:

$$1\sigma^2 2\sigma^2 3\sigma^2 4\sigma^2 5\sigma^2 1\pi^4$$
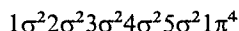
A set of calculated orbital energies and approximate descriptions is given in Table 28. The two degenerate π orbitals are orthogonal and occupy most of the space surrounding the CN group. The 3σ bond is mainly due to the overlap of the 2s orbitals on the carbon and nitrogen centers and forms the third member of the triple bond. The 4σ orbital is largely CH bonding and the 5σ approximates a lone pair on the nitrogen atom. The approximate form of the molecular orbitals is shown in Fig. 43.

The bonding in the isoelectronic HCP molecule is expected to be similar to that in HCN. The 22 electrons are distributed in the molecular orbitals as:

$$1\sigma^2 2\sigma^2 3\sigma^2 4\sigma^2 1\pi^4 5\sigma^2 6\sigma^2 7\sigma^2 2\pi^4$$
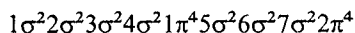
Table 28. Energies and approximate descriptions of the molecular orbitals of HCN [184].

MO	Energy (au)	Approximate description
1σ	−15.6471	1s on nitrogen
2σ	−11.3353	1s on carbon
3σ	−1.2181	2s on carbon + 2s on nitrogen + C−N σ bonding
4σ	−0.7770	C−H bonding
5σ	−0.5287	N lone pair
$1\pi_x$	−0.4764	C−N π bond
$1\pi_y$	−0.4764	C−N π bond
$2\pi_x$	0.2949	LUMO
$2\pi_y$	0.2949	LUMO
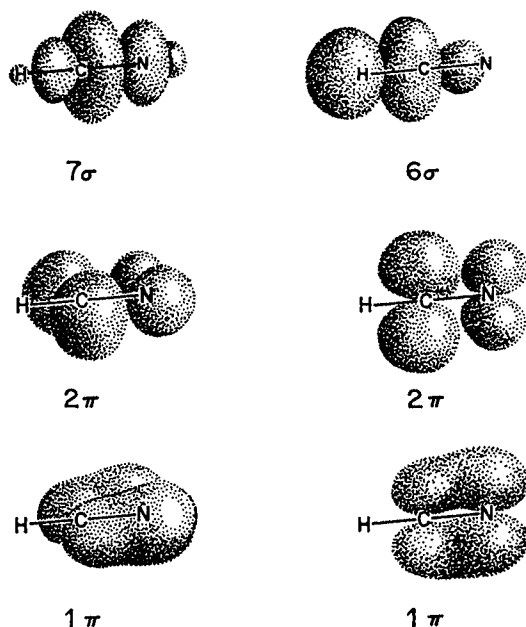
Fig. 43. Schematic representations of the molecular orbitals of HCN

The five HCP valence orbitals (5σ through 2π) are dominated by localized bonding descriptions similar to those of HCN (Table 28). The only differences are that the 6σ bond in HCP has some P−C bond character in addition to the C−H bond contribution, and the lone pair electrons are more diffuse on the phosphorus than on nitrogen. The molecular structures of HCN, HCP and a number of substituted species have been determined by microwave techniques. Although studies of the nitriles are well advanced due to the stability of the species and the ease of obtaining the various isotopomers, data on the phosphaalkynes are less complete. The latter are studied by pyrolysis of organophosphorus precursors in flow systems, making isotopic substitution experiments more difficult and costly. In many cases,

molecular parameters are transferred from similar molecules to arrive at a structure that is consistent with the observed rotational constants, but is not unique. A comparison of various nitrile and phosphaalkyne structures is given in Table 29.

Although the structures and bonding of the nitriles and phosphaalkynes are in many ways very similar, there is at least one example of a substantial difference in the two species. It concerns the ground state bending potentials. It is well known that the nitriles can unimolecularly isomerize to isonitriles. The isomerization is thought to be the result of large amplitude internal bending. The potential function has been derived from the large body of available experimental data [201] and has been found to agree well with the results of ab initio calculations [202]. The potential, shown in Fig. 44a, has a barrier to HCN isomerization of 17319 cm^{-1} and a maximum at a bending angle of 87 degrees relative to the linear conformation.
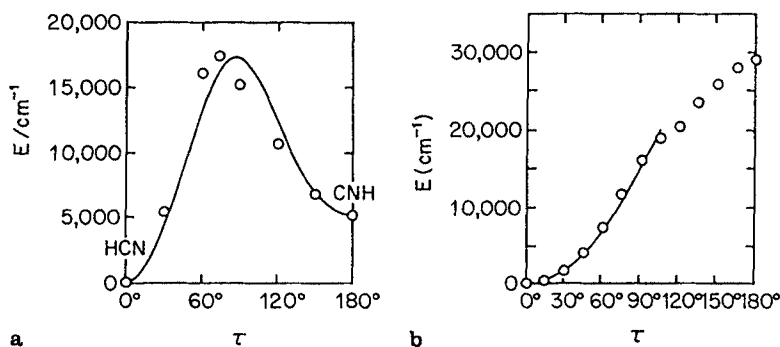
Fig. 44a. The ground state bending potential for HCN. The solid line is that obtained from a fit of HCN/CNH data, the circles are ab initio results; **b.** The ground state bending potential for HCP. The solid line is that obtained from a fit of experimental data, the circles are ab initio results

The bending potential of HCP has recently been studied using experimental and ab initio data [203]. In sharp contrast to the behavior of HCN, the HCP potential, illustrated in Fig. 44b, shows no sign of turning over to form a minimum for CPH. The ab initio calculations predict that linear CPH corresponds to a local maximum approximately 30000 cm^{-1} higher in energy than HCP. Thus, the ground state bending potentials of HCN and HCP are very different, despite the similarities in most other spectroscopic parameters.

High resolution gas phase infrared spectra have been reported for a variety of nitriles but only for three phosphaalkynes, HCP, FCP and CH_3CP. The linear triatomic species have $C_{\infty v}$ geometries and the vibrations are numbered such that v_1 and v_3 are the stretching modes and v_2 the bend. The degeneracy of the bending mode (Π_u) leads to the complications of vibrational angular momentum which appear in the vibration-rotation spectra. A summary of relevant vibrational data for both groups of molecules is given in Table 30.

229

Table 29. Structural data for substituted nitriles and phosphaalkynes.

Nitrile	$r(C \equiv N)$ (Å)	$r(X{-}C)$ (Å)	μ (D)	Ref.
HCN	1.15512(15)	1.06316(10)	2.986	185, 186)
CH_3CN	1.1567(6)	1.4617(6)	3.913(2)	187, 188)
FCN	1.15594(10)	1.26504(10)	2.1203(10)	189, 190)
CF_3CN	1.158ᵃ	1.464(20)	—	191)
$N \equiv C{-}C \equiv N$	1.154(17)	1.389(30)	0.0	192)
$HC \equiv C{-}C \equiv N$	1.1585(10)	1.3775(10)	3.724(30)	193)
$CH_2 = CH{-}C \equiv N$	1.1637(10)	1.4256(10)	$3.68(7)\mu_a$	194)

Phosphaalkyne	$r(C \equiv P)$ (Å)	$r(X{-}C)$ (Å)	μ (D)	Ref.
HCP	1.5421(5)	1.0667(5)	0.390(5)	195)
CH_3CP	1.544(4)	1.465(3)	1.499(1)	196)
FCP	1.541(5)	1.285(5)	0.279(1)	197)
CF_3CP	1.542ᵃ	1.460ᵃ	—	183)
$N \equiv C{-}C \equiv P$	1.544ᵃ	1.382ᵃ	3.44(3)	198)
$HC \equiv C{-}C \equiv P$	1.544ᵃ	1.382ᵃ	0.745(5)	199)
$CH_2 = CH{-}C \equiv P$	1.544ᵃ	1.432ᵃ	1.183(2)	200)

ᵃ these parameters transferred from other molecules and are consistent with the derived rotational constants.

Table 30. Vibrational data for various nitriles and phosphaalkynes.ᵃ

$XC \equiv N$	$v(CX$ stretch)	$v(C \equiv N$ stretch)	v(bend)	Ref.
HCN	3311.4775(15)	2096.855(12)	711.979(1)	204, 205, 206)
DCN	2630.303(2)	1925.265(2)	569.046(1)	205, 207)
FCN	1076.492007(13)	2318.81	450.92	189, 190)
CH_3CN	915.40	2270.6	364.71	208)

$XC \equiv P$	$v(CX$ stretch)	$v(C \equiv P$ stretch)	v(bend)	Ref.
HCP	3216.88952(32)	1278.2798(12)	674.69990(34)	209)
DCP	2419.42515(33)	1231.40260(55)	525.220421(22)	210, 211)
FCP	801.339(7)	1670.842(9)	375.252(6)	212)
CH_3CP	750ᵇ	1558.724(25)	302ᵇ	213, 214, 215)

ᵃ in cm^{-1}. ᵇ from spectra taken in the solid phase.

4.2 The Excited States

The electronic spectra of the nitriles occur for the most part in the far ultraviolet, making experimental studies difficult. Not surprisingly, the excited states of the HCN molecules are the most fully characterized of this group. Of the phosphaalkyne series, only the spectra of HCP/DCP have been reported. In a single paper, Johns et al. [216] reported the identification and analysis of *seven* electronic transitions of HCP in the UV-visible, making it one of the best characterized polyatomic molecules in this regard. The ground state electronic configurations of HCN and HCP

Table 31. Electron configurations and terms for the electronic states of HCN and HCP.

Linear geometry		Bent geometry	
Configuration	States	Configuration	States
... $\sigma^2\pi^4$	$^1\Sigma^+$	... $a'^2a'^2a''^2$	$^1A''$
... $\sigma^2\pi^3\pi^*$	$^{1,3}\Delta$	... $a'^2a'^2a''a'^*$	$^{1,3}A''$
		... $a'^2a'^2a''a''^*$	$^{1,3}A'$
	$^{1,3}\Sigma^+$	... $a'^2a'a''^2a'^*$	$^{1,3}A'$
	$^{1,3}\Sigma^-$	... $a'^2a'a''^2a''^*$	$^{1,3}A''$
... $\sigma\pi^4\pi^*$	$^{1,3}\Pi$	... $a'a'^2a''^2a'^*$	$^{1,3}A'$
		... $a'a'^2a''^2a''^*$	$^{1,3}A''$

are both ... $\sigma^2\pi^4$ which is a $^1\Sigma^+$ state. Promotion of a π electron yields a variety of possible excited states which may be of either bent or linear geometry. The various terms are summarized in Table 31.

The geometries of the excited states of HAB molecules can be qualitatively predicted using Walsh diagrams [217]. Such predictions are in general agreement with the results of detailed ab initio calculations for HCN [218] as outlined in Table 32.

The ultraviolet spectrum of HCN consists of a weak set of bands between 200 and 170 nm and a much stronger system in the 150 to 130 nm region. Herzberg and Innes [179] made a detailed high resolution study of the weak bands for both HCN and DCN. Long progressions in the bending mode v_2' were observed and analysis established that the first excited state was bent, with a bond angle of 125°. The spectrum becomes increasingly diffuse to shorter wavelengths due to a strong predissociation in the $\tilde{A}$ state. This diffuseness sets in earlier and is more pronounced for HCN than DCN. Herzberg and Innes proved that the transition, with band origin at 191.4 nm in HCN, was $\tilde{A}^1A'' \leftarrow \tilde{X}$ and ascribed it to the $a'' \rightarrow a'$ excitation correlating with the linear $^1\Delta$ state. A second transition, observed only in DCN, was analyzed and assigned as $\tilde{B}^1A''(^1\Sigma^-) \leftarrow \tilde{X}$. The strong band system was also analyzed by Herzberg and Innes [179] and assigned as a transition to the A' component of the $^1\Pi$ state. Most of the vibronic bands are diffuse but rotational structure was resolvable in the lower members of the long upper state bending progression. A bond angle of 141° was derived for this state.

Table 32. Theoretical predictions of the excited state energies and geometries of HCN.

State	T_e (eV)	r_e(HC) (Å)	r_e(CN) (Å)	$\star$ (HCN) (deg)
$^1\Sigma^+$	0.00	1.055	1.180	180.0
$^3A'$	4.42	1.081	1.294	128.6
$^3A''$	5.46	1.099	1.365	117.0
$^3A'$	5.91	1.063	1.320	160.0
$^1A''$	6.48	1.096	1.318	127.2
$^1A'$	6.78	1.102	1.287	124.9
$^3A''$	6.85	1.061	1.314	157.4
$^3A'$	6.98	1.081	1.250	132.6
$^3\Pi$	7.41	1.045	1.237	180.0

Subsequent ab initio calculations [218, 219] cast serious doubt on some of the assignments. In particular, they predicted that the second A'' state should be about 0.75 eV higher than the assigned $\tilde{B}^1A''$ state, that it should be nearly linear rather than strongly bent, and that the only state of the correct geometry and energy is of species $^1A'$. One way to rationalize all the discrepancies is to assign the bending progression of the $\tilde{B} \leftarrow \tilde{X}$ system as the $(1, v_2, 0)$ upper state progression of the $\tilde{A} \leftarrow \tilde{X}$ band system. This explanation was rejected by Herzberg and Innes because it leads to anomalous anharmonicity constants. However, recent spectra of $D^{13}CN$ and $DC^{15}N$ analyzed by Bickel and Innes [220] firmly established that this explanation is correct and that the $\tilde{B} \leftarrow \tilde{X}$ system is in fact part of the $\tilde{A} \leftarrow \tilde{X}$ transition, resolving the discrepancy in favor of both the Walsh and ab initio predictions. Furthermore, the $\tilde{A} \leftarrow \tilde{X}$ transition has been reassigned as $^1A''(^1\Sigma^-) \leftarrow \tilde{X}$ on the basis of calculated energies [219]. Transitions to excited triplet states of HCN have not been reported. Current assignments are presented in Table 33 in conjunction with the most recent ab initio predictions.

The ultraviolet spectrum of HCP is similar to that of HCN but occurs at longer wavelengths, facilitating spectroscopic studies. The triplet-singlet transitions of HCP are also observable, because of the greater spin-orbit coupling of phosphorus relative to nitrogen. Due to these favorable circumstances, the excited states of HCP are more extensively characterized than those of HCN and most other polyatomic molecules. HCP exhibits a variety of weak bands between 410 and 285 nm and a much stronger absorption starting at 285 nm and extending to shorter wavelengths [216]. The main system is assigned as $\tilde{A}^1A'' \leftarrow \tilde{X}^1\Sigma^+$ with the upper state correlating with $^1\Sigma^-$ in the linear conformation. The excited state has a bent equilibrium configuration but exhibits quasilinearity. The only other singlet-singlet transition observed is to the $^1A'$ state correlating with the $^1\Sigma^+$ linear state of the $\sigma^2\pi^3\pi^*$ configuration. Three triplet-singlet transitions with this same upper state configuration are also observed. Two other triplet-singlet transitions have been analyzed, one of which is assigned as $^3\Pi—^1\Sigma^+$ with the $\sigma\pi^4\pi^*$ upper state configuration. A summary of the observed states and their geometries is given in Table 34.

Table 33. Experimental [179, 220] data and theoretical predictions [219] for the excited states of HCN.[a]

State	T_0 (eV)	r(HC) (Å)	r(CN) (Å)	∡(HCN) (deg)	Linear configuration
$\tilde{X}$	0.0	1.064	1.156	180	$^1\Sigma^+$
	(0.0)	(1.058)	(1.188)	(180)	
$\tilde{A}^1A''$	6.48	1.140	1.297	125	$^1\Sigma^-$
	(6.73)	(1.085)	(1.330)	(123)	
$2^1A'$	—	—	—	—	$^1\Delta$
	(7.52)	(—)	(1.351)	(120)	
$2^1A''$	—	—	—	—	$^1\Delta$
	(7.99)	(—)	(1.337)	(180)	
$\tilde{C}^1A'$	8.14	—	—	141	$^1\Pi$
	(—)	(—)	(—)	(—)	

[a] calculated values in parentheses.

Table 34. Excited state energies and geometries of HCP.

State	T_0 (cm^{-1})	v_1	v_2	v_3	r(CP) (Å)	⋌ (HCP) (deg)
		(a) ... $\sigma^2\pi^4$ configuration				
$\tilde{X}^1\Sigma^+$	0	3217	675	1278	1.5421	180
		(b) ... $\sigma^2\pi^3\pi^*$ configuration				
$\tilde{a}^3\Sigma^+$	24440	2700	443	943	1.67	180
$\tilde{c}^3\Sigma^-$	31023.9	—	—	927.8	1.668	180
$\tilde{A}^1A''(^1\Sigma^-)$	34745.6	—	566.6	953.9	1.69	130
$\tilde{d}^3\Delta_1$	35926.9	—	—	967.6	1.635	180
$\tilde{C}^1A'(^1\Sigma^+)$	40247.6	—	615.4	969.4	1.69	113
		(c) ... $\sigma\pi^4\pi^*$ configuration				
$\tilde{b}^3\Pi$	30430	—	—	963	1.67	180
$^3\Pi^a$	35976.3	—	—	953.5	1.67	180

^{a} the configuration of this state is in doubt.

Comparison of the excited states of HCP and HCN is hampered by the lack of data on the triplet states of the latter. The $\tilde{A}^1A''$ states are exact analogs and the $\tilde{C}^1A'$ states are similar although Johns et al. [216] note that the transition to the $\tilde{C}$ state in HCP is much weaker than that in HCN. The observed HCP triplet states can only be compared with calculated HCN states and predictions based on Walsh diagrams. The relevant data are given in Table 35. The agreement is poor, although the geometries of the HCP triplet states are not very well established.

The isomerization of HCN in the excited state has been studied theoretically by Ross and Bunker [201]. They fitted excited state energy levels to a semirigid bender model, using a combination of experimental data and ab initio predictions. The general results are shown in Fig. 45, from which it is clear that HCN does exhibit a second minimum in the bending potential. It is unfortunate that a similar study has not been undertaken to determine the excited state potential of HCP.
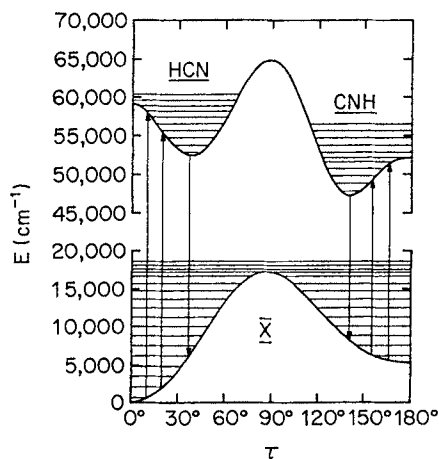
Fig. 45. Ground and excited state bending potentials for HCN/CNH

Table 35. Comparison of geometries of the triplet states of HCP with theoretical predictions for similar states of HCN.

State	HCP geometry [216]	Walsh diagram prediction [217]	HCN Ab initio bond angle
$\tilde{a}^3\Sigma^+$	linear	bent	122[a]
$\tilde{b}^3\Pi$	linear	linear	180[b]
$\tilde{c}^3\Sigma^-$	linear	slightly bent	157[b].
$\tilde{d}^3\Delta_1$	linear	bent	120[a]

[a] ref. 221. [b] ref. 218.

5 Conclusions

5.1 The Ground State

The general effects of substitution on the ground states of the carbonyls, ketenes and nitriles can be examined by correlating structural and vibrational data from the spectroscopic data base presented in Sects. 2 to 4 of this article.

5.1.1 Molecular Structure

A correlation of the C=X bond lengths for the carbonyls and ketenes as a function of substituents is presented in Fig. 46. The double bond elongates on substitution by sulfur and selenium, as expected due to the increasing size of the terminal atom and the inherent weakness of bonds involving 2p–3p or 2p–4p π overlap. The elongation is about 0.4 Å on substituting sulfur for oxygen and only about 0.15 Å more on selenium substitution. This trend of a more moderate variation on replacing sulfur with selenium is noted for many parameters that show changes on substitution.

The π bond strengths of atoms in the second and third periods have been recently estimated by calculations of cis-trans rotation barriers and hydrogenation energies [222]. The authors conclude that the efficacy of π bonding is in the order $0 > N \cong C \gg S > P > Si$. A comparison of their recommended π bond energies is shown in Table 36. The lower π bond strength in combinations involving carbon and elements of the third period is clearly evident.

Table 36. Calculated π bond strengths [222].

Bond	Energy (Kcal/mol)
C=C	65
C=O	77
C=S	52
C=Si	38
C=N	63
C=P	43
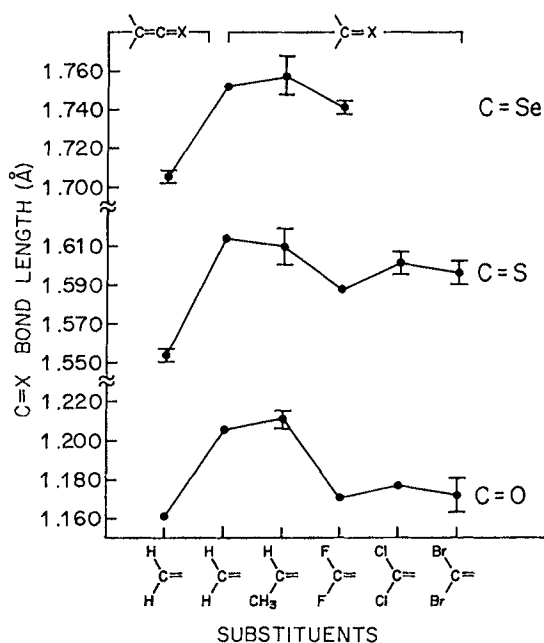
Fig. 46. Correlation diagram of the C=X bond lengths in various ketene and carbonyl compounds, X = O, S, Se

The effect of substituents on the C=X bond length is parallel in the carbonyl series, with electron withdrawing groups decreasing the bond lengths. Oberhammer and Boggs [223] have studied these effects for C=O and C=S compounds using fully optimized ab initio geometries for a variety of tetraatomic species. The authors attempted to find simple correlations between the electronic and geometric structures of these molecules. Although their calculations reproduced experimental bond lengths very well, they concluded that no systematic correlation could be found between overlap populations for individual bonds and their bond lengths.

The effect of S and Se substitution in the ketene series is also shown in Fig. 46. The trend is the same as in the carbonyls but the double bond is shorter in the ketenes, due to the partial triple bond character in the C=C=X moiety. It is unfortunate that more data are not available for substituted thio- and selenoketenes to extend the observed trends.

Substituting phosphorus for nitrogen in the nitriles causes a 0.4 Å elongation of the triple bond which shows little variation with substituents. The longer C≡P bond is attributable to the larger atomic radius of phosphorus and the more diffuse nature of C≡P bonding [224].

Variations in the geometric parameters around the substituents are also informative. The HCH angle in the carbonyls increases only slightly on S and Se substitution and is less than the 120° expected for strictly sp^2 hybridization on carbon. In contrast, the corresponding angle in the ketenes is greater than 120° and decreases substantially on sulfur substitution, with little change on going to selenium. In the

carbonyls, there are no in-plane b_2 π orbitals which can interact with the in-plane substituents. In the ketenes, there are such orbitals which are delocalized onto the substituents, pulling them towards the $C=C=X$ frame and opening the bond angle. Sulfur or selenium in place of oxygen decreases the π bonding character and appears to allow the substituents to move closer together.

The trend in $C-X$ bond lengths is also opposite in the carlonyl and ketene series. Sulfur and selenium decrease the $C-H$ bond lengths in the carbonyls but clearly increase them in the ketenes. The same trend of decreasing $C-X$ bond length is observed in the tetraatomic halogenated carbonyls. It is tempting to ascribe this reversal in behavior between the carbonyls and ketenes to π delocalization in the latter, as in the rationale for the variation in bond angle. Although a closing of the HCH angle and corresponding increase in the CH bond length in S or Se substituted ketenes appears reasonable, it does not rationalize the fact that the $C-H$ bond lengths are essentially identical in CH_2S/CH_2CS and CH_2Se/CH_2CSe. The drop in the $C-X$ distance on replacing O by S in the carbonyls cannot be explained by variations in calculated σ and π electron densities on the carbon atom [223].

In the nitriles, the $X-C$ bond length is insensitive to the change from nitrogen to phosphorus, as might be expected since the triple bond is substituent invariant. The only noticeable exception is FCN/FCP where the $F-C$ distance changes by 0.02 Å. The trend is reflected in the dipole moments which, although substantially smaller in the phosphaalkynes, show similar variations with substituents in $C\equiv N$ and $C\equiv P$ molecules.

In larger polyatomic carbonyls, the effect of sulfur and selenium substitution on other structural parameters can be explored. In the acetaldehyde series, internal rotation is the molecular motion of most interest. In the oxygen, sulfur and selenium species, the equilibrium geometry is one with hydrogen on the CH_3 group eclipsing the $C=X$ group. The trend is for modest increases in the barrier to internal rotation on sulfur and selenium substitution. In general, the potential function for internal rotation is very similar in the three molecules.

5.1.2 Molecular Vibrations

The $C=X$ stretching frequencies closely parallel changes in the $C=X$ bond lengths in the carbonyl/thiocarbonyl/selenocarbonyl series. In the ketenes some unexpected trends are evident. The nominal $C=O$ stretch in ketene is substantially higher than the normal $C=O$ frequency of $\sim 1700 \text{ cm}^{-1}$, as might be expected if the $C=O$ moiety has substantial triple bond character. However, the normal coordinate analysis of Moore and Pimentel [225] and the general harmonic force field calculations of Duncan et al. [163] show that the normal mode is actually a combination of $C=O$ and $C=C$ stretching motions. The $C=C$ stretch in ketene is 500 to 600 cm^{-1} lower than expected due to this mixing. In thioketene, the opposite trends are observed. The $C=S$ stretching frequency is lower than expected and the $C=C$ frequency higher. This can be explained in the context of perturbation theory, in which two mutually interacting levels repel each other. The higher level ($C=O$ in ketene, $C=C$ in thioketene) is displaced upwards in energy and the lower ($C=C$ in ketene and $C=S$ in thioketene) down by the off-diagonal interaction.

Duncan [226] has shown that there is an accurate correlation between the difference of the symmetric and antisymmetric $C-H$ stretching frequencies in molecules con-
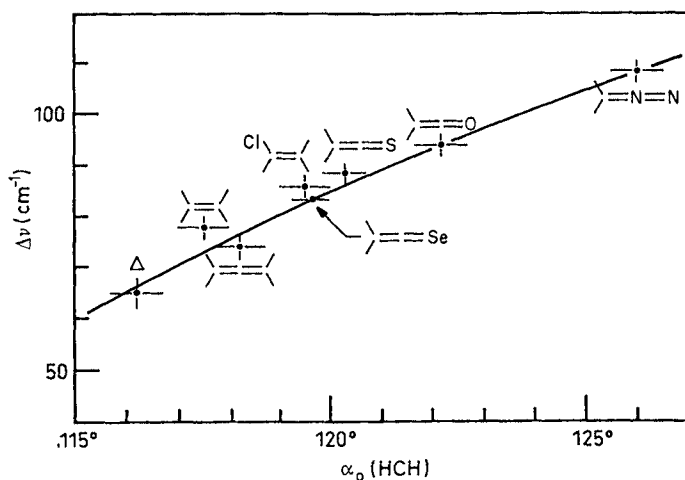
Fig. 47. Correlation diagram of the HCH angle and the difference in symmetric and antisymmetric C—H stretching frequencies in molecules containing the $H_2C=$ group

taining the $H_2C=$ group and their HCH angles. Addition of the available thioketene and selenoketene data to the correlation diagram give the plot shown in Fig. 47. Allowing for the likely possibility of a Fermi resonance in the CH_2CS v_1 band, the correlation is satisfactory. The difference between the as yet unobserved CH stretching frequencies of selenoketene is predicted to be ~ 85 cm^{-1}.

In the HCN/HCP series, the representative $C \equiv N$ and $C \equiv P$ stretching frequencies are 2097 and 1278 cm^{-1}, respectively. The higher values for the fluorine and methyl substituted compounds have been shown by force field analysis to be due to substantial vibrational coupling. Harmonic force constants are available for several nitrile and phosphaalkyne compounds and are shown in Table 37. The much lower $C \equiv P$ stretching force constants relative to the corresponding $C \equiv N$ values establish the relative weakness of the CP triple bond. This likely reflects the poor $p\pi - p\pi$ overlap inherent in multiple bonds involving elements beyond the second row of the periodic table. Calculated electron density plots of the P—C and N—C π-bonding orbitals [224] clearly show considerably more diffuse bonding between the carbon and phosphorus, in accord with the spectroscopic results. The substituent-functional group stretching force constants are not substantially different for the two types of molecules, consistent with conclusions based on bond lengths.

Table 37. Harmonic force constants of $C \equiv N$ and $C \equiv P$ compounds.

Constant[a]	HCN	FCN	CH_3CN	HCP	FCP	CH_3CP
$f(C \equiv Y)$	18.774	16.960	18.40	9.184	8.071	8.887
$f(X—C)$	6.230	9.332	5.236	5.483	8.343	5.184
Reference	[212]	[212]	[208]	[212]	[212]	[215]

[a] in mdyn Å^{-1}.

In comparing the effect on the ground state of substituting heavier atoms into the three types of functional groups, the main conclusion is that there are few surprises. The expected trends in bond lengths and vibrational frequencies are observed on substituting sulfur or selenium for oxygen. In cases where anomalies are found, they can be satisfactorily explained without invoking any unusual or new attributes to the substituted species. The comparison of the nitriles and phosphaalkynes is also straightforward. Substituent effects on the properties of the functional groups parallel each other on substitution down the periodic table. The only major difference concerns the ground state bending potentials of HCN and HCP. Although HCN can isomerize to CNH, it appears that there is no secondary minimum in the HCP potential so that CPH is not expected to be observable. This intriguing variation hints that the molecules substituted with heavier atoms should not be considered simple clones of the more conventional analogs. This point of view is strongly reinforced by consideration of excited state properties.

5.2 The Excited States

The first major conclusion concerning the excited states is that species substituted with atoms from the third and fourth periods have substantially lower S_1—S_0 excitation energies and are therefore experimentally more accessible. This trend is shown in the form of a bar graph in Fig. 48. In the carbonyls, sulfur shifts the n—π^* electron promotion from the near ultraviolet into the visible. Selenium substitution moves the transition to even longer wavelengths. In CH_2CO/CH_2CS the shift is less dramatic, although the lack of definitive T_0 values makes the comparison less valid. If electronic transition maxima are compared, a shift of $\sim 12,000 \text{ cm}^{-1}$, from 31,500 to 19,500 cm^{-1}, is found. Similarly, HCP has its first allowed transition in the near UV at about 290 nm while the corresponding system in HCN occurs in the vacuum UV at 190 nm.

The much lower excitation energy in the thiocarbonyls can be explained by the much higher energy of the n orbital in the sulfur (3p) versus oxygen (2p). This effect is enhanced for excitation into the π^* orbital, since it is calculated to be
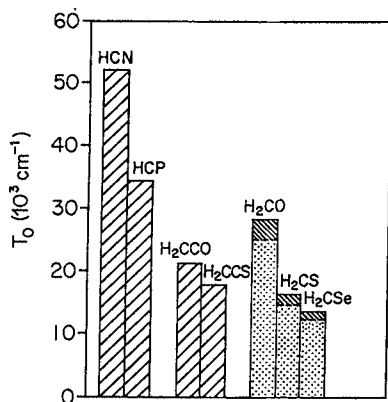
Fig. 48. S_1—S_0 excitation energies for various compounds. The dotted regions show the corresponding T_1—S_0 excitation energies

somewhat more stable in CH_2S than in CH_2O [227]. In the ketenes the excitation is also predominantly $n \rightarrow \pi^*$ although the n orbital has some π character, which appears to moderate the effect of changing from oxygen to sulfur. The excitation is $\pi \rightarrow \pi^*$ in the nitriles and the lower energy in the phosphaalkynes is due primarily to the higher energy of the π orbital as evident from ab initio and photoelectron data [228].

The lower excitation energies and pronounced differences in upper state characteristics have made studies of the electronic spectra of the heavy atom substituted species often more informative than studying the conventional functional groups directly. These benefits often outweigh the advantage of greater ground state chemical stability in the compounds incorporating only second row atoms. For example, in CH_2S, bands of all three possible polarizations are readily observable in the $S_1 - S_0$ spectrum, whereas in CH_2O the type-B bands predominate. The magnetic dipole allowed 0—0 band of CH_2S has been rotationally analyzed while the corresponding band in CH_2O is too weak and overlapped for detailed assignments to be made. The thioformaldehyde spectrum is also ideally located for laser experiments since the band system falls within the fundamental tuning range of most dye lasers. Most of the formaldehyde bands are only accessible by frequency doubling.

Lower excitation energies generally result in a lesser degree of photochemical activity in the excited state. In CH_2O, near the S_1 origin, the quantum yield of the molecular products $H_2 + CO$ is about 0.7 [229]. In CH_2S, the quantum yield of fluorescence is believed to be ~ 1 [230], and calculations suggest that photodissociation cannot take plane from S_1 [231]. Thioketene has a discrete vibronic band system, suggesting that the excited state is longer lived than that of ketene. The same trend is found for HCP, which does not exhibit the strong predissociation found in the HCN spectrum.

A second major conclusion is that substitution enhances the spin-forbidden singlet-triplet transitions. This effect is to be expected from even the most naive considerations of heavy atom induced spin-orbit coupling. However, the magnitude of the enhancement is occasionally surprising. In HCP, five singlet-triplet transitions have been identified while none are known for HCN. In formaldehyde, the $T_1 \leftarrow S_0$ bands are much weaker than the singlet system, in CH_2S the two are comparable, and in CH_2Se the singlet-triplet bands dominate the spectrum, with a substantial decrease in the singlet-triplet splitting down the group. In contrast, the spin-forbidden bands have not been positively identified in ketene or thioketene.

The third major conclusion is that substitution down the period can have a substantial effect on the excited state molecular geometry. The best example of this effect is formaldehyde versus thioformaldehyde. Figure 49 summarizes the geometric changes on excitation to the S_1 state in the two species. CH_2O adopts a non-planar geometry with an out-of-plane angle of 34° and a barrier to inversion of 350 cm^{-1}. Surprisingly, thioformaldehyde is found to be planar with no inversion barrier in the excited state, although the out-of-plane bending potential is highly anharmonic. Similar results are found for the T_1 states of the two molecules. CH_2Se also appears to be planar in the excited T_1 state. In all cases, qualitative Walsh diagrams predict a nonplanar excited state. These predictions are based on stabilization of the π^* orbital by out-of-plane bending. However, as was shown by Bruna et al. [227], in CH_2S the magnitude of the orbital energy change on bending is very
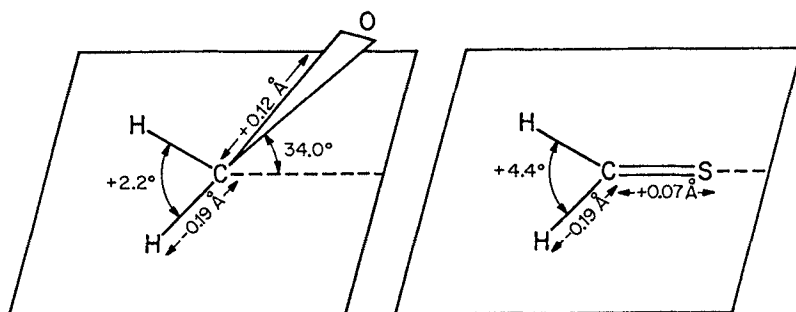
Fig. 49. Geometric changes on excitation to the S_1 state for formaldehyde and thioformaldehyde

small and does not strongly stabilize the excited state. Thus, the quantitative aspects of the calculated Walsh diagrams for formaldehyde and thioformaldehyde are different as shown by the geometries.

The other geometric parameters in the S_1 state also show variations in the two molecules. The elongation of the double bond on excitation is substantially larger in CH_2O, consistent with the greater n orbital stability, the less localized nature of the n orbital and the less stable π^* orbital in formaldehyde. Although the CH bond contracts by 0.19 Å in both molecules, the HCH angle opens by 4.4° in thioformaldehyde and only 2.2° in formaldehyde.

In the halogenated carbonyls, the inversion barrier in the S_1 state decreases substantially on substitution by S or Se. For example, in $CF_2O/CF_2S/CF_2Se$ the barriers are $8200/3076/2483$ cm^{-1} while the out-of-plane angle stays constant. The decreasing stabilization of the π^* orbital is clearly evident. The effect of electronegative substituents on a given chromophore is to increase the inversion barrier in the S_1 state.

The effect of sulfur substitution in the aliphatic carbonyls is to simplify the absorption spectra, making them more amenable to analysis. This is a consequence of two effects. First, the sulfur compounds have less out-of-plane distortion, making the Franck-Condon profile of the spectrum less extensive and the transitions to low v' much stronger. Second, the $T_1 \leftarrow S_0$ spectra are stronger, making them the preferred bands for analysis since Herzberg-Teller induced bands are absent, drastically simplifying the vibronic structure compared to the singlet-singlet system. Since the major interest in these spectra, and consequently the major difficulty, is the torsional activity, inherent simplifications are of great benefit. A subsidiary benefit is that the thione T_1 states usually phosphoresce strongly, so that further information can be obtained from the resolved emission spectrum. The much lower torsional barrier in T_1 thioacetaldehyde (94 cm^{-1}) compared to acetaldehyde (625 cm^{-1}) and a similar trend in the acetones can be attributed to less pyramidal distortion on excitation in the sulfur compounds.

Ketene and thioketene excited state geometries are unknown although the Franck-Condon profiles of the $S_1 \leftarrow S_0$ transitions suggest that the latter does not distort as much on excitation. Analysis of the vibronically discrete thioketene spectrum suggests an in-plane bent structure as predicted for ketene on the basis of ab initio calculations.

The excited state geometries appear similar in HCN/HCP although the linearity of the HCP triplet states is contrary to ab initio predictions for most of the corresponding HCN states. The elongation of the $C \equiv X$ bond on excitation is about the same in both species.

A fourth major conclusion is that substitution facilitates the observation and analysis of higher valence and Rydberg states. In the aldehydes and ketones, the absorption bands due to the $\pi - \pi^*$ excitation are at very high energies and have not been identified in the prototype, formaldehyde. Similarly, the Rydberg transitions of the oxygen compounds do not have discrete rovibronic structure. However, in the thiones, both the $\pi - \pi^*$ and Rydberg transitions can be identified and, in favorable cases, vibrationally and even rotationally analyzed. Some of the tetraatomic thiocarbonyl compounds are unique in that they not only have descrete $\tilde{B} \leftarrow \tilde{X}$ band systems but also fluoresce strongly from the $\tilde{B}$ state. From emission and absorption studies, some of the geometric parameters of the S_2 states can be determined and these are presented in Table 38 in comparison with the lower states. The simple notion of progressively decreasing bond order on $n - \pi^*$ and $\pi - \pi^*$ excitation is confirmed by the decrease in $C = S$ vibrational frequency and elongation of the bond on excitation.

Table 38. Geometric parameters of the S_0, S_1 and S_2 states of selected thiocarbonyl compounds.

Molecule	State	$C = S$ bond order	$C = S$ stretching frequency (cm^{-1})	$\Delta r(C = S)$ (Å)	Inversion barrier (cm^{-1})	Out-of-plane angle (deg)
CH_2S	S_0	2.0	1059	0	0	0
	S_1	1.5	820	0.14	0	0
	S_2	1.0	483	0.48	?	?
CF_2S	S_0	2.0	1368	0	0	0
	S_1	1.5	1101	0.12	3100–3400	30.5–34.1
	S_2	1.0	?	?	High	?
$CClFS$	S_0	2.0	1257	0	0	0
	S_1	1.5	877 or 964	0.2 or 0.15	1556	37
	S_2	1.0	567	0.48	> 2000	≫ 0
CCl_2S	S_0	2.0	1139	0	0	0
	S_1	1.5	907	0.13	620	32
	S_2	1.0	504	0.50	730	30

The rotational analysis of the the $n - 4s$ Rydberg state of CH_2S [50] is another example of the detailed characterization of higher states. The decrease in the $C = S$ bond length (0.007 Å) and increase in the HCH angle (5.81°) are substantially different from the trends observed on valence excitation. The dipole moment was also determined from the Stark effect [232] and found to point in the direction opposite to that in the ground state, as suggested by theoretical estimates for the corresponding state of CH_2O [48].

In HCN/HCP, the geometry and vibrational frequencies of the $\tilde{C}$ state of the phosphorus compound are better established due to the lack of predissociation in the

HCP spectrum. The substantial number of triplet states of HCP which have been analyzed also attests to the generality of this conclusion regarding the higher states of the substituted species.

5.3 Concluding Remarks

It is clear from the material presented in this review that substitution of progressively heavier atoms within a group into a chromophore can have a substantial effect on the spectroscopic properties of the molecule. This is particularly true of the electronic excited states, although some differences have been noted in the ground states as well. It is for this reason that the literature on heavy atom substituted chromophores has been expanding rapidly in recent years. The general instability, toxicity, unpleasant odors and low steady state concentrations of these species, which historically were major impediments to their study, are only minor irritations when modern spectroscopic techniques are applied.

We look forward to the addition of other chromophores substituted with heavy atoms to the short list compiled in this work. The preparation of gas phase telluroketones appears imminent. A variety of silicon substituted compounds have been reported [233] including silanones ($RR'Si=O$), silanethiones ($RR'Si=S$), silaisonitriles (RNSi), silenes ($R'R''Si=CR_1R_2$) and others. Phosphorus compounds such as phosphaallenes ($RC=P=X$), phosphaalkenes ($RR'C=PR''$) and diphosphenes ($RP=PR'$) have been synthesized by a number of groups [234]. A few compounds containing As, Sb, Bi, and Ge atoms have also been reported [235]. We are confident that many of these new species will have properties which are sufficiently at variance with those of conventional organic chromophores to make spectroscopic studies both novel and rewarding.

6 Acknowledgments

7 References

1. Gordy W, Cook RL (1984) "Microwave molecular spectra", Wiley, New York
2. Green S (1981) Ann. Rev. Phys. Chem. *32*: 103
3. Oka T (1978) J. Mol. Spectrosc. *72*: 172
4. Dieke GH, Kistiakowsky GB (1934) Phys. Rev. *45*: 4

5. Herzberg G (1945) "Molecular spectra and molecular structure, (vols I–III) Van Nostrand Reinhold, New York
6. Gusel'nikov LE, Nametkin NS (1979) Chem. Rev. *79*: 539 and references therein
7. Kroto HW (1982) Chem. Soc. Rev. *11*: 435
8. Moule DC, Walsh AD (1975) Chem. Rev. *75*: 67
9. Clouthier DJ, Ramsay DA (1983) Ann. Rev. Phys. Chem. *34*: 31
10. Robin MB (1985) Higher Excited States of Polyatomic Molecules, vol III. Academic, Orlando, FL
11. Lee ECK, Lewis RS (1980) Advances in Photochemistry *12*: 1
12. Steer RP (1981) Rev. Chem. Intermed *4*: 1
13. Davy H (1817) Ann. Chem. Phys. *4*: 347
14. Emeleus HJ (1926) J. Chem. Soc. 2948
15. Zitomer F (1968) Anal. Chem. *40*: 1091
16. Callear AB, Connor J, Dickson DR (1969) Nature *221*: 1238
17. Johnson DR, Powell FX (1970) Science *169*: 679
18. Back TG, Barton DHR, Britten-Kelly MR, Guziec FS (1976) J. Chem. Soc., Perkin Trans. 1 *19*: 2079
19. Hass A, Koch B, Welcman W (1976) Z. Anorg. Allg. Chem. *427*: 114
20. Hutchinson M, Kroto MW (1978) J. Mol. Spectrosc. *70*: 347
21. Bock H, Aygen S, Rosmus P, Solouki B, Weissflog E (1985) Chem. Ber. *117*: 187
22. Brown RD, Godfrey PD, McNaughton D (1985) Chem. Phys. Letters *118*: 29
23. Brown RD, Godfrey PD, McNaughton D, Taylor PR (1986) J. Mol. Spectrosc. *120*: 292
24. Judge RH, Clouthier DJ, Moule DC (to be published)
25. Walsh AD (1953) J. Chem. Soc. 2306
26. Brand JCD (1956) J. Chem. Soc. 858
27. Coon JB, Naugle NW, McKenzie RD (1966) J. Mol. Spectrosc. *20*: 107
28. Altmann SL (1967) Proc. Roy. Soc., Ser. A *298*: 184
29. Callomon JH, Innes KK (1963) J. Mol. Spectrosc. *10*: 166
30. Jones VT, Coon JB (1969) J. Mol. Spectrosc. *31*: 137
31. Jensen P, Bunker PR (1982) J. Mol. Spectrosc. *94*: 114
32. Judge RH, King GW (1979) J. Mol. Spectrosc. *74*: 175
33. Judge RH, King GW (1979) J. Mol. Spectrosc. *78*: 51
34. Cohen AD, Reid Rl (1957) J. Chem. Soc. 2386
35. Hougen JT (1964) Can. J. Phys. *42*: 433
36. Birss FW, Ramsay DA, Till SM (1978) Can. J. Phys. *56*: 781
37. Judge RH, Moule DC, King GW (1980) J. Mol. Spectrosc. *81*: 37
38. Judge RH, Moule DC (1986) J. Am. Chem. Soc. *106*: 531
39. Glinski RJ, Mishalanie EA, Birks JW (1986) J. Am. Chem. Soc. *108*: 531
40. Clouthier DJ, Judge RH, Moule DC (1987) Chem. Phys. Letters *114*: 417
41. Price WC (1935) J. Chem. Phys. *3*: 256
42. Lessard CR, Moule DC (1976) J. Mol. Spectrosc. *60*: 343
43. Taylor S, Wilden DG, Comer J (1982) J. Chem. Phys. *70*: 291
44. Allison K, Walsh AD (1957) Chem. Inst. Canada Symp. Ottawa
45. Bell S, Crighton JS (1985) J. Chem. Soc., Faraday Trans. 2 *81*: 1813
46. Langhoff PW, Langhoff SR, Corcoran CT (1977) J. Chem. Phys. *67*: 1722
47. Langhoff PW, Orel AE, Rescigno TN, McKoy BV (1978) J. Chem. Phys. *69*: 4689
48. Harding LB, Goddard III WA (1977) J. Amer. Chem. Soc. *97*: 677
49. Drury CR, Lai JYK, Moule DC (1982) Chem. Phys. Letters *87*: 520
50. Drury CR, Moule DC (1982) J. Mol. Spectrosc. *92*: 469
51. Collins S, Back TG, Rauk A (1985) J. Am. Chem. Soc. *107*: 6589
52. Nakata M, Kohata K, Fukuyama T, Kuchitsu K, Wilkins CJ (1980) J. Mol. Struct. *68*: 271
53. Christen D, Oberhammer H, Zeil W, Haas A, Darmadi A (1980) J. Mol. Struct. *66*: 203
54. Nakata M, Kohata K, Fukuyama T, Kuchitsu K (1980) J. Mol. Spectrosc. *83*: 105
55. Nakata M, Fukuyama T, Kuchitsu K (1982) J. Mol. Struct. *81*: 121
56. Nakata M, Fukuyama T, Wilkins CJ, Kuchitsu K (1981) J. Mol. Struct. *71*: 195
57. Christen D (1980) J. Mol. Struct *66*: 211
58. Huisman PAG, Klebe KJ, Mijlhoff FC, Renes GH (1979) J. Mol. Struct. *57*: 71

59. Davis RW, Gerry MCL (1983) J. Mol. Spectrosc. *97*: 117
60. Oberhammer H (1980) J. Chem. Phys. *73*: 4310
61. Gleisberg F, Haberl A, Zeil W (1975) Z. Naturforsch. *30A*: 549
62. Thakur K B, Narahari Rao K, Freidl RR, Rinsland CP, Malathy Devi V (1987) J. Mol. Spectrosc. *123*: 255
63. Mallinson PD, McKean DC, Holloway JH, Oxton IA (1975) Spectrochim. Acta *31A*: 143
64. Downs AJ (1963) Spectrochim. Acta *19*: 1165
65. Haas A, Willner H, Burger H, Pawelke G (1977) Spectrochim. Acta *33A*: 937
66. Hopper MJ, Russell JW, Overend J (1968) J. Chem. Phys. *48*: 3765
67. Frenzel CA, Blick K E, Bennett CR, Neidenzu K (1970) J..Chem. Phys. *53*: 198
68. Brand JCD, Callomon JH, Moule DC, Tyrrell J, Goodwin TH (1965) Trans. Faraday Soc. *61*: 2365
69. Darmadi A, Haas A, Willner H, Schnockel H (1981) Z. Naturforsch. *36B*: 1261
70. Hauswirth W, Willner H (1979) Spectrochim. Acta *35A*: 263
71. Nielsen AH, Burke TG, Woltz PJH, Jones EA (1952) J. Chem. Phys. *20*: 596
72. Moule DC, Subramaniam CR (1969) Can. J. Chem. *47*: 1011
73. Stratton RF, Nielsen AH (1960) J. Mol. Spectrosc. *4*: 373
74. Brema JL, Moule DC (1972) Spectrochim. Acta *28A*: 809
75. Maker PD, Niki H, Breitenbach H, Savage CM (1984) 39th Symp. on Mol. Spectroscopy, Ohio State University
76. Carroll DG, Vanquickenborne LG, McGlynn SP (1966) J. Chem. Phys. *45*: 2777
77. Judge RH, Moule DC (1983) J. Chem. Phys. *78*: 4806
78. Moule DC, Foo PD (1971) J. Chem. Phys. *55*: 1262
79. Clouthier DJ, Moule DC (1981) J. Mol. Spectrosc. *87*: 471
80. Simard B, Hackett PA, Steer RP (in press) J. Mol. Spectrosc.
81. Moule DC (1976) in: Durig JR (ed) Vibrational spectra and structure, vol 6, Elsevier, New York
82. Judge RH, Moule DC (1985) J. Mol. Spectrosc. *113*: 302
83. Subramaniam CR, Moule DC (1974) J. Mol. Spectrosc. *53*: 443
84. Moule DC, Mehra AK (1970) J. Mol. Spectrosc. *35*: 137
85. Boluk MY, Moule DC, Clouthier DJ (1983) Can. J. Chem. *61*: 1743
86. Fischer G (1969) J. Mol. Spectrosc. *29*: 37
87. Judge RH, Moule DC (1985) J. Mol. Spectrosc. *113*: 77
88. Fischer G, Sorek Y (1979) J. Mol. Spectrosc. *74*: 136
89. Condirston DA, Moule DC (unpublished results)
90. McGlynn SP, Azumi T, Kinoshita M (1969) Molecular spectroscopy of the triplet state, Prentice-Hall, Englewood Cliffs, NJ
91. DiGiorgio VE, Robinson GW (1959) J. Chem. Phys. *31*: 1678
92. Moule DC (1970) Can. J. Chem. *48*: 2623
93. Moule DC, Subramaniam CR (1973) J. Mol. Spectrosc. *48*: 336
94. Simard B, Steer RP, Judge RH, Moule DC (in press) Can. J. Chem.
95. Vasudevan K, Grein F (1978) Int. J. Quantum Chem. *14*: 717
96. Workman GL, Duncan ABF (1970) J. Chem. Phys. *52*: 3204
97. Dixon RN, Western CM (1986) J. Mol. Spectrosc. *115*: 74
98. Judge RH, Moule DC (1980) J. Mol. Spectrosc. *80*: 363
99. Clouthier DJ, Knight A R, Steer RP, Judge RH, Moule DC (1980) J. Mol. Spectrosc. *83*: 148
100. Lessard CR, Moule DC (1973) Spectrochim. Acta *29A*: 1085
101. Lee EKC, Lewis RS (1980) Advan. Photochem. *12*: 1
102. Kroto HW, Landsberg BM (1976) J. Mol. Spectrosc. *62*: 346
103. Hutchinson H, Kroto HW (1978) J. Mol. Spectrosc. *70*: 347
104. Kilb RW, Lin CC, Wilson EB (1957) J. Chem. Phys. *26*: 1695
105. Harmony MD, Laurie VW, Kuczkowski RL, Schwendeman RH, Ramsay DA, Lovas FJ, Lafferty WJ, Maki AG (1979) J. Phys. Chem. Ref. Data *8*: 619
106. Hollenstein H, Gunthard HsH (1971) Spectrochim. Acta, Part A *27A*: 2027
107. Wiberg KB, Walters V, Colson SD (1984) J. Phys. Chem. *88*: 4723
108. Crighton JS, Bell S (1985) J. Mol. Spectrosc. *112*: 315
109. Rao VR, Rao IA (1954) Indian J. Phys. *28*: 491
110. Innes KK, Giddings LE (1961) J. Mol. Spectrosc. *7*: 435

111. Hubbard LM, Bocian DF, Birge RR (1981) J. Am. Chem. Soc. *103*: 3313
112. Noble M, Apel EC, Lee EKC (1983) J. Chem. Phys. *78*: 2219
113. Baba M, Hanazaki I, Nagashima U (1985) J. Chem. Phys. *82*: 3938
114. Noble M, Lee EKC (1984) J. Chem. Phys. *81*: 1632
115. Baba M, Nagashima U, Hanazaki I (1985) J. Chem. Phys. *83*: 3514
116. Judge RH, Moule DC, Bruno AE, Steer RP (1983) Chem. Phys. Lett *102*: 385
117. Judge RH, Moule DC, Bruno AE, Steer RP (1987) J. Chem. Phys. *87*: 60
118. Schuh MD, Speiser S, Atkinson GH (1984) J. Phys. Chem. *88*: 2224
119. Moule DC, Ng KHK (1985) Can. J. Chem. *63*: 1378
120. Smeyers YG, Niño A, Bellido MN (unpublished)
121. Walsh AD (1946) Proc. Roy. Soc. *A185*: 176
122. Lucazeau G, Sandorfy C (1970) J. Mol. Spectrosc. *35*: 214
123. Crighton JS, Bell S (1985) J. Mol. Spectrosc. *112*: 304
124. Noller CR (1952) Chemistry of organic compounds. W. B. Saunders, Philadelphia, p 271
125. Swalen JD, Costain CC (1959) J. Chem. Phys. *31*: 1562
126. Peter R, Dreizler H (1965) Z. Naturforsch *A20*: 301
127. Nelson R, Pierce L (1965) J. Mol. Spectrosc. *18*: 344
128. Iijima T (1972) Bull. Chem. Soc. Japan *45*: 3526
129. Fately WG, Miller FA (1962) Spectrochim. Acta *18*: 977
130. Smith DR, McKenna BK, Moller KD (1966) J. Chem. Phys. *45*: 1904
131. Groner P, Guirgis GA, Durig JR (1986) J. Chem. Phys. *86*: 565
132. Crighton JS, Bell S (1986) J. Mol. Spectrosc. *120*: 383
133. Dellipane G, Overend J (1966) Spectrochim. Acta *22*: 593
134. Hollenstein H, Gunthard HH (1980) J. Mol. Spectrosc. *84*: 457
135. Kroto HW, Landsberg BM, Suffolk RJ, Vodden J (1974) Chem. Phys. Letters *29*: 265
136. Garrigou-Lagrange C, Andrieu CG, Mollier Y (1976) Spectrochim. Acta *A32*: 477
137. Noyes Jr WA, Duncan ABF, Manning WM (1934) J. Chem. Phys. *2*: 717
138. Baba M, Hanazaki I, Nagashima U (1985) J. Chem. Phys. *82*: 3938
139. Fabian J, Meyer R (1964) Spectrochim. Acta *20*: 299
140. Paone S, Moule DC, Bruno AE, Steer RP (1984) J. Mol. Spectrosc. *107*: 1
141. Kopper H (1936) Z. Phys. Chem. *B34*: 396
142. Howard EG (1962) U.S. Patent No. 3035030. May 15
143. Georgiou K, Kroto HW, Landsberg BM (1974) J. Chem. Soc. Comm. 739
144. Bock H, Solouki B, Bert G, Rosmus P (1977) J. Am. Chem. Soc. *99*: 1663
145. Winnewisser M, Schäfer E (1980) Z. Naturforsch. *35a*: 483
146] Raasch MS (1972) J. Org. Chem. *37*: 1347
147. Elam EU, Rash FH, Doughtery JT, Goodlett VW, Brannock KC (1968) J. Org. Chem. *33*: 2738
148. Del Bene JE (1972) J. Am. Chem. Soc. *94*: 3713
149. Dykstra CE, Schaefer III HF (1976) J. Am. Chem. Soc. *98*: 2689
150. Tanaka K, Yoshimine M (1980) J. Am. Chem. Soc. *102*: 7655
151. Strausz O, Gosavi RK, Bernardi F, Mezey PG, Goddard JD, Csizmadia IG (1978) Chem. Phys. Lett. *53*: 211
152. Siegbahn PEM, Yoshimine M, Pacansky J (1983) J. Chem. Phys. *78*: 1384
153. Gosavi RK, Strausz OP (1983) Can. J. Chem. *61*: 2596
154. Krantz A (1973) J. Chem. Soc., Chem. Commun. 670
155. Bak B, Nielsen OJ, Svanholt H, Holm H (1978) Chem. Phys. Lett., *53*: 374
156. Mallinson PD, Nemes L (1976) J. Mol. Spectrosc. *59*: 470
157. Johnson HR, Strandberg MWP (1952) J. Chem. Phys. *20*: 687
158. Georgiou K, Kroto HW, Landsberg BM (1979) J. Mol. Spectrosc. *77*: 365
159. Bak B, Nielsen OJ, Svanholt H, Holm A (1978) Chem. Phys. Lett. *55*: 36
160. Laureni J, Krantz A, Hajdu RA (1976) J. Am. Chem. Soc. *98*: 7872
161. Gershinowitz H, Wilson EB (1937) J. Chem. Phys. *5*: 500
162. Duncan JL, Ferguson AM, Harper J, Tonge KH, Hegelund F (1987) J. Mol. Spectrosc. *122*: 72
163. Duncan JL, Ferguson AM, Harper J, Tonge KH (1987) J. Mol. Spectrosc. *125*: 196
164. Kroto HW, McNaughton D (1985) J. Mol. Spectrosc. *114*: 473
165. Torres M, Safarik I, Clement A, Gosavi RK, Strausz OP (1984) Can. J. Chem. *62*: 2777
166. Clouthier DJ, unpublished results from gas phase mid- and far-IR spectra

167. Johns JWC, Stone JMR, Winnewisser G (1972) J. Mol. Spectrosc. *42*: 523
168. Nemes L, (1978) J. Mol. Spectrosc. *72*: 102
169. Dixon RN, Kirby GH (1966) Trans. Faraday Soc. *62*: 1406
170. Laufer AH, Keller RA (1971) J. Am. Chem. Soc. *93*: 61
171. Noyes WA, Unger I (1964) Pure Appl. Chem. *9*: 461
172. Allen WD, Schaefer III HF (1986) J. Chem. Phys. *84*: 2212
173. Clouthier DJ (1987) J. Phys. Chem. *91*: 1354
174. Chadwick BM, Edwards HGM (1973) in: Barrow RF, Long DA, Millen DJ (eds) Molecular spectroscopy, vol 1, The Chemical Society, London, p 446
175. Milligan DE, Jacox ME (1963) J. Chem. Phys. *39*: 712
176. Arrington CA, Ogryzlo EA (1975) J. Chem. Phys. *63*: 3670
177. Blackman GL, Brown RD, Godfrey PD, Gunn HI (1976) Nature *261*: 395
178. Maki AG, Sams RL (1981) J. Chem. Phys. *75*: 4178
179. Herzberg G, Innes KK (1957) Can. J. Phys. *35*: 842
180. Ashfold MNR, Macpherson MT, Simons JP (1979) in: Topics in Current Chemistry, vol 86, p 29, Springer, Berlin Heidelberg New York
181. Gier TE (1961) J. Am. Chem. Soc. *83*: 1769
182. Hopkinson MJ, Kroto HW, Nixon JF, Simmons NPC (1976) Chem. Phys. Lett. *42*: 460
183. Burckett St. Laurent JCTR, Cooper TA, Kroto HW, Nixon JF, Ohashi O, Ohno K (1982) J. Mol. Struct. *79*: 215
184. Palke WE, Lipscomb WN (1966) J. Am. Chem. Soc. *88*: 2384
185. Winnewisser G, Maki AG, Johnson DR (1971) J. Mol. Spectrosc. *39*: 149
186. Bhattacharya BN, Gordy W (1960) Phys. Rev. *119*: 144
187. Demaison J, Dubrulle A, Boucher D, Burie J (1979) J. Mol. Spectrosc. *76*: 1
188. Steiner AP, Gordy W (1966) J. Mol. Spectrosc. *21*: 291
189. Whiffen DH (1978) Spectrochim. Acta *34A*: 1165
190. Maki AG, Freund SM (1977) J. Mol. Spectrosc. *66*: 493
191. Sheridan J, Gordy W (1952) J. Chem. Phys. *20*: 591
192. Maki AG (1965) J. Chem. Phys. *43*: 3193
193. Costain C (1958) J. Chem. Phys. *29*: 864
194. Wilcox WW, Goldstein JH, Simmons JW (1954) J. Chem. Phys. *22*: 516
195. Tyler JK (1964) J. Chem. Phys. *40*: 1170
196. Kroto HW, Nixon JF, Simmons NPC (1979) J. Mol. Spectrosc. *77*: 270
197. Kroto HW, Nixon JF, Simmons NPC (1980) J. Mol. Spectrosc. *82*: 185
198. Cooper TA, Kroto HW, Nixon JF, Ohashi O (1980) J. Chem. Soc. Chem. Comm. 333
199. Kroto HW, Nixon JF, Ohno K (1981) J. Mol. Spectrosc. *90*: 512
200. Ohno K, Kroto HW, Nixon JF (1981) J. Mol. Spectrosc. *90*: 507
201. Ross SC, Bunker PR (1983) J. Mol. Spectrosc. *101*: 199; (1984) J. Mol. Spectrosc. *105*: 369
202. Pearson PK, Schaefer III HF, Wahlgren U (1975) J. Chem. Phys. *62*: 350
203. Lehmann KK, Ross SC, Lohr LL (1985) J. Chem. Phys. *82*: 4460
204. Maki AG (1975) J. Mol. Spectrosc. *57*: 308
205. Wang VJ, Overend J (1973) Spectrochim. Acta *29A*: 687
206. Maki AG, Blaine LR (1964) J. Mol. Spectrosc. *12*: 45
207. Maki AG, Plyler EK, Thibault R (1964) J. Opt. Soc. Am. *54*: 869
208. Duncan JL, McKean DC, Tullini F, Nivellini GD, Perez Pena J (1978) J. Mol. Spectrosc. *69*: 123
209. Cabana A, Doucet Y, Garneau J, Pepin C, Puget P (1982) J. Mol. Spectrosc. *96*: 342
210. Lavigne J, Pepin C, Cabana A (1984) J. Mol. Spectrosc. *104*: 49
211. Lavigne J, Pepin C, Cabana A (1983) J. Mol. Spectrosc. *99*: 203
212. Ohno K, Matsuura H, Murata H, Kroto HW (1983) J. Mol. Spectrosc. *100*: 403
213. Ohno K, Matsuura H, Murata H (1984) J. Phys. Chem. *88*: 342
214. Ohno K, Yamamoto Y, Matsuura H, Murata H, Chem. Lett. *1984*: 413
215. Ohno K, Matsuura H, McNaughton D, Kroto HW (1985) J. Mol. Spectrosc. *111*: 415
216. Johns JWC, Shurvell HF, Tyler JK (1969) Can. J. Phys. *47*: 893
217. Walsh AD (1953) J. Chem. Soc. 2288
218. Schwenzer GM, O'Neil SV, Schaefer III HF, Baskin CP, Bender CF (1974) J. Chem. Phys. *60*: 2787
219. Peric M, Peyerimhoff SD, Ruenker RJ (1977) Can. J. Chem. *55*: 3664

220. Bickel GA, Innes KK (1984) Can. J. Phys. *62*: 1763
221. Laidig WD, Schaefer III HF (1980) J. Chem. Phys. *73*: 1470
222. Schmidt MW, Truong PN, Gordon MS (1987) J. Am. Chem. Soc. *109*: 5217
223. Oberhammer H, Boggs JE (1979) J. Mol. Struct. *55*: 283
224. Robert J, Marsmann H, Absar I, Wazer JR (1971) J. Am. Chem. Soc. *93*: 3320
225. Moore CB, Pimentel GC (1963) J. Chem. Phys. *38*: 2816
226. Duncan JL (1970) Spectrochim. Acta *26 A*: 429
227. Bruna PJ, Peyerimhoff SD, Buenker RJ, Rosmus P (1974) Chem. Phys. *3*: 35
228. Cambi R, Von Niessen W (1983) Chem. Phys. Lett. *101*: 412
229. Moore CB, Weisshaar JC (1983) Ann. Rev. Phys. Chem. *34*: 525
230. Bruno AE, Steer RP (1983) J. Chem. Phys. *78*: 6660
231. Pope SA, Hillier IH, Guest MF (1985) J. Am. Chem. Soc. *107*: 3789
232. Goetz W, Moule DC, Ramsay DA (1981) Can. J. Phys. *59*: 1635
233. Raabe G, Michl J (1985) Chem. Rev. *85*: 419 (A recent review of silicon compounds)
234. Appel R, Knoll F, Ruppert I (1981) Angew. Chem. Int. Ed. *20*: 731 (A review)
235. Jutzi P (1975) Angew. Chem. Int. Ed. *14*: 232 (A review of the older literature)

Theory of Reaction Mechanisms

Paul L. Corio

Department of Chemistry, University of Kentucky, Lexington, KY 40506-0055, U.S.A.

1 Introduction

The concept of a reaction mechanism was undoubtedly a product of nineteenth chemistry, but it was not until the turn of the century, when the idea was inseparably joined with chemical kinetics, that the possibility of meaningful conclusions was established by the experiments of Lapworth [1]. At about the same time, Bodenstein and Lind [2] were studying the gas-phase reaction of hydrogen and bromine, obtaining a rate law which was mechanistically interpreted thirteen years later by Christiansen [3], Herzfeld [4], and Polanyi [5]. These triumphs, together with the subsequent successes of Rice and Herzfeld [6, 7] mechanisms for the decomposition of organic molecules, provided considerable impetus to the idea that it was only necessary to discover the correct mechanisms in order to account for most chemical reactions.

Although the importance of these investigations cannot be overestimated, they were concerned with specific reactions in which considerations of the energy were especially important. Indeed, energy has traditionally been the guiding principle in the construction of reaction mechanisms. Chemists deal with specific reactions, and energy considerations introduce specificity into the matter. Which bonds have to be broken? What are their energies? What is the activation energy? What is the available thermal or photochemical energy? It is not surprising, therefore, that some time elapsed before reaction mechanisms were considered from more general points of view [8−11].

We review here some recent research [12−15] which, despite its theoretical simplicity, provides unambiguous answers to several important questions: How many components can there be in a mechanism with a finite number of steps? How many intermediates? What is the relation between the observed stoichiometric relation and the underlying mechanism? What is the mechanistic significance of multiple stoichiometries, such as

$$4\,C_2H_6 \rightarrow 2\,CH_4 + 3\,C_2H_4 + 2\,H_2\,,$$

$$3\,C_2H_6 \rightarrow 2\,CH_4 + 2\,C_2H_4 + H_2\,?$$
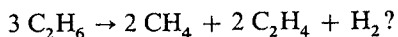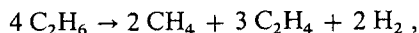
And how do the answers to these questions change when the experimental conditions are changed?

The theory also provides criteria for the construction of consistent reaction mechanisms, and shows how to construct all mechanisms consistent with a given set of reaction components. It turns out that there are, in general, infinitely many consistent reaction mechanisms, but they are all expressible in terms of a finite number of parameters. Moreover, if one imposes the restriction that the molecularity of any mechanistic step must not exceed three or four, only a finite number of mechanisms is possible.

The principal assumptions are that the reaction occurs in a closed, isothermal system, that the reaction indeed admits a description in terms of a finite number of mechanistic steps, and that the laws of mass and charge conservation are valid.

2 Stoichiometric Relations

2.1 Uncatalyzed Reactions

A *stoichiometry* may be defined as a balanced chemical reaction. In this sense, the term may be applied to the chemical equation describing the overall transformation of reactants into products, as well as each balanced step of a proposed reaction mechanism. To avoid ambiguity, we shall use the term and all of its inflected forms only in connection with the observed transformation of reactants to products. Supposing, then, that ϱ distinguishable reactants $X_1, X_2, \dots, X_\varrho$, of known composition, react and ultimately form π distinguishable products $X_{\varrho+1}, X_{\varrho+2}, \dots, X_{\varrho+\pi}$, of determinable composition, the observed stoichiometric relation may be written

$$s_1 X_1 + s_2 X_2 + \dots + s X_\varrho \rightarrow s_{\varrho+1} X_{\varrho+1} + s_{\varrho+2} X_{\varrho+2} + \dots + s_{\varrho+\pi} X_{\varrho+\pi}.$$

$$(2.1)$$
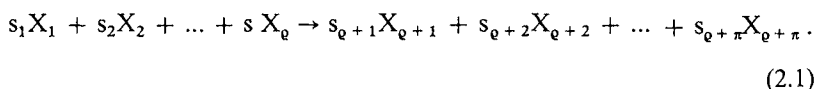
Assuming, for the moment, that (2.1) involves no ionic species, a system of linear, homogeneous equations for the stoichiometric coefficients s_j is obtained from it by requiring conservation of the atoms comprising reactants and products:

$$\sum_{j=1}^{p+\pi} M_{ij} s_j = 0, \qquad i = 1, 2, \dots,$$

$$(2.2)$$

where the absolute value of M_{ij} is the number of atoms of type i in X_j, and j ranges over all distinct atoms. These equations are not, in general, independent. The number v of independent equations, that is, the number of independent mass conservation conditions, is equal to the rank of the system (2.2). Although v is often equal to the number of distinct atoms, it can be smaller. In an isomerization, for instance, Eqs. (2.2) are (nonzero) multiples of each other, so there is only one independent mass conservation condition whatever the number of atoms. In practice, the value of v can often be inferred by inspection; but as the number of equations increases, the only reliable procedure is to compute the rank of the matrix $M = (M_{ij})$

$$v = \text{rank } M,$$

$$(2.3)$$

and for this computation reactants and produces *must* be known. Thus, $v = 1$ for the isomerization of butane to isobutane, but $v = 2$ for the decomposition for butane to ethane and ethylene.

The rank of the matrix M is given by the number of rows or columns in the non-vanishing determinant of highest order contained in M, or by the number of nonzero rows (columns) in any equivalent matrix derived from M by elementary row (column) operations [16].

For the oxidation of oxalic acid by iodine,

$$s_1 I_2 + s_2 (COOH)_2 \rightarrow s_3 HI + s_4 CO_2 \,, \tag{2.4}$$
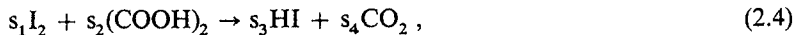
$$M = \begin{pmatrix} 2 & 0 & -1 & 0 \\ 0 & 2 & 0 & -1 \\ 0 & 2 & -1 & 0 \\ 0 & 4 & 0 & -2 \end{pmatrix}$$

whose rows give the coefficients for the conservation of iodine, carbon, hydrogen, and oxygen atoms, respectively. The determinant of M is zero, but that of the 3×3 matrix in the upper left-hand corner is nonzero, so that $v = 3$. Alternatively, by subtracting the second row from the third, and twice the second from the fourth, we find that M is row-equivalent to

$$\begin{pmatrix} 2 & 0 & -1 & 0 \\ 0 & 2 & 0 & -1 \\ 0 & 0 & -1 & 1 \\ 0 & 0 & 0 & 0 \end{pmatrix}$$

which confirms that $v = 3$. Although both methods yield the desired result without difficulty in this particular example, the determination of v by row or column operations on M is usually much more expeditious.

When the reaction involves ions, a charge conservation condition is adjoined to the system (2.2), and the formula (2.3) will give the number of independent conservation conditions. For the reduction of permanganate ion by hydrogen peroxide in an acidic medium

$$s_1 MnO_4^- + s_2 H_2 O_2 + s_3 H^+ \rightarrow s_4 Mn^{2+} + s_5 O_2 + s_6 H_2 O \,. \tag{2.5}$$

$$M = \begin{pmatrix} 1 & 0 & 0 & -1 & 0 & 0 \\ 4 & 2 & 0 & 0 & -2 & -1 \\ 0 & 2 & 1 & 0 & 0 & -2 \\ -1 & 0 & 1 & -2 & 0 & 0 \end{pmatrix},$$

whose rows give the coefficients for the conservation of manganese, oxygen, hydrogen, and charge, respectively. An easy computation shows that M is row equivalent to

$$\begin{pmatrix} 1 & 0 & 0 & -1 & 0 & 0 \\ 0 & 2 & 0 & 4 & -2 & -1 \\ 0 & 0 & 1 & -4 & 2 & -1 \\ 0 & 0 & 0 & 1 & -2 & 1 \end{pmatrix},$$

so that $v = 4$.

2.2 Multiple Stoichiometries

Equations (2.2) are consistent when the ineger

$$\varphi = \varrho + \pi - \nu , \tag{2.6}$$

called the *multiplicity*, satisfies the condition $\varphi \geq 1$. When this is the case, there are exactly φ independent solutions of Eqs. (2.2), that is, the multiplicity is equal to the number of independent stoichiometric relations [12]. Every stoichiometry, including the observed stoichiometry, is a linear combination of φ independent stoichiometric relations.

To illustrate these ideas, consider the decomposition of dinitrogen pentoxide, for which the observed stoichiometry is

$$s_1 N_2O_5 \rightarrow s_2 NO_2 + s_3 N_2O_4 + s_4 O_2 . \tag{2.7}$$
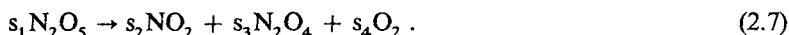
The equations for conservation of nitrogen and oxygen are

$$2s_1 - s_2 - 2s_3 = 0 ,$$
$$5s_1 - 2s_2 - 4s_3 - 2s_4 = 0 , \tag{2.8}$$

whose rank is 2, so that $\varphi = \varrho + \pi - \nu = 4 - 2 = 2$. Indeed, 2 independent solutions of (2.8) are $(s_1, s_2, s_3, s_4) = (2, 4, 0, 1)$, and $(s_1', s_2', s_3', s_4') = (0, -2, 1, 0)$, corresponding, respectively, to the independent stoichiometries

$$2 N_2O_5 \rightarrow 4 NO_2 + O_2 , \tag{2.9}$$

$$2 NO_2 \rightarrow N_2O_4 . \tag{2.10}$$

In the second stoichiometry, NO_2 has been transposed to the left-member to render its coefficient positive. The most general stoichiometry for the decomposition is a linear combination of (2.9) and (2.10)

$$2c_1 N_2O_5 \rightarrow 2(2c_1 - c_2) NO_2 + c_2 N_2O_4 + c_1 O_2 . \tag{2.11}$$
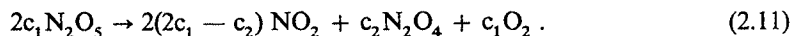
It must be emphasized that there need not be ϱ rectants and π products in each reaction of a set of φ independent stoichiometries, such as (2.9) and (2.10). On the other hand, the observed stoichiometry *must* contain ϱ reactants and π products. Thus the coefficients c_1, c_2 in (2.11) must be real numbers satisfying

$$c_1, c_2 > 0 , \qquad 2c_1 - c_2 > 0 . \tag{2.12}$$

Since NO_2 dimerizes to N_2O_4, it might appear that reactions (2.9) and (2.10) provide a better representation of overall reaction. However, experimental observations of the reaction products detect NO_2, N_2O_4, and O_2, so reaction (2.7) is the more accurate description of the observed stoichiometry. The equilibration of N_2O_4 and NO_2 represents an experimental fact in addition to the observed stoichiometry.

The following prescription is a systematic procedure for obtaining φ independent solutions of Eqs. (2.2): (a) select any set of ν independent equations, rearranging and relabeling them, if necessary, so the determinant formed with the first ν coefficients in each equation is nonzero; (b) transpose the remaining φ unknowns to the right-hand members and successively assign to them the φ sets of values $(1, 0, \ldots, 0)$, $(0, 1, \ldots, 0), \ldots, (0, 0, \ldots, 1)$; (c) solve each of these ν inhomogeneous systems of linear equations by Cramer's rule. The solutions of Eqs. (2.8) cited previously were obtained by this procedure.

If the jth solution of an independent set is denoted $S_j = (s_{1j}, s_{2j}, \ldots, s_{\varrho + \pi, j})$, the stoichiometry $S = (s_1, s_2, \ldots, s_{\varrho + \pi})$ may be expressed uniquely in the form

$$S = \sum_{j=1}^{\varphi} c_j S_j . \tag{2.13}$$

This linear combination of particular solutions is also a solution of equations (2.2) since the latter are linear. Moreover, any multiple of S is also a solution, so that only the ratios of the c_i are significant. The existence of solutions μS, where $\mu > 0$, means that the reaction defined by the stoichiometry S can, in so far as only mass and charge conservation are concerned, be carried out on any desired scale.

When the product distribution is determined by the kinetics, the ratios of the c_i may be determined by integrating the rate equations which, in general, will require numerical methods. In particular instances, the integration may be carried out analytically. The mechanism

$$A \rightarrow B , \qquad 2A \rightarrow C \tag{2.14}$$

is a nontrivial illustration, but we first observe, as will be shown in Sect. 3.4, that the multiplicity of a reaction mechanism with n steps in which there are no reaction intermediates is equal to n, and that the n reactions themselves constitute a set of φ independent stoichiometries. Thus the most general stoichiometry associated with mechanism (2.14) is

$$(c_1 + 2c_2) A \rightarrow c_1 B + c_2 C . \tag{2.15}$$

Integrating the rate equations for mechanism (2.14) and passing to the limit as $t \rightarrow \infty$, we find that

$$\frac{c_1}{c_1 + 2c_2} = \frac{B_\infty - B_0}{A_0} = \frac{k_1}{2k_2 A_0} \ln \left(1 + \frac{2k_2 A_0}{k_1} \right), \tag{2.16}$$

where A_0 and B_0 denote the concentrations of A and B at $t = 0$, B_∞ the concentration of B in the limit as $t \rightarrow \infty$, and k_1, k_2, respectively, denote the rate constants for the unimolecular and bimolecular steps of the mechanism. For $k_1/2k_2 A_0 \gg 1$, c_2/c_1 is close to zero, so that $(B_\infty - B_0)/A_0$ is close to 1, which means that the stoichiometry conforms to the first step: $A \rightarrow B$. For $k_1/2k_2 A_0 \ll 1$, c_1/c_2 is close to zero, and the stoichiometry conforms to the second step: $2A \rightarrow C$.

When the product distribution is thermodynamically determined, the ratios of the c_i may be determined by equilibrium computations and related to the kinetic parameters by straightforward procedures [17-24].

Multiple stoichiometries are not at all uncommon. The oxidation of permanganate ion by hydrogen peroxide [Eq. (2.5)] is another example. Here, $\varrho + \pi - v = 6 - 4 = 2$, and two independent stoichiometries, from which all others can be constructed, are

$$2\,MnO_4^- + 5\,H_2O_2 + 6\,H^+ \to 2\,Mn^{2+} + 5\,O_2 + 8\,H_2O\,,$$

$$2\,MnO_4^- + H_2O_2 + 6\,H^+ \to 2\,Mn^{2+} + 3\,O_2 + 4\,H_2O\,. \tag{2.17}$$
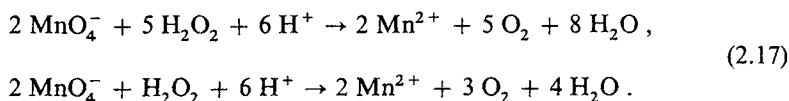
Other examples are the autoxidation of t-butyl alcohol to acetic acid, acetone, carbon dioxide, and water ($\varphi = 3$), and the pyrolysis of ethane to methane, ethylene, and hydrogen ($\varphi = 2$).

When $\varrho + \pi - v \leq 0$, equations (2.2) are inconsistent unless $s_1 = s_2 = \ldots = s_{\varrho + \pi} = 0$. For example, $s_1 C_6 H_6 \to s_2 C_6 H_5 CH_3$ leads to the equations $6s_1 = 7s_2$, $6s_1 = 8s_2$, which are obviously inconsistent, unless $s_1 = s_2 = 0$. In this case $\varrho + \pi - v = 2 - 2 = 0$. Similarly, $s_1 CH_3 OH \to s_2 C_6 H_5 OH$ violates mass conservation ($\varrho + \pi - v = 2 - 3 = -1$), unless $s_1 = s_2 = 0$. To avoid a vacuous discussion, we shall always assume that the stoichiometric coefficients are not all zero.

2.3 Catalyzed Reactions

We now suppose the reaction is catalyzed, and that the coefficients of the catalysts are $s_j, s_k, \ldots$, in the left-member of the stoichiometric relation, and $s'_j, s'_k, \ldots$, in the right-member. If M' is the matrix of coefficients defined by the stoichiometric relation when the catalysts are *omitted*, then

$$v = \text{rank } M' + \text{the number of catalysts}\,. \tag{2.18}$$

To prove this formula, observe first that the system of equations for the stoichiometric coefficients always has the following particular solutions: $s_j = s'_j \neq 0$, all other $s_i = 0$; $s_k = s'_k \neq 0$, all other $s_i = 0$; and similarly for each catalyst. These solutions express the conservation of each catalyst and are independent, so that each catalyst accounts for at least one conservation conditions; in fact, each catalyst accounts for one and only one conservation condition. For in the full matrix M derived from the equations for the stoichiometric coefficients, each catalyst determines a row whose only nonzero entries are 1 and -1, and since the contribution of this catalyst to any other conservation condition is always a multiple of this row, such contributions can always be removed by elementary row operations. Thus the system of equations for the stoichiometric coefficients can be reduced to a system in which certain equations do not contain the coefficients of any catalysts, whereas each of the remaining (independent) equations involves one and only one catalyst. This proves Eq. (2.18).

It is, of course, possible to determine ν directly by computing the rank of the full matrix M, but the procedure suggested by Eq. (2.18) is generally simpler and quicker.

Consider the dehydrogenation of ethanol to ethylene and water. The reaction is catalyzed by aluminium oxide, but for greater generality we shall suppose the reaction is simultaneously catalyzed by a compound with the formula $M_xO_yH_z$:

$$s_1C_2H_5OH + s_2Al_2O_3 + s_3M_xO_yH_z \rightarrow s_4C_2H_4 + s_5H_2O + s_6Al_2O_3$$

$$+ s_7M_xO_yH_z \, . \tag{2.19}$$
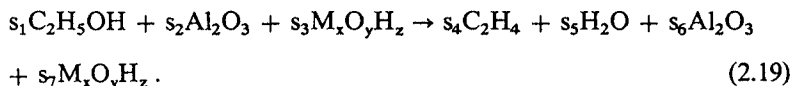
The equations for conversion of C, H, O, Al, and M, respectively, are

$$s_1 \qquad\qquad -s_4 \qquad\qquad\qquad = 0 \, ,$$

$$6s_1 \qquad +zs_3 \;\; -4s_4 \;\; -2s_5 \qquad\qquad -zs_7 \;\; = 0 \, ,$$

$$s_1 \; +3s_2 \; +ys_3 \qquad\quad -s_5 \;\; -3s_6 \;\; -ys_7 \;\; = 0 \, , \tag{2.20}$$

$$s_2 \qquad\qquad\qquad\qquad -s_6 \qquad\quad = 0 \, ,$$

$$s_3 \qquad\qquad\qquad\qquad -s_7 \;\; = 0 \, .$$

The catalysts contribute to the conservation of hydrogen and oxygen, [the second and third of Eqs. (2.20)], but it is clear that these contributions can be eliminated by elementary operations using the fourth and fifth equations. The system can thus be reduced to an equivalent system in which $s_2, s_3, s_6,$ and s_7 do not appear in the first three equations, and in which $s_1, s_4,$ and s_5 do not appear in the fifth or sixth equations, which are obviously independent. Consequently, $\nu = 2$ plus the rank of

$$M' = \begin{pmatrix} 1 & -1 & 0 \\ 6 & -4 & -2 \\ 1 & 0 & -1 \end{pmatrix} ,$$

which is 2, so that $\nu = 4$. On the other hand, the full matrix M is

$$M = \begin{pmatrix} 1 & 0 & 0 & -1 & 0 & 0 & 0 \\ 6 & 0 & z & -4 & -2 & 0 & -z \\ 1 & 3 & y & 0 & -1 & -3 & -y \\ 0 & 1 & 0 & 0 & 0 & -1 & 0 \\ 0 & 0 & 1 & 0 & 0 & 0 & -1 \end{pmatrix} ,$$

and a straightforward computation shows that its rank is indeed 4.

The preceding discussion shows that knowledge of the observed stoichiometric relation here implies knowledge of reactants, products, and catalysts, including in

the latter molecular isomers and polymorphic substances. In computing the sum $\varrho + \pi$, each catalyst is to be counted only once, even though it is regenerated by the reaction. This is, perhaps, more readily appreciated from the mechanistic point of view where a catalyst participates in the reaction and would only be counted as one of the reaction components. The traditional representation of the observed stoichiometric relation:

$$\text{reactants} \xrightarrow{C, C', C''...} \text{products} \tag{2.21}$$

clearly shows that each of the catalysts $C, C', C'', \ldots$ is to be counted only once among the reactants and products. It follows that the multiplicity $\varphi = \varrho + \pi - \nu$ is unchanged by the presence of catalysts.

Finally, it should be mentioned that if we were *only* concerned with equilibrium systems [25, 26], the foregoing considerations would have been superfluous. But catalysts participate in reaction mechanisms and failure to determine ν by formula (2.18) would lead to serious inconsistencies; more precisely, failure to take the contributions of catalysts to the number of conservation conditions would lead to correct results only for uncatalyzed reactions, even though the correct multiplicity would be obtained in either case.

2.4 Change of Basis

Equation (2.13) expresses the observed stoichiometric relation in terms of a particular set of φ independent stoichiometries. If S'_j, $j = 1, 2, \ldots, \varphi$, is another set of φ independent stoichiometries, the observed stoichiometry can also be expressed in the form

$$S = \sum_{j=1}^{\varphi} c'_j S'_j. \tag{2.22}$$

To relate the c_j of (2.13) to the c'_j of (2.22), we note that the S'_j can be written as linear combination of the S_j:

$$S'_j = \sum_{i=1}^{\varphi} T_{ij} S_i, \qquad j = 1, 2, \ldots, \varphi. \tag{2.23}$$

Substituting for S'_j in Eq. (2.22) and comparing with Eq. (2.13), it follows that

$$c_i = \sum_{j=1}^{\varphi} T_{ij} c'_j, \qquad i = 1, 2, \ldots, \varphi. \tag{2.24}$$

These results show that the observed stoichiometry can be expressed in terms of any convenient set of independent stoichiometries, so that no fundamental significance can be ascribed to any particular set of φ independent stoichiometries. Moreover, any conditions satisfied by the c_j of Eq. (2.13) impose a corresponding set of

conditions on the c_j' by virtue of Eq. (2.24). If, for example, in the decomposition of dinitrogen pentoxide, we take

$$S_1' = S_1 + 2S_2\,, \qquad S_2' = -S_1 - S_2 \qquad\qquad (2.25)$$

where $S_1 = (2, 4, 0, 1)$ and $S_2 = (0, -2, 1, 0)$, corresponding to stoichiometries (2.9) and (2.10), respectively, then S_1' and S_2', respectively, correspond to

$$2\,N_2O_5 \rightarrow 2\,N_2O_4 + O_2\,, \qquad\qquad (2.26)$$

$$2\,NO_2 + O_2 + N_2O_4 \rightarrow 2\,N_2O_5\,. \qquad\qquad (2.27)$$

In terms of these reactions, the observed stoichiometry is

$$2(c_1' - c_2')\,N_2O_5 \rightarrow -2c_2'\,NO_2 + (2c_1' - c_2')\,N_2O_4 + (c_1' - c_2')\,O_2\,. \qquad\qquad (2.28)$$
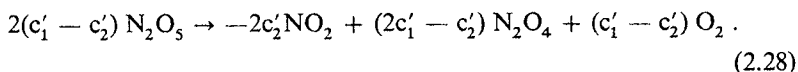
The T_{ij} are obtained from Eqs. (2.25) and on introducing them into Eqs. (2.24), we obtain

$$c_1' - c_2' = c_1\,, \qquad 2c_1' - c_2' = c_2\,. \qquad\qquad (2.29)$$

It is easy to show that when conditions (2.12) are satisfied, the coefficient of each substance in stoichiometry (2.28) is positive.

3 Mechanisms and Stoichiometries

3.1 General Relations

The observed stoichiometric relation is characterized by specifying reactants and products, including catalysts, and the number of conservation conditions; the integers ϱ, π, ν epitomize these properties. There are also integer parameters associated with a proposed reaction mechanism [14], namely, $\varkappa$, the number of chemical components, ι, the number of intermediate species, and n, the number of independent chemical reactions. Catalysts are to be counted among the $\varkappa$ components, so no special symbol is required for them.

A mechanism also implies a definite number of conservation conditions, and a method for deriving them is described in Sect. 3.3. It is evident, however, that since the reaction has been assumed to occur in a closed system, consistency demands that the number of conservation conditions implied by the mechanism must be equal to the number of conservation conditions implied by the observed stoichiometry; in other words, ν is an invariant property of the system.

The number of independent chemical reactions may be interpreted as the number of independent first-order differential equations required to specify the kinetics of the system. From this point of view, n represents the number of degrees of freedom,

so that $n = \varkappa - v$. Furthermore, the number of reaction components minus the number of intermediates must be equal to the sum of the numbers of reactants and products in the observed stoichiometric relation. It follows that [12,14]

$$\varkappa = \varrho + \pi + \iota = n + v, \tag{3.1}$$

$$\varphi = \varrho + \pi - v = n - \iota \geqq 1, \tag{3.2}$$

$$\varkappa \geqq \varrho + \pi \geqq 2. \tag{3.3}$$

Equations (3.1) reveal the intimate relations subsisting between the integer para-meters characterizing the observed stoichiometry and those characterizing the under-lying mechanism. They also reflect the principal assumptions made here, namely, the reaction occurs in a closed, isothermal system, involving a finite number of distinguishable components, and admits a traditional description in terms of a mechanism with a finite number of steps, that is, a description in terms of traditional concepts: reactants, products, catalysts, intermediates, mechanism, and stoichio-metry. There are six parameters and two equations, so that, in general, four of them must be specified to determine all six. The four parameters cannot, however, be specified arbitrarily. For although one can choose four parameters from $\varkappa$, ϱ, π, v, ι, n in 15 ways, four of these choices do not lead to the determination of all six para-meters. For example, if $\varkappa$, ϱ, π, and ι are given, n and v are still undetermined. The other cases are $\varkappa$, ϱ, n, v (π and ι undetermined); $\varkappa$, π, n, v (ϱ and ι undetermined); $\varkappa$, ι, n, v (ϱ and π undetermined).

The relations (3.2) follow from the equality of the second and third members of (3.1) and the consistency condition discussed in Sect. 2.1. These relations give the mechanistic interpretation of the multiplicity of the observed stoichiometry, and show that the consistency condition $\varphi \geqq 1$ is equivalent to $n - \iota \geqq 1$. Thus, the existence of a nontrivial stoichiometric relation manifests itself in the reaction mechanism by the requirement that the number of reaction intermediates cannot equal or exceed the number of independent reaction. It will be shown in Sect. 3.4 that this is precisely the condition required to deduce the stoichiometric relation(s) from the mechanism.

The inequalities (3.3) obviously state that there must be at least one reactant and at least one product.

Examples

1. The stoichiometric relation for the reaction of nitrogen dioxide with chlorine monoxide in the gas phase and in solution is [27]

$$Cl_2O + 2\,NO_2 \rightarrow NO_3Cl + NO_2Cl \tag{3.4}$$
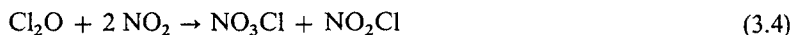
From this relation, it follows that $\varrho + \pi = 4$, and $v = 3$. Introducing these results into (3.1), we find $\varkappa = 4 + \iota = n + 3$, so that $\iota = n - 1$. The proposed two-step mechanism with OCl as an intermediate is consistent with this result:

$$NO_2 + Cl_2O \rightarrow NO_2Cl + OCl,$$
$$NO_2 + OCl \rightarrow NO_3Cl. \tag{3.5}$$
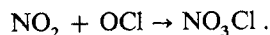
2. For the gas-phase reaction of hydrogen and bromine [2-5] the known stoichiometry

$$H_2 + Br_2 \rightarrow 2\, HBr \,, \tag{3.6}$$

together with Eqs. (3.1) imply $\varkappa = 3 + \iota = n + 2$, so that a mechanism with two intermediates must have three steps and five components. The classical mechanism chain conforms to these conditions:

$$Br_2 + M \rightleftharpoons 2\, Br + M \,,$$

$$Br + H_2 \rightleftharpoons HBr + H \,, \tag{3.7}$$

$$H + Br_2 \rightarrow HBr + Br \,.$$

Note that although M participates in the physics of the reaction, it does not participate in the chemistry, so it is not counted among the components. Bromine molecules could serve the function of M, but in that event Br_2 would be included among the components by virtue of its dissociation in the first step, not by assuming the collisional function of M. It should also be noted that forward and reverse reactions of any reversible mechanistic step are to be counted as a *single* step of the mechanism. The reason is that n in Eqs. (3.1) represents the number of independent reactions; the forward and reverse reactions of a reversible step sum to the null reaction, so they are not (algebraically) independent.

3. For an application of Eqs. (3.1), consider the mechanism for the gas-phase decomposition of N_2O_5 in which NO and NO_3 are intermediates:

$$N_2O_5 \rightleftharpoons NO_2 + NO_3 \,,$$

$$NO_2 + NO_3 \rightarrow NO_2 + NO + O_2 \,,$$

$$NO + NO_3 \rightarrow 2\, NO_2 \,, \tag{3.8}$$

$$2\, NO_2 \rightleftharpoons N_2O_4 \,.$$
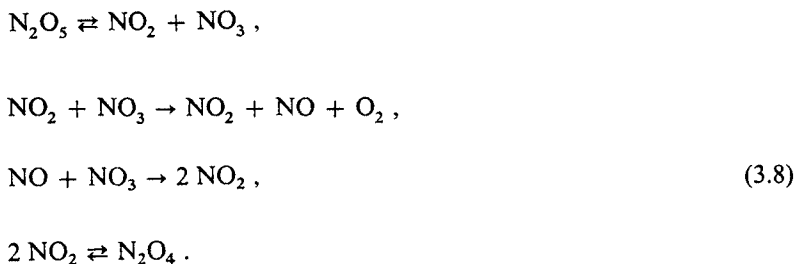
Only the first three steps are customarily cited [28], but we have shown that the multiplicity is two, so we must have $n - \iota = 2$. A mechanism with three steps and two intermediates is inconsistent. If there are two intermediates, there *must* be four steps, and the reversible conversion of NO_2 and N_2O_4 seems an obvious choice for a fourth step.

4. The vapor phase decomposition of nitric acid follows the stoichiometry

$$4\, HNO_3 \rightarrow 4\, NO_2 + 2\, H_2O + O_2 \,. \tag{3.9}$$
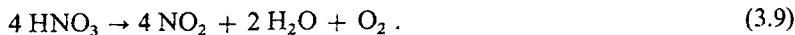
Since $\varrho + \pi = 4$, and $\nu = 3$, Eqs. (3.1) demand that $\varkappa = 4 + \iota = n + 3$. The following 4-step mechanism[29] with intermediates HO, NO, and NO_3 conforms to this requirement:

$$HNO_3 \rightleftarrows HO + NO_2 \,,$$

$$HO + HNO_3 \rightarrow H_2O + NO_3 \,,$$

$$NO_2 + NO_3 \rightarrow NO_2 + NO + O_2 \,, \tag{3.10}$$

$$NO + NO_3 \rightarrow 2\,NO_2 \,.$$
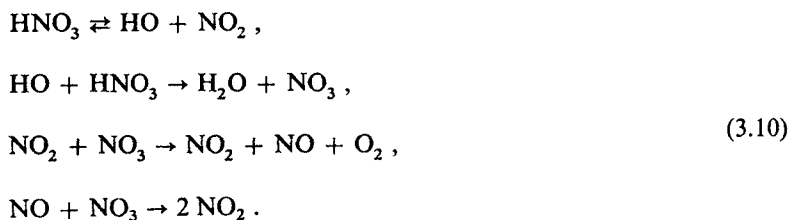
5. The pyrolysis of acetaldehyde conforms closely to the stoichiometry

$$CH_3CHO \rightarrow CH_4 + CO \,, \tag{3.11}$$

but small amounts of ethane and hydrogen are detected and their inclusion among the reaction products requires a stoichiometry of multiplicity 2. Indeed, two independent stoichiometries are

$$4\,CH_3CHO \rightarrow 2\,CH_4 + 4\,CO + C_2H_6 + H_2 \,, \tag{3.12}$$

$$3\,CH_3CHO \rightarrow CH_4 + 3\,CO + C_2H_6 + H_2 \,. \tag{3.13}$$
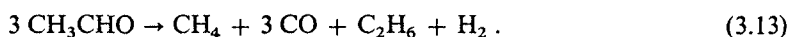
The stoichiometry (3.11) is the difference of reactions (3.12) and (3.13), so that reaction (3.11) and either of reactions (3.12) or (3.13) are alternative pairs of independent stoichiometries. Since $\varrho + \pi = 5$, and $\nu = 3$, Eqs. (3.1) require that $\varkappa = 5 + \iota = n + 3$. The following mechanism[30] with six steps and four intermediates (CH_3, CHO, H, CH_3CO) is consistent with this requirement:

$$CH_3CHO \rightarrow CH_3 + CHO \,,$$

$$CHO \rightarrow CO + H \,,$$

$$H + CH_3CHO \rightarrow H_2 + CH_3CO \,,$$

$$CH_3 + CH_3CHO \rightarrow CH_4 + CH_3CO \,, \tag{3.14}$$

$$CH_3CO \rightarrow CH_3 + CO \,,$$

$$2CH_3 \rightarrow C_2H_6 \,.$$
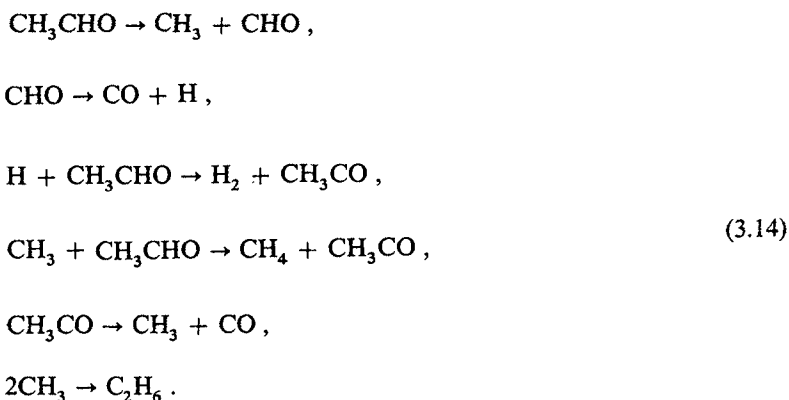
6. The pyrolysis of ethane to ethylene, methane, and hydrogen requires that $\varrho + \pi = 4$, $\nu = 2$ (carbon and hydrogen conservation). It follows from (3.1) that

any mechanism for the pyrolysis must satisfy $\varkappa = 4 + \iota = n + 2$. The five-step chain mechanism

$$C_2H_6 \rightarrow 2\,CH_3\,,$$

$$CH_3 + C_2H_6 \rightarrow CH_4 + CH_3CH_2\,,$$

$$CH_3CH_2 \rightarrow C_2H_4 + H\,, \qquad\qquad (3.15)$$

$$H + C_2H_6 \rightarrow H_2 + CH_3CH_2\,,$$

$$H + CH_3CH_2 \rightarrow C_2H_6\,.$$
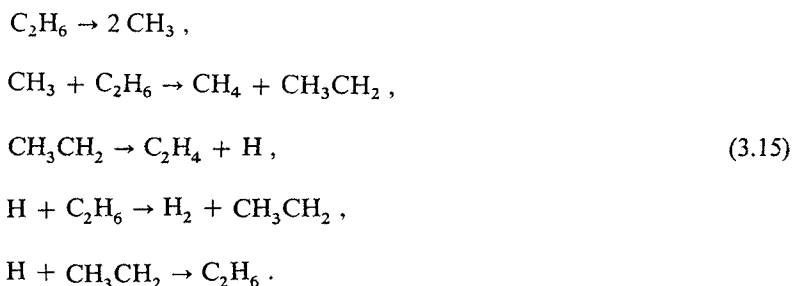
in which H, CH_3, and CH_3CH_2 are intermediates, is consistent with these conditions.

7. The case of a catalyzed reaction is illustrated by

$$V^{3+} + Fe^{3+} \rightarrow V^{4+} + Fe^{2+}\,, \qquad\qquad (3.16)$$

which is catalyzed by the cupric ion, so that $v = 4$ (conservation of vanadium, iron, and charge, together with one catalyst). Here, $\varrho + \pi = 5$, and Eqs. (3.1) require that $\varkappa = 5 + \iota = n + 4$. The kinetics suggest a two-step mechanism [31] with Cu^+ ion as an intermediate:

$$V^{3+} + Cu^{2+} \rightarrow V^{4+} + Cu^+\,.$$

$$Cu^+ + Fe^{3+} \rightarrow Fe^{2+} + Cu^{2+}\,. \qquad\qquad (3.17)$$

8. The commercial synthesis of acetic acid by the insertion of carbon monoxide into methyl alcohol

$$CH_3OH + CO \rightarrow CH_3COOH \qquad\qquad (3.18)$$

illustrates a more complex catalyzed reaction. The suggested mechanism is [32]

$$CH_3OH + HI \rightarrow CH_3I + H_2O\,,$$

$$CH_3I + [Rh(CO)_2I_2]^- \rightarrow [CH_3Rh(CO)_2I_3]^-\,,$$

$$[CH_3Rh(CO)_2I_3]^- \rightarrow [CH_3CORh(CO)I_3]^-\,,$$

$$[CH_3CORh(CO)I_3]^- + CO \rightarrow [CH_3CORh(CO)_2I_3]^-\,, \qquad (3.19)$$

$$[CH_3CORh(CO)_2I_3]^- \rightarrow [Rh(CO)_2I_2]^- + CH_3COI\,.$$

$$CH_3COI + H_2O \rightarrow CH_3COOH + HI\,.$$
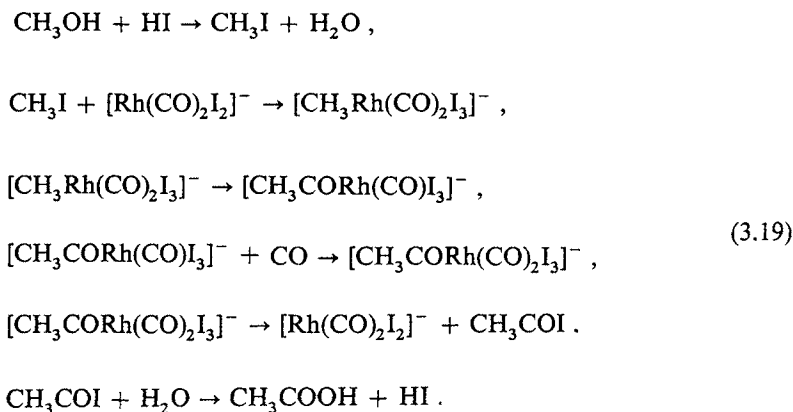
According to the mechanism, HI, H_2O, and $[Rh(CO)_2I_2]^-$ are catalysts, so that $\varrho + \pi = 6$ (three catalysts plus the three components of the stoichiometry). and $v = 5$, by virtue of Eq. (2.18). Thus the proposed six-step mechanism with 11 components and 5 intermediates is consistent with Eq. (3.1).

9. The chemical components of a reaction mechanism may include molecules or atoms in excited states, which are counted as distinct components, as in the mechanism [33] for the conversion of *ortho* and *para* hydrogen:

$$Hg(^3P) + H_2 \rightarrow Hg(^1S) + 2 H ,$$

$$H + p\text{-}H_2 \rightarrow o\text{-}H_2 + H ,$$
(3.20)

$$2H \rightarrow H_2 .$$
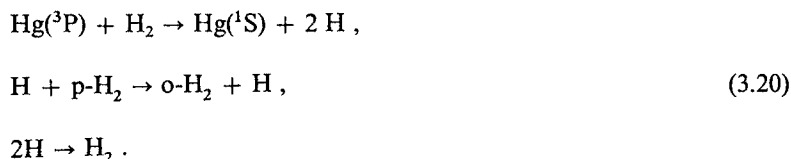
In the first and third steps, H_2 denotes molecules that are *ortho* or *para*, that is, these steps are indifferent to the nuclear orientation; hence H_2 is counted as a separate component, giving a total of six components in the mechanism. The stoichiometry is

$$Hg(^3P) + p\text{-}H_2 \rightarrow o\text{-}H_2 + Hg(^1S) ,$$
(3.21)

and H_2, as the mechanism indicates, functions as a catalyst. Thus $\varrho + \pi = 5$, $v = 3$ (hydrogen, mercury, and one catalyst), $n = 3$, $\iota = 1$, so that Eqs. (3.1) are satisfied.

10. The relation $\varphi = n - \iota$ shows that the multiplicity varies with the number of intermediates. This is illustrated by the following two-step mechanisms in which reversible and irreversible reactions are used to alter the function of a component from an intermediate to a product:

$$A \rightarrow B , \quad B \rightarrow C ;$$
(3.22)

$$A \rightleftarrows B , \quad B \rightarrow C ;$$
(3.23)

$$A \rightarrow B , \quad B \rightleftarrows C ;$$
(3.24)

$$A \rightleftarrows B , \quad B \rightleftarrows C .$$
(3.25)

Since $\varkappa = 3$, and $n = 2$, there is only one mass conservation condition in each case, so that $\varphi = 2 - \iota$. In mechanisms (3.22) and (3.23), B is the only intermediate, so $\varphi = 1$, corresponding to the stoichiometry $A \rightarrow C$. In mechanisms (3.24) and (3.25), however, B is a product, so $\varphi = 2$, and two independent stoichiometries are $A \rightarrow B$, $B \rightarrow C$.

The general relations (3.1), (3.2), and (3.3) are conditions that must be observed if the terms *reactant, product, stoichiometry, intermediate, catalyst,* and *independent mechanistic step* are to be used consistently. The examples show that they have been implicitly observed in many instances, but it is important that they be taken into

account explicitly to guard against inconsistencies. For example, in the photo-chemical decomposition of iodomethane, the observed stoichiometry is

$$9 \, CH_3I \rightarrow 3 \, CH_4 + C_2H_6 + C_2H_4 + CH_2I_2 + CH_3I + 3 \, I_2 \,. \quad (3.26)$$
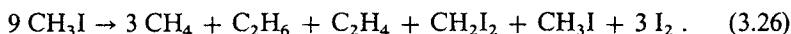
The reaction is not catalyzed, so that $\varkappa = 7 + \iota = n + 3$. Although the reaction has been the subject of several kinetic studies [34], and the proposed mechanism explains some features of the kinetics, it has 15 components, seven intermediates, and 15 independent reactions, violating Eqs. (3.1). If there are seven intermediates, there *must* be 14 components, and 11 independent reactions. That a mechanism may explain salient features of the kinetics while being inconsistent clearly demonstrates how easily inconsistent mechanisms can slip through the sieve of experiment. On the other hand, mechanisms consistent with the general relations may not be consistent with experiment.

One feature of the general relations merits special emphasis: they apply when the reaction is diffusion controlled, when there is a rate determining step, or, indeed, no matter what the rates of the individual mechanistic steps. The general relations are independent of the details of the kinetics.

3.2 Dependent and Independent Reactions

The integer n refers to the number of linearly *independent* reactions in the mechanism. Reactions that are linearly *dependent* may be expressed as linear combinations of n independent mechanistic reactions, just as the observed stoichiometric relation may be expressed as a linear combination of φ independent stoichiometries. The reactions $A \rightarrow B$ and $B \rightarrow A$, for instance, are linearly dependent, since the second is -1 times the first. In general, forward and reverse reactions of a reversible mechanistic step are dependent, hence the rule given in Example 2.

To determine whether the reactions of a given mechanism are dependent or in-dependent, transpose the reactants from the left-member of each mechanistic step to the right-member, changing the sign of each coefficient. Components and reactions are then numerically ordered in any convenient manner, so that the mechanism may be symbolically written

$$\sum_{i=1}^{K} \sigma_{i\alpha} X_i = 0, \qquad \alpha = 1, 2, \ldots, \quad (3.27)$$

where $\sigma_{i\alpha}$ is the net coefficient of component X_i in step α, taken with a plus or minus sign according as X_i is a product or a reactant, and the index α ranges over all mechanistic steps. The number of independent steps in the mechanism is equal to the rank of the matrix $\sigma = (\sigma_{i\alpha})$. In this computation the reactions of the mechanism are regarded as vectors with $\varkappa$ components without regard to the reversibility or irreversibility of the steps, so the symbols $\rightarrow$ and $\rightleftarrows$ have no effect on the computation. It should also be noted that when the reactions are written in the form (3.27), the array of coefficients displayed is *not* the matrix σ, but its transpose $\tilde{\sigma}$. Nevertheless,

either matrix may be used to determine the number of linearly independent reactions, since the row rank of a matrix equals its column rank [35]:

$$n = \text{rank}\,\sigma = \text{rank}\,\tilde{\sigma} \tag{3.28}$$

Using this criterion, it may be shown that the reactions in each of the illustrative mechanisms of the preceding section are indeed independent.

Although many mechanisms consist entirely of independent reactions, it is often *essential* that dependent steps be included to avoid ambiguity. In the cyclic conversion of three isomers

$$A \rightleftarrows B, \qquad B \rightleftarrows C, \qquad C \rightleftarrows A, \tag{3.29}$$

$$\tilde{\sigma} = \begin{pmatrix} -1 & 1 & 0 \\ 0 & -1 & 1 \\ 1 & 0 & -1 \end{pmatrix}.$$

The rank of σ is 2, but any two reactions of the mechanism fail to disclose its cyclic nature. Note, moreover, that Eqs (3.1) are satisfied when $n = 2$. Incidentally, the multiplicity is 2, and any two reactions of the mechanism constitutes a pair of linearly independent stoichiometries.

The mechanism

$$A \rightarrow 2\,B,$$

$$B + C \rightarrow D + E,$$

$$A + D \rightarrow B + E, \tag{3.30}$$

$$C \rightarrow 2\,D,$$

also consists of dependent reactions, since

$$\tilde{\sigma} = \begin{pmatrix} -1 & 2 & 0 & 0 & 0 \\ 0 & -1 & -1 & 1 & 1 \\ -1 & 1 & 0 & -1 & 1 \\ 0 & 0 & -1 & 2 & 0 \end{pmatrix}$$

whose rank is 3. Any three steps of the mechanism are independent, but all four steps are necessary to define the function of each component. If the first step is omitted, B is changed from a product to a catalyst; if the third step is omitted B is changed from a product to an intermediate, and similarly with D if the fourth step is omitted.

In general, a mechanism should include dependent steps only to make the function each component unambiguous, or to exhibit some particular aspect of the mechanism

itself, as illustrated by mechanisms (3.29) and (3.30). It should be recognized, however, that dependent steps will contribute to the kinetics, so that care should be taken to avoid redundant steps. In specific instances, it should be possible to settle such matters without difficulty.

Consider the oxidation of iodide ion by hypochlorite ion in aqueous, alkaline solution. The observed stoichiometry is [36]

$$I^- + OCl^- \rightarrow OI^- + Cl^- ,$$ (3.31)

and a proposed mechanism is [36, 37]

$$OCl^- + H_2O \rightleftarrows HOCl + OH^- ,$$

$$I^- + HOCl \rightarrow HOI + Cl^- ,$$ (3.32)

$$OH^- + HOI \rightarrow H_2O + OI^- .$$
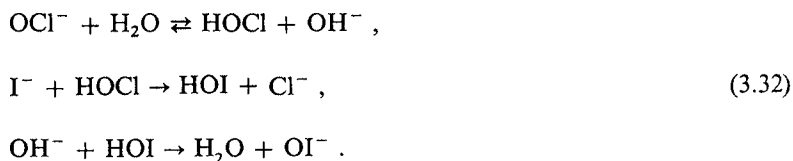
The mechanism includes three intermediates ($HOCl$, HOI, OH^-), and indicates that the water molecule functions as a catalyst; hence the observed stoichiometry and formula (2.18) yield $v = 3 + 1 = 4$. But $\varkappa = 8$, $\varrho + \pi = 5$, and $n = 3$, so that Eqs. (3.1) are not satisfied. In fact, the stoichiometry and the mechanism specify different values for v, since the mechanism implies five conservation conditions: chlorine, oxygen, hydrogen, iodine, and charge. Here we have a mechanism that is inconsistent with the observed stoichiometry.

The mechanism can be remedied by means of the experimental fact that OH^- inhibits the reaction, so that H^+ is a catalyst. Introducing H^+ into the reaction by means of the equation

$$H^+ + OH^- \rightleftarrows H_2O .$$ (3.33)

the value of v as determined by means of (2.18) becomes equal to $3 + 2 = 5$, so that mechanism and stoichiometry now imply the same number of conservation conditions. The number of components is increased to 9, the number of independent reactions is increased to 4, and $\varrho + \pi = 4 + 2 = 6$, so that Eqs. (3.1) are satisfied. One minor difficulty remains: if hydrogen is a catalyst, there must be a mechanism for its regeneration. This difficulty is removed by adjoining the *dependent* reaction

$$HOI \rightarrow H^+ + OI^- .$$ (3.34)

This is preferred to the dependent reaction $HOCl \rightarrow H^+ + OCl^-$, because with the second step of (3.32) as ratedetermining, the new mechanism will conform to the observed kinetics.

3.3 Conservation Conditions

The invariant v may be deduced from the observed stoichiometry. Consistency requires that the value obtained with formula (2.18) be equal to that determined by

the mechanism. When the mechanism is given explicitly, the value of v is obtained by writing out all the conservation conditions, and then determining how many of them are independent. The computation is straightforward and will be illustrated with the mechanism for the oxidation of iodide ion by hypochlorite ion, reactions (3.32), (3.33), and (3.34). The conservation conditions for chlorine, iodine, hydrogen, oxygen, and charge, respectively, are

$$[OCl^-] \quad\quad +[HOCl] \quad\quad\quad\quad +[Cl^-] \quad\quad\quad\quad = c_1 \,,$$

$$[I^-] \quad +[HOI] \quad\quad +[OI^-] \quad\quad = c_2 \,,$$

$$2[H_2O] +[HOCl] +[OH^-] \quad\quad +[HOI] \quad\quad\quad\quad +[H^+] = c_3 \,,$$

$$[H_2O] +[HOCl] +[OH^-] \quad\quad +[HOI] \quad\quad +[OI^-] \quad\quad = c_4 \,,$$

$$[OCl^-] \quad\quad\quad +[OH^-] +[I^-] \quad\quad +[Cl^-] +[OI^-] -[H^+] = c_5 \,,$$

where the c's are constants determined by the initial conditions. The value of v is equal to the rank of the matrix determined by the coefficients of the concentrations:

$$\begin{pmatrix} 1 & 0 & 1 & 0 & 0 & 0 & 1 & 0 & 0 \\ 0 & 0 & 0 & 0 & 1 & 1 & 0 & 1 & 0 \\ 0 & 2 & 1 & 1 & 0 & 1 & 0 & 0 & 1 \\ 0 & 1 & 1 & 1 & 0 & 1 & 0 & 1 & 0 \\ 1 & 0 & 0 & 1 & 1 & 0 & 1 & 1 & -1 \end{pmatrix}.$$

The rank of this matrix is 5, which confirms the assertion in the preceding section that the mechanism implies $v = 5$.

The conservation conditions can be derived with equal facility when the mechanism is formulated abstractly by Eqs. (3.27). Let X_i denote the molar concentration of component X_i, and let r_α be the forward rate of mechanistic step α in moles per unit volume per unit time. (Here, and subsequently, italicized Roman capitals denote molar concentrations.) The contribution of step α to the time derivative of X_i is zero if X_i does not appear in that step, or is unaltered by it; otherwise $(\partial X_i/\partial t)_\alpha = \sigma_{i\alpha} r_\alpha$. The total time derivative $dX_i/dt \equiv \dot{X}_i$ is obtained by summing over all mechanistic steps:

$$\dot{X}_i = \sum_\alpha \sigma_{i\alpha} r_\alpha \,, \quad\quad i = 1, 2, \ldots, \varkappa \,. \quad\quad\quad (3.35)$$

Now the jth conservation condition may be written

$$\sum_{i=1}^{\varkappa} a_{ji} X_i = c_j \,, \quad\quad\quad\quad\quad\quad (3.36)$$

267

where the a_{ji} are *numerical* coefficients, and c_j is a constant that may be evaluated in terms of the initial concentrations. Differentiating (3.36) with respect to the time, and substituting from (3.35), we obtain

$$\sum_{\alpha} \left\{ \sum_{i=1}^{\varkappa} a_{ji}\sigma_{i\alpha} \right\} r_{\alpha} = 0 \tag{3.37}$$

If the r_{α} are independent, functionally or linearly, it would follow that the coefficient of each r_{α} must vanish. The same conclusion also applies when the r_{α} are dependent; for otherwise the dependent r's could be expressed in terms of independent r's, and these expressions would necessarily involve the kinetic parameters characterizing the rates. On setting the coefficients of the independent r's equal to zero, we would then obtain a system of equations for the a_{ji} that contain the kinetic parameters, contradicting the fact that the a_{ji} are *numerical* coefficients independent of the time, the concentrations, and all details of the kinetic process. It follows that the coefficients of *all* r_{α} must vanish:

$$\sum_{i=1}^{\varkappa} a_{ji}\sigma_{i\alpha} = 0, \qquad \alpha = 1, 2, \dots, n. \tag{3.38}$$

It is permissible to extend the range of α only over the independent reactions of the mechanism, because the rank of σ is n, so that any additional equations that occur are expressible in terms of those given by equations (3.38). Furthermore, since we have a system of linear equations of rank n in $\varkappa$ components, there will be exactly $\nu = \varkappa - n$ independent solutions.

Equations (3.38) are easily written out when the mechanism is given, since the coefficients of the a_{ji}, that is, the $\sigma_{i\alpha}$, may be easily read from the mechanism when all reactants are transformed to the right-hand members. In the case of mechanism (3.30), for example, we have

$$\begin{aligned}
-a_{j1} + 2a_{j2} &= 0, \\
-a_{j2} - a_{j3} + a_{j4} + a_{j5} &= 0, \\
-a_{j1} + a_{j2} \qquad\quad - a_{j4} + a_{j5} &= 0, \\
-a_{j3} + 2a_{j4} &= 0,
\end{aligned} \tag{3.39}$$

where the subscripts 1, 2, 3, 4, 5, refer to components A, B, C, D, E, respectively. The reactions of the mechanism are linearly dependent, so that Eqs. (3.39) are also linearly dependent. In fact, the sum of the first two minus the third equals the fourth. Any three of Eqs. (3.39) are linearly independent, and if we solve them, the remaining equation will be satisfied. Taking the first three equations and applying the procedure suggested in Sect. 2.2, we obtain two independent solutions $(a_{11}, a_{12}, a_{13}, a_{14}, a_{15}) = (-2, -1, 2, 1, 0)$, $(a_{21}, a_{22}, a_{23}, a_{24}, a_{25}) = (2, 1, 0, 0, 1)$, that is, the conservation conditions are

$$-2A - B + 2C + D = c_1, \qquad 2A + B + E = c_2. \tag{3.40}$$

This proves that mechanism (3.30), for which $\varkappa = 5$ and $n = 3$, conforms to $\varkappa = n + v$. The discussion in the following section will establish that the mechanism also conforms to $\varkappa = \varrho + \pi + \iota$.

3.4 Stoichiometry of a Mechanism

The stoichiometric relation(s) implied by a mechanism can be derived by algebraic elimination of the reaction intermediates. Since any dependent reactions in the mechanism can be expressed as linear combinations of the n independent mechanistic steps, we need only consider the elimination of intermediates from the n independent reactions of the mechanism.

In the special case when there are no intermediates, the multiplicity equals n, and the n independent steps of the mechanism provide the required number of independent stoichiometries, the general stoichiometry being given by Eq. (2.13). If the observed stoichiometry is expressible in this form, the mechanism is qualitatively consistent with it.

Turning to the general case, let us assume that $\iota \neq 0$, and let n^* be the number of reactions in the mechanism *without* intermediates. These reactions provide n^* independent stoichiometries, and since there must be exactly $n - \iota$ independent stoichiometries, the remaining $n - n^* - \iota$ stoichiometries have to be obtained by eliminating the intermediates from the other $n - n^*$ reactions of the mechanism.

The integer n^* may have any one of the values $1, 2, \ldots, n - \iota - 1$, but the value $n - \iota$ is excluded. For if $n^* = n - \iota$, the mechanism provides the required $n - \iota$ independent stoichiometries and ι other independent reactions containing the intermediates. The existence of ι reactions containing the intermediates leads to a contradiction. Indeed, if such reactions did exist, it would be impossible to eliminate the intermediates from them, because if that were possible we would exceed the number of allowed independent stoichiometries. This means each intermediate occurs only once in each of the supposed ι reactions; for if an intermediate occurred twice, once, say, in each of two different mechanistic steps, it would be possible to eliminate it algebraically and obtain another stoichiometry. But if each intermediate occurs only once in each of the reactions, the intermediates are functioning as reactants and products. This contradiction proves

$$n - n^* - \iota \geq 1, \qquad \iota \neq 0. \tag{3.41}$$

To eliminate the intermediates when $\iota \neq 0$, each of the $n–n^*$ reactions containing intermediates is multiplied by an unknown constant, and the resulting equations summed. On equating the coefficients of corresponding intermediates in each member, a system of ι linear, homogeneous equations in $n–n^*$ unknowns is obtained. The consistency condition (3.41) ensures that this system of equations has $n - n^* - \iota$ independent solutions. Substituting into the equation obtained by the summation process, we obtain one stoichiometric relation for each independent solution. The stoichiometries obtained need not contain exactly ϱ reactants and π products, but it must be possible, for a consistent mechanism, to represent the observed stoichiometry in the form of (2.13).

To illustrate the procedure, we apply it to mechanism (3.14), multiplying the first step by a, the second by b, and so on, obtaining the stoichiometric relation in the form

$$(a + c + d)\, CH_3CHO \rightarrow (b + e)\, CO + cC_2H_4 + dCH_4 + fCH_2H_6 \,,$$
$$(3.42)$$
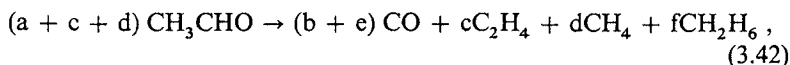
and the following system of equations for elimination of the intermediates CH_3, CHO, H, and CH_3CO:

$$a - d + e - 2f = 0 \,,$$

$$c + d - e = 0 \,, \qquad (3.43)$$

$$a = b = c \,,$$

Two independent solutions of these equations are $(a_1, b_1, c_1, d_1, e_1, f_1) = (0, 0, 0, 1, 1, 0)$, and $(a_2, b_2, c_2, d_2, e_2, f_2) = (1, 1, 1, 1, 2, 1)$, and, when substituted into (3.42), yield stoichiometries (3.11) and (3.13), respectively.

When the stoichiometric relation is obtained, catalysts will appear in opposite members with equal coefficients. For example, the mechanism

$$A + B \rightarrow C \,,$$
$$C \rightarrow B + D \,, \qquad (3.44)$$

admits two conservation conditions

$$B + C = c_1 \,, \qquad (3.45)$$
$$A + C + D = c_2 \,,$$

expressing the conservation of A and B, respectively. Since C is the only intermediate, the multiplicity is one, and the elimination of C yields the stoichiometric relation in the form $A + B \rightarrow B + D$. Note that $\varkappa = 4$, and $\iota = 1$, so that $\varrho + \pi = 3$, showing that

$$A \xrightarrow{B} D \qquad (3.46)$$

better representation of that fact that a catalyst is counted only once in the sum $\varrho + \pi$.

3.5 Classification of Reaction Mechanisms

Reaction mechanisms can be sorted into classed by fixing one or more of the parameters n, $\varkappa$, ν, ϱ, π, ι. The number of mechanistic types in a class will be denoted $(\alpha\beta\gamma \ldots)$, where letters enclosed within parentheses are the fixed parameters defining the class. Obviously only those classifications containing a finite number of

mechanistic types will be useful, and since the stipulated parameters must satisfy Eqs. (3.1), we can appeal to these equations to decide the issue for any particular choice of parameters. In particular, Eqs. (3.1) show that fixing n does not delimit the values of the other parameters, so that there are infinitely many mechanistic types having the same number of independent mechanistic steps. The same conclusion holds for all of the remaining parameters except $\varkappa$, for which

$$(\varkappa) = \frac{1}{6}\varkappa(\varkappa - 1)(2\varkappa - 1). \tag{3.47}$$

Observe that the expression in the right-hand member is the sum of the squares of the first $\varkappa - 1$ integers.

The proof of Eq. (3.47) follows easily from the following tableau:

$$
\begin{array}{ccccccc}
\varrho + \pi = 2 & 3 & 4 & 5 & \ldots \varkappa - 1 & \varkappa \\
\iota \quad = \varkappa - 2 & \varkappa - 3 & \varkappa - 4 & \varkappa - 5 & \ldots 1 & 0 \\
 & 1 & 1 & 1 & \ldots 1 & 1 \\
 & & 2 & 2 & \ldots 2 & 2 \\
 & & 3 & 3 & \ldots 3 & 3 \\
 & & & 4 & \ldots 4 & 4 \\
 & & & & \cdot & \cdot \\
 & & & & \cdot & \cdot \\
 & & & & \cdot & \cdot \\
 & & & & \varkappa - 2 & \varkappa - 2 \\
 & & & & & \varkappa - 1 \\
\end{array}
$$

The first row gives all the values of $\varrho + \pi$ from 2 up to the fixed value of $\varkappa$, and the second the corresponding of $\iota = \varkappa - \varrho - \pi$. The entries below the second row in any given column are the values of v allowed by the value of $\varrho + \pi$ heading the column, in all $\varrho + \pi - 1$ values, since $1 \leqq v \leqq \varrho + \pi - 1$. The value of n is, of course, given by $\varkappa - v$. Now each value of $\varrho + \pi$ can be partitioned into individual values of ϱ and π in exactly $\varrho + \pi - 1$ ways, which may be associated with any of the $\varrho + \pi - 1$ values of v. Thus, for a fixed value of $\varkappa$, the total number of integer sets satisfying Eqs. (3.1) is obtained by summing $(\varrho + \pi - 1)^2$ over all values of $\varrho + \pi$ from 2 to $\varkappa - 1$. This proves Eq. (3.47).

The mechanistic types for several values of $\varkappa$ are given in Table 1 for $\varkappa = 2, 3, 4, 5, 6$, and it will be observed that the number increases rapidly with $\varkappa$, thus (6) = 55, but (10) = 285. In any case, however, it is advisable to begin constructing a mechanism by fixing the number of components, as this ensures only a finite number of mechanistic types need be considered. It must be emphasized that Table 1 *does not* give the number of possible mechanisms for a given value of κ, but the number of mechanistic types in the class defined by fixing κ. Thus there are five types of mechanisms in the class defined by setting $\kappa = 3$, but only one type when $\kappa = 2$, and the latter includes, among others, all mechanisms of the form mA → B. Never-

Paul L. Corio

Table 1. Integer Sets Satisfying Equations (3.1) for κ = 2, 3, 4, 5, 6

κ	n	ν	ϱ	π	ι	κ	n	ν	ϱ	π	ι	κ	n	ν	ϱ	π	ι	κ	n	ν	ϱ	π	ι
2	1	1	1	1	0	5	4	1	1	1	3	6	5	1	1	1	4	6	5	1	1	5	0
3	2	1	1	1	1	5	4	1	1	2	2	6	5	1	1	2	3	6	5	1	2	4	0
3	2	1	1	2	0	5	4	1	2	1	2	6	5	1	2	1	3	6	5	1	3	3	0
3	2	1	2	1	0	5	3	2	1	2	2	6	4	2	1	2	3	6	5	1	4	2	0
3	1	2	1	2	0	5	3	2	2	1	2	6	4	2	2	1	3	6	5	1	5	1	0
3	1	2	2	1	0	5	4	1	1	3	1	6	5	1	1	3	2	6	4	2	1	5	0
4	3	1	1	1	2	5	4	1	2	2	1	6	5	1	2	2	2	6	4	2	2	4	0
4	3	1	1	2	1	5	4	1	3	1	1	6	5	1	3	1	2	6	4	2	3	3	0
4	3	1	2	1	1	5	3	2	1	3	1	6	4	2	1	3	2	6	4	2	4	2	0
4	2	2	1	2	1	5	3	2	2	2	1	6	4	2	2	2	2	6	4	2	5	1	0
4	2	2	2	1	1	5	3	2	3	1	1	6	4	2	3	1	2	6	3	3	1	5	0
4	3	1	1	3	0	5	2	3	1	3	1	6	3	3	1	3	2	6	3	3	2	4	0
4	3	1	2	2	0	5	2	3	2	2	1	6	3	3	2	2	2	6	3	3	3	3	0
4	3	1	3	1	0	5	2	3	3	1	1	6	3	3	3	1	2	6	3	3	4	2	0
4	2	2	1	3	0	5	4	1	1	4	0	6	5	1	1	4	1	6	3	3	5	1	0
4	2	2	2	2	0	5	4	1	2	3	0	6	5	1	2	3	1	6	2	4	1	5	0
4	2	2	3	1	0	5	4	1	3	2	0	6	5	1	3	2	1	6	2	4	2	4	0
4	1	3	1	3	0	5	4	1	4	1	0	6	5	1	4	1	1	6	2	4	3	3	0
4	1	3	2	2	0	5	3	2	1	4	0	6	4	2	1	4	1	6	2	4	4	2	0
4	1	3	3	1	0	5	3	2	2	3	0	6	4	2	2	3	1	6	2	4	5	1	0
						5	3	2	3	2	0	6	4	2	3	2	1	6	1	5	1	5	0
						5	3	2	4	1	0	6	4	2	4	1	1	6	1	5	2	4	0
						5	2	3	1	4	0	6	3	3	1	4	1	6	1	5	3	3	0
						5	2	3	2	3	0	6	3	3	2	3	1	6	1	5	4	2	0
						5	2	3	3	2	0	6	3	3	3	2	1	6	1	5	5	1	0
						5	2	3	4	1	0	6	3	3	4	1	1						
						5	1	4	1	4	0	6	2	4	1	4	1						
						5	1	4	2	3	0	6	2	4	2	3	1						
						5	1	4	3	2	0	6	2	4	3	2	1						
						5	1	4	4	1	0	6	2	4	4	1	1						

theless, some interesting conclusions can be drawn from Table 1. For instance, for a given κ, the number of mechanistic types decreases as the number of intermediates descreases, but this decrease is countered by an increase in the number of independent reactions. If mechanistic types were selected randomly, mechanistic types without intermediates would prevail more and more as κ increased. We shall see presently, in fact, that the number of mechanistic types without intermediates is, for given κ, equal to $(κ - 1)^2$.

Classifications of reaction mechanisms with two fixed parameters contain a finite number of mechanistic types only when one of the parameters is κ. Specifically,

$$(κn) = (κν) = (nν) = \frac{1}{2} (κ - ν) (κ + ν - 1), \qquad (3.48)$$

$$(κϱ) = (κπ) = \frac{1}{2} (κ - ϱ) (κ + ϱ - 1), \qquad (3.49)$$

$$(κι) = (κ, ϱ + π) = (ϱ + π - 1)^2 = (κ - ι - 1)^2 . \qquad (3.50)$$

272

The proof of each of these formulas can be easily established by a procedure similar to that used in the proof of Eq. (3.47). Note that although $\varkappa$ does not appear explicitly in (nv), fixing n and v fixes $\varkappa$. Equations (3.1) may be used to change the arguments of any of these formulas, and in the last member of Eqs. (3.49), ϱ can be replaced with π.

Equations (3.49) are especially useful when the number of reactants is known, but analytical problems lead to some uncertainty regarding the number of products in the observed stoichiometric relation. If, by any means, a reasonable value be assigned to $\varkappa$, the formula tells us at once how many mechanistic types are consistent with these parameters, all of which can be quickly written down. For example, if $\varrho = 3$, and $\varkappa$ is taken as 5, formula (3.49) gives $(\varkappa\varrho) = 7$, which may be confirmed by reference to Table 1.

The following formulas hold when three or four parameters are fixed

$$(\varkappa\iota n) = (\varkappa\iota v) = \varkappa - \iota - 1 = \varrho + \pi - 1 , \tag{3.51}$$

$$(\varkappa\varrho\iota) = (\varkappa\pi\iota) = (\varkappa\varrho\pi) = \varkappa - 1 , \tag{3.52}$$

$$(\varkappa\iota v n) = \varkappa - \iota - 1 , \tag{3.53}$$

$$(\varkappa\varrho\pi v) = \varkappa - \varrho , \tag{3.54}$$

$$(\varkappa\pi n v) = \varkappa - \pi , \tag{3.55}$$

$$(\varkappa\iota n v) = \varkappa - \iota - 1 . \tag{3.56}$$

There is only one mechanistic type for any other choice of four fixed parameters.

Finally, let us note that since the smallest value of $\varrho + \pi$ is 2, the largest value of $\iota = \varkappa - 2$. But $n - \iota \geqq 1$, so the largest value of ι also equals $n - 1$. Equating these values, we find $\varkappa - n = v = 1$, so that, $\varrho + \pi = 2$, $v = 1$, $n = \varkappa - 1$, $\iota = \varkappa - 2$, and $\varphi = 1$. Similarly, the largest value of $v = \varrho + \pi - 1$, which is also equal to $\varkappa - 1$. Equating these values, we find $n = \varkappa - v = 1$, so that $\varkappa = \varrho + \pi$, $\iota = 0$, $n = 1$, $v = \varkappa - 1$, $\varphi = 1$. Both cases can be easily verified by examining the first and last entries for a given $\varkappa$ in Table 1.

4 Modification and Design of Reaction Mechanisms

4.1 Modification of a Mechanism

A reaction mechanism will, in general, vary with varying experimental conditions. Nevertheless, Eqs. (3.1), which we now write in the form

$$v = \varkappa - n = \varrho + \pi - n + \iota ,$$

provide useful information regarding the allowed changes. Since v is invariant, only $\varkappa$, ϱ, π ι and n vary with experimental conditions. In particular, it follows from the first equality that $\varkappa$ and n must both increase or decrease by the same integral aliquot. If $\varkappa'$ and n' denote the new values of $\varkappa$ and n, and δ the change in these quantities, then

$$\varkappa' = \varkappa + \delta, \qquad n' = n + \delta. \tag{4.1}$$

Similarly, the equality of the first and third members yields

$$\varrho' + \pi' = \varrho + \pi + \varepsilon, \qquad \iota' = \iota + \delta - \varepsilon, \tag{4.2}$$

where ε is the change in $\varrho + \pi$, and the change in ι has been expressed in terms of ε and δ by means of the condition

$$\varrho' + \pi' - n' + \iota' = \varrho + \pi - n + \iota.$$

The integers δ, ε, which may be positive or negative, must be such that $\varkappa' \geqq \varrho' + \pi' \geqq 2$, $n' \geqq 1$, $\iota' \geqq 0$, and

$$\varrho' + \pi' - v = n' - \iota' \geqq 1.$$

It follows that if the changes in any two of $\varkappa$, $\varrho + \pi$, ι, or any two of n, $\varrho + \pi$, ι are determined, the changes in the other parameters can be calculated from Eqs. (4.1) and (4.2). The change in the multiplicity is, from the definition of ε and the invariance of v,

$$\varphi' = \varphi + \varepsilon.$$

Several interesting facts are immediate consequences of Eqs. (4.1) and (4.2). If there is no change in the number of components, there must be no change in the number of independent reactions, so that all changes are confined to the number of intermediates and the sum $\varrho + \pi$, both of which change in such a way that $\varrho + \pi + \iota$ is invariant. If there is no change in the sum $\varrho + \pi$, then $\varkappa$, ι, and n all increase or decrease by the same amount. If there is no change in ι, then n, $\varkappa$, and $\varrho + \pi$ all increase or decrease by the same amount. These particular cases, as well as Eqs. (4.1) and (4.2), can be verified by an examination of those entries of Table 1 with the same value of v.

Equations (4.1) and (4.2) can also be used when it is desired to modify a reaction mechanism. Suppose, for example, that $\varkappa$, ϱ, π, ι, n are the parameters of a mechanism conforming to Eqs. (3.1) for a specified value of v, then Eqs. (4.1) and (4.2) show how those parameters are required to change in order that $\varkappa'$, ϱ', π', ι', n' also satisfy Eqs. (3.1), while v remains unchanged.

As an illustration, consider the gas phase reaction of hydrogen and iodine

$$H_2 + I_2 \rightleftarrows 2\,HI \tag{4.3}$$

If the process is indeed bimolecular, then Eq. (4.3) represents the stoichiometry and the mechanism, so that $\varkappa = 3 = \varrho + \pi$, $\nu = 2$, $\iota = 0$. It was suggested [38], however, that at high temperatures another mechanism occurred

$$I_2 \rightleftarrows 2\,I\,,$$

$$I + H_2 \rightleftarrows HI + H\,, \qquad\qquad (4.4)$$

$$H + I_2 \rightleftarrows HI + I\,,$$

for which $\varkappa' = 5$, $n' = 3$, $\iota' = 2$, $\varrho' + \pi' = \varrho + \pi$. This mechanism, regarded as a modification of (4.3), conforms to (4.1) and (4.2) with $\delta = 2$, $\varepsilon = 0$. Similar considerations apply to another suggested mechanism [39]:

$$I_2 \rightleftarrows 2\,I\,,$$

$$I + H_2 \rightarrow H_2I\,, \qquad\qquad (4.5)$$

$$I + H_2I \rightarrow 2\,HI\,.$$

Equations (4.1) and (4.2) also apply when a mechanism is modified by making some reactions reversible or irreversible, since such changes will, in general, alter the mechanistic function of some components. Consider the mechanism

$$A + B \rightleftarrows C\,,$$

$$\qquad\qquad (4.6)$$

$$C \rightleftarrows B + D\,.$$

In this case, we have $\varkappa = 4$, $n = 2$, $\iota = 0$, $\nu = 2$, and $\varrho + \pi = 4$. The multiplicity is two, and the two mechanistic steps provide two independent stoichiometries. When the second step is irreversible, or when both steps are irreversible, C functions as an intermediate, and B as a catalyst. The stoichiometry is now

$$A \xrightarrow{B} D\,, \qquad\qquad (4.7)$$

and its multiplicity is $n - \iota = \varrho + \pi - \nu = 1$. The change in mechanism is consistent with Eqs. (4.1) and (4.2), for since $\varkappa' = \varkappa$, and $n' = n$, we have $\delta = 0$, $\varepsilon = -1$.

4.2 The Gas Phase Decomposition of Ozone

Although Eqs. (3.1) are useful for verifying the consistency of a given mechanism, and provide useful general constraints to be observed in the construction of mechanisms, they offer little practical assistance in the actual construction of a mechanism. On the other hand, Eqs. (3.38) provide a system of linear homogeneous equations satisfied by the mechanistic coefficients $\sigma_{i\alpha}$ for the independent reactions of a mechanism. Normally, these equations would be used to derive the conservation

conditions from values of the $\sigma_{i\alpha}$ defined by the mechanism, but if the conservation conditions can be written down, then the question arises as to how the equations can be solved to obtain the mechanistic coefficients, that is, the $\sigma_{i\alpha}$. To study this question, we shall consider a reaction that is simple enough to illustrate the essential ideas without involving lengthy computations, namely, the decomposition of ozone in the gas phase with atomic oxygen as the only intermediate. We shall also assume that the reaction is indifferent to the electronic state of atomic oxygen.

There is only one conservation condition:

$$3[O_3] + 2[O_2] + [O] = \text{constant} . \tag{4.8}$$

Since $\varkappa = 3$, and $v = 1$, there can only be two independent reactions, so that Eqs. (3.38) and (4.8) yield

$$\begin{aligned}
3\sigma_{11} + 2\sigma_{21} + \sigma_{31} &= 0 , \\
3\sigma_{12} + 2\sigma_{22} + \sigma_{32} &= 0 ,
\end{aligned} \tag{4.9}$$

where $\sigma_{1\alpha}$, $\sigma_{2\alpha}$, and $\sigma_{3\alpha}$ denote the coefficients of onzone, molecular oxygen, and oxygen atoms, respectively, in mechanistic step α. Alternatively, we have to find all solutions in integers of

$$3x + 2y + z = 0 , \tag{4.10}$$

and select pairs of independent solutions from the set of all solutions. One difficulty is immediately obvious: Eq. (4.10) admits infinitely many solutions in integers. Although the solution to the problem is not unique, the theory of homogeneous linear equations shows that the general solution is expressible in terms of a finite number of particular solutions. If we can write down a formula giving *all* solutions to the problem, then the formula also contains the desired solution, and all that remains is to formulate some means for sifting it from the formula. But the issue is *still* unsettled if we apply the customary procedure for solving linear homogeneous equations. To see this, observe that $(2,-2,2)$ and $(2,-3,0)$ are solutions of equation (4.10), and they are independent, since the rank of

$$\begin{pmatrix} 2 & -2 & -2 \\ 2 & -3 & 0 \end{pmatrix} \tag{4.11}$$

is 2. It would appear that the general solution of (4.10) is given as a linear combination of $(2,-2,-2)$ and $(2,-3,0)$ with integer coefficients, namely,

$$x = 2t + 2u , \qquad y = -2t - 3u , \qquad z = -2t , \tag{4.12}$$

where t and u assume the values 0, ± 1, $\pm 2,- \ldots$ But $(1,-1,-1)$ is a solution of (4.10) that is *not* contained in the solution-set (4.12). Equations (4.12) yield infinitely many solutions of (4.10), but they *omit* infinitely many solutions, namely, all solutions in which x and z are odd integers.

On the other hand, linear combinations of the two particular (independent) solutions $(-1,3,-3)$, $(0,1-2)$ give *all* solutions in the form

$$x = -t , \qquad y = 3t + u , \qquad z = -3t - 2u , \qquad (4.13)$$

where t and u again take on all integer values. The solution $(1,-1,-1)$ *is* contained in this set of solutions, being given by $t = -1$, $u = 2$, and it is easily shown that the solutions $(2,-2,-2)$, $(2,-3,0)$ are also contained in Eqs. (4.13).

The distinction between Eqs. (4.12) and (4.13) is that, in the latter case, the 2×2 determinants formed from the matrix of particular solutions

$$\begin{pmatrix} -1 & 3 & -3 \\ 0 & 1 & -2 \end{pmatrix} \qquad (4.14)$$

have the greatest common divisor 1, that is, they are relatively prime, whereas the determinants formed similarly from the matrix (4.1) are not.

Using Eq. (4.13), we can express the solutions of Eqs. of (4.9) in terms of four integer parameters

$$\sigma_{11} = -p , \qquad \sigma_{21} = 3p + q , \qquad \sigma_{31} = -3p - 2q ;$$

$$\sigma_{12} = -r , \qquad \sigma_{22} = 3r + s , \qquad \sigma_{32} = -3r - 2s . \qquad (4.15)$$

In order that these solutions be independent, the rank of the matrix

$$\begin{pmatrix} -p & 3p + q & -3p - 2q \\ -r & 3r + 2s & -3r - 2s \end{pmatrix}$$

must equal 2, so that p, q, r, s are subject to the condition

$$qr - ps \neq 0 \qquad (4.16)$$

As p, q, r, s take all integral values 0, ± 1, ± 2, . . ., subject to (4.16), we obtain *all* solutions of (4.9). In terms of chemical reactions, equations (4.15) imply

$$pO_3 \rightarrow (3p + q) O_2 - (3p + 2q) O ,$$

$$rO_3 \rightarrow (3r + s) O_2 - (3r + 2s) O . \qquad (4.17)$$
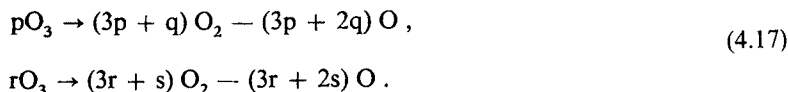
The possible cases can be delimited further by the following considerations (i) since the mechanism is to describe the decomposition of ozone, O_3 must appear by itself in the left-hand number of the first reaction; (ii) the intermediate O must appear in the right-hand member of the first reaction, but in the left-hand member of the second reaction; (iii) molecular oxygen may or may not appear in the right-hand member of the first step; (iv) if O_2 does not appear in the right-hand member of the

first-step, it must appear in the right-hand member of the second step. These requirements lead to the following additional conditions on p, q, r, s:

$$p > 0 , \tag{4.18}$$

$$3p + 2q < 0 , \tag{4.19}$$

$$3r + 2s > 0 , \tag{4.20}$$

$$3p + q \geqq 0 , \tag{4.21}$$

$$3r + s > 0 , \quad \text{if} \quad 3p + q = 0 . \tag{4.22}$$

Let us consider the implications of these relations for the first of reactions (4.17), supposing that molecular oxygen appears in the right-hand member. The appropriate relations are (4.18), (4.19), and (4.21) with the upper sign. The restrictions imposed by these inequalities can be quickly surveyed by a graphical representation in the qp-plane, Fig. 1. The solution domain is defined by the lines $p = 1$, $3p + q = 0$, and $3p + 2q = 0$, namely, the allowed values of p and q must lie above the line $p = 1$ and above the line $3p + q = 0$, but below the line $3p + 2q = 0$, the dashed lines in Fig. 1. The heavy dots are solutions allowed by the conditions $p > 0$, $3p + 2q > 0$, $3p + q > 0$. The reactions corresponding to some of these solutions are

$$O_3 \rightarrow O_2 + O ; \quad p = 1 , \quad q = -2 ; \tag{4.23}$$

$$\left. \begin{array}{l} 2\,O_3 \rightarrow 2\,O_2 + 2\,O , \\[2mm] 2\,O_3 \rightarrow O_2 + 4\,O ; \end{array} \right\} \quad p = 2 , \quad q = -4, -5 ; \tag{4.24}$$

$$\left. \begin{array}{l} 3\,O_3 \rightarrow 4\,O_2 + O , \\[2mm] 3\,O_3 \rightarrow 3\,O_2 + 3\,O , \\[2mm] 3\,O_3 \rightarrow 2\,O_2 + 5\,O , \\[2mm] 3\,O_3 \rightarrow O_2 + 7\,O ; \end{array} \right\} \quad p = 3 , \quad q = -5, -6, -7, -8 . \tag{4.25}$$
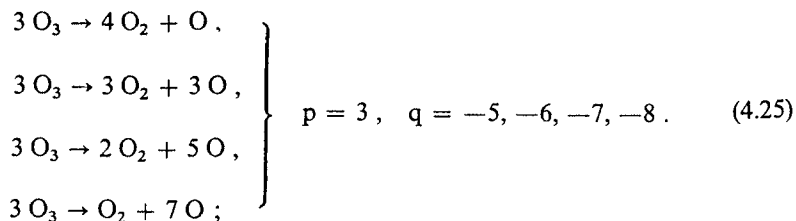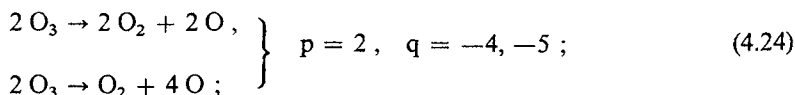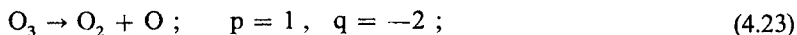
Note that multiples of equation (4.23) appear in equations (4.24) and (4.25), because the points corresponding to them, namely, (1, —2), (2, —4), (3, —6) all lie on a common ray within the solution domain. This will also occur with other solutions, being a natural consequence of the fact that equations (4.13) give all solutions of (4.10), including multiples of solutions.

The solutions for which molecular oxygen does not appear in the right-hand member of the first mechanistic step are shown in Fig. 1 by the open dots.
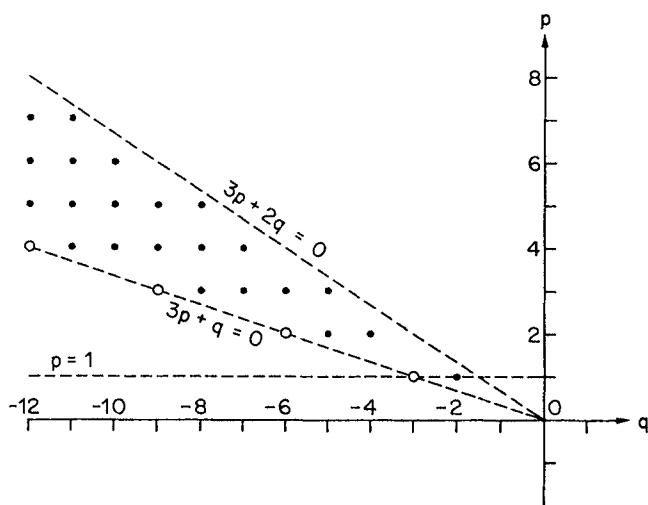
Fig. 1. Diagram for determining the integers p, q for the first step of the ozone decomposition: $pO_3 \rightarrow (3p + q) O_2 - (3p + 2q)$. The allowed values of p, q are determined by the lines $p = 1$, $3p + q = 0$, $3p + 2q = 0$

These solutions lie on or above the line $p = 1$, on the line $3p + q$, but below the line $3p + 2q$, so all constraints are satisfied. Since these solutions lie on the same ray, they are all multiples of

$$O_3 \rightarrow 3 O, \qquad p = 1, \qquad q = -3q. \tag{4.26}$$
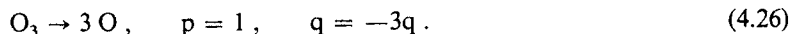
For the second step of the mechanism, the integer r may be positive negative, or zero, subject to the inequality (4.20). There are two cases to consider, according as $3p + q$ is greater than or equal to zero. If $3p + q > 0$, then all allowed solutions for r, s must lie above the line $3r + 2s = 0$ (Fig. 2). The allowed reactions include

$$O_3 + O \rightarrow 2 O_2, \qquad r = 1, \qquad s = -1, \tag{4.27}$$

$$2 O \rightarrow O_2, \qquad r = 0, \qquad s = 1, \tag{4.28}$$

$$O_3 + 3 O \rightarrow 3 O_2, \qquad r = 1, \qquad s = 0. \tag{4.29}$$
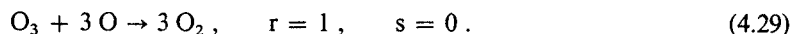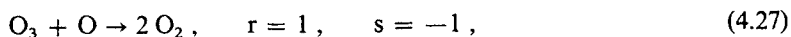
If $3p + q = 0$, then $3r + s$ must be greater than zero. But $3r + 2s$ must always be greater than zero, so that, for negative s, the allowed values of the parameters must lie above the line $3r + 2s = 0$, whereas the allowed parameters must lie above the line $3r + s = 0$ for positive s. For example,

$$O_3 + O \rightarrow 2 O_2 \qquad r = 1, \qquad s = -1. \tag{4.30}$$
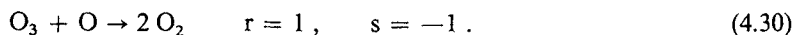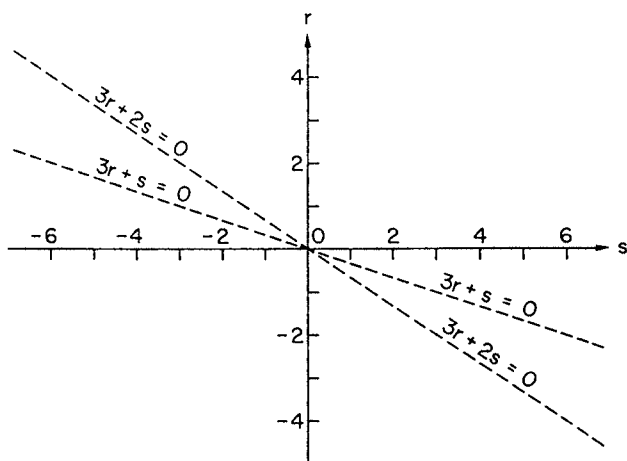
Fig. 2. Diagram for determining the integers r, s for the second step of the ozone decomposition: $rO_3 \rightarrow (3r + s) O_2 - (3r + 2s) O$. The allowed values of r, s are determined by the lines $3r + s = 0$, $3r + 2s = 0$

The allowed pairs of reactions for a two-step decomposition must also satisfy the condition (4.16). If we select from the reactions listed only those pairs that are at most bimolecular in the forward reaction, we have the following possible mechanisms

$$\left. \begin{array}{l} O_3 \rightarrow O_2 + O \\ O_3 + O \rightarrow 2\,O_2 \end{array} \right\}. \qquad (I)$$

$$\left. \begin{array}{l} O_3 \rightarrow O_2 + O \\ 2\,O \rightarrow O_2 \end{array} \right\} \qquad (II)$$

$$\left. \begin{array}{l} 2\,O_3 \rightarrow O_2 + 4\,O \\ O_3 + O \rightarrow 2\,O_2 \end{array} \right\} \qquad (III)$$

$$\left. \begin{array}{l} 2\,O_3 \rightarrow O_2 + 4\,O \\ 2\,O \rightarrow O_2 \end{array} \right\} \qquad (IV)$$

$$\left. \begin{array}{l} O_3 \rightarrow 3\,O \\ O_3 + O \rightarrow 2\,O_2 \end{array} \right\} \qquad (V)$$

$$\left. \begin{array}{l} O_3 \rightarrow 3\,O \\ 2\,O \rightarrow O_2 \end{array} \right\} \qquad (VI)$$

Mechanism (I) with a reversible first step has been found to provide a satisfactory description of the decomposition over a considerable range of concentrations [40].

4.3 General Considerations

To formulate the general problem, we write out Eq. (3.38) for mechanistic step α, namely,

$$a_{11}\sigma_{1\alpha} + a_{12}\sigma_{2\alpha} + ... + a_{1\varkappa}\sigma_{\varkappa\alpha} = 0 ,$$

$$a_{21}\sigma_{1\alpha} + a_{22} \quad \sigma_{2\alpha} + ... + a_{2\varkappa}\sigma_{\hat{E}\alpha} = 0 ,$$

$$\cdot \qquad \cdot \qquad \cdot \qquad \cdot \tag{4.31}$$

$$a_{v1}\sigma_{1\alpha} + a_{v2}\sigma_{2\alpha} + ... + a_{v\varkappa}\sigma_{\varkappa\alpha} = 0 .$$

The rank of this system is v, and its solution in integers gives the coefficients of the components in the αth mechanistic step. We shall assume that the $\varkappa$ components participating in the reaction, including intermediates, are known or assumed, so that we can write down the conservation conditions for mass and charge, the former being easily written out as atoms conservations. The rank of this system of linear relations gives the value of v, and from any set of v linearly independent conservation conditions, we obtain the a_{ij} of Eq. (4.31). In particular, the a_{ij} are all integers, and can be so chosen that their greatest common divisor is 1. Moreover, the a_{ij} in the equations for the atom conservations will be positive integers. Since the integer $\varkappa$ is given, and v can be determined, the mechanism contains exactly $n = \varkappa - v$ linearly independent mechanistic reactions. Starting with the system (4.31) for step α, we construct n particular solutions x_{rs}^α, $(r = 1, 2, ... , n; s = 1, 2, ... , \varkappa)$, such that all determinants contained in the matrix with elements x_{rs}^α have the greatest common divisor 1. The general solution of Eq. (4.31) may then be expressed in the form [41, 42]

$$\sigma_{s\alpha} = \sum_{r=1}^{n} \xi_r x_{rs}^\alpha , \qquad s = 1, 2, ..., \varkappa , \tag{4.32}$$

where the ξ_r are integers. From this representation we construct n independent solutions, one for each value α, as we did in the case of the ozone mechanism. Since the mechanism consists of n independent steps, the matrix $(\sigma_{s\alpha})$ is of rank n, that is, the construction of n independent sets $(\sigma_{1\alpha}, \sigma_{2\alpha}, ... , \sigma_{\varkappa\alpha})$, $\alpha = 1, 2, ... , n$, can in fact be accomplished.

Equations (4.32) yield an infinite number of reaction mechanism, all consistent with the conservation conditions. There are, however, a number of delimiting conditions that considerably reduce the number of possible mechanisms. If, for example, the subscript s in $\sigma_{s\alpha}$ denotes a component identified as a reactant, then $\sigma_{s\alpha} < 0$, for some mechanistic step α. It may, of course, also be true that $\sigma_{s\alpha} < 0$ for several steps, but, in general, the condition is only guaranteed for one step; there will, however, be one such condition for each reactant. Similarly, for each component identified as a product, $\sigma_{s\alpha} > 0$, for some step α. On the other hand, if s refers to an intermediate, then $\sigma_{s\alpha} > 0$, for some reaction α, but $\sigma_{s\beta} < 0$ for some reaction $\beta \neq \alpha$. In this way, we obtain $\sigma + \pi + 2\iota$ inequalities on the solutions of (4.32). These conditions, as well as

other possible conditions that might arise in particular instances, can be handled rather efficiently by computer programs now being written [14].

It is important to recognize what cannot be provided by the method of construction proposed here.

1. It is not possible to determine the reversibility of a step; it is possible, however, to include both options, that is, reversibility or irreversibility, in a computer program, though this would introduce 2^n additional contingencies in a mechanism with n steps.

2. It is not possible to determine if a mechanistic step contains a substance like M in mechanism (3.7), which serves a collisional function, but is otherwise chemically inert.

3. The method of analysis determines a set of n independent reactions consistent with the mass conservation conditions, but it cannot supply a *dependent* step that would indicate the mechanism is cyclic, or that a particular component is an intermediate rather than a product.

4. The nature of the intermediates cannot be determined. Such determinations depend upon energy considerations which have been avoided to maintain generality.

5 References

1. Lapworth A (1904) J. Chem. Soc. 85: 30
2. Bodenstein M, Lind SC (1907) Z. Phys. Chem. 57: 168
3. Christiansen JA (1919) Kongel. Danske Videnskab, Selskab., Math.-fysi. Medd. 1: 14
4. Herzfeld KF (1919) Z. Elektrochem. 25: 301; (1919) Ann. Physik. 59: 635
5. Polanyi M (1920) Z. Elektrochem. 26: 50
6. Rice FO, Herzfeld KF (1934) J. Am. Chem. Soc. 56: 284
7. Rice FO, Herzfeld KF (1935) The aliphatic free radicals, Johns Hopkins, Baltimore
8. Horiuti J, Nakamura T (1957) Z. Phys. Chem. 11: 358
9. Horiuti J (1973) Ann. N.Y. Acad Sci. 213: 5
10. Happel, Sellers PH (1982) Ind. Eng. Chem. Fundam. 21: 67
11. Côme (1983) in: Bamford CH, Tipper CFH (eds) Comprehensive chemical kinetics, Elsevier, Oxford, vol 24 chapt 3
12. Corio PL (1970) Trans. Ky. Acad. Sci. 32: 51
13. Barbara TM, Corio PL (1980) J. Chem. Ed. 57: 243
14. Corio PL (1984) J. Phys. Chem. 88: 1825
15. Corio PL (unpublished research)
16. Birkhoff GD, MacLane S (1977) A survey of modern algebra, 4th eds. MacMillan, New York, p 185
17. Manes M, Hofer LJE, Weller S (1950) J. Chem. Phys. 10: 1355
18. Hollingsworth CA (1952) J. Chem. Phys. 20: 921, 1649
19. Horiuti J (1957) Z. Phys. Chem. 11: 358
20. Denbigh KG (1981) The principles of chemical equilibrium, 4th edn, Cambridge University Press, London chapt 15
21. Blum EH, Luus R (1964) Chem. Eng. Sci. 19: 322
22. Boyd RK (1977) Chem. Rev. 77: 93
23. Hammett LP (1970) Physical organic chemistry, 2nd edn, McGraw-Hill, New York, p 54
24. Corio PL (1983) J. Phys. Chem. 87: 2416
25. Jouget E (1921) J. Ec. Polytech., Paris, II 21: 61
26. Brinkley SR Jr (1946) J. Chem. Phys. 14: 563, 586
27. Martin H (1966) Angew. Chem. Int. Ed., 78

28. Frost AA, Pearson RG (1961) Kinetics and mechanism, 2nd edn, Wiley, New York, p 380
29. Johnston HS (1966) Gas phase reaction rate theory, Ronald, New York, p 312
30. Steacie EWR (1954) Atom and free radical reactions, 2nd edn, Rheinhold, New York, p 206
31. Ashmore PG (1963) Catalysis and inhibition of chemical reactions, Butterworths, London, p 60
32. Huheey JE (1983) Inorganic chemistry, 3rd edn, Harper and Row, New York, p 658
33. Farkas L, Sachsee H (1935) Z. Phys. Chem. B 55: 222
34. Benson SW (1960) The foundations of chemical kinetics, McGraw-Hill, New York, p 398
35. Birkhoff GD, MacLane S (1977) A survey of modern algebra, 4th edn, MacMillan, New York, p 250
36. Chia Y-T, Connick RE (1956) J. Phys. Chem. Soc. 63: 1518
37. Anbar M, Taube H (1958) J. Am. Chem. Soc. 80: 1073
38. Benson SW, Srinivasan R (1955) J. Chem. Phys. 23: 200
39. Sullivan JH (1967) J. Chem. Phys. 46: 73
40. (a) Benson SW, Axworthy AE (1957) J. Chem. Phys. 26: 1718; (b) Reference 34, p 400
41. Smith HJS (1861) Phil. Trans. London 151: 293
42. Skolem T (1938) Diophantische Gleichungen, Springer, Berlin, p 4

other possible conditions that might arise in particular instances, can be handled rather efficiently by computer programs now being written [14].

It is important to recognize what cannot be provided by the method of construction proposed here.

1. It is not possible to determine the reversibility of a step; it is possible, however, to include both options, that is, reversibility or irreversibility, in a computer program, though this would introduce 2^n additional contingencies in a mechanism with n steps.

2. It is not possible to determine if a mechanistic step contains a substance like M in mechanism (3.7), which serves a collisional function, but is otherwise chemically inert.

3. The method of analysis determines a set of n independent reactions consistent with the mass conservation conditions, but it cannot supply a *dependent* step that would indicate the mechanism is cyclic, or that a particular component is an intermediate rather than a product.

4. The nature of the intermediates cannot be determined. Such determinations depend upon energy considerations which have been avoided to maintain generality.

5 References

1. Lapworth A (1904) J. Chem. Soc. 85: 30
2. Bodenstein M, Lind SC (1907) Z. Phys. Chem. 57: 168
3. Christiansen JA (1919) Kongel. Danske Videnskab, Selskab., Math.-fysi. Medd. 1: 14
4. Herzfeld KF (1919) Z. Elektrochem. 25: 301; (1919) Ann. Physik. 59: 635
5. Polanyi M (1920) Z. Elektrochem. 26: 50
6. Rice FO, Herzfeld KF (1934) J. Am. Chem. Soc. 56: 284
7. Rice FO, Herzfeld KF (1935) The aliphatic free radicals, Johns Hopkins, Baltimore
8. Horiuti J, Nakamura T (1957) Z. Phys. Chem. 11: 358
9. Horiuti J (1973) Ann. N.Y. Acad Sci. 213: 5
10. Happel, Sellers PH (1982) Ind. Eng. Chem. Fundam. 21: 67
11. Côme (1983) in: Bamford CH, Tipper CFH (eds) Comprehensive chemical kinetics, Elsevier, Oxford, vol 24 chapt 3
12. Corio PL (1970) Trans. Ky. Acad. Sci. 32: 51
13. Barbara TM, Corio PL (1980) J. Chem. Ed. 57: 243
14. Corio PL (1984) J. Phys. Chem. 88: 1825
15. Corio PL (unpublished research)
16. Birkhoff GD, MacLane S (1977) A survey of modern algebra, 4th eds. MacMillan, New York, p 185
17. Manes M, Hofer LJE, Weller S (1950) J. Chem. Phys. 10: 1355
18. Hollingsworth CA (1952) J. Chem. Phys. 20: 921, 1649
19. Horiuti J (1957) Z. Phys. Chem. 11: 358
20. Denbigh KG (1981) The principles of chemical equilibrium, 4th edn, Cambridge University Press, London chapt 15
21. Blum EH, Luus R (1964) Chem. Eng. Sci. 19: 322
22. Boyd RK (1977) Chem. Rev. 77: 93
23. Hammett LP (1970) Physical organic chemistry, 2nd edn, McGraw-Hill, New York, p 54
24. Corio PL (1983) J. Phys. Chem. 87: 2416
25. Jouget E (1921) J. Ec. Polytech., Paris, II 21: 61
26. Brinkley SR Jr (1946) J. Chem. Phys. 14: 563, 586
27. Martin H (1966) Angew. Chem. Int. Ed., 78

28. Frost AA, Pearson RG (1961) Kinetics and mechanism, 2nd edn, Wiley, New York, p 380
29. Johnston HS (1966) Gas phase reaction rate theory, Ronald, New York, p 312
30. Steacie EWR (1954) Atom and free radical reactions, 2nd edn, Rheinhold, New York, p 206
31. Ashmore PG (1963) Catalysis and inhibition of chemical reactions, Butterworths, London, p 60
32. Huheey JE (1983) Inorganic chemistry, 3rd edn, Harper and Row, New York, p 658
33. Farkas L, Sachsee H (1935) Z. Phys. Chem. B 55: 222
34. Benson SW (1960) The foundations of chemical kinetics, McGraw-Hill, New York, p 398
35. Birkhoff GD, MacLane S (1977) A survey of modern algebra, 4th edn, MacMillan, New York, p 250
36. Chia Y-T, Connick RE (1956) J. Phys. Chem. Soc. 63: 1518
37. Anbar M, Taube H (1958) J. Am. Chem. Soc. 80: 1073
38. Benson SW, Srinivasan R (1955) J. Chem. Phys. 23: 200
39. Sullivan JH (1967) J. Chem. Phys. 46: 73
40. (a) Benson SW, Axworthy AE (1957) J. Chem. Phys. 26: 1718; (b) Reference 34, p 400
41. Smith HJS (1861) Phil. Trans. London 151: 293
42. Skolem T (1938) Diophantische Gleichungen, Springer, Berlin, p 4

Author Index Volumes 101–150

Contents of Vols. 50–100 see Vol. 100
Author and Subject Index Vols. 26–50 see Vol. 50

The volume numbers are printed in italics